eman ta zabal zazu

Universidad del País Vasco
Euskal Herriko Unibertsitatea

Hippocampal Neural Stem Cells: From Origin to Disease

Postnatal and on-site generation of adult hippocampal neural stem cells and blocking of the epidermal growth factor receptor to preserve neurogenesis in temporal lobe epilepsy

Doctoral thesis opting to the PhD degree, presented by

Oier Pastor Alonso

2020

Supervisors:

Dr. Juan Manuel Encinas Pérez

Dr. José Ramón Pineda Martí

(c)2020 OIER PASTOR ALONSO

This doctoral thesis has been performed thanks to the usage of a UPV/EHU fellowship for the hiring of predoctoral researchers during 2016-2020

The experimental work has been financed by grants given by the Spanish Ministry of Economy and Competitiveness (http://www.mineco.gob.es) and FEDER funds (SAF-2015-70866-R and RYC-2012-11137).

TABLE OF CONTENTS

TABLE OF CONTENTS

1. LIST OF ABBREVIATIONS 3

2. SUMMARY 11

3. INTRODUCTION 17

3.1. Hippocampal formation (HPF): The brain seahorse 17

3.1.1. Anatomy and circuitry 17

3.1.2. Cognitive functions 20

3.1.3. DG: The complex gate 20

3.2. History of adult neurogenesis: 50 years to acceptance 22

3.3. Adult hippocampal neurogenic cascade 24

3.3.1. From neural stem cells (NSCs) to newborn neurons 25

3.3.2. NSCs: SCs? 28

3.3.3. Modulating factors of AHN 29

3.4. Adult hippocampal neurogenic niche: Development in rodents 31

3.4.1. Cortical hem (CH): First steps towards the HPF 31

3.4.2. Building the DG 32

3.4.3. Origin of adult NSCs 35

3.4.3.1. Embryonic origin of NSCs 36

3.4.3.2. Postnatal proliferation: generating adult NSCs 38

3.4.3.3. Dividing mechanisms of adult NSC precursors: Cyclin D2 (cD2) 40

3.4.3.4. Adult NSCs vs dNSCs 43

3.5. The hippocampal neurogenic niche in humans 44

3.5.1. Development of the human hippocampal neurogenic niche 45

3.5.2. hAHN: To be or not to be 47

TABLE OF CONTENTS

"Hippocampal NSCs: from Origin to Pathology"

3.6. Adult hippocampal neurogenic niche in pathology: Epilepsy 53

3.6.1. Mesial temporal lobe epilepsy (MTLE) 55

3.6.1.1. Rodent models of MTLE 57

3.6.1.2. MTLE-HS 58

3.6.1.3. MTLE and NSCs 61

3.6.2. Possible mechanisms in MTLE-HS 63

3.6.2.1. Fibroblast growth factor receptor (FGFR) 64

3.6.2.2. EGFR 65

3.6.2.3. Zinc (Zn^{+2}) as a mediator of EGFR activation after KA 72

3.6.2.4. Blocking EGFR signaling 76

4. HYPOTHESES AND OBJECTIVES 81

5. MATERIALS AND METHODS 89

5.1. Animals 89

5.2. Human Samples 90

5.3. Stereotaxic intrahippocampal injections 90

5.3.1. Postnatal SFFV-RV infections 90

5.3.2. Adult stereotaxic intrahippocampal injections 91

5.4. Treatments 92

5.4.1. Intranasal administration of the EGFR inhibitor Gefitinib 92

5.4.2. Subcutaneous administration of the Zn^{+2} chelator TPEN 92

5.4.3. BrdU administration 93

5.5. Cell cultures 93

5.6. RNA extraction RT-qPCR 94

5.6.1. RNA extraction and reverse transcription 94

5.6.2. RT-qPCR 94

5.7. IHC 95

5.7.1. Rodent brain tissue 95

5.7.2. Cell cultures 96

5.7.3. Human tissue 96

5.8. WB 100

5.9. ELISA 102

5.10. Danscher stainning 103

5.11. Image analysis 103

5.11.1. Quantitative analysis of cell populations 103

5.11.2. Morphological analysis of NSCs: SHOLL analysis 105

5.12. Statistical analysis 105

6. RESULTS 109

6.1. cD2 is essential for the formation of the adult NSC population 109

6.1.1. In the absence of cD2, adult NSC population failed to form 109

6.1.2. Cell death is not increased in the absence of *cD2* 116

6.2. Postnatal on-site generation of the adult DG NSC population 117

6.2.1. SFFV-RV infections to identify the spatial origin of adult NSCs 118

6.2.2. Only DG-located precursors contributed to generate adult NSCs 122

6.2.3. Divergent spatial contribution to the DG from DMS progenitors 128

6.3. LPA_1 as a differential marker of adult NSCs 129

6.3.1. NSCs acquired LPA_1 expression during the postnatal period 130

6.3.2. The cellular specificity of LPA_1-EGFP expression switched from postnatal to adult stages 132

6.4. Human DG development is almost ended by mid-gestation 133

6.4.1. The DMS was present in the early human development (GW14) 133

6.4.2. Differential spatial patterns during DG development 135

6.4.3. DG formation is restricted to the GCL by GW30 137

6.4.4. A RGC scaffold was still present in the DG early after birth 138

6.5. FGFR1 was not involved in the early response of the neurogenic niche after MTLE induction 140

6.6. EGFR was involved in the early response of the neurogenic niche after MTLE induction 143

6.6.1. Increased expression and activation of the EGFR signaling pathway were early events after the induction of MTLE 143

6.6.2. EGFR participated in the proliferating activity of cultured NSPCs 147

6.6.3. Pharmacological blockage of EGFR ameliorated the pathological response of NSCs after MTLE 153

6.7. The role of Zn^{+2} on the NSC activation and React-NSC induction after MTLE 159

6.7.1. The levels of Zn^{+2} increased in the neurogenic niche in MTLE 159

6.7.2. Zn^{+2} promoted proliferation in NSPCs in a dose-dependent manner 162

6.7.3. The intrahippocampal administration of Zn^{+2} mimicked the alterations produced in the neurogenic niche in MTLE 163

6.7.4. The effect of Zn^{+2} on the neurogenic niche was EGFR-mediated 167

6.7.5. Zn^{+2} chelation in MTLE increased cell death in the GCL 170

6.8. HB-EGF was massively released in the DG after KA 171

7. DISCUSSION 181

7.1. Adult NSCs are genereated on-site in the DG after birth 181

7.1.1. Cyclin D2 is fundamental for the postnatal generation of adult NSCs 181

7.1.2. dNSCs divide on-site in the DG to generate adult NSCs 184

7.1.3. LPA_1 differentiates adult NSCs from dNSCs 189

7.2. Human and mouse DG share similitude in their formation 191

7.2.1. The DG formation is almost completed between GW14-GW30 192

7.2.2. The human DG develops differently along the longitudinal axis 193

7.2.3. RGCs remain in the DG early after birth: Potential role as NSCs? 194

7.3. EGFR is involved in the early response of NSCs in MTLE 195

7.3.1. EGFR, but not FGFR, overexpression is an early event after KA 196

7.3.2. EGFR mediates the massive activation and induction of React-NSCs 198

7.4. Zn^{+2} as a mechanism in the early response of the neurogenic niche and the NSCs in MTLE 203

7.4.1. Zn^{+2} effect can be driven by EGFR activation 204

7.4.2. Zn^{+2} chelation as a therapeutic approach in MTLE 207

7.5. Massively released HB-EGF can activate EGFR in NSPCs in MTLE 207

8. CONCLUSIONS 213

9. BIBLIOGRAPHY 219

1. LIST OF ABBREVIATIONS

1. LIST OF ABBREVIATIONS

AHN	Adult hippocampal neurogenesis
ANOVA	Analysis of variance
ANP	Amplifying neural progenitor
AP	Anteroposterior
AREG	Amphiregulin
ASCL1	Achaete-Scute Family BHLH Transcription Factor 1
ATP	Adenosine tryphosphate
BBB	Blood brain barrier
BDNF	Brain-derived neurotrophic factor
BLBP	Brain lipid-binding protein
BMP	Bone morphogenetic protein
BTC	Betacellulin
BrdU	5-bromo-2'-deoxyuridine
BSA	Bovin Serum Albumin
CA	Cornu ammonis
cD	Cyclin D
CDK	Cyclin dependent kinase
CH	Cortical hem
CNS	Central nervous system
CR	Cajal retzius
CSK	C-terminal Src kinase
CX	Cortex
CXCL	Chemokine ligand
CXCR	Chemokine receptor
CTRL	Control
D	Dorsal
DCX	Doublecortin
DG	Dentate gyrus
DMS	Dentate migratory stream
DMSO	Dimethyl sulfoxide
DNA	Deoxyribonucleic acid
DNe	Dentate neuroephitelium
dNSC	Developmental neural stem cell

LIST OF ABBREVIATIONS

"Hippocampal NSCs: from Origin to Pathology"

DV	Dorsoventral
EHU/UPV	Euskal Herriko unibertsitatea/Univesidad del País Vasco
E*x*	Embryonic day *x*
EC	Entorhinal cortex
EEG	Electroencephalograph
EGF	Epidermal growth factor
EGFP	Enhanced green fluorescent protein
EGFR	Epidermal growth factor receptor
EM	Electron microscopy
EMX	Empty spiracles homeobox
EPGN	Epigenin
EPR	Epiregulin
ERK	Extracellular signal regulated kinases
FDJ	Fimbrio-dentate junction
FI	Fimbria
FGF	Fibroblast growth factor
FGFR	Fibroblast growth factor receptor
FOXG	Forkhead box G
GABA	Gamma-aminobutyric acid
GC	Granule cell
GCD	Granule cell layer dispersion
GCL	Granule cell layer
GEFI	Gefitinib
GFP	Green fluorescent protein
GFAP	Glial fibrillary acidic protein
GPCR	G protein-coupled receptor
GW	Gestational week
hAHN	Human adult hippocampal neurogenesis
HATA	Hippocampus-amygdala transition area
[3H]-TdR	Tritium
HB-EGF	Heparin binding EGF-like growth factor
HCL	Chlorhydric acid
HF	Hippocampal fissure
HH	Hedgehog
HNe	Hippocampal neuroepithelium
HOPX	Homeodomain protein box

HP	Hippocampus
HPF	Hippocampal formation
HS	Hippocampal sclerosis
HuB	HTLV-I U5RE binding protein
HVC	High vocal center
IHC	Immunohistochemistry
ILAE	International league against epilepsy
KA	Kainic acid or kainate
L	Lateral
LHX	LIM homeobox
LL	Laterolateral
LV	Lateral ventricle
M	Medial
MAM	Methylazoxymethanol
MAPK	Mitogen activated protein kinase
MEK	Mitogen-activated protein kinase kinase (MAPK/ERK)
ML	Molecular layer
MMP	Matrix metalloproteinase
mRNA	Messenger ribonucleic acid
MT	Methallothionein
MTLE	Mesial temporal lobe epilepsy
MF	Mossy fiber
ML	Molecular layer
NB	Neuroblast
NESTIN	Neuroectodermal stem cell intermediate marker
NGN	Neurogenin
NSC	Neural stem cell
NSPC	Neural stem and progenitor cell
OB	Olfactory bulb
OPC	Oligodendrocyte precursor cell
P*x*	Postnatal day *x*
PBD	Phosphotyrosine binding domains
PBS	Phosphate buffered saline
PFA	Paraformaldehyde
PKB	Protein kinase B
PI_3K	Phosphoinositie 3-kinase

LIST OF ABBREVIATIONS

"Hippocampal NSCs: from Origin to Pathology"

PIP-3	Phosphatidylinositol-3,4,5-triphosphate
PSA-NCAM	polysialic neural cell adhesion molecule
PP	Perforant path
REACT-NSC	Reactive neural stem cell
RGC	Radial glia cell
RT-qPCR	Real time quantitative polymerase chain reaction
SAL	Saline
SC	Stem cell
ScRNA-seq	Single cell ribonucleic acid sequencing
SDF	Stromal cell-derived factor
SE	Status epilepticus
SEM	Standard error mean
SH2	Src homology 2
SFFV-RV	Spleen-focus forming virus gamma-retroviruses
SHH	Sonic hedgehog
SGZ	Subgranular zone
SMO	Smoothened
SOX2	Sex determining region Y box 2
SPZ	Subpial zone
STAT	Signal transducers and activator of transcription proteins
SUB	Subiculum
SuFu	Suppressor of fused
SVZ	Subventricular zone
TBR	T-box brain protein
TBS-T	Tris-buffered saline (TBS) and Polysorbate 20 (Tween)
TLE	Temporal lobe epilepsy
TKI	Tyrosine kinase inhibitors
TGFα	Transforming growth factor α
TNT	Phosphate buffered saline with 0.05% Triton-X100
TPEN	*N*,*N*,*N′*,*N′*-tetrakis(2-pyridylmethyl) ethylenediamine
UCSF	University of California, San Francisco
UPV/EHU	University of the Basque Country
V	Ventral
VEGF	Vascular endothelial growth factor
VGLUT	Vesicular glutamate transporter
vHPF	Ventral hippocampal formation

VZ	Ventricular zone
WB	Western blot
WNT	Wingless related interaction site
WT	Wild type
Zn^{+2}	Zinc
ZnT	Zinc transporter

2. SUMMARY

2. SUMMARY

The brain of most mammals is capable of producing newly born neurons during the whole life, including postnatal and adult periods, throughout a process called adult neurogenesis. It is now well-established that the core cells that fundament the whole adult neurogenic process are adult neural stem cells (NSCs). These cells give birth to neurons that integrate into the existent circuitry in at least two regions of the brain; the subventricular zone (SVZ) of the lateral ventricles (LVs) and the subgranular zone (SGZ) of the dentate gyrus (DG). The DG is part of the hippocampal formation (HPF) and therefore, the neurogenic process here is termed adult hippocampal neurogenesis (AHN).

In mice, it was described that the AHN diminishes over time. Indeed, a dramatic neurogenic decline is associated with aging and it has been proposed to occur mainly because of NSC depletion, due to the ultimate astrocytic or neuronal differentiation of those NSCs that enter the cell cycle ("get activated") to generate neuronal precursors. Although self-replication of NSCs is possible in the adult SGZ it is not enough to outpower the progressive depletion of the NSC population. Therefore, the total neurogenic capacity of an individual will be determined by the initial number of NSCs. Although the origin of adult NSCs is not well known, the generally accepted view in the field is that they, as well as the process of AHN, are a remnant from the embryonic hippocampal development.

In humans, the actual occurrence and extent of AHN has been historically subject of fierce debate. Recently, the debate got rekindled due to a controversial work reporting the absence of AHN from childhood onwards. However, other authors have reported the presence of doublecortin (DCX)-expressing cells in the SGZ of the adult DG, inferring thus the presence of AHN. The two opposing views remain under debate up to this day.

In the first part of this thesis, we address the developmental origin of adult NSCs. For that, we studied the postnatal development of the DG in a knock-out mouse for cyclin D2 (cD2) crossed with a Nestin-Green fluorescent protein (GFP) transgenic line of mice in which NSCs are readily visualized. We also used region-targeted retroviral infections to permanently label dividing cells and their progeny in different regions of the postnatal brain. The results indicated that the adult population of NSCs is

generated on-site in the DG around postnatal days 2-7 through a cD2 dependent process. This suggests that adult NSCs comprise a separated population from developmental progenitors, being generated postnatally in an independent manner. Therefore, the process of postnatal and AHN is not a mere continuation of the embryonic development. These results are also supported by the differential expression of a biomarker that is not present in developmental NSCs. Using the transgenic lysophosphatidic acid receptor 1 (LPA_1)-Enhanced green fluorescent protein (EGFP) mouse model, we observed that LPA_1 starts to be expressed in NSCs only from postnatal day 10-14 (P10-P14) onwards, and then its expression remains throughout adulthood in hippocampal NSCs.

As mentioned, the existence of AHN in humans recently became a hot topic in the field with strongly controversial results being reported. Addressing the issue from a developmental point of view, we described that human and mouse developmental processes may follow different temporal dynamics, although sharing similar formation patterns. In contrast to mouse, where the DG develops mainly postnatally, in humans it is almost completely formed by mid-gestation. However, radial glia cell (RGC) populations are still present early after birth. Indeed, the existence of a population of NSCs in the human DG after birth (independent on the temporal extent) could be of great importance in pathological conditions.

The loss, disruption or alteration of the hippocampal neurogenic niche arguably results in the impairment of all the related tasks such as learning, memory, pattern separation, axiety, etc. In fact, the pathological alteration of AHN has been related to different neurodegenerative diseases such as epilepsy, Parkinson's, Alzheimer's, Huntington's or dementia. In all these pathologies at least part of the symptoms could be potentially caused or favored by reduced or altered AHN. Indeed, my host laboratory has recently shown how seizure-induced neuronal hyperactivity induces NSCs to become reactive NSCs (React-NSCs), drastically changing their mitotic and morphological properties and ultimately generating reactive astrocytes at the almost complete expense of neurogenesis.

In the second part of this thesis, using a model of mesial temporal lobe epilepsy (MTLE) in which a single injection of kainic acid (KA) is delivered into the HPF, we studied the role of the epidermal growth factor receptor (EGFR) signaling pathway in the onset of the neurogenic niche pathological response to seizures. EGFR is upregulated in NSCs early after seizures, and using the reversible EGFR inhibitor

Gefitinib (used for the treatment of glioma) after MTLE induction, we show that the massive proliferating activity and React-NSC induction is significantly ameliorated, suggesting a major role of the pathway in this process. Importantly, neurogenesis, measured by the presence of DCX-expressing immature neurons is recovered in the MTLE mice that were administered with Gefitinib. Furthermore, we demonstrate that the increased release of zinc (Zn^{+2}) after seizures also contributes to the induction of React-NSCs, either by direct stimulation of EGFR or by potentially promoting the cleavage of membrane-bound heparin binding-epidermal growth factor (HB-EGF), a natural ligand of EGFR..

3. INTRODUCTION

3. INTRODUCTION

3.1. Hippocampal formation (HPF): The brain seahorse

3.1.1. Anatomy and circuitry

It was 1587 when the anatomist Giulio Cesare Arantius found deep inside the medial temporal lobe of the human brain a curious structure that strongly resembled a seahorse. Acknowledging this similarity he took the Greek word for this sea creature and named the region "*hippocampu*s" (HP) (Arantius, 1587). Since then, this archicortical structure has been continuously raising the interest of uncountable researchers that have worked to unravel its morphological and functional properties. Nowadays, the term HP refers to a structure that was also termed "*cornu ammonis"* (CA) or "*ammon's horn*" due to its similarity to a ram horn and after the Egyptian god Amun Knepth, whose symbol was a ram (de Garengeot, 1742). Curiously, the CA nomenclature was thereafter maintained to define the subfields of the HP (CA1, CA2, CA3 and CA4) **(Figure I1 A)**.

The HP is functionally connected to related brain regions that together comprise the HPF, first represented by Camillo Golgi (Golgi, 1886) and thoroughly described by Santiago Ramón y Cajal (Ramón y Cajal, 1893, 1911) and his student Raphael Lorente de Nó (Lorente de Nó, 1934). Based on their studies, we nowadays know that the HPF is formed by different structures other than HP, that include the subiculum, presubiculum, parasubiculum, entorhinal cortex (EC), alveolus, hippocampal fissure (HF), hippocampal tail, HP-amygdala transition area (HATA) and also the dentate gyrus (DG) (Iglesias et al., 2015) **(Figure I1 A)**. These structures, although varying in size, are present in all mammals from rodents to humans **(Figure I1 B)**.

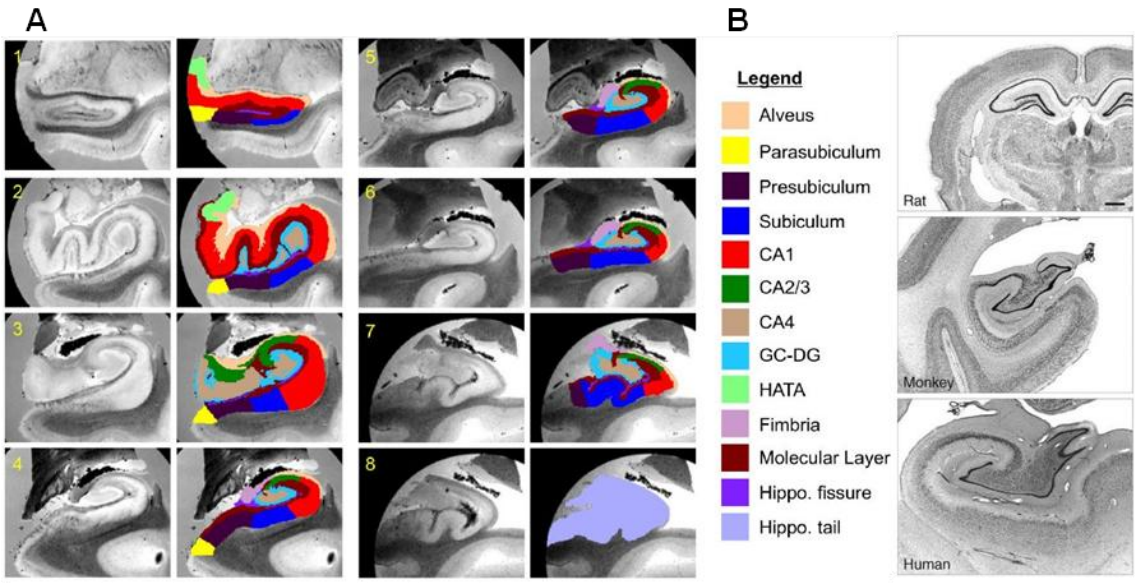

Figure I1. A) Different subfields of the HPF. **B)** HPF of rat, monkey and human (modified from Iglesias et al., 2015 and Savage et al., 2013).

The studies performed by Theodore Wilhelm Blackstad and colleagues on the 60s shed light on the HPF circuitry. They described how the different structures are linked mostly by unidirectional connections (Blackstad, 1956, 1958; Blackstad et al., 1970) and portrayed the main circuit of the HPF, the so-called "*trisynaptic circuit*" (Andersen et al., 1966). Stellate and pyramidal neurons from the EC project their output to the dendrites of the DG excitatory granule cells (GCs) through the perforant path (PP). GCs extend their axons, the mossy fibers (MFs), to CA3, where Schaffer collateral axons send the major input to CA1 field (Andersen et al., 1966; Steward and Scoville, 1976). Moreover, CA1 neurons project back to EC deep layers and to the subiculum, which in turn close the loop connecting to the cortical areas that originally projected to the HPF (Köhler, 1985a) **(Figure I2)**. More recently, it was described a disynaptic circuit where EC excitatory inputs directly reach CA2 neurons, which in turn send strong output to CA1 (Chevaleyre and Siegelbaum, 2010). Also, the subiculum has been shown to be a modulator of the neurotransmission along the PP (Köhler, 1985b; Shipley, 1975).

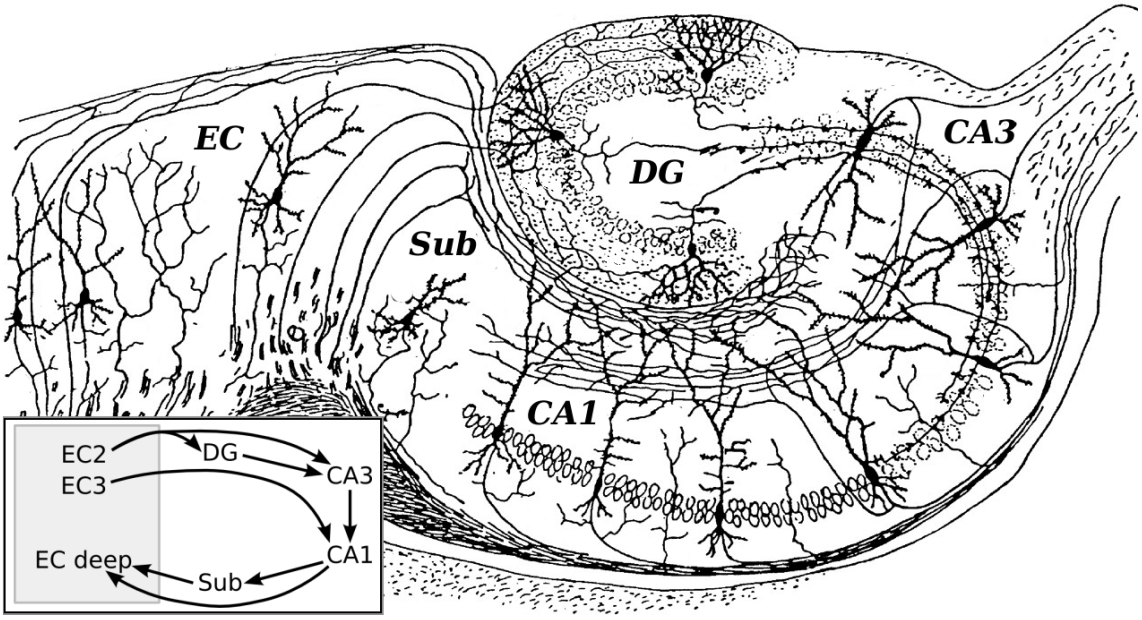

Figure I2. The hippocampal circuitry first performed by Santiago Ramón y Cajal (1909) visualizing neurons using Golgi. Later, Theodore Blackstad and colleagues will further describe these connections (see inset) (Blackstad, 1956, 1958; Blackstad et al., 1970) and Per Andersen will baptized them as the "*trisynaptic circuit".*

Following the concept of trisynaptic circuit, Per Andersen and its collaborators postulated that hippocampal circuitry exists in a transversal way, repeating along the septotemporal axis and creating slices, or lamella, of interconnected regions. They called this theory "*the lamellar hypothesis of the hippocampal connectivity*" (Andersen et al., 1971). Although this hypothesis supposed one of the first important steps in the way to define hippocampal connectivity, years later several studies demonstrated that this was an extremely simple theory and that the HPF showed both internal regional complex connectivity patterns and external connections to other brain regions such as the septum, hypothalamus, amygdala and neocortex (Sloviter and Lømo, 2012).

During the early 2000s, the field of hippocampal neuroanatomy took a huge step forward by combining genomic and neuroanatomical experiments such as microarray analysis and microdissection techniques. Hence, several authors provided molecular basis for the previously defined anatomic hippocampal subfields, revealing differential region-specific molecular expression between and within the adult mouse hippocampal subfields (Datson et al., 2001, 2004; Lein et al., 2004, 2005, 2007; Zhao et al., 2001). Furthermore, this heterogeneity on the molecular expression has been demonstrated also along the septotemporal axis (Leonardo et al., 2006; Thompson et al., 2008). These discoveries were crucial to facilitate functional studies on the different structures and neuronal subtypes of the HPF.

3.1.2. Cognitive functions

The HPF is involved in important cognitive functions, as it has been shown through animal and human studies. After Alf Brodal questioned for the first time the widely held view that the HPF was a specific part of the olfactory system (Brodal, 1947), important advances were made underlying its role in learning and memory. In 1957, William Beecher Scoville and Brenda Milner studied patients who underwent bilateral surgery to remove both hippocampi as a solution to their psychosis or, in the famous case of H.M., constant seizures caused by epilepsy. They reported severe loss of recent memory consequent to hippocampal extraction (Scoville and Milner, 2000). Since then, the importance of the HPF in these cognitive processes has been long addressed in rodents and humans and it is a widely accepted concept nowadays (Jarrard, 1993; Moscovitch et al., 2005). Nevertheless, spatial representation and anxiety has also been reported to be dependent on the HPF functionality (McNaughton and Gray, 2000; Moser et al., 2017). Specifically, the ventral HPF (vHPF) has been reported to participate in anxiety-related behaviors while the dorsal HPF (dHPF) relates more to memory and learning processes (Bannerman et al., 2004).

3.1.3. DG: The complex gate

The DG is the most medial area of the HPF (Medina and Abellán, 2009; Puelles, 2001) and its main input region. As part of the archicortex, it is a structure divided in three layers and comprised by a principal layer called granule cell layer (GCL), formed by a dense population of excitatory GCs and also inhibitory pyramidal basket cells located at the border between GCL and the next layer of the DG; a polymorphic layer named hilus, mainly populated by mossy cells (inhibitory) and excitatory neurons, that serves as a connecting region for CA and DG; and the molecular layer (ML), a relatively cell-free layer mainly populated by the GC dendrites, PP fibers and few interneurons, as well as glial cells (Amaral et al., 2007; Lorente de Nó, 1934) **(Figure I3)**. Thus, the DG is a complex structure in which the functionality of the HPF highly relies. Several authors have described the DG as the gate of the HPF, where incoming inputs get filtered by the dentate-hilar complex, therefore modulating pattern separation and specific memory creation (Acsády and Káli, 2007; Hsu, 2007). When a stimulus reaches the DG, GCs activate following a sparse coding. A small number of cells get activated each time, thus enabling a sensitive pattern separation capacity both in rodents and humans (Bakker et al., 2008; Chawla et al., 2005; Leutgeb et al., 2007).

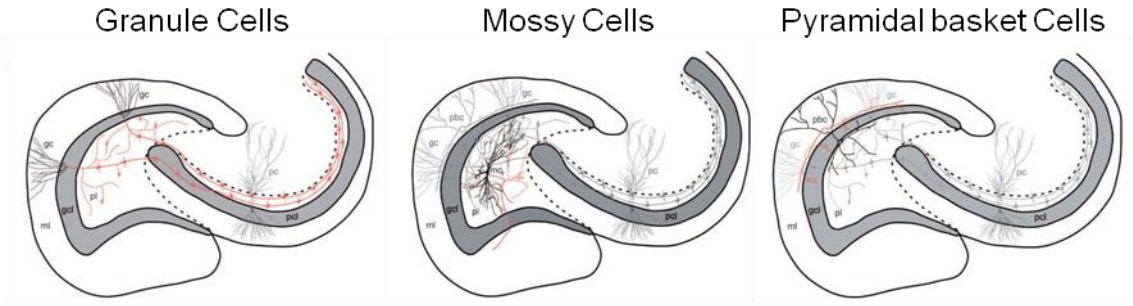

Figure I3. Different neuronal types in the DG (modified from Amaral et al., 2007).

One of the main characteristics that distinguish the DG as a unique structure in mammalian brain is the capacity to generate newborn neurons during the whole life. Thus, neurons are added continuously to the already existing circuit in a process known as adult hippocampal neurogenesis (AHN), modulating several brain functions in the normal and pathological brain. However, a role for newborn neuron generation in the adult brain was not first described in mammals but in birds. The pioneering studies of Fernando Nottebohm and colleagues were the first step on the study of the involvement of adult neurogenesis in learning and memory associated with spatial information. The formation of new neurons in the high vocal center (HVC) of avian brain was demonstrated to be related to hormonal patterns, seasonal and sex differences and also complex experiences that affect song learning (Goldman and Nottebohm, 1983; Nottebohm, 2004).

Over the last two decades AHN has been associated with memory and learning. The generation and integration of new neurons in the hippocampal circuit have been suggested to help weakening old memories, strengthening the capacity to learn new things and acquire new information (Abrous and Wojtowicz, 2015; Akers et al., 2014; Drew et al., 2013; Gould et al., 1999a; Shors et al., 2001; Treves et al., 2008; Vivar and van Praag, 2013). Also, it has been long related the relevance of AHN for pattern separation, facilitating the spatial and temporal contextual memory (Deng et al., 2010; Vivar et al., 2016) and encoding temporally related memories (Aimone et al., 2006; Becker and Wojtowicz, 2007; Clemenson et al., 2015). However, this idea has recently been discussed (Becker, 2017). In fact, there is controversy between rodent studies that relate, or do not, AHN to different cognitive functions. Therefore, the variability between studies makes it difficult to draw conclusions on the specific role of AHN, though it seems safe to claim its relation to learning and memory in general terms.

3.2. History of adult neurogenesis: 50 years to acceptance

In 1958, Bernard Messier and colleagues discovered clusters of dividing cells underlying the ependyma of the lateral ventricle (LV) in mice (Messier et al., 1958), and these cells were further suggested to be a continuous source of glia in rats (Bryans, 1959). Later, Ian Smart and Charles Phillipe Leblond continued these studies in mice reporting that subependymal cells did divide, although they did not add a significant population of new cells to the adult brain, possibly balanced by cell death (Smart and Leblond, 1961). However, even though their discoveries were fundamental for the posterior research and findings, they failed to find adult newborn neurons and they did not report any cell division in the DG.

It was not until the 60-70s when the generation of newborn cells in the adult brain, which nobody considered it possible until then, appeared on the spotlight of the neuroscience field, with Joseph Altman as the visible head of several studies that laid the groundwork of adult neurogenesis. Using thymidine labeled with tritium (a radioactive isotope of hydrogen; ([^{3}H]-TdR) he studied brain lesions in rats and found neuronal cells in the DG that unequivocally retained this radiolabelled signal. This finding led him to wonder for the first time about the possibility of new neuronal production in the adult HPF and brain in general (Altman, 1962a, 1962b). He quickly performed another study in adult rats and cats in which he found high rates of ependymal cell multiplications in the LVs and frequent labeling of GCs in the DG (Altman, 1963). During the following decade, combining [^{3}H]-TdR and histological analyzes, he and his collaborators described that effectively the observed dividing cells were generating new neurons in the LVs, from where they migrated to the olfactory bulb (OB) to supply with new neuronal populations (Altman, 1969a; Altman and Das, 1965). They also described adult neurogenesis happening in the caudate nucleus and cerebellum of rats (Altman, 1969b; Das and Altman, 1971). Finally, in collaboration with his colleague Gopal Das, they found adult neurogenesis in the DG of rats, cats, and guinea pigs (Altman and Das, 1965, 1967).

Subsequent studies using previous [^{3}H]-TdR techniques combined to electron microscopy (EM) supported the idea that the [^{3}H]-TdR labeled cells in the adult rat DG and OB were in fact young neurons and not any other cell type (Kaplan and Hinds, 1977). Moreover, additional evidence was provided by Kaplan and colleagues when they found adult neurogenesis in the visual cortex (Kaplan, 1981) and in the DG of 9-month old rats (Kaplan and Bell, 1983), being product of dividing neuroblasts (NBs)

(Kaplan and Bell, 1984). More importantly, it was later demonstrated the existence of adult neurogenesis in higher vertebrates, after finding dividing cells in the subependymal layer of the LVs in rhesus monkey (Kaplan, 1983).

However, adult neurogenesis was yet to find several setbacks on its way to acceptance. The skepticism of the field was well represented first in the book published by Hubert Korr in which against the evidence of newborn neuron generation in the adult rodent brain he reviewed previous works where adult neurogenesis was indeed not found and posed under doubt the interpretation about [^{3}H]-TdR labeled cells being neurons (Korr, 1980). Moreover, Pasko Rakic reported the non-existence of adult neurogenesis in higher vertebrates. He analyzed the HPF of rhesus monkey and described how only a few cells divided in the DG after birth, doing so only during the first postnatal months and not in the adult life (Eckenhoff and Rakic, 1988; Rakic, 1985). He reported the absence of adult-born neurons in any other brain region and charged against the previous study of Michael Kaplan, also in rhesus monkey, arguing misinterpretation of the nature of the dividing cells. He claimed that glial cells had been taken for neurons and damaged cells for dividing cells (as during the mechanism of deoxyribonucleic acid (DNA) reparation, damaged cells remove the damaged nucleotide and insert the correct one, or in this case [^{3}H]-TdR, without implying mitotic process) (Rakic, 1985). That same year, Kaplan published a work defending his method based on ultrastuctural analysis through EM as the only valid method for the assessment of the neuronal nature of an adult-born cell and therefore discrediting the absence of adult neurogenesis claimed by Rakic (Kaplan, 1985). The field was polarized and immersed in a fierce debate and adult neurogenesis would have to wait many more years to become widely accepted.

One of the main findings that allowed important discoveries in the field was the development of a monoclonal antibody directed against 5-bromo-2'-deoxyuridine (BrdU), a synthetic nucleoside analog of thymidine, allowing immunohistochemical staining of cells which have incorporated this compound into their DNA during replication (Gratzner et al., 1982). The use of BrdU was introduced and adapted by Miller and Nowakowski for studying cell proliferation, migration and time of origin of cells in the developing brain (Miller and Nowakowski, 1988). A year later, they used BrdU labeling to successfully find AHN in juvenile rodent brains, although they interpreted their results as hilar proliferation during the development of the DG without linking it to adult neurogenesis (Nowakowski et al., 1989).

During the 90s, BrdU was successfully employed to demonstrate the existence of adult neurogenesis in rodents in both the subventricular zone (SVZ) of the LV (Corotto et al., 1993) and subgranular zone (SGZ) of the DG (Cameron et al., 1993; Kuhn et al., 1996; Seki and Arai, 1993) **(Figure I4)**. More importantly, towards the end of the decade Elizabeth Gould et al. published several works using BrdU and showing the existence of AHN in treeshrews and old world monkeys (Gould et al., 1997, 1999b, 1999a) and in the SVZ of macaques (Gould et al., 1999c). This time, the discoveries were supported by other authors, including Pasko Rakic and colleagues (Kornack and Rakic, 1999, 2001; Pencea et al., 2001), although they reported that AHN in old world monkeys was, relatively, ten times lower than in rodent studies (Kornack and Rakic, 1999). Thus, in spite of the unsettled opinion about the correct usage and interpretation of BrdU during the next years (Nowakowski, 2000), almost half a century after Altman's discoveries the concept of adult neurogenesis in the mammalian SVZ and SGZ got fully accepted and started to be intensely studied. After 50 years struggling to outweigh the heavy power of an already established idea; the "everything may die, nothing may be regenerated" dogma was dead (Gross, 2000).

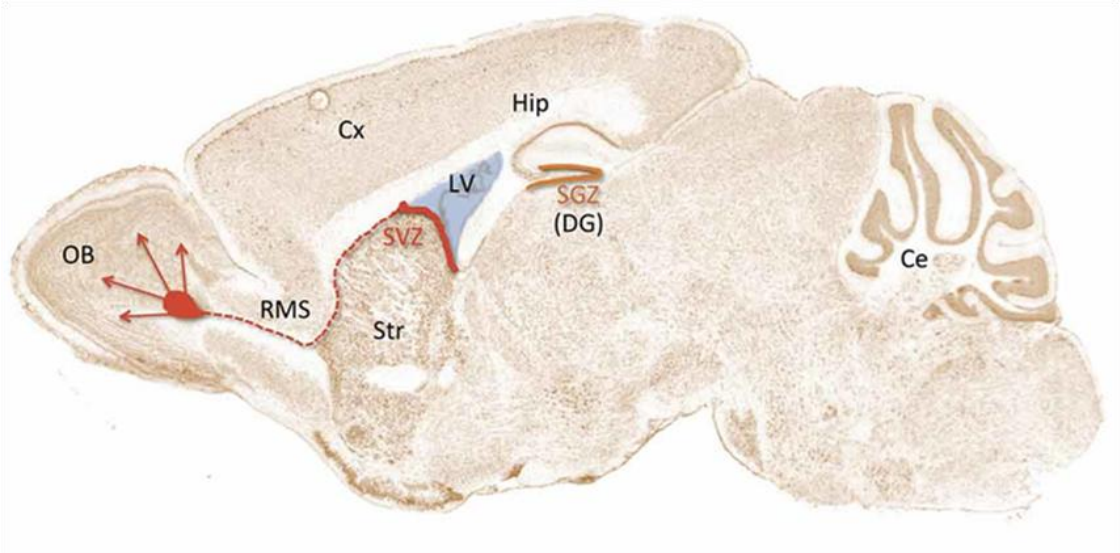

Figure I4. Adult neurogenic niches in the SVZ of the LV wall and SGZ of the hippocampal DG.

3.3. Adult hippocampal neurogenic cascade

The discovery of the *in vitro* neurogenic capabilities of cells residing in the adult SVZ and the DG (Palmer et al., 1997; Reynolds and Weiss, 1992; Richards et al., 1992) rapidly brought discussion over the existence of undifferentiated, multipotent stem cells (SCs) (potentially producing neurons, astrocytes and oligodendrocytes) with endless or prolonged self-renewing capacity along the entire life of an individual

(McKay, 1997; Seaberg and Van Der Kooy, 2003; Watt and Hogan, 2000; Weiss et al., 1996). SCs are able to divide both symmetrically, producing two cells committed to the same fate, or asymmetrically, giving two distinct cell types**.** The intermediate cell type between the SC and the finally differentiated cell is called progenitor. Opposing SC properties, progenitors are unipotent and have limited self-renewal capacity. From a functional perspective, they serve to amplify the final progeny and allow SCs to keep their multipotent nature (Watt and Hogan, 2000; Weiss et al., 1996).

3.3.1. From neural stem cells (NSCs) to newborn neurons

In the adult DG, radial glia cells (RGCs) expressing the glial fibrillary acid protein (GFAP) (Kosaka and Hama, 1986; Rickmann et al., 1987) were found to be capable of dividing, although this proliferating capacity was initially related to gliogenesis (Cameron et al., 1993; Kaplan and Bell, 1984). However, years later Arturo Alvarez-Buylla and colleagues described for the first time, using BrdU to label and trace mitotic cells, that GFAP-positive radial astrocytes acted as SCs and were indeed generating newborn neurons in the SGZ of the adult DG (Seri et al., 2001).

Shortly after, transgenic lines of mice in which NSCs could be labeled based on the expression of the specific neuroepithelial SC marker neuroectodermal stem cell intermediate marker (Nestin) were developed (Lendahl et al., 1990). These new transgenic mice allowed for a detailed characterization of the SGZ radial astrocytes that immunostaining alone could not provide. Thus, the neurogenic radial astrocytes that represented the first step of the adult neurogenic cascade were called type-1 cells (Filippov et al., 2003; Kronenberg et al., 2003). They were defined as those cells showing a characteristic morphology, with the soma located in the SGZ and a process extending towards the ML that branched once reaching the outer region of the GCL, creating a broccoli-like crown (Filippov et al., 2003; Mignone et al., 2004) **(Figure I5 A)**. In addition to GFAP and Nestin, they have been described to show expression of other markers such as Vimentin, Brain Lipid-Binding Protein (BLBP) and Sex determining region Y box 2 (Sox2), as well as to lack expression of the mature astrocyte marker S100β (Encinas and Enikolopov, 2008; Filippov et al., 2003; Gould et al., 1992; Yamaguchi et al., 2000). These cells have also been referred to as quiescent neural progenitors, as at the population level they are mainly quiescent, with only the 2-5% of them dividing in a given moment (Encinas et al., 2011a). The term progenitor was also preferred because it had been only demonstrated that they gave rise to neurons and not other cell type and therefore they did not comply with the definition of SC.

Currently, they are generally accepted as *bona fide* NSCs (and this is the way we will refer to them from now on) as they are considered to be multipotent and can self-renew. Nonetheless, their SC nature is still discussed, as we will later address.

The mechanisms and dynamics by which NSCs divide have been long addressed by the scientific community, aiming to unravel the cell division patterns in the adult SGZ. Using inducible lineage tracing combined with BrdU labeling and later two-photon *in vivo* imaging, it has been reported that once activated, NSCs divide an average of 3 times (Encinas et al., 2011a; Pilz et al., 2018), giving birth (asymmetrically in most occasions) to a copy of themselves and a rounded daughter cell lacking GFAP and Vimentin expression (Encinas et al., 2006; Kempermann et al., 2004; Kronenberg et al., 2003; Seki et al., 2007). While the fate of this progenitors is neurogenic, activated NSCs finally differentiate into astrocytes thereby losing their neurogenic capabilities (Encinas et al., 2011a) **(Figure I5 B)**. Depletion of activated NSCs by neurogenic symmetric division is also possible (Pilz et al., 2018) and in fact it has been suggested using mathematical modeling that the astrocytic differentiation of NSCs might not account for all the depletion of the NSC pool (Ziebell et al., 2018). This study also supported that the oscillation between quiescence and activation would better explain the maintenance and exhaustion of the NSC pool. However the *in vivo* data by (Encinas et al., 2011a; Pilz et al., 2018) support the contrary. Once activated the vast majority of NSCs will divide several times consecutively and then exit the NSC pool through astrocytic or neurogenic differentiation. Nonetheless, the dynamics of NSC activation and depletion can change with age. NSCs could become more quiescent overtime and therefore their exhaustion would be slowed down (Kalamakis et al., 2019; Martín-Suárez et al., 2019) so that even in the aged brain NSCs, and neurogenesis, remain. Different mechanisms are involved in this change of behaviour, ranging from the increase in neuroinflammatory modulators (Kalamakis et al., 2019; Martín-Suárez et al., 2019) to age-related increase of glucocorticoid receptors by NSCs (Schouten et al., 2019).

In any case, the modulation of the activation of NSCs will determine the level of neurogenesis in a given time point but also have consequences in the long term. Understanding the mechanisms underlying NSC activation will also be of special relevance in those pathological situations in which NSC activation is abnormally increased. According to previous findings Achaete-Scute Family BHLH Transcription Factor 1 (Ascl1) is essential for the regulation of cell cycle in NSCs, showing a dynamic expression along the different cell stages of the hippocampal neurogenic cascade (Kim

et al., 2011). The induction of Ascl1 expression when NSCs receive activating signals provokes the subsequent entrance into a proliferating state. Moreover, blockage of Ascl1 renders NSCs unresponsive to activating stimuli (Andersen et al., 2014) and the destabilization of Ascl1 by the E3 ubiquitin ligase Huwe1 provokes the return of NSCs to a quiescent state (Urbán et al., 2016). In addition, the level of activated Notch1 plays a fundamental role in the NSC choice to remain quiescent or divide. Low levels of activated Notch1 promote NSC activation, although the complete ablation of Notch1 also provokes the transition of NSCs to an intermediate progenitor or neuronal state (Breunig et al., 2007a; Guentchev and McKay, 2006). Bone Morphogenetic Proteins (BMPs) are also involved in the maintenance of NSCs quiescence, preventing them from getting activated and preserving the neurogenic capacity of the niche (Mira et al., 2010), as well as gamma-aminobutyric acid (GABA), which is also important as a niche signal to maintain adult NSCs quiescence (Song et al., 2012). Interestingly, epidermal growth factor receptor (EGFR) has been shown to be expressed in activated NSCs (Jhaveri et al., 2015; Okano et al., 1996; Walker et al., 2016) and since its ligand epidermal growth factor (EGF) can modulate the proliferation of NSCs in the SVZ (Craig et al., 1996; Reynolds and Weiss, 1992), it seems logic to conclude that EGFR signaling pathway may play a role in the activation of hippocampal NSCs as it will be discussed in detail later.

After NSCs enter mitosis, they give birth to intermediate progenitors known as amplifying neural progenitors (ANPs), also called type-2 cells (Filippov et al., 2003), that expand themselves through symmetric divisions actively dividing around 2-5 times at a population level (Encinas et al., 2011a; Pilz et al., 2018). ANPs, modulated by GABA-induced excitatory tonic input (Tozuka et al., 2005), exit cell cycle to differentiate into doublecortin (DCX) and polysialic acid neural cell adhesion molecule (PSA-NCAM) expressing type-3 NBs. These NBs also start to express markers that will retain as mature neurons, such as Prox1 (particular to GCs) and NeuN (Encinas et al., 2006; Filippov et al., 2003; Kempermann et al., 2004; Seri et al., 2004). Importantly, around two thirds of cells transitioning from ANP to NB undergo apoptosis, being efficiently phagocytosed by microglia in a process critical for AHN (Sierra et al., 2010, 2014). The surviving newborn neurons undergo several morphological changes during the posterior three weeks. They evolve from being a round cell with short processes to a multipolar cell with multiple neurites, to finally extend an apical dendrite until it branches in the ML and the axon towards CA3 (Seri et al., 2004; Stanfield and Trice, 1988; Zhao et al., 2006a). Thus, together with the onset of glutamatergic input, new

GCs get integrated into the already existing hippocampal circuit (Van Praag et al., 2002) **(Figure I5 B)**.

The different steps of the neurogenic cascade have been assessed also at transcriptomic level by the use of single cell ribonucleic acid-sequencing (scRNA-seq). First, it was described that quiescent NSCs display a different molecular program once activated, decreasing their extrinsic signaling capacity and therefore becoming less responsive to environmental input (Shin et al., 2015). Further studies showed specific molecular changes across the different steps of the neurogenic cascade from quiescent NSCs to mature neurons, supporting the transition across each of the cellular types previously described (Artegiani et al., 2017; Hochgerner et al., 2018).

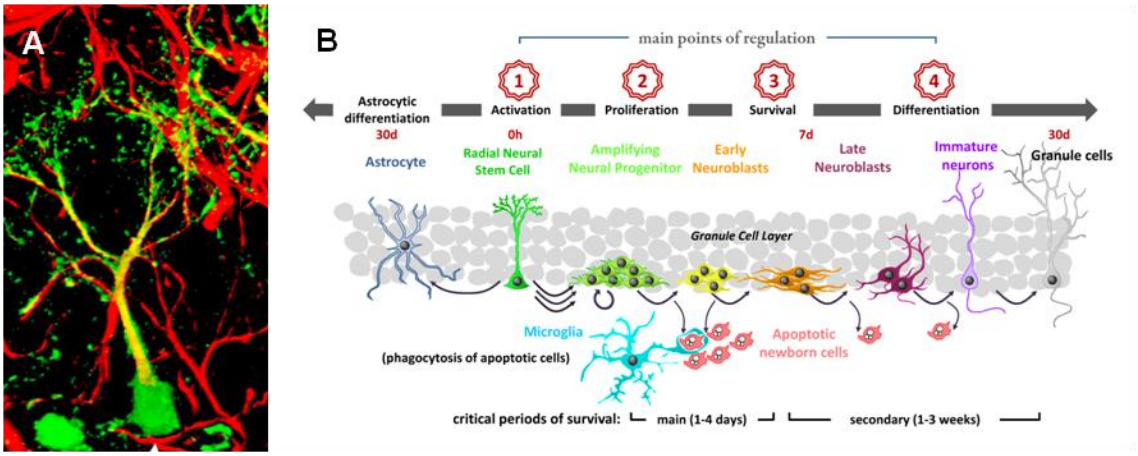

Figure I5. A) Nestin (green)- and GFAP (red)-expressing NSC with the soma located in the SGZ and the process extending towards the ML, where it arborizes forming a broccoli-like crown. **B)** Hippocampal neurogenic cascade. NSCs, with radial morphology, are mostly quiescent, but once activated they divide several times consecutively asymmetrically to give rise to ANPs that either die by apoptosis or slowly differentiate into mature granule cells (modified from Encinas et al., 2011 and Encinas and Sierra 2012).

3.3.2. NSCs: SCs?

As mentioned, the multipotency of the SGZ NSCs remains an opened debate in the field. NSCs have been shown to generate both neurons and astrocytes (Bonaguidi et al., 2011; Encinas et al., 2011b) and some authors have claimed that they possess self-renewing capabilities (Bonaguidi et al., 2011). Moreover, some studies were able to artificially induce oligodendrocytes from SGZ neural stem and progenitor cells (NSPCs) either by overexpression of Ascl1, Olig2 and Sox10 (Braun et al., 2015) or inactivation of Neurofibromin 1 (Sun et al., 2015), being remarkable their functional capability to remyelinate cells (Braun et al., 2015). However, this multipotency has

been opposed by studies indicating that SGZ NSCs are not able to give oligodendrocytes in several different *in vitro* conditions, and that they only undergo self-renewal when co-culturing with embryonic tissue, being influenced by developmental niche inputs that modulate them (Clarke and Van Der Kooy, 2011; Seaberg and Van der Kooy, 2002; Seaberg and Van Der Kooy, 2003).

Michael Bonaguidi et al. interpreted their results that self-renewal of NSCs took place in the DG based on the close proximity of clonally labeled NSCs. By minimal sparse labeling of NSCs in inducible Nestin-GFP transgenic mice (labeling initially just one or two cells per DG) they concluded that two NSCs located proximal to each other could only came from the same precursor cell and therefore that NSCs have the capacity to symmetrically divide generating two copies of them. However, since NSC show a natural cluster organization (Mineyeva et al., 2018), this conclusion seems to be premature and it calls for further research. Even more if we take into account that other studies have reported the absence of NSC self-renewal (Encinas et al., 2011a). More recently, chronic *in vivo* imaging has shown that NSCs are capable to symmetrically divide and expand themselves, although the majority of divisions are asymmetric. Nonetheless, NSCs do not return to quiescence once they get activated (Pilz et al., 2018), meaning that the natural progressive depletion cannot be counterbalanced by symmetric division of NSCs.

We understand that the SC nature of SGZ NSCs implies more than a semantic issue, significantly affecting the way we investigate and draw conclusions regarding these cells. Establishing whether they are life-long SCs or on the contrary a differentiated cell type with neurogenic capabilities will be important for addressing future investigations from the correct scope.

3.3.3. Modulating factors of AHN

The hippocampal neurogenic cascade can be modulated by multitude of factors, either augmenting or reducing the generation of newborn neurons. Among the stimuli that promotes AHN there are dietary restriction (Lee et al., 2000a), enriched environment (Kempermann et al., 1998; Nilsson et al., 1999), hippocampal-dependent learning-tasks (Gould et al., 1999a; Lemaire et al., 2000), physical exercise (Hodge et al., 2008; Kronenberg et al., 2003; Van Praag et al., 1999), Fluoxetine (Encinas et al., 2006) and deep brain stimulation (Encinas et al., 2011b). Also, any stimulus causing neuronal hyperactivity will lead to an increase in cell proliferation and neurogenesis (Deisseroth et al., 2004). Normally, the increase in AHN happens by an effect upon

ANPs, thereby preserving quiescent NSCs intact and the neurogenic reservoir conserved.

On the contrary, several drugs (alcohol, nicotine, opiates) have been associated with decrease in AHN. Likewise, stressful experiences have been reported to reduce AHN as well (Gould et al., 1998, 1999b; Tanapat et al., 2013), relating this effect to the release of glucocorticoids in response to stressors (Gould and Gross, 2002). However, one of the most studied phenomenon provoking a decrease in AHN is the age itself (Altman and Das, 1965; Barker et al., 2005; Beccari et al., 2017; Encinas et al., 2011a; Kalamakis et al., 2019; Kempermann et al., 1998; Seki and Arai, 1995) **(Figure I6)**. As it was previously mentioned, once activated NSCs divide and end up losing their neurogenic capabilities by ultimately differentiating into astrocytes or neurogenic progenitors. Taking into account that the proportion of active NSCs remains constant over time, the continuous and exponential depletion of NSCs is the main driving force underlying the age-related decline in AHN (Encinas and Sierra, 2012; Encinas et al., 2011a). Despite the potential NSC ability to self-renew, previously discussed, it is not enough to overcome the NSC loss at a population level (Bonaguidi et al., 2011; Encinas et al., 2011a; Pilz et al., 2018). Altogether, these dynamics suggest the importance of the initial number of NSCs, as they will determine the total hippocampal neurogenic output in the life of an individual. It is therefore crucial to shed light upon a fundamental question that has been intriguing the field during several decades. When and how are adult hippocampal NSCs generated?

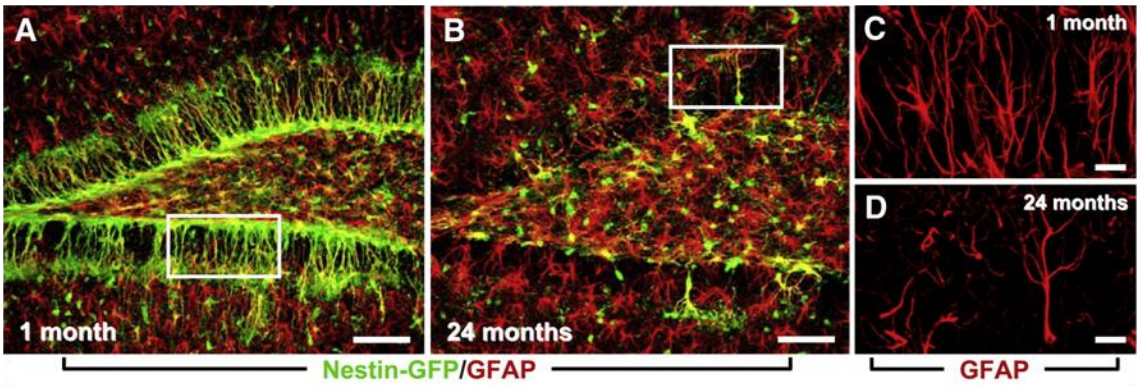

← **Previous page. Figure I6.** Depletion of NSC population with age. **A)** Young DG full of NSCs along the SGZ. **B)** Elderly DG in which there are only few remaining NSCs. **C-D)** Close confocal pictures of the GCL of young (C) and old (D) mice (taken from Encinas et al., 2011).

3.4. Adult hippocampal neurogenic niche: Development in rodents

3.4.1. Cortical hem (CH): First steps towards the HPF

During telencephalon development, the dorsal midline region invaginates at embryonic day 8.5 (E8.5) to give rise to paired telencephalic vesicles. Concomitantly, the dorsal telencephalon is subdivided along the medial-lateral axis into three regions. The most lateral region, called cortical neuroepithelium forms the cerebral cortex. The medial tissue becomes reorganized and subdivided into the most medial part, the choroid plexus epithelium and a longitudinal strip of neuroepithelium generated in the intermediate part, termed the CH by Elizabeth Grove and colleagues. The medial location of the CH is defined by its rich expression of proteins from the two main superfamilies related to axis generation and SC proliferation during embryonic development: The protein families of Wingless-related integration site (Wnt) and transforming growth factor ß (Tgfß), to which BMPs belong. Hence, CH is a fundamental region to provide patterning cues to the adjacent developing HPF (Furuta et al., 1997; Grove et al., 1998) **(Figure I7)**.

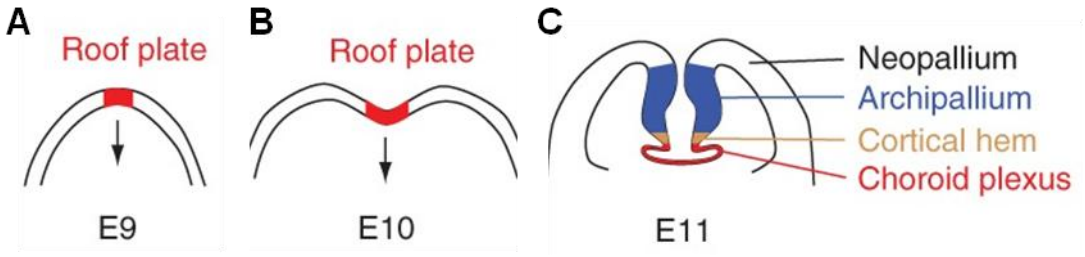

Figure I7. A-B) At E9, the roof plate starts to invaginate in response to Wnt and BMP signalization (Furuta et al., 1997; Grove et al., 1998). **C)** At E11, the different regions of the medial telencephalon are already observable, including the CH (modified from Grove et al., 1998).

The instrumental role of the CH on normal hippocampal development was proven by studies using different mutant mice for the Wnt signaling pathway, in which HPF failed to normally develop (Galceran et al., 2000; Lee et al., 2000c; Zhou et al., 2004). Moreover, in another study where the CH was completely ablated basing on the *Wnt3a* and empty spiracles homeobox 1 (*Emx1*) co-expression (restricted to CH in the telencephalon), the HPF was also absent at mid gestation. These results showed that the CH comprises the first step in the HPF development (Yoshida et al., 2006). Moreover, the activation of Wnt signaling outside the prospective HPF, as in the cortical neuroepithelium, causes the appearance of hippocampal phenotypes in

neocortical territory, with upregulated subset of hippocampal markers (Machon et al., 2007).

BMP has also been reported to be a critical regulator of CH activity working as a suppressor of different Wnt-inhibiting signals such as fibroblast growth factor 8 (Fgf8) or LIM homeobox 2 (Lhx2), and therefore conserving the CH identity (Monuki et al., 2001; Shimogori et al., 2004). In fact, *Lhx2* expression is restricted to the cortical neuroepithelium cells, and not CH. In its absence, the CH expands at the expense of the cortical neuroepithelium, causing detailed hippocampal field specification in the neocortex (Bulchand et al., 2001; Mangale et al., 2008). Similar effects were described in the absence of forkhead box G1 (Foxg1), where mice showed an expanded CH (Muzio and Mallamaci, 2005). These findings strongly support the role of the CH as hippocampal organizer.

The CH is also a source for Cajal-Retzius (CR) cells that migrate to cortical regions to form a neuronal layer critical for the laminar organization of the neocortex (García-Moreno et al., 2007; Takiguchi-Hayashi et al., 2004; Yoshida et al., 2006; Zhao et al., 2006b). Interestingly, CR cells were described to be present in the HPF and more specifically in the prospective ML of the developing DG (Del Río et al., 1995; Soriano et al., 1994). From this strategic location, they orchestrate the development of the DG via reelin (Brunne et al., 2014; Förster et al., 2002; Frotscher et al., 2003; Sibbe et al., 2009; Stanfield and Cowan, 1979; Wang et al., 2018; Zhao et al., 2004), p73 (Meyer et al., 2004) and stromal cell-derived factor 1 (SDF1) (Berger et al., 2006; Li et al., 2009) and also play a role in hippocampal synaptogenesis (Borrell et al., 1999; Del Rio et al., 1997; Del Río et al., 1996)

3.4.2. Building the DG

Several authors, including Joseph Altman himself, performed pioneering studies to describe the development of the DG. It was described how neurons travel from the LV wall into the DG following a migration route along the fimbria. However, it was under debate whether those migrating neurons divided or not along the way (Altman and Das, 1965, 1966, 1966; Schlessinger et al., 1975; Stanfield and Cowan, 1979). It was not until the early 90s that Joseph Altman and Shirley Bayer described thoroughly the origin, migration and settling of the principal cells comprising the HPF, with special emphasis on the DG (Altman and Bayer, 1990a, 1990b). Thus, they established the basis for future research on the topic.

Dorsal to the CH, the ventricular region gets defined by two morphogenetically distinct components. The dentate neuroepithelium (DNe) originates from a ventricular indentation called the dentate notch. Here is where the first progenitor pool that will generate GCs arises, also known as the primary dentate matrix (Altman and Bayer, 1990c; Nakahira and Yuasa, 2005; Seki et al., 2014). Following the ventricle dorsally, the ammonic neuroepithelium will give rise to the pyramidal neurons of CA in a process that will end before birth. Also, the CH will develop into the fimbrial glioepithelium, giving rise to glial cells of the fimbria. Together, these three structures form the hippocampal neuroepithelium (HNe) from which the majority of HPF arises (Altman and Bayer, 1990c) **(Figure I8)**.

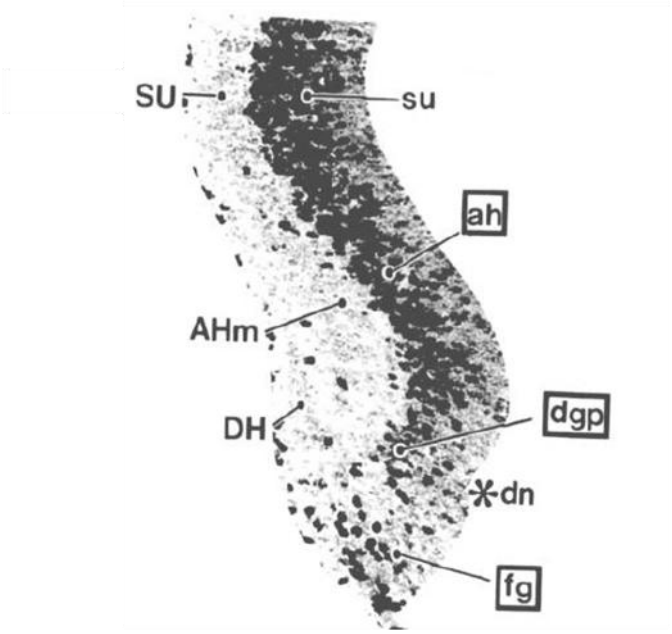

Figure I8. The three different regions of the HNe as were first described by Joseph Altman: Ammonic neuroepithelium, DNe and fimbrial neuroepithelium (modified from Altman and Bayer 1990). ah: Ammonic neuroepithelium. *AHm: Ammonic migration. dgp: primary dentate neuroepithelium. DH: Dentate hilus cells. dn: Dentate notch. fg: fimbrial glioepithelium. SU: Subiculum. su: Subicular neuroepithelium.*

From the ventricular zone (VZ) of the DNe developmental NSCs (dNSCs) exit the contact with the ventricle, forming a migration route along the subpial region towards the prospective DG known as dentate migratory stream (DMS). These dNSCs constitute the secondary dentate matrix (Altman and Bayer, 1990a; Hodge et al., 2013; Li et al., 2009; Nakahira and Yuasa, 2005; Seki et al., 2014) **(Figure I9 A-B)**. They proliferate all the way until they reach the HF. Once there, they form a transient neurogenic niche that will generate the first GCs. These primitive neurons will allocate

in the outer layer of the GCL comprising the skeleton of the structure (Hodge et al., 2013; Li et al., 2009; Seki et al., 2014).

Around birth, a second migration route takes place, where dNSCs exit the subpial region at the fimbrio-dentate junction (FDJ) level to enter the hilus and form the so-called tertiary dentate matrix **(Figure I9 C-D)**. As the secondary dentate matrix gets depleted, this new dNSC pool will give rise to the neurons that will build the GCL from superficial (outer) to deeper (inner) layers (Altman and Bayer, 1990a; Hodge et al., 2013; Nakahira and Yuasa, 2005; Namba et al., 2005, 2007, 2011; Seki et al., 2014; Sugiyama et al., 2013). Still, the role of the secondary matrix during the early postnatal period remains under debate. It is not clear whether it remains active giving birth to GCs or on the contrary acts as a mere source from which tertiary matrix dNSCs arise.

As a final step in the GCL formation, it has been reported that immature neurons migrate tangentially from the tertiary matrix to find their right position into the GCL (Namba et al., 2007, 2019). However, the main mechanism by which they reach the GCL is radial migration (Nakahira and Yuasa, 2005; Namba et al., 2019), guided by elongated RGCs that describe the path for the migrating cells. As the postnatal development proceeds, the tertiary matrix disappears from the hilus, and a layer of neuronal precursors gets restricted to the SGZ under the GCL, being responsible for neurogenesis throughout the adulthood (Altman and Bayer, 1990a; Hodge et al., 2013; Li et al., 2009; Namba et al., 2005; Nicola et al., 2015; Seki et al., 2014; Sugiyama et al., 2013).

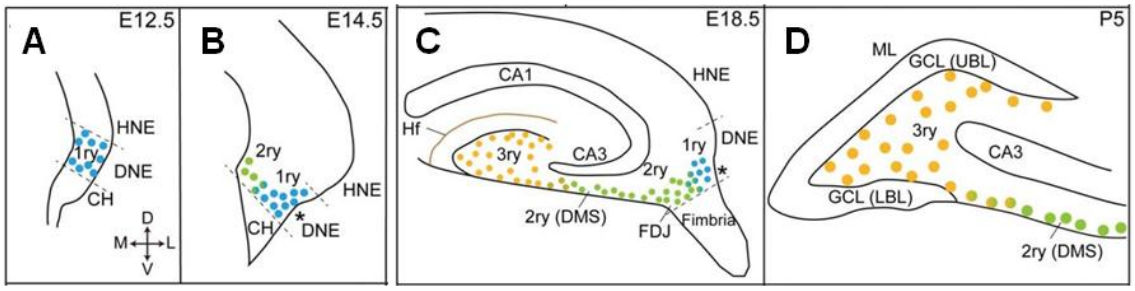

Figure I9. A-D) Temporal evolution of the different progenitor matrixes that form the DG. The primary matrix (in blue) arises from the DNe and gives rise to the secondary matrix (in green) that extends along the fimbria and connects to the DG, forming the DMS. Inside the DG, the tertiary matrix (in yellow) of progenitors ends the formation of the DG postnatally (modified from Sugiyama et al. 2013).

Thus, while the majority of neurons that form the HPF are generated during embryonic gestation, the vast majority of the GCL neurons are born after birth (Angevine, 1965; Bayer, 1980; Bayer and Altman, 1974). Postnatal neurogenesis

follows a sharp peak early after birth and then it drops off later by the second week (Bayer and Altman, 1974), being crucial for the formation of the initial connections between MFs and CA3 neurons (Amaral and Dent, 1981; Gaarskjaer, 1985). Interestingly, the sequence of neuron formation in the GCL is unique and contrary to any other cortical area or layer, following three distinct morphogenetic gradients. First, neurons populate the GCL in an "outside-in" pattern where the superficial neurons are formed earlier than the deeper ones (Angevine, 1965; Schlessinger et al., 1975). Second, GCs at the tip of suprapyramidal layer of the GCL are the first ones to get generated, following a dorsal to ventral gradient in the generation of the GCL. Finally, caudal (or temporal) regions are formed earlier than rostral (or septal) ones (Bayer, 1980; Schlessinger et al., 1975).

The neuronal migration described during the DG development, with progenitor pools forming different germinal matrixes fixes spatio-temporally with the formation of glial scaffolds described by Cowan and colleagues (Rickmann et al., 1987). They and others described how a primary RGC scaffold arise from the DNe to the subpial zone (SPZ) and contact the HF invagination point earlier than the first GCs start to migrate. This serves as a tangential migration scaffold for the dNSCs that form the secondary germinal matrix after detaching from the neuroepithelium (Nakahira and Yuasa, 2005; Rickmann et al., 1987; Sievers et al., 1992).

Together with neuronal precursors, glial precursors migrate from the VZ along the DMS, giving rise to the secondary RGC scaffold that appears fanning out in the hilus from the FDJ, extending towards the GCL in a suprapyramidal to infrapyramidal pattern (Yuasa, 2001). This allows new GCs of the tertiary matrix to reach the GCL. Interestingly, it has been suggested a mechanism whereby RGC fibers get "unattractive" while they get old, explaining the suprapyramidal to infrapyramidal formation pattern of the GCL and why neurons follow secondary rather than primary RGC scaffold postnatally (Eckenhoff and Rakic, 1984; Rickmann et al., 1987; Sievers et al., 1992).

3.4.3. Origin of adult NSCs

In the rodent SVZ neurogenic niche, adult NSCs are originated from neuronal precursors during the early development. Around E14 RGCs proliferate generating glutamatergic neurons that allocate in cortical, septal and striatal regions. RGCs enter quiescence after several divisions, acquiring a dormant state until they get re-activated at postnatal or adult stages when they give rise to GABAergic OB neurons. Arturo

Alvarez-Buylla et al. named this process the "set-aside" model in which embryonic progenitors stop their cell cycle and activate again after a long period generating a completely different type of neuron (Fuentealba et al., 2015; Furutachi et al., 2015). Despite the considerable advances done on the origin of SVZ adult NSCs, this same topic remains one of the most intriguing unresolved aspects of DG development.

3.4.3.1. Embryonic origin of NSCs

The DG comprises a neurogenic niche with a remarkable difference compared to the SVZ. It is located far from the ventricle. In fact, the adult SGZ of the DG remains completely dissociated from its embryonic germinative zone (Altman and Bayer, 1990a). When the DG development started to be described, it was published that adult hippocampal NSCs were generated from precursors residing in the DNe during development, either by direct translocation (Eckenhoff and Rakic, 1984) or indirectly following the above described DG-forming migration processes (Altman and Bayer, 1990a) until they end up located in the SGZ of the DG postnatally (Nicola et al., 2015; Sugiyama et al., 2013). Thus, it has been the generally accepted view in the field, as stated by Gage and collaborators (Gonçalves et al., 2016), that adult NSCs and neurogenesis are a remnant from the embryonic development of the HPF.

Supporting this view, it has been described how GFAP is expressed by spindle-shaped neuronal precursors along the different germinal matrixes that form the DG during embryonic and postnatal development. Thus, it was suggested that these astrocyte-like cells migrate from the DNe to the SGZ, comprising the precursor population that generates GCs throughout the whole life (Matsue et al., 2018; Seki et al., 2014). However, BLBP has been referred as a differential factor between prenatal and postnatal dNSCs. After birth, neuronal precursors acquire BLBP expression before getting established in the SGZ (Matsue et al., 2018; Nicola et al., 2015; Seki et al., 2014). This finding could mean either that migrating dNSCs acquire new characteristics before getting established in the SGZ, or on the contrary that a new subpopulation of NSCs arises from the embryonic dNSCs postnatally.

Further studies have identified the putative dNSCs migrating from DNe to SGZ using other markers and transgenic mouse models: Nestin, the intermediate precursor marker eomesodermin, also known as T-box brain protein 2 (Tbr2) (Hodge et al., 2008, 2012) and neurogenin-2 (Ngn2) have been described to label neuronal precursors across all the dentate germinal matrixes (Galichet et al., 2008; Hodge et al., 2013; Li et al., 2009). In this line, Samuel Pleasure and colleagues suggested that some of them

migrate from the DNe, maintaining their undifferentiated state due to neurogenic inhibiting signals, until they reach the SGZ at postnatal stages and remain there during adulthood (Pleasure et al., 2000a). Moreover, they described that dNSCs dwell in a transient neurogenic zone located in the SPZ between the HF and the FDJ for at least one week before establishing in the SGZ (Li et al., 2009) **(Figure I10)**. In the absence of Ngn2 (Galichet et al., 2008) reelin or chemokine ligand 12/chemokine receptor 4 (Cxcl12/Cxcr4) signaling (Brunne et al., 2014; Hodge et al., 2013; Li et al., 2009) the SPZ to SGZ NSC transition was not completed, triggering an excessive accumulation of precursors in the subpial region and the absence of adult NSC pool. Also, using a knock-out mouse model for *Tbr2* it was shown that its expression in CR cells is necessary for their establishment surrounding the outer edge of the forming GCL. From this strategic location, Tbr2-positive CR cells contribute to the RGC scaffold establishment, dNSC guidance and adult NSC pool generation (Hodge et al., 2013) **(Figure I10)**.

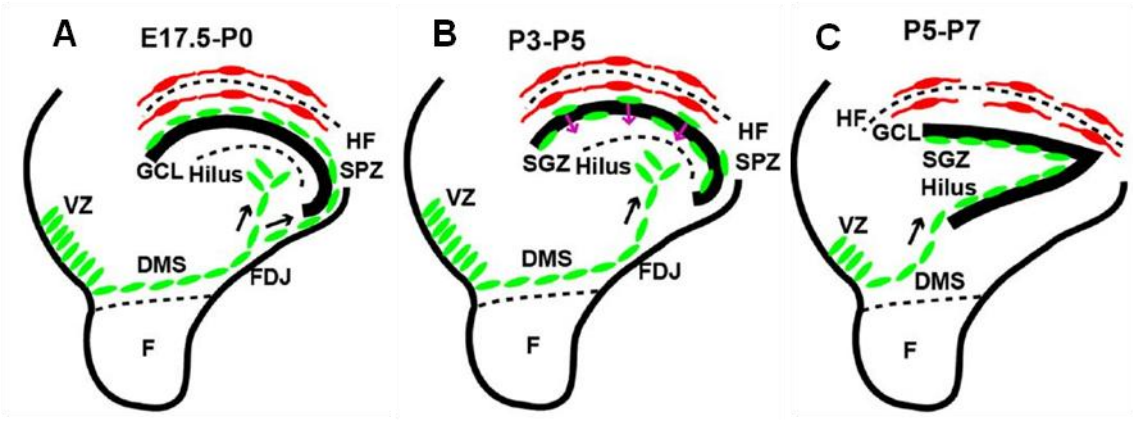

Figure I10. A-C) Guided by CR cells located in the SPZ along the HF, the precursors of adult NSCs migrate from the DNe into the DG until they allocate along the SGZ forming the adult NSC population (modified from Hodge et al., 2013).

Homeodomain protein box (Hopx) is expressed in DG adult NSCs (Shin et al., 2015) and distinguishes them from SVZ NSCs. Also, a role for Hopx in the regulation of AHN was suggested through interaction with Notch signaling (Li et al., 2015). Recently, Daniel Berg et al. reported that Hopx-positive dNSCs migrate from the DNe to the SGZ, contributing to the formation of the DG throughout the embryonic and postnatal development to later become quiescent and constitute the adult NSC population. More importantly, they claimed that Hopx-positive progenitors generate GCs exclusively, highlighting their specificity and bias to this particular neuronal lineage. Basing on these results, they supported the notion that AHN is the lifelong extension of the

embryonic and postnatal development, defending a "continuous" model in which Hopx-positive NSCs give GCs throughout the whole life, from development to adulthood (Berg et al., 2019).

Regarding the spatial origin of the adult NSCs, the work of Samuel Pleasure and colleagues reporting a new temporo-septal progenitor migratory stream came as a challenging idea to the field. They described that adult NSC precursors migrate from the VZ close to the ventral DG towards the dorsal DG at embryonic and perinatal stages, getting established in the SGZ postnatally. They migrate in a sonic hedgehog (Shh)-reponsive manner, as indicated by the impaired formation of adult NSC pool in the absence (or defects in regulators) of this signaling pathway (Li et al., 2013). Shh is a well known member of the hedhehog (Hh) family and it has been shown to be highly implicated in the growth and development of the neocortex promoting RGC and progenitor expansion, but the work of Samuel Pleasure and colleagues brought the signaling pathway into the focus of hippocampal development. In fact, they opposed the general view of the field and suggested that DNe progenitors contribute only to the formation of the outer GCL shell, the initial one, while the inner shell and adult NSC population originate from dNSCs migrating from the ventral DG in a Shh-reponsive way. They propose a model in which both streams connect perinatally in the FDJ of the DG, opening the possibility for different spatial origins for adult NSCs (Li et al., 2013).

3.4.3.2. Postnatal proliferation: generating adult NSCs

Regardless of their embryonic origin, postnatal proliferation has been demonstrated to be critical for the formation of the adult NSC pool in the DG. Using BrdU it was reported that although some dNSCs divide embryonically and then enter quiescence until adulthood, the majority of them divide at early postnatal stages before acquiring adult characteristics between P7-P14 (Mathews et al., 2010). Furthermore, using dual birth-dating methods it was reported that adult NSC precursors have a proliferation peak towards the end of the first postnatal week, suggesting that this time is a key period for the generation of adult NSCs (Ortega-Martínez and Trejo, 2015). Indeed, it was described that in rats, adult NSCs arise from dividing non-radial precursors located in the hilus at postnatal day 5 (P5) (Brunne et al., 2010; Namba et al., 2005, 2011). Using intrahippocampal retroviral infections, Takashi Namba and colleagues defined that hilar GFAP-expressing dNSCs generate neurons, astrocytes and also adult NSCs dividing in symmetric and asymmetric patterns (Namba et al., 2005, 2011). Complementing the previous studies, it was also reported using retroviral infections that dividing dNSCs from the hippocampal VZ, the postnatal region derived

from the DNe, contribute to the formation of the DG with neurons, astrocytes and also adult NSCs at P5 (Navarro-Quiroga et al., 2006). However, this result was controversial since other authors described that the postnatal hippocampal VZ does not contribute to the adult NSC population, and instead adult NSC precursors migrate from the DNe into the hilus during the embryonic period (Clarke and Van Der Kooy, 2011). Also, a recent report described that during early postnatal stages, adult NSC precursors divide to expand themselves in a Shh-depending way before becoming quiescent to form the adult NSC pool (Noguchi et al., 2019). Together, these results suggest that blocking proliferation at early postnatal stages would signify the loss of adult NSC population, directly acting on their generation window.

However, several studies have reported reversible effects upon GC production after proliferation blocking insults during the postnatal period, such as low irradiation (although the obtained results could be biased by the proneurogenic physical activity to which the treated animals are subjected) (Naylor et al., 2008), administration of the cell proliferation suppresser methylazoxymethanol (MAM) (Ciaroni et al., 2002) or an induced transitory hypothyroidism model (Zhang et al., 2009). These results showed postnatal reduction of GC production, but AHN was not impaired at long-term, suggesting that a unique or transitory proliferation blockage is not enough to affect the adult NSC pool generation and long-term neurogenic capacity. On the other hand, a recent study suggested that pharmacogenetic ablation of proliferating GFAP-expressing cells during the first postnatal week has devastating effects upon adult NSC. Incapable to divide, dNSCs do not fully form the adult NSC population, provoking the lack of neurogenic capacity during adulthood. Interestingly, when proliferating GFAP-positive cells were ablated during the third postnatal week there was no effect over the number of adult NSCs, although they became less neurogenic both at short- and long-term (Youssef et al., 2019). The authors argued that progenitors are more proliferative at P0-P7 than at P14-P21 and therefore the effect on ablated progenitors is stronger during that period. However, they might be affecting different populations in their two paradigms (dNSCs vs adult NSCs), which would explain their differential outcomes. Besides, they do not provide any spatial resolution about the progenitors they are affecting. Nonetheless, this work provides basis for the need of a sustained proliferation blockage during postnatal development to significantly impact on the adult NSC generation, leading us to hypothesize that they might be generated in a gradual way.

3.4.3.3. Dividing mechanisms of adult NSC precursors: Cyclin D2 (cD2)

The mechanisms by which dNSCs divide and give birth to adult NSCs remain unknown. It has been previously suggested that Shh signaling pathway is involved in the postnatal proliferation of precursors that will form the DG as well as the adult NSC pool. Smoothened (Smo) and Supressor of Fused (SuFu) regulate Shh activity controlling dNSC proliferation. Deregulation of this signaling pathway leads to a premature entrance into quiescence of the dNSCs, failing to expand and triggering a reduced adult NSC pool and a smaller GCL (Han et al., 2008; Noguchi et al., 2019). Other factors such as GABA or BMP have been explored as quiescence regulators in the adult mouse brain, whereas their role upon postnatal proliferation remains unexplored (Mira et al., 2010; Song et al., 2012).

The D-type cyclins (D1, D2 and D3) govern the G1 to S phase transition of the mammalian cell cycle, a step largely involved in controlling cell proliferation and differentiation **(Figure I11)**. Specifically, D-type cyclin activation is the first response after a cell receives mitogenic stimulus to leave quiescent state, triggering the activation of cyclin-dependent kinase 4 and 6 (CDK4 and CDK6) (Pardee, 1989). Interestingly, D-type cyclins have been described to be quite redundant and highly compensatory. Thus, mice lacking one of the three show normal embryogenesis, although there are specific phenotypes associated to older ages (Ekholm and Reed, 2000; Sherr, 1995; Sherr and Roberts, 2004). In fact, even the lack of all D-type cyclins was described to be irrelevant for mouse embryogenesis up to E16.5, meaning that embryonic cell cycle progression happens, or can happen, in a cyclin D-independent way (Kozar et al., 2004).

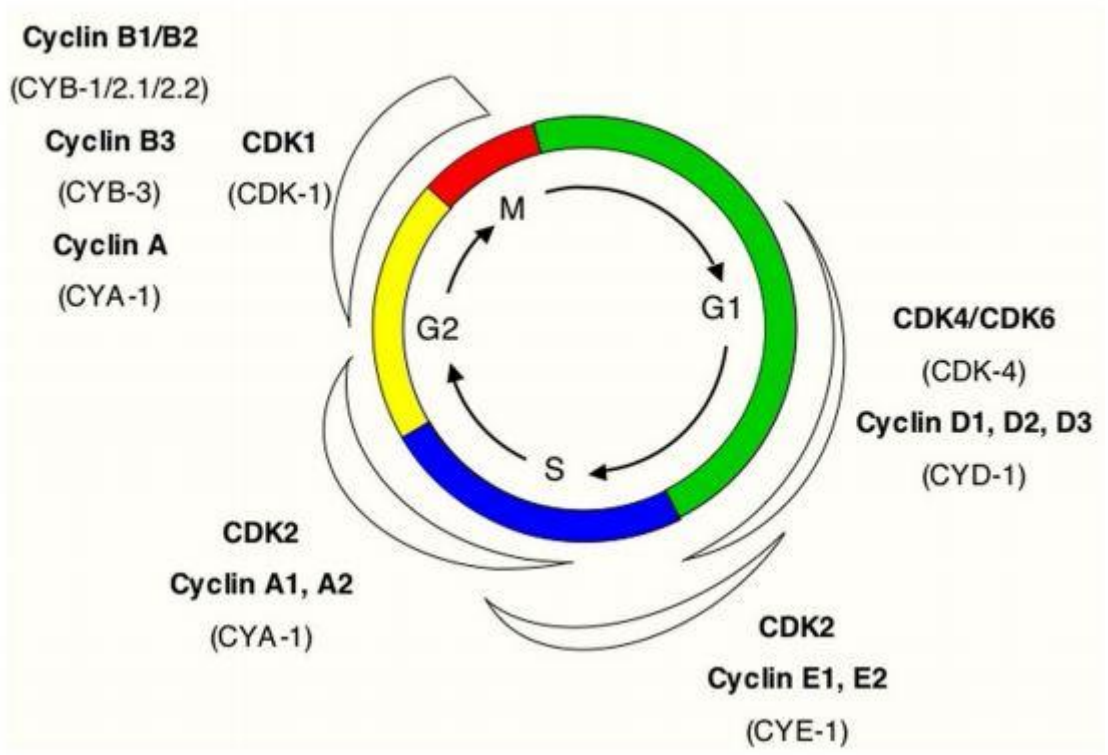

Figure I11. The role of the different cyclins in the regulation of the different phases of cell cycle. Cyclin D1, D2 and D3 in combination with CDK4 and CDK6 regulate the transition from G1 to S phase (Modified from van den Heuvel, 2005).

In the mammalian brain, cD2 has been shown to be involved in the correct development of the cerebellum. In its absence, reduced proliferation and increased apoptosis processes trigger a diminished GC and interneuron population by the second postnatal week (Huard et al., 1999). Likewise, the neocortex shows aberrant development in *cD2* knock-out mice (*cD2*KO), showing lengthening of G1 phase, shortening of S phase and premature cell cycle-exit of the embryonic progenitors, triggering their early differentiation into neurons (Glickstein et al., 2007a, 2009). Likewise, cD2 was described to pay a role in the apical progenitor maintenance during neocortex development. After asymmetric divisions, cD2 would be inherited by one of the daughter cells thereby keeping the apical progenitor fate (Tsunekawa et al., 2012). In addition, posterior work showed that cD2 activity during neocortex development is at least in part regulated by Smo, critical regulator of the Shh pathway. In Smo absence, cD2 is down-regulated leading to progenitor expansion failure and neocortical development defects (Komada et al., 2013). Together, these results highlight the role of *cD2* to maintain the undifferentiated state and guide the expansion of progenitors during neocortex development and open the possibility for similar regulation mechanisms in the DG.

In the developing DG, cD2 appears expressed especially along the DMS and around the HF, while cD1 shows stronger expression in the secondary and tertiary germinal matrixes. Postnatally, both cD1 and cD2 show expression in the tertiary matrix, getting restricted to the SGZ with DG maturation (Glickstein et al., 2007b). Interestingly, at early postnatal stages *cD2*KO transgenic mice show similar levels of proliferating cells in the DG than WT animals (Kowalczyk et al., 2004). However, and despite the expression of cD1 in the SGZ (Glickstein et al., 2007b), AHN has been reported to be almost absent in the *cD2* deficient mice (Ansorg et al., 2012; Kowalczyk et al., 2004) **(Figure I12)**. It remains unresolved whether this lack of neurogenic capacity is due to the inability of adult NSCs to generate newborn neurons or on the contrary, consequence of a developmental failure in the postnatal expansion of dNSCs and posterior generation of adult NSC pool.

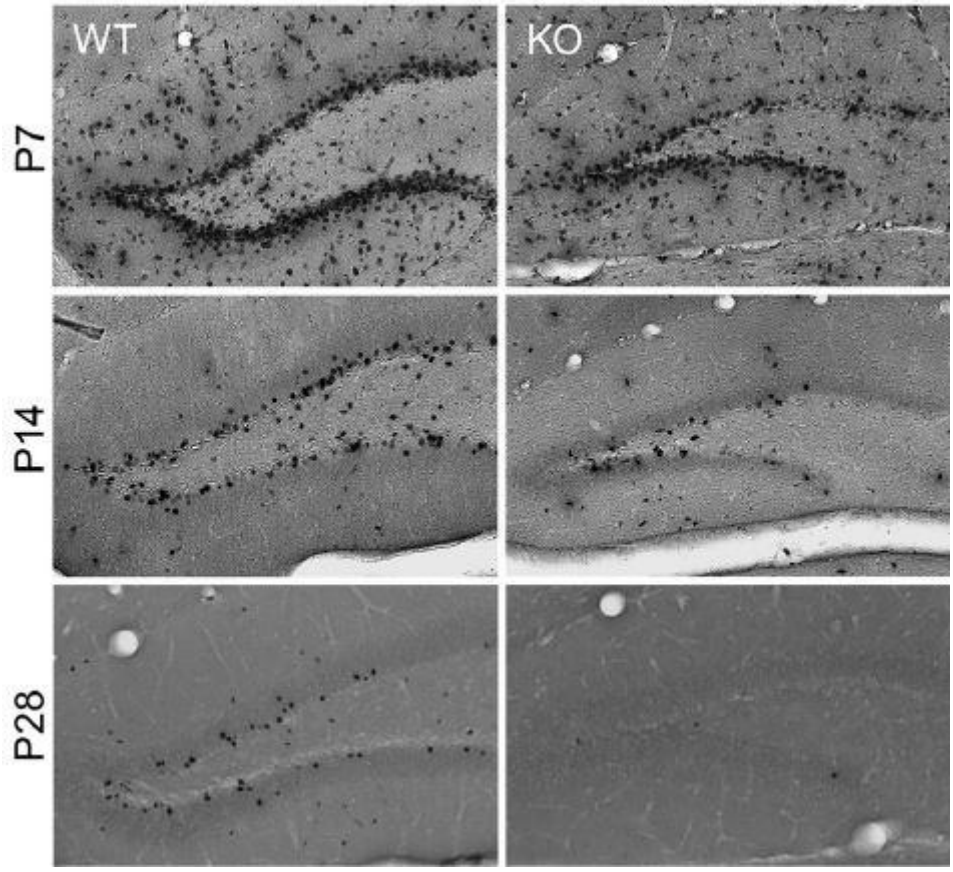

Figure I12. In the absence of cD2, proliferation in the DG starts to decay during the first postnatal two weeks, and AHN is absent at P28 (modified from Ansorg et al. 2012). *Dots show dividing cells that have incorporated BrdU.*

3.4.3.4. Adult NSCs vs dNSCs

Shedding light upon the origin of adult DG NSCs will help to solve one of the main questions remaining in the field: Is AHN a remnant from the developmental neurogenesis forming the DG or is it an independent process built as a unique biological phenomenon? Addressing this question could be essential to understand the functions of the AHN and its role in several normal and pathological conditions.

The postnatal appearance of a new structure away from the ventricle and capable to persist giving newborn neurons during the whole life have led some authors to pinpoint the principal differences between the developmental and adult neurogenesis (Nicola et al., 2015). However, since the SGZ is the endpoint of the whole plethora of developmental processes and structures to form the DG, it is the current accepted view in the field that AHN is the last remaining step in the formation of the DG. In other words, a continuation of the developmental neurogenesis program (Berg et al., 2019; Matsue et al., 2018; Nicola et al., 2015; Seki et al., 2014).

A recent work using powerful technology as scRNA-seq described that the neurogenic process follows similar paths both in adult and developmental scenarios. In other words, ANPs, NBs and immature neurons are molecularly highly similar at embryonic, perinatal and adult stages (Hochgerner et al., 2018). These results have been used to support the idea of AHN being a remnant from development (Berg et al., 2019). However, Sten Linnarson and colleagues also identified a switch in the molecular properties of the NSCs from embryonic to postnatal/adult age. They described that coinciding with NSCs getting established in the SGZ, they undergo molecular changes (higher quiescence and switch on marker expression) becoming clearly distinguishable from dNSCs (Hochgerner et al., 2018). Supporting this, Jennifer Gilley et al. found cell-autonomous changes from early postnatal to young/adult mice, observing different transcriptional profiles between both ages (Gilley et al., 2011). Altogether, these results lead us to think about adult and developmental neurogenesis being different processes, at least at NSC level.

The main issue when addressing the dNSC transition from developmental to adult is the lack of valid specific markers to differentiate both populations. Several works have shown that BLBP expression switches from embryonic to postnatal stages, where progenitors start to express it (Matsue et al., 2018; Nicola et al., 2015; Seki et al., 2014), although the differential expression between early postnatal dNSCs and adult NSCs remains unclear. Sten Linnarson et al. showed in their scRNA-seq data

that some markers were specific among quiescent NSCs compared to the active ones (Hochgerner et al., 2018). As quiescence has been described to be a hallmark of adult NSCs, we hypothesize that these markers could be differentiating adult NSCs from developmental precursors. Interestingly, Lysophosphatidic acid receptor 1 (LPA_1) was one of those markers (Hochgerner et al., 2018), which has been reported to specifically label NSCs in the adult DG using the LPA_1-Enhanced green fluorescent protein (EGFP) mouse model (Valcárcel-Martín et al., 2020; Walker et al., 2016) **(Figure I13)**. Although its role in adult NSC function remains mostly unknown, LPA_1 deletion has been shown to reduce AHN in normal conditions (Matas-Rico et al., 2008) and the massive activation of NSCs after seizures (Valcárcel-Martín et al., 2020). Furthermore, during embryonic development, LPA_1 has been involved in cortical neural progenitor proliferation, cell migration and survival (Estivill-Torrús et al., 2008). For all these reasons, LPA_1 seems to be a good candidate to specifically label NSCs ones they acquire quiescence at a population level and become adult.

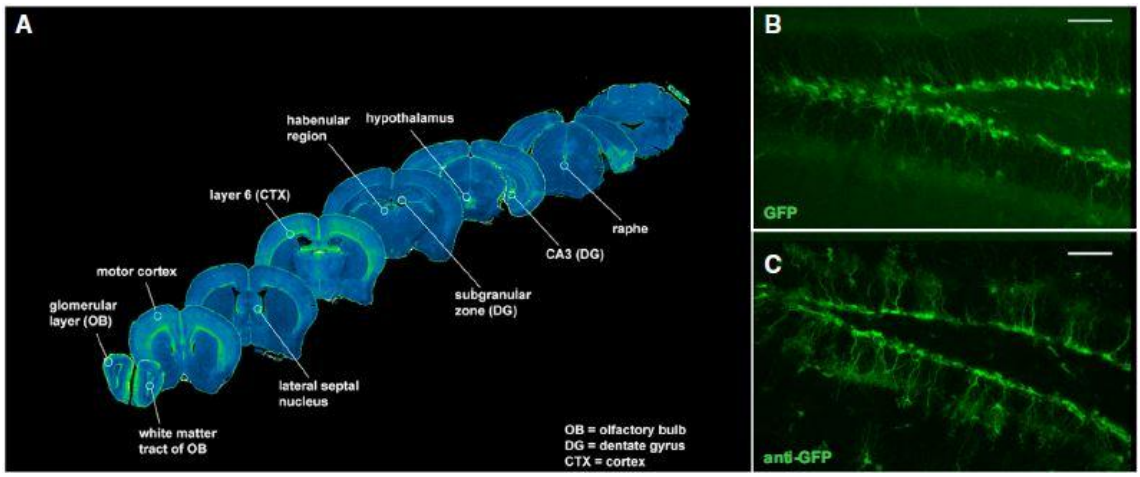

Figure I13. A) Using the LPA_1-EGFP transgenic mouse model, LPA_1 expression can be observed both in the SVZ of the LV and in the DG. **B-C)** LPA_1 specifically labels NSCs in the adult DG, both in the absence (B) and presence of an anti-GFP antibody (modified from Walker et al. 2015).

3.5. The hippocampal neurogenic niche in humans

Animal models, including rodents, represent a well-known system to address the formation and development of the HPF during the entire (animal) life. However, what happens in humans? With the objective to translate all the information from rodent models into our knowledge about our own brain, it is fundamental to search for the similarities and differences that both share. One of the major differences of the HPF between rodents and higher mammals, worth to bear in mind when comparing both systems, resides in its spatial location. In contrast to rodents, the human HPF develops

along the ventral midline of the hemisphere (Abraham et al., 2004; Kier et al., 1997; Strange et al., 2014; West, 1990) **(Figure I14)**. Dorsally, the prospective HPF fades at early prenatal stages due to the emergence and progressive growth of the corpus callosum, remaining in the adulthood as an atrophic remnant called the *induseum griseum* (Meyer et al., 2019; Rakic and Yakovlev, 1968). Thus, the vHPF is the one that develops into the well-known functional structure of the adult brain (Abraham et al., 2004; Kier et al., 1997; Meyer et al., 2019). However, the different stages in the development of the human HPF remain largely unexplored.

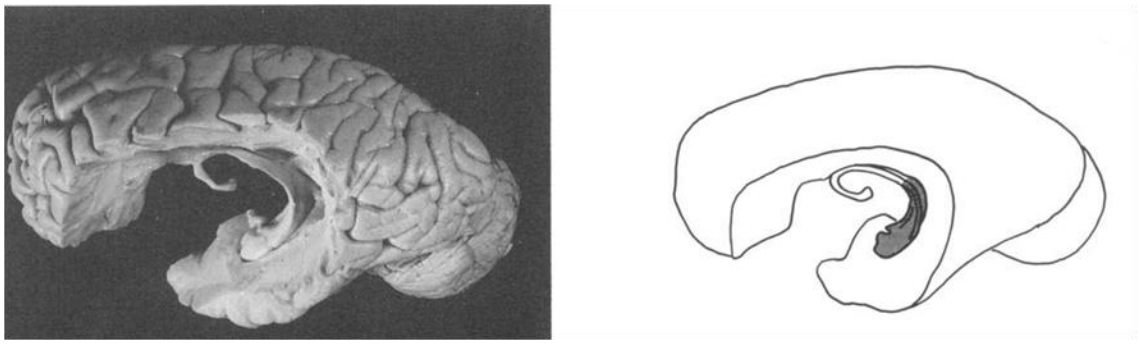

Figure I14. Picture of the human HPF after the removal of the overlaying cortex. It is observable (coloured in gray in the schematic of the right) that the HPF is more prominent in the ventromedial position (modified from West, 1990).

3.5.1. Development of the human hippocampal neurogenic niche

The CH serves as embryonic signaling center for the formation of rodent HPF and it is defined by the expression of Bmp and Wnt family proteins (Grove et al., 1998; Lee et al., 2000c). Likewise, a CH-like structure was identified during early development of human fetuses by the overlapping expression of Bmp7 and Wnt2b in a dorsal region close to the ventricle, suggesting that the major patterning cues seen in rodents were conserved also in humans (Abu-Khaklil et al., 2004). Later on, this structure was also ventrally observed, and it was described to be the source of CR cells that will help in the formation of the primary ammonic and dentate structures (Abraham et al., 2004). Importantly, this ventral CH has not been identified in rodents (where it exists only dorsally), suggesting the uniqueness and relevance of this structure in humans compared to mammals with more prominent dHPF (Abraham et al., 2004).

One of the most important events of the early human hippocampal development is the appearance of a slight inward curve in the ventromedial region around gestational week 11/12 (GW11/12) that will represent the HF. At this stage, ammonic

and subiculum plates already express layer specific markers and the EC is also discernible (Cipriani et al., 2016; Humphrey, 1967; Meyer et al., 2019). At GW13/14, the wide-opened prospective HF thickens to form a "diffuse zone" (Humphrey, 1967) mainly populated by CR cells coming from the CH (Abraham et al., 2004). At this stage, the unfolded HPF surrounds the HF, formed by now clearly discernible cytoarchitectonic regions and a distinguished cell layer of pyramidal neurons forming the primordial CA (Arnold and Trojanowski, 1996; Kier et al., 1997). During the following weeks, the DG and CA fold into the temporal lobe (Kier et al., 1997) and the two structures and subiculum approximate each other across the HF, that gets fused (Humphrey, 1967; Kier et al., 1997) **(Figure I15)**. At GW16 CA fields start to clearly differentiate from each other (Kier et al., 1997; Kostović et al., 1989) and by GW24 the HPF already resembles the adult structure (Arnold and Trojanowski, 1996; Humphrey, 1967; Kier et al., 1997; Seress et al., 2001) and has established both septal (fimbria-fornix) and entorhinal (PP) synaptic connections (Kostović, 1986; Kostović et al., 1989).

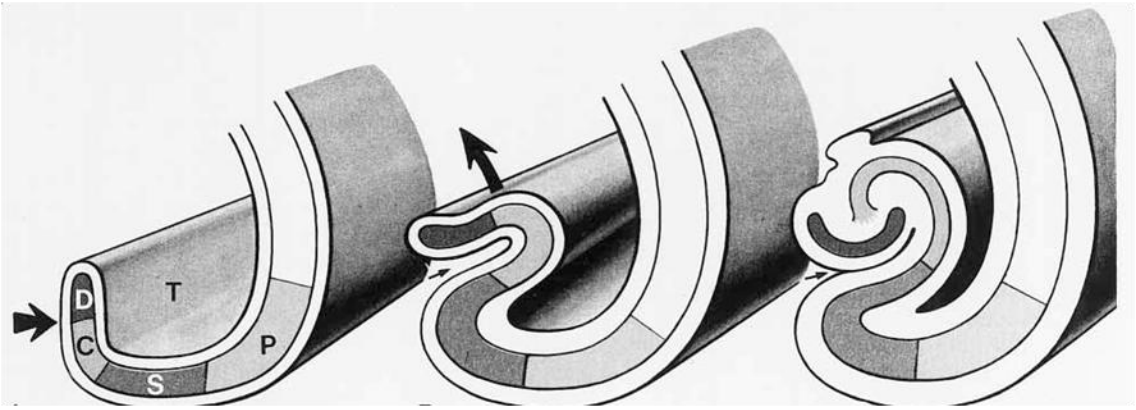

Figure I15. At early fetal stages (GW11/12), the HPF starts to fold from the region between DG and CA (large arrow) and the HF is generated (small arrow) at GW13/14. Later, at GW18, the HF gets obliterated and the HPF adopts the form that will maintain during the adulthood (modified from Kier et al., 1997).

The DG follows unique and differentiated patterns from the rest of the HPF. At GW9, proliferating progenitors form the primary dentate matrix next to the CH, although the distinction between the ammonic neuroepithelium and the DNe has not been clearly established yet at this early time point. Around GW11/12, a non-proliferative neuronal layer appears in the prospective DG, so-called the "dentate plate" (Abraham et al., 2004; Cipriani et al., 2017). Interestingly, although the dentate plate has been demonstrated in the developing HPF of monkeys (Eckenhoff and Rakic, 1984) it has never been described in rodents. Then, Vimentin- and Nestin-positive RGC fibers from the primary dentate matrix extend into the SPZ below the HF, crossing the forming GCL and contacting the dentate plate. Thus, the primary glial scaffold gets established,

coinciding with the appearance of the secondary dentate matrix adjacent to the DNe, composed of Pax6- and Tbr2-expressing proliferative progenitors. At GW13/14, the secondary dentate matrix progenitors start to migrate and form the DMS. Proliferating cells extend from the DNe towards the SPZ and populate the hilus of the prospective DG (Abraham et al., 2004; Cipriani et al., 2017, 2018; Seress et al., 2001; Sorrells et al., 2018). At this stage, the DG reaches the peak of neurogenesis (Yang et al., 2014). Later at GW17/18 a more condensed GCL starts to be distinguishable and the tertiary dentate matrix gets formed in the hilar region of the DG. By GW22, proliferation disappears from the DNe and DMS and is almost entirely restricted to the hilus (Sorrells et al., 2018).

Like in rodents, human DG is the last hippocampal region to get formed and GCs are added to the GCL from GW30 on and at least until early after birth (Arnold and Trojanowski, 1996; Humphrey, 1967; Seress et al., 2001), with remaining Nestin-expressing cells populating the hilus and GCL (Cipriani et al., 2018; Sorrells et al., 2018) and the last waves of NB migration to the GCL taking place during the first postnatal eight months (Seress, 1988; Seress et al., 1992). Nonetheless, the formation of GCL is considered to be practically completed by mid-gestation and cell proliferation occurring during the second half of gestation and at postnatal stages is not especially prominent (Arnold and Trojanowski, 1996; Humphrey, 1967; Seress et al., 2001; Sorrells et al., 2018). The existence of a postnatal neurogenic niche has always attracted scientific attention and many authors have tried to unravel the extent and relevance of postnatal human AHN (hAHN), seduced by the implication of its therapeutic potential.

3.5.2. hAHN: To be or not to be

The development and formation of an adult neurogenic niche in the mammalian DG has been of great interest for the scientific community. However, it was not until 1998 that the first evidence of hAHN appeared. In their seminal study, Peter Erikson et al. analyzed postmortem hippocampal samples of cancer patients (average age of 64.4 ± 2.9 years) to whom BrdU had been intravenously administered to label proliferative tumor cells. Unexpectedly, they found BrdU-positive cells in the GCL of the DG, with a substantial part of them co-staining for neuronal markers. With this appealing results, they claimed that new neurons were generated in this region during the whole human life (Eriksson et al., 1998). During the following years opposite results were reported, showing a residual expression of *MKI67* (the gene that encodes nuclear protein Ki67,

necessary for cellular proliferation) in the SGZ of adult epileptic patients (Del Bigio, 1999). In spite of this, the work of Erikson and colleagues was gladly received in the community and became the milestone for the animal studies of the following decade. In addition, several *in vitro* studies supported the presence of neural progenitors in the human DG capable to generate neurons (Coras et al., 2010; Hermann et al., 2006; Moe et al., 2005; Palmer et al., 2001; Roy et al., 2000).

At the beginning of this last decade, Rolf Knoth and collaborators characterized the pattern of expression of the immature neuronal precursor marker DCX throughout the human adulthood. They found that DCX expression was present in the GCL across different adult ages, although it progressively decreased over time. The unusual localization of DCX to the nucleus of the labeled cells, however, raised concerns about the specificity of the immunodetection. Based on their findings, Knoth et al. speculated about the similitude of the neurogenic patterns between rodents and humans, although they were unable to find any radially-oriented glia cell in the SGZ (Knoth et al., 2010). Another study led by Kathryn Mathews et al. supported their conclusions after the characterization of the levels of messenger ribonucleic acid (mRNA) of both *DCX* and *MKI67* genes at different time-points across the life, showing its age-related downregulation (Mathews et al., 2017). However, it was not until 2013 that one of the most important works regarding hAHN came out. Kirsty Spalding et al. assessed the generation of hippocampal cells in humans by taking advantage of the atmospheric carbon 14 (^{14}C) released from the cold-war rising nuclear-bomb tests and its integration in genomic DNA. They presented an integrated model reporting that 700 neurons are added per day in the adult human DG with a modest decline with aging, corroborating the previous studies and establishing solid grounds on the existence of hAHN (Spalding et al., 2013). The adequacy of the modeling has however been challenged and a corrected curve with much sharper decline, more in agreement with animal data, has been proposed (Lipp and Bonfanti, 2016).

Recently, when hAHN seemed well-rooted and almost undoubted, new works have claimed the lack of such process, stirring the scientific community and raising new questions in the field. The first one was based on immunohistochemistry (IHC) results reporting that after 3 years of age, microglia is the only proliferating cell type in the human DG (Dennis et al., 2017). These results brought disbelief and controversy to the field (Dennis et al., 2017; Marucci, 2017), although the community was not truly shaken until the appearance of the work of Arturo Álvarez-Buylla and colleagues. Analyzing both light and EM images of samples from different fetal, perinatal and adult ages, they

described a huge decline of DCX-positive cells from fetal stages to first years of life, with negligible amounts of DCX cells remaining by 7-13 years of age (Sorrells et al., 2018) **(Figure I16 A)**. They did not observe progenitors adjacent to the GCL during adulthood, nor a dense layer similar to the rodent SGZ. Thus, they concluded that "*neurogenesis in the DG does not continue, or is extremely rare, in adult humans*" (Sorrells et al., 2018). Furthermore, another work came out same year claiming that although morphologically, antigenically and topographically diverse progenitor pools are present in the human DG from development to adulthood, their neurogenic potential is minimal, indicated by the very few DCX-positive cells being present in the adult DG (Cipriani et al., 2018). Reacting to these studies, a big part of the community focused on reminding that "*the absence of evidence is not evidence of absence*" and giving relevance to the strong evidence showed in the past (Kempermann et al., 2018; Lee and Thuret, 2018). On the other side of the coin, new criticism arouse about the existence of hAHN, also pointing to the previous groundbreaking works (Eriksson et al., 1998; Spalding et al., 2013) and their possible technical issues that misled to a wrong conclusion (Duque and Spector, 2019). The lack of evidence for NSCs in the adult human DG, the high variability between samples and the fact that, as explained by previous studies (Breunig et al., 2007b), cells could incorporate BrdU by processes not associated with cell division (by cell damage for instance) were argued against the well-established idea of hAHN (Duque and Spector, 2019; Sorrells et al., 2018). In fact, some authors (Dennis et al., 2016) indicated that even the studies arguing in favor of hAHN (Knoth et al., 2010; Spalding et al., 2013) reported low levels of new added neurons, even 10-times lower than in laboratory animals (Spalding et al., 2013). It was the start of another chapter (perhaps the last) on the story of the controversy of adult neurogenesis.

Soon after Sorrells et al. claimed absence of hAHN, a publication came out reporting that neurogenesis does actually persist in the adult DG. They showed presence of dividing progenitor cells using Ki67 in combination with Nestin and Sox2 markers, and also DCX- and PSA-NCAM-positive cells that could potentially be immature neurons (Boldrini et al., 2018). Hence, Maura Boldrini et al. and others defended the evidence of hAHN and attributed the contradictory results with Alvarez-Buylla and colleagues (Sorrells et al., 2018) to variations between both studies in duration of postmortem delay, fixation and sample preservation methods and staining protocols. They also criticized the absence of case information in Alvarez-Buylla's work, arguing that pathological circumstances could be affecting their results

(Kempermann et al., 2018; Kuhn et al., 2018; Tartt et al., 2018). The debate was opened, and Alvarez-Buylla and colleagues quickly followed-up calling into question some of the labeling from Boldrini's paper and highlighting the outside-GCL location of the Nestin/Sox2-positive cells. They also pointed out the importance of doing correct interpretations of the obtained results, suggesting that apart from the specific antibody expression, parameters like morphology or location should be taken into account when categorizing a neuron as mature or immature (Paredes et al., 2018).

In this scenario, a new paper got the focus of the community, reporting abundant hAHN in adult cases up to the ninth decade of life. They based their work on DCX and Calretinin (another immature neuron marker) expression and claimed the presence of newborn neurons in a methodologically thorough work in which fixation protocols were tightly controlled (Moreno-Jiménez et al., 2019) **(Figure I16 B)**. They tried different antibodies for DCX and several fixation times getting a really complete IHC method that they published in an extended way short after (Flor-García et al., 2020). Meanwhile, another report supported these results finding DCX-expressing cells spread in the GCL throughout the dorsal-ventral axis in elderly individuals. Also, they reported the presence of Sox2 and Nestin-positive cells, which they claim to be progenitors, although Nestin was restricted exclusively to the anterior DG (Tobin et al., 2019). These new findings brought again strong belief into the hAHN occurrence and its potential role in normal and pathological conditions. Some authors like Paul Lucassen et al. defended the massive evidence showing its existence over the reports claiming its absence (Lucassen et al., 2020), while others highlighted that the scientific community "*should not let questions about the extent of adult neurogenesis once again impede our progress toward understanding the phenomenon and how it might be harnessed to improve human health*" (Snyder and Drew, 2020).

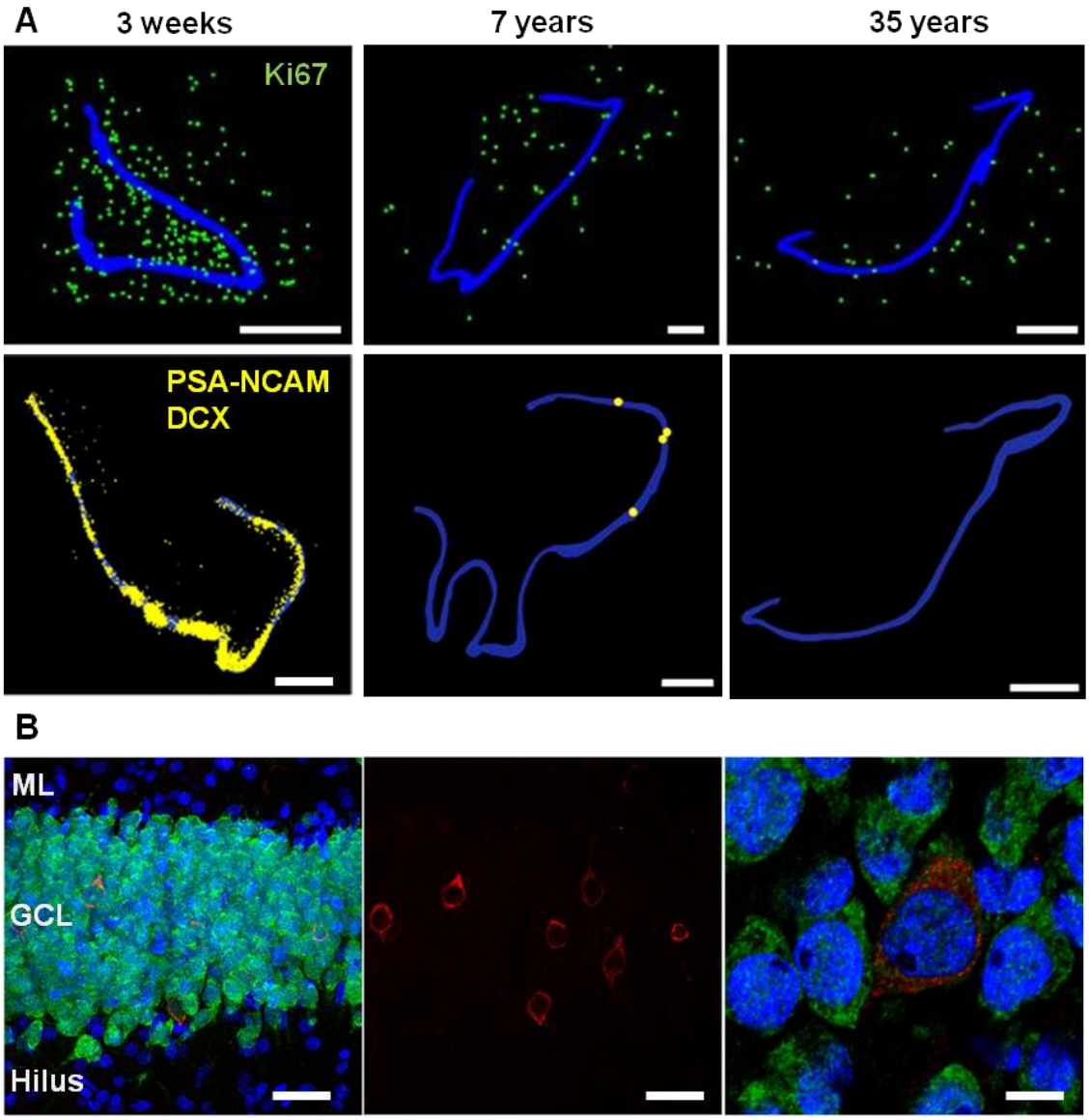

Figure I16. A) Decline of proliferating cells and immature neurons from childhood to adulthood suggesting the absence of adult neurogenesis in humans, as reported by Sorrells et al. (2018). **B)** Presence of DCX – expressing cells (in red) in the GCL of adult humans (47-83 year old), colocalizing with DAPI (blue) and NeuN (green) staining. These results suggest the presence of immature neurons in the GCL, as reported by Moreno-Jiménez et al. (2019) (modified from Sorrells et al., 2018 and Moreno-Jiménez et al., 2019). *GCL: Granule cell layer. ML: Molecular layer.*

On the other hand, other authors chose a different view, focusing on the limitations to overcome in future studies when addressing hAHN. David Petrik and Juan Manuel Encinas, for instance, stressed that Sox2 and Nestin may not be the best candidates for the detection of NSCs due to their wide expression in other cell types like oligodendrocyte precursor cells (OPCs) or astrocytes (Clarke and Van Der Kooy, 2011; Encinas et al., 2011a; Komitova and Eriksson, 2004; Petrik and Encinas, 2019). Thus, new specific markers should be necessary to define a given cell as a NSC in the adult human DG. Regarding immature neuronal markers, Gerd Kempermann and colleagues already showed concern years ago when they reported DCX-expressing cells to be present in the adult DG and cautiously conclude that "*Such data would not offer proof of adult neurogenesis in humans, because it is based on the assumption that humans and rodents share marker expression patterns in adult neurogenesis*" (Knoth et al., 2010). In agreement, a recent paper showed high levels of PSA-NCAM-positive cells in adult control and epileptic cases, although few DCX-, HTLV-I U5RE binding protein (HuB; another immature neuron marker)- and Ki67- expressing cells were observed. Hence, authors suggested that PSA-NCAM-expressing immature-type neurons were not recently generated neurons and that hAHN is indeed sparse, so they enforced the need of different interpretations of IHC results between rodents and humans (Seki et al., 2019). Furthermore, DCX have been reported to be expressed in glial cells, such as microglia or astrocytes, in different conditions (Liu et al., 2018; Verwer et al., 2007; Zhang et al., 2014) and to be re-expressed by already mature neurons by neural excitation or drug administration, being therefore independent of hAHN process (Hagihara et al., 2019). Also, the presence of DCX-positive cells does not assure that neurogenesis takes place, as these could be cells generated even during development that maintain the expression of DCX. They might undergo very long periods of maturation and integration as it has been demonstrated in the brain of rodents and sheep (Piumatti et al., 2018; La Rosa et al., 2019; Benedetti et al. 2019).

Despite all the controversy, there is agreement over a certain postnatal period in which neurogenesis still happens in the human DG (Cipriani et al., 2018; Knoth et al., 2010; Sorrells et al., 2018), and unlike in the adulthood, early life exposures to social and chemical stress have been shown to produce long-lasting effects on brain function, potentially including hippocampal disfunction (Cooper et al., 2015; Dorn et al., 2014; Rees and Inder, 2005). This suggests a neonatal temporal window when pathological insults could irreversibly affect a yet unformed HPF. In fact, opposing the results observed in adult epileptic conditions (Fahrner et al., 2007; Seki et al., 2019),

evidence was provided for increased neurogenesis in pediatric patients with early onset of temporal lobe epilepsy (TLE) (Blümcke et al., 2001), possibly derived from Nestin-expressing astroglial cells remaining from fetal development (Cipriani et al., 2018; Kruglyakova et al., 2005; Sorrells et al., 2018).

In TLE, despite the demonstration of no enhanced hAHN (Fahrner et al., 2007; Seki et al., 2019) reorganization of neurons (Seki et al., 2019) and astroglial populations (Crespel et al., 2005; Liu et al., 2018; Verwer et al., 2015) have been shown. Indeed, in rodent models NSCs have been reported to actively contribute to gliosis after seizures (Muro-García et al., 2019; Sierra et al., 2015). All the above indicates the relevance of shedding light into human DG development to understand how different neuronal and glial populations are arranged during initial formation, regardless of the neurogenic capacity of the adult niche. Likewise, understanding of pathological mechanisms closely related to hippocampal functionality such as TLE and their effect on different cell populations of the DG will help to unravel functional properties associated to this structure.

3.6. Adult hippocampal neurogenic niche in pathology: Epilepsy

To describe such a complex pathology like epilepsy, it is worth to start by its definition. Scientific history tells us how difficult it is to get a consensus when defining something and it is not different in this case. A conceptual definition of epilepsy was provided by the "international league against epilepsy" (ILAE) in 2005 for the first time, as a "*disorder of the brain characterized by an enduring predisposition to generate epileptic seizures and by its psychosocial consequences*". For a condition to be considered and treated as epilepsy, two unprovoked seizures had to be reported more than 24 h apart (Fisher et al., 2005). However, this definition was revisited in 2014 and the ILAE started to consider epilepsy a brain disease, in which either two unprovoked seizures occurred more than 24 h apart, the risk of further seizures after one unprovoked seizure was higher than 60% or an epilepsy syndrome was diagnosed (Fisher et al., 2014).

This widened definition brought controversy into the field, mainly focused on the treatment of epilepsy as a disease rather than a disorder. On behalf of ILAE, Robert Fisher explained that the disease word can be misunderstood to reflect contagiousness and might carry more stigma than it does a disorder, but ILAE interpreted that 'disease' better conveyed the gravity of epilepsy (Fisher, 2015). Still, part of the community was not convinced. Adam Noble et al. carried out a survey in which they questioned several

epileptic patients and reported that the significant majority of them preferred other terms rather than 'disease'. Thus, they concluded that ILAE was at odds with what patients want and discussed the implications of it (Noble et al., 2017). However, the definition provided by ILAE (Fisher et al., 2014) is the one that currently stands as the official one.

However it is defined, epilepsy imposes a substantial public health burden with an estimated number of 65 million people affected worldwide, being the developing countries the most impacted areas (Ngugi et al., 2010). Besides its prevalence, side effects and more importantly comorbidities such as cognitive impairment, depression or psychiatric disorders make epilepsy a major health concern (Gaitatzis et al., 2004; LaFrance et al., 2008). It is worth to mention that the risk of suicide has been demonstrated to be increased in most of people with epilepsy (Bell et al., 2009). The probability of premature death is 10 times higher in people with epilepsy than in the general population (Fazel et al., 2013). Furthermore, some studies have shown that between 30-40% of patients become resistant to antiepileptic drugs (Kwan and Brodie, 2000). Despite a tremendous increase in the number of new drugs developed for epilepsy in the last decades, the efficacy of the treatment has not improved in the last 70 years.

Regarding the mechanisms underlying epilepsy, it is well-known that it is the result of synchronized increased neuronal activity. This hyperactivity is provoked by an imbalance wherein excitatory neurotransmission, mostly through glutamatergic signaling, is increased or the inhibitory neurotransmission, through GABAergic signaling, is decreased (Dalby and Mody, 2001; Isokawa et al., 1997; Sharma et al., 2007a). Thus, a seizure, the defining event of epilepsy, was described as "*a transient occurrence of signs and/or symptoms due to abnormal excessive or synchronous neuronal activity in the brain*" (Fisher et al., 2005). Nonetheless, there are different types of seizures, which lead to different types of epilepsy.

Since the first modern classification was proposed in 1964 (Gastaut and Poirier, 1964), seizures have been classified according to different standards for many years. In 2015, ILAE made a new classification both for seizure (Fisher et al., 2017) and types of epilepsy (Scheffer et al., 2017). Thus, they classed them depending on parameters such as the type: Focal, generalized, both focal and generalized or unknown, and the region where seizures take place (Fisher et al., 2017; Scheffer et al., 2017). Again, some authors manifested their disagreement with the ILAE criteria of classification

(Lüders et al., 2019), which again was addressed by Robert Fisher. Indeed, he faced the debate stating that "*controversy about seizure classifications will continue until science explains why there are different types of seizures. Until then, every classification is a compromise, reflecting consensus and pragmatism*".

One of the few consensuses in the scientific community is that TLE is the most common subtype of focal epilepsy in human patients and the most likely to be resistant to drug treatment. Importantly, it is closely associated to the HPF and related structures (Falconer et al., 1964; Savage, 2014; Wiebe, 2000).

3.6.1. Mesial temporal lobe epilepsy (MTLE)

Different subclassifications of focal seizures arising from the temporal lobe have been proposed, finally leading to the distinction between two types of TLE depending on their site of origin: The lateral neocortical type and the medio-basal type, also known as MTLE (Yu et al., 2003). Although symptomatology commonly overlaps and spreads from lateral to mesial cortex (and vice versa), this is a useful distinction. MTLE arises from HPF or related structures in the majority of the cases and is mostly associated with specific memory impairment, although general intellectual impairment can often be discerned (Hermann et al., 1997). In most cases, MTLE associated seizures consist of non-lateralized manifestations such as oral automatisms, papillary dilatation, impaired consciousness and generalized rigidity (Williamson et al., 1993).

MTLE is the most pharmacoresistant among the different subtypes of epilepsy and therefore many patients (up to 30%) undergo surgery to resect the HPF and in most instances also the anterior parahippocampal gyrus (Wieser, 2004). However, this intervention is expensive and not always practicable. Furthermore, even though surgery can control seizures and improve quality of life in appropriately selected patients (Arruda et al., 1996; Garcia et al., 1994; Jeha et al., 2006; McIntosh et al., 2004; Quirico-Santos et al., 2013), there are still cases that do not respond to neither medical nor surgical treatment and are classed as "intractable epilepsy". In these cases, comprehensive care is required to address the adverse effects of medical treatment, quality of life issues and comorbid disorders (Schuele and Lüders, 2008). The pathological evolution of MTLE is comprised by three different critical stages: *Status epilepticus* (SE), the latent period and the chronic period **(Figure I17 A)**. The SE is the initial phase in which a precipitant injury afflicting the HPF or related areas leads to seizure activity lasting more than 5 minutes during which full consciousness does not recover **(Figure I17 B)**. It is divided in two different phases; A first one characterized by

generalized convulsive tonic-clonic seizures and a second one associated to minor behavioral symptoms concomitant to continuous electrical discharges, increase in intracranial pressure and decrease in cerebral blood flow recover (Lowenstein, 1999; Seinfield et al., 2016). The latent period is the seizure-free time between the SE and the clinical manifestation of the first spontaneous seizure, characterized by strong presence of interictal spikes in electroencephalograph (EEG) recordings (Chauvière et al., 2012; Wang et al., 2019; White et al., 2010). Finally, patients start to show chronic occurrence of clusters of seizures that can happen many times a day over multiple consecutive days, known as spontaneous recurrent seizures **(Figure I17 C)** (Haut, 2006; Williams et al., 2009). The study of MTLE in human tissue, as for any other pathological condition, is limited. Therefore, different animal models have been developed to reproduce the electroencephalographic, behavioral and neuropathological features of this disease (Kandratavicius et al., 2014; Lévesque et al., 2016).

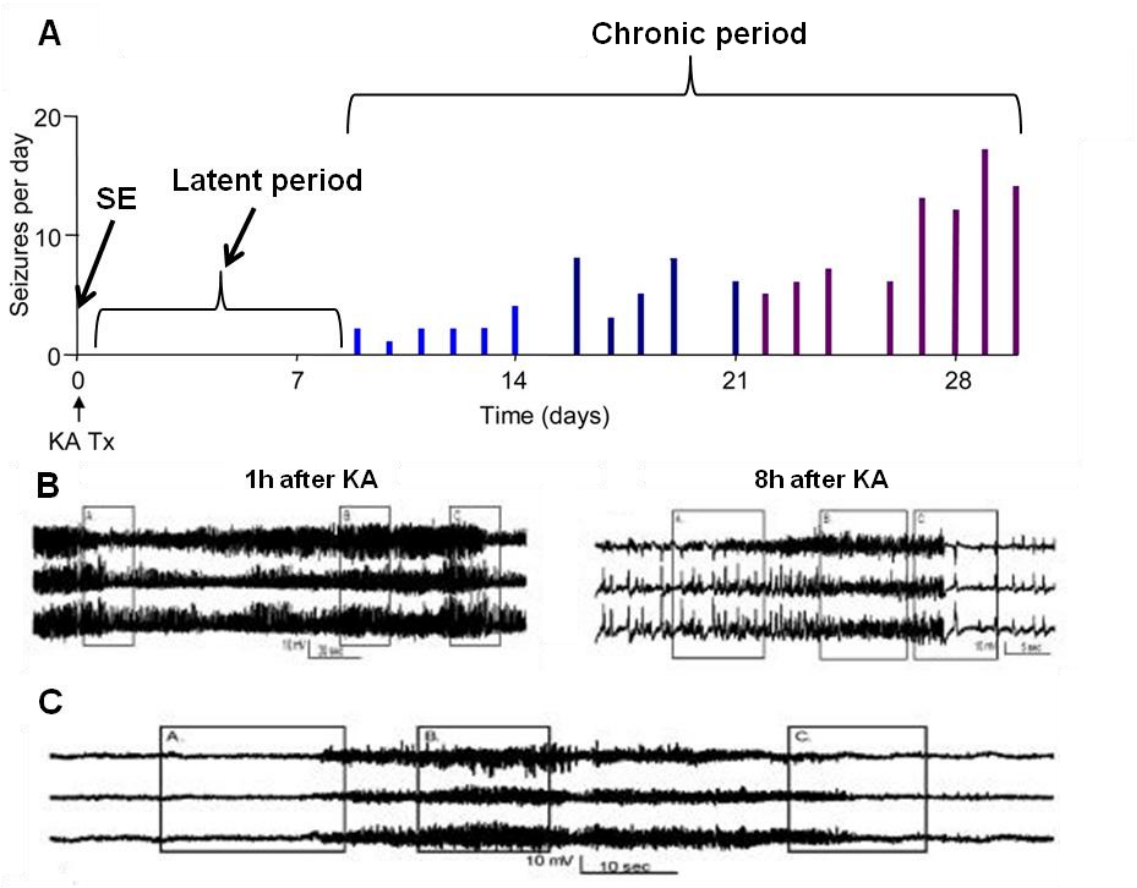

Figure I17. A) The pathological evolution of MTLE in rodents. After the SE induced by kainic acid (KA) administration, a seizure-free latent period lasts around one week until the first spontaneous seizure appears, leading to the chronic period in which spontaneous recurrent seizures take place. **B)** KA-induced seizures during the SE. Electrographic spikes were continuous, but decreased in frequency from 1h to 8h

following KA treatment. **C)** Electrographic spikes of a spontaneous seizure recorded 12 weeks after SE (modified from White et al., 2009 and Williams et al., 2010).

3.6.1.1. Rodent models of MTLE

The most widely used models to reproduce MTLE in rodents are administration of pilocarpine or KA. In both models, in the first days after intraperitoneal or intracerebral injection of the chemoconvulsants animals alternate between seizure-free periods and high-seizure rates (Arida et al., 1999; Babb et al., 1995; Bouilleret et al., 1999; Cavalheiro, 1995; Goffin et al., 2007; Williams et al., 2009).

Pilocarpine is a cholinergic muscarinic receptor agonist that in 1983 was showed to induce SE in rodents after systemic intraperitoneal administration. It affects several regions including the olfactory cortex, amygdale, thalamus, neocortex, *substantia nigra* and also the HPF. Approximately 2 weeks after the initial SE, animals suffer spontaneous seizures (Turski et al., 1983). Although pilocarpine has been mainly used intraperitoneally in rats (Arida et al., 1999; Cavalheiro, 1995; Goffin et al., 2007; Parent et al., 1997, 2006), it has been also administered intrahippocampally (De Furtado et al., 2002).

KA is a cyclic analog of L-glutamate and an agonist of the ionotropic KA receptor. Ben Ari and colleagues used its administration as the first MTLE model in rats (Ben-Ari et al., 1979). They reported SE after an intraamygdalar KA injection and appearance of spontaneous seizures thereafter. Similar results were obtained using an intrahippocampal injection model (Cavalheiro et al., 1982) and also intraperitoneal systemic injections, although the brain damage was more generalized in the latter (Babb et al., 1995). Later, the intrahippocampal method was thoroughly implemented for the study of MTLE in mice, replicating human EEG features, cell death and inflammation (Abiega et al., 2016; Bouilleret et al., 1999; Sierra et al., 2015). In mice, the intraamygdalar injection of KA replicates the effects of the intrahippocampal injection of KA on the DG and the observations in the DG and neurogenic niche of MTLE patients (Muro-García et al., 2019).

Both models (Pilocarpine and KA) and their different experimental applications (intraperitoneal, intraamygdaloid or intrahippocampal) represent valid methods for human MTLE replication in rodents. However, the KA intrahippocampal injection model has been described to be the one that more reliably reproduces human MTLE and consequent hippocampal sclerosis (HS) in mice, mimicking the effect of hippocampal

focal seizures and their extended damage over related healthy tissue (Lévesque and Avoli, 2013).

3.6.1.2. MTLE-HS

MTLE is highly associated with a pathology termed HS, characterized by hardening of the HPF (Blümcke et al., 2013; Thom, 2014). In 1880, Wilhelm Sommer reviewed the accumulating data and published a landmark paper recognizing the relevance of this lesion in the tissue. He highlighted neuronal loss in CA as the main observation (Sommer, 1880). In the following decades this concept was extended with new reported forms of HS with neuronal loss and gliosis affecting also the DG (Margerison and Corsellis, 1966; Spielmeyer, 1927). Currently, there is a classification of different HS types (Blümcke et al., 2013; Thom, 2014) **(Figure I18)** and it is studied with high interest, as its exact relation with seizures (cause or consequence) remains intriguingly unknown (Blümcke et al., 2002; Cendes et al., 2014; Sano and Malamud, 1953; Thom, 2014).

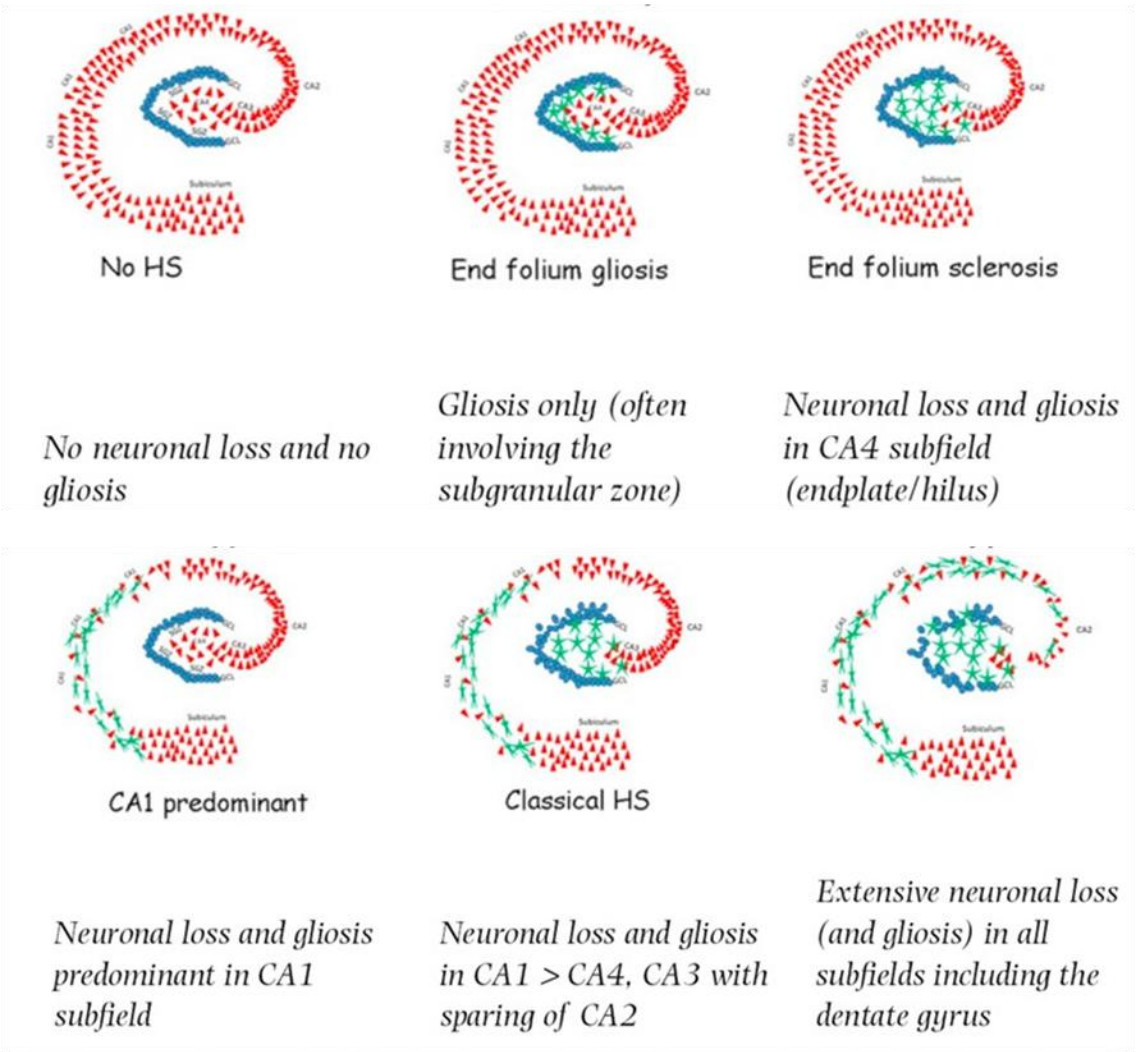

Figure I18. Classification of the different types of HS (modified from Thom, 2014).

The most obvious and classically studied change that occurs with HS is neuronal loss in different regions of the HPF, specially CA subfields and DG. Pyramidal cells, excitatory mossy cells and interneurons undergo cell death at variable degrees depending on the case and the HS type (Blumcke et al., 2000; de Lanerolle et al., 1989; Mathern et al., 1996; Steve et al., 2014; Thom et al., 2002). Together with neuronal loss, GCL dispersion (GCD) (Houser, 1990; Kobow et al., 2009; Lurton et al., 1998), MF sprouting and synaptic reorganization are key neuropathological aspects of HS (Malmgren and Thom, 2012; Sutula et al., 1989). Focusing on these neuronal effects, most antiepileptic drugs produce their therapeutic effect either by reducing neuronal excitation or potentiating neuronal inhibition (Rogawski and Löscher, 2004). However, the neuronal approach is not always effective and the patient can become medically refractory (Kwan and Brodie, 2006; Schuele and Lüders, 2008). Therefore several authors have highlighted the importance of new approaches focusing on

reactive astrogliosis, another critical pathological consequence of HS and MTLE (Binder and Steinhäuser, 2006; Rassendren and Audinat, 2016; Wilcox et al., 2015).

Proliferation and hypertrophy of astrocytes that form the glial scar has been highly studied as one of the hallmarks of MTLE (Binder and Steinhäuser, 2006; Rassendren and Audinat, 2016; Wilcox et al., 2015). In control conditions, astrocytes can release calcium from internal stores following activation of a variety of G-coupled receptors. This triggers the release of different factors that can modulate neuronal signaling, such as glutamate, d-serine and adenosine triphosphate (ATP) (Halassa et al., 2007). In epileptic conditions, changes in astrocyte numbers and densities have long been reported, with high increase especially in the DG (Briellmann et al., 2002). Moreover, they undergo morphological changes like process thickening and increase their expression of intermediate filament proteins such as GFAP, (Wilhelmsson et al., 2006) both characteristics of reactive astrocytes (Sofroniew, 2009) **(Figure I19)**. Following reactivation, glutamate transport currents are altered (Takahashi et al., 2010) and they decrease glutamine synthetase expression (Eid et al., 2019), which leads to an excessive release of extracellular glutamate, causing general neuronal hyperexcitation. Also, in seizure-related pathologies their domain organization gets disrupted (Oberheim et al., 2008) and water and potassium homeostasis dysregulated (Lee et al., 2012). Interestingly, soon after KA-induced SE, astrocytes start to express a number of specific subunits of KA receptors (Vargas et al., 2013).

The exact role of astrocytes in the development of epilepsy has been long discussed in the last decades (Gibbons et al., 2013). In fact, it has been proposed not only that they have fundamental roles in modulating seizures by altering the electrical excitability and excitotoxic levels of the epileptogenic focus (de Lanerolle and Lee, 2005), but also that they may contribute in the genesis of epilepsy and seizures, as well as in the pathways targeted by antiepileptic drugs (Lee et al., 2012; Tian et al., 2005). However, the assessment of astrogliosis contribution needs to be carefully done, as it is not a single-or-none response (Sofroniew, 2009). Astrogliosis should be regarded as a complex process in which numerous subtle and reversible changes take place in a continuous way. Moreover, depending on the circumstances reactive astrocytes can mediate beneficial functions that include protecting neurons or restricting the spread of inflammation and infection (Sofroniew, 2009).

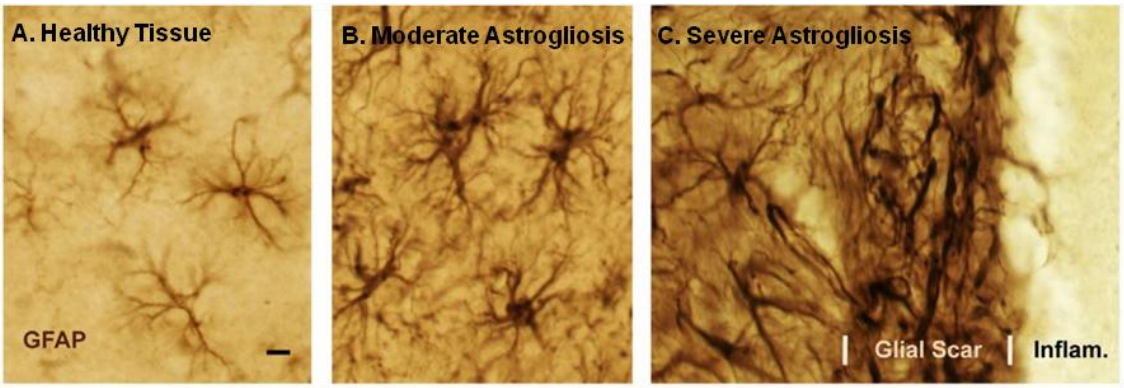

Figure I19. Morphological changes of GFAP-expressing astrocytes in the mouse neocortex. Compared to healthy conditions, astrocytes show process thickening and stronger expression of GFAP in conditions of moderate astrogliosis. They form a glial scar around the inflamed area when the astrogliosis is severe (taken from Sofroniew, 2009).

3.6.1.3. MTLE and NSCs

Adult hippocampal NSCs have been shown to get activated in different animal models in which seizures were provoked and neuronal activity enhanced (Gray and Sundstrom, 1998; Hüttmann et al., 2003; Lugert et al., 2010; Segi-Nishida et al., 2008; Sierra et al., 2015). In fact, it has been proposed that neuronal activity and NSC proliferation are coupled, the first triggering the latter (Deisseroth et al., 2004). Likewise, tonic GABA promotes quiescence of NSCs and its reduction favors their activation (Song et al., 2012). In rats to which pilocarpine was intraperitoneally administered following systemic injections, seizure induced SGZ proliferation has been associated with increased newborn neuron generation at short-term (Hattiangady et al., 2004; Parent et al., 1997). Moreover, these neurons have been reported to accelerate their morphological development and abnormally migrate into ectopic locations, mainly ML and hilus (Overstreet-Wadiche et al., 2006). Their aberrant integration into the existent circuit contributes to increased synapses in the hippocampal circuit that trigger cognitive impairment (Althaus et al., 2019; Jessberger et al., 2005, 2007; Parent et al., 1997, 2006; Scharfman et al., 2000). However, these enhanced neurogenesis is driven by effects upon DCX-positive migrating late-stage progenitors rather than NSC activation itself (Jessberger et al., 2005). Indeed, the increased neurogenesis observed shortly after acute seizures returns to baseline levels by about 2 months after the initial seizure episode in rats (Jessberger et al., 2007), although slightly augmented neurogenesis has also been reported to be maintained after spontaneous recurrent seizures (Cha et al., 2004).

On the contrary, it has been reported that chronic epileptic seizures impair AHN rather than stimulating it (Hattiangady et al., 2004; Heinrich et al., 2006; Kralic et al., 2005; Sierra et al., 2015). In both intraventricular and intraperitoneal KA injections in rats, after an initial burst of progenitor cells proliferation, neurogenesis becomes absent at long-term (Hattiangady et al., 2004). In addition, given that the authors failed to observe a decrease in Sox2 or Vimentin-expressing NSCs in the SGZ of chronically epileptic animals, the decrease in the neurogenic capacity was attributed to a change of the neurogenic niche towards a hostile environment for the NSCs (Kuruba and Shetty, 2007).

In mouse models in which KA was injected intrahippocampally, more characteristics of MTLE and HS were reproduced: 1) The mitotic activity following injury was indeed not neurogenic, contributing to previously reported microgliosis and astrocytosis (Heinrich et al., 2006; Kralic et al., 2005; Lee et al., 2003). 2) The production of newborn neurons sharply decreased in a disrupted neurogenic niche, at that time explained as "induced quiescence of NSCs" (Kralic et al., 2005). 3) In previous studies of my host lab, Juan Manuel Encinas and colleagues applied this intrahippocampal model using constitutive and inducible Nestin-GFP transgenic mice, corroborating the massive activation of NSCs and a drastic alteration of their neurogenic program. After seizures affecting the HPF and adjacent areas, NSCs undergo a dramatic shift in their morphology, acquiring a reactive phenotype (hypertrophic and multibranched) and switching from neurogenic state to a gliogenic one. Indeed, reactive NSCs (React-NSCs) tend to divide symmetrically generating more copies of them, which finally differentiate into reactive astrocytes by division or direct transformation. Therefore, the transformation of NSCs into React-NSCs contributes to the hippocampal gliosis and leads to the long-term impairment of neurogenesis (Muro-García et al., 2019; Sierra et al., 2015; Valcárcel-Martín et al., 2020) **(Figure I20)**.

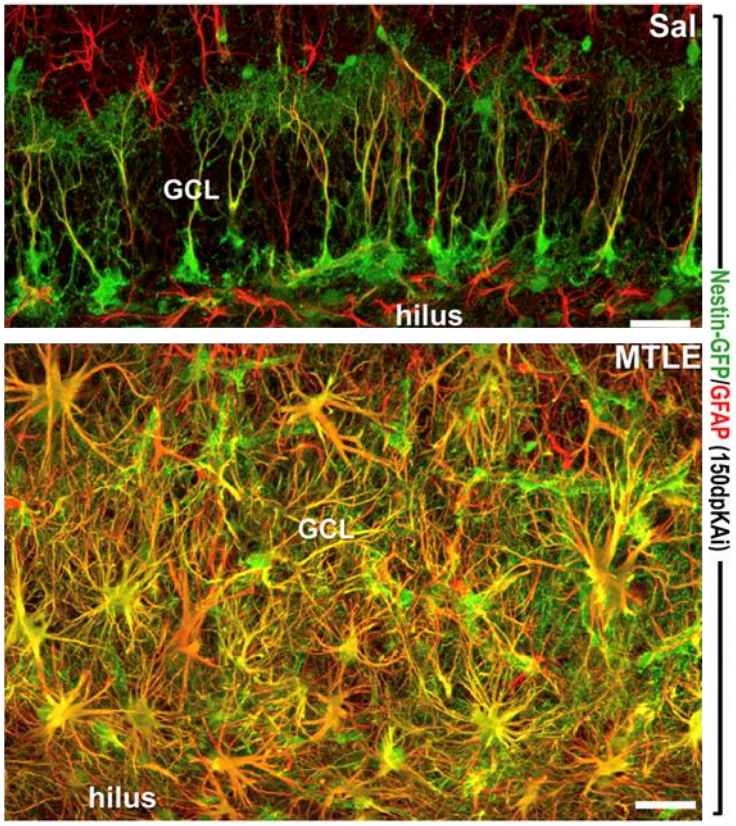

Figure I20. 150 days after KA-induced MTLE, the hippocampal neurogenic niche gets completely disrupted. NSCs get massively activated, producing React-NSCs and contributing to the gliosis in the GCL (modified from Sierra et al., 2015).

Despite the importance of the NSC pool disruption and its potential contribution to the pathological consequences in chronic epilepsy, the mechanisms underlying these alterations remain unknown. Alternatively, growth factors have been long known to regulate the formation of new neurons by modulating SC and progenitor proliferation, differentiation and survival (Calof, 1995). Moreover, seizure-induced expression of trophic factors by surrounding tissue, such as brain-derived neurotrophic factor (BDNF), vascular endothelial growth factor (VEGF) and others could indirectly induce NSC proliferation (Gall, 1993; Gall et al., 1991).

3.6.2. Possible mechanisms in MTLE-HS

EGF was long ago reported to be mitogenic on cultured astrocytes (Simpson et al., 1982). Later, both EGF and fibroblast growth factor 2 (FGF2) were shown to stimulate proliferation of cultured embryonic SC and progenitors (Reynolds et al., 1992; Tropepe et al., 1999) and several studies reported also the mitogenic effect of both factors in NSCs derived from the adult rodent brain (Kuhn et al., 1997; Palmer et al., 1995). Importantly, EGF also provokes the expansion of SVZ NSCs after its *in vivo*

administration (Craig et al., 1996). Altogether, these results suggest a possible role for these factors and their signalization pathway in the activation of NSCs and astrocytes, thereby being potentially relevant in the context of epilepsy.

3.6.2.1. Fibroblast growth factor receptor (FGFR)

FGF2 is part of a bigger family of growth factors composed by 18 different FGFs forming different subfamilies. Although they share a 30-60% homology, different N- and C-terminals regulate their specific receptor binding (Beenken and Mohammadi, 2009). FGFs have been reported to bind four different FGFRs: FGFR1, FGFR2 (Dionne et al., 1990), FGFR3 (Keegan et al., 1991) and FGFR4 (Partanen et al., 1991; Stark et al., 1991). All of them consist of an extracellular ligand binding region containing three immunoglobulin-like domains and an intracellular split tyrosine kinase domain. FGFR1 and FGFR2 are the ones with higher affinity to FGF2 (Dionne et al., 1990; Johnson et al., 1990), while FGFR3 has lower affinity for it (Keegan et al., 1991) and FGFR4 binds to FGF1 but not to FGF2 (Partanen et al., 1991). Importantly, FGF2 needs to previously bind to heparan sulfate to properly bind to FGFRs (Rapraeger et al., 1991).

FGF2 has been long demonstrated to be increased after seizures in different rodent models. Following a focal electrolytic lesion in the hilus that triggered seizures, FGF2 was shown to be increased in several brain regions, including DG. Interestingly, although the majority of cells showing FGF2 expression were astroglia, GCs also showed increased expression of FGF2 (Gall et al., 1994). In this line, within the first 24 h after an intraperitoneal KA injection FGF2 was augmented in astrocytes and neuronal populations of the DG (Gómez-Pinilla et al., 1995a; Riva et al., 1994; Van Der Wal et al., 1994). Moreover, FGFR1 was also increased especially in astroglial populations, suggesting an interplay between FGF2 and FGFR1 in the seizure-mediated glial response (Gómez-Pinilla et al., 1995b; Van Der Wal et al., 1994). Supporting these observations, cultured astrocytes showed increased FGF2 and FGFR1 levels in the presence of glutamate (Pecháň et al., 1993), which is known to be abnormally released into the extracellular medium after seizures (Eid et al., 2019; Meldrum et al., 1999).

Indeed, FGF2 and FGFR1 have been shown to be involved in the reactivity of astrocytes after a focal injury in rodents (Gómez-Pinilla et al., 1995b). Also, after its subcutaneous administration FGF2 promotes neurogenesis in the postnatal rat cerebellum (Tao et al., 1996) and in the HPF and SVZ both at postnatal and adult stages (Wagner et al., 1999). In fact, when administered intraventricularly, FGF2 promotes expansion of the progenitor population, enhancing neurogenesis and

newborn neurons in the OB (Kuhn et al., 1997). Therefore, it seems fair to hypothesize that FGFR1 stimulation could be playing a role in the aberrant neurogenesis and reactive astrogliosis that occurs after seizures (Sierra et al., 2015). Interestingly, FGF2 has been described to induce responsiveness to EGF during embryonic development, possibly mediated by induced EGFR expression (Ciccolini and Svendsen, 1998).

3.6.2.2. EGFR

EGFR (Also known as HER or ErbB1) is the first receptor of the ErbB family, also comprised by three more transmembrane receptor kinases that were described as related to EGFR: ErbB2 (Semba et al., 1985), ErbB3 (Kraus et al., 1989; Plowman et al., 1990) and ErbB4 (Plowman 1993). EGFR was discovered in 1978 by Graham Carpenter and colleagues. Using a cell-free membrane preparation, they reported for the first time a receptor tyrosine kinase that was bound to EGF, triggering phosphorylation of endogenous and exogenous proteins (Carpenter et al., 1978). Later, the complete amino acid sequence of the receptor was presented, opening a new way for further research on its cellular role and signaling pathway (Ullrich et al., 1984).

Each of the ErbB receptor kinases are single chain transmembrane polypeptide proteins that have three different domains: 1) A cysteine-rich extracellular domain that acts as binding site for the ligands that will trigger the receptor activation, 2) a transmembrane domain involved in the dimerization between receptors after ligand stimulation and 3) a large cytoplasmic tyrosine kinase domain that phosphorylates tyrosine residues on substrate proteins, triggering the correspondent signaling pathway that will end up provoking the cellular outcome (Bessman et al., 2014; Herbst, 2004; Riese and Stern, 1998; Yarden and Sliwkowski, 2001) **(Figure I21)**.

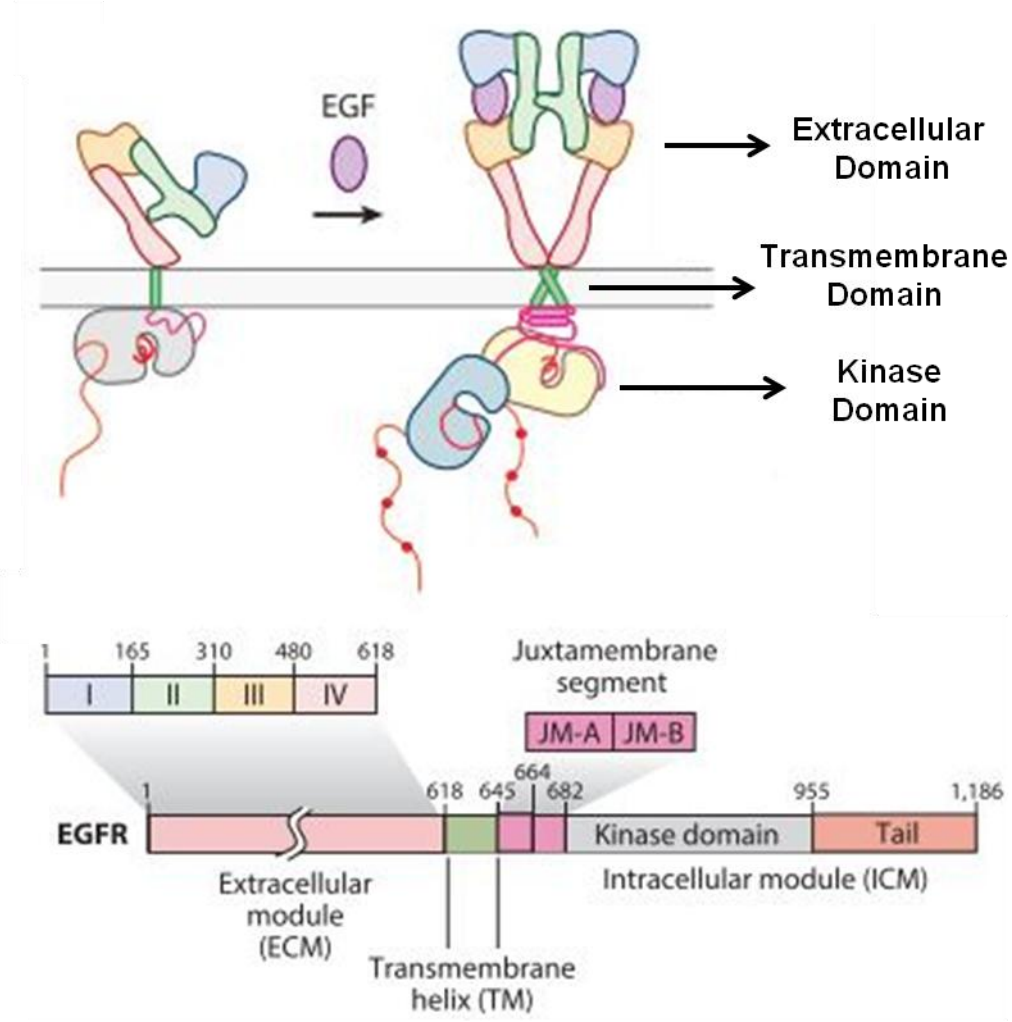

Figure I21. The structure of EGFR before and after binding to a ligand. The four different domains that comprise the extracellular module form a dimer (as it will be later explained) in order to bind to the ligand. Then, the transmembrane domain and the juxtamembrane segment trigger the activation of the tyrosine kinase domain (Intracellular module) activating different downstream signaling pathways (modified from Kovacs et al., 2015).

ErbB receptors can be activated by multiple ligands, with the exception of ErbB2 that is considered an orphan receptor and thus, its action is restrained to heterodimerization with the other receptors of the family. All ligands are synthesized from one transmembrane precursor and once expressed at the plasma membrane they are subjected to the proteolytic cleavage of their ectodomain. Thus, the soluble growth factor that will trigger the whole cellular response is generated (Carpenter, 2000). EGFR in particular can be activated by seven different growth factors that are classified in two different subtypes. The high-affinity ligands are EGF, transforming growth factor alfa (TGFα), heparin-binding EGF-like growth factor (HB-EGF) and betacellulin (BTC), while the low-affinity ligands are epiregulin (EPR), epigen (EPGN) and amphiregulin

(AREG) (Harris et al., 2003; Jones et al., 1999; Riese and Stern, 1998). The affinity of the ligands to EGFR is not exclusive and differs between them. For example, BTC also shows high-affinity to ErbB4, whereas EGF, TGFα and HB-EGF have narrow specificity to EGFR (Jones et al., 1999). However, ligand affinities get more complex considering one fundamental characteristic for the functionality of ErbB receptors: Dimerization.

Before being stimulated by a ligand, ErbB receptors remain as tethered monomers. When a ligand activates them they bind together, forming dimers that are essential to trigger the whole intracellular signaling thereafter (Bessman et al., 2014; Herbst, 2004; Riese and Stern, 1998; Yarden and Sliwkowski, 2001). In this process, receptors can bind to their equals, forming homogeneous dimers or homodimers. Nonetheless, the capacity of the receptors to cross-talk and generate heterodimers with different receptors of the family has been long studied (Earp et al., 1995; Karunagaran et al., 1996; Tzahar et al., 1996). This interplay is not meaningless for the resulting cellular dynamics since it affects the tyrosine phosphorilation sites and hence which signaling proteins are engaged. For instance, even though ErbB2 cannot bind to any ligand, it has the capacity to form heterodimers with the rest of the receptors after they are activated, provoking strong responses (King et al., 1988; Stern and Kamps, 1988; Wada et al., 1990). Indeed, it has been described that homodimeric receptor combinations are the less mitogenic and transforming ones, being the heterodimers the most potent complexes to elicit this cellular output (Pinkas-Kramarski et al., 1996). In adittion, different receptor combinations can affect the binding preference of a ligand, modifying the whole cellular functions (Jones et al., 1999).

Once the intracellular machinery has started, the different ErbB family members possess distinct complements of tyrosine phosphorylation sites that make them elicit diverse, although sometimes overlapping, sets of responses (Jones et al., 2006). Nonetheless, similar to the non-existent capacity of ErbB2 to bind to any ligand, ErbB3 has lost robust kinase activity over the evolutionary course, remaining catalytically inactive (Jura et al., 2009). Thus, its signalization capacity is also restricted to heterodimerization. Soon after the discovery of EGFR (Carpenter et al., 1978) several tyrosine residues were described in the intracellular carboxyl-terminal tail of the receptor, identified as autophosphorylation sites in the activated EGFR (Carpenter, 1983). During the following years, these autophosphorylation sites were further described (Y992, Y1068, Y1086, Y148 and Y1173)(Downward et al., 1984; Margolis et al., 1989; Walton et al., 1990) and it was also reported the existence of specific tyrosine residues (Y845, Y891, Y920 and Y1101) that despite not being able to

autophosphorylate, they had the capacity to be trans-phosphorylated by other kinases (Biscardi et al., 1999; Stover et al., 1995). Moreover, phosphorylation of serine (S967, S971 and S1002) and threonine (T654 and T669) residues were also found in EGFR (Heisermann and Gill, 1988; Hunter et al., 1984; Kuppuswamy et al., 1993).

Interestingly, apart from direct ligand binding ErbB receptors can also get indirectly activated. G protein-coupled receptors (GPCRs) can get activated and indirectly promote phosphorylation of specific tyrosines on ErbB receptors (Carpenter, 1999, 2000; Gschwind et al., 2001). After GPCR activation, the non-receptor tyrosine kinase Src was described to directly associate and phosphorylate EGFR tyrosine kinases (Thomas and Brugge, 1997). Furthermore, it was demonstrated that angiotensin II (Eguchi et al., 1998) or LPA (Luttrell et al., 1996) were able to quickly increase the detected amount of Src coprecipitated with EGFR. Indeed, this GPCR-derived EGFR tyrosine phosphorylation was decreased by overexpression of either a dominant-negative Src construct or C-terminal Src kinase (CSK), a regulatory kinase that inhibits Src function (Luttrell et al., 1996). Therefore, the Src-EGFR complexes provoked by GPCR activation were defined as a mechanism for EGFR trans-activation. This process was initially thought to occur only in an intracellular ligand-independent manner due to its rapid onset (Carpenter, 1999). However, it was later described that trans-activation can indeed be mediated by ligand induction (Carpenter, 2000; Gschwind et al., 2001). In a pair of groundbreaking works, Norbert Prenzel and colleagues reported that after GPCR agonist binding, mettalloproteinases get quickly stimulated and cleavage the HB-EGF precursor protein (pro-HB-EGF), ultimately leading to EGFR activation by the soluble HB-EGF and the consequent biological outcome (Gschwind et al., 2002; Prenzel et al., 1999). This process was termed triple membrane passing signal event (Prenzel et al., 1999).

EGFR dimerization and ligand activation can trigger a plethora of intracellular responses in an extensive downstream signaling pathway. The described tyrosine phosphorylation sites act as docking sites for several signaling molecules containing a phosphotyrosine-binding sequence, such as Src homology 2 (SH2) or phosphotyrosine-binding domains (PBD) (Olayioye, 2000; Shoelson, 1997). Next, depending on the receptor stimulation process, different downstream signaling pathways will activate.

The most important and studied one is possibly the mitogen-activated protein kinases (MAPK) pathway **(Figure I22 A)**. This well-known signaling pathway starts with

the activation of RAS proteins that lead to the phosphorylation of RAF kinases, which in turn phosphorylate MAPK/extracellular signal regulated kinases (ERK) (MEK). Finally, MEK induces ERK1/2 activation leading to the production of several cell-cycle associated transcription factors and the accumulation of cD catalyzing the division of the cell (Downward, 2003). Moreover, ERK1/2 phosphorylate a wide number of substrates and translocate them to the nucleus, where they modulate the action of multiple proteins and transcription factors that play critical roles in the regulation of proliferation, survival and cell metabolism (Deschênes-Simard et al., 2014; Lewis et al., 1998; Morrison, 2012).

Another pathway among the downstream signaling of EGFR is the Akt **(Figure I22 A)**, also known as protein kinase B (PKB), signaling pathway. In this case, phosphoinositide 3-kinase (PI_3K) docks to a phosphorylated kinase in EGFR and stimulates the generation of phosphatidylinositol-3,4,5-triphosphate (PIP-3), which in turn promotes the activation of Akt (Cully et al., 2006). Thus, Akt modulates cell survival through suppression of apoptosis and can participate in other cellular processes such as proliferation, metabolism, cell growth and motility (Dibble and Cantley, 2015; Morgensztern and McLeod, 2005).

The family of signal transducers and activator of transcription proteins (STATs) **(Figure I22 B)** has been also shown to be part of the EGFR downstream signaling (David et al., 1996). Particularly, STAT3 can bind to multiple tyrosine residues of EGFR and get phoshporylated (Park et al., 1996; Zhong et al., 1994). Once activated, STAT3 forms a dimer with another STAT3 protein and gets internalized. Interestingly, it has been reported to play a role in the proliferative capacity and reactivity of astrocytes in different conditions (De La Iglesia et al., 2008; Priego et al., 2018). Furthermore, STAT3 can also be activated through Akt signaling pathway (Kim et al., 2013), suggesting that the interplay between different signaling pathways can be critical for the final cellular outcome.

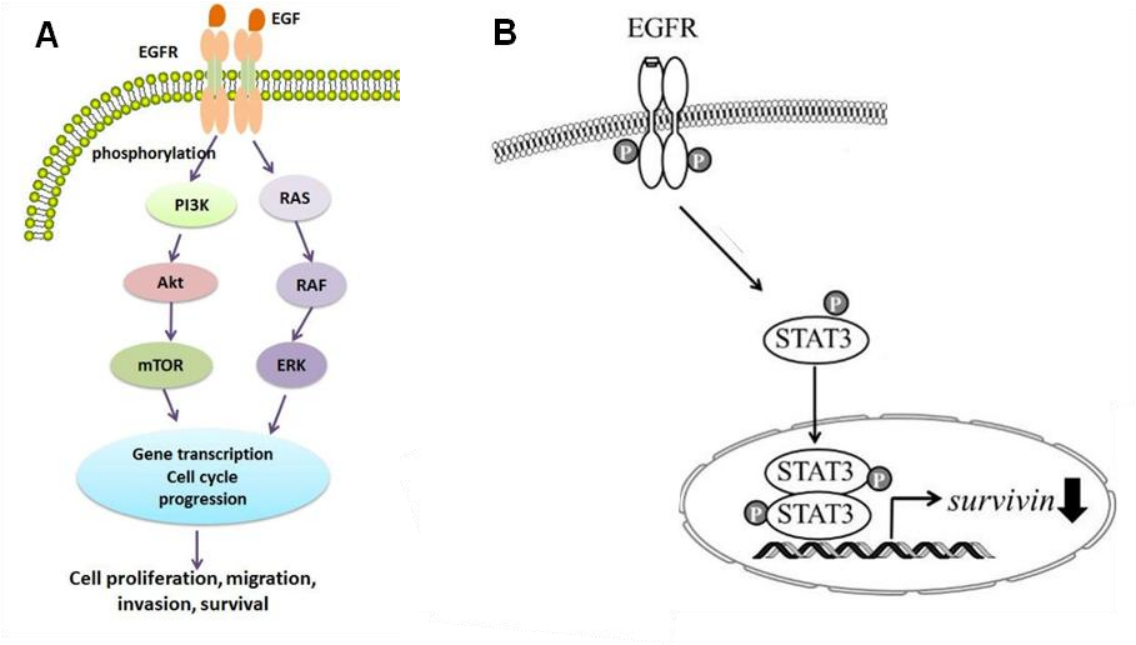

Figure I22. Downstream signaling pathways of EGFR. **A)** A simplified version of the Akt and ERK1/2 downstream signaling pathways that mostly lead to cell proliferation, migration and survival. **B)** The STAT3 downstream signaling pathway that after being activated forms a dimer with another STAT3 and plays a role in cellular processes such as survival (modified from Yamashita et al., 2017; Zulkifli et al., 2017).

EGFR was reported to be ubiquitous in the mammal brain, starting to be expressed in astroglia at P16 and reaching its maximum immunoreactive expression at P19, while it becomes much weaker or almost absent thereafter (Gómez-Pinilla et al., 1988; Nieto-Sampedro et al., 1988). On the contrary, in adult and aged rats and also in humans, strong EGFR signal was reported in cortical neurons, being abundant in the cingulate, frontal, frontoparietal and striate cortical regions (Gómez-Pinilla et al., 1988; Werner et al., 1988). However, even if the expression of EGFR in glial cells is negligible in normal conditions, the situation changes in pathological conditions.

EGFR has been highly studied in the context of cancer diseases. Its overexpression has been reported in several types of human tumors, including head and neck, breast, ovarian, prostate, bladder, non-small-cell lung cancer, pancreatic an renal cell carcinomas and squamous carcinomas (Arteaga, 2011; Nicholson et al., 2001; Salomon et al., 1995; Sasaki et al., 2009; Sharma et al., 2007b). In addition, the EGFR amplification has been demonstrated to be highly important in glioblastomas (Lee et al., 2006; Libermann et al., 1985; Vivanco et al., 2012). Taking this into account, it seems that the relevance of EGFR for cellular proliferation and reactivity in pathologic conditions could be applied to the understanding of MTLE. However, not much is known about the role of EGFR in this disease. Juan Manuel Encinas and

colleagues performed gene expression (whole genome arrays) analysis and showed that three days after an intrahippocampal KA injection 46 different signaling pathways were upregulated in the mouse HPF. Interestingly, the ErbB signaling pathway, to which EGFR belongs, was one of them (Sierra et al., 2015). Nonetheless, one of the hallmarks of MTLE, which is the massive extracellular release of glutamate that causes neuronal hyperexcitation (Eid et al., 2019; Meldrum et al., 1999), could affect EGFR expression. In glioblastoma-derived glial cells glutamate induces a significant increase of EGFR mRNA and protein levels, while treatment with EGFR inhibitors such as Gefitinib reversed the effect of glutamate on cell proliferation (Schunemann et al., 2010). In hypothalamic astrocytes activation of metabotropic or AMPA glutamate receptors causes the recruitment of ErbB receptors to the cell membrane, trans-activating them and increasing their cellular expression (Dziedzic et al., 2003). Likewise, in cultured rat cortical astrocytes, the glutamate receptor mGluR5, when activated, forms a signaling complex with EGFR and together induce the activation of ERK2 signaling pathway (Peavy et al., 2001).

Being reactive astrogliosis one of the main features of MTLE-HS (Binder and Steinhäuser, 2006; Rassendren and Audinat, 2016; Wilcox et al., 2015), it is remarkable that following the first days after different focal brain injury models, EGFR has been reported to be increased in astroglia in both rats (Nieto-Sampedro et al., 1988; Río et al., 1995) and humans (Ferrer et al., 1996). Also, receptor expression was shown in rats in reactive astrocytes and microglia within the first three days after ischemia (Planas et al., 1998), suggesting a role of the receptor in the glial reactive response.

As previously mentioned, in a rodent MTLE model NSCs have also been shown to massively activate and contribute to the reactive astrogliosis, losing their neurogenic capabilities (Sierra et al., 2015). Interestingly, isolating EGFR-expressing cells was demonstrated that EGFR plays a fundamental role in the regulation of the adult SVZ neurogenic niche, where EGFR expression correlates with activated NSCs (Codega et al., 2014; Pastrana et al., 2009). During embryonic development, EGFR affects the migration capacity of cortical progenitors at embryonic stages (Burrows et al., 1997; Caric et al., 2001; Ciccolini et al., 2005) and modulates progenitor proliferation, maturation and cell fate, inducing them to differentiate towards astrocytic lineage at neuronal expense. However, this effect on glial cell fate is dependent on the presence of high extracellular ligand amount (Burrows et al., 1997; Viti et al., 2003). Supporting the role of EGFR on glial vs neuronal differentiation, it was reported that SVZ

progenitors divide asymmetrically in terms of EGFR expression during development. Thus, after mitosis, a cell containing high levels of EGFR would be fated towards astrocytic lineage while its low EGFR-expressing sister cell would not (Sun et al., 2005). Moreover, another study demonstrated that overexpression of EGFR in the SVZ disrupts the neurogenic niche stability, expanding the neural precursor population but reducing the NSC number and therefore losing the long term neurogenic potential (Aguirre et al., 2010). Using a knock-out mouse model for EGFR, Maria Sibilia and colleagues found a reduced number of astrocytes in the developing cortex, with impaired proliferative capacity when cultured *in vitro* (Sibilia et al., 1998). Indeed, they demonstrated later that the increased apoptosis displayed by cortical astrocytes was due to a defective Akt signaling, which consequently affected also neuronal survival. Moreover, they found this effect to be restricted to cortical astrocytes, with midbrain astrocytes being unaffected (Wagner et al., 2006). Furthermore, these mice were found to be more susceptible to intraperitoneal KA-induced epileptic seizures (Robson et al., 2018).

EGFR has been reported to modulate progenitor migration and proliferation in the developing HPF (Carrillo-García et al., 2014; Sibilia et al., 1998). In the adult DG, EGFR expressing cells were shown to colocalize with the proliferating cells in the SGZ (Okano et al., 1996), and it was used to isolate active NSCs (Jhaveri et al., 2015; Walker et al., 2016), although it was claimed that in contrast to SVZ, in the DG EGFR can be expressed also by quiescent NSCs (Jhaveri et al., 2015). Regardless of the identity of NSC subpopulations expressing EGFR, the functionality of the receptor in the hippocampal neurogenic niche remains largely unknown, especially in MTLE-HS conditions. We suggest that activation of EGFR mediates in the pathological consequences of this disease.

3.6.2.3. Zinc (Zn^{+2}) as a mediator of EGFR activation after KA

Among metal ions, Zn^{+2} is well-known to be critical for brain development during fetal and postnatal periods and also for the correct brain function in the adulthood, including modulation of the neurogenic process both at developmental and adult stages (Levenson and Morris, 2011; Sandstead, 2012; Sandstead et al., 2000). About the 80% of the total Zn^{+2} in the brain exists in metalloproteins such as metallothioneins (MTs) that act as storage units for Zn^{+2}, while the 20% left exists in the presynaptic vesicles of a subclass of glutamatergic neurons to serve as a signal factor in the intracellular cytosolic compartment as well as in the extracellular compartment (Frederickson, 1989; Frederickson and Danscher, 1990; Kambe et al., 2015; Maret, 2017; Takeda and

Tamano, 2009) **(Figure I23 A)**. This synaptic Zn^{+2} is histochemically reactive and it can be revealed by Danscher's sulfide-silver staining method (Danscher, 1981).

We know since the serendipitous discovery of Helmut Maske that Zn^{+2} presence in the HPF is one of the most intense in the brain (Maske, 1955). The majority of the Zn^{+2} in the HPF can be found widespread through the different areas, including subiculum and EC (Frederickson et al., 1983; Slomianka, 1992). Around 10% of the total hippocampal Zn^{+2} and the majority of synaptic Zn^{+2} can be found in the giant boutons of the MFs in the hilus, where it is contained in presynaptic vesicles (Frederickson et al., 1983; Sindreu et al., 2003). Also, around half of Schaffer collaterals was shown to contain Zn^{+2} in presynaptic vesicles (Sindreu et al., 2003) **(Figure I23 B).**

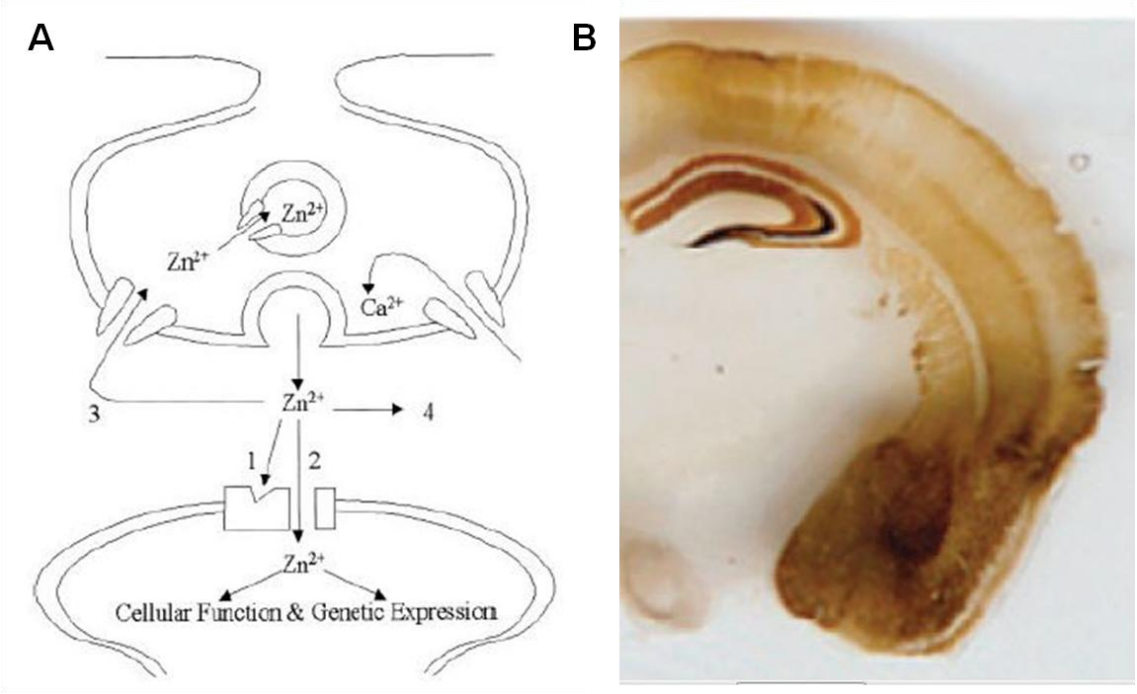

Figure I23. A) Once Zn^{+2} gets released into the synaptic cleft, it can modulate the postsynaptic neuron either directly (1) or through receptor binding (2). It can be reuptaken by the presynaptic cell (3) or released into the extracellular space (4). **B)** Synaptic Zn^{+2} is mainly expressed in the HPF, especially in the MFs, and also in the amygdala (modified from Takeda et al, 2013 and Burdette et al., 2000).

After an electrical impulse that triggered neuronal excitation in hippocampal slices, Zn^{+2} was demonstrated to be released into the extracellular space (Assaf and Chung, 1984), primarily from MFs (Aniksztejn et al., 1987). In fact, the released Zn^{+2} was shown to be re-uptaken by MFs, suggesting a role of Zn^{+2} in neural signaling processes for the first time (Howell et al., 1984). Years later, using novel methods for Zn^{+2} staining and tracing, it was found that after electrical stimulation, the released Zn^{+2}

crosses the synaptic cleft and enters postsynaptic neurons, potentially triggering intracellular responses (Li et al., 2001).

Since all the Zn^{+2} containing neurons in the brain are glutamatergic, Zn^{+2} and glutamate are thought to be contained in the same vesicle and get released together (Paoletti et al., 2009; Qian and Noebels, 2005). Indeed, expression of vesicular glutamate transporter 1 (VGLUT-1) was reported in the synaptic vesicles containing Zn^{+2} (Sindreu et al., 2003). Thus, Zn^{+2} could act as a modulator in glutamatergic neurotransmission. Indeed, in a series of *in vivo* experiments, the released Zn^{+2} from Schaffer collaterals and MFs after neuronal stimulation was shown to negatively modulate calcium signaling at presynaptic level, acting as a negative feed-back factor, and also at postsynaptic level. Consequently, the blocking of calcium signaling leads to the suppression of glutamate release (Minami et al., 2006; Takeda et al., 2003, 2006). Supporting these results, chelation of Zn^{+2} using *N*,*N*,*N′*,*N′*-tetrakis (2-pyridylmethyl) ethylenediamine (TPEN), a membrane-permeable Zn^{+2} chelator, increased presynaptic calcium signaling (Quinta-Ferreira and Matias, 2004). Also, Zn^{+2} has been proposed to activate presynaptic ATP sensitive potassium channels, thereby protecting neurons from hyperactivation, excessive glutamate release and excitotoxicity (Bancila et al., 2004). In addition to suppressing extracellular glutamate release, Zn^{+2} has the opposite effect upon GABA (Takeda et al., 2004), leading to the decrease of the general circuit activity, in which Zn^{+2} acts as a neuromodulator.

In the context of epilepsy, after seizures induced by amygdalar and hippocampal kindling, the amount of Zn^{+2} was shown to increase in the hippocampal area within the first two weeks after seizure induction (Kasarskis et al., 1987; Mody and Miller, 1985). In mice, when KA was intraperitoneally injected, the increase of Zn^{+2} was also observed in the HPF within the first three days after injection. Also, MT1 and MT2, which recapture Zn^{+2} from both intracellular and extracellular spaces, were also highly increased (Carrasco et al., 2000). In fact, in a mouse model of congenital TLE, Zn^{+2} levels were lowered in the DG (Fukahori et al., 1988). Altogether, these findings suggest that increased levels of Zn^{+2} may play a role during the onset of seizures, while it would disappear thereafter. Indeed, in the intrahippocampal KA administration model of MTLE, Zn^{+2} increased in the HPF during the first 2 weeks post-injection, followed by a progressive decline with a complete loss of staining at 56 days after KA administration (Mitsuya et al., 2009).

The exact role of Zn^{+2} in the seizure-induced hippocampal response remains controversial. Some studies from the 70s-80s indicated a pro-convulsive effect of Zn^{+2}, basing on elevated Zn^{+2} levels in non-human primates moderately sensitive to photically induced seizures (Alley et al., 1981) or the generation of seizures after intraventricular Zn^{+2} injection in rats (Donaldson et al., 1971) and rabbits (Pei et al., 1983). On the contrary, Zn^{+2}-deficient diet contributes to increased seizures in a congenital TLE mouse model, while enriching the diet with Zn^{+2} has the opposite effect (Fukahori and Itoh, 1990). Likewise, subcutaneously-administered Zn^{+2} lowers the risk of noise-induced seizure incidence in rats, even though no effect was observed when seizures were induced by intraperitoneal KA administration (Morton et al., 1990). However, taking a different approach and instead of administering Zn^{+2}, chelating it after subcutaneous KA administration or electrical stimulation of the PP, aggravated the seizures induced in both models (Mitchell and Barnes, 1993; Mitchell et al., 1990). Moreover, it has been reported that in knock-out mice for MT1 and MT2 or MT3, where the recapture of Zn^{+2} is impaired, the seizures after intraperitoneal KA injections were aggravated (Carrasco et al., 2000; Cole et al., 2000). The same effect was reported in knock-out mice for Zn^{+2} transporter 3 (ZNT3), in which Zn^{+2} is absent from the presynaptic vesicles (Cole et al., 2000).

Remarkably, Zn^{+2} was demonstrated to activate EGFR signaling through different ways. In fibroblast cell lines as well as human skin A431 and bronchial epithelial cells, Zn^{+2} was shown to induce EGFR phosphorylation at tyrosines Y845, Y1068 and Y1173 through trans-activation in a c-src dependent manner (Samet et al., 2003). Moreover, Zn^{+2} was reported to provoke the extracellular release of HB-EGF, indirectly triggering the EGFR activation (Wu et al., 2004). As previously mentioned, HB-EGF is a potent mitogen ligand of EGFR that is membrane-anchored under its precursor form and can be converted into a soluble and an active form through metalloproteinase cleavage (Gschwind et al., 2002; Prenzel et al., 1999). Interestingly, HB-EGF is increased in the DG after intraperitoneal KA administration as soon as within the first 24 h, while it decreases thereafter (Opanashuk et al., 1999). This early increase of HB-EGF could be relevant, given that HB-EGF is known to affect proliferation, differentiation and morphology of cultured astrocytes (Jia et al., 2018; Kornblum et al., 1999; Puschmann et al., 2014), as well as to promote neurogenesis in the SGZ when it is intraventricularly administered (Jin et al., 2002).

We herein propose that Zn^{+2} might play a role in the initial stage of MTLE-HS, either by direct activation of EGFR or by the extracellular releasing of HB-EGF. Aiming

to understand this process, the next step would be to block EGFR signalization in the context of seizures to investigate the specific role of the receptor activation.

3.6.2.4. Blocking EGFR signaling

Inhibition of EGFR has been demonstrated to be a useful approach to ameliorate the reactive gliosis in spinal cord injury models (Li et al., 2014; Qu et al., 2012). Furthermore, being EGFR highly implicated in the evolution of different cancer diseases (Arteaga, 2011; Nicholson et al., 2001; Salomon et al., 1995; Sasaki et al., 2009; Sharma et al., 2007b), different potential strategies aiming to target EGFR have been developed. Among these approaches, monoclonal antibodies and tyrosine kinase inhibitors (TKI) are the most advanced ones, both resulting in the effective blockade of the EGFR downstream signaling transduction. Between both strategies, the TKI have been more extensively studied (Chen, 2013).

Gefitinib (ZD1839) was the first EGFR-targeted small-molecule TKI being approved with the aim to reduce tumor proliferation. It reversibly targets EGFR at the ATP binding site within the tyrosine kinase that acts as an activator of the signaling pathway. Its side effects use to range from mild to moderate, consisting of a dose-dependent skin rash and diarrhea (Wakeling et al., 2002). Also, Afatinib, an irreversible EGFR inhibitor has been recently approved and clinically tried (Watanabe et al., 2018; Yang et al., 2015). Here, we suggest that the use of Gefitinib and Afatinib could potentially ameliorate the pathological consequences of MTLE-HS, especially the NSC massive activation and reactive gliosis.

4. HYPOTHESES AND OBJECTIVES

4. HYPOTHESES AND OBJECTIVES

Hippocampal NSCs represent the first step of the adult neurogenic cascade, acting as a non-renewable source of new neurons during the lifespan of most mammals. Thus, the initial size of NSC population will determine the total potential neurogenic output throughout lifetime. Moreover, once the NSC population is generated, pathophysiological conditions such as epilepsy can alter their properties, strongly affecting neurogenesis. Based on these premises and our preliminary data we hypothesize that:

1. Adult NSCs are generated *de novo* during the early postnatal stages of DG development.
2. Adult NSCs are generated on-site in the early postnatal DG.
3. Adult NSCs generation in the early postnatal DG requires the expression of cD2.
4. The expression and activity of the FGFR1 and EGFR signaling pathways increase after seizures, playing a fundamental role in the massive activation and induction of React-NSCs.
5. The efficient inhibition of EGFR by Gefitinib prevents the massive activation and induction of React-NSCs after seizures.
6. The massive release of Zn^{+2} after seizures induces the EGFR-mediated activation and induction of React-NSCs.
7. The massive release of HB-EGF after seizures induces the EGFR-mediated activation and induction of React-NSCs.

General objective 1: To study the development and formation of adult NSCs in the mouse.

Objective 1.1. To analyze the role of cD2 on the postnatal formation of the adult NSC population. For this purpose we will use a double transgenic mouse model that results from the crossing of *cD2*KO mouse and a Nestin-GFP mouse that expresses GFP under the regulatory element of Nestin, a NSC marker. We will analyze in a comparative manner (WT vs *cD2*KO) the development of NSCs (number and division dynamics) and cell death in the SGZ+GCL along different postnatal time points by means of confocal microscopy-based quantitative image analysis.

Objective 1.2. To study the contribution of early postnatal NSPCs from different spatial locations (DMS and DG) to the adult NSC population. For this purpose, we will develop and validate a method to perform cell labelling by region-targeted retroviral infections in the DMS and the DG early after birth. We will analyze the identity of the labelled progeny at later time points by confocal microscopy-based quantitative image analysis.

Objective 1.3. To characterize the expression of LPA_1 in the dNSCs and adult NSCs in the DG. For this purpose we will use a transgenic mouse model in which EGFP is driven by the expression of LPA_1. We will analyze the expression of LPA_1-EGFP in the DG and specifically in the NSCs at different postnatal time points by means of confocal microscopy-based quantitative image analysis.

General objective 2: To study the development of the hippocampal neurogenic niche in humans.

Objective 2.1. Analyze different dNSC populations along the human HPF development. For this purpose, we will perform IHC in human embryonic and early postnatal hippocampal samples and explore the development of the different progenitor matrixes that will form the DG by means of confocal microscopy-based quantitative image analysis.

General objective 3: To study mechanisms of induction of React-NSCs in MTLE.

Objective 3.1. To study the potential implication of FGFR1 in the hippocampal response early after the induction of MTLE. For this purpose, we will analyze through real time-quantitative polymerase chain reaction (RT-qPCR) and western blot (WB) the mRNA and protein levels of FGFR1 at different early time points after the intrahippocampal injection of KA as a model of MTLE.

Objective 3.2. To study the potential implication of the EGFR signalling pathway in MTLE. For this purpose we will analyze through RT-qPCR and WB the

mRNA and protein levels of EGFR and its downstream signalling pathways Akt, ERK1/2 and STAT3 at different early time points after the induction of MTLE. We will also study EGFR expression in Nestin-GFP mice and Nestin-GFP-derived NSPCs by IHC and confocal microscopy-based quantitative image analysis.

Objective 3.3. To test the efficacy of Gefitinib to block the EGFR signalling pathway in NSPCs *in vitro*. For this purpose we will culture NSPCs and assess the effect of the EGFR inhibitor Gefitinib over the proliferating capacity of Nestin-GFP-derived NSPCs. Using WB and confocal microscopy-based quantitative image analysis we will determine the efficiency of Gefitinib in the EGFR signalling pathway blockage and its effect over NSPC proliferation capacity measured by BrdU incorporation.

Objective 3.4. To analyze the effect of Gefitinib *in vivo* on NSCs and neurogenesis in MTLE. For this purpose, we will administrate Gefitinib to adult mice during the first three days after the induction of MTLE by intrahippocampal KA injection. After the treatment, we will evaluate the number, activation and morphological complexity of NSCs, as well as the presence of NBs in the SGZ+GCL by confocal microscopy-based quantitative image analysis.

Objective 3.5. To evaluate the potential action of Zn^{+2} on NSCs in MTLE. For this purpose we will first evaluate the amount of Zn^{+2} and MTs, the metalloproteins in charge of Zn^{+2} storage, in the HPF by means of Danscher staining and RT-qPCR respectively early after the induction of MTLE. We will study the effect of Zn^{+2} administration *in vitro* on NSPCs and *in vivo* in the NSCs of the DG by means of confocal microscopy-based quantitative image analysis.

Objective 3.6. To determine the potential EGFR-mediated induction of React-NSCs by Zn^{+2}. For this purpose, we will determine the phosphorylation of various EGFR tyrosine sites (Y845 and Y1068) by WB after Zn^{+2} administration to NSPCs *in vitro.* We will also evaluate by confocal microscopy-based quantitative image analysis *in vivo* the potential restoration by Gefitinib administration of the Zn^{+2}-induced proliferation in the SGZ.

Objective 3.7. To evaluate the effect of Zn^{+2} quelation on NSCs and neurogenesis in MTLE. For this purpose we will use the Zn^{+2} quelator TPEN, administrating it to adult mice during seven days after the induction of MTLE and evaluating the potential prevention of the GCD and cellular death by confocal microscopy-based quantitative image analysis *in vivo.*

Objective 3.8. To evaluate HB-EGF as a possible mechanism for EGFR activation in MTLE. For this purpose we will quantify using the enzyme-linked immunosorbent assay (ELISA) the amount of HB-EGF released *in vivo* within the first three days after the induction of MTLE and *in vitro* by NSPCs in proliferating conditions. We will also resort to IHC to check the distribution of HB-EGF inside the DG after KA intrahipocampal injection and to WB to measure the activation of the EGFR signalling pathway in NSPCs after the HB-EGF administration.

5. MATERIALS AND METHODS

5. MATERIALS AND METHODS

5.1. Animals

All the animals used in the present study were maintained with *ad libitum* access to food and water in a colony room at a constant temperature (19–22°C) and humidity (40–50%) on a 12:12h light/dark cycle. All procedures were approved by the University of the Basque Country (UPV/EHU) Ethics Committee (Leioa, Spain) and the Diputación Foral de Bizkaia under protocol M20/2015/236 and followed the European directive 2010/63/UE and NIH guidelines.

Nestin-GFP transgenic mice were generated in the laboratory of Grigori Enikolopov at Cold Spring Harbor Laboratory (Cold Spring Harbor, NY, USA), who kindly provided the strain, and have been thoroughly characterized before (Mignone et al., 2004)

LPA_1-EGFP transgenic mice, generated by the GENSAT project at Howard Hughes Medical Institute (The Rockefeller University, NY, USA) (Gong et al., 2003), were provided by Gerd Kempermann at the Center for Regenerative Therapies Dresden (Technische Universität Dresden, Dresden, Germany). The characterization of the expression of LPA_1-GFP in adult NSCs has been characterized elsewhere (Valcárcel-Martín et al., 2020; Walker et al., 2016).

Both animal strains were crossed with C57BL/6 mice for at least 10 generations in order to homogenize genetic variability. Nestin-GFP mice were used for the postnatal characterization of the DG neurogenic niche, spleen-focus forming virus gamma-retrovirus (SFFV-RV) injections and also for MTLE experiments whereas LPA_1-GFP mice were used only for the postnatal characterization of the DG neurogenic niche.

In order to characterize the role of cD2 in the postnatal development of the DG, knock-out mice for the ccnd2 (Sicinski et al., 1996), referred to as cD2KO, were crossed with a different version of the Nestin-GFP mice (Yamaguchi et al., 2000) in the laboratory of Anja Urbach (Universitätsklinikum Jena, Jena, Germany). Heterozygous offspring of this breeding were mated with each other to obtain Nestin-GFP-positive mice homozygous for the cD2KO or wild type (WT) littermates. Their brains were fixed

at different time points during postnatal development (P0, P7, P14 and P28) and sent to us for the histological analysis.

5.2. Human Samples

Gestational (GW14 and GW30) and early postnatal (3 weeks) *post-mortem* control cases were collected by Mercedes Paredes after previous written consent of their progenitors and in strict observance of the legal and institutional ethical regulations of the University of California, San Francisco (UCSF) Committee on Human Research. Protocols were approved by the Human Gamete, Embryo and Stem Cell Research Committee (Institutional Review Board) at UCSF. As previously described (Sorrells et al., 2018), all samples from the temporal lobe were cut from the amygdaloid complex to the posterior end of the inferior horn of the LV into approximately 1.5-cm blocks, fixed in 4% paraformaldehyde (PFA)(Sigma-Aldrich, #441244) for an additional two days, cryoprotected in a 30% sucrose solution, and then frozen in embedding medium (OCT) for its histological analysis.

5.3. Stereotaxic intrahippocampal injections

5.3.1. Postnatal SFFV-RV infections

We optimized a method to perform intrahippocampal injections in accordance to our requirements: 1) The need to inject independently in two different regions (DG and DMS) of the HPF, and 2) Its adaptation to the varying size of these regions during early postnatal development. To achieve that we tested different coordinates from a wide variety of published experimental approximations that have previously implemented stereotaxic intrahippocampal injections in neonatal mice (Jiang et al., 2017; Xu et al., 2012).

We traced the lineage of postnatal hippocampal progenitors with mCerulean- and mCherry-expressing SFFV-RVs, kindly given by Diego Gómez-Nicola (University of Southampton, UK) (Gomez-Nicola et al., 2014a; Weber et al., 2012). P2 and P5 old mice were anaesthetized by hypothermia by placing them in ice for 2 minutes and then secured to a platform placed in the stereotaxic apparatus. Aided by a fiber optic light, Lambda was localized by head transillumination and it was used as reference to inject, using a heat-pulled glass microcapillar at the following stereotaxic coordinates: for DG, -1 mm anteroposterior (AP), ±1.2 mm laterolateral (LL), -1.7 mm dorsoventral (DV); for the DMS -0.9 mm AP, ±1.4 mm LL, -1.7 mm DV. The microcapillar was introduced percutaneously to inject 0.3 µl of SFFV-RV in each hippocampal region at 0.3 µl/min

rate flow. After surgery, mice were quickly placed in a warm water bath first and later on a thermal blanket until their respiration, color of the skin and locomotor activity returned to normal. Finally, in order to facilitate re-acceptance of the mother, they were impregnated with a mixture of the mother´s own stool, bedding and water prior to returning them to the breeding cage. The whole procedure for each pup was carried out in less than 10 minutes to minimize as much as possible maternal stress. No pups were rejected or abused by the dam. However, and despite mortality was almost negligible, all the pups that did not recover from anesthesia corresponded to the P5 age group, suggesting a major susceptibility to hypothermia at this age.

The implemented method allows the delivery of viral particles in the targeted anatomical regions, yet the injection accuracy is not 100% due to the variability in each animal size and methodological limitations. Therefore, given the proximity of both injection sites and the small size of the pups at these postnatal stages, we employed also *a posteriori* criteria to assign correctly injected animals to each group; to classify an injection as "DG" we ensured that no cells were labeled by the SFFV-RV in the DMS. On the other hand, to classify injections to the "DMS" group, SFFV-RV-positive cells needed to be populating the entire stream above the fimbria from the injection site into the DG. Furthermore, the path of the microcapillar was observable in several cases, assuring the identification of the injection site. Injections that only reached the meninges were differentiated from DMS injections due to their location forming a stream under the ventral blade of the DG and the characteristic elongated morphology of the cells in this region.

5.3.2. Adult stereotaxic intrahippocampal injections

Intrahippocampal KA injections were performed as previously described (Sierra et al., 2015). Briefly, animals were anesthetized intraperitoneally with a mixture of Ketamine- (75 mg/kg; Ketamine, #581140) and Medetomidine- (1 mg/kg; Sedastart, Pfizer) induced anesthesia and received a single subcutaneous dose of analgesic Buprenorphine (1 mg/kg; Buprecare, Animalcare Lted., #582039). Mice were ensured to be in deep anesthesia by checking for regular, relaxed respiration and the lack of response to tail/toe pinch. Then, the hair over the scalp was shaved and after positioning the mice in the stereotaxic apparatus, povidone iodine was applied to clean and disinfect prior a surgical incision to separate the skin over the scalp. Stereotaxic coordinates were taken from the reference point Bregma. The hippocampal region was selected at the following coordinates: -1.8 mm AP, -1.6 mm LL and -1.9 mm DV. In

order to reach the desired position, the skull was perforated using a 0.6 mm micromotor high-speed drill.

To induce SE 50 nl of a 20 mM solution of KA (Sigma-Aldrich, #K0250/K3375) were delivered using a nanoinjector (Nanoject II, Drummond Scientific, #3-000-205A) attached to a pooled glass microcapilar filled with mineral oil as previously described (Sierra et al., 2015). To assess the role of Zn^{+2} in the neurogenic niche, 5, 20 and 30 nM were administered using a stainless steel cannula (outer diameter, 0.28 mm) connected to a Hamilton microsyringe (Hamilton, #84250). For EGFR inhibition Afatinib dimaleate (Selleck Chemicals, #S7810) was diluted with saline to a concentration of 70 µM and injected intrahipocampally prior KA injection. In each case, a solution in 0.9% sterile NaCl was used for control animals. The cannula was left for 5 minutes to avoid the reflux along the cannula tract and then the skin over the mice skull was sutured and the animals were placed in a thermal blanket until they got recovered from anesthesia.

5.4. Treatments

5.4.1. Intranasal administration of the EGFR inhibitor Gefitinib

10 mg/Kg of Gefitinib (Selleck Chemicals, #S1025) were diluted with 0.5% Methylcellulose and 0.2% Tween 80 following manufacturer instructions and intranasally administered starting immediately after stereotaxia and twice a day for the first three days, as previously described (Hanson et al., 2013; Pineda et al., 2013). 10 µl of the solution were administered into the right nostril using a pipette tip and holding the mice as previously described (Hanson et al., 2013). To avoid that the mice snorted out solution drops, administration was performed in several series, waiting a few seconds between each administration while keeping the animal immobilized. Pipette tips were replaced for every animal in order to avoid dose excesses.

5.4.2. Subcutaneous administration of the Zn^{+2} chelator TPEN

To chelate extracellular Zn^{+2}, TPEN solution was freshly prepared in 10% ethanol (10% ethyl alcohol in normal physiological saline, Merck, #616394) and injected subcutaneously under the nape skin of the animals twice a day at 5 mg/kg (9–10 am and 17–18 pm) as previously described (Kim et al., 2012). Administration was done for one week after KA intrahippocampal injection. For control animals, an equivalent volume of 10% ethanol was administered each time.

5.4.3. BrdU administration

BrdU (Sigma, #B5002-1G) was diluted in sterile saline and administered intraperitoneally at 150 mg/kg three consecutive times separated by 3 h intervals. For the analysis three days after KA or Zn^{+2} intrahippocampal injection and seven days after Zn^{+2} intrahippocampal injection, BrdU was given 24 h before sacrifice in order to label proliferating cells. For the experiments 14 days after KA or Zn^{+2} intrahippocampal injection, BrdU was administered right after the last Gefitinib administration (third day after KA/Zn^{+2}) in order to see the fate of newly generated cells born after the end of treatments. In the *in vitro* experiments, a pulse of at 10 µM BrdU for 1 h was performed before cell fixation in order to label proliferating cells.

5.5. Cell cultures

NSPC cultures were obtained using an adaptation of the protocol previously described for HPF and SVZ (Jhaveri et al., 2015; Pineda et al., 2013) in which a mix of Papain and DNAse enzymatic solution (20.000 U; 195 U/µl) was preheated (37ºC and 5% CO_2) for extracellular matrix digestion and Ovomucoid was used to halt enzymatic activity avoiding serum, instead of DMEM/F-12 medium. Briefly, hippocampi were extracted from either C57BL/6 or Nestin-GFP mice, pooled and placed in ice-cooled phosphate buffered saline (PBS)-Glucose (50 µl glucose 30% into 50 ml PBS), cut into small pieces of approximately 2 mm. Next, the sample was placed into a 15 ml tube, washed to minimize risk of contamination and incubated with the previously-heated enzymatic digestion for 15 minutes at 37ºC. The sample was mechanically agitated every 5 min to avoid aggregation of the tissue.

Afterwards, supernatant was discarded and the enzymatic reaction halted using 950 µl of the Papain inhibitor Ovomucoid. Then, cells were disaggregated by pipette tip mechanical dissociation. The resultant cell suspension was filtered into a 15 ml tube and cells were centrifuged 10 min at 200G, the pellet was resuspended in 500 µl of Neurocult proliferation medium enriched with 10% proliferation supplement (Stem Cell Technologies, #05702), 2% B27, 0.24% Heparin (Stem Cell Technologies, #07980), 0.8% EGF and 0.2% FGF (Peprotech, #P01132 and #P15655) of the total volume and placed in T25 flask with 5 ml of Neurocult enriched medium. Cells were maintained at standard conditions in a humidified 37ºC incubator containing 5% CO_2.

NSPC cultures were then passaged every 7 days by enzymatic disaggregation with Accutase (Stem Cell Technologies, #7920) in presence of the antibiotics Penicillin 100 U/ml and Streptomycin 150 µg/ml (Gibco, #15140 and #15122), as previously described (Pineda et al., 2013). NSPC cultures were maintained for a maximum of 4 total passages in order to preserve heterogeneous population and avoid cell selection issues. For IHC assays, NSPCs were seeded into 12 mm coverslips coated with Laminin (Sigma, #L2020) as previously described (Silvestre et al., 2012). For the assessment of cell signalization by WB in control and KA conditions, 400,000 NSPCs per condition were used. For proliferation/inhibition assays, the number of NSPCs was reduced to 25,000 cells per well in order to reduce cell density and avoid inhibition of cell proliferation by cell-to-cell contact. In order to study the effects of Zn^{+2} over EGFR signaling pathway and its inhibition (using Gefitinib), cells were rinsed and cultured with starved media without growth factors during 2 h to downregulate EGFR downstream signaling. Then, cells were preincubated with 2 µM Gefitinib and/or stimulated either with 200 µM of Zn^{+2}, 100 ng/ml of HB-EGF and 20 ng/ml of EGF for 2 h.

5.6. RNA extraction RT-qPCR

5.6.1. RNA extraction and reverse transcription

Hippocampi dissected at different time points (0 h 1.5 h 12 h 24 h 72 h post KA injection) were immediately frozen with RLT buffer. Total RNA extraction and DNAse treatment to eliminate genomic DNA residues were carried out following manufacturer's instructions (Qiagen). The quantity of RNA was measured using the Nanodrop 2000. Next, 1.5 µg of RNA were retrotranscribed using random hexamers and Superscript III Reverse Transcriptase kit (Invitrogen, #10432122), accordingly to manufacturer's instructions using a Veriti Thermal Cycler (Applied Biosystems, #4375305).

5.6.2. RT-qPCR

RT-qPCR was performed on a BioRad CFX96 using Power SybrGreen (BioRad, #1708880) for complementary DNA amplification and the primers shown in **Table 1**. The protocol was 3 min at 95^{o}C for denaturing, 45 cycles of 10 sec at 95^{o}C for annealing and 30 sec at 60^{o}C. Each sample was normalized to endogenous GAPDH and HPRT expression. Each reaction was performed at least twice in duplicate.

GENE	GENE BANK	AMPLICON SIZE	SEQUENCE
HPRT	NM_013556.2	150	Fwd:5'-GTTGGGCTTACCTCACTGCT-3' Rev:5'-TCATCGCTAATCACGACGCT-3'
GAPDH	NM_001289726.1	153	Fwd:5'-CCAGTATGACTCCACTCACG-3' Rev:5'-GACTCCACGACATACTCAGC-3'
EGFR	NM_007912.4	165	Fwd:5'-GCCAACTGTACCTATGGATGT-3' Rev:5'-GGCCCAGAGGATTTGGAAGAA-3'
FGFR1	NM_001079908.2	88	Fwd:5'-CCAAACCCTGTAGCTCCCTA-3' Rev:5'-TGAACTTCACCGTCTTGGCA-3'
FGFR2	NM_010207.2	105	Fwd:5'-CCGAATGAAGACCACGACCA-3' Rev:5 -TCGGCCGAAACTGTTACCTG-3'
MTH1	NM_013602.3	86	Fwd:5'-TCACCACGACTTCAACGTCC-3' Rev:5'-CAGTTGGGGTCCATTCCGAG-3'
MTH2	NM_008630.2	133	Fwd:5'-GCATCTGCAAAGAGGCTTCC-3' Rev:5'-AGTTGTGGAGAACGAGTCAGG-3'
MTH3	NM_013603.2	77	Fwd:5'-GCTGCTGGACTGGATATGGA-3' Rev:5'-TTGCATTTGTCCGAGCAGGT-3'

Table 1. List of primers used for RT-qPCR.

5.7. IHC

5.7.1. Rodent brain tissue

IHC was performed as previously described using the methods optimized for the use in transgenic mice (Encinas and Enikolopov, 2008; Encinas et al., 2011a). In brief, animals were transcardially perfused with 30 ml of PBS 1X followed by 30 ml of 4% PFA in PBS, pH 7.4. Next, the brains were removed and postfixed for 3 h at room temperature in the same fixative solution, transferred to PBS-0.2% sodium azide and kept at 4ºC. Serial 50 µm-thick sagittal sections were cut using a Leica VT 1200S vibrating blade microtome (Leica Microsystems GmbH). For postnatal SFFV-RV experiments, serial 70 µm-thick coronal sections were cut to properly visualize the extension of the SFFV-RV infection. For the IHC, sections were incubated with blocking

and permeabilization solution (PBS containing 0.25% Triton-X100 and 3% bovin serum albumin (BSA)) for 3 h at room temperature and then incubated overnight with the primary antibodies (diluted in the same solution) at 4ºC. After the incubation, the primary antibody was removed and the sections were washed with PBS three times for 10 minutes. Next, the sections were incubated with fluorochrome-conjugated secondary antibodies diluted in the permeabilization and blocking solution for 3 h at room temperature. After washing with PBS, the sections were mounted on gelatin coated slides with Fluorescent Mounting Medium (DakoCytomation, #S302380). For the BrdU analysis and Nestin-including experiments, sections were treated with 2M chlorhydric acid (HCl) during 20 minutes at 37ºC and immediately incubated with 0.1M tetraborate for 10 minutes at room temperature before the staining. Aferwards, the sections were washed with PBS and the staining followed as describe above. GFP signal from Nestin-GFP and LPA_1-EGFP transgenic mice, as well as the mCerulean signal from SFFV-RV, was detected with an antibody against GFP for enhancement and better visualization. Likewise, mCherry signal from SFFV-RV was detected with an antibody against DsRed for enhancement and visualization. The complete list of primary and secondary antibodies is indicated in **Tables 2 and 3**.

5.7.2. Cell cultures

After every treatment, cell cultures were fixed with PFA 4% dissolved in PBS-4% sucrose. Next, the coverslips with cells attached were incubated with PBS-0.3% Triton-X100 1% BSA during 3 minutes at room temperature for permeabilization and incubated with the primary antibody diluted in 0.2% Triton-X100 and 3% BSA in PBS over night at 4ºC. After, they were washed with PBS three times and incubated with the secondary antibody containing DAPI in the same solution for 2 h at room temperature. Finally, the coverslips were mounted upside down on glass slides with Fluorescent Mounting Medium. For the BrdU experiments, cells were treated before the staining using 2M HCl during 5 minutes at 37ºC and immediately incubated with 0.1M tetraborate for 10 minutes at room temperature. Aferwards, sections were washed with PBS and the staining followed as describe above. The list of antibodies can be found in **Tables 2 and 3**.

5.7.3. Human tissue

Blocks of human brain tissue were cut into 30 µm-thick sections using a cryostat and then directly attached to pre-frozen (-20ºC) Superfrost glass slides (1 section per slide) and stored at -80ºC until use. For each case, a minimum of three sections were

colored with Cresyl Violet staining to confirm anatomical landmarks and orientation of the sample. IHC was conducted following the protocol previously described (Sorrells et al., 2018).

Prior to IHC, frozen slides were allowed to equilibrate to room temperature for 3 h and then baked at 65ºC for 30 min. After rehydrating the slides using 0.05% Triton-X100 in PBS (TNT buffer), they were post-fixed with 4% PFA for 45 min. Slides were rinsed with TNT and distilled water and then the endogenous peroxidase was quenched using a solution of 1% H_2O_2 in PBS for 30 min. For the epitopes requiring antigen retrieval an additional incubation with 10 mM sodium citrate buffer, pH 6.0 at 95ºC for 10 min, and then the slides were cooled down at room temperature. After that, slides were washed with TNT for 10 min three times and re-placed in 1% H_2O_2 in PBS for 1 h 30 min to ensure proper quenching of the endogenous peroxidase. Unspecific unions were blocked with 0.1 M Tris-HCl, pH 7.5, 0.15 M NaCl, 0.5% blocking reagent from PerkinElmer (TNB solution) for 1 h and then the slides were incubated with the primary antibodies diluted in TNB overnight at 4 °C **(Table 4)**.

Next day after the overnight incubation, slides were washed with TNT for 10 min three times and incubated with secondary antibodies in TNB. For the strongest signals directly coupled secondary antibodies were used. For the weakest signals, an amplification of staining intensity was performed using the Tyramide signal amplification kit (PerkinElmer). Briefly, biotinylated secondary antibodies (Jackson Immunoresearch Laboratories) were incubated for 2.5 h at room temperature. Then, the binding of streptavidin–horseradish peroxidase (diluted at 1:200 in TNB) was allowed for 30 min. Finally, tyramide-working solution with the conjugated fluorophores (FITC: 1:50; Cy3: 1:100; Cy5: 1:100) was incubated for 5 min and the reaction terminated with the Reaction Stop Reagent.

The IHC protocol was performed sequentially for different antibodies, incubating the strongest primary antibody and its respective secondary antibody in the first place. Therefore, after the tyramide-working solution incubation, slides were re-fixed for another 30 minutes and incubated in 3% H_2O_2 H_2O_2 in PBS, re-initiating the protocol for the rest of primary antibodies. Finally, once all antibodies were incubated, sections were thoroughly washed with TNT, dehydrated, mounted and coverslipped.

PRIMARY ANTIBODIES FOR IHC		
ANTIBODY	**COMPANY**	**DILUTION**
Chicken anti-GFP	Aves Laboratories #GFP-1020	1:1000
Rabbit anti-NeuN	Abcam #ab177487	1:500
Rabbit anti-Ki67	Vector Laboratories #ab16667	1:750
Rabbit anti-GFAP	Dako #Z0334	1:1000
Rat anti-BrdU	AbD Serotech #MCA2060GA	1:1000
Goat anti-DCX	St. cruz Biotech. #sc-8067	1:750
Chicken anti-Nestin	Aves Laboratories #NES	1:1000
Rabbit anti-GFP	Abcam #ab6556	1:1000
Goat anti-GFAP	Abcam #ab53554	1:1000
Rabbit anti-BLBP	Abcam #ab32423	1:1000
Rabbit anti DsRed	Abcam #MA5-15257	1:2000
Rabbit anti-EGFR	Abcam #ab131498	1:1000
Rabbit anti-FGFR	Cell Signaling #34725	1:200
Rabbit anti-HB-EGF	Cell Signaling #85672	1:400

Table 2. Primary antibodies used for mice tissue and cell cultures.

SECONDARY ANTIBODIES FOR IHC		
ANTIBODY	**COMPANY**	**DILUTION**
AlexaFluor 488 Goat anti-chicken	Molecular Probes #A11039	1:500
Alexa Fluor 568 Donkey anti-chicken	Invitrogen #A11042	1:500
AlexaFluor 680 Goat anti-rabbit	Molecular Probes #111605003	1:500
Alexa Fluor 488 Donkey anti-rabbit	Invitrogen #A21206	1:500
Alexa Fluor 568 Donkey anti-rabbit	Invitrogen #A10042	1:500
AlexaFluor 594 Goat anti-rat	Molecular Probes #112295167	1:500
Alexa Fluor 568 Donkey anti-goat	Invitrogen #A11057	1:500
Alexa Fluor 680 Donkey anti-goat	Invitrogen #21084	1:500
DAPI	Sigma #32670	1:1000

Table 3. Secondary antibodies used for mice tissue and cell cultures.

PRIMARY ANTIBODIES FOR IHC		
ANTIBODY	**COMPANY**	**DILUTION**
Rabbit anti-Tbr2	Abcam Inc #ab23345	1:1000
Chicken anti-GFAP	Abcam #ab134436	1:750
Rabbit anti-Ki67	BD Pharmigen #550609	1:200
Rabbit anti-Hopx	Sigma-Aldrich #HPA030180	1:200
Rabbit anti-S100B	Sigma-Aldrich #HPA015768	1:750
Mouse anti-Nestin	Covance #AB291466	1:250
Mouse anti-Vimentin	Sigma-Aldrich #V2258	1:1000

Table 4. Primary antibodies used for human tissue.

5.8. WB

Depending on the experiment, hippocampal tissue or cultured NSPCs were collected at indicated time points in RIPA buffer mixed with protease inhibitor cocktail and phosphatase inhibitors. Each sample was conserved at -80ºC until its use. The day of the experiment, samples were homogenized and centrifuged at 14000 rpm for 10 min. Supernatant protein (20 µg) was loaded in a 10% Tris-Glycine gels and transferred to a nitrocellulose membrane (Life technologies, #88018). Ponceau staining (Sigma-Aldrich, #P7170) was carried out in the membranes to check the correct protein and band migration. To stain our proteins of interest, membranes were blocked in 5% nonfat dry milk in TBS-T (150 mM NaCl, 20 mM Tris-HCl, pH 7.5, 0.05% Tween 20) for 1 h and then incubated with the primary antibodies **(Table 5)** for 2 h. After three

washes in TBS-T, membranes were incubated with secondary antibodies **(Table 6)** for another hour and visualized by ECL SuperSignal (Thermo Fisher, #34095) Western blotting analysis system.

PRIMARY ANTIBODIES FOR WB		
ANTIBODY	**COMPANY**	**DILUTION**
Rabbit anti-ß-actin	Cell Signaling #4970	1:1000
Mouse anti-EGFR	Abcam #ab8465	1:1000
Rabbit anti-AKT	Cell signaling #9272	1:1000
Rabbit anti-ERK	Cell signaling #9102	1:1000
Rabbit anti-STAT3	Cell signaling #12640	1:2000
Rabbit anti-FGFR1	Cell signaling #9740	1:1000
Rabbit anti-MT1/2	Thermo Fisher #MA1-25479	1:1000
Rabbit anti-pEGFR (Y1068)	Cell Signaling #2234	1:1000
Rabbit anti-pEGFR (Y845)	Cell Signaling #2231	1:1000
Rabbit anti-pAKT (Ser473)	Cell Signaling #3787	1:1000
Rabbit anti-pERK (Y202/204)	Cell Signaling #9101	1:2000
Rabbit anti-pSTAT3 (Y 705)	Cell Signaling #9145	1:1000

Table 5. Primary antibodies used for WB.

SECONDARY ANTIBODIES FOR WB		
ANTIBODY	**COMPANY**	**DILUTION**
HRP-conjugated anti-rabbit	Life technologies #65-6120	1:1000
HRP-conjugated anti-mouse	Life technologies #62-6520	1:1000

Table 6. Secondary antibodies used for WB.

5.9. ELISA

To measure HB-EGF levels in the NSPC cultures or in brain tissue exposed to KA at different time points, we used the R&D DuoSet Immunoassay as described previously (Luzuriaga et al., 2019). Either cellular pellet or brain tissue were lysed using a buffer containing Hepes 25 mM, 5 $MgCl_2$ 5 mM EGTA 1 mM, EDTA 1.3 mM, PMSF 1 mM and a protease and phosphatase cocktail inhibitors (Thermo Fisher, #88665 and #78420).

For cell cultures, 250,000 cells were seeded in a 96 well plate using 150 µl of culture media deprived of growth factors. The cell containing media was collected 72 h after plating. After centrifuging 10 min at 14,000 rpm at 4ºC, 100 µl of the lysed cell pellet and/or supernatant were diluted 1:1 in reagent diluent for the analysis. In parallel conditions, right after 72 h of culture, the number of cells was counted using a Bio-Rad TC20 automated cell counter, as well as trypan blue to mark and exclude death cells. We therefore determined the amount of HB-EGF per cell at the end of the experiment.

For analysis of HB-EGF levels in brain tissue, mice were deeply anesthetized in a CO_2 chamber at 0 h, 1.5 h, 12 h, 24 h and 72 h post-KA or saline administration (n=4 per condition). Their hippocampus was extracted on ice and rapidly frozen using dry ice. Samples were homogenized in lysis buffer and immediately centrifuged (20 min at 14,000 rpm at 4ºC). Supernatants were collected and the total protein content was analyzed using the BCA protein assay kit (Pierce, #23227). 100 µg of protein were loaded for each point diluted 1:1 in reagent diluent buffer.

Both *in vitro* and *in vivo* quantifications were performed using the following four parameter logistic (4-PL) curve fit:

$$y = d + \frac{a - d}{1 + \left(\frac{x}{c}\right)^b}$$

Where *x* and *y* were the independent and dependent variables respectively, *a* and *d* were the minimum and maximum values measured, *c* was the point of inflection halfway between *a* and *d* and *b* was the Hill's slope of the curve (steepness of the curve at point c).

For *in vitro* analyses the values were normalized and expressed as µg of HB-EGF per ml and for *in vivo* analyses the values were calculated as µg of HB-EGF per µg of tissue protein.

5.10. Danscher stainning

For indirect autometallographic Danscher method, 20 mg/kg of sodium selenite was injected intraperitoneally 30 minutes before PFA 4%-Glutaraldehyde 0.5% perfusion and the tissue processed by serial cutting of 50 µm slices. The staining was developed as previously described (López-García et al., 2002). Granule size and quantification was carried out determining the ROI of the GFP cell region (15-20 cells per condition) and particle analyzer using ImageJ software.

5.11. Image analysis

Most of fluorescence immunostaining images were collected using the 40X oil-immersion objective of a Leica SP8 laser scanning confocal microscope. For the quantification of total areas of the DG the 10X objective was used to completely visualize the DG in each section. For the pictures of developing mouse DG in which DMS is illustrated, and for all human pictures, the 3DHistech panoramic digital slidescanner was used. The signal from each fluorochrome was collected sequentially, and brightness, contrast, and background were adjusted equally for the entire image using the software of the confocal microscopy Leica LAS X Life Science.

5.11.1. Quantitative analysis of cell populations

Quantitative analysis of cell populations *in vivo* was performed by design-based (assumption free, unbiased) stereology using a modified optical fractionator sampling scheme as previously described (Encinas and Enikolopov, 2008; Encinas et al., 2006, 2011a).

For cell densities, quantifications were done maintaining the same z-stack size between conditions. The values were normalized to the volume of the SGZ+GCL in the counted area. For total numbers, the whole area of the DG was determined for every slice of a single series and then multiplied by the thickness of the GCL, that was measured at least in three points in each slice. The obtained value was multiplied by 5 to obtain the volume of the whole DG.

For experiments during postnatal stages prior to P14, where NSCs are still not morphologically adult-like (Brunne et al., 2013; Nicola et al., 2015), cells were quantified as dNSCs when they had their soma located inside the GCL, and fulfilled the following criteria: Expression of the well-described NSC markers Nestin-GFP and GFAP (Encinas and Enikolopov, 2008; Kronenberg et al., 2003; Seri et al., 2001) and presence of a radial process extended towards the ML. From P14 on, NSCs were counted following previously described criteria for their identification (Encinas and Enikolopov, 2008; Kronenberg et al., 2003).To identify proliferating cells, it was used the marker Ki67. NSCs positive for the criteria described above and positive for this marker were counted as proliferating dNSCs/NSCs. 3-4 pictures of 1024x1024 frame size z-stacks were chosen randomly in the GCL of 3-5 medial DG slices (depending on the age of the animal). For adult tissue sections, 3-4 z-stacks located at random positions in the DG were collected per hippocampal section, and 4-6 sections per series were analyzed, depending on the experiment. For cultured NPSCs, 5 pictures of 4 µm-thick random z-stacks of the coverslips were collected per sample and condition.

For the experiments using SFFV-RV infections, we quantified all cells infected in the GCL for each condition. We also quantified the number of NSCs in the infected area (region with SFFV-RV-positive cells) to obtain the percentage of NSCs infected with the SFFV-RV per condition.

To measure cell death, apoptotic cells were defined as cells with abnormal nuclear morphology (pyknotic/karryorhectic). In MTLE experiments, GCD was measured in DAPI- and NeuN-stained sections.

For the anaysis of EGFR expression after KA administration, an open-source plug-in for ImageJ was used. In brief, the area was measured as the pixels occupied by EGFR. Using the same "noise-tolerance" for all conditions the area was quantified with "find maxima" option obtaining the total area occupied by EGFR.

The proliferation of cultured NSPCs was measured by the incorporation of BrdU. The relative proportions of BrdU-positive NSPCs were referred to the total number of cells (DAPI staining) quantified per coverslip and conditions. The proliferation in all the conditions was refered to the basal proliferation of the control condition.

5.11.2. Morphological analysis of NSCs: SHOLL analysis

3D confocal images were exported and cell morphology analyzed using NeuronStudio 0.9.92 software (Rodriguez et al., 2006). Results were exported into Excel to pool all the cells and GraphPad Prism v5 was used for graph representation and statistical analysis.

5.12. Statistical analysis

SigmaPlot was used for statistical analysis, except for the morphological analyses for which GraphPad Prism v5 was used. For analysis of pairs of groups the Student's t test was performed, resorting to U-Mann Whitney test when data were non parametric. When more than two groups were present, one-way analysis of variance (ANOVA) test of all groups was performed to determine the overall effect of each factor, resorting to Kruskal-Wallis test when data were no parametric. Two-way ANOVA was performed to detect interaction between factors. In all cases, all pairwise multiple comparisons (Holm-Sidak, Dunn or Student-Newman-Keuls test) were used as a *post hoc* test to determine the significance between groups in each factor or comparisons versus control group (Holm-Sidak, Dunn, Dunnet or Tukey test) to determine the significance of each factor compared to the control group. A logarithmic transformation of the data was performed when required to comply with ANOVA assumptions (normality and homocedascity). $p<0.05$ was considered as statistically significant. Results were presented as mean ± standard error mean (SEM). The number of independent experiments is shown in the respective section.

6. RESULTS

6. RESULTS

6.1. cD2 is essential for the formation of the adult NSC population

To investigate the role of postnatal cell proliferation on the formation of adult NSCs, we examined the development of the DG in the presence (WT) or absence of *cD2* (*cD2*KO); a relevant factor involved in the transition from G1 to S phase during cell cycle (Matsushime et al., 1992; Meyerson and Harlow, 1994; Sherr, 1995). *cD2*KO mice have been shown before to have only residual AHN left (Ansorg et al., 2012), but it is unknown whether this is due to an impairment in the neurogenic capacity of adult NSCs or in contrast, to a failure in the formation of the NSC pool during development. Here, we visualized NSCs on the Nestin-GFP/*cD2*KO mutant mice and compared to the Nestin-GFP/WT at five different postnatal time points (P0, P7, P10, P14 and P28) **(Figures R1-R3)**. We defined as NSCs those cells located inside the GCL, expressing both Nestin-GFP and GFAP markers and extending a radial process towards the ML.

6.1.1. In the absence of cD2, adult NSC population failed to form

The embryonic development, up to early postnatal stages, of the DG in *cD2*KO mice is similar to the WT (Kowalczyk et al., 2004), which makes this mouse a valuable tool to assess the relevance of postnatal proliferation in the formation of the hippocampal neurogenic niche. Indeed, the overall proliferation is decreased in the GCL of the *cD2*KO from P7 onwards and AHN is almost completely absent (Ansorg et al., 2012). Therefore, we wondered whether the absence of AHN was due to an impaired neurogenic capacity of the NSCs or to a failure in the formation/establishment of the NSC population during the postnatal period. We assessed the number and proliferation dynamics (by Ki67 expression) of the NSCs present in the GCL at different ages (P0, P7, P10, P14 and P28) **(Figures R1-R3)** in *cD2*KO and WT mice using stereology, strict marker expression and morphological criteria to define NSCs (expression of both Nestin and GFAP, soma inside the GCL, extended process towards the ML and broccoli-like crown). As well, we measured the volume of the GCL using DAPI. Since at least during the postnatal period the distinction between dNSCs and adult NSCs remains unclear (as we will further address later) and the precise moment of generation of adult NSCs is not known, we based on temporal criteria to differentiate them. The population of NSCs is considered adult at a population level at

P14 (Nicola et al., 2015) and therefore, before P14 we referred to the NSCs in the GCL as dNSCs, and as adult NSCs after P14.

Our results showed that at P0 the morphology of dNSCs was similar between both conditions, as well as the number of dNSCs located in the GCL and the volume of the GCL **(Figure R1 A-F)**. However, these similarities shifted at P7. In the absence of *cD2*, a smaller GCL was clearly observable, the dNSCs were significantly fewer than in the WT and they showed an abnormal morphology with a shorter process **(Figure R1 I-N)**. We also assessed whether cell division was specifically altered in dNSCs using the cell cycle marker Ki67 to quantify the proliferating dNSCs at each time point. The total number and proportion of dNSCs that remained cycling in *cD2*KO mice was not significantly different from the WT neither at P0 nor P7, although a trend towards a reduced total number of proliferating dNSCs was observable at P7 **(Figure R1 G-H;O-P)**.

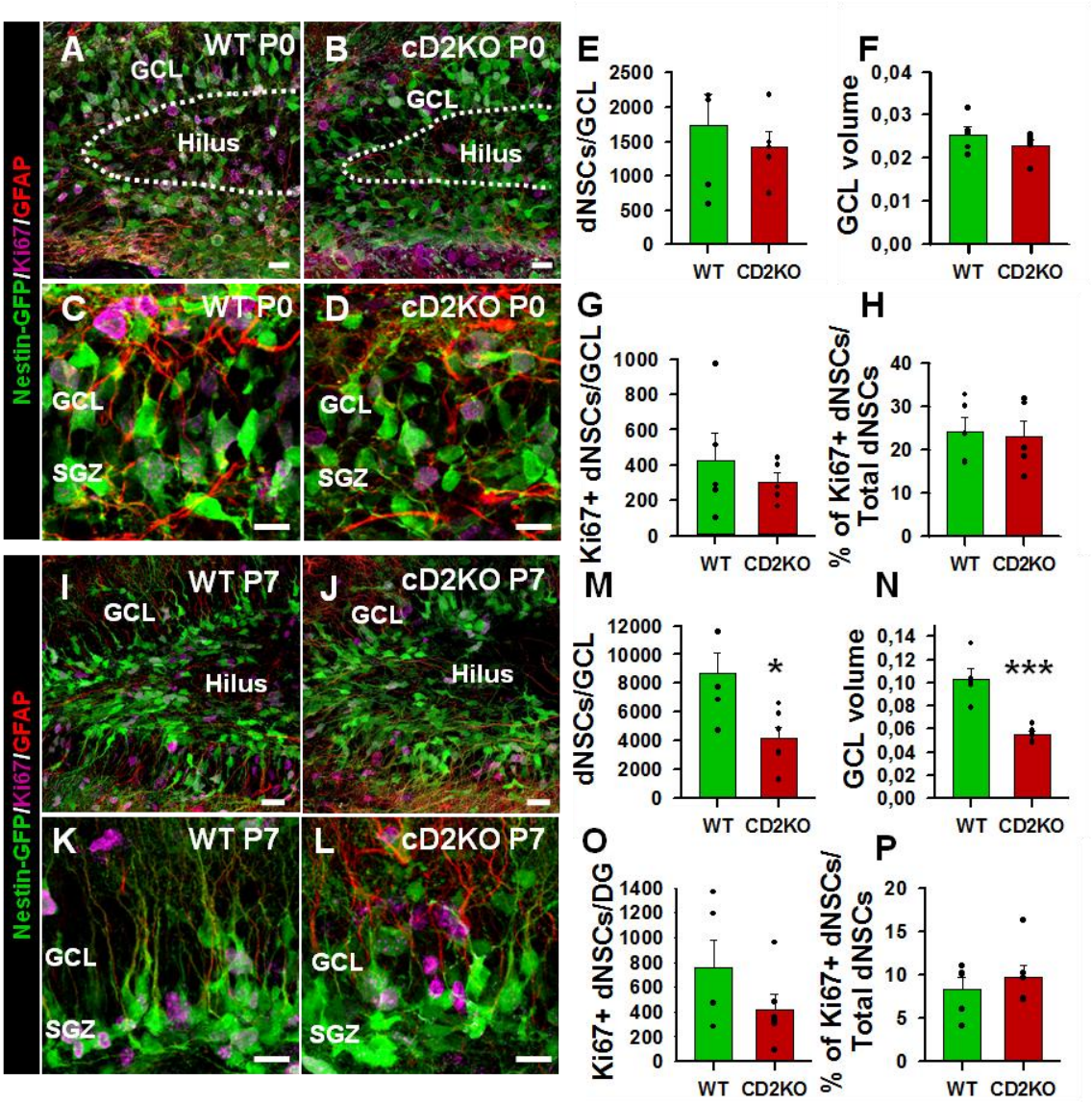

Figure R1. In the *cD2*KO mice, dNSCs failed to properly expand during the first postnatal week. A-D) Representative confocal images of the dNSCs (Nestin-GFP /GFAP) and proliferating cells (Ki67) in the DG of WT and *cD2*KO mice at P0. **E)** Quantification of the total number of dNSCs in the GCL of WT and *cD2*KO mice at P0. **F)** Quantification of the GCL volume of WT and *cD2*KO mice at P0. **G)** Quantification of the total number of cycling dNSCs in the GCL of WT and *cD2*KO mice at P0. **H)** Quantification of the percentage of cycling dNSCs in the GCL of WT and *cD2*KO mice at P0. **I-L)** Representative confocal images of the dNSCs (Nestin-GFP /GFAP) and proliferating cells (Ki67) in the DG of WT and *cD2*KO mice at P7. **M)** Quantification of the total number of dNSCs in the GCL of the DG of WT and *cD2*KO mice at P7. **N)** Quantification of the GCL volume of WT and *cD2*KO mice at P7. **O)** Quantification of the total number of cycling dNSCs in the GCL of WT and *cD2*KO mice at P7. **P)** Quantification of the percentage of cycling dNSCs in the GCL of WT and *cD2*KO mice at P7. *GCL: Granule cell layer. SGZ: Subgranular zone. Scale bars are of 10 µm. *p<0.05 and ***p<0.001 Student 's t-test. Bars show mean ± SEM. Dots show individual data.*

RESULTS

"Hippocampal NSCs: from Origin to Pathology"

At P14, when the hippocampal neurogenic niche is already considered to be adult-like (Nicola et al., 2015), NSCs in the *cD2*KO were morphologically distinct **(Figure R2 A-D)** and the number was significantly lower compared to the WT **(Figure R2 E)**. Likewise, the GCL volume was highly smaller in the absence of *cD2* **(Figure R2 F)** and the total number of proliferating NSCs was also significantly reduced **(Figure R2 G)**, although the percentage of proliferating NSCs among the total NSCs was unaltered **(Figure R2 H)**. Moreover, the differences observed at P14 were aggravated later at P28 and the few remaining cells in the *cD2*KO were morphologically aberrant **(Figure R2 I-L)**. At P28, the number of NSCs was more than 3-fold lower and the GCL volume was 50% smaller **(Figure R2 M-N)**. Also, NSC proliferation was clearly impaired with a negligible number of proliferating NSCs and a reduced percentage of proliferating NSCs **(Figure R2 O-P)**.

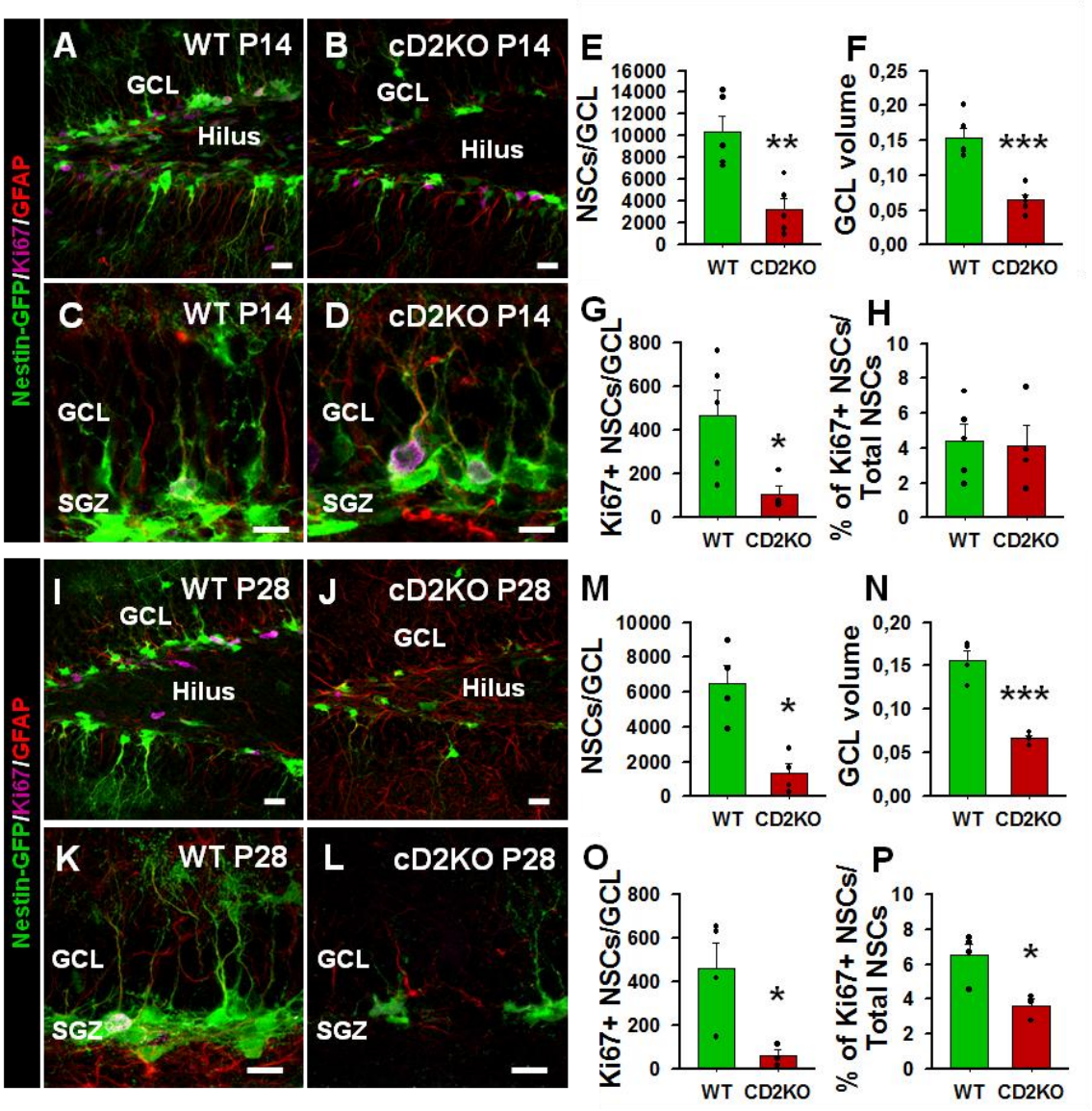

Figure R2. In the absence of *cD2*, the adult NSC population did not get fully generated, leading to its early depletion at P28. A-D) Representative confocal images of the NSCs (Nestin-GFP /GFAP) and proliferating cells (Ki67) in the DG of WT and *cD2*KO mice at P14. **E)** Quantification of the total number of NSCs in the GCL of the DG of WT and *cD2*KO mice at P14. **F)** Quantification of the GCL volume of WT and *cD2*KO mice at P14. **G)** Quantification of the total number of cycling NSCs in the GCL of WT and *cD2*KO mice at P14. **H)** Quantification of the percentage of cycling NSCs in the GCL of WT and *cD2*KO mice at P14. **I-L)** Representative confocal images of the NSCs (Nestin-GFP /GFAP) and proliferating cells (Ki67) in the DG of WT and *cD2*KO mice at P28. **M)** Quantification of the total number of NSCs in the GCL of the DG of WT and *cD2*KO mice at P28. **N)** Quantification of the GCL volume of WT and *cD2*KO mice at P28. **O)** Quantification of the total number of cycling NSCs in the GCL of WT and *cD2*KO mice at P28. **P)** Quantification of the percentage of cycling NSCs in the GCL of WT and *cD2*KO mice at P28. *GCL: Granule cell layer. SGZ: Subgranular zone. Scale bars are of 10 µm. *p<0.05, **p<0.005 and ***p<0.001 Student's t-test. Bars show mean ± SEM. Dots show individual data.*

In summary, in the absence of *cD2* the DG was not correctly formed and dNSCs failed to expand between P0-P14 **(Figure R3 A-F; I-J)**. Therefore, the *cD2*KO DG hosted substantially fewer NSCs from P14 onwards, resulting in the almost depletion of the NSC population at P28 that explains the absent AHN in these mice **(Figure R3 G-I)**. In addition, a trend towards fewer NSCs entering cell cycle was observed in the *cD2*KO from P7 on, being statistically significant from P14 on **(Figure R3 K)**. However, the percentage of dividing NSCs was unaltered until P28, when a trend towards lower dividing NSCs was observed in the *cD2*KO **(Figure R3 L)**. Hence, we hypothesized that the observed diminished size of the adult NSC pool in the *cD2*KO could be due to a reduced expansion of the dNSCs, or on the contrary due to aberrant dNSC dynamics at early postnatal stages (related to cell survival and apoptosis) that would impede its correct formation.

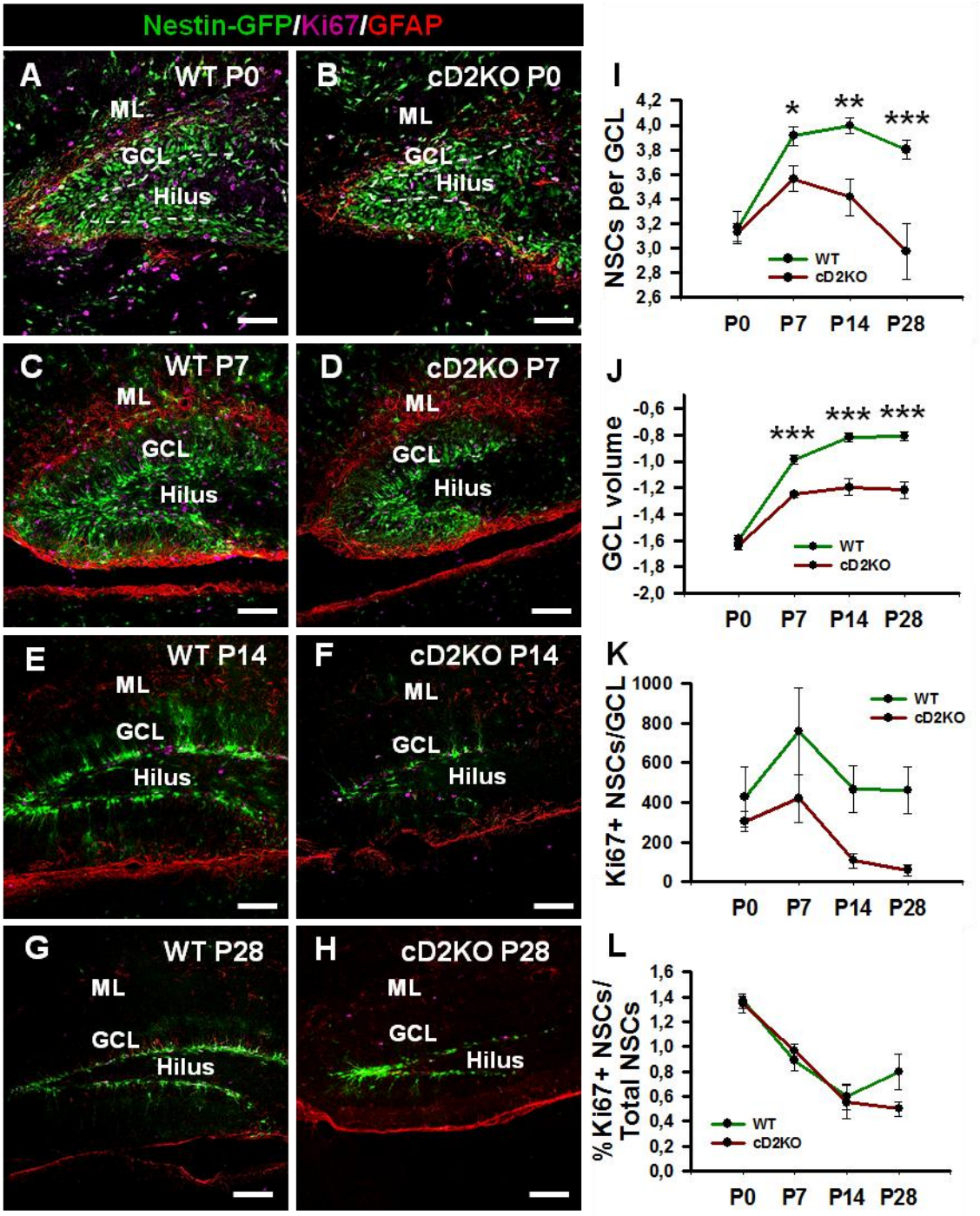

Figure R3. Mice lacking *cD2* failed to generate the adult NSC population during the first two postnatal weeks. A-H) Representative confocal images of the DG and the neurogenic niche of WT and *cD2*KO mice from P0 to P28. **I)** Quantification of the total number of NSCs in the GCL of the DG of WT and *cD2*KO mice from P0 to P28 **J)** Quantification of the GCL volume of WT and *cD2*KO mice from P0 to P28. **K)** Quantification of the total number of cycling NSCs in the GCL of the DG of WT and *cD2*KO mice from P0 to P28. **L)** Quantification of the percentage of cycling NSCs in the GCL of WT and *cD2*KO mice from P0 to P28. *GCL: Granule cell layer. ML: Molecular layer. Scale bars are of 100 µm. *p<0.05, **p<0.01 and ***p<0.001. Two-way ANOVA followed by all pairwise comparisons by Holm-Sidak post hoc test. Dots show mean ± SEM. To comply with homoscedasticity all data were Log_{10} transformed.*

6.1.2. Cell death is not increased in the absence of *cD2*

We next moved to investigate whether the abnormally reduced postnatal expansion of the NSC population in *cD2*KO mice could be accounted by possible increased cell death of dNSCs. To evaluate cell death, we quantified the density of pyknotic nuclei in the GCL at each time point (P0, P7, P14, P28) **(Figure R4 E-F)**, as pyknosis involves the irreversible condensation of chromatin in cells undergoing necrosis or apoptosis (Burgoyne, 1999). The results showed no alterations in the density of pyknotic cells neither at P0 nor at P7 **(Figure R4 F)**. However, after P14 there were less pyknotic nuclei in the *cD2*KO **(Figure R4 A-D; F)**, which could be attributable to the fact that there were fewer NSCs and lower neurogenesis. Therefore, in the absence of *cD2* dNSCs developed following the same apoptotic dynamics than in the WT, whereas after P14 cell death is reduced in the *cD2*KO consistent with a reduced neurogenic niche and reduced proliferative capacity.

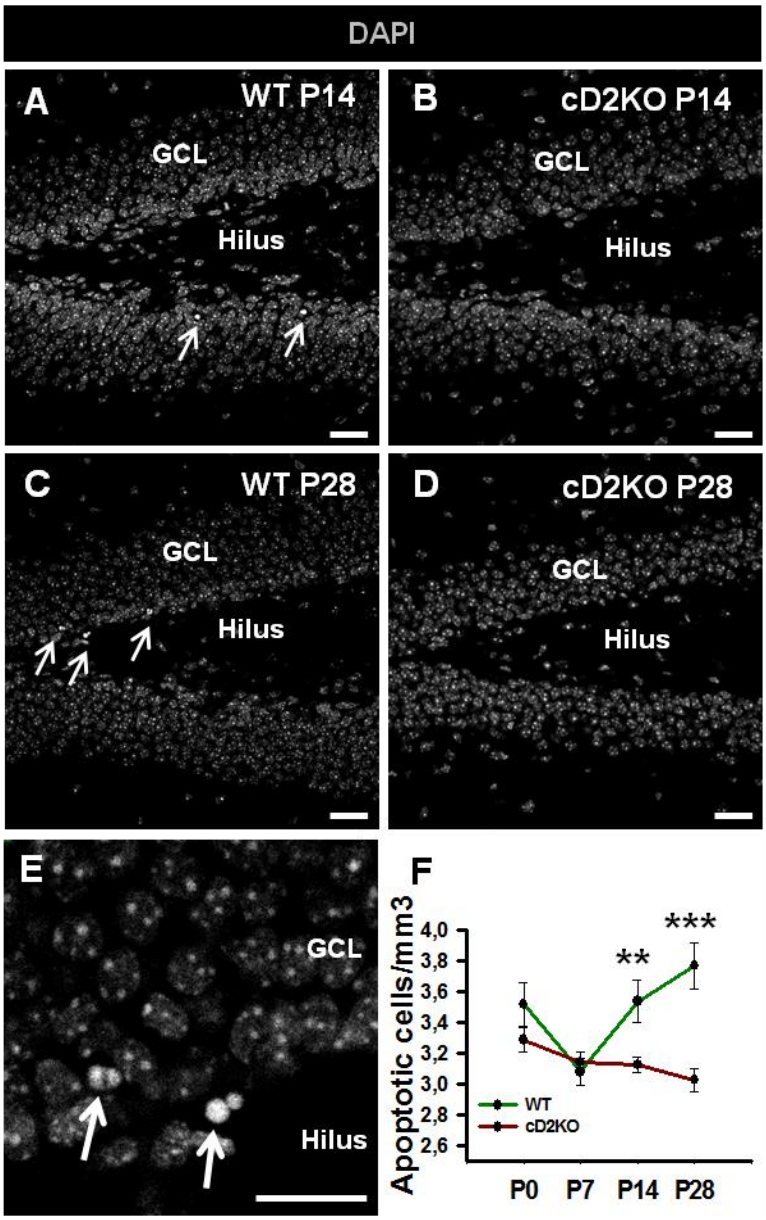

Figure R4. The absence of *cD2* did not affect the cellular apoptotic dynamics until the complete formation of the neurogenic niche. A-D) Representative confocal images of the GCL of WT and *cD2*KO mice at P14. Arrows point to apoptotic cells in the WT mice. **E)** Representative confocal image of an apoptotic cell. **F)** Quantification of the cell death density at different time points during the DG postnatal formation (P0, P7, P14, P28). *GCL: Granule cell layer. Scale bars are of 10 µm in A-D and 5 µm in E. **p<0.01 and ***p<0.001. Two-way ANOVA followed by all pairwise comparisons by Holm-Sidak post hoc test. Dots show mean ± SEM. To comply with homoscedasticity all data were* Log_{10} *transformed.*

6.2. Postnatal on-site generation of the adult DG NSC population

Our previous results indicated that early postnatal proliferation, in a *cD2*-dependent manner, was essential for the adult NSC pool formation. Nonetheless, during the formation of the DG, including the postnatal period, several transitory neurogenic/gliogenic niches get generated in different regions of the HPF (Hodge et al., 2013; Li et al., 2013). One of these transient neurogenic/gliogenic niches is the DMS, a migratory stream formed during the early embryonic period by dNSCs and progenitors that migrate from the DNe into the DG. Importantly, the DMS remains active during the early postnatal period (Hodge et al., 2013; Li et al., 2013; Nakahira and Yuasa, 2005;

Sugiyama et al., 2013). Therefore, the adult NSC precursors could be proliferating in the DMS or be already inside the DG early after birth. Taking this into account, we next moved to evaluate the contribution of the precursors located in these two regions of the HPF to the formation of the DG and especially to the adult neurogenic niche, i.e. progenitors located inside the DG and the ones coming from the DMS during the postnatal development (Altman and Bayer, 1990a; Berg et al., 2019; Hodge et al., 2013; Sugiyama et al., 2013).

6.2.1. SFFV-RV infections to identify the spatial origin of adult NSCs

Aiming to differentially label dividing dNSCs located inside the DG or the DMS, we resorted to the intrahippocampal administration of SFFV-RVs, which are exclusively incorporated by cells undergoing mitotic phase (Weber et al., 2012). To test the accuracy of the injections and the efficiency and diffusion of the SFFV-RV, we infected mice *in vivo* by intrahippocampal injections of a SFFV-RV-mCherry vector at P2 and P5 and studied the location of SFFV-RV-infected cells shortly after (two days post-infection) **(Figure R5 A)**.

We set up two different injection paradigms. First, we injected inside the DG to stain dividing cells exclusively in the hilus and GCL. This led to infections in which labeled cells were completely excluded from the DMS **(Figure R5 B-C)**. In the second paradigm we injected outside the DG, in the DMS. These injections labeled dividing cells settled in the DMS without infecting any cell inside the DG **(Figure R5 D-E)**. Thus, these two injection paradigms were probed to be effective to reveal independently the differential lineage of the dNSCs located in the two hippocampal regions.

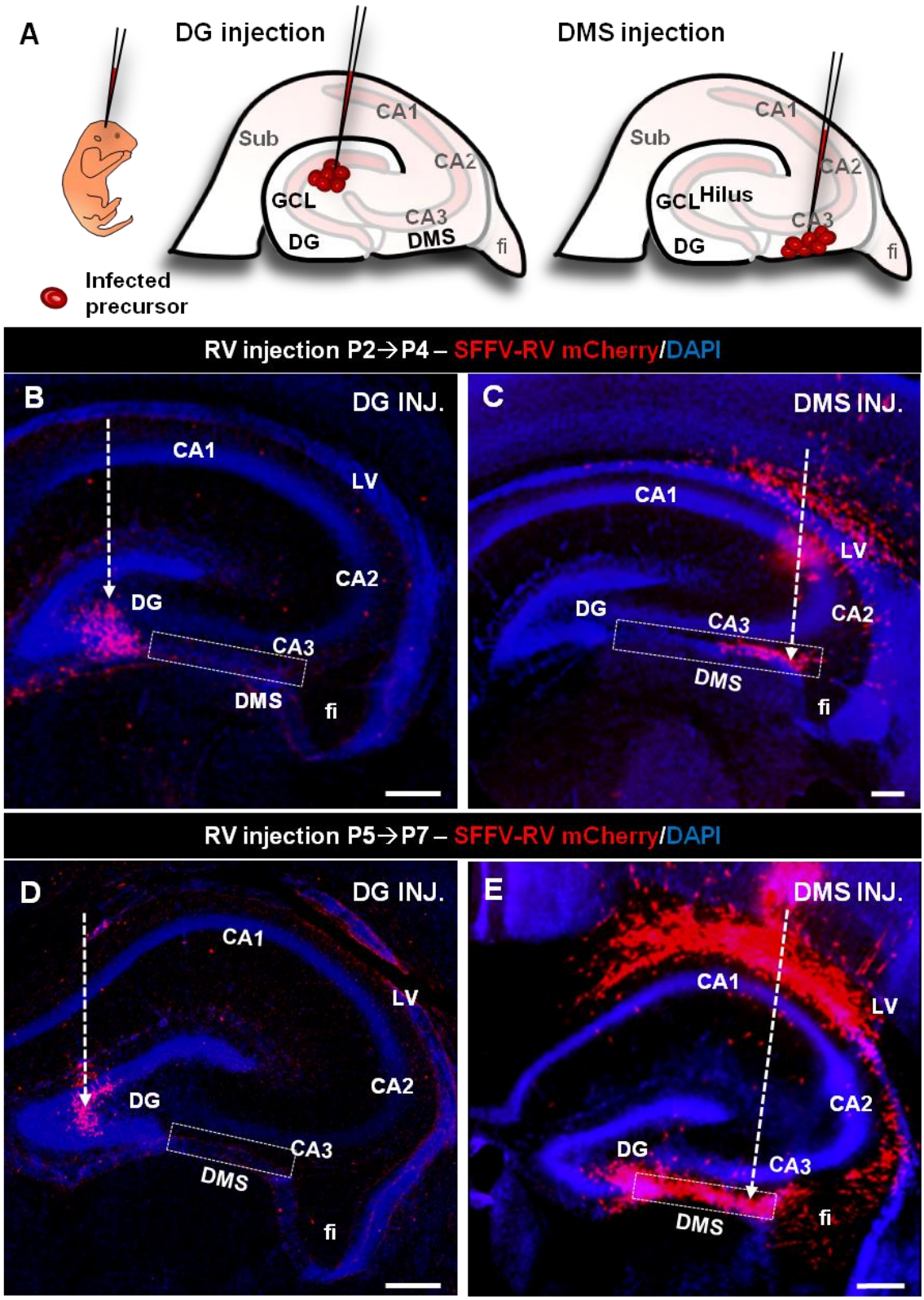
A
DG injection
DMS injection
CA1
Sub
CA2
GCL
Hilus
CA3
DG
DMS
fi
Infected precursor
RV injection P2→P4 – SFFV-RV mCherry/DAPI
B
DG INJ.
LV
C
DMS INJ.
RV injection P5→P7 – SFFV-RV mCherry/DAPI
D
E

← Previous page. Figure R5. Postnatal SFFV-RV infections as a tool to spatially label different HPF dNSC populations. A) Schematics of the experimental paradigm. **B-E)** Fluorescence slide scanner images showing different spatial stereotaxic SFFV-RV-infections. Pups were injected at P2 either inside the DG (A) or in the DMS (B) and the injection site was evaluated at P4. **C-D)** Fluorescence slide scanner images showing different spatial stereotaxic SFFV-RV-infections. Pups were injected at P5 either inside the DG (C) or in the DMS (D) and the injection site was evaluated at P7. The square delimitates the DMS and the arrow the injection path. At both ages, infected cells were never observed in both DG and DMS, indicating that the injections were exclusive from each other. *CA: Cornu ammonis. DG: Dentate gyrus. DMS: Dentate migratory stream fi: fimbria. GCL: Granule cell layer. LV: Lateral ventricle. Scale bars are of 10 µm.*

To further demonstrate the lineage-tracing independency of these two paradigms, we performed both injection types in the same HPF at P2 and distinguished each injection paradigm by different fluorescent reporter genes-encoding SFFV-RVs. We injected a SFFV-RV-mCherry vector in the DMS and a SFFV-RV-mCerulean vector in the DG, thus enabling the visual distinction of the cell lineages derived from each region **(Figure R6 A)**. We evaluated the lineage of the infected cells at P14, a period in which the population of NSCs is already established in the SGZ (Nicola et al., 2015). The different localization of the injections (DG vs DMS) led to independently labeled cell populations that did not show any overlapping, even though the lineage of both populations ended up located in the GCL. Indeed, the cells infected by injections in the DG were more restricted to the medial portions of the rostrocaudal axis, whereas the cells infected in the DMS injection model were observable from rostral to caudal regions of the DG **(Figure R6 B-E)**, suggesting again that the different injections led to different cell populations, even if all were located in the DG at P14.

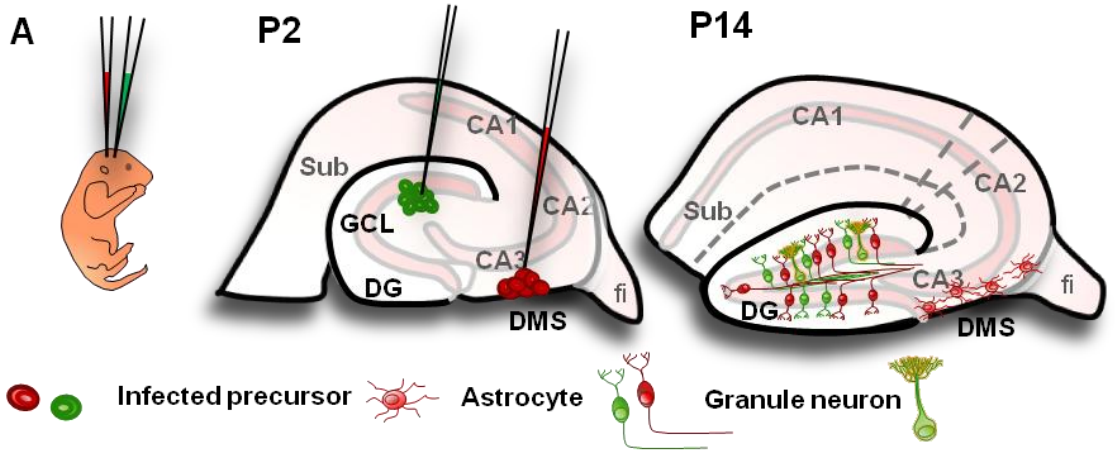
A
P2
P14
CA1
Sub
GCL
CA2
CA3
DG
DMS
fi
Infected precursor
Astrocyte
Granule neuron

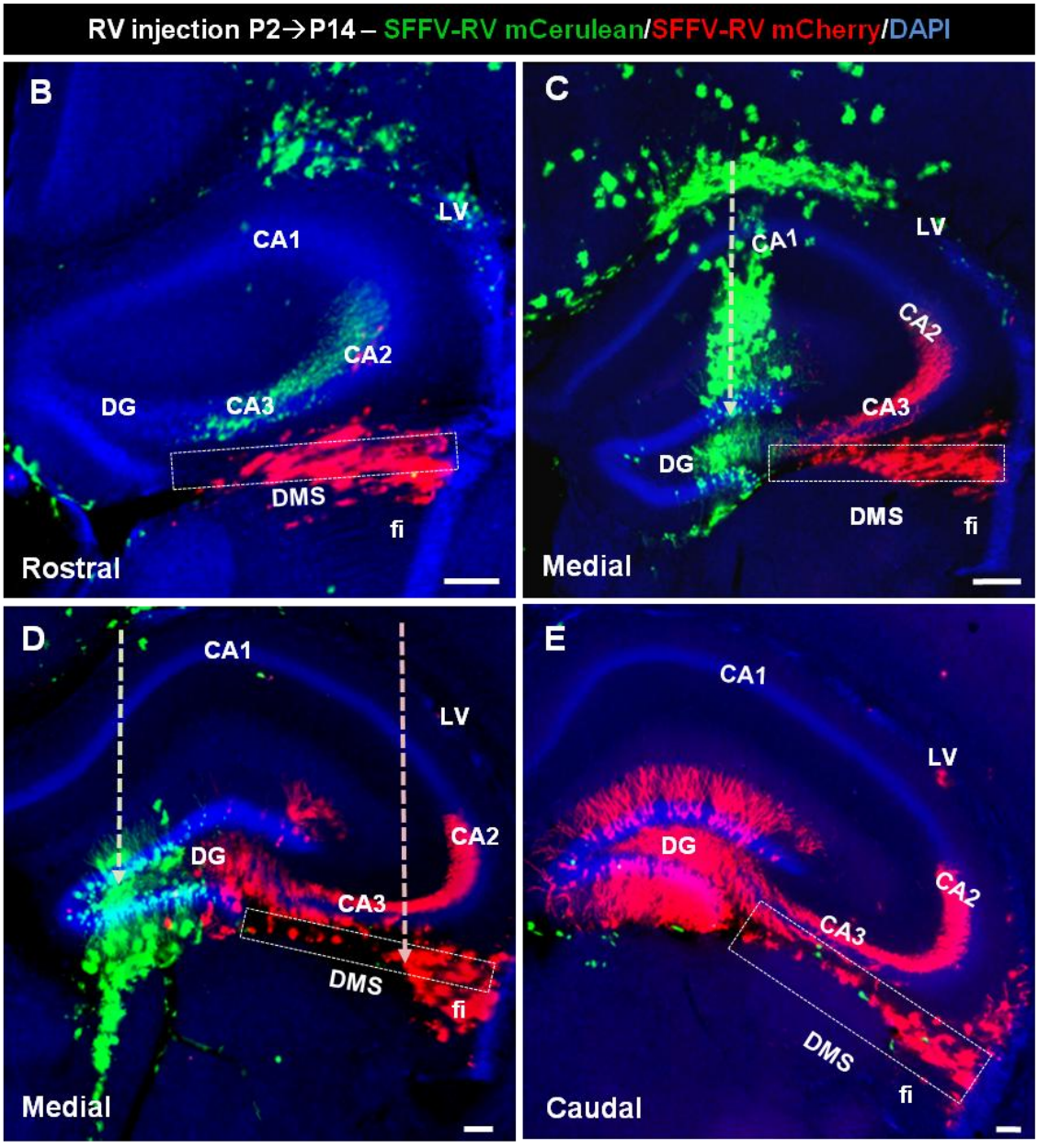
RV injection P2→P14 – SFFV-RV mCerulean/SFFV-RV mCherry/DAPI
B
Rostral
C
Medial
D
Medial
E
Caudal
CA1
LV
CA2
CA3
DG
DMS
fi

← Previous page. Figure R6. Postnatal SFFV-RV infections exclusively labeled cells in the injected region. A) Schematics of the experimental paradigm **B-E)** Fluorescence slide-scanner images showing different spatial stereotaxic SFFV-RV-infections in the same animal. Images are shown in the rostrocaudal axis in a representative way of the extension of the infection. Pups were injected at P2 either inside the DG (green) or in the DMS (red) and the location of the infected cells was evaluated at P14. The square delimitates the DMS and the arrows show the injection path. Infected cells coming from independent regions never overlapped, although the final destination of most cells was the GCL in both injection models. This indicated that the injections were exclusive from each other. *CA: Cornu ammonis. DG: Dentate gyrus. DMS: Dentate migratory stream. fi: fimbria. GCL: Granule cell layer. LV: Lateral ventricle. Scale bars are of 10 µm.*

6.2.2. Only DG-located precursors contributed to generate adult NSCs

Once the method was set up and in order to identify the spatial origin of the adult NSC population, we studied the full postnatal lineage of the infected hippocampal cells that were dividing in the DMS or in the DG at P2 and P5. For that purpose, the SFFV-RV-mCherry vector was used and the fate of the infected cells was evaluated at P14. In both time points, after DG injections the DG appeared full of SFFV-RV-infected cells at the medial and medial-caudal levels, near the site where the injection was performed. As expected, there was not a single infected cell within the DMS **(Figure R7 A)**. At the same time, we could also identify many of them as neurons by morphology and absence of expression of NSC/astrocytic markers and we observed the axons of these infected GCs reaching the rostral DG in the hilar region **(Figure R7 A)**. On the other hand, after DMS injections the labeled lineage appeared fully populating the GCL, with neuron-like properties, at the medial and caudal portions of the DG, and the axons of the GCs reaching the rostral part. In contrast to what was observed in the DG injection model, the DMS was full of SFFV-RV-mCherry-expressing cells from rostral to caudal levels, presumably due to glial differentiation of the postnatally mitotic dNSCs **(Figure R7 B)**.

Despite both injection models resulted in infected cells populating the GCL at P14, some differences were observable. After DG injections at P2, cells were distributed all over the GCL including the SGZ, while DMS-injected cells were restricted to the upper part of the GCL, leaving the SGZ completely empty. Moreover, the SFFV-RV-mCherry-labeled cells had different cellular fates in each injection model. In DG infections, the majority of infected cells were neurons (neuronal morphology with dendrites and axons and absence of expression of either Nestin-GFP or GFAP). However, the 4-5% of the SFFV-RV-mCherry-positive cells among both the total SFFV-RV-mCherry-positive cells and the total NSCs were adult NSCs, identified by their

positive labeling for Nestin-GFP and GFAP, radial morphology and their soma located in the SGZ. On the contrary, we saw a negligible number of NSCs infected by the SFFV-RV in DMS infections **(Figure R7 C-F; Figure R9)**.

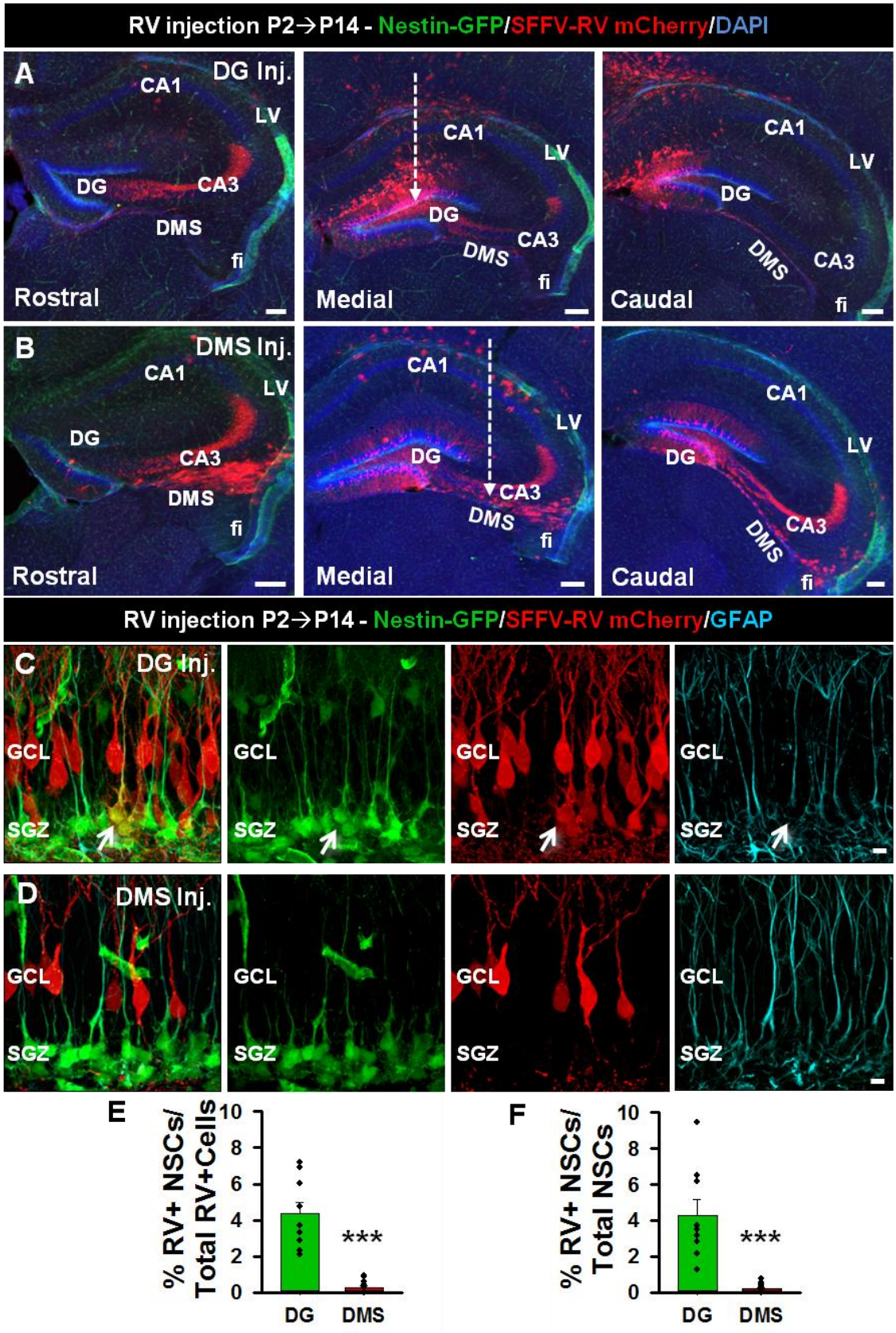
RV injection P2→P14 - Nestin-GFP/SFFV-RV mCherry/DAPI
A
DG Inj.
CA1
LV
DG
CA3
DMS
fi
Rostral
Medial
Caudal
B
DMS Inj.
RV injection P2→P14 - Nestin-GFP/SFFV-RV mCherry/GFAP
C
D
GCL
SGZ
E
F
% RV+ NSCs/ Total RV+Cells
% RV+ NSCs/ Total NSCs
***
0
2
4
6
8
10

← Previous page. Figure R7. The vast majority of adult NSC precursors were located inside the DG at early postnatal stages. A-B) Fluorescence slide-scanner images showing the spatial destination of SFFV-RV-infected cells in the DG (A) or in the DMS (B) from rostral to caudal. Pups were injected at P2 and the spatial destination of the infected cells was assessed at P14. The arrow marks the injection path. **C-D)** Confocal images showing the morphology and NSC marker expression (Nestin-GFP and GFAP) of the SFFV-RV-infected cells located in the GCL. Arrows point to a SFFV-RV-infected NSC. **E)** Quantification of the percentage of SFFV-RV-positive NSCs among the total SFFV-RV-positive cells. **F)** Quantification of the percentage of SFFV-RV-positive NSCs among the total NSCs. *CA: Cornu ammonis. DG: Dentate gyrus. DMS: Dentate migratory stream fi: fimbria. GCL: Granule cell layer. LV: Lateral ventricle. SGZ: Subgranular zone Scale bars are 200 µm in A-B and 10 µm in C-D. ***p<0.001. Student's t-test. Bars show mean ± SEM. Dots show individual data.*

The observed region-dependent differences were maintained at P5. When precursors were infected inside the DG at this age, the SFFV-RV-mCherry-positive cells were found more restricted to the lower part of the GCL and along the SGZ at P14 **(Figure R8 A-D)**. As before, most of them were identified as neurons. Importantly, 3-4% of the SFFV-RV-mCherry-positive cells were NSCs **(Figure R8 E; Figure R9)**, corresponding in turn to the 2% of the total adult NSC population **(Figure R8 F; Figure R9)**. On the other hand, following the same pattern than at P2, when precursors were infected in the DMS, the vast majority of the SFFV-RV-mCherry-positive cells located in the GCL at P14 were neurons with identifiable dendrites and axons that lacked Nestin-GFP and GFAP labeling **(Figure R8 C-F)**. This set of *in vivo* fate-mapping studies strongly suggested that the adult NSC population was directly generated from dNSCs located exclusively inside the DG early after birth, even though there were progenitors coming from the DMS that contributed to the neuronal formation of the DG. In combination with the *cD2* data we postulated that a population of dNSCs located in the DG generated the adult NSC population directly and on-site through *cD2*-dependent mitosis during the early postnatal period. Therefore, we concluded that adult NSCs are a different population from dNSCs that gets independently generated after birth and AHN is not a mere remnant of developmental neurogenesis but a distinct phenomenon.

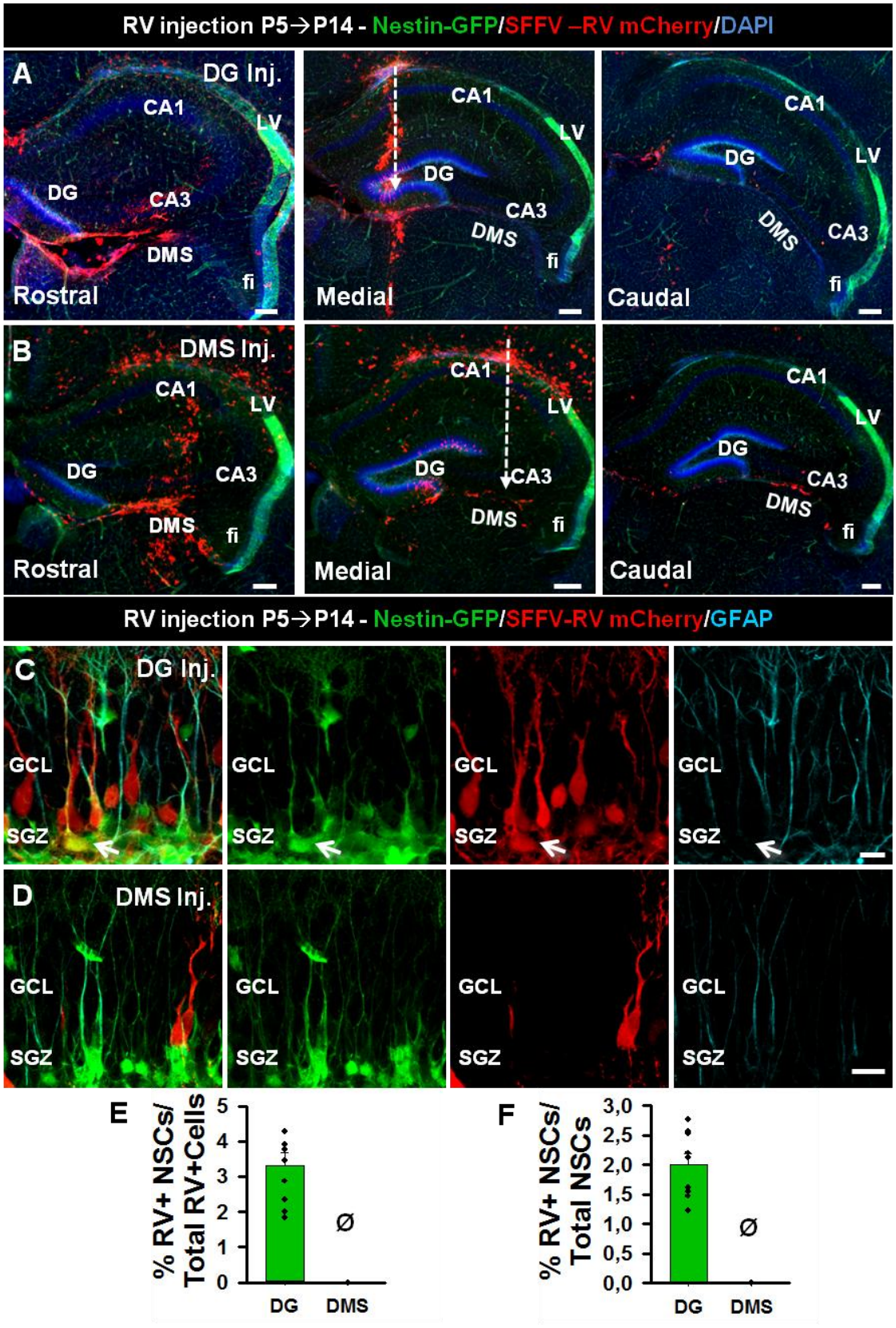
RV injection P5→P14 - Nestin-GFP/SFFV –RV mCherry/DAPI
A
DG Inj.
CA1
LV
DG
CA3
DMS
fi
Rostral
Medial
Caudal
B
DMS Inj.
RV injection P5→P14 - Nestin-GFP/SFFV-RV mCherry/GFAP
C
D
GCL
SGZ
E
% RV+ NSCs/ Total RV+Cells
F
% RV+ NSCs/ Total NSCs
Ø

← Previous page. Figure R8. All adult NSC precursors were located inside the DG before the end of the first postnatal week. A-B) Fluorescence slide scanner images showing the spatial destination of SFFV-RV-infected cells in the DG (A) or in the DMS (B) from rostral to caudal. Pups were injected at P5 and the spatial destination of the infected cells was assessed at P14. The arrow marks the injection path. **C-D)** Confocal images showing the morphology and NSC marker expression (Nestin-GFP and GFAP) of the SFFV-RV-infected cells located in the GCL. Arrows point to a SFFV-RV-infected NSC. **E)** Quantification of the percentage of SFFV-RV-positive NSCs among the total SFFV-RV-positive cells. **F)** Quantification of the percentage of SFFV-RV-positive NSCs among the total NSCs. *CA: Cornu ammonis. DG: Dentate gyrus. DMS: Dentate migratory stream fi: fimbria. GCL: Granule cell layer. LV: Lateral ventricle. SGZ: Subgranular zone. Scale bars are 200 µm in A-B and 10 µm in C-D. Student's t-test. Bars show mean ± SEM. Dots show individual data.*

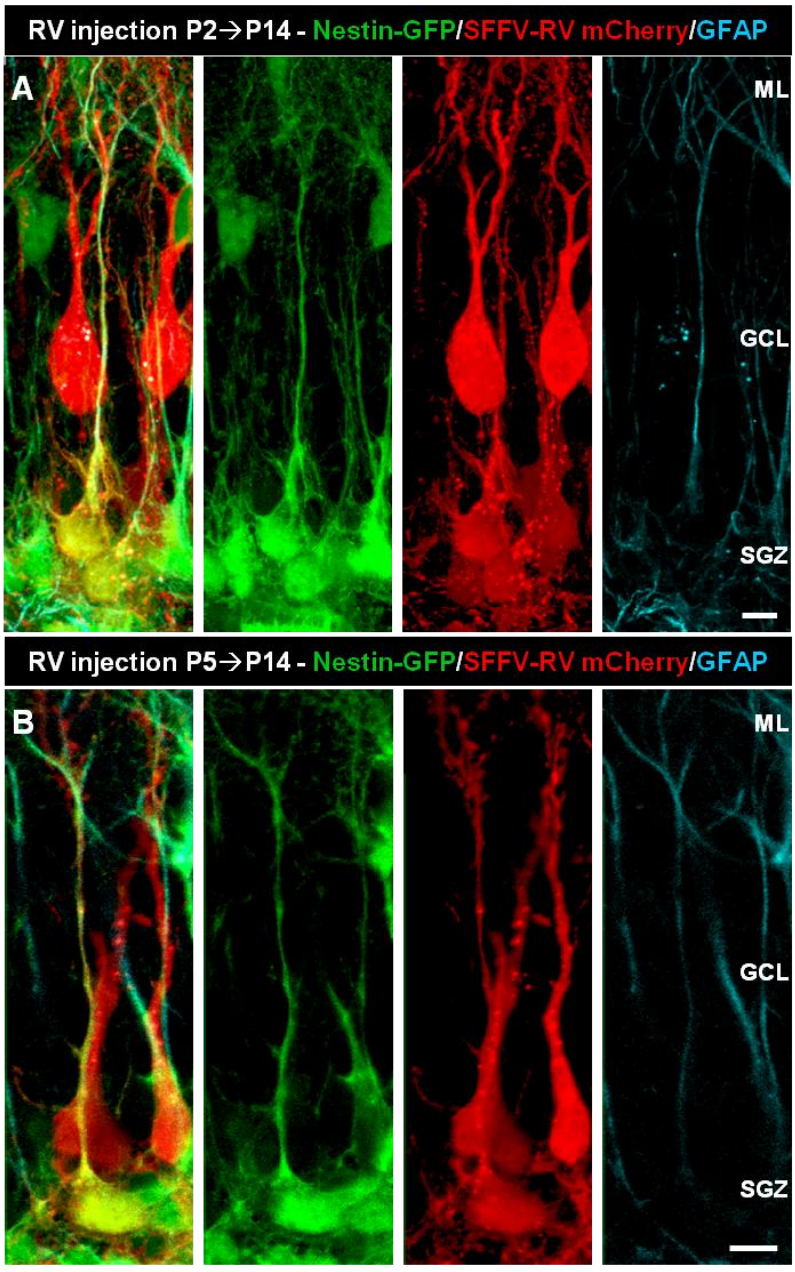

← Previous page. Figure R9. The SFFV-RV infections effectively labeled NSCs when injecting inside DG. A-B) Confocal images showing SFFV-RV-infected NSCs in the GCL. Injecting the SFFV-RV at P2 and P5 inside the DG, several Nestin-GFP and GFAP-expressing cells were labeled. The soma in the SGZ, the process towards the ML and the broccoli-like crown arborizing in the ML were perfectly identifiable. *GCL: Granule cell layer. ML: Molecular layer. SGZ: Subgranular zone. Scale bars 10 µm.*

6.2.3. Divergent spatial contribution to the DG from DMS progenitors

Our previous results indicated that the precursors that will give rise to adult NSCs are already located inside the DG at early postnatal stages. However, the DMS remained active during these postnatal stages, so we next moved to further explore the extent of the DMS precursor contribution to the GCL. After SFFV-RV-mCherry infections in the DMS at P2 and P5, we assessed the differential spatial fate preference of the divided cells at P14.

At both ages, neuron-like cells were more densely packed in the ventral arm of the DG than in the dorsal arm. SFFV-RV-infected cells were mainly grouped near the edge of the ventral arm, while scattered cells could be observed throughout the rest of the GCL **(Figure R10 A-B)**. Moreover, ventral and dorsal SFFV-RV-mCherry-expressing cells diverge in their morphology. The ventral ones were settled down at different positions between the SGZ and ML and the majority of them had a short apical process from dendrites rapidly spread into the ML. On the contrary, the dorsal ones were commonly positioned in the lower half of the GCL and had longer processes from which dendrites spread into the ML **(Figure R10 A-B)**.

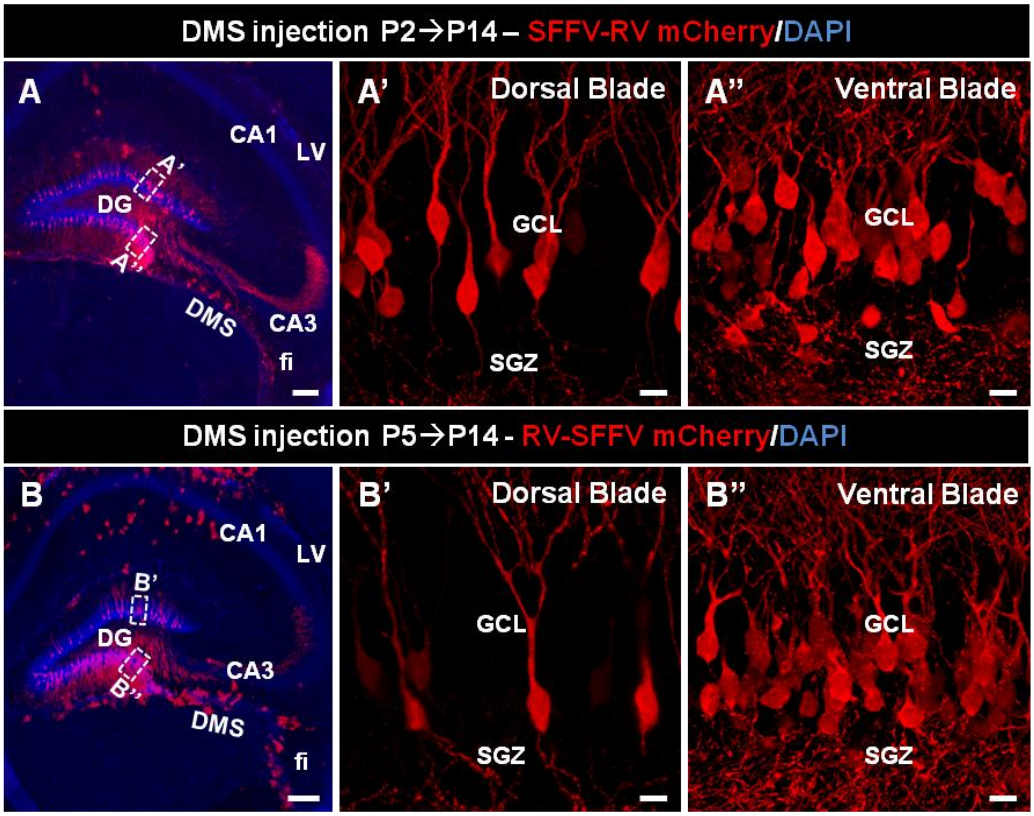

Figure R10. Divergent spatial contribution to the DG from DMS progenitors. A-B) Representative fluorescent slide-scanner images showing at P14 the spatial distribution of the progeny from P2 and P5 SFFV-RV-labeled DMS precursors. Neurons were observable widespread throughout the whole GCL. However, while in the dorsal arm individual, well-separated cells populated the GCL (A', B'), the ventral arm of the DG appeared full of packed cell clusters (A'', B''). *CA: Cornu ammonis. DG: Dentate gyrus. DMS: Dentate migratory stream. GCL: Granule cell layer. LV: Lateral ventricle. SGZ: Subgranular zone. Scale bars 10 µm.*

6.3. LPA_1 as a differential marker of adult NSCs

We had previously established that during early postnatal stages dNSCs proliferate inside the DG in a *cD2*-dependent manner. Taking that into account we next hypothesized that adult NSCs comprise a new independent population in the DG, rather than being a remnant from developmental dNSCs. However, one of the main issues when assessing the developmental dynamics of NSCs is the lack of markers for the differential identification of dNSCs and adult NSCs. Recently, LPA_1 has been reported to selectively label adult hippocampal NSCs (Walker et al., 2016). Since LPA_1 acts as a modulator of AHN (Matas-Rico et al., 2008) and also cortical development (Estivill-Torrús et al., 2008), we aimed to assess its expression during the postnatal development of the DG using the LPA_1-EGFP mouse model (Gong et al., 2003).

6.3.1. NSCs acquired LPA_1 expression during the postnatal period

We analyzed the DG and the neurogenic niche at five different postnatal time points (P4, P7, P10, P14 and P21). LPA_1-EGFP expression was widespread throughout the hilus at P4, while it was almost negligible in the GCL. Later at P7, the expression of LPA_1-EGFP started to switch from the hilar region to the GCL. By P14, the switch was completely evident and LPA_1-EGFP expression was restricted to the SGZ **(Figure R11 A)**. Interestingly, as there was no LPA_1-EGFP expression in the GCL at P4, none of the Nestin-expressing and radially oriented dNSCs that were located there were LPA_1-EGFP-positive. However, after P7 onwards, some dNSCs started to acquire LPA_1-EGFP expression. Remarkably, at P14, when the NSC population becomes adult (Nicola et al., 2015), almost all NSCs expressed LPA_1-EGFP **(Figure R11 B)**. These results suggested that LPA_1 could be a potential marker to distinguish the transition of NSCs from developmental to adult.

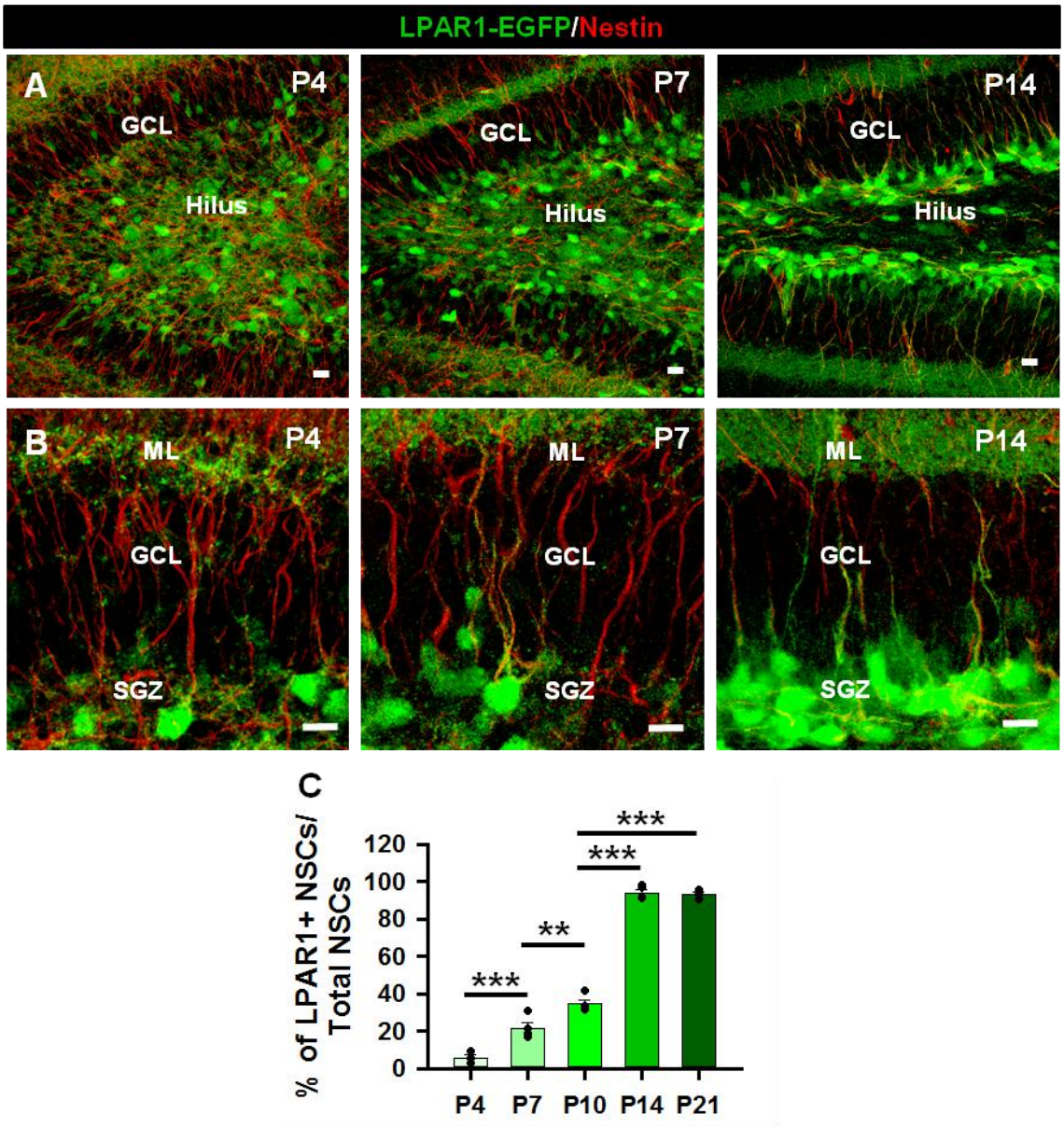

Figure R11. LPA_1-EGFP expression differentially labeled adult NSCs from dNSCs. A-B) Representative confocal images of the LPA_1-EGFP expression in the whole DG (A) and specifically in the GCL (B) at P4, P7 and P14. The majority of dNSCs were negative for LPA_1-EGFP, whereas almost the entire population of NSCs expressed it at P14. **C)** Quantification of the percentage of dNSCs/NSCs (defined as Nestin-positive, radially oriented cells) expressing LPA_1-EGFP at P4, P7, P14 and P21. There was a significant increase in the percentage of LPA_1-EGFP-expressing NSCs from developmental stages (P4 and P7) to P14. *GCL: Granule cell layer. SGZ: Subgranular zone. ML: Molecular layer. Scale bars are of 10 µm. **p<0.01, ***p<0.001. One-way ANOVA followed by all pairwise comparisons by Holm-Sidak post hoc test. Bars show mean ± SEM. Dots show individual data.*

6.3.2. The cellular specificity of LPA_1-EGFP expression switched from postnatal to adult stages

We next evaluated the nature of the hilar LPA_1-EGFP-expressing cells, hypothesizing that they could correspond to neuronal populations because of their morphology. Indeed, the results showed that there was a switch in the cell-specific expression of LPA_1-EGFP. At P4-P7, the majority of LPA_1-EGFP cells in the hilus were positive for the mature neuronal marker NeuN **(Figure R12 A-B)**, while thereafter, coinciding with the period in which NSCs started to express LPA_1-EGFP, only a few LPA_1-EGFP-expressing cells were also positive for NeuN **(Figure R12 C-D)**.

Altogether, these results showed a spatial and cellular switch in the expression of LPA_1-EGFP from the early postnatal period (P4-P7) to the end of the neurogenic niche formation (P14). The expression was mainly neuronal during early postnatal development, whereas it got restricted to the NSCs from P14 on. Thus, we suggest LPA_1 as a valuable tool for the differentiation of dNSCs and adult NSCs, potentially playing a role in the transition of NSCs from developmental to adult. These results also support the notion of adult NSCs being altogether a distinct population from dNSCs.

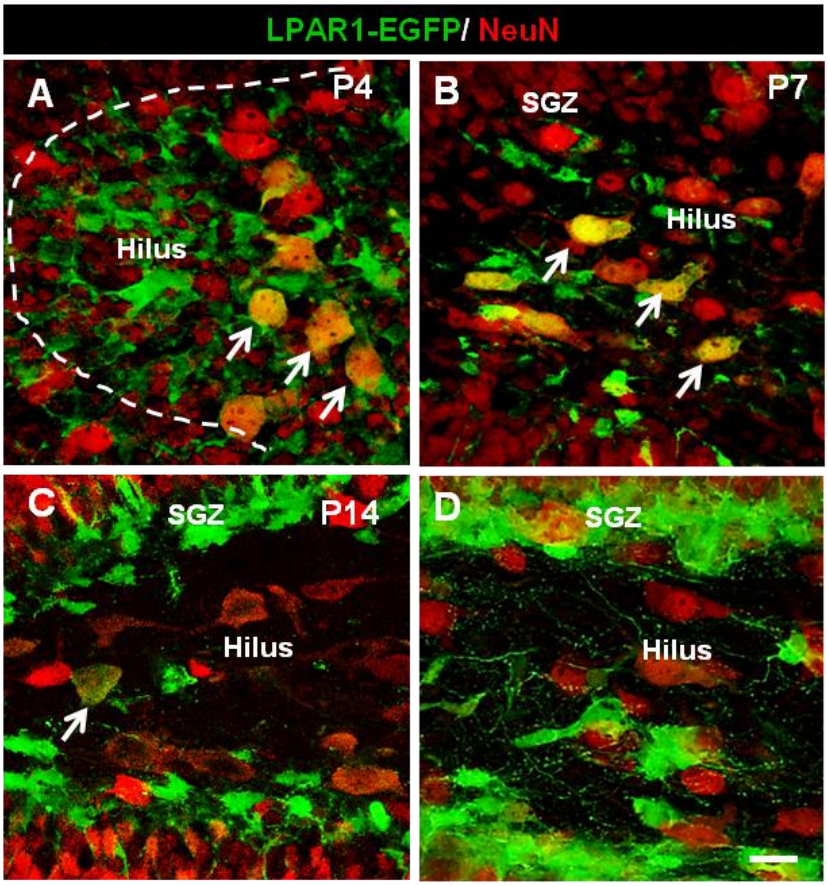

← Previous page. Figure R12. LPA_1-EGFP expression in the DG switched at early postnatal stages. A-D) Representative confocal images of the NeuN- and LPA_1-EGFP- expressing cells in the hilar region at different postnatal time points. While several big cells appeared expressing both LPA_1-EGFP and NeuN in the hilus at early postnatal stages, they gradually lost LPA_1-EGFP expression with time. The dashed line delimitates the SGZ. Arrows point at those cells co-expressing both NeuN and LPA_1-EGFP. *Scale bars are of 10 µm.*

6.4. Human DG development is almost ended by mid-gestation

Our previous results pointed towards the generation in the early postnatal DG of an independent neurogenic NSC population that will remain in the SGZ during the whole life of the mouse, being different from the dNSCs that form the DG and other regions from the HPF during the embryonic and early postnatal development development. Our next step was to investigate whether these results could be translated to humans. In a context in which the existence of AHN in humans remains controversial (Moreno-Jiménez et al., 2019; Sorrells et al., 2018), shedding light upon the formation patterns of the DG and its neurogenic niche would help us to explore the extent of the AHN in humans.

6.4.1. The DMS was present in the early human development (GW14)

In collaboration to Mercedes Paredes from the UCSF, who kindly let us access to human samples, we proceeded to histologically characterize the development of the human DG and more specifically the potential presence of different dNSC populations. Previous works have already shown proliferating progenitors and neurogenic RGCs forming the DMS at GW14 (Cipriani et al., 2017, 2018; Sorrells et al., 2018). Furthermore, this is the embryonic time period when hippocampal neurogenesis reaches its peak (Yang et al., 2014). Here, we further characterized the HPF at this age, using RGC and progenitor cell markers. Although at this age both dHPF and vHPF are observable, the ventral region is the one that more prominently evolves and thereby the one in which we focused our analysis **(Figure R13 A)**.

We observed that overlapping Nestin- and GFAP-positive fibers extended from the DNe to the DG, forming a RGC scaffold along the DMS. Nestin-expressing cells were also located inside the prospective DG, mainly in the outer limb and populating the ML close to the HF **(Figure R13 B)**. Moreover, **the** GFAP-expressing fibers showed also HOPX expression, which labeling reached the DG through the FDJ, even though the GCL was free of HOPX staining **(Figure R13 C)**. HOPX has been suggested to be a specific marker for GC precursors in mice from embryonic stages to adulthood (Berg

et al., 2019) and these results opened the possibility of a similar HOPX-positive progenitor population in humans.

S100ß labels mature astrocytes in the adult mouse brain, although it has also been proposed as a neuronal precursor marker during postnatal DG development in mice (Namba et al., 2005). Here, we observed that S100ß-expressing cells were located along the DMS close to Tbr2-positive intermediate progenitors **(Figure R13 D)**. Regarding proliferating cells, using the mitotic marker Ki67, they appeared distributed throughout the whole HPF, although a strong presence of Ki67-positive cell clusters was observable surrounding the FDJ towards the hilus **(Figure R13 E)**.

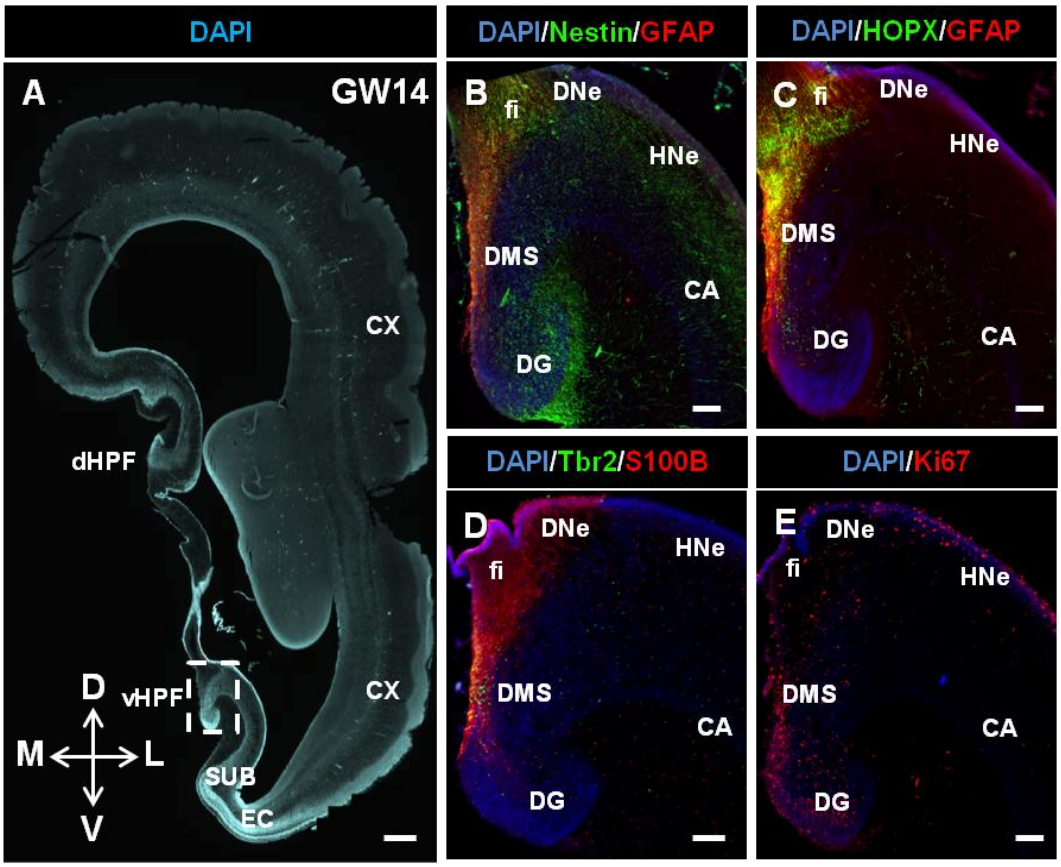

Figure R13. RGC and progenitors formed the DMS during the early development of the human HPF. **A)** Fluorescent slide-scanner image showing a hemisphere of a GW14 brain. The vHPF is marked by the dashed square. **B)** Nestin (green)- and GFAP (red)-expressing cells in the HPF at GW14. GFAP-expressing fibers were present along the DMS, while Nestin-expressing fibers can be also observed in the prospective ML of the DG. **C)** Likewise, HOPX-expressing cells were also populating the DMS, largely colocalizing with GFAP-expressing fibers and **D)** S100β-expressing cells and Tbr2-expressing progenitors were also distributed along this region. **E)** Ki67-expressing cells (proliferating cells) were distributed from the DNe to the DG. *CA: Cornu ammonis. Cx: Cortex. D: Dorsal. DG: Dentate gyrus. dHPF: Dorsal hippocampal formation. DMS: Dentate migratory stream. DNe: Dentate neuroepithelium. EC: Entorhinal*

cortex fi: fimbria. GCL: Granule cell layer. HNe: Hippocampal neuroepithelium. L: Lateral. M: Medial. SUB: Subiculum. V: Ventral. vHPF: Ventral hippocampal formation. Scale bars are 500 µm for A and 100 µm for B-E.

6.4.2. Differential spatial patterns during DG development

We next moved to describe the distribution of the progenitor cell and proliferation markers along the anteroposterior axis of the HPF. Remarkably, in the anterior HPF the majority of Ki67- expressing cells can be found attached to the DNe and the HNe (also known as the ammonic neuroepithelium), while sparse nuclei populated the DMS and DG **(Figure R14 A)**. However, at more medial positions Ki67-expressing nuclei were more concentrated in the DMS and the hilus, even though there were proliferating cells still remaining in the DNe **(Figure R14 B)**. This trend became more evident at posterior regions where the majority of the Ki67-expressing cells were restricted to the DG, especially at the edge of the inner limb where the DMS connects to the DG, but distributed also along the GCL and reaching the outer limb **(Figure R14 C)**. The different pattern of cellular expression between anterior and posterior regions of the HPF was not restricted to proliferating cells, being the HOPX-positive cells distributed in a similar manner. While in anterior regions they were attached to the DNe extending their processes along the DMS above the fimbria **(Figure R14 D)**, in posterior regions they can be observed inside the DG almost entirely restricted to the hilar region **(Figure R14 E)**. On the contrary, GFAP-expressing cells remained restricted to the DMS at the different anteroposterior levels **(Figure R14 D-E)**.

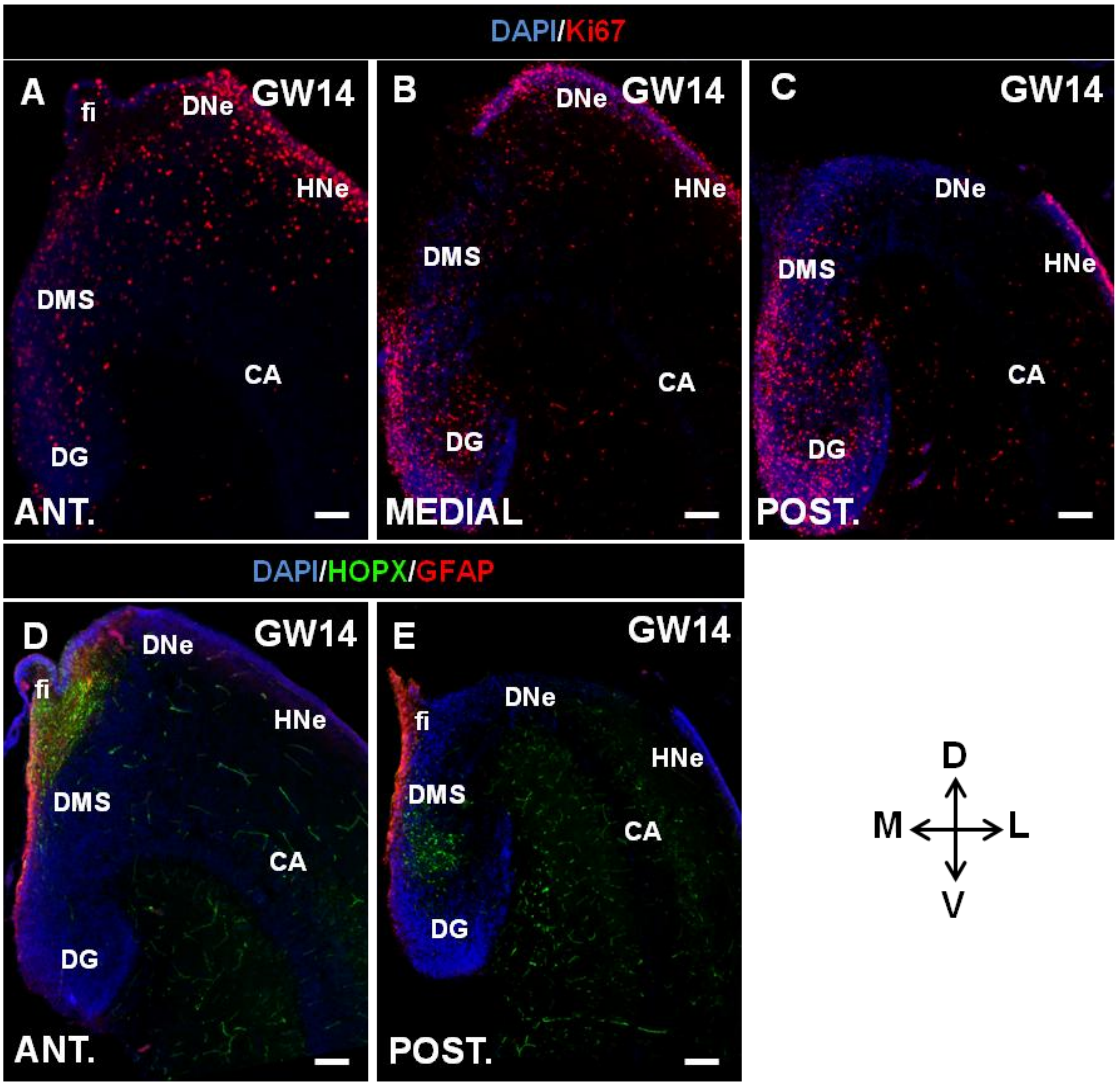

Figure R14. Differential expression patterns along the anteroposterior axis of the HPF during early development. A-C) Fluorescent slide-scanner image showing the expression of proliferating (Ki67) cells at different levels along the anteroposterior axis (from left to right, anterior to posterior). In the anterior part, Ki67-expressig cells were mainly located in the DNe and HNe, while they switched to the DMS and DG at posterior slices. **D-E)** HOPX-expressing cells followed the same pattern. They were restricted to the DNe and DMS in the anterior HPF but they got into the DG in the posterior part. On the contrary, GFAP expression conserved the same pattern along the whole axis, being restricted to the DMS. *CA: Cornu ammonis. D: Dorsal. DG: Dentate gyrus. DMS: Dentate migratory stream. DNe: Dentate neuroepithelium. fi: fimbria. GCL: Granule cell layer. HNe: Hippocampal neuroepithelium L: Lateral. M: Medial. V: Ventral. Scale bars are 100 µm.*

Altogether, the cellular expression patterns in GW14 embryos suggested a similar distribution of progenitors than in mice at embryonic and early postnatal stages, forming the DMS from the DNe to the DG. However, heterogeneous cell populations can be observed attending to their spatial location (inside or outside the DG) and marker expression. Likewise, the development of the DG followed different temporal

patterns along the anteroposterior axis. Next, we wanted to observe how these progenitor populations develop at later stages, after mid-gestation.

6.4.3. DG formation is restricted to the GCL by GW30

Aiming to explore the development of the progenitors during DG formation at mid-late embryonic stages, we moved to analyze the HPF of a GW30 embryo. At this age, the dHPF is still observable, although smaller than the vHPF that folds following the previously described patterns (Humphrey, 1967) **(Figure R15 A)**. In contrast to the observations at GW14, at this age Nestin-expressing cells appeared completely populating the hilus, fanning out extending their fibers towards the GCL and ML. Remarkably, remaining Nestin-positive fibers were observable horizontally oriented along the DNe and through the DMS above the fimbria **(Figure R15 B)**. Else, HOPX staining covered the entire HPF, suggesting a wide and non-specific cellular expression of the marker at this age compared to GW14. In the DG, HOPX-expressing cells appeared located in the hilus, extending processes towards the ML in a similar way than Nestin-expressing cells. Curiously, the inner limb of the DG lacked HOPX-expressing cells, while they entirely covered the outer limb. On the other hand, strong expression of GFAP can be observed along the remaining DMS **(Figure R15 C)**. Likewise, strong expression of S100β was present in the inner limb of the DG where the DMS ended **(Figure R15 D)**, following a similar pattern than HOPX expression **(Figure R15 C)**. The expression of S100β showed a differential pattern along the GCL, with cells located in the outer limb rather than in the inner limb **(Figure R15 D)**. Importantly, Tbr2-expressing progenitors and Ki67-positive proliferating cells were restricted to the hilar region, surrounding the GCL and forming a layer below **(Figure R15 D-E)**, which indicates that at GW30 the formation of the DG is mostly completed, resembling the late postnatal stages (P7-P14) of the mouse DG development.

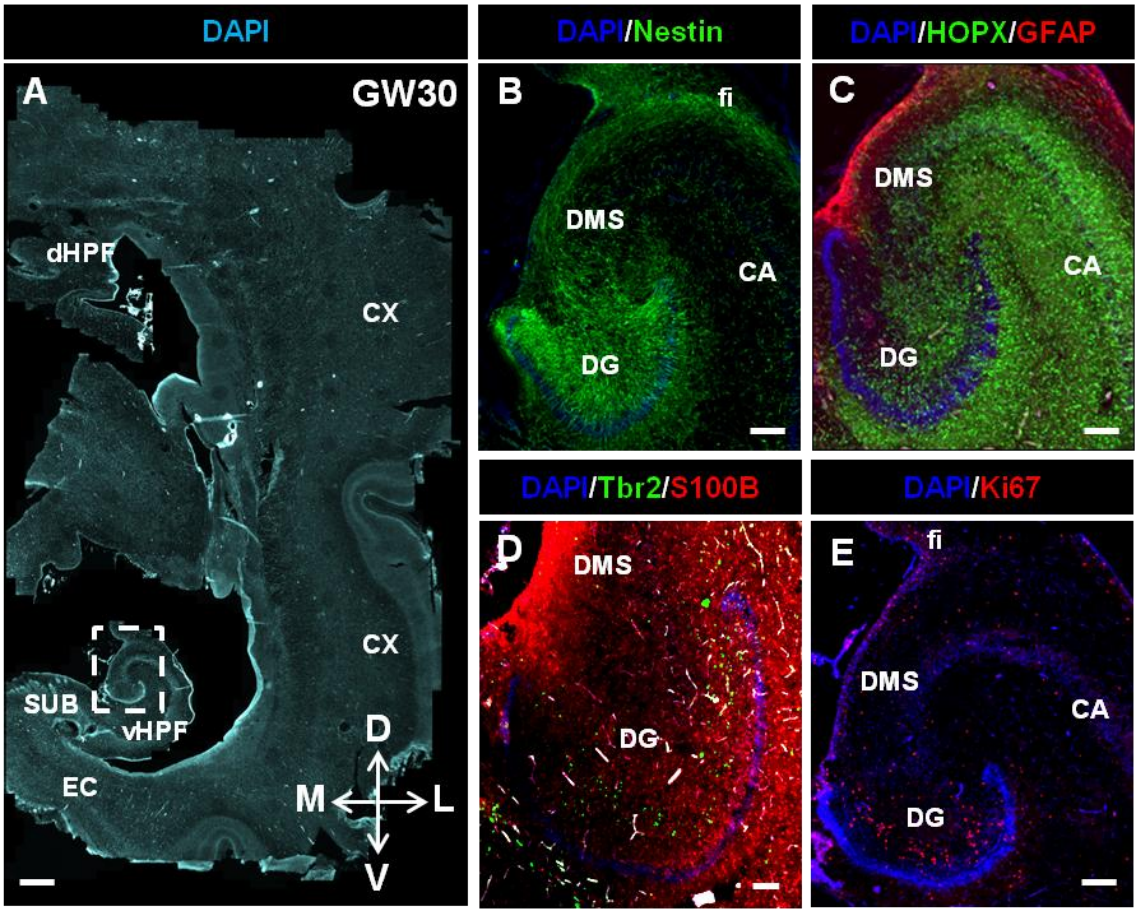

Figure R15. RGCs and progenitors were restricted to the hilus at GW30. A) Fluorescent slide-scanner image showing one hemisphere of a GW30 brain. The vHPF was marked by the dashed square. **B)** Nestin-expressing cells appeared fanning out inside the DG at GW30. They formed a scaffold that crossed the hilus and GCL towards the ML. **C)** GFAP-expressing fibers were present along the DMS, while HOPX expressing cells were observable throughout the whole HPF, including DG forming RGC scaffold similar to the Nestin one. **D)** S100β-positive cells were widespread throughout the GCL and ML, although the expression was much stronger in the outer limb of the DG than in the inner one. In contrast, cells positive for the intermediate progenitor marker Tbr2 formed a wide layer beneath the GCL. **E)** Likewise, proliferating cells were now restricted to the hilus, forming a wide layer beneath the GCL. *CA: Cornu ammonis. Cx: Cortex. D: Dorsal. DG: Dentate gyrus. dHPF: Dorsal hippocampal formation. DMS: Dentate migratory stream. EC: Entorrhinal cortex. fi: fimbria. GCL: Granule cell layer. L: Lateral. M: Medial. SUB: Subiculum. V: Ventral. vHPF: Ventral hippocampal formation. Scale bars are 500 µm for A and 100 µm for B-E.*

6.4.4. A RGC scaffold was still present in the DG early after birth

Despite the HPF gets already formed for the most part before birth, resembling the adult structure already at the neonatal period **(Figure R16 A)**, the last waves of migratory NBs reach the GCL and establish their synapses during the first years after birth, forming the hippocampal circuitry (Cipriani et al., 2018; Seress et al., 2001;

Sorrells et al., 2018). One month after birth, RGCs populated the hilus beneath the GCL, with their processes crossing the GCL towards the ML. Interestingly, while Vimentin staining can be observed distributed along the entire GCL, Nestin expression was restricted to the inner limb of the DG, suggesting potential heterogeneity among the remaining RGC populations **(Figure R16 B-C)**. Also, Ki67-positive proliferating cells were distributed throughout the hilus, although we did not observe any discernible SGZ as the one present in the adult mouse **(Figure R16 D)**, supporting the previous results of Arturo Alvarez-Buylla and colleagues (Sorrells et al., 2018). Altogether, the results indicated that there might be heterogeneous RGC populations in the human DG after birth, although proliferation took place mainly in the hilus suggesting that those populations would be mainly quiescent.

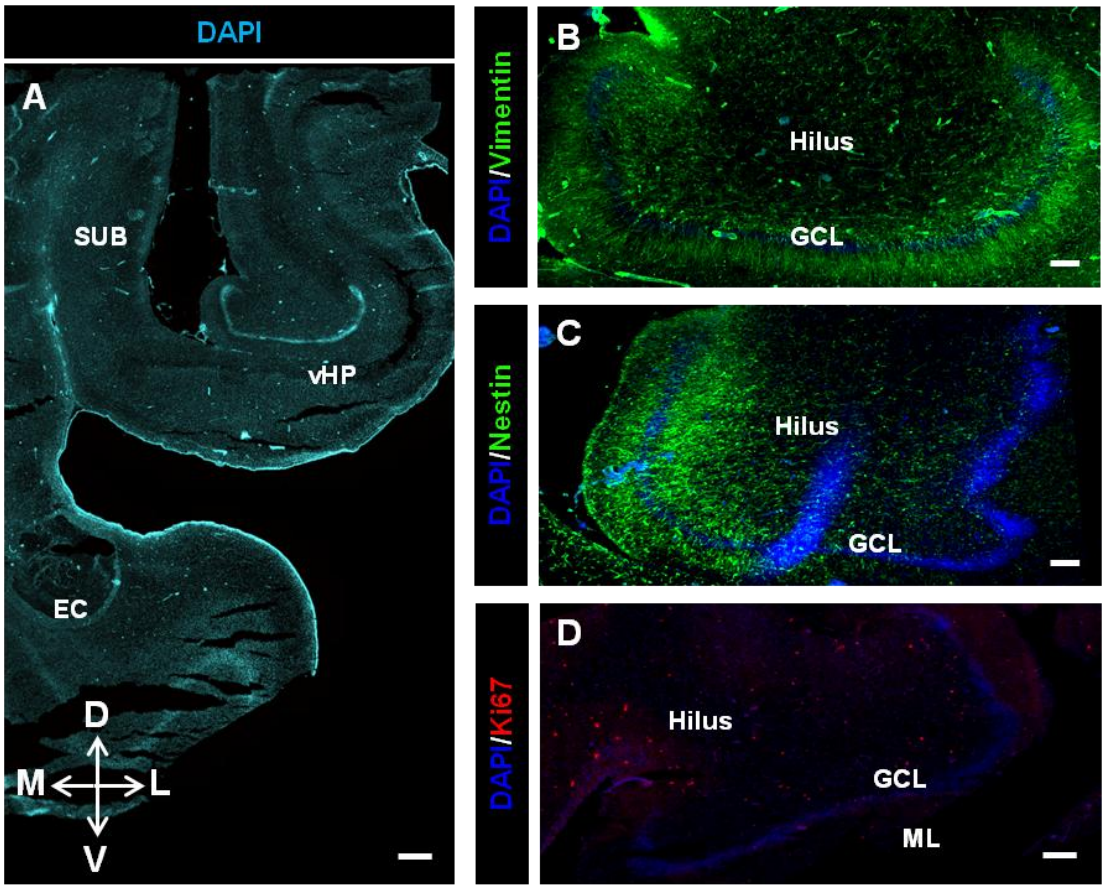

Figure R16. Early after birth, there were RGCs and proliferating cells in the DG. A) Fluorescent slide scanner image showing the HPF of a 1 month old brain. **B-C)** Vimentin- and Nestin-expressing cells in the DG 1 month after birth. There were fibers expressing both RGC markers crossing the GCL from the hilus to the ML. **D)** Regarding proliferation, we observed Ki67-expressing cells inside the DG at this age, although they populated the hilus rather than the GCL. D: Dorsal. *DG: Dentate gyrus. EC: Entorhinal cortex. GCL: Granule cell layer. L: Lateral. M: Medial. ML: Molecular layer. SUB: Subiculum. V: Ventral. vHPF Ventral hippocampal formation. Scale bars are 500 µm for A and 50 µm for B-D.*

The results obtained in the first part of this thesis indicated that in mouse, adult hippocampal NSCs comprise a differentiated cell population from the dNSCs that participate in the formation of the DG during the developmental period. Moreover, the formation of adult NSCs takes place precisely inside the DG early after birth. Else, in humans, hippocampal proliferation is already restricted to the DG before birth, suggesting that the potential formation of a neurogenic niche in the GCL would be already completed. Despite the recent controversy regarding the existence of NSCs and neurogenesis in adult humans (Moreno-Jiménez et al., 2019; Sorrells et al., 2018), the existence of RGCs expressing NSC markers during the first years after birth is not under debate (**Figure R16**; Blümcke et al., 2001; Cipriani et al., 2018; Sorrells et al., 2018). Indeed, Nestin-expressing cells have been reported to increase in the DG after infantile seizures, suggesting a possible role of these cells in response to pathological insults.

Thus, we moved back to explore in mice the role that a possible population of NSCs could have in the DG in response to pathological stimuli such as seizures. In mouse, adult hippocampal NSCs get massively activated and become reactive after seizures (Muro-García et al., 2019; Sierra et al., 2015), although the mechanism leading to this outcome remains unknown. Here, using an MTLE mouse model in which seizures are induced by KA intrahippocampal injection (Bouilleret et al., 1999; Sierra et al., 2015), we explored two possible receptors (FGFR1 and EGFR) that might be acting on the early response of NSCs.

6.5. FGFR1 was not involved in the early response of the neurogenic niche after MTLE induction

The FGFR1 signaling pathway, especially in response to its high-affinity ligand FGF2, has been demonstrated to be a modulator of the mitotic activity of cultured NSPCs and astrocytes (Reynolds and Weiss, 1992; Tropepe et al., 1999). In fact, the increase of both FGF2 and FGFR1 were observed after intraperitoneal KA injections, especially in reactive glial cells (Van Der Wal et al., 1994; Gómez-Pinilla et al., 1995). Thus, we consider that FGFR1 could be playing an important role on the activation and induction of React-NSCs that takes place as an early response in mouse models of MTLE (Muro-García et al., 2019; Sierra et al., 2015).

Here, we aimed to evaluate the expression of FGFR1 in a well-characterized model of MTLE (Bouilleret et al., 1999; Sierra et al., 2015). For that, we administered 1 nM of either KA (MTLE group) or saline (as control group) intrahippocampally to adult

mice and collected their hippocampi at different time points after the injection **(Figure R17 A)**. In contrast to what we expected, FGFR1 was not altered at either the mRNA or protein levels within the first 72 h after the KA injection, as measured by RT-qPCR and WB respectively **(Figure R17 B-C)**. In addition, we also checked the FGFR2 mRNA levels, as it also has high affinity to FGF2 (Dionne et al., 1990; Johnson et al., 1990) and thereby a possible activation route for the FGFR signaling pathway, but we observed no differences within the first 72 h after KA administration **(Figure R17 C)**. Wondering about the possibility that the analysis of the whole HPF might be masking or diluting a possible alteration of FGFR1 specifically in the DG, we moved to assess the FGFR1 expression in tissue by IHC at 24 h post-KA injection. We considered 24 h to be the best time point to observe FGFR1 alterations in the neurogenic niche, given that after KA administration proliferation in the neurogenic niche starts to be increased at 24 h and reaches its peak at 72 h (Sierra et al., 2015). Therefore, we considered that in order to trigger the response FGFR1 should be increased at 24 h. However, we detected no differences between the control animals and the ones injected with KA **(Figure R17 D)**, indicating that FGFR1 was not involved in the early response after the induction of MTLE.

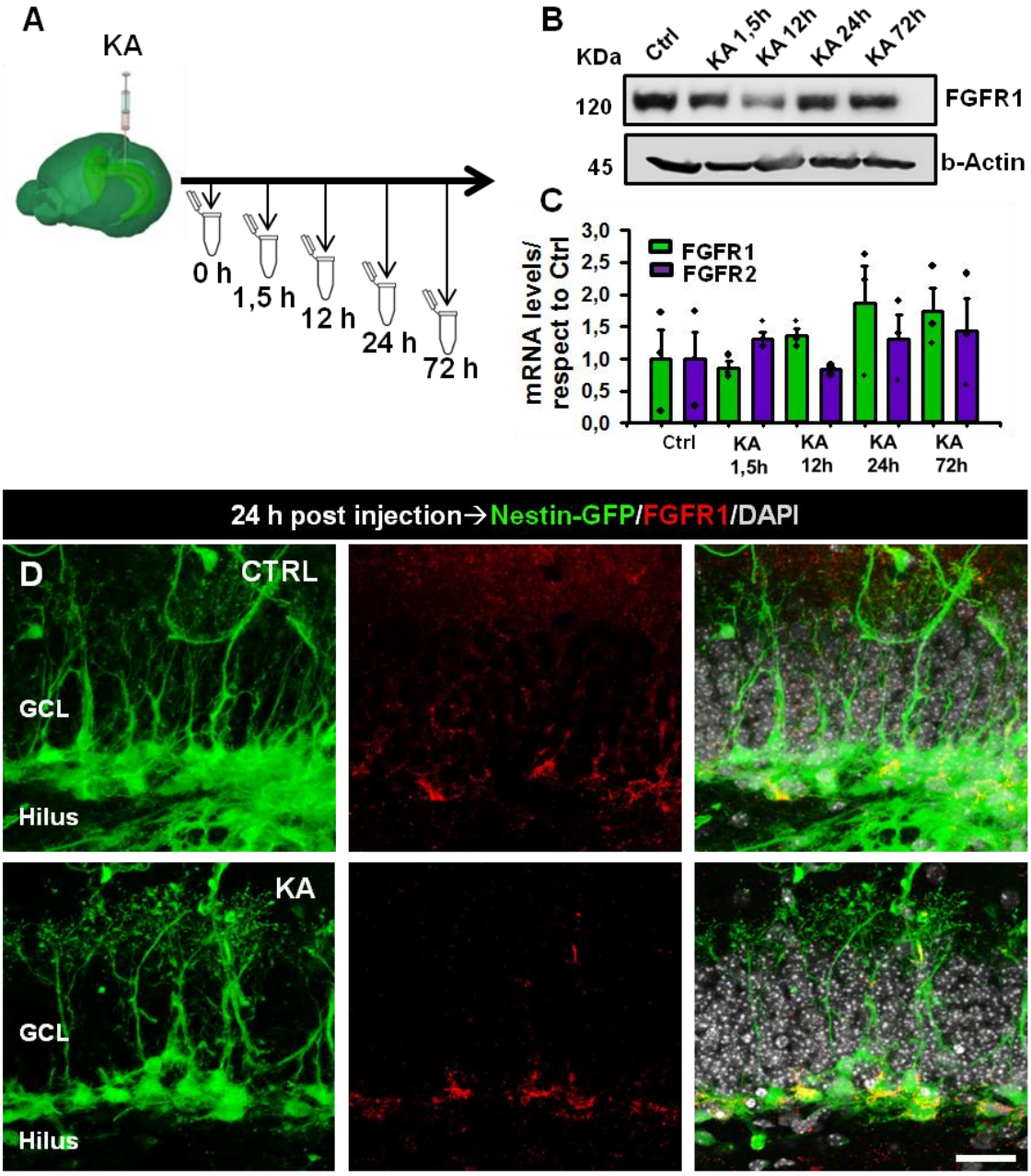

Figure R17. FGFR1 levels were not altered after KA administration. A) Schematic of the time course followed for hippocampi collection after KA injection. **B)** WB analysis showed that FGFR1 protein levels were not altered within the first 72 h after KA injection. **C)** RT-qPCR analysis showed no changes in FGFR1 mRNA expression during the first 72 h after KA injection. In addition, the mRNA levels of FGFR2 were also unaltered. **D)** Representative confocal pictures showing the GCL and Nestin-GFP-expressing cells after saline (control) or KA administration. There were no changes in the FGFR1 expression 24 h after KA injection. *CTRL: Control. GCL: Granule cell layer. KA: Kainic acid. Scale bars are of 20 µm. There were no statistical differences in (C) as indicated by one-way ANOVA followed by Holm-Sidak post hoc test versus control group. Bars show mean ± SEM. Dots show individual data.*

6.6. EGFR was involved in the early response of the neurogenic niche after MTLE induction

Thus, in light of the previous results discarding FGFR1 as a candidate to regulate the response of the neurogenic niche and NSCs after seizures, we moved to evaluate our next candidate, the EGFR signaling pathway, which is also involved in cultured NSPC proliferation (Reynolds and Weiss, 1992; Tropepe et al., 1999), being its nuclear expression strongly correlated with highly proliferating cells (Lin et al., 2001). EGFR has been demonstrated to be highly mitogenic for astrocytes (Simpson et al., 1982) and it is highly involved in the development of glioblastoma (Lee et al., 2006; Libermann et al., 1985; Vivanco et al., 2012). Moreover, EGFR increases in astroglia after different focal injury models both in rats and humans (Ferrer et al., 1996; Nieto-Sampedro et al., 1988; Río et al., 1995) and importantly, the expression of ErbB family (to which EGFR belongs) increases in the HPF after KA (Sierra et al., 2015). However, the precise implication of EGFR in the hippocampal response after seizures is not known and thus, we proceeded to evaluate possible alterations in the EGFR signaling pathway in a MTLE mouse model.

6.6.1. Increased expression and activation of the EGFR signaling pathway were early events after the induction of MTLE

We sought to evaluate EGFR expression following the same experimental paradigm than before; we administered either KA or saline (control group) intrahippocampally and collected the hippocampi thereafter following a temporal time-course (1.5 h, 12 h, 24 h, 72 h) **(Figure R18 A)**. We assessed the mRNA levels of EGFR through RT-qPCR analysis, observing a 2-3-fold increase at 1.5 h, 24 h and 72 h post-KA administration **(Figure R18 B)**. Next, since the levels of EGFR were increased after KA we proceeded to measure the activation of the EGFR pathway by WB. We evaluated the amount of EGFR phosphorylation (activation) on its Y845 residue, highly involved in EGFR-mediated mitogenesis (Biscardi et al., 1999; Sato et al., 1995; Tice et al., 1999), and the results revealed a progressive increase of the proportion of phosphorylated EGFR Y845 among the total EGFR, becoming significant from 24 h onwards **(Figure R18 C-D)**.

EGFR Y845 phosphorylation modulates the activation of several downstream signaling pathways, including STAT3, Akt and ERK1/2, involved in glial reactivity responses, cell survival and apoptosis or cellular proliferation (Goffin and Zbuk, 2013; Lill and Sever, 2012; Meloche and Pouysségur, 2007; Priego et al., 2018). Our WB

analyzes demonstrated a significant increase of the phosphorylated levels of STAT3 respect to the total amount of STAT3 12 h post-KA administration, decreasing thereafter **(Figure R18 C-E)**. Regarding the Akt signaling pathway, the ratio of phosphorylated Akt respect to the total Akt was significantly increased from 24 h after KA onwards **(Figure R18 C-F)**. Similarly, phosphorylated ERK1/2 increased at the 1.5 h timepoint after KA administration and kept increasing until the last time point checked (72 h after KA). Importantly, these changes were subdued to the total amount of protein (as we measured the ratio of phosphorylation among the total amount), which might be altered in different manners. Indeed, whereas the WB showed a tendency to increase in the total amount of EGFR and STAT3, Akt and ERK1/2 tended to decrease **(Figure R18 C)**. In any case, we could conclude that the expression of EGFR not only increased in the HPF early after inducing MTLE, but it also got highly phosphorylated at least in its Y845 site. Moreover, several downstream signaling pathways of EGFR (STAT3, Akt and ERK1/2) got also phosphorylated early after KA, suggesting a possible important role of the signaling pathway in the hippocampal response after seizures.

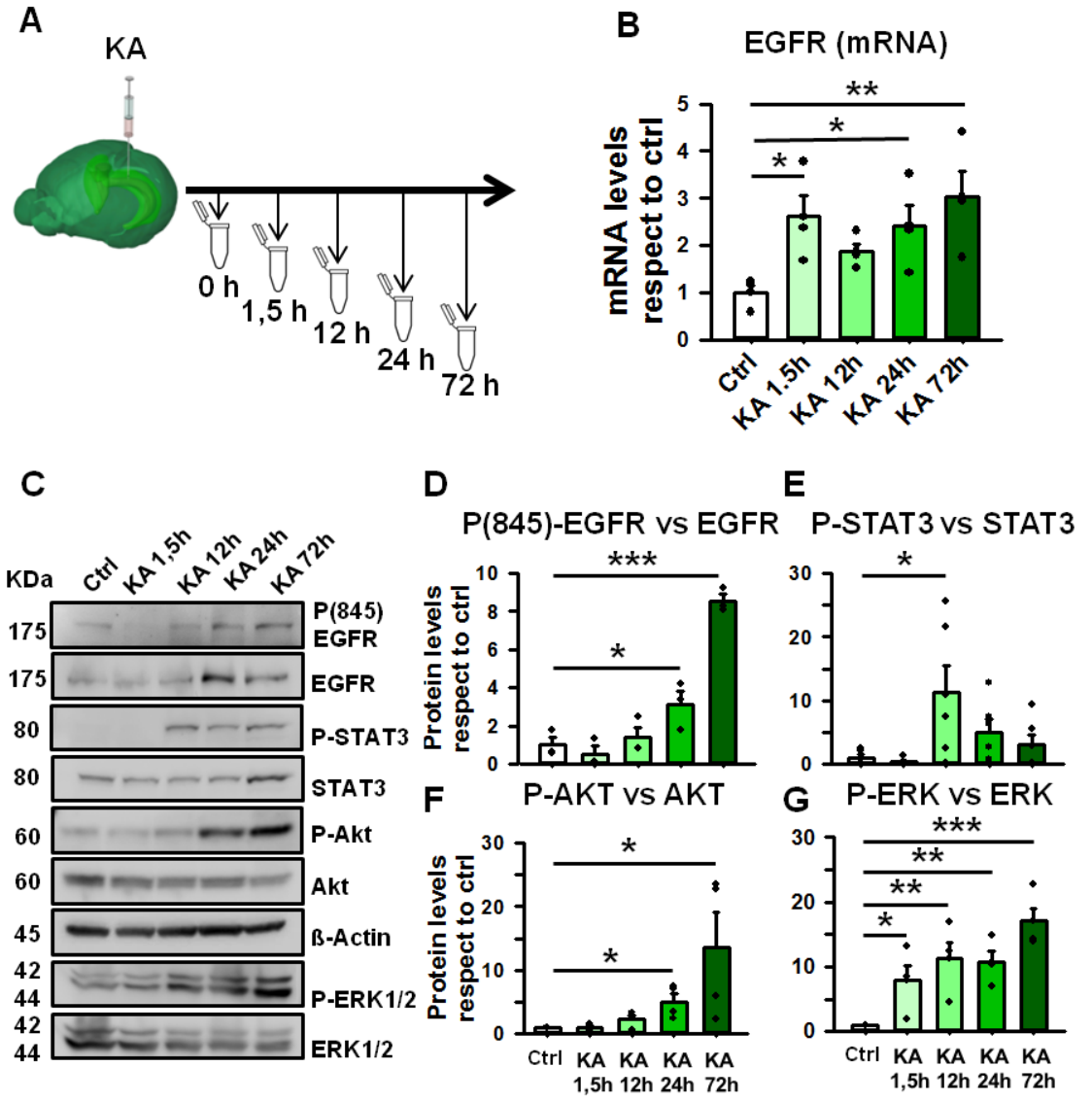

Figure R18. The increased expression and activation of the EGFR signaling pathway were early events of MTLE. A) Schematic illustrating the time course for the hippocampi collection after KA injection. **B)** RT-qPCR showed the increase of mRNA levels of EGFR at different time points after KA administration. **C)** WB showed changes in the total and phosphorylated amount of protein for EGFR (and its tyrosine site EGFR Y845), STAT3, Akt and ERK1/2 at different time points after KA. **D-G)** Quantifications of the proportion of phosphorylated isoforms compared to the total amount of protein for EGFR (and its tyrosine site EGFR Y845) and its downstream signaling pathways STAT3, Akt and ERK1/2. The data in each graph was normalized taking the mean of the control group as 1 ± SEM. **p<0.05*, ***p<0.01 and ***p<0.001. One-way ANOVA followed by multiple comparisons versus control group by Holm-Sidak post hoc test in (A), (D) and (G). Kruskal-Wallis followed by multiple comparisons versus control group by Dunnet post hoc test in (E) and (F). Bars show mean ± SEM. Dots show individual data.*

Once confirmed that the expression of EGFR was increased and that several of its downstream signaling pathways (STAT3, Akt, ERK1/2) were activated in the HPF early after the KA-induced MTLE, our next hypothesis was that EGFR expression would be increased specifically in the NSCs, playing a role in their massive activation and reactive transformation. To check this, we performed intrahippocampal injections of either KA or saline (control group) in Nestin-GFP transgenic mice and analyzed the EGFR expression in the neurogenic niche 24 h later. For that, we combined IHC and confocal microscopy, measuring the colocalization of EGFR-positive pixels with the area covered by Nestin-GFP-expressing cells that corresponded to the RGC-like adult NSCs and ANPs.

In control conditions, EGFR expression was tightly restricted to a limited number of Nestin-GFP-expressing cells. In sharp contrast, 24 h after KA EGFR expression increased noticeably in the neurogenic niche and especially in the Nestin-GFP-expressing NSCs and ANPs **(Figure R19 A)**. Indeed, after KA the quantification of the number of EGFR-positive pixels showed a tendency to increase in the whole GCL, not only in the Nestin-GFP-expressing cells, **(Figure R19 B)** and also a significant increase in the hilus **(Figure R19 C)**. More importantly, the colocalization of EGFR with Nestin-GFP-expressing NSCs, identified by morphological criteria (Mignone et al., 2004), was increased by 450% after KA **(Figure R19 D)**, strongly suggesting a role of the receptor in the response of NSCs after seizures.

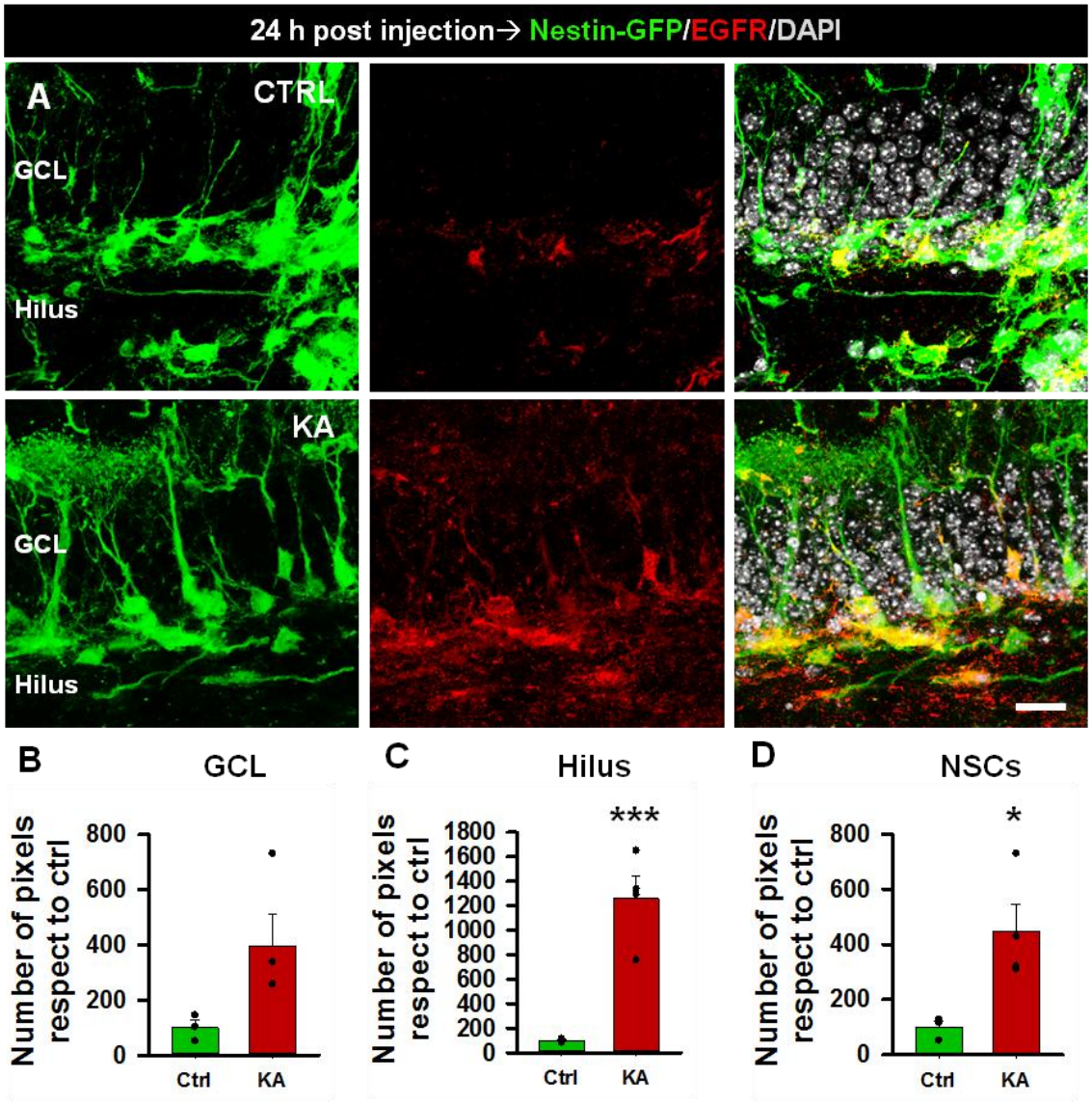

Figure R19. EGFR increased in NSCs after KA administration. A) Representative confocal images 24 h after saline (CTRL) or KA injections. **B-D)** Quantifications of EGFR expression (in pixels) in different regions of the DG (GCL and hilus) and the colocalization with NSCs. The data in each graph was normalized taking the mean of the control group as 100 ± SEM. *GCL: Granule cell layer. KA: Kainic acid. SAL: Saline. Scale bars 20 µm.* *p<0.05 and ****p<0.001*. *Mann Whitney test in (B) and Student's t test in (C) and (D). Bars show mean ± SEM. Dots show individual data.*

6.6.2. EGFR participated in the proliferating activity of cultured NSPCs

The obtained results suggested a potential action of EGFR on NSCs after seizures, due to its increase in the neurogenic niche and particularly in NSCs after KA administration. Thus, seeking to unravel the role of the receptor we moved to isolate and enrich hippocampal NSPCs *in vitro* adapting previously optimized methods (Pineda et al., 2013). This approach allowed us to check the presence of EGFR and

directly modulate its signaling without the interference of external niche signals (ions, molecules or circuital electrical activity).

As expected, we isolated NSPCs from 2-month-old Nestin-GFP mice and confirmed that after being cultured for one week EGFR was present in all cells **(Figure R20 A)**. Therefore, once demonstrated the presence of EGFR in NSPCs artificially induced to proliferate, we sought to assess the effect of EGFR inhibition in their proliferating capacity. Having the NSPCs in continuous proliferating conditions and with the EGFR signaling activated upon EGF and FGF stimulation, we checked the effect of the pharmacological inhibition of EGFR signaling using the reversible inhibitor Gefitinib, that efficiently blocks phosphorylation of all the tyrosine sites of EGFR (Pedersen et al., 2005). In this case, trying to get a more global sense of the effect of Gefitinib upon EGFR inhibition, we checked not only the Y845 phosphorylation site, as we did before, but also the autophosphorylation site Y1068, which is well-known to regulate the EGFR-mediated cell proliferation (Downward et al., 1984). Furthermore, we tested ERK1/2 phosphorylation as well, since it is the downstream signaling pathway of EGFR that is more directly related with cell proliferation (Meloche and Pouysségur, 2007). The results showed by WB analysis that the addition of 2 µM Gefitinib for 1 h into cultured NSPCs efficiently reduced EGFR phosphorylation at both residues Y845 and Y1068, as well as ERK1/2 phosphorylation **(Figure R20 B-E)**. Thus, the effect of Gefitinib upon NSCs was revealed, as well as its potential therapeutic effect as a candidate to reverse the massive activation and React-NSC induction after seizures.

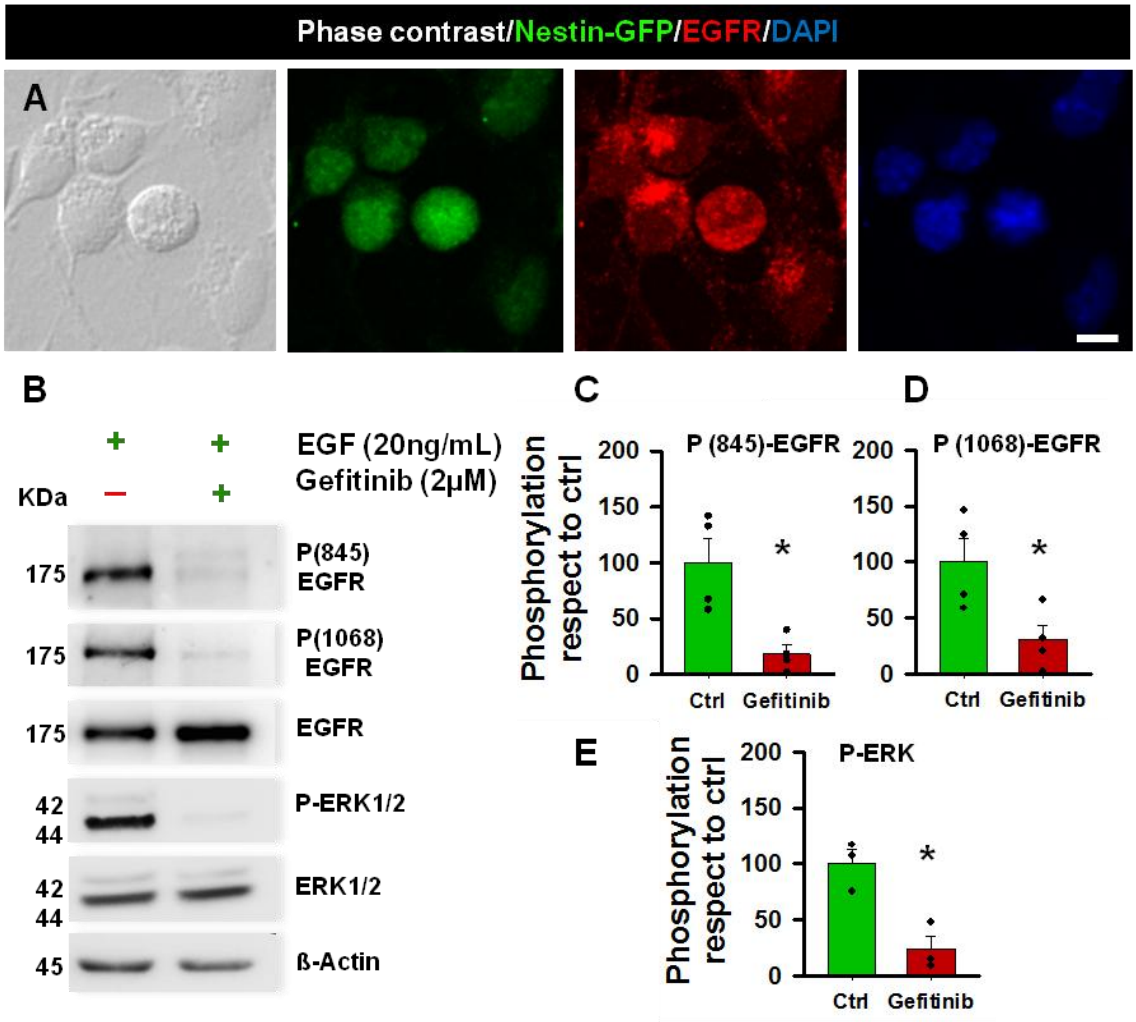

Figure R20. Gefitinib efficiently shut off EGFR signaling in cultured NSPCs. A) Representative confocal images showing EGFR expression in cultured Nestin-GFP-expressing NSPCs. **B)** Representative WB images of EGFR and ERK1/2 and their activation in NSPCs stimulated with EGF and FGF and in presence of the EGFR inhibitor Gefitinib. **C-E)** Quantification of the phosphorylated isoforms compared to the total amount of protein levels for EGFR (Y845 and Y1068) and its downstream signaling pathway ERK1/2. The data in each graph was normalized taking the mean of the control group as 100 ± SEM. *Scale bar 20 µm. *p<0.05. Mann Whitney test in (C). Student's t test in (D) and (E). Bars show mean ± SEM. Dots show individual data.*

Our results indicated so far that EGFR was present in cultured hippocampal NSPCs and that Gefitinib can efficiently block its signalization activity. Next, we aimed to shed light into the potential role of EGFR on the proliferating activity of the NSPCs. EGFR has been shown to be present in activated NSCs of the SVZ (Codega et al., 2014; Pastrana et al., 2009), but its role on the hippocampal NSCs remains unknown. Thus, following with our *in vitro* experimental paradigm, we measured first the intensity of EGFR expression in both mitotic and non-mitotic NSPCs, and then evaluated the

functional effect of Gefitinib on them using BrdU to assess the proportion of proliferating NSPCs. According to the results, EGFR expression increased in cultured NSPCs undergoing mitosis compared to those in interphase, identified by the chromosomal disposition by DAPI staining **(Figure R21 A-C)**. Moreover, the NSPCs that incorporated BrdU 1 h before fixation were reduced in a 37% in presence of 2 μM Gefitinib compared to those in presence of vehicle (dimethyl sulfoxide; DMSO) **(Figure R21 D-E)**, confirming the essential relevance of EGFR for NSPC proliferation and its effective blockage by Gefitinib.

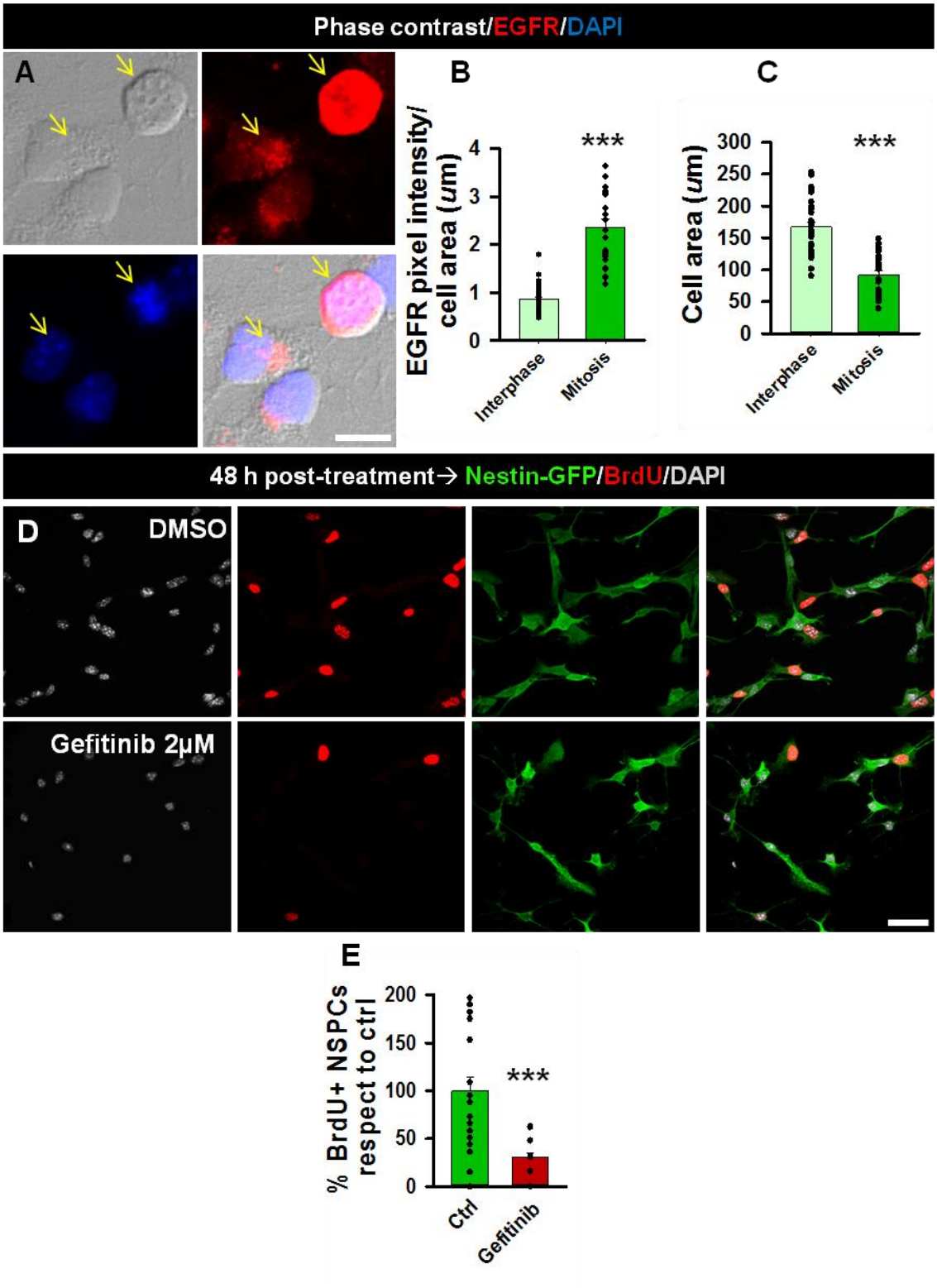

Figure R21. The EGFR-mediated proliferation activity of NSPCs was reduced in the presence of Gefitinib. A) Confocal representative images of mitotic and non-mitotic NSPCs (identified by chromosome disposition using DAPI) showing higher intensity of EGFR in mitotic NSPCs. Arrows point location of the cells (C). **B-C)** Quantifications of the EGFR intensity in the area of the cell (B) and the total cellular area in mitotic and non-mitotic NSPCs. **D)** Representative confocal images showing the decrease in the number of

proliferating cells (as shown by BrdU incorporation) in Gefitinib-treated NSPCs respect to control NSPCs treated with DMSO. **E)** Quantification showing the decrease of BrdU- positive NSPCs in the presence of Gefitinib respect to the control group (DMSO-treated NSPCs). The data in each graph was normalized taking the mean of the control group as 100 ± SEM. *Scale bar 20 µm. ***p<0.001. Mann Whitney in (B) and (E). Student's t test in (C). Bars show mean ± SEM. Dots show individual data.*

Given that Gefitinib, a reversible inhibitor of EGFR, was effectively able to reduce proliferation in NSPCs, we sought to explore whether Afatinib, an irreversible inhibitor of EGFR, would have a stronger effect. Afatinib potently suppresses the kinase activity of EGFR and it was designed to overcome the resistance that tumor patients developed to the reversible inhibitors like Gefitinib, due to mutations in the kinase domain (Li et al., 2008). In sharp contrast with the results obtained using Gefitinib, 2µM of Afatinib inhibitor induced massive cell death of the NSPCs at 48 h, indicated by the almost complete loss of NSPCs, as well as the rounded morphology, small size and nuclear DNA condensation of the few remaining ones **(Figure R22 A)**. Interestingly, the quantification showed a reduction in the percentage of BrdU-positive cells in the presence of Afatinib, although conclusions on the effectiveness of Afatinib on mitosis cannot be drawn due to the high cellular loss provoked by its administration **(Figure R22 B)**.

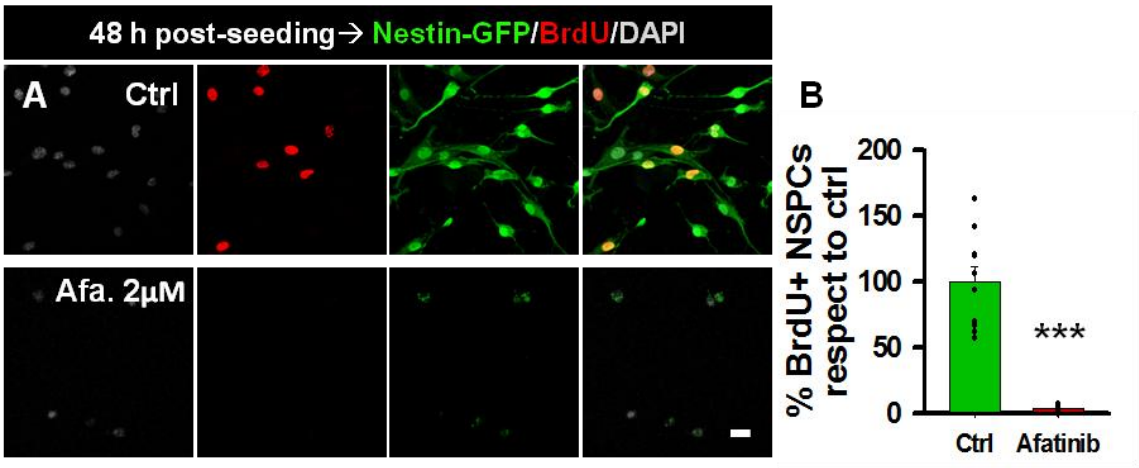

Figure R22. Irreversible blockage of EGFR by Afatinib led to cell death in NSPCs. A) Representative confocal images showing the normal growth and incorporation of BrdU of NSPCs in control conditions and the devastating effects produced by Afatinib, provoking massive cell loss. **B)** Quantification showing the reduction of BrdU-positive cells in the condition treated with Afatinib respect to the control condition. The data in each graph was normalized taking the mean of the control group as 100 ± SEM. *Scale bar 20 µm. ***p<0.001. Mann Whitney. Bars show mean ± SEM. Dots show individual data.*

Therefore, based on the results we concluded that Gefitinib was the appropriate candidate to inhibit EGFR in experimental MTLE *in vivo* and evaluate the effect of its

blockage over the neurogenic niche. The adverse effect of Afatinib *in vitro* dissuaded us to try it as a potential therapeutic strategy.

6.6.3. Pharmacological blockage of EGFR ameliorated the pathological response of NSCs after MTLE

Given the massive cell death provoked by Afatinib we chose to continue with Gefitinib to evaluate the effect of EGFR inhibition over the neurogenic niche and NSCs after intrahippocampal KA administration. In order to reduce the risk of lesion by direct injection (as a higher volume than for KA would be required), seeking to facilitate the potential applicability in humans and because Gefitinib does not cross the blood brain barrier (BBB) we resorted to intranasal administration (Chen, 2013; McKillop et al., 2004). This direct route to brain has been previously used for other anti-epileptic drug treatments validating its effectiveness (Barakat et al., 2006).

Previous studies have reported that proliferation increases early on (24 h) and reaches the peak at 72 h after the intrahippocampal injection of KA (Sierra et al., 2015). Although it was reported that a single dose of Gefitinib can reduce cell proliferation for 72 h (Pedersen et al., 2005), we administered it every 12 h starting right after the induction of MTLE in order to maximize its presence in the tissue when the peak of proliferation is observed (Sierra et al., 2015) **(Figure R23 A)**. As expected, the results showed that 72 h after KA proliferation was highly reduced in the DG (hilus and GCL+SGZ) when Gefitinib was administered compared to control animals treated just with the intranasal vehicle DMSO **(Figure R23 B)**. Further, the specific analysis of the neurogenic niche showed that the density of Ki67-expressing cells located in the SGZ and the percentage of NSCs expressing Ki67 were also significantly reduced in mice treated with Gefitinib right after KA administration **(Figure R23 C and R23 D)**. These results indicated that EGFR mediates the massive activation of NSCs and general proliferative activity that takes place in the neurogenic niche after seizures and furthermore, its blockage by the use of Gefitinib might be a potential candidate to preserve the NSC population and neurogenesis at mid and long-term.

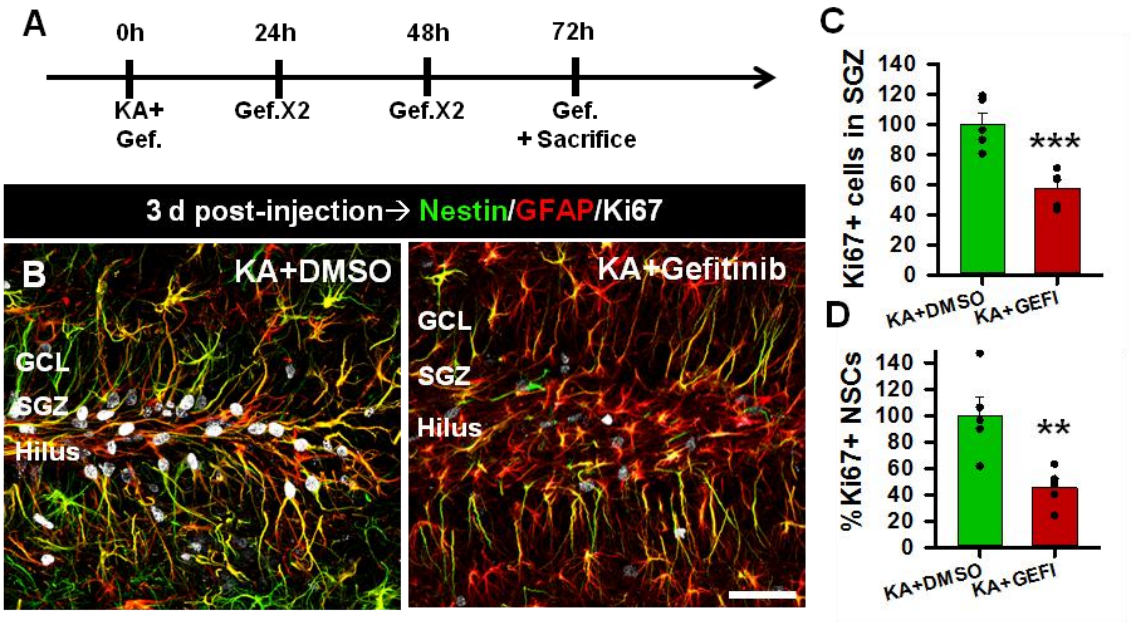

Figure R23. Administration of Gefitinib reduced the proliferation triggered in the neurogenic niche and NSCs after KA administration. A) Schematic of the experimental paradigm. After intrahippocampal administration of KA Gefitinib or DMSO (CTRL) were administered every 12 h until the moment of sacrifice 72 h post-KA. **B)** Representative confocal images showing the DG after KA administration in animals treated with either CTRL or Gefitinib. **C-D)** Quantifications of the density of Ki67-expressing cells in the SGZ (C) and the percentage of NSCs expressing Ki67 (D) both in KA+CTRL and KA+Gefitinib groups. The data in each graph was normalized taking the mean of the KA+CTRL group as 100 ± SEM. *CTRL: Control. GCL: Granule cell layer. GEFI: Gefitinib. KA: Kainic acid. SGZ: Subgranular zone. Scale bar 20 µm. **p>0.01, ***p<0.001. Student's t test. Bars show mean ± SEM. Dots show individual data.*

Given that the general proliferation in the SGZ and the early activation of NSCs was prevented when Gefitinib was administered right after inducing MTLE, we wondered whether the treatment with Gefitinib would be able to protect NSCs at mid-term, avoiding the characteristic React-NSC induction that leads to the exhaustion of the neurogenic capacity of the niche (Muro-García et al., 2019; Sierra et al., 2015; Valcárcel-Martín et al., 2020). Thus, we recapitulated the treatment with either DMSO or Gefitinib during the first 72 h after KA or saline (control group) administration, but this time the Nestin-GFP mice were sacrificed at 14 d after KA administration **(Figure R24 A)**.

At mid-term two of the main consequences in the MTLE model are the GCD and the lack of production of newly generated DCX-positive immature neurons (Muro-García et al., 2019; Sierra et al., 2015). Here, we show that the total number of DCX-expressing cells was reduced by 4-fold in the KA-injected animals treated with DMSO (KA+CTRL) in comparison to the saline-injected animals treated with DMSO

(CTRL+CTRL). Interestingly, in the KA-injected animals that were treated with Gefitinib (KA+GEFI) the total number of DCX-expressing cells was recovered up to control levels, strongly suggesting that Gefitinib-induced EGFR inhibition can conserve the neurogenic capacity of the hippocampal niche at mid-term after seizures. As a control measure for the effect of Gefitinib on the neurogenic niche in control conditions, we administered it after injecting the animals with saline (CTRL+GEFI). In this case, the total number of DCX-expressing cells was no different than in the saline-injected animals treated with DMSO (CTRL+CTRL), suggesting that the inhibition of EGFR by Gefitinib in control conditions does not affect neurogenesis **(Figure R24 B-C)**. We also analyzed the GCD (measured by DAPI staining as the thickness of the GCL from the hilus to the ML) in saline- and KA-injected animals after the treatment with either DMSO or Gefitinib. The results showed GCD when animals were injected with KA (KA+CTRL) respect to the control animals injected with saline (CTRL+CTRL). Following the same trend as observed before in the DCX-expressing cell numbers, when KA-injected animals were treated with Gefitinib (KA+GEFI) the observed GCD returned to control levels **(Figure R24 B-D)**. As expected, the GCD was similar in the saline-injected animals treated with DMSO (CTRL+CTRL) or Gefitinib (CTRL+GEFI). We concluded that the Gefitinib-induced inhibition of EGFR after KA administration is able to protect the neurogenic niche, at least in terms of DCX-expressing cell numbers and GCD. Furthermore, the induction of React-NSCs seemed to be reduced in KA-injected animals treated with Gefitinib in comparison to the ones treated with DMSO **(Figure R24 B)**, leading us to wonder whether EGFR could play a role in the React-NSC induction after KA, and whether the inhibition of the receptor using Gefinitib could protect them at mid-term.

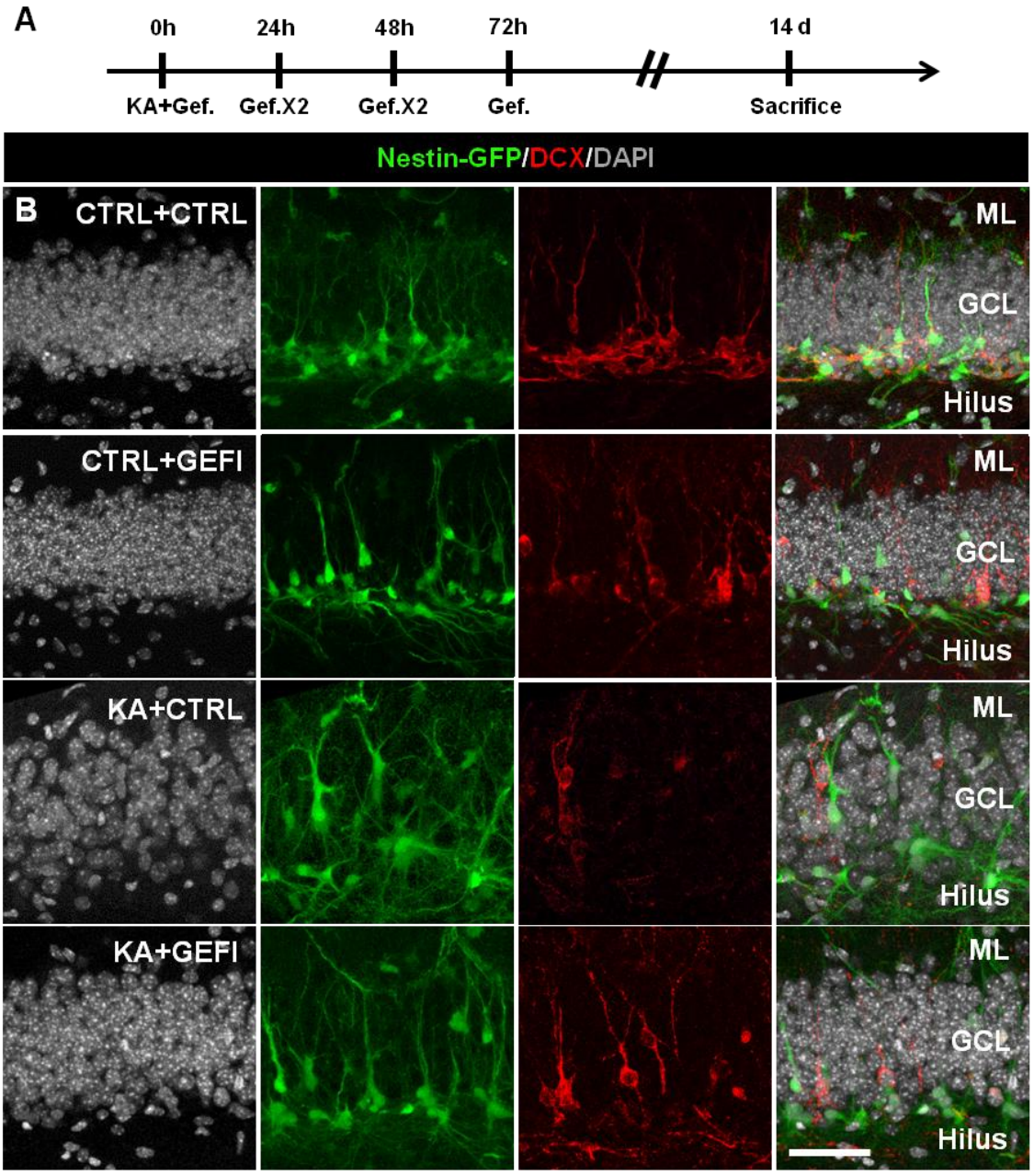
A
0h
24h
48h
72h
14 d
KA+Gef.
Gef.X2
Gef.X2
Gef.
Sacrifice
Nestin-GFP/DCX/DAPI
B
CTRL+CTRL
CTRL+GEFI
KA+CTRL
KA+GEFI
ML
GCL
Hilus

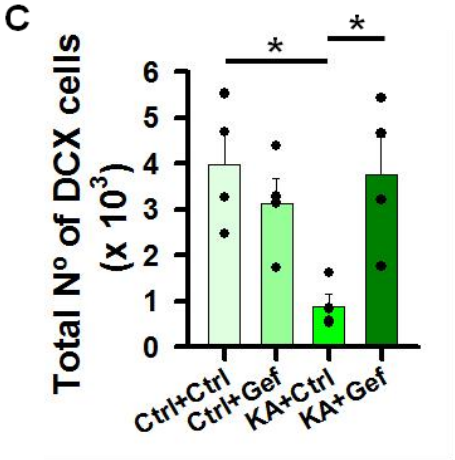
C
Total Nº of DCX cells (x 10³)
0
1
2
3
4
5
6
*
*
Ctrl+Ctrl
Ctrl+Gef
KA+Ctrl
KA+Gef

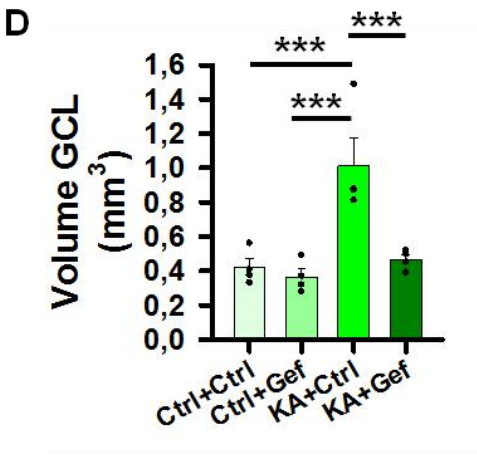
D
Volume GCL (mm³)
0,0
0,2
0,4
0,6
0,8
1,0
1,2
1,4
1,6
***
***
***
Ctrl+Ctrl
Ctrl+Gef
KA+Ctrl
KA+Gef

← Previous page. Figure R24. The intranasal treatment with Gefitinib protected the neurogenic niche 14 d after KA administration. A) Schematic of the experimental paradigm. After the intrahippocampal administration of either saline (control) or KA, Gefitinib or its vehicle (DMSO) were administered every 12 h during 72 h and the animals were sacrificed 14 d post-injection, forming four different experimental groups (CTRL+CTRL; CTRL+GEFI; KA+CTRL; KA+GEFI). **B)** Representative confocal images showing the DG after DMSO or Gefitinib administration in animals injected with either saline or KA. **C-D)** Quantifications of the total number of DCX-expressing cells in the GCL of each group (C) and the GCD (measured by DAPI) in each group (D). *CTRL: Control. GCL: Granule cell layer. GEFI: Gefitinib. KA: Kainic acid. ML: Molecular layer. SGZ: Subgranular zone. Scale bar 20 µm. *p<0.05, ***p<0.001. One-way ANOVA followed by multiple comparisons versus control group by Holm-Sidak post hoc test in (C) and Kruskal-Wallis followed by all pairwise comparisons by Student-Newman-Keuls post hoc test in (D). Bars show mean ± SEM. Dots show individual data.*

Thus, we next focused on the React-NSC induction after KA administration, evaluating the potential effect of Gefitinib treatment to revert it. We followed the same paradigm than before, injecting intrahippocampally saline or KA and intranasally treating the animals with either DMSO or Gefitinib within the first days after the injections, forming a total of four different groups (CTRL+CTRL; CTRL+GEFI; KA+CTRL; KA+GEFI). To evaluate the NSCs and their potential conversion into React-NSCs at mid-term we sacrificed the animals 14 days after the intrahippocampal injection **(Figure R25 A)**. One of the hallmarks of reactive astrocytes is the hypertrophied morphology with enlarged soma and thickened processes (Sofroniew, 2009) and NSCs were described to undergo similar changes after seizures, being a characteristic of the React-NSCs (Muro-García et al., 2019; Sierra et al., 2015). Therefore, to assess these morphological changes in our model we resorted to 3D Sholl analysis (Rodriguez et al., 2006), measuring the length, branching points and the process volume of the NSCs in Nestin-GFP mice.

The intrahippocampal administration of KA followed by intranasal administration of the Gefitinib vehicle DMSO as a control (KA+CTRL) provoked an increase in the process length, volume and number of branching points of NSCs compared to the control group (CTRL+CTRL), which translates in observably thicker and more arborized cells after KA, a characteristic morphology of a reactive phenotype in general and React-NSCs in particular **(Figure R25 B-E)**. Importantly, as we observed before in a general assessment of the neurogenic niche (GCD and DCX-expressing cell number), the reactive morphology induced by KA administration on the Nestin-GFP-expressing NSCs is reverted by Gefitinib administration (KA+GEFI). Noteworthy, even though NSCs in the KA+GEFI group did not show differences compared to the CTRL+CTRL and CTRL+GEFI group for the selected morphological criteria, it can be

appreciated that they lost their broccoli-like crown, another hallmark of React-NSCs. Nonetheless, we can conclude that EGFR was involved in the induction of React-NSCs and its inhibition via intranasal Gefitinib administration was able preserve the normal morphology of the NSCs at mid-term (14 d), although losing their characteristic broccoli-like crown **(Figure R25 B-E)**. On the other hand, Gefitinib administration in saline-injected animals (CTRL+GEFI) provoked changes in the NSCs too, decreasing their volume and the number of branching points in comparison to the control group (CTRL+CTRL) **(Figure R25 D-E)**.

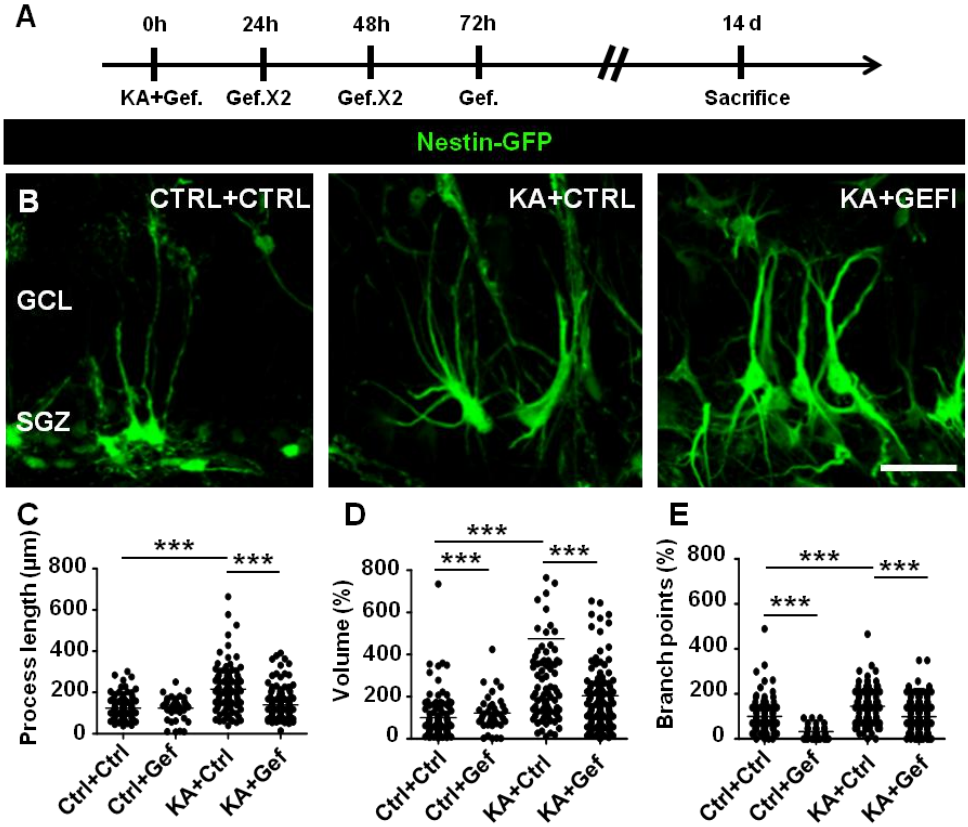

Figure R25. Gefitinib administration reduced the KA-induced React-NSC transformation at mid-term. A) Schematic of the experimental paradigm. After intrahippocampal administration of either saline (control animals) or KA, Gefitinib or its vehicle (DMSO) were administered every 12 h during 72 h and the animals were sacrificed 14 d post-injection, forming four different experimental groups (CTRL+CTRL; CTRL+GEFI; KA+CTRL; KA+GEFI). **B)** Representative confocal images showing the morphology of Nestin-GFP-expressing cells of each experimental group. **C-E)** Quantifications through 3D Sholl analysis of the length of the Nestin-GFP-expressing NSCs (C), the volume of the Nestin-GFP-expressing NSCs (D) and the number of branching points of the process of Nestin-GFP-expressing NSCs (E) in each experimental group. The data in each graph was normalized taking the mean of the CTRL+CTRL group as 100 ± SEM. *CTRL: Control. GCL: Granule cell layer. GEFI: Gefitinib. KA: Kainic acid. SGZ: Subgranular zone. Scale bar 20 µm. ***p<0.001. One-way ANOVA followed by multiple comparisons versus control group by Holm-Sidak post hoc test. Bars show mean ± SEM. Dots show individual data.*

6.7. The role of Zn^{+2} on the NSC activation and React-NSC induction after MTLE

Once demonstrated the participation of EGFR signaling pathway in the early response that takes place in the neurogenic niche and NSCs in the mouse model of MTLE, we moved on to look for possible mechanisms that could lead to its activation. In this line, we drew our focus towards Zn^{+2}, which has been reported to trigger EGFR signaling directly and also indirectly by promoting HB-EGF release (Samet et al., 2003; Wu et al., 2004). Moreover, Zn^{+2} has been reported to act as neuroprotector, preventing hyperactivation of the general neuronal circuit (Bancila et al., 2004; Takeda et al., 2003). Indeed, after seizures, when neuronal activity is exacerbated, Zn^{+2} has been shown to be increased in the HPF (Carrasco et al., 2000; Kasarskis et al., 1987; Mody and Miller, 1985). Nonetheless, its effect upon glial cells is unknown. We wondered about a possible role of Zn^{+2} over neurons to modulate the hyperactivation induced after seizures and we proposed it as an alternative mechanism that regardless of its role in neurons, might be triggering the EGFR-mediated massive activation and React-NSC induction after seizures.

6.7.1. The levels of Zn^{+2} increased in the neurogenic niche in MTLE

First, seeking to evaluate whether the described release of Zn^{+2} in the HPF after seizures (Carrasco et al., 2000; Kasarskis et al., 1987; Mody and Miller, 1985) specifically affected the neurogenic niche, we resorted to the Danscher staining to measure levels of histochemically reactive (free) Zn^{+2}. The Danscher staining requires an injection of sodium selenite at a very controlled time (30 minutes prior to the sacrifice) in all conditions in order to precipitate free Zn^{+2} without varying the size of Zn^{+2} granules (Danscher, 1981). Thus, we measured the amount of Zn^{+2} colocalizing with Nestin-GFP-expressing cells in the GCL+SGZ 72 h after either saline or KA intrahippocampal administration, when the peak of cell proliferation after KA administration has been reported to occur (Sierra et al., 2015). The results showed that Zn^{+2} was almost absent in the GCL+SGZ in control animals injected with saline, being restricted to the hilus where MFs contain synaptic vesicles with Zn^{+2} (Frederickson et al., 1983; Sindreu et al., 2003) and therefore with very little colocalization with Nestin-GFP-expressing cells. In contrast, after KA administration Zn^{+2} granules were spread throughout the GCL+SGZ, partially colocalizing with Nestin-GFP-expressing NSCs **(Figure R26 A)**. Indeed, the quantification of Zn^{+2} granules, measured in pixels, confirmed these observations. We first checked the size of Zn^{+2} granules as a control for the quality of the Danscher staining technique, observing no statistically significant

differences between saline and KA injections and thus discarding possible differences due to variability in the technique **(Figure R26 B)**. On the other hand, the number of Zn^{+2} granules colocalizing with Nestin-GFP-expressing cells in the GCL showed an almost 2-fold increase after KA administration compared to the control condition **(Figure R26 C)**. Therefore, we concluded that after KA Zn^{+2} was released and accumulated in the neurogenic niche close to or in the NSCs, which opened the possibility for a possible interaction between them.

Furthermore, given that the amount of Zn^{+2} increased in the HPF and specifically in the neurogenic niche after KA, we hypothesized that the expression of MTs would also be increased in these conditions. MTs are metalloproteins in charge of decreasing the intracellular labile Zn^{+2} levels, controlling Zn^{+2} homeostasis in the central nervous system (CNS) (Kägi and Schäffer, 1988; Vašák and Hasler, 2000). To test our hypothesis, we followed the same experimental timeline than in the previous experiments, sacrificing the animals at different time points after KA administration (1,5 h, 12 h, 24 h, 72 h) **(Figure R26 D)**. We determined the protein levels of MT1 and MT2 through WB and the results showed that the expression of both MT1 and MT2 begun to increase 12 h after KA in comparison to control levels **(Figure R26 E)**. Likewise, we determined mRNA levels of MT1, MT2 and also MT3 through RT-qPCR. In this case, the mRNA levels of MT1 increased after KA becoming significant from 24 h onwards. In addition, although not statistically significant, the same tendency can be observed for MT2. In contrast**,** the mRNA levels of MT3 were not altered at any of the time points after KA administration **(Figure R26 E-F)**. Altogether, the results suggested a massive release of Zn^{+2} in the HPF after KA that the system tried to contain through the increase of MT levels. Nonetheless, regarding its accumulation in the GCL, Zn^{+2} might be affecting NSCs, triggering or participating in their early response to the onset of MTLE.

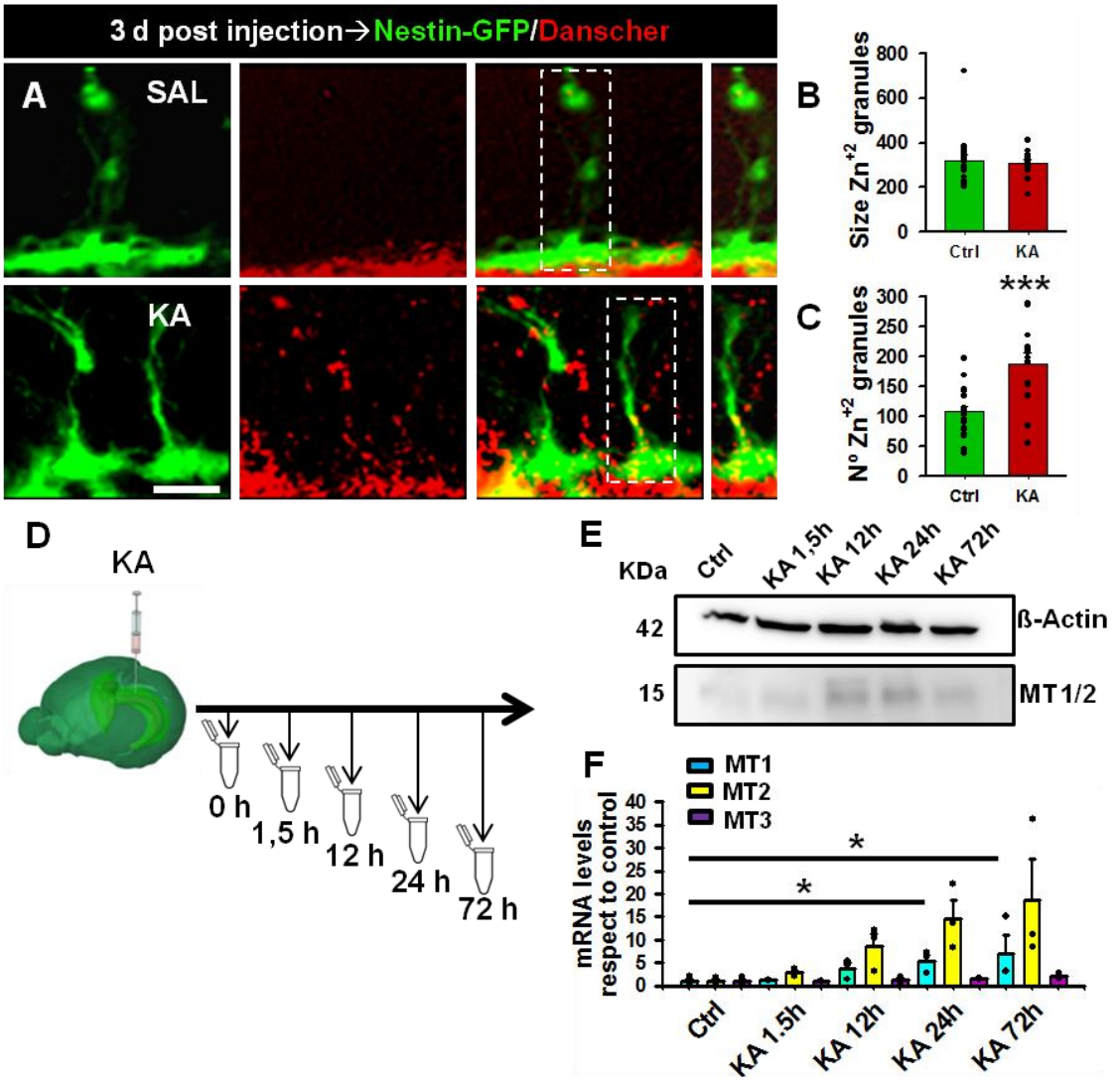

Figure R26. Zn^{+2} accumulated in the neurogenic niche after KA administration. A) Representative fluorescent microscope images showing the increase of Zn^{+2} in the neurogenic niche and its overlapping with NSCs 72 h after KA administration. Images were pseudo-colored (Zn^{+2} in red) for visualization purposes. **B)** Quantification of the size of Zn^{+2} granules as a control measure of the quality of the Danscher technique. The lack of significant differences between the control and KA group indicated an efficient application of the technique. **C)** Quantification of the number of Zn^{+2} granules colocalizing with Nestin-GFP-expressing cells, showing a significant increase after KA. **D)** Schematic of the experimental timeline. Hippocampi were collected at different time points after intrahippocampal KA administration **E)** WB of the hippocampi collected at different time points after KA administration showed increase in MT1 and MT2 expression from 12 h after KA onwards. **F)** RT-qPCR of the hippocampi collected at different time points after KA administration showing a tendency of MT1 and MT2 levels, but not MT3, to increase after 12 h. The data in each graph was normalized taking the mean of the control group as 1 ± SEM. *SAL: Saline. KA: Kainic acid. Scale bar 20 µm. *p<0.05, ***p<0.001. Student's t test in (B-C). Kruskal-Wallis followed by multiple comparisons versus control by Dunnet post hoc test for MT1 and MT3 and One way ANOVA followed by multiple comparisons versus control by Dunnet post hoc test for MT2 in (F). Bars show mean ± SEM. Dots show individual data.*

6.7.2. Zn^{+2} promoted proliferation in NSPCs in a dose-dependent manner

Next, we moved to evaluate the possible effect of Zn^{+2} over NSCs. For that, we resorted to cultured NSPCs to manipulate them in proliferating conditions and evaluate the effect exerted by the addition of different doses of Zn^{+2} (5, 10 and 400 μM). We cultured 25,000 NSPCs into laminin-coated coverslips, treated them with the correspondent dose of Zn^{+2} and gave them a BrdU pulse 1 h before fixation in order to determine cell proliferation. The results showed that after treating NSPCs with 5 μM Zn^{+2} there was an almost 3-fold increase in the number of cells that incorporated BrdU **(Figure R27 A-B)**. However, subsequent increase in the Zn^{+2} doses (10 μM and 400 μM) provoked a deleterious effect upon the NSPCs leading to a clear loss of cytoplasmic Nestin-GFP and the presence of bright and small pycnotic nuclei that suggested cell death **(Figure R27 A-B)**. These results indicated that Zn^{+2} induced proliferation in NSPCs at low doses but caused cell death at higher doses. In light of the obtained results, we wondered about the possible role of Zn^{+2} over NSCs in MTLE conditions *in vivo*.

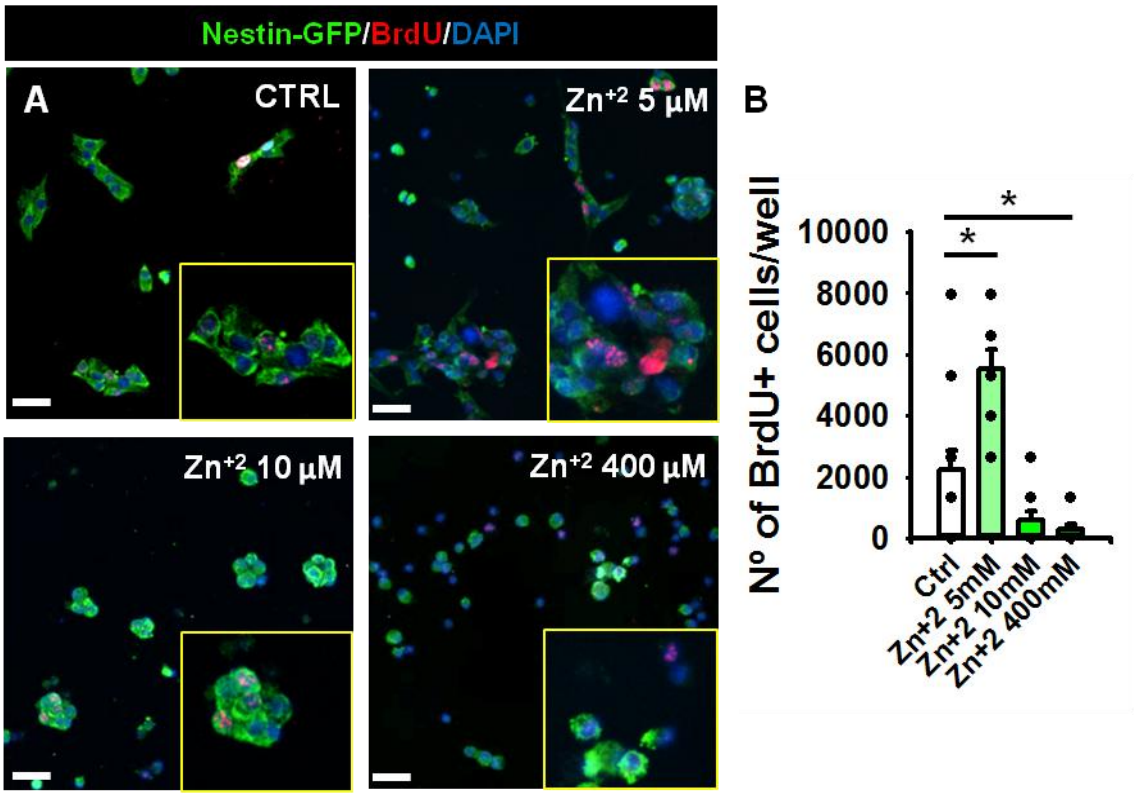

Figure R27. Zn^{+2} affected NSPCs in a dose-dependent manner. A) Representative confocal images showing proliferating NSPCs. Images illustrate a higher number of NSPCs that incorporated BrdU after a treatment with 5 μM of Zn^{+2}, while the number decreased with higher doses. Likewise, the small and rounded nuclei observed when NSPCs were treated with 10 μM or 400 μM indicated that these doses of

Zn^{+2} caused cellular death. **B)** Quantification of the total number of NSPCs that incorporated BrdU in each experimental condition. There was a significant increase when cells were treated with 5 µM of Zn^{+2}, while the number decreased with higher doses. CTRL: Control. *Zn^{+2}: Zinc. Scale bar 20 µm. *p<0.05. Kruskal-Wallis followed by multiple comparisons versus control by Dunn post hoc test. Bars show mean ± SEM. Dots show individual data.*

6.7.3. The intrahippocampal administration of Zn^{+2} mimicked the alterations produced in the neurogenic niche in MTLE

Taking into account that after KA administration Zn^{+2} spread in the GCL, colocalizing with Nestin-GFP-expressing cells, and that *in vitro* it can affect cultured NSPCs promoting their proliferation, we next moved to evaluate the effects of Zn^{+2} administration *in vivo* on the neurogenic niche, hypothesizing that it may be playing an important role on the massive activation and React-NSC induction that is observed after seizures. To test this, we injected intrahippocampally saline (control group) or different doses of Zn^{+2} (5, 20 or 30 nM) and we checked the effects over the neurogenic niche and NSCs 7 days later. 24 h before sacrificing the animals we injected BrdU intraperitoneally to identify proliferating cells **(Figure R28 A)**. The results showed no observable effect of Zn^{+2} over the neurogenic niche at 5 nM (data not shown) but in contrast, a strong dose-dependent effect causing the alteration of the neurogenic niche could be observed with higher doses. With the doses of 20 nM and 30 nM GCD, increase of BrdU-positive cells and the reactive-like morphology and displacement of the NSCs were observable **(Figure R28 B-D)**, replicating some of the main effects that define the KA-induced response in the neurogenic niche.

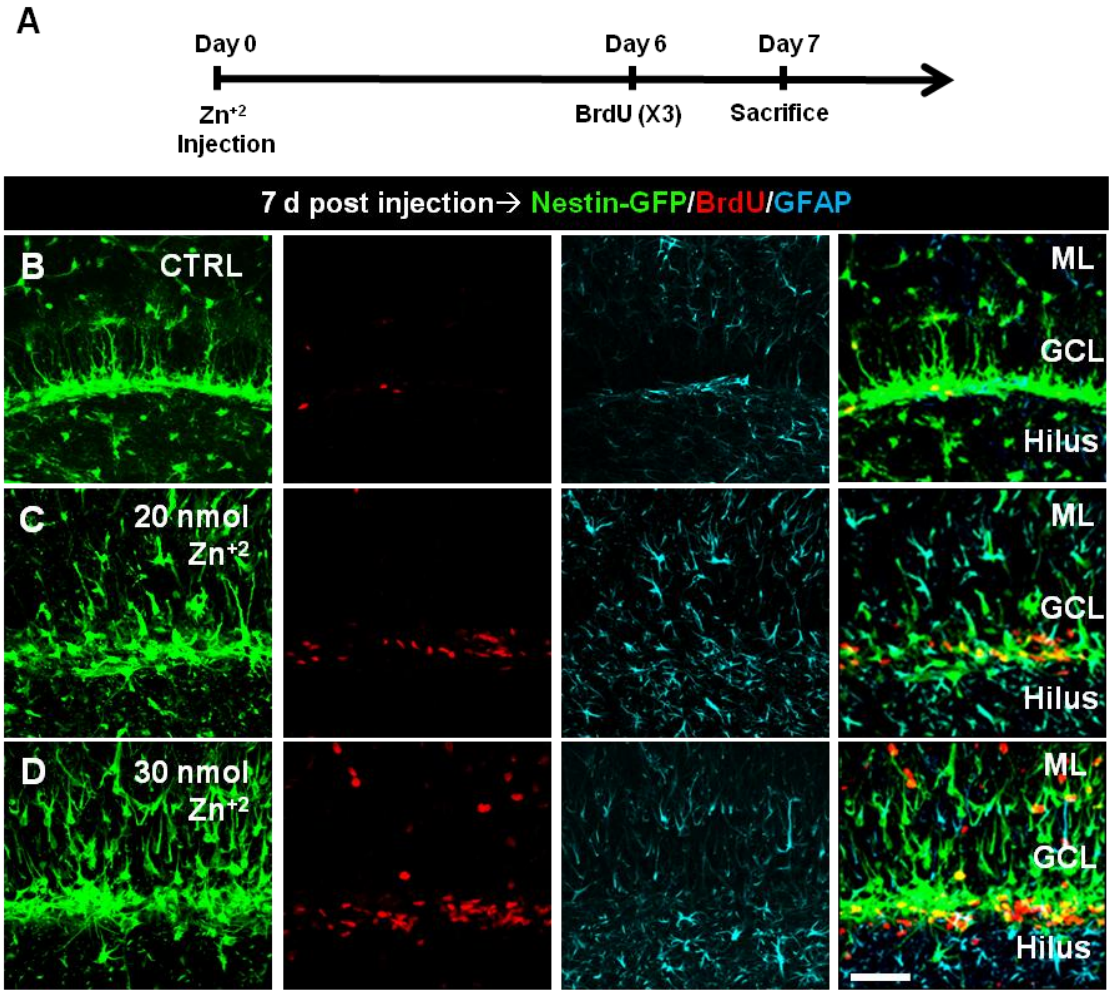

Figure R28. Intrahippocampal Zn^{+2} disrupted the neurogenic niche in a dose-dependent manner. A) Schematic of the experimental timeline. Nestin-GFP mice were sacrificed 7 d after intrahippocampal Zn^{+2} administration. 24 h before the sacrifice 3 BrdU intraperitoneal injections were administered, separated by 3 h intervals in order to mark the proliferating cells. **B-D)** Representative confocal images showing the effect of intrahippocampal saline (CTRL) (B), 20 nM of Zn^{+2} (C) or 30 nM of Zn^{+2} (D) administration. It can be observed that Zn^{+2} affected the neurogenic niche provoking GCD, increase of BrdU-positive cells and morphological and spatial alterations in the NSCs, becoming reactive-like and abandoning the SGZ towards the ML. *GCL: Granule cell layer. ML: Molecular layer. Zn^{+2}: Zn^{+2}. Scale bar 20 µm.*

To further characterize the effects produced by Zn^{+2}, we decided to follow this study using the minimal amount (20 nM) that produced alterations in the neurogenic niche. We followed the previous experimental timeline, sacrificing mice 7 d after Zn^{+2} intrahippocampal administration and injecting BrdU intraperitoneally 24 h prior to the sacrifice **(Figure R29 A-B)** and we assessed the replication of some of the main characteristics that define the neurogenic niche disruption after seizures. We first evaluated the GCD (Houser, 1990) basing on DAPI staining and measuring the

thickness of the GCL and then we evaluated the number of cells that incorporated BrdU in the neurogenic niche. The results showed significant nuclei dispersion in the GCL of the Zn^{+2}-injected animals compared to saline-injected control animals **(Figure R29 D)**. Moreover, there was an almost 4-fold increase in the density of cells that incorporated BrdU in the neurogenic niche after Zn^{+2} administration **(Figure R29 E)**. These results further proved that Zn^{+2} administration provoked changes in the neurogenic niche that shared similitude with the effects observed after KA administration.

We next moved to assess the effect of Zn^{+2} administration specifically upon NSCs. We quantified the density of NSCs in the GCL in both experimental groups and also the proportion of NSCs that incorporated BrdU. Interestingly, the density of NSCs 7 days post-Zn^{+2} infusion showed a tendency to reduce **(Figure R29 F)**, but the proportion of BrdU-positive NSCs respect to the total number of NSCs did not show significant differences **(Figure R29 G)**. This suggested an effect of Zn^{+2} over the neurogenic niche without affecting NSC activation, which would be differentially regulated. Yet, we cannot exclude a transitory activation of the NSCs early after Zn^{+2} administration that will shut off earlier than 7 d post-injection, a time-point when NSCs would acquire control activation levels again.

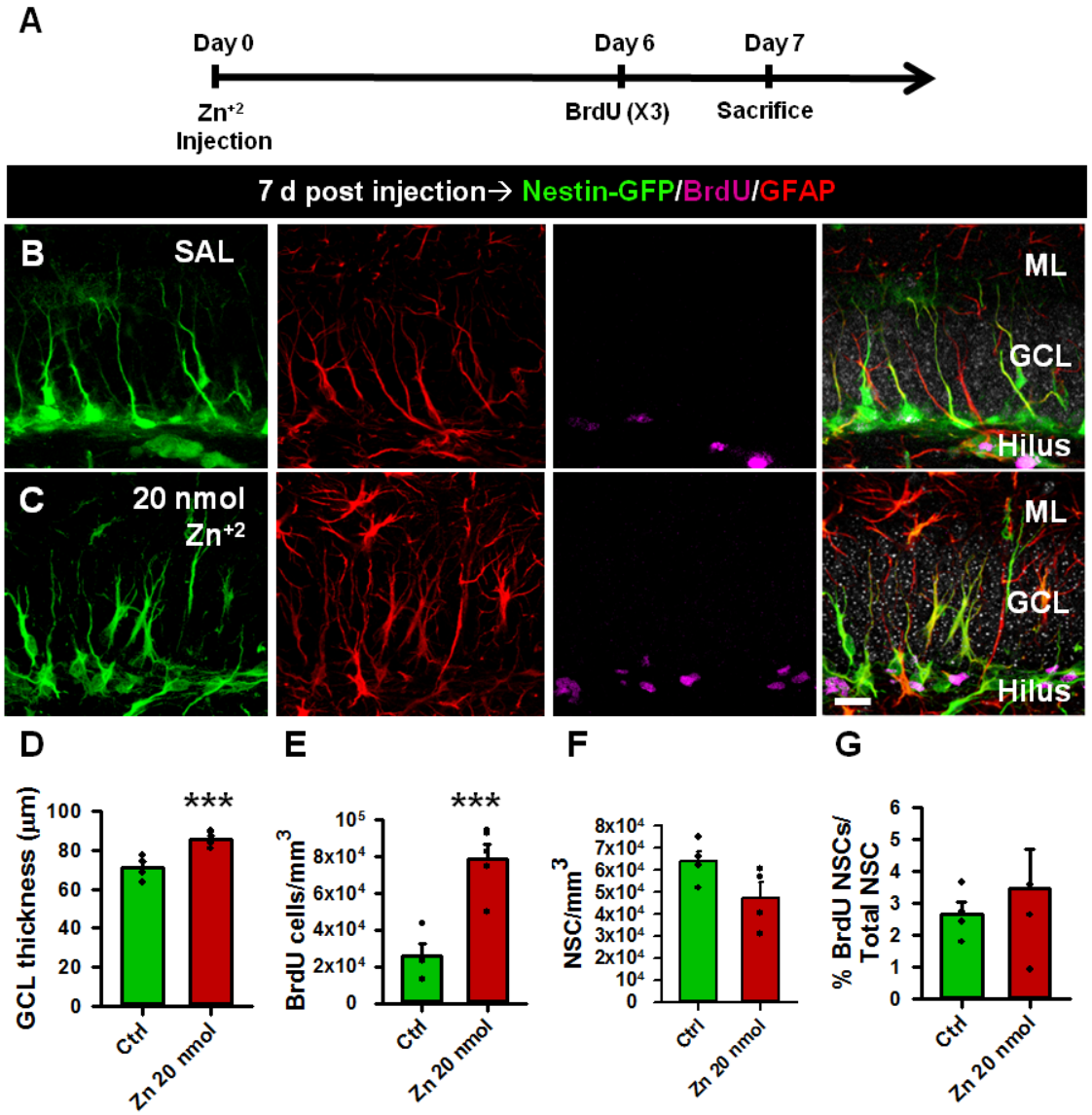

Figure R29. The intrahippocampal administration of Zn^{+2} recapitulated some of the KA-induced effects in the neurogenic niche. A) Schematic of the experimental timeline. Nestin-GFP mice were sacrificed 7 d after intrahippocampal Zn^{+2} administration. 24 h before the sacrifice 3 BrdU intraperitoneal injections were administered, separated by 3 h intervals in order to mark the proliferating cells. **B-C)** Representative confocal images of the neurogenic niche after saline (CTRL) (B) or 20 nM Zn^{+2} (C) intrahippocampal administration. **D)** Quantification of the GCD based on DAPI staining. The results showed a significant increase in the GCL thickness after intrahippocampal Zn^{+2} administration. **E)** The quantification of the density of BrdU-positive cells showed a significant increase in the neurogenic niche after Zn^{+2} administration. **F)** Quantification of the density of NSCs. The results showed a trend to decrease in the density of NSCs after Zn^{+2}, although it was not significant. **G)** Quantification of the percentage of activated NSCs over the total NSC number. The results showed no statistical differences. *GCL: Granule cell layer. ML: Molecular layer. Zn^{+2}: Zinc. Scale bar 20 µm. ***p<0.001. Student's t test. Bars show mean ± SEM. Dots show individual data.*

6.7.4. The effect of Zn^{+2} on the neurogenic niche was EGFR-mediated

Our previous results showed that Zn^{+2} was massively released after KA, getting accumulated into the neurogenic niche and being able to provoke its disruption in a similar manner to what occurs in the experimental MTLE model. Moreover, other studies indicate that Zn^{+2} can stimulate the EGFR signaling pathway (Samet et al., 2003; Wu et al., 2004), meaning that their interplay could be driving or contributing to the response observed in the neurogenic niche and NSCs after seizures. To test whether the presence of Zn^{+2} could modulate NSCs in an EGFR-mediated way, we resorted again to cultured NSPCs. In order to observe a potential effect of Zn^{+2} over EGFR, we first needed to shut down the growth factor signaling that is normally active in cultured NSPCs to maintain them in proliferating conditions, due to the application of EGF and FGF in the medium. For this purpose, we incubated the NSPCs with growth factor-starved media and our preliminary data showed a remarkable loss of phosphorylated ERK1/2 at 2 h (data not shown). Thus, NSPCs were dissociated and incubated in growth factor-starved media for 2 h in order to silence the growth factor-induced EGFR activation and properly test the potential activation of the receptor by Zn^{+2} administration.

We evaluated the capacity of Zn^{+2} to activate EGFR on NSPCs by following an adaptation of the protocol previously described (Wu et al., 2004). In addition to the starved group (Stvd), we administered either 100 ng/ml EGF as a control of the EGFR activation (EGF) or 200 μM Zn^{+2} (Stvd+ Zn^{+2}) creating two additional groups. Furthermore, we added another group in which NSPCs were pretreated with 2 μM Gefitinib for 60 min prior to the 200 μM Zn^{+2} administration (Stvd+ Zn^{+2}+Gef). Protein extracts were blotted sequentially against EGFR Y845 and Y1068 and also against the total EGFR in order to perform the ratio of receptor phosphorylation **(Figure R30 A)**. Interestingly, Zn^{+2}-administrated NSPCs showed a mild phosphorylation of the residue Y845 in comparison to the starved NSPCs, being fully blocked in presence of Gefitinib **(Figure R30 C)**. However, Y1068 phosphorylation was triggered in the presence of EGF, but not in the presence of Zn^{+2} **(Figure R30 D)**.

Furthermore, we analyzed the downstream signaling pathway of EGFR ERK1/2, highly related with cell proliferation (Downward et al., 1984). The results showed that Zn^{+2} exposure in starved conditions was able to increase the phosphorylated ERK1/2 signaling and importantly, the inhibition of EGFR reduced its phosphorylation to basal levels **(Figure R30 B; E)**. These results suggested that on NSPCs Zn^{+2} was able to

directly activate EGFR on its Y845 phosphorylation site and it can also activate its downstream signaling pathway ERK1/2, while inhibiting EGFR was sufficient to interrupt this phosphorylation loop and inactivate the receptor.

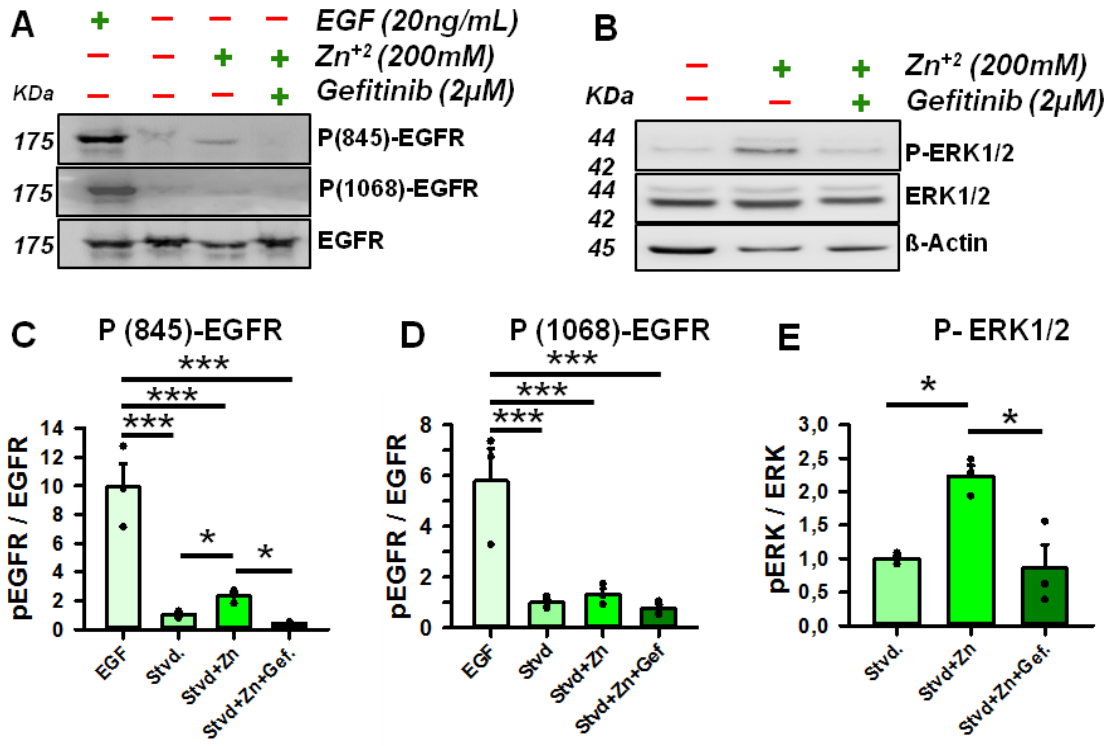

Figure R30. Zn^{+2} triggered the activation of EGFR signaling pathway on NSPCs. A) WB for Y845-EGFR, Y1068-EGFR and total EGFR in EGF-stimulated, starved, Zn^{+2}-stimulated, and Zn^{+2}-stimulated after Gefitinib treatment conditions. **B)** WB for P-ERK1/2, total ERK1/2 and the control ß-Actin in starved, Zn^{+2}-stimulated, and Zn^{+2}-stimulated after Gefitinib treatment conditions. **C)** Quantification of the WB showing a 10-fold decrease in the ratio of Y845-EGFR respect to the total EGFR in NSPCs treated with EGF compared to starved cells. Likewise, Zn^{+2} increased the Y845 phosphorylation significantly, although this activation was blocked by Gefitinib pre-treatment. **D)** Quantification of the WB showing a 6-fold increase in the ratio of Y1068-EGFR respect to the total EGFR in NSPCs treated with EGF compared to starved cells. In this case, Zn^{+2} was not able to trigger Y1068-EGFR activation, and the previous treatment with Gefitinib did not cause any alteration neither. **E)** Quantification of the WB showing stimulation of P-ERK1/2 ratio respect to the total ERK1/2 in presence of Zn^{+2}, and its consequent inhibition after Gefitinib pre-treatment.**p<0.05 and ***p<0.001. Kruskal-Wallis followed by all pairwise comparisons by Student-Newman-Keuls post hoc test in (C-D).One-way ANOVA followed by all pairwise comparisons by Holm-Sidak post hoc test in (E). Bars show mean ± SEM. Dots show individual data.*

Observing that Zn^{+2} was capable of stimulating EGFR on NSPCs, at least in the Y845 phosphorylation site, we next moved to assess whether the neurogenic niche disruption that we observed after Zn^{+2} administration *in vivo* could be driven by EGFR

activation. For this purpose, we tested the effect of EGFR inhibition in Nestin-GFP mice that received a single dose of Zn^{+2} 20 nM intrahippocampally administering Gefitinib intranasally during the first 72 h post-injection following the same paradigm used for KA-administration experiments **(Figure R23-R25)**. 24 h before sacrifice the animals received three doses of intraperitoneal BrdU in order to track dividing cells **(Figure R31 A)**. As expected, the results showed that the intrahippocampal Zn^{+2} administration significantly increased the density of cells that incorporated BrdU in the neurogenic niche. Importantly, EGFR inhibition via Gefitinib administration reduced this Zn^{+2}-induced increase of BrdU-positive cells, while Gefitinib administration to saline-injected mice did not cause any alteration **(Figure R31 B-C)**. These results demonstrated the involvement of EGFR in the Zn^{+2}-induced response of the neurogenic niche, suggesting the possible interplay between both factors in MTLE conditions.

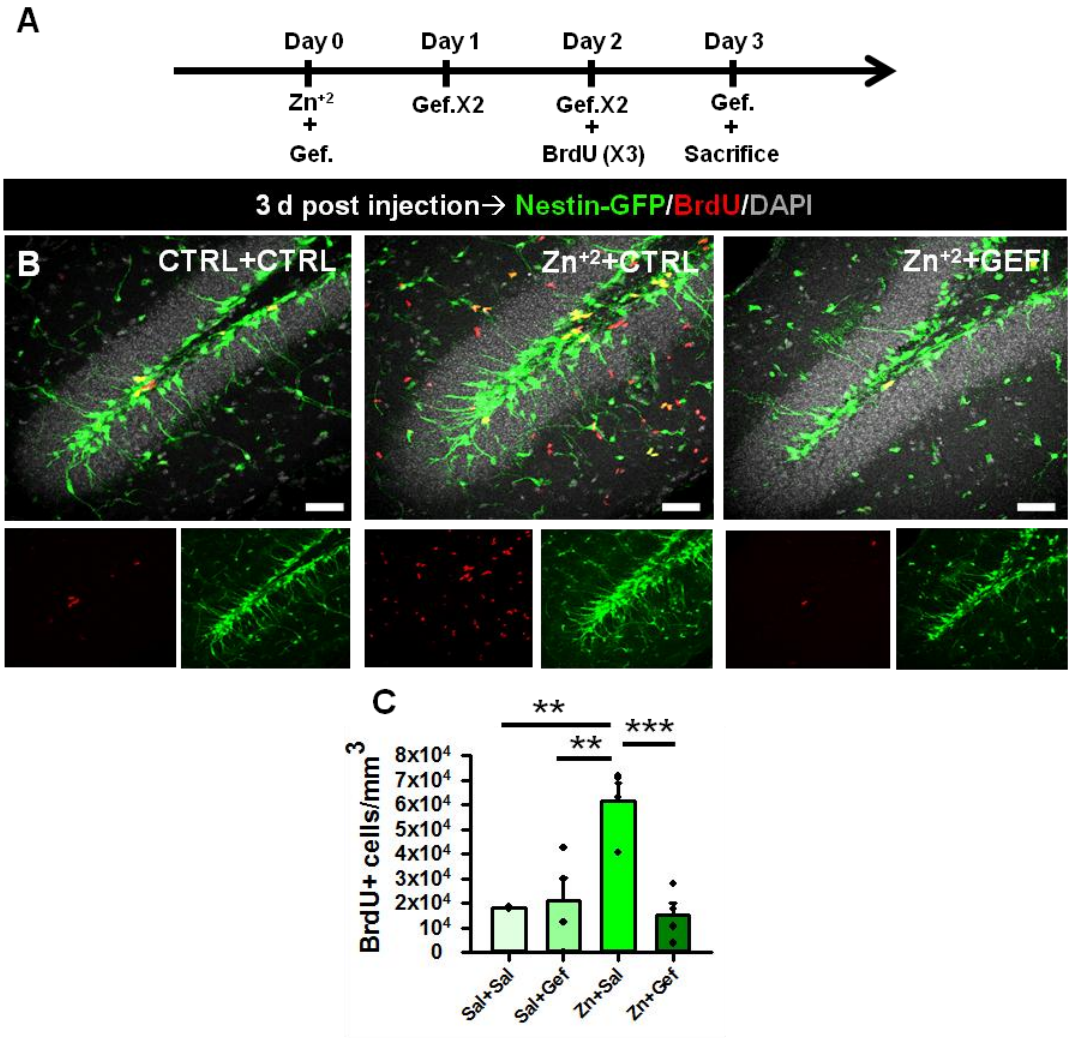

← Previous page. Figure R31. Zn^{+2} promoted proliferation in the neurogenic niche of the DG in an EGFR-mediated manner. A) Schematic of the experimental timeline. Nestin-GFP mice were sacrificed 72 h after intrahippocampal saline (CTRL) or Zn^{+2} administration after receiving 6 intranasal treatments with DMSO (CTRL) or Gefitinib in 12 h intervals. 24 h before the sacrifice 3 BrdU intraperitoneal injections were administered, separated by 3 h intervals in order to mark the proliferating cells. **B)** Representative confocal pictures of the DG of mice intrahippocampally injected with saline (CTRL) or Zn^{+2} and intranasally treated with DMSO (CTRL) or Gefitinib. **C)** Quantification of the density of BrdU-positive cells in the GCL showing an increase after intrahippocampal Zn^{+2} administration compared to control animals injected with saline. The increase in the density of BrdU-positive cells was reduced with Gefitinib treatment after Zn^{+2} administration. CTRL: Control. *SAL: Saline. Zn^{+2}: Zn^{+2}. Scale bar 20 µm. **p<0.01. ***p<0.001. One-way ANOVA followed by all pairwise comparisons by Holm-Sidak post hoc test. Bars show mean ± SEM. Dots show individual data.*

6.7.5. Zn^{+2} chelation in MTLE increased cell death in the GCL

Considering the high presence of Zn^{+2} in the GCL at 72 h post KA and its effects over the neurogenic niche, mediated by the EGFR signaling pathway, we speculated that Zn^{+2} chelation could be a valid strategy to minimize the alterations observed in the neurogenic niche after KA administration. To test this hypothesis, we performed intrahippocampal injections of either saline (CTRL) or KA and administered subcutaneously 5 mg/kg of the Zn^{+2} chelating agent TPEN or its vehicle saline (CTRL) as previously described (Kim et al., 2012) twice a day during 7 consecutive days, sacrificing the animals right after the treatment. We evaluated the density of pyknotic cells in the GCL as a measure of the efficiency of TPEN. The results showed that the number of dying cells identified by condensed DAPI staining tended to increase after KA (KA+CTRL) compared to saline–injected mice (CTRL+CTRL). On the other hand, the TPEN administration after an intrahippocampal injection of saline (CTRL+TPEN) did not provoke any alteration in the GCL. Unexpectedly, dead cells in the GCL increased in the animals injected with KA and treated thereafter with TPEN (KA+TPEN) compared to the control groups (CTRL+CTRL; CTRL+TPEN) and showed a tendency to increase compared to the KA-injected animals treated with vehicle (KA+CTRL) **(Figure R32 A-B)**. Therefore, these results revealed that chelation of Zn^{+2} further increased cell death, discarding this strategy as a potential therapeutic approach in MTLE.

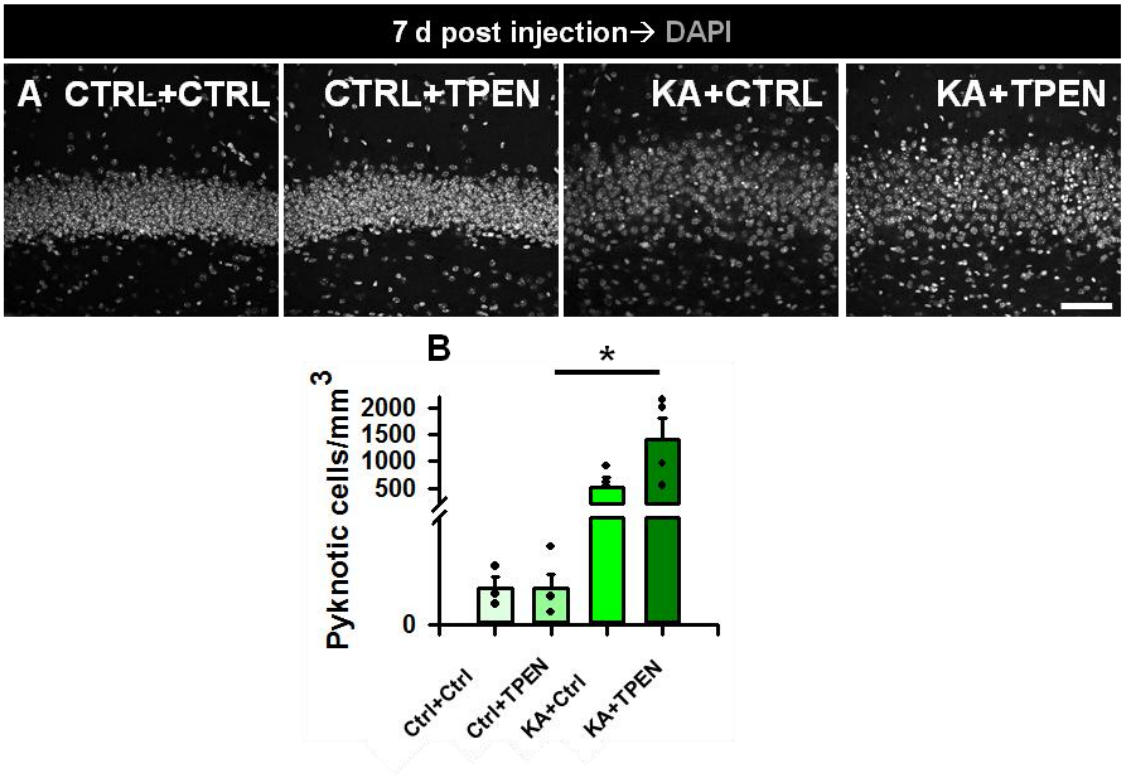

Figure R32. Chelation of Zn^{+2} in MTLE further increased cell death in the GCL. A) Representative confocal pictures of the GCL after intrahippocampal saline (CTRL) or KA injections and vehicle or TPEN subcutaneous treatments (CTRL or TPEN). **B)** Quantification of the density of pyknotic cells in the GCL. There was a significant increase of pyknotic cells after KA that TPEN treatment further increased. *CTRL: Control. KA: Kainic acid. SAL: Saline. Scale bar 20 µm. *p<0.05. Kruskal-Wallis followed by all pairwise comparisons by Dunn post hoc test. Bars show mean ± SEM. Dots show individual data.*

The obtained results suggested that EGFR and Zn^{+2} played an important role in the response of the neurogenic niche after seizures. Indeed, Zn^{+2} was able to stimulate the phosphorylation of EGFR on its Y845 tyrosine site, suggesting it as a possible mechanism that contributes to the activation of EGFR after seizures. Interestingly, cellular internalization of Zn^{+2} has been reported to trigger the release of HB-EGF from the cell membrane, which is a potent ligand for EGFR (Samet et al., 2003; Wu et al., 2004). Thus, we proceeded to evaluate whether HB-EGF could be mediating the activation of EGFR after KA administration.

6.8. HB-EGF was massively released in the DG after KA

The previous results pointed towards an integrated role of Zn^{+2} and EGFR in the response after KA. Given that cellular reuptake of Zn^{+2} can trigger the release of HB-EGF from the cell membrane (Samet et al., 2003; Wu et al., 2004), and Zn^{+2} was massively released in the GCL after seizures, we decided to explore whether HB-EGF

could be triggering the EGFR-mediated effect in MTLE. HB-EGF is able to affect proliferation, differentiation and morphology of cultured astroglia (Jia et al., 2018; Kornblum et al., 1999; Puschmann et al., 2014) and it has been reported to be upregulated after intraperitoneal KA administration (Opanashuk et al., 1999). Moreover, HB-EGF intensely stimulates astroglial migration (Faber-Elman et al., 1996). Therefore, given that after KA we already found that NSCs increased the EGFR expression and were later mislocalized and disorganized, we sought to characterize HB-EGF changes in the DG in our intrahippocampal KA administration model.

Following the same experimental timeline than before, we administered KA intrahippocampally to 2-month old Nestin-GFP mice and collected the injected hippocampi at different times after KA (1.5 h, 12 h, 24 h, 72 h) **(Figure R33 A)**. To evaluate the amount of released HB-EGF in the HPF we measured the HB-EGF in tissue at each time point after KA through ELISA and compared the results to the amount of HB-EGF in saline-injected (CTRL) animals. The results showed a statistically significant increase of around 25% at 12 h after KA compared to the control condition in which mice were injected with saline. However, this increase reached its peak at 24 h and rapidly decreased thereafter **(Figure R33 B)**. Since the ELISA approach gave us information about the overall HB-EGF levels in the whole HPF rather than in the neurogenic niche, we resorted to IHC in order to evaluate the presence of the ligand specifically in the DG 72 h after saline or KA injection. The results showed that HB-EGF staining was enriched in the immediate upper ML and the hilar region, although the GCL did not show observable differences compared to control **(Figure R33 C)**. However, we cannot exclude the occurrence of a transitory increase of HB-EGF in the GCL prior to 72 h after KA administration. Therefore, HB-EGF could be playing a role specifically in the DG. Given the high expression observed in the ML and its reported role as chemoattractant (Faber-Elman et al., 1996), we speculated of a possible role of HB-EGF in the migration of NSCs towards the ML after seizures.

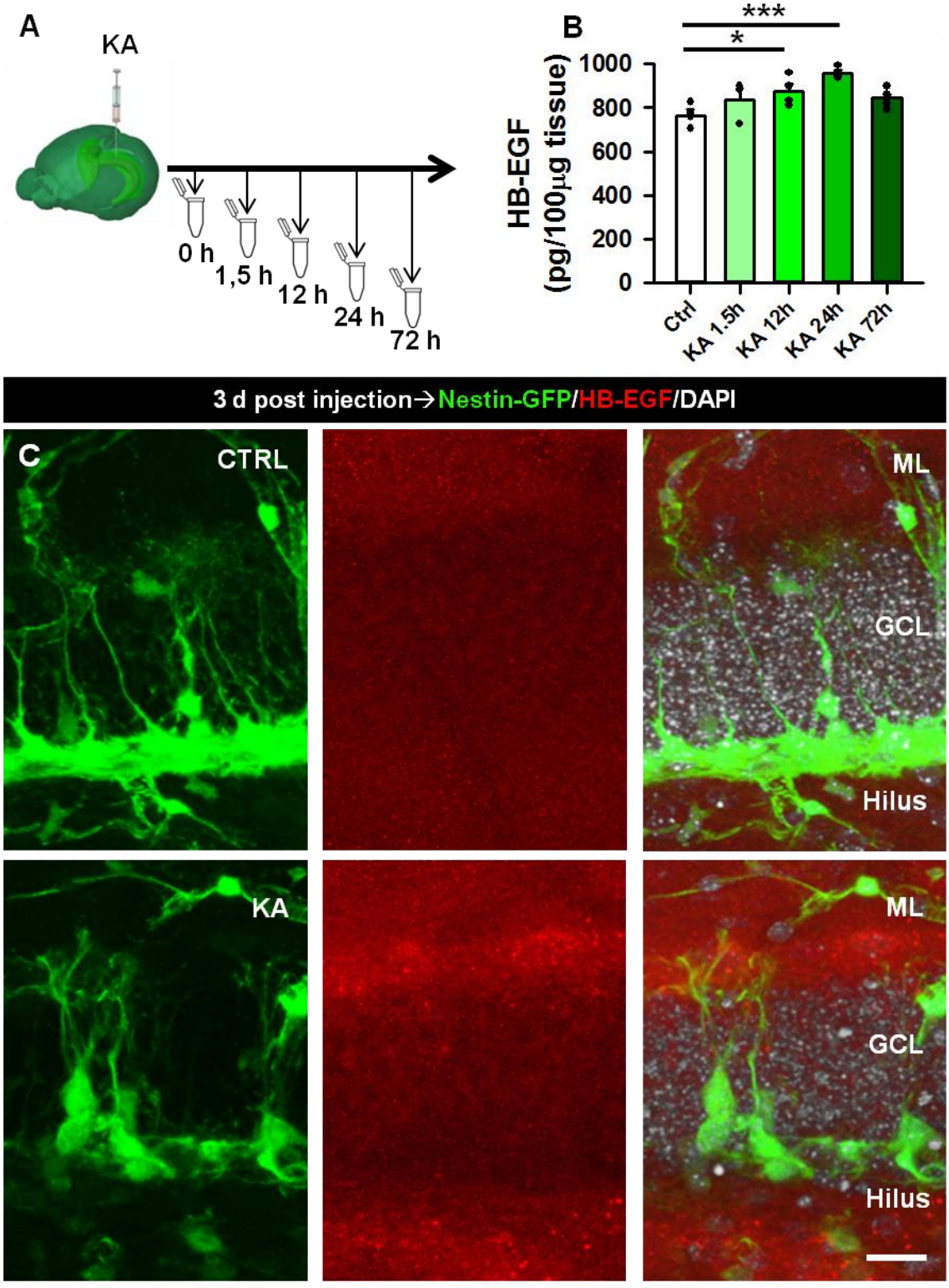

Figure R33. HB-EGF increased in the DG early after KA administration. A) Schematic of the experimental timeline. Hippocampi were collected at different time points after intrahippocampal KA administration. **B)** Measurement of the amount of HB-EGF in tissue through ELISA at different time points after KA administration. There was a significant increase at 12 h and 24 h after KA in the number of pg/µg of HB-EGF, decreasing thereafter. **C)** Representative confocal pictures of HB-EGF expression in the DG.

The staining showed that while HB-EGF increased in the ML and hilus after KA administration, the GCL remained unaltered compared to control animals injected with saline. *GCL: Granule cell layer. KA: Kainic acid. ML: Molecular layer. SAL: Saline. Scale bar 20 µm. ***p<0.001. One-way ANOVA followed by multiple comparisons versus control group by Holm-Sidak post hoc test. Bars show mean ± SEM. Dots show individual data.*

Given that HB-EGF was released in the DG after KA administration, we next moved to assess the potential contribution of NSCs in the release of HB-EGF after KA and the capacity of HB-EGF to activate EGFR and its downstream signaling pathway ERK1/2 in cultured hippocampal NSPCs. We maintained cultured NSPCs in proliferating conditions and analyzed through IHC the presence of HB-EGF in the NSPCs. The results showed that even though HB-EGF expression was present in some cultured NSPCs in comparison to the control condition without primary HB-EGF antibody, the majority of NSPCs did not show any HB-EGF labeling **(Figure R34 A)**. However, given that NSPCs were constantly maintained in proliferating conditions, we wondered about the possibility of HB-EGF being constantly released from the cell membrane and acting as a ligand for EGFR. Thus, we evaluated the HB-EGF amount by ELISA separately in NSPCs (Pellet), their culture media (Supernatant) and compared the results to a culture media without NSPCs as a control group (Media). The results showed a significant increase of around 200% in the amount of HB-EGF in the cultured media containing NSPCs (Supernatant) compared to the control media (Media) and cellular pellet (Pellet), demonstrating that NSPCs were able to release HB-EGF to the extracellular media in proliferating conditions **(Figure R34 B)**.

Next, to test whether HB-EGF was able to trigger the activation of EGFR signaling pathway, we first starved NSPCs from EGF and FGF to shut off the EGFR signaling pathway. Then, we stimulated the starved NSPCs with HB-EGF and also with HB-EGF and Zn^{+2} together, aiming to get the most similar condition to *in vivo* and test the capacity of HB-EGF to activate EGFR in NSPCs. Furthermore, we added another experimental group pre-treating the NSPCs with Gefitinib and then exposing them to HB-EGF and Zn^{+2}. We measured the activation of EGFR on its phosphorylation sites Y845 and Y1068 and also the phosphorylation of the EGFR downstream signaling pathway ERK1/2. The results showed that HB-EGF was able to strongly phosphorylate EGFR at both Y845 and Y1068 residues, as well as ERK1/2. Remarkably, Zn^{+2} stimulation did not produce any significant additive effect, probably prevailed by the excess of HB-EGF. Finally, the pre-treatment with Gefitinib was able to block phosphorylation on Y845 and Y1068 even in the concomitant presence of both Zn^{+2} and HB-EGF, as well as to reduce the phosphorylation of ERK1/2 **(Figure R34 C-D)**.

These results pointed towards the possible interaction of HB-EGF and EGFR to trigger the effects observed in the neurogenic niche after KA administration, perhaps regulated by Zn^{+2}-induced release of HB-EGF.

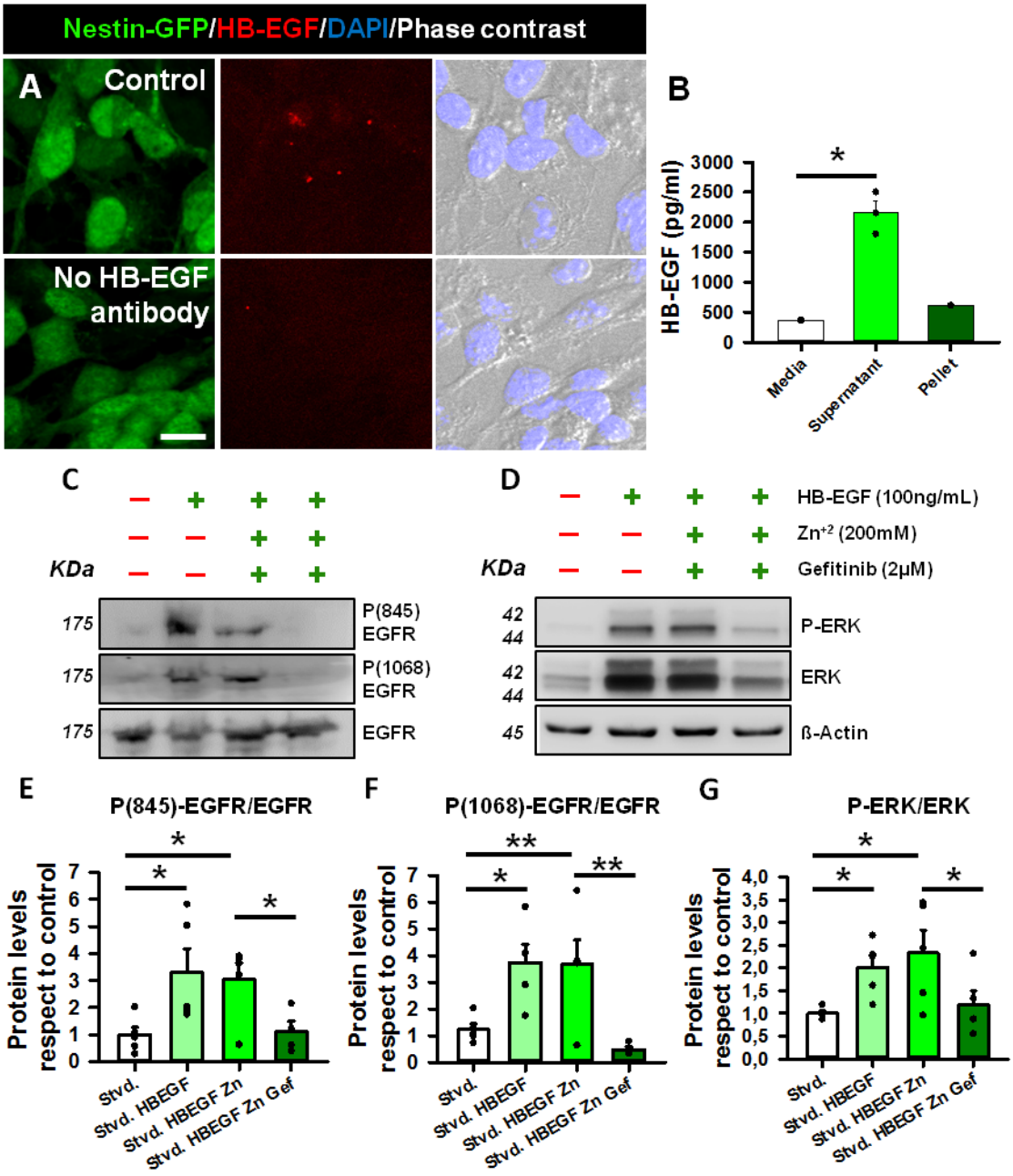

Figure R34. HB-EGF triggered the activation of the EGFR signaling pathway in cultured NSPCs. A) Representative confocal pictures of the HB-EGF expression on cultured NSPCs after IHC both with primary HB-EGF antibody and without the primary antibody. **B)** Quantification by ELISA of the amount of HB-EGF in culture media without NSPCs (media), media from cultured NSPCs (supernatant) and the pellet of cultured NSPCs (pellet). The results showed a significant increase in the amount of HB-EGF in the media from cultured NSPCs, showing that NSPCs released the ligand in proliferative conditions. **C-D)** WB showing increasing levels of phosphorylated EGFR Y845, EGFR Y1068 and the downstream signaling

pathway ERK1/2 in the conditions treated with HB-EGF. **E-G)** Quantifications of phosphorylation levels compared to the total amount of protein levels for EGFR (Y845 and Y1068) and the downstream signaling pathways ERK1/2. The control group was normalized to 100% ± SEM. *Scale bar 20 µm. *p<0.05* and ***p<0.01. Kruskal-Wallis followed by multiple comparisons versus control group by Tukey post hoc test in (B). One-way ANOVA followed by multiple comparisons versus control group by Holm-Sidak post hoc test in (E), (F) and (G). Bars show mean ± SEM. Dots show individual data.*

The results obtained in the second part of this thesis pointed to EGFR as one of the relevant mediators in the seizure-induced React-NSC transformation taking place in the DG that leads to the total loss of the neurogenic capacity. Our work opened an avenue towards EGFR activation as an alternative mechanism for the hippocampal response to MTLE. Indeed, we found the intranasal administration of Gefitinib to be a valid method to inhibit EGFR, overcoming the BBB and ameliorating the dramatic effects of seizures over the hippocampal neurogenic niche (Loss of DCX, GCD and React-NSC induction). Further, we proposed Zn^{+2} and HB-EGF, and the interaction between them, to play a role in the induction of EGFR activation, as they were found to be massively released into the extracellular media after seizures. Keeping in mind that the triggering of the hippocampal response after seizures will involve more than a single actor, our results shed light into one of the governing mechanisms of the React-NSC induction and loss of neurogenesis. These findings pave the way for further research focused on other pathways, including other ErbB receptors, that could be modulated by Zn^{+2} and HB-EGF.

7. DISCUSSION

7. DISCUSSION

7.1. Adult NSCs are genereated on-site in the DG after birth

In the rodent DG, adult NSCs give rise to new neurons postnatally and during the whole life of the organism (Altman and Das, 1965; Kempermann et al., 2015). However, after getting activated adult NSCs lose their neurogenic capacity by differentiating into astrocytes or directly into neurons (Encinas et al., 2011a; Pilz et al., 2018) and despite their presumed capacity to self-replicate (Bonaguidi et al., 2011), they undergo gradual exhaustion over time until they get depleted at a population level (Encinas and Sierra, 2012). Thus, the formation and establishment of the adult hippocampal NSC population during the developmental period will determine the adult neurogenic potential of an individual. The general believe in the field is that AHN is a remnant process from the embryonic development, yet the specific spatial origin of adult NSCs remains unknown and somehow controversial (Berg et al., 2019; Gonçalves et al., 2016; Hodge et al., 2013; Li et al., 2013; Matsue et al., 2018). Furthermore, the DG is one of the brain regions that get mainly formed postnatally. The majority of neurons reach the GCL at early postnatal stages (Bayer, 1980) and the blockage of the proliferation of postnatal progenitors impedes the formation of the adult NSC population, therefore abolishing AHN (Youssef et al., 2019). Interestingly, mice lacking cD2, a relevant factor for cell cycle, show lack of AHN in the DG (Ansorg et al., 2012). Thus, we hypothesized that adult NSCs are not a remnant from the embryonic development but a whole new population generated through cD2-dependent proliferation at early postnatal stages. We found our hypothesis to be true by analyzing the postnatal development of the neurogenic niche in the absence of cD2.

7.1.1. Cyclin D2 is fundamental for the postnatal generation of adult NSCs

To assess the relevance of cD2 in the formation of adult NSC population we analyzed the postnatal DG at different time points (P0, P7, P14, P28) in a Nestin-GFP mouse model lacking cD2 (*cD2*KO) using tissue kindly sent by Anja Urbach, in whose laboratory both transgenic lines were crossed. In the *cD2*KO mice, the embryonic development of the DG is close to normal, getting formed as in the WT (Kowalczyk et al., 2004). In fact, we did not find any difference neither in the dNSC number nor in the proliferating dynamics within the GCL of the *cD2*KO mouse at P0. This might be due to a compensatory action exerted by the other D-type cyclins (Ciemerych et al., 2002), as

the three D-type cyclins are expressed in cultured NSPCs derived from P5 hippocampi, while in NSPCs derived from adult hippocampi the whole system relies on the cD2 (Kowalczyk et al., 2004). However, in B-lymphocytes only cD3 (and not cD1) compensates for the loss of cD2 and induces proliferation with a slower cell cycle (Lam et al., 2000), opening the possibility for a non-essential role of cD2 during the embryonic development of the DG, potentially explaining the lack of effect in its absence, rather than compensation from the other D-type cyclins.

After birth, in normal conditions dNSCs proliferate and expand themselves until P14, when the NSC population becomes "adult" (Nicola et al., 2015). Our results indicate that in normal conditions the number of NSCs progressively increases during the first postnatal weeks, confirming previous data that reported an outgrowth in the total number of NSCs from P7 to P28 (Gilley et al., 2011). In the absence of cD2, this expansion fails to happen, leading to an almost entirely depleted population of adult NSCs. Moreover, the remaining ones divide at lower proportion than in the WT. This could be due to a premature senescence of the neurogenic niche, at least in terms of the NSC number and their activation rate. Indeed, the remaining adult NSCs are morphologically different and resemble the senescent-like and aged-associated phenotype of the omega NSCs (Martín-Suárez et al., 2019). Our results are in agreement with a previous model that ablated dividing GFAP-positive cells during the first postnatal week, provoking the absence of NSCs in the adult DG (Youssef et al., 2019). Thus, we suggest that dNSCs divide and generate *de novo* adult NSCs in the postnatal DG (P0-P14), in a process dependent of cD2, and hypothesize that any insult affecting dNSC proliferation during this period will affect the neurogenic niche in a long-lasting fashion **(Figure D1)**.

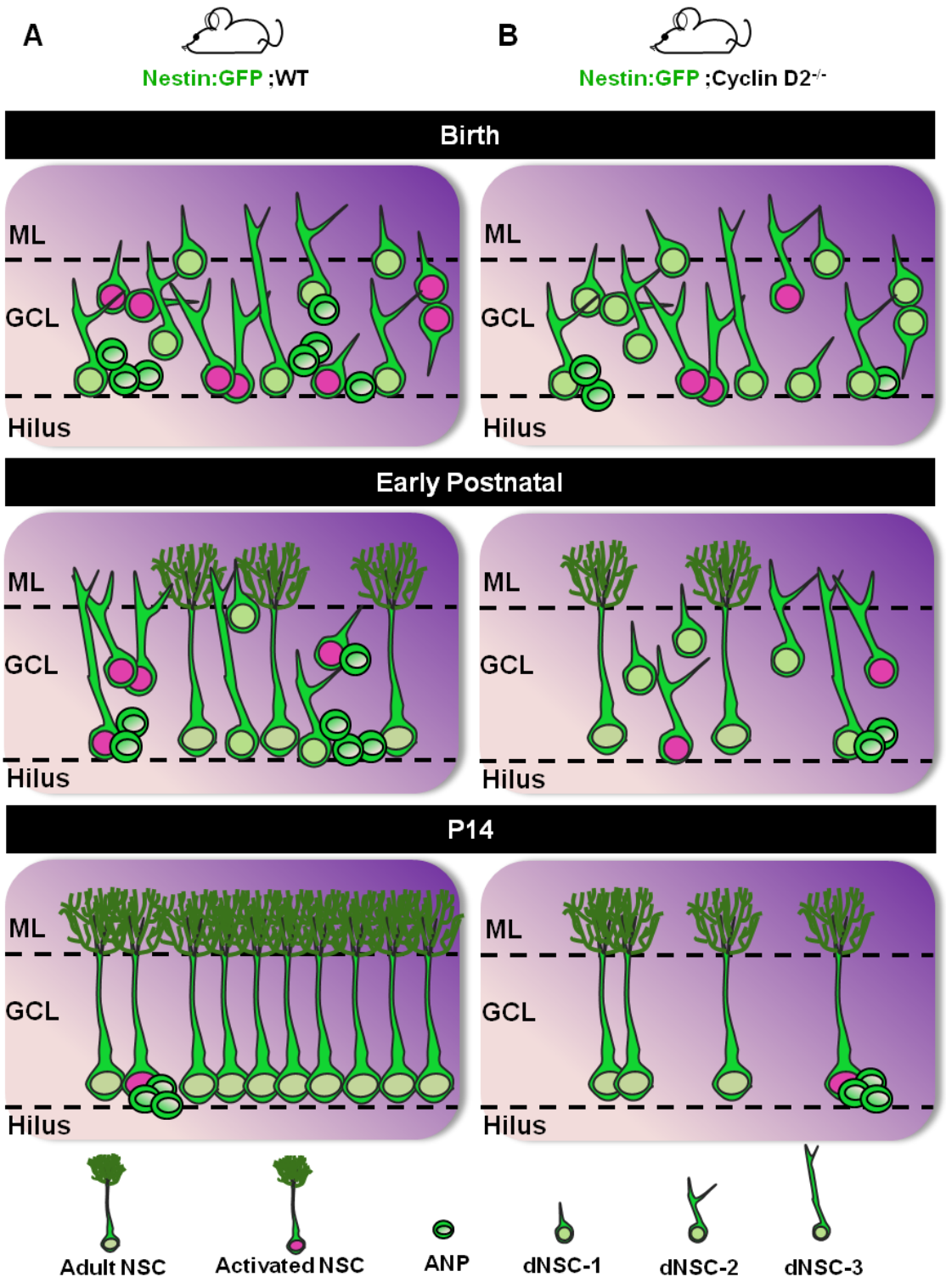

Figure D1. cD2-mediated proliferation is essential for the generation of adult NSCs. A) After birth and during the first 14 postnatal days, dNSCs proliferate and give rise to adult NSCs that locate in the SGZ, giving birth to newborn neurons during the whole lifetime. **B)** In the absence of cD2, proliferation is impaired during the early postnatal period, affecting to the generation of adult NSCs that translates in a diminished initial pool size that will affect the neurogenic capacity during the whole lifetime.

We next wondered whether the loss of adult NSCs could be due to increase cell death rather than to impaired cell proliferation. In the cerebellum, GCs and stellate interneurons are reduced in *cD2*KO mice, due to both reduction in primary neurogenesis and increase in apoptosis (Huard et al., 1999). However, *cD2*KO mice do not show increased cell death in the GCL at early postnatal stages. On the contrary, cell death tends to decrease suggesting that the failure in the generation of adult NSCs is due to a lack of expansion of dNSCs rather than cell death. We interpret the decreased cell death as a reflection of a reduced number of NSCs being generated, as apoptosis is high in this cell type and correlates with both their number and their proliferation (Sierra et al., 2010).

D-type cyclins constitute a molecular bridge between extracellular mitogenic signaling and the activity of cell cycle machinery (Matsushime et al., 1994; Tanguay and Chiles, 1996) and their loss forces the cell into a quiescent state (Andreu et al., 2015; Kippin et al., 2005). Furthermore, studies of different brain regions have shown association of cD2 with the maintenance of the undifferentiated state of NSCs and their expansion at the expense of their neuronal differentiation, being the latter more related to cD1 (Glickstein et al., 2007b, 2009; Lukaszewicza and Anderson, 2011; Ross et al., 1996; Tsunekawa et al., 2012). We propose that in the absence of cD2 dNSCs are not capable to proliferate during the early postnatal period, entering quiescence without expanding and failing to generate adult NSC population. Nevertheless, the generation of adult NSCs is not completely abolished and a limited pool gets formed in the *cD2*KO mice and therefore we cannot exclude a potential role of other mechanisms, including the other D-type cyclins.

7.1.2. dNSCs divide on-site in the DG to generate adult NSCs

Having established that dNSCs need to proliferate during the early postnatal period to generate adult NSCs, we next wondered about the specific location where this proliferative stage takes place. One of the hallmarks of the DG development is the formation of the DMS by dNSCs and progenitors that get detached from the DNe during the embryonic development. Although dNSCs enter the DG already at embryonic stages, forming a new progenitor matrix inside the DG, the DMS is still active during the early postnatal period (Altman and Bayer, 1990a; Berg et al., 2019; Hodge et al., 2013; Li et al., 2009; Sugiyama et al., 2013). Thus, we aimed to assess the migration and division dynamics, as well as the contribution of the postnatal dNSCs

from the DMS compared to the ones that have already reached the DG during the postnatal formation of the DG.

In order to trace the lineage of dNSCs from both HPF regions, we resorted to SFFV-RVs, a well-known tool to birth-date newborn cells. SFFV-RVs only infect mitotic cells and the limited diffusion of the virus particles allows the regional infection of dNSCs and progenitors (Gomez-Nicola et al., 2014b; Weber et al., 2012). We injected postnatal mice at P2 and P5 either inside the DG or in the DMS aiming to assess possible fate differences related to the spatial location of dNSCs. In both injection models (DMS and DG), SFFV-RV-infected cells were restricted to the targeted area inside the HPF, demonstrating the usefulness of the technique. In some animals, the VZ got infected due to the flowing back when removing the capillary after the injection. However, the infected area outside the HPF is not a source of DG progenitors and thereby we considered it not to be affecting the experimental purposes. Furthermore, we used two different SFFV-RVs expressing different fluorescent markers (SFFV-RV-mCherry and SFFV-RV-mCerulean) to test the capacity of the model to independently label dNSCs from each region. This dual injection model has been previously used to label progenitors to study the neuronal formation of the DG, although performing each injection separately at different ages (Mathews et al., 2010). We implemented it to spatially differentiate dNSCs during a single experimental procedure. Indeed, the progeny of the dNSCs from the different regions showed no overlapping at P14, demonstrating the independent and restricted efficacy of the infections. When infections were done in the DMS, the viral particles showed high diffusion covering the DMS from septal to temporal regions, while inside the DG the diffusion was highly restricted to the injection site. In both models, axons from labeled GCs were visible even in adjacent slices where GC somas were not present.

Next, to better assess the cellular identity of the SFFV-RV-labeled progeny we performed the same experiments in Nestin-GFP mice. Previous studies, through the use of SFFV-RV infections too, have proposed that at P5 proliferative GFAP-positive astrocytes from the DG give rise mostly to granule neurons and stellate astrocytes, but also to adult NSCs (Namba et al., 2005). Likewise, DG progenitors from P7 organotypic slices give rise to neurons, astrocytes and radial GFAP-positive cells (Yokose et al., 2011). Our results confirmed previous discoveries, additionally reporting that while precursors of neuronal and astroglial populations are both in the DMS and DG, adult NSC precursors are confined to the DG by birth. In contrast, injecting an EGFP-expressing retrovirus in the hippocampal VZ of P5 mice, neuronal and astroglial

lineage were reported in the DG at P10 and P45, as well as the presence of EGFP-positive cells located in the SGZ with radial morphology and Nestin expression on at least one of them (Navarro-Quiroga et al., 2006). However, we believe that since neurons born at P5 locate in the inner part of the GCL and extend their axons towards the ML, the identification of adult NSCs by a radial process extending towards the ML and a soma located in the SGZ can be confusing. Moreover, the authors showed one single Nestin-positive cell with radial orientation that lacked the broccoli-like crown. We consider that adult NSC markers are shared by other cell populations, as pericytes or astrocytes in the case of Nestin (Clarke and Van Der Kooy, 2011; Encinas et al., 2011a; Komitova and Eriksson, 2004; Petrik and Encinas, 2019), being therefore necessary the use of more than one marker and strict morphological criteria to identify adult NSCs as such. Although we do not completely rule out the possibility that some isolated adult NSC precursors might come from the DNe/DMS at postnatal stages, as we observed when injecting the SFFV-RV in the DMS at P2, we consider the sole presence of isolated adult NSC-like cells insufficient to make claims at a population level. Moreover, other studies that electroporated the DNe of neonatal (Ito et al., 2014) and E16.5 (Sugiyama et al., 2013) mice did not find any other cell type in the GCL but neurons. We propose that at E16 all the adult NSC precursors are already detached from the DNe, on the DMS or already in the DG, involved in a migratory process that gets completed at P2 or before.

When we discuss about the developmental origin of the adult NSCs, the DMS is not the only pathway from which they have been reported to migrate into the DG. An alternative route following the SPZ has been described by some authors, with progenitors forming the so-called "transient subpial neurogenic niche" along the HF, prior to migrating downwards into the DG (Hodge et al., 2013; Li et al., 2009). In a groundbreaking work, Samuel Pleasure and coworkers described another migratory stream coming from the vHPF at embryonic stages. They claimed that progenitors coming from the DNe contribute to the formation of the outer shell of the suprapyramidal blade of the DG, while the temporoseptal pathway contributes to the inner shell of the GCL and SGZ, including adult NSCs. Cell migration from outside the HPF into the DG has also been described. During development, the caudal ganglionic eminence is source of hilar interneurons and neurons of the GCL that reach the DG postnatally attracted by FGF signalization (Aguirre et al., 2004; Cuccioli et al., 2015; Pleasure et al., 2000b). Given the neuronal contribution of the ganglionic eminence, it seems logic to think that progenitors could also be migrating into the DG to contribute

to the adult NSC population. In our injection models, we found that adult NSC precursors proliferate inside the DG at P2-P5, and not in the DMS. Moreover, as our method does not provide 100% accuracy regarding the site of injection and variability ensued, it led to several off-target injections that gave us valuable information. When the injection site was the transient subpial neurogenic zone, we observed later few neurons in the GCL but never adult NSCs, and we did not observe any cell migration to the dorsal DG when progenitors were labeled in the ventral DG (data not shown). However, the possibility of a heterogeneous adult NSC population with different spatial origins during embryonic gestation is a possibility that calls for further exploration **(Figure D2)**.

One could also argue that with SFFV-RV injections we are missing quiescent dNSCs that could be migrating towards the DG from outside. We think that given the importance of proliferation for the adult NSC pool generation after birth (Ortega-Martínez and Trejo, 2015; Youssef et al., 2019), and the role of cD2 previously discussed, dNSC migration without proliferation during this period seems improbable. Our studies show that regardless of where they initially come from, there is a population of dNSCs that enter mitosis inside the DG to give rise to adult NSCs early after birth, while the dNSCs coming from the DNe at this period are only neurogenic. In summary, we think that adult NSCs are generated as a whole new population in a differentiated process that takes place postnatally inside the DG, meaning that adult NSCs are not a mere continuation of the embryonic development.

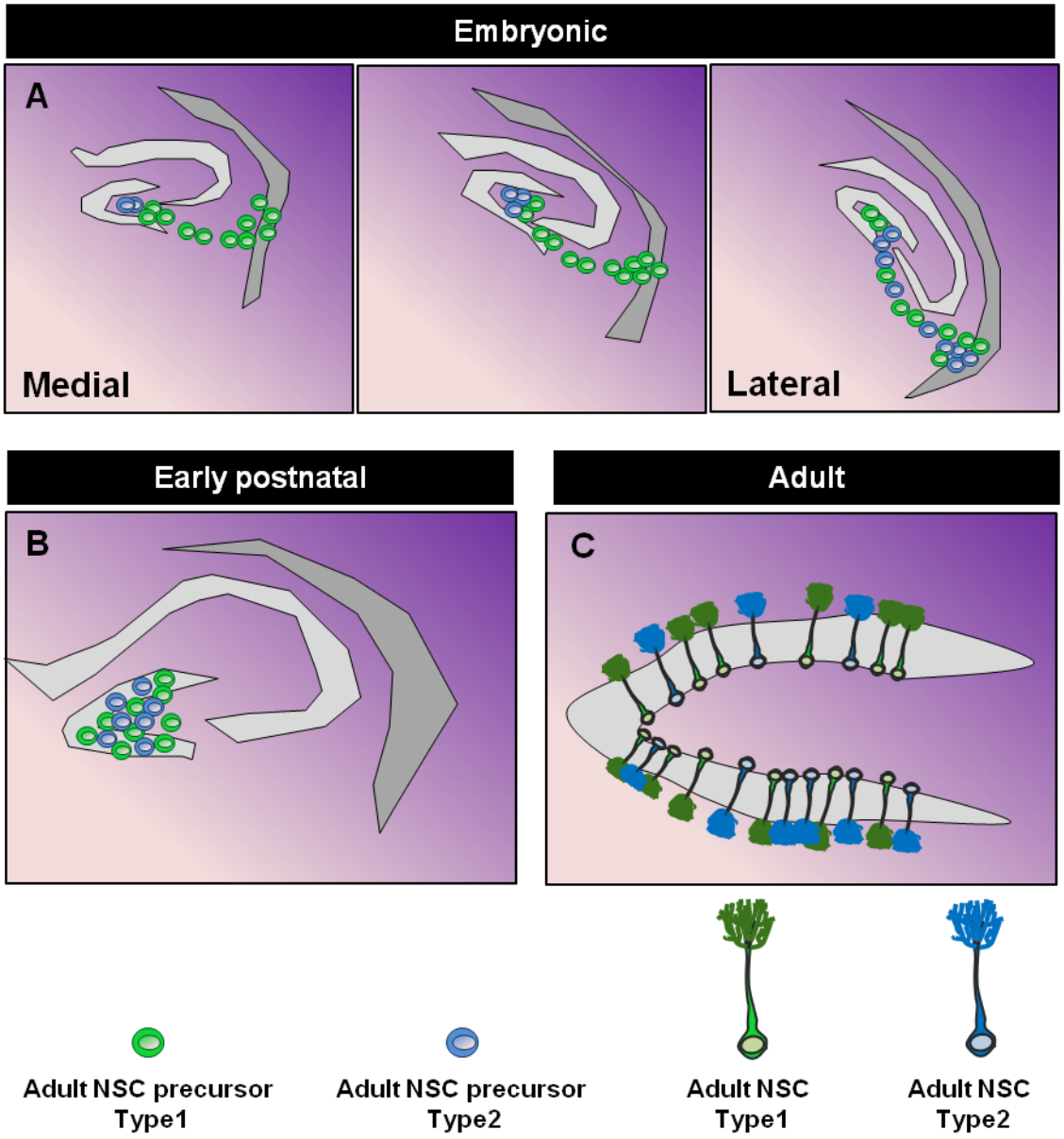

Figure D2. Heterogeneous origin of adult NSCs. A) During the embryonic period, various sources have been described as the origin of NSCs. On the one hand, the more classic view indicating the DNe as the source from where progenitors (in green) migrate into the DG until they locate in the SGZ (Altman and Bayer, 1990a; Berg et al., 2019; Hodge et al., 2013; Li et al., 2009; Sugiyama et al., 2013). On the other hand, adult NSCs have been described to migrate from ventricular area of the vHPF in a shh-responsive manner (in blue) (Li et al., 2013). The pictures represent the HPF from medial to lateral in a coronal view, from left to right. **B)** This would mean that heterogeneous populations of progenitors (Shh-responsive and non-responsive) migrate following different dynamics during the embryonic period and get into the DG. Regardless of their different precedence, the adult NSC precursors gather inside the DG after birth, proliferating there, on-site, to give rise to the adult NSC pool. **C)** The different origin might involve heterogeneous populations of adult NSCs sharing their location in the SGZ and responding differently to external or internal stimulus.

Despite our main focus in this study was to determine the spatial developmental origin of adult NSCs, the majority of the cells generated from the infected dNSCs in both DMS and DG were neurons, leading to observations into the neuronal formation of the GCL. The GCL is well-known to form following an outside-in pattern, where the outer layer is the one formed by the earliest born GCs (Angevine, 1965; Schlessinger et al., 1975). In addition, this formation gets completed following a supra-to-infrapyramidal layer pattern. Around P0, NBs migrate to the marginal zone of the suprapyramidal blade of the DG and later complete the GCL formation migrating towards the infrapyramidal blade, that gets formed during the early postnatal period (Bayer, 1980; Schlessinger et al., 1975). In our injection models we found that dNSCs coming from the DMS give rise to neurons that populate both the ventral and dorsal blade of the DG. However, the organizational pattern is quite different in each place. While in the dorsal blade neurons locate in the inner part of the GCL forming an easily observable layer, they gather up in the ventral blade forming packed cell clusters that extend from the hilus to the ML. This supports the dorsal-to-ventral organizational dynamic previously described and suggests that postnatal neurogenesis is determinant for the formation of the ventral GCL and therefore key for the region-related functions during the adulthood.

7.1.3. LPA_1 differentiates adult NSCs from dNSCs

During the last years, the developmental origin of adult NSCs has been studied assuming that adult neurogenesis is a mere continuation from the developmental neurogenesis (Berg et al., 2019; Hochgerner et al., 2018; Nicola et al., 2015; Seki et al., 2014). Progenitors forming the DG during development have been reported to share molecular features with adult NSCs (Pleasure et al., 2000a). Notch1 and Notch2 have been suggested to be involved in maintaining the proliferative and undifferentiated stage of dNSCs during development until they become adult (Breunig et al., 2007a; Nelson et al., 2020) and protein expression markers such as GFAP (Seki et al., 2014) or Hopx (Berg et al., 2019) have been claimed as common markers for dNSCs and adult NSCs under the idea of a single population of NSCs giving birth to GCs during the whole life. In contrast, although defending adult neurogenesis as a developmental continuum, some authors have outlined the postnatal apparition of a "new structure" which corresponds to different functionality in the SGZ (Nicola et al., 2015). In this line, there are cell autonomous differences, as well as different transcriptional profiles and cell properties between P7 and P28 Nestin-GFP-expressing NSCs (Gilley et al., 2011) and some dNSCs undergo protein expression changes from

the embryonic to postnatal development, such as expression of BLBP (Matsue et al., 2018). However, the lack of specific markers for NSCs leads to possible biases in the result interpretation, so the specific identification and lineage tracing of the dNSCs that will give rise to adult NSCs remain a challenge in the field.

Using the LPA_1-EGFP transgenic mouse, LPA_1 has been proposed to specifically label adult NSCs in the DG (Walker et al., 2016). We have recently validated the expression of LPA_1-EGFP as a true reflection of LPA_1 expression and its validity as a specific marker of NSCs (Valcárcel-Martín et al., 2020). Thus, we postulated LPA_1 as a possible candidate to specifically distinguish adult NSC precursors during development and a potential option to track them down. Surprisingly, we found that LPA_1-EGFP expression is spread all over the hilus during the early postnatal development and later switches to the SGZ and specifically to adult NSCs between P10 and P14. During the early postnatal period LPA_1-EGFP labels NeuN-positive neurons in the hilus, while dNSCs in the GCL express Nestin but not LPA_1-EGFP. By P14, LPA_1-EGFP expression is almost absent from the hilus, while almost all of adult NSCs express it. Therefore, even though LPA_1 is not useful to trace adult NSC precursors from development stages, it reveals as a valuable tool to specifically distinguish between dNSCs and adult NSCs and further supports the notion of adult NSCs and adult neurogenesis being qualitatively different from dNSCs and developmental neurogenesis. Indeed, Sten Linnarson and coworkers showed using scRNA-seq that RGCs (NSCs) undergo a clear shift in the molecular expression from the second postnatal week on, when they become closer to astrocytes. Importantly, this shift is defined also by LPA_1 expression (Hochgerner et al., 2018), as we observe through IHC. Although the role of LPA_1 in progenitors modulating proliferation and adult neurogenesis has been outlined (Estivill-Torrús et al., 2008; Matas-Rico et al., 2008) and our recent data show that the seizure-induce massive activation of NSCs is reduced in mice lacking expression of LPA_1 (Valcárcel-Martín et al., 2020), its role during development is unclear. Regardless, we propose that dNSCs enter mitosis during the first postnatal week inside the DG and modulated by cD2 give rise to a brand new population of cells, known as adult NSCs, that start to express LPA_1 **(Figure D3)**.

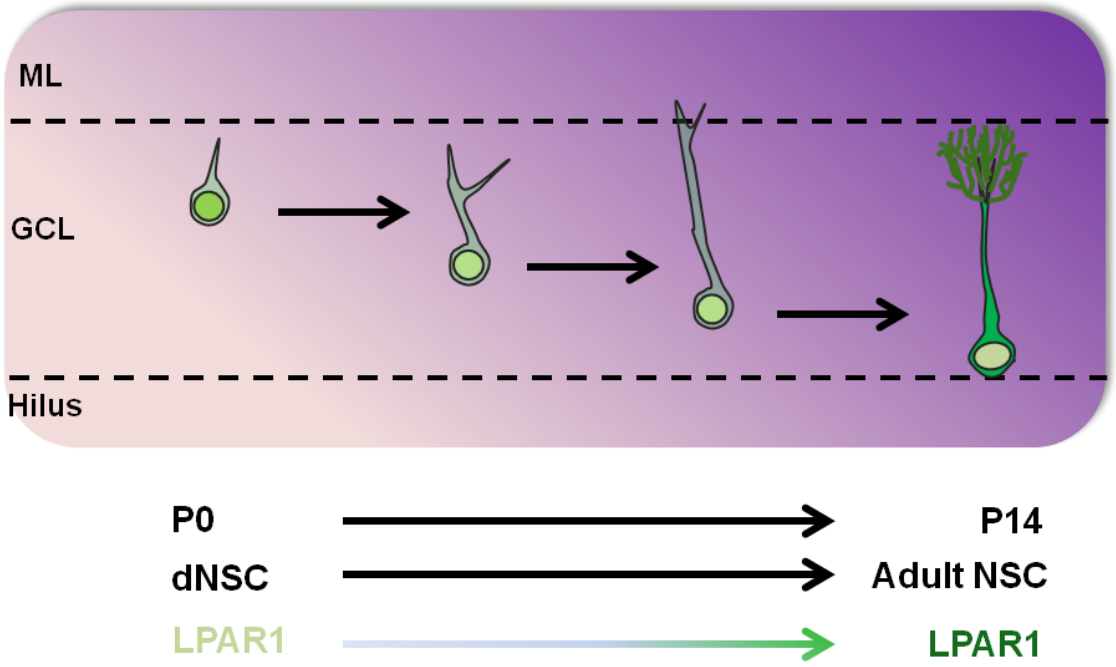

Figure D3. LPA_1 specifically differentiates adult NSCs from dNSCs. Early after birth, dNSCs divide to generate adult NSCs. During this process dNSCs do not express LPA_1, whereas they acquire its expression when they become adult-like around the second postnatal week.

We thus consider that adult NSCs comprise a differentiated SC type with specific functions different from the dNSCs, and this should be taken into account when studying them. The identity and actual SC nature of adult NSCs has been debated before, stating that rather than considering them as undifferentiated cells, it may be more productive to think of them as appropriately differentiated for their specific tissue niches (Clarke and Van Der Kooy, 2011; Seaberg and Van Der Kooy, 2003; Weiss et al., 1996). Defining the origin and identity of adult NSCs influences the way we study them in rodents, and the way we extrapolate this knowledge into humans. Therefore, this represents a more serious question than simple semantics. Regarding the recent controversy on the absence of adult neurogenesis in the human brain, we should consider the existence of adult NSCs in terms of the generation of a specific cell type with specific functions during development, rather than SC endurance over lifetime.

7.2. Human and mouse DG share similitude in their formation

The existence of newborn neuron generation in the human adult DG has recently come to a new historical hotspotand the community has been shaken mainly due to two studies claiming opposite results, i.e. presence and absence of DCX-positive NBs in the adult GCL (Moreno-Jiménez et al., 2019; Sorrells et al., 2018). We

understand the NSC pool formation as the foundation of lifelong neurogenesis and as such, we consider the study of this process as key to assess the extension and relevance of the postnatal neurogenic niche and neurogenesis. We think that by applying our knowledge from mouse to human we could determine how, if so, dNSCs give rise to a new population of adult neurogenic cells. One of the unique characteristics of human (and primate) DG formation is the generation of the dentate plate during the early embryonic development (Abraham et al., 2004; Cipriani et al., 2017). However, probably the most important difference between rodents and human HPF lies on the spatial location. During the early gestational period the human HPF extends both at dorsal and ventral level. However, before mid-gestation the dorsal part of the HPF gets constraint due to the growth of the corpus callosum. Thus, the HPF ends up placed at a ventromedial level, with a prominent anterior part and a narrow posterior part known as the *induseum griseum* or the hippocampal tail (Meyer et al., 2019; Rakic and Yakovlev, 1968). These differences could lead us to think of a completely different developmental process in both species. Yet, the human HPF shows similar migratory dynamics than mice, with RGCs and progenitors moving from the DNe into the DG, forming the DMS (Sorrells et al., 2018). We hypothesized that despite possible differences between mouse and human HPFs, both are developed following similar patterns, and therefore adult NSCs would be generated in a similar fashion.

7.2.1. The DG formation is almost completed between GW14-GW30

The study of human tissue poses obvious hurdles for the identification and tracking of dNSCs. We first proceeded to study potential dNSC and progenitor populations in humans through IHC. To better characterize the DG formation and identify the potential formation of a population similar to mouse adult NSCs, we analyzed the cellular expression of dNSC, intermediate progenitor and proliferating cell markers across the human embryonic and early postnatal development. At GW14, the cellular distribution in the HPF resembles the mouse late embryonic/early postnatal development. Hopx-, GFAP-, S100ß- and Nestin-expressing fibers are clearly positioned above the fimbria and SPZ, forming a RGC scaffold that extends along the DMS, surrounded by progenitors and proliferating cells. Remarkably, while GFAP, S100ß and Hopx expression terminates when the fibers contact the medial blade of the DG, the presence of Nestin-positive fibers covers also the hilus and part of the lateral blade of the GCL, suggesting the presence of an independent dNSC population that invades the DG earlier than the rest. Interestingly, at GW30 intermediate progenitors

and proliferating cells appear restricted to the DG forming a layer below the GCL, as it happens during the late postnatal development (P10-P14) in mouse. In contrast, the DMS is almost devoid of proliferating cells, although remaining Nestin-expressing fibers can be observed all the way above the fimbria without any observable attachment to the DNe, fanning out into the ML once they reach the hilus. On the other hand, the expression of Hopx and S100ß, markers of adult NSC precursors in mouse (Berg et al., 2019; Namba et al., 2005), changes and gets spread out all over the HPF, suggesting their lack of specificity as dNSC markers at mid-gestation. Curiously, we observed lack of both Hopx and S100ß in the medial blade of the DG, precisely where DCX-positive immature neurons concentrate at that age (Sorrells et al., 2018). Previous studies have reported that the DG gets completely formed before mid-gestation (GW30-32), with a peak of proliferation at GW14 that goes decreasing thereafter, and is almost absent by term (Arnold and Trojanowski, 1996; Yang et al., 2014). Our observations support the idea that the human DG gets formed sharing certain similitude with mouse during the early-mid gestation (GW14-GW30), with dNSCs and progenitors detaching from the DNe and forming different matrixes (DNe, DMS, FDJ, DG) until they get restricted into the hilus, close to the GCL.

7.2.2. The human DG develops differently along the longitudinal axis

The spatial location is one of the most striking differences comparing mouse and human HPF. The anterior-posterior axis in humans is homologous to the ventral-dorsal axis in the mouse, where the dorsal part is well-developed and more prominent than the ventral, while in humans it is the opposite (Fanselow and Dong, 2010; Poppenk et al., 2013; Strange et al., 2014). In mice, cognitive functional differences have been well described comparing the involvement of the vHPF and dHPF (Bannerman et al., 2002; Strange et al., 2014). Likewise, the response to pathological insults, such as SE, varies depending on the position in the longitudinal axis (Häussler et al., 2012) and the maturation of the adult newborn neurons, as well as perinatal interneurons, is also different. This heterogeneity has also been reported in humans, presenting genetic, functional and connectivity differences between the anterior and posterior HPF (Fanselow and Dong, 2010; Strange and Dolan, 1999; Vogel et al., 2020). Interestingly, we found that at GW14 the anterior part of the ventral DG appears to develop slower than its more posterior counterpart. In the anterior DG, the expression of Ki67 is observable mostly in the DNe, with some cells in the DMS but none inside the prospective DG. This pattern changes when looking at more posterior positions, where Ki67 cells disappear from the DNe to spread all over the DMS and

have already entered the DG. This pattern is also observable with Hopx-positive cells located gradually closer to the DG in an anterior to posterior trend. Moreover, these differences are inconspicuous at GW30, arguing in favor of an already close to an end developmental formation of the DG in both the anterior and posterior poles. Therefore, the window between GW14-GW30 would be essential in the formation of the DG, with temporal differences along the longitudinal axis that may imply further functional distinctions. We wonder whether these differences might also affect in the potential generation of a NSC niche in the GCL.

7.2.3. RGCs remain in the DG early after birth: Potential role as NSCs?

After birth, the presence of NSCs in the human DG, and their actual neurogenic capacity is under debate. Although some authors have reported a lack of Nestin-expressing cells at term (Arnold and Trojanowski, 1996; Yang et al., 2014), the majority of the literature reports that RGCs are still present in the DG during the first years after birth. Proliferating BLBP- and Nestin-expressing cells have been reported in the hilus and other regions of the HPF (Blümcke et al., 2001; Cipriani et al., 2018; Sorrells et al., 2018). Our results support previous findings of a potential NSC population with Vimentin- and Nestin-positive cells populating the DG 3 weeks after birth. In contrast to what we observe in the mouse SGZ, these cells have their nuclei located in the hilus and extend their fibers towards the ML, crossing the GCL. In addition, the few Ki67-positive cells that are observable inside the DG at this age are spread throughout the hilus, meaning that the Nestin- and Vimentin- expressing RGCs would be mainly quiescent. We speculate that they form the ultimate RGC scaffold, comparable to the secondary RGC scaffold in mouse, helping the last waves of immature neurons to migrate from the hilus into the GCL (Seress et al., 2001). However, their neurogenic capacity remains under debate, and their endurance during adulthood is currently a hot topic. Arturo Alvarez-Buylla and colleagues defend that NSCs are absent in the GCL in cases older than 7 years. They reported that although BLBP- and Vimentin-expressing cells are present in the ML (but not in the GCL), they do not proliferate (Sorrells et al., 2018). Opposite to this view, other authors reported presence of Nestin-expressing cells inside and outside the DG during adulthood. However, while some defended their NSC nature and ability to proliferate (Boldrini et al., 2018; Tobin et al., 2019) others claimed that they lack neurogenic capacity (Cipriani et al., 2018). Given that the formation of the GCL seems to be finished by GW30, we wonder whether the postnatal RGCs that we observe could represent a population equivalent to adult NSCs in mouse, following similar activation/depletion dynamics that drive the niche to a

deforestation during the first years of childhood (Encinas and Sierra, 2012; Encinas et al., 2011a), leaving an almost barren neurogenic niche comparable to the aged SGZ in mouse.

Regardless of their presence during adulthood, the early postnatal NSCs might play an important role in the hippocampal response in normal and also pathological conditions, such as epilepsy. Indeed, the developing human brain has a predominance of excitation over inhibition and is therefore at higher risk of developing seizures, particularly during the first month of life (Holmes, 2009; Rakhade and Jensen, 2009). Seizure occurrence during neonatal age appear to play a significant role in later developing epilepsy, intellectual disability and headache (Oh et al., 2019). Interestingly, Nestin expression strikingly increases in the hilus and GCL of TLE patients younger than 2 year old compared to adult and control cases, suggesting a significant role of this population in the pathological response provoked by epilepsy (Blümcke et al., 2001), although this overexpression of Nestin could be attributed to the generation of reactive astrocytes. Thus, we next moved to study the NSCs in normal and pathologic conditions. We explored possible mechanisms involved in the massive activation and induction of React-NSCs in a mouse model of MTLE.

7.3. EGFR is involved in the early response of NSCs in MTLE

We have used in the laboratory a context of pathophysiological relevance, epilepsy (MTLE specifically), to study novel properties of NSCs and we have started to unveil the mechanisms driving the response of adult NSCs and their neurogenic niche in this pathological context. Seizures induce NSCs to drastically change their morphology and to become functionally proinflammatory (Martín-Suárez et al., in preparation); to get massively activated; to switch to a symmetric mode of cell division and to ultimately differentiate into reactive astrocytes abandoning their neurogenic program (Muro-García et al., 2019; Sierra et al., 2015; Valcárcel-Martín et al., 2020). MTLE is one of the most common epilepsies (Falconer et al., 1964; Savage, 2014; Wiebe, 2000) and it is resistant to drug treatment in high proportion of cases (35%), having one of the worse prognosis (Wieser, 2004). Thus, our study might be useful not only to answer fundamental questions about the role of NSCs in pathological conditions, but also to shed light about MTLE and potential strategies to prevent its negative effects over the HPF.

In the mouse model of MTLE induced by intrahippocampal or intra-amygdalar injection of KA, neuronal hyperexcitation induces NSCs to develop a hypertrophic

cytoplasm and a multibranched phenotype with overexpression of Nestin, GFAP and LPA_1 (Muro-García et al., 2019; Sierra et al., 2015; Valcárcel-Martín et al., 2020). At the same time, they get activated in much higher proportion than in normal conditions. Thus, NSCs transform into React-NSCs which end up differentiating into reactive astrocytes. Strikingly, in MTLE React-NSCs change their mode of division from the typical asymmetric manner of normal NSCs that is ANP-generating and neurogenic to a symmetric mode that generates more React-NSCs (Sierra et al., 2015). It is remarkable that just the initial episode of seizures triggers the induction of React-NSCs and their massive activation. Furthermore, the conversion of NSCs into React-NSCs and their posterior differentiation into reactive astrocytes contribute to the development of HS in the DG, a hallmark of MTLE that correlates with bad prognosis and resistance to antiepileptic drugs (Quirico-Santos et al., 2013; Sierra et al., 2015; Thom, 2014). Previous research of the lab on mouse and human MTLE show a very similar reactive transformation in both species, although we cannot make any claim about the possible transformation of NSCs into React-NSCs in epilepsy patients (Muro-García et al., 2019). The induction of React-NSCs after seizures does not only contribute to the HS, but also leads to the complete loss of neurogenic capacity in the SGZ. In fact, the few neurons that are newly born get aberrantly located outside the GCL (Overstreet-Wadiche et al., 2006; Parent et al., 2006). Despite all this, the mechanisms by which NSCs transform into React-NSCs are still unknown. We have described before that lack of LPA_1 reduces the massive activation of NSCs by seizures (Valcárcel-Martín et al., 2020) and other research lines of the laboratory are now exploring ATP through purinergic 2X receptors (ATP-P2XR pathway) as a key mechanism for the induction of React-NSCs (Martín-Suárez et al., in preparation 2020). Nonetheless, an additional molecular signaling in which we have more insight gained is that of the EGFR. Here, we have explored the possibility of FGFR1 and EGFR as important players in the neurogenic niche and NSC response in MTLE. Both have been reported as potent mitogenic factors for hippocampal NSCs and astroglia (Reynolds and Weiss, 1992; Tropepe et al., 1999). Moreover, ErbB family, to which EGFR belongs, has been reported to increase within the first three days after an intrahippocampal injection of KA (Sierra et al., 2015). We hypothesized that both FGFR and EGFR would play a role in the massive activation and reactive transformation of NSCs in MTLE.

7.3.1. EGFR, but not FGFR, overexpression is an early event after KA

To induce seizures adult mice were injected with KA, provoking as soon as 30 minutes convulsive seizures (SE) that keep repeating up to 6 h after the injection. In

addition, mice develop unprovoked spontaneous chronic seizures after a few days, becoming epileptic (Bouilleret et al., 1999; Sierra et al., 2015). Following focal seizures, KA induces cell death, inflammation and GCD, all hallmarks of HS (Abiega et al., 2016; Bouilleret et al., 1999; Sierra et al., 2015). Although there are other widely used models of epilepsy such as pilocarpine we discarded this option due to their high mortality rate and the difficulty to replicate it due to the high variability (Curia et al., 2008; Lévesque et al., 2016). Pilocarpine is a systemic injection with a high spectrum of action being uncontrollable in terms of the region of the brain which is going to be affected. In contrast, the intrahippocampal injection of KA is directly delivered in the ML in a very small volume, restricting the area of action and without systemic alterations as those induced by the intraperitoneal alternative. Indeed, the intraperitoneal injection of KA in mice, although more consistent in rats, induces high mortality and too wide variability in mice. Previous research of the laboratory using both the intrahippocampal (Sierra et al., 2015) and intra-amygdalar (Muro-García et al., 2019) single injection of KA show that the dramatic effect on (ipsi and contralateral) hippocampal NSCs and the neurogenic niche is driven by neuronal hyperexcitation and not because of the injection of KA itself. Further, working with a model of generalized epilepsy (Dravet syndrome, a rare but devastating infant epilepsy), React-NSCs and aberrant neurogenesis are also induced (Martín-Suárez et al., 2020).

We measured the protein and mRNA levels of two different isoforms of our first candidate FGFR (FGFR1 and FGFR2), within the first three days after KA administration. Both FGFR1 and FGFR2 have high affinity for the FGF2 ligand and their interaction promotes astroglial inflammation and glutamate release (Gómez-Pinilla et al., 1995a; Tao et al., 1996), both hallmarks of MTLE (Eid et al., 2019; Meldrum et al., 1999). Also, FGF2 is well-known to induce proliferation of hippocampal NSPCs *in vitro* (Kalluri et al., 2005; Reynolds and Weiss, 1992; Tropepe et al., 1999). Unexpectedly, we did not find any alteration either in the mRNA or protein levels of FGFR1 or FGFR2 in the HPF after KA. Furthermore, looking for possible particular alterations in the DG that the analysis of the whole HPF could be masking, we analyzed FGFR1 levels in the neurogenic niche 24 h after KA, with no observable differences in the FGFR1 expression in the GCL and in Nestin-GFP cells. Thus, we discarded FGFR as a mediator of the early neurogenic niche response in MTLE. Although we cannot rule out the possibility of FGFR1 activation without needing to increase its expression, we moved on to the study of EGFR and its downstream signaling pathway.

EGFR is highly involved in cell proliferation, playing a key role in the growth of several tumors types (Arteaga, 2011; Nicholson et al., 2001; Salomon et al., 1995; Sasaki et al., 2009; Sharma et al., 2007b). Moreover, it promotes proliferation of NSCs from both the SVZ and DG (Reynolds et al., 1992; Tropepe et al., 1999) and can induce astroglial differentiation (Sun et al., 2005). Importantly, the expression of ErbB family, from which EGFR is part, increases within the first three days after a KA intrahippocampal injection (Sierra et al., 2015). Here, following the same experimental timeline as before, we show that mRNA and protein expression levels of the receptor increase within the first three days after KA in the whole HPF, suggesting a role of EGFR in MTLE. In normal conditions, EGFR is expressed in neuronal populations of the HPF, with higher intensity in the neurons of CA2 (Tucker et al., 1993), making us wonder whether the increase of EGFR in MTLE can affect specifically to the neurogenic niche and NSCs. Interestingly, the expression of EGFR also increases in the GCL after KA, with EGFR observable in the nuclei and processes of the Nestin-GFP-expressing NSCs. In fact, EGFR interaction with any of its ligands induces the internalization and trafficking of the receptor to early endosomes, mitochondria or nucleus where it can act as transcriptional regulator, tyrosine kinase and mediator of other physiological processes (Gazzeri, 2018; Roepstorff et al., 2009), suggesting that the nuclear location of EGFR in NSCs might be due to its prior activation. Moreover, we show that not only the total amount of EGFR is increased after KA, but there is also higher phosphorylation of the tyrosine site Y845, which has been reported to control cell cycle and promote activation, especially via MAPK and Akt. Indeed, the EGFR downstream signaling pathways Akt, ERK1/2 and STAT3 were also activated, which are implicated in cell proliferation, survival and astroglial reactivity (Deschênes-Simard et al., 2014; Dibble and Cantley, 2015; De La Iglesia et al., 2008; Lewis et al., 1998; Morgensztern and McLeod, 2005; Morrison, 2012; Priego et al., 2018). We conclude that the increase of EGFR levels together with an increased activation of the receptor and its downstream signaling pathways play an important role in the early response that takes place in the HPF and specifically in the neurogenic niche of the DG of mice subjected to MTLE.

7.3.2. EGFR mediates the massive activation and induction of React-NSCs

In light of the high upregulation and activation of the EGFR signaling pathway in MTLE, we next sought to manipulate it in NSPCs resorting to cultures. We extracted the HPF from adult mice and grew neurospheres in proliferating conditions as previously described (Jhaveri et al., 2015; Pineda et al., 2013). Although the presence

of EGFR in NSPCs from both SVZ and DG has been long known (Reynolds et al., 1992; Tropepe et al., 1999), opposite results with NSPCs not being responsive to EGF due to a lack of EGFR have been also described (Kalluri et al., 2005), suggesting a possible differential action of the receptor depending on the cell line. Therefore, we first confirmed the clear expression of EGFR in our model of NSPCs directly derived from the mouse DG. Furthermore, the labeling was more intense in cells undergoing mitosis, arguing in favor of the role of EGFR in cell division.

Next, we used the reversible inhibitor Gefitinib, widely used to revert tumor proliferation (Chen, 2013; Singh et al., 2016), to modulate the EGFR signaling pathway. We found that Gefitinib is able to turn off the Y845 phoshorylation site of EGFR and also the phosphorylation of ERK1/2, the downstream signaling pathway more closely related to cellular proliferation (Deschênes-Simard et al., 2014; Lewis et al., 1998; Morrison, 2012). Moreover, the addition of Gefitinib in the culture media drastically reduces the proliferation of NSPCs in terms of BrdU integration into the DNA. Thus, observing the efficiency of Gefitinib to block EGFR, we decided to try an irreversible inhibitor, Afatinib, also used to stop tumor proliferation in cancer (Watanabe et al., 2018; Yang et al., 2015). However, even though Afatinib apparently reduces the proliferating capacity of NSPCs it can be due to its dramatic effect on cell viability. Therefore, we conclude that because the irreversible blockage of EGFR leads to NSPC death, its reversible blockage through the use of Gefitinib poses an interesting alternative in order to manipulate the proliferation and the induction of React-NSCs.

The massive activation and proliferation of the NSCs has been reported to reach its peak three days after the KA administration, when React-NSCs have been induced, accompanying the total disruption of the neurogenic niche and leading to very reduced and aberrant neurogenesis remaining (Sierra et al., 2015). Taking this into account, we administered Gefitinib during the first three days after KA starting from the moment right after the injection. As we expected, mice treated with Gefitinib showed decreased cellular proliferation (including NSCs) in the SGZ three days after KA. Then, we wondered whether the neurogenic capacity would be preserved at mid-term after KA (14 d). Interestingly, mice treated with Gefitinib preserved the population of DCX cells in the GCL and SGZ, otherwise greatly reduced in the MTLE mice treated with vehicle. Indeed, the increased morphological complexity characteristic of React-NSCs was also diminished. Moreover, GCD was prevented. The mechanism underlying GCD is still unknown but our data suggest that EGFR is also involved in this process directly or indirectly. In favor of a direct implication, both EGFR signaling and its natural ligand

HB-EGF have been previously shown to regulate developmental migratory processes in the cortex and in the HPF (Aguirre et al., 2004; Caric et al., 2001; Fox and Kornblum, 2005; Kornblum et al., 1999), as well as to confer migratory properties to non-migratory neural progenitors during the postnatal period (Aguirre et al., 2005). Also, EGFR is implicated in migratory functions during the adulthood in regions such as the RMS or the white matter of the hippocampus (Craig et al., 1996; Sibilia et al., 1998) and HB-EGF has been demonstrated to induce migration of immature neurons upon receptor binding (Sugiura et al., 2005; Zhou et al., 2012). Our results show that during the first events after intrahippocampal KA delivery there is an increase of both EGFR and HB-EGF ligand and progressive neuronal and neurogenic niche dispersion. Niche disorganization produces aberrant ectopic circuitry leading to strong consequences. Indeed, neuronal circuits generated after aberrant neurogenesis has been related to play a role in the susceptibility and recurrence of seizures (Jessberger and Parent, 2015), although it has been also suggested that aberrant neurogenesis is not causative of GCD (Fahrner et al., 2007). The mechanisms responsible for neurogenic niche alteration include the migratory properties of NSCs, the mislocalization of the newly generated neurons and the altered pattern of vasculogenesis, which are all key aspects to support neural activity. Their fine characterization is of utmost importance to understand how these alterations can affect normal neuronal circuitry. We hypothesize that reactive gliosis, in turn controlled by EGFR, is driven by GCD and therefore results reduced by Gefitinib.

Some studies have pointed that the absence of EGFR provokes hypersensitivity to epileptic seizures (Robson et al., 2018) and that although NSPCs present their proliferative capacity impaired, they are more prone to differentiate into astrocytes (Robson et al., 2018; Sibilia et al., 1998). Nonetheless, these results were reported using the intraperitoneal model of KA, in which the location of seizures can be more widespread than in MTLE, and a knock-out mouse model for EGFR (Robson et al., 2018). Thus, we postulate that the absence/blockage of EGFR could have different effects in different brain areas and that while a reversible inhibition of EGFR might be beneficial in MTLE, the whole absence of the receptor might lead a completely different and adverse scenario, as the one we observe with the use of Afatinib. In addition, due to recurrent seizures taking place over time in MTLE (Sierra et al., 2015), we cannot exclude the possibility that the neurogenic niche gets disrupted in the long-term even with the initial blocking of EGFR. Although in turn a longer administration of Gefitinib could be proposed. Indeed, given that seizures trigger a plethora of responses within

the HPF, and regarding that blocking of EGFR causes a partial reduction of the effect on the neurogenic niche, we do not consider EGFR to be a unique or the main protagonist governing the induction of React-NSCs, but a part of a more complicated network in which other factors, including other ErbB receptors, ATP and LPA_1 can be playing important roles. However, we do demonstrate the participation of the EGFR signaling pathway in the initiation of the process and the capacity to restrain the adverse effects caused in the neurogenic niche at short-mid-term by blocking it **(Figure D4)**.

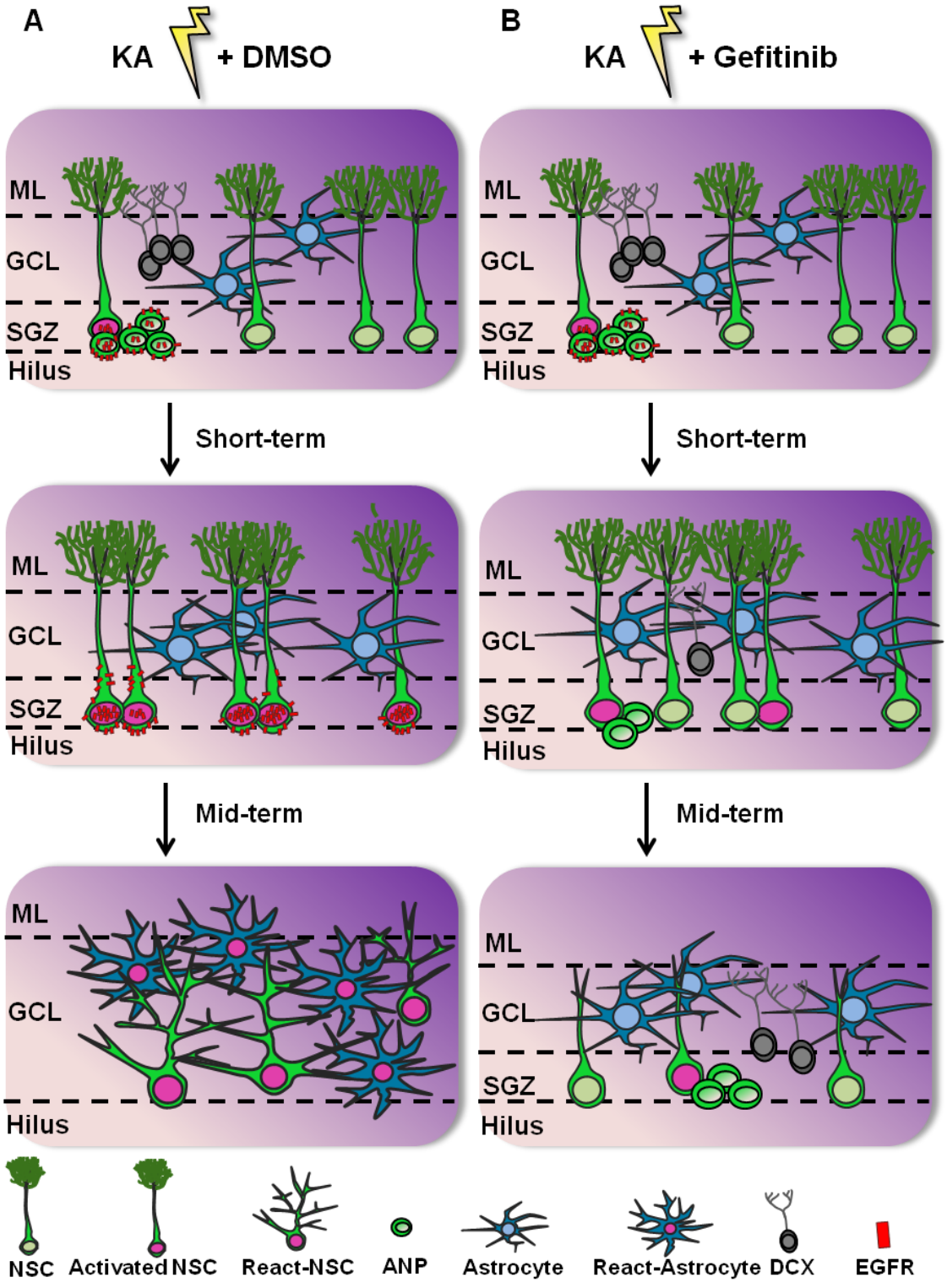

Figure D4. Gefitinib ameliorates the adverse effects provoked by KA in the neurogenic niche and NSCs. A) When KA is intrahippocampally administered the neurogenic niche gets altered. While in normal conditions 2-4% of NSCs get activated (Encinas et al., 2011a), this percentage increases short after KA. This massive activation is preceded by an increase of EGFR expression in NSCs. EGFR, usually present in activated NSCs and ANPs (Jhaveri et al., 2015; Pastrana et al., 2009) switches its expression and it is observable in many NSCs after KA. These early events provoke GCD, induction of React-NSCs and

reactive astrocytes and the complete loss of neurogenic capacity of the niche at mid-term. **B)** The administration of Gefitinib during the first days after KA leads to the reversible blocking of EGFR signaling (illustrated as the absence of the receptor for visualization purposes), thus ameliorating the GCD provoked by KA at mid-term and the induction of React-NSCs. Likewise, the neurogenic capacity of the niche is preserved. Nonetheless, even though the NSCs are not converted into React-NSCs, they lose their characteristic broccoli-like crown, indicating that the effect of KA is not completely reverted.

7.4. Zn^{+2} as a mechanism in the early response of the neurogenic niche and the NSCs in MTLE

Exploring further potential mechanisms that could elicit the response over the NSCs and neurogenic niche after seizures, we drew our attention towards trace metals. Their involvement in convulsive disorders has been previously studied, with iron being the first one reported to induce epileptiform activity and recurrent seizures in different mammalian species (Lange et al., 1980; Willmore et al., 2020). Here we focus on Zn^{+2}, which has been described to be released in the HPF after seizures (Kasarskis et al., 1987; Mody and Miller, 1985) and can also potentially act as modulator of neuronal activity (Bancila et al., 2004; Takeda et al., 2004), also being able to induce cell death (Koh et al., 1996; Lee et al., 2000b). Finally, Zn^{+2} has been shown to interact with the EGFR pathway, activating the receptor both directly and indirectly through the release of HB-EGF (Samet et al., 2003; Wu et al., 2004). We used the Danscher staining method to analyze the amount of Zn^{+2} accumulated in the GCL and in the NSCs after KA. The increase in the granules of Zn^{+2} in the GCL and their colocalization with Nestin-GFP suggest for the first time a possible role of the released Zn^{+2} over the neurogenic niche and NSCs. We also observed the increase of MT1 and MT2 in the HPF, both in charge of encapsulating Zn^{+2}. In contrast, we did not observe any alteration on the levels of MT3, which could be due to differences in the location and regulation respect to MT1 and MT2 (Aschner et al., 1997; Hidalgo et al., 1997). Supporting our results, MT1 and MT2 have been previously reported to increase in the HPF after intraperitoneal KA (Carrasco et al., 2000). Indeed, their absence provokes aggravation of seizures (Carrasco et al., 2000; Cole et al., 2000). Altogether, our results suggest a possible role of Zn^{+2} in the neurogenic niche and on NSCs after seizures. Nonetheless, the system tries to tightly regulate this response, in sight of the increased levels of MT1 and MT2 expression, probably because even though Zn^{+2} could be beneficial in epilepsy by reducing glutamatergic synaptic activation (Bancila et al., 2004; Minami et al., 2006; Takeda et al., 2003), it can also exert neurotoxic effects (Bitanihirwe and Cunningham, 2009; Konoha et al., 2006; Mizuno and Kawahara, 2013).

We assessed the specific effect of Zn^{+2} over the NSCs. For that, we cultured NSPCs *in vitro* and applied Zn^{+2} at different concentrations. We found that low Zn^{+2} concentrations (5 µM) promotes proliferation of NSPCs but these effect switches in a dose-dependent manner, with concentrations higher than 10 µM leading to massive cell death in the cultures. The obtained results agree with previous findings in which cell death was observed in response to Zn^{+2} (Koh et al., 1996; Lee et al., 2000b) and suggests a detrimental effect of Zn^{+2} that is massively released in MTLE. To check the effect on NSCs *in vivo* and given the dose-dependent opposite effect observed *in vitro*, we injected different concentrations of Zn^{+2} intrahippocampally in the DG and analyzed the neurogenic niche 7 d after the injection. Given that the peak of proliferation after KA takes place 3 d after the injection (Sierra et al., 2015), we selected this time point to ensure the correct visualization and assessment of the potential effect of Zn^{+2} upon the niche. We found that Zn^{+2} administration triggers an increase of dividing cells in the SGZ, as well as the morphological induction of React-NSCs and GCD in a dose-dependent manner, thus mimicking the effect of the injection of KA. Therefore, to continue our experiments we picked the lowest dose (20 mM) with which we observed the mentioned effects. Even though Zn^{+2} mediates the morphological transformation of NSCs into React-NSCs, the massive activation or entrance of NSCs into cell cycle is not recapitulated by Zn^{+2} injection. Nonetheless, we could not exclude the option of an early direct effect on NSCs in which they get activated, returning to normal levels thereafter in the absence of further stimuli. In contrast to the KA model, animals do not manifest seizures after Zn^{+2} administration which would explain an early and transitory activation of NSCs that we would be missing analyzing the tissue 7 d after the injection, since we administer BrdU 24 h before sacrifice. Instead, we would be observing the ANP proliferation after the first burst of NSC activation, that in the absence of recurrent seizures do not get massively activated anymore.

7.4.1. Zn^{+2} effect can be driven by EGFR activation

We have described the implication of EGFR and Zn^{+2} in the early events that occur in the hippocampal neurogenic niche after seizures. Interestingly, as indicated before, Zn^{+2} can promote the activation of EGFR either directly and also indirectly by provoking the release of the EGFR natural ligand, HB-EGF, from the cell membrane (Samet et al., 2003; Wu et al., 2004). We hypothesized that the response of the neurogenic niche and especially NSCs could be driven by the interplay of both factors. Resorting to *in vitro* NSPCs, we discovered that Zn^{+2} directly phosphorylates EGFR on the Y845 phosphorylation site, but not on Y1068. Importantly, Zn^{+2} is also able to

strongly provoke the phosphorylation of the ERK1/2, highly related with cellular proliferation (Deschênes-Simard et al., 2014; Lewis et al., 1998; Morrison, 2012). Nevertheless, even though ERK1/2 is one of the downstream signaling pathways of EGFR, Zn^{+2} can also affect this pathway directly through intracellular action (Park and Jae-Young, 1999; Tice et al., 1999). Furthermore, we tested the capacity of Gefitinib to ameliorate the effects that Zn^{+2} provoke on the neurogenic niche. We followed the paradigm previously used for the Gefitinib administration, within the first 3 d post-injection. Our results showed that the Zn^{+2}-induced increase in cell proliferation was reduced in the SGZ by administration of Gefitinib. Moreover, the induction of React-NSCs seemed to be ameliorated. We propose that when Zn^{+2} is injected intrahippocampally, in a model that does not cause recurrent seizures, its EGFR-mediated effect is exerted upon the cells that express EGFR in normal conditions, i.e. ANPs and the few already active NSCs (Jhaveri et al., 2015; Walker et al., 2016). In contrast, KA-induced seizures provoke the increase of EGFR in NSCs, opening the way for extracellular Zn^{+2} to massively activate them. Moreover, since the administration of Zn^{+2} alone let the majority of NSCs untouched and does not cause seizures, we speculate that its effect will be transitory, provoking a boost of neurogenesis that will return to basal levels with time, as it occurs in other models where ANPs, but not NSCs, are induced to activation (Deisseroth et al., 2004; Gould et al., 1999a; Lee et al., 2000a; Lemaire et al., 2000; Nilsson et al., 1999; Van Praag et al., 1999) **(Figure D5)**. Regardless, our results indicate that the effect of Zn^{+2} over the neurogenic niche, at least proliferation, is mediated by the activation of EGFR signaling pathway, shedding light upon a new mechanism and its therapeutic modulation.

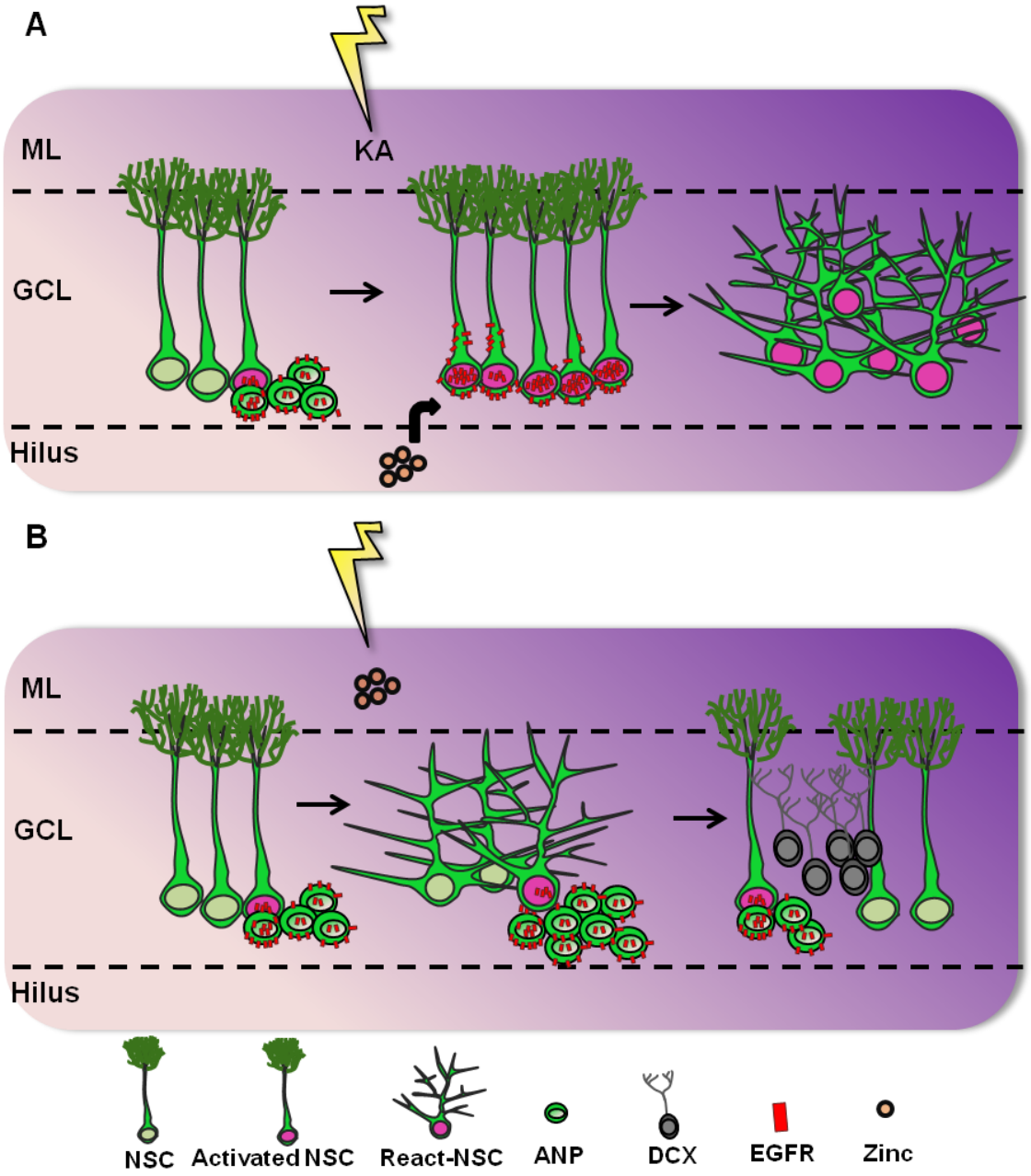

Figure D5. Zinc alone does not provoke the long-term depletion of the neurogenic capacity. A) The intrahippocampal administration of KA provokes the increase of EGFR in NSCs and the massive liberation of Zn^{+2} into the GCL. Consequently, Zn^{+2} binds to NSCs inducing React-NSC transformation and proliferation via EGFR. Thus, React-NSCs symmetrically divide, losing their neurogenic capacity. **B)** In the absence of KA, EGFR expression is restricted to the activated NSCs and ANPs. Moreover, the proliferation induced by intrahippocampal administration of Zn^{+2} is limited to the cells expressing EGFR, provoking the massive division of ANPs. However, Zn^{+2} induces the transformation of NSCs into React-NSCs even in the absence of EGFR, suggesting the implication of other mechanisms or the direct effect of Zn^{+2} upon NSCs. Nevertheless, since the intrahippocampal administration of Zn^{+2} does not provoke seizures, it represents a single insult and its effects will be diluted with time, potentially leading to the recovery of the neurogenic capacity.

7.4.2. Zn^{+2} chelation as a therapeutic approach in MTLE

We next wondered about the possibility of Zn^{+2} being key protagonist in the response of the neurogenic niche after seizures and about the potential beneficial action of its chelation. Therefore, administrated TPEN, a membrane permeable Zn^{+2} chelator (Kim et al., 2012), in our model of MTLE. We tested *in vitro* the possibility of trying Clioquinol, another Zn^{+2} chelator (Bareggi and Cornelli, 2012), but we were inclined to the use of TPEN due to the high level of cell death induced by Clioquinol (data not shown). Thus, we administered TPEN subcutaneously during 7 d after intrahippocampal KA administration, but instead of the expected improvement, we observed a devastating effect in the GCL. In the animals treated with TPEN, not only the GCD is not reduced but the cell death tends to increase. Moreover, the reactivity of the niche, including React-NSCs, was not ameliorated, possibly affected by the huge amount of cellular death undergoing in the GCL. These results are probably due to the neuroprotective effect that Zn^{+2} exerts in a context of neuronal hyperactivation as MTLE, and support the studies observing an increase of the apoptotic cells and worsening of seizures in mice lacking Zn^{+2} (Carrasco et al., 2000; Minami et al., 2006; Takeda et al., 2003). The obtained results indicate that while Zn^{+2} can be one of the mechanisms contributing to the induction of React-NSCs, GCD and hyperproliferation in the SGZ, its quelation is not an effective therapeutic approach in MTLE, as it might counteract the neuroprotective role of Zn^{+2} in the GCL.

7.5. Massively released HB-EGF can activate EGFR in NSPCs in MTLE

So far, we had explored two mechanisms regulating the response of the neurogenic niche and NSCs after seizures: EGFR and its signaling pathway and Zn^{+2}. Interestingly, one of the ways for the possible interplay between both mechanisms involves HB-EGF (Samet et al., 2003; Wu et al., 2004), one of the natural ligands of EGFR (Jones et al., 1999). Therefore, we decided to assess the levels of HB-EGF release in our MTLE model. In normal conditions, HB-EGF expression is present in all the principle layers of the DG from birth to P7, whereas from P14 on it is mainly concentrated in the GCL. Moreover, after seizures induced by intraperitoneal KA, the expression increases during the first 24 h post-injection in the GCL, the ML and also CA1 and CA3. The expression decreases thereafter, yet it remains elevated in vulnerable regions of the HPF and the amygdaloid complex (Opanashuk et al., 1999). Supporting these observations, we observed in our MTLE model an increase of HB-EGF in the HPF within the first 24 h post-KA followed by a return to control levels at 72

h. Nonetheless, the increased HB-EGF levels were maintained in the ML and the hilus at 72 h post-injection, suggesting a possible sustained effect of the ligand in these regions. We propose a model in which after seizures, EGFR is upregulated in NSCs and further activated by the massively released Zn^{+2}, either by direct action or indirect liberation of HB-EGF **(Figure D6)**.

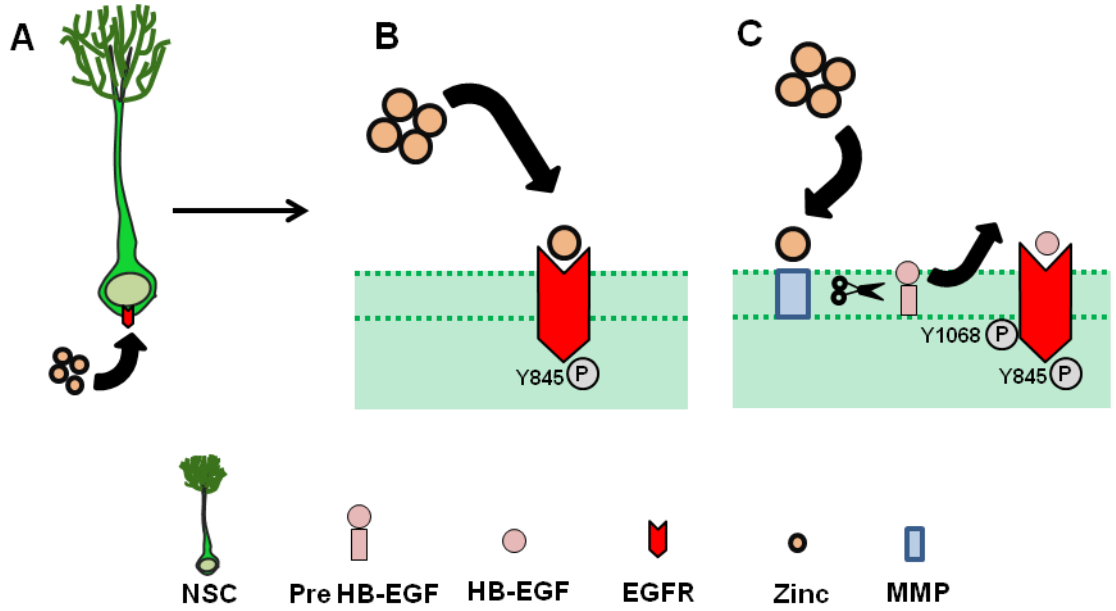

Figure D6. Zn^{+2} activates EGFR through different manners. A) After seizures, massively released Zn^{+2} activates EGFR, which expression is increased in NSCs. **B)** Zn^{+2} can directly activate EGFR, phosphorylating the receptor on its tyrosine kinase Y845 (Samet et al., 2003; Wu et al., 2002). **C)** Zn^{+2} also provokes the release of HB-EGF from its cell-membrane anchored form, probably through matrix metalloproteinase (MMP) shedding (Sanderson et al., 2006; Wu et al., 2004). Indeed, HB-EGF is a potent neuroprotective EGFR ligand that is massively released in the DG after seizures.

We next sought to evaluate the effect of HB-EGF on NSCs resorting to cultured NSPCs. First, we observed that cultured NSPCs release HB-EGF to the media in proliferating conditions. The levels of HB-EGF were highly increased in the media compared to the cellular pellet, suggesting a constant release of HB-EGF from the cell membrane in proliferating conditions. Moreover, after NSPCs are starved from growth factors and EGFR and ERK signaling have been shut off, HB-EGF is capable of stimulating the EGFR signaling pathway again by increasing phosphorylation in both Y845 and Y1068 sites. In contrast, the additional administration of Zn^{+2} does not increase the effect probably due to the prevailing excessive effect of HB-EGF. Nonetheless, although HB-EGF is mainly related to proliferation and migratory processes, ErbB ligands may have different signal transduction cascades depending on the ErbB family receptor they activate/stimulate (Kochupurakkal et al., 2005;

Willmarth and Ethier, 2006; Wilson et al., 2012) and thereby further research would be necessary to properly assess the respond of hippocampal NSCs to HB-EGF. On top of that, we consider worth bearing in mind the possible action of HB-EGF on ErbB4, another receptor of the EGFR family to which HB-EGF can bind. Although the effect on cellular proliferation is not induced by the binding to ErbB4, cellular chemotaxis is, therefore potentially affecting the GCD and React-NSC migration towards the ML (Elenius et al., 1997).

We postulate that HB-EGF might play an important role in the GCD and NSC activation that occur after seizures. The massive liberation of this ligand can provoke an increased activation of the EGFR signaling pathway, triggering the consequent cellular responses (proliferation, reactivation, migration). We do not postulate this as being the only mechanism taking place in MTLE, as we understand that such a complex response has to be driven by a plethora of different mechanims. Indeed, several potential mechanisms could be playing a role through EGFR. LPA_1, a selective marker of adult DG NSCs (Walker et al., 2016) that plays a role in the activation of seizure-induced React-NSCs (Valcárcel-Martín et al., 2020), and its activation by LPA could play a role by EGFR transactivation (Cunnick et al., 1998; Daub, 1997; Daub et al., 1996) in the Y845 phosphorylation site (Gotoh et al., 1992; Tice et al., 1999) in a similar manner than we observe with Zn^{+2}. Additionally, there are diverse ligands capable of producing distinct cellular EGFR-mediated responses (Wilson et al., 2009); Neuregulin-1, another natural ligand of EGFR, selectively increases proliferation and overall neurogenesis in the mouse DG, yet its effects are restricted to the ventral part (Mahar et al., 2016). TGF-α, also a natural ligand of EGFR that is synthesized in the developing and mature brain (Brown et al., 1990) mimics the effects of EGF on NSPCs *in vitro* (Reynolds and Weiss, 1992). Although we did not explore these mechanisms herein, we cannot leave out the possibility of them playing a role in MTLE. We consider that our results open interesting avenues for the study of potential therapies that will preserve the neurogenic niche and neurogenesis, which is our ultimate goal, with special focus in the EGFR signaling pathway. We believe that future alternatives should aim to target more than a unique pathway to avoid compensatory mechanisms, yet studies like ours contribute to the knowledge and help to establish a first stone to pave the way towards a therapeutic alternative.

8. CONCLUSIONS

8. CONCLUSIONS

1. Adult NSCs are generated postnatally as a new population independent from dNSCs rather than remaining as a mere residue from the DG development.

- Adult NSCs are generated during the early postnatal period in a cD2 dependent manner.

- Progenitors located inside the DG early after birth contribute to the generation of the adult NSC pool, while progenitors coming from the DMS are strictly neurogenic.

- The postnatal onset of LPA_1 expression in the SGZ distinguishes adult NSCs from dNSCs.

2. The formation of sequential progenitor matrixes (DNe, DMS, DG) share similar features during the development of human and mouse DG.

- During the human early embryonic development (GW14) heterogeneous populations of dNSCs populate different regions of the HPF (DNe, DMS, DG).

- In humans, Tbr2-expressing progenitors and Ki67-expressing proliferating cells are restricted to the hilus (close to the GCL) before birth.

- Nestin-expressing RGCs remain in the human DG early after birth, although with residual proliferating capacity.

3. The massive activation and induction of React-NSCs in MTLE is regulated by Zn^{+2}- and HB-EGF-induced activation of EGFR.

- EGFR, but not FGFR, is involved in the early response of the HPF after KA administration.

CONCLUSIONS

"Hippocampal NSCs: from Origin to Pathology"

- The increase in the expression and the activation of EGFR and its downstream signaling pathway (STAT3, Akt, ERK1/2) is a key event within the first three days after KA administration.

- Gefitinib is able to inhibit EGFR and its downstream signaling pathway ERK1/2 in NSPCs *in vitro*, effectively blocking their proliferation.

- The intranasal administration of Gefitinib after KA reduces the proliferation in the neurogenic niche and GCD, as well as the activation and reactive transformation of NSCs.

- Zn^{+2} is massively released in the DG after KA administration, accumulating in the GCL close to NSCs.

- Zn^{+2} stimulates proliferation of NSPCs *in vitro* in a dose-dependent manner, causing cell death in high doses.

- Intrahippocampal injection of Zn^{+2} induces proliferation in the SGZ, GCD and reactive transformation of NSCs.

- Zn^{+2} administration into cultured NSPCs induces direct phosphorylation of EGFR in its tyrosine site Y845, but not Y1068.

- The intranasal administration of Gefitinib reverts the massive proliferation in the SGZ provoked by intrahippocampal Zn^{+2} administration.

- Quelation of Zn^{+2} by repeated subcutaneous injections of TPEN after KA administration induces additional cell death, invalidating it as a potential therapy for MTLE.

- HB-EGF is massively released in the DG after KA administration, accumulating in the ML and hilus.

- HB-EGF administration into cultured NSPCs induces strong activation of both EGFR tyrosine sites Y845 and Y1068, as well as its downstream signaling pathway ERK1/2.

9. BIBLIOGRAPHY

9. BIBLIOGRAPHY

A

Abiega, O., Beccari, S., Diaz-Aparicio, I., Nadjar, A., Layé, S., Leyrolle, Q., Gómez-Nicola, D., Domercq, M., Pérez-Samartín, A., Sánchez-Zafra, V., et al. (2016). Neuronal Hyperactivity Disturbs ATP Microgradients, Impairs Microglial Motility, and Reduces Phagocytic Receptor Expression Triggering Apoptosis/Microglial Phagocytosis Uncoupling. PLoS Biol. *14*, 1–48.

Abraham, H., Pérez-García, C.G., and Meyer, G. (2004). p73 and Reelin in Cajal-Retzius Cells of the Developing Human Hippocampal Formation. Cereb. Cortex *14*, 484–495.

Abrous, D.N., and Wojtowicz, J.M. (2015). Interaction between neurogenesis and hippocampal memory system: New vistas. Cold Spring Harb. Perspect. Biol. *7*, 1–24.

Abu-Khaklil, A., Fu, L., Grove, E.A., Zecevic, N., and Geschwind, D.H. (2004). Wnt genes define distinct boundaries in the developing human brain: Implications for human forebrain patterning. J. Comp. Neurol. *474*, 276–288.

Acsády, L., and Káli, S. (2007). Models, structure, function: the transformation of cortical signals in the dentate gyrus. Prog. Brain Res. *163*, 577–599.

Aguirre, A., Rizvi, T.A., Ratner, N., and Gallo, V. (2005). Overexpression of the epidermal growth factor receptor confers migratory properties to nonmigratory postnatal neural progenitors. J. Neurosci. *25*, 11092–11106.

Aguirre, A., Rubio, M.E., and Gallo, V. (2010). Notch and EGFR pathway interaction regulates neural stem cell number and self-renewal. Nature *467*, 323–327.

Aguirre, A.A., Chittajallu, R., Belachew, S., and Gallo, V. (2004). NG2-expressing cells in the subventricular zone are type C-like cells and contribute to interneuron generation in the postnatal hippocampus. J. Cell Biol. *165*, 575–589.

Aimone, J.B., Wiles, J., and Gage, F.H. (2006). Potential role for adult neurogenesis in the encoding of time in new memories. Nat. Neurosci. *9*, 723–727.

Akers, K.G., Martinez-canabal, A., Restivo, L., Yiu, A.P., Cristofaro, A. De, Hsiang, H.L., Wheeler, A.L., Guskjolen, A., Niibori, Y., Shoji, H., et al. (2014). and Infancy. *598*, 598–603.

BIBLIOGRAPHY

"Hippocampal NSCs: from Origin to Pathology"

Alley, M.C., Killam, E.K., and Fisher, G.L. (1981). The influence of D-penicillamine treatment upon seizure activity and trace metal status in the Senegalese baboon, Papio papio. J. Pharmacol. Exp. Ther. *217*, 138–146.

Althaus, A.L., Moore, S.J., Zhang, H., Du, X., Murphy, G.G., and Parent, J.M. (2019). Altered Synaptic Drive onto Birthdated Dentate Granule Cells in Experimental Temporal Lobe Epilepsy. J. Neurosci. *39*, 7604–7614.

Altman, J. (1962a). Are New Neurons Formed in the. Science (80-.). *135*, 0–1.

Altman, J. (1962b). Autoradiographic Regenerative Cells Study Proliferation with Tritiated of Degenerative of Neuroglia Thymidine. Exp. Neurol. *318*, 302–318.

Altman, J. (1963). Autoradiographic investigation of cell proliferation in the brains of rats and cats. Anat. Rec. *145*, 573–591.

Altman, J. (1969a). Autoradiographic and histological studies of postnatal neurogenesis. IV. Cell proliferation and migration in the anterior forebrain, with special reference to persisting neurogenesis in the olfactory bulb. J Comp Neurol 433–457.

Altman, J. (1969b). Autoradiographic and histological studies of postnatal neurogenesis. 3. Dating the time of production and onset of differentiation of cerebellar microneurons in rats. J Comp Neurol *136*, 269–293.

Altman, J., and Bayer, S.A. (1990a). Migration and distribution of two populations of hippocampal granule cell precursors during the perinatal and postnatal periods. J. Comp. Neurol. *301*, 365–381.

Altman, J., and Bayer, S.A. (1990b). Prolonged sojourn of developing pyramidal cells in the intermediate zone of the hippocampus and their settling in the stratum pyramidale. J. Comp. Neurol. *301*, 343–364.

Altman, J., and Bayer, S.A. (1990c). Mosaic organization of the hippocampal neuroepithelium and the multiple germinal sources of dentate granule cells. J Comp Neurol *301*, 325–342.

Altman, J., and Das, G.D. (1965). Autoradiographic and histological evidence of postnatal hippocampal neurogenesis in rats. J Comp Neurol *124*, 319–335.

Altman, J., and Das, G.D. (1966). Autoradiographic and Histological Studies o Postnatal Neurogenesis. J. Comp. Neurol. *126*, 337–389.

Altman, J., and Das, G.D. (1967). Postnatal neurogenesis in the guinea-pig. Nature *214*, 1098–1101.

Amaral, D.G., and Dent, J.A. (1981). Development of the mossy fibers of the dentate gyrus: I. A light and electron microscopic study of the mossy fibers and their expansions. J. Comp. Neurol. *195*, 51–86.

Amaral, D.G., Scharfman, H.E., and Lavenex, P. (2007). The dentate gyrus: fundamental neuroanatomical organization (dentate gyrus for dummies). Prog. Brain Res. *163*, 3–22.

Andersen, J., Urbán, N., Achimastou, A., Ito, A., Simic, M., Ullom, K., Martynoga, B., Lebel, M., Göritz, C., Frisén, J., et al. (2014). A Transcriptional Mechanism Integrating Inputs from Extracellular Signals to Activate Hippocampal Stem Cells. Neuron *83*, 1085–1097.

Andersen, P., Blackstad, T.W., and Lömo, T. (1966). Location and identification of excitatory synapses on hippoeampal pyramidal cells. Exp. Brain Res. *1*, 236–248.

Andersen, P., Bliss, T.V.P., and Skrede, K.K. (1971). Lamellar organization of hippocampal excitatory pathways. Exp. Brain Res. *13*, 222–238.

Andreu, Z., Khan, M.A., González-Gõmez, P., Negueruela, S., Hortigüela, R., San Emeterio, J., Ferrõn, S.R., Martínez, G., Vidal, A., Fariñas, I., et al. (2015). The cyclin-dependent kinase inhibitor p27kip1 regulates radial stem cell quiescence and neurogenesis in the adult hippocampus. Stem Cells *33*, 219–229.

Angevine, J. (1965). Time of neuron origin in the hippocampal region. An autoradiographic study in the mouse. Exp. Neurol. *11*, 1–39.

Aniksztejn, L., Charton, G., and Ben-Ari, Y. (1987). Selective release of endogenous zinc from the hippocampal mossy fibers in situ. Brain Res. *404*, 58–64.

Ansorg, A., Witte, O.W., and Urbach, A. (2012). Age-dependent kinetics of dentate gyrus neurogenesis in the absence of cyclin D2. BMC Neurosci. *13*, 1–13.

Arantius, J.C. (1587). De humano foetu liber. Venetiis: Apud lacobum brechtanum.

Arida, R.M., Scorza, F.A., De Araujo Peres, C., and Cavalheiro, E.A. (1999). The course of untreated seizures in the pilocarpine model of epilepsy. Epilepsy Res. *34*, 99–107.

Arnold, S.E., and Trojanowski, J.Q. (1996). Human fetal hippocampal development: I. Cytoarchitecture, myeloarchitecture, and neuronal morphologic features. J. Comp. Neurol. *367*, 274–292.

Arruda, F., Cendes, F., Andermann, F., Dubeau, F., Villemure, J.G., Jones-Gotman, M., Poulin, N., Arnold, D.L., and Olivier, A. (1996). Mesial atrophy and outcome after

amygdalohippocampectomy or temporal lobe removal. Ann. Neurol. *40*, 446–450.

Arteaga, C.L. (2011). ERBB receptors in cancer: signaling from the inside. Breast Cancer Res. *13*, 304.

Artegiani, B., Lyubimova, A., Muraro, M., van Es, J.H., van Oudenaarden, A., and Clevers, H. (2017). A Single-Cell RNA Sequencing Study Reveals Cellular and Molecular Dynamics of the Hippocampal Neurogenic Niche. Cell Rep. *21*, 3271–3284.

Aschner, M., Cherian, M., Klaassen, C., Palmiter, R.D., Erickson, J., and Bush, A. (1997). Metallothioneins in brain--the role in physiology and pathology. Toxicol Appl Pharmacol *Feb*, 229–242.

Assaf, S.Y., and Chung, S.H. (1984). Release of endogenous Zn2+ from brain tissue during activity. Nature *308*, 734–736.

B

Babb, T.L., Pereira-Leite, J., Mathern, G.W., and Pretorius, J.K. (1995). Kainic acid induced hippocampal seizures in rats: comparisons of acute and chronic seizures using intrahippocampal versus systemic injections. Ital. J. Neurol. Sci. *16*, 39–44.

Bakker, A., Kirwan, C.B., Miller, M., and Stark, C.E.L. (2008). Pattern separation in the human hippocampal CA3 and dentate gyrus. Science (80-.). *319*, 1640–1642.

Bancila, V., Nikonenko, I., Dunant, Y., and Bloc, A. (2004). Zinc inhibits glutamate release via activation of pre-synaptic K ATP channels and reduces ischaemic damage in rat hippocampus. J. Neurochem. *90*, 1243–1250.

Bannerman, D.M., Deacon, R.M.J., Offen, S., Friswell, J., Grubb, M., and Rawlins, J.N.P. (2002). Double dissociation of function within the hippocampus: Spatial memory and hyponeophagia. Behav. Neurosci. *116*, 884–901.

Bannerman, D.M., Rawlins, J.N.P., McHugh, S.B., Deacon, R.M.J., Yee, B.K., Bast, T., Zhang, W.N., Pothuizen, H.H.J., and Feldon, J. (2004). Regional dissociations within the hippocampus - Memory and anxiety. Neurosci. Biobehav. Rev. *28*, 273–283.

Barakat, N.S., Omar, S.A., and Ahmed, A.A.E. (2006). Carbamazepine uptake into rat brain following intra-olfactory transport. J. Pharm. Pharmacol. *58*, 63–72.

Bareggi, S.R., and Cornelli, U. (2012). Clioquinol: Review of its mechanisms of action and clinical uses in neurodegenerative Disorders. CNS Neurosci. Ther. *18*, 41–46.

Barker, J.M., Wojtowicz, J.M., and Boonstra, R. (2005). Where's my dinner? Adult

neurogenesis in free-living food-storing rodents. Genes, Brain Behav. *4*, 89–98.

Bayer, S.A. (1980). Development of the hippocampal region in the rat I. Neurogenesis examined with 3H- thymidine autoradiography. J. Comp. Neurol. *190*, 87–114.

Bayer, S.A., and Altman, J. (1974). Hippocampal development in the rat: Cytogenesis and morphogenesis examined with autoradiography and low-level X-irradiation. J. Comp. Neurol. *158*, 55–79.

Beccari, S., Valero, J., Maletic-Savatic, M., and Sierra, A. (2017). A simulation model of neuroprogenitor proliferation dynamics predicts age-related loss of hippocampal neurogenesis but not astrogenesis. Sci. Rep. *7*, 1–13.

Becker, S. (2017). Neurogenesis and pattern separation: time for a divorce. Wiley Interdiscip. Rev. Cogn. Sci. *8*, 1–15.

Becker, S., and Wojtowicz, J.M. (2007). A model of hippocampal neurogenesis in memory and mood disorders. Trends Cogn. Sci. *11*, 70–76.

Beenken, A., and Mohammadi, M. (2009). The FGF family: Biology, pathophysiology and therapy. Nat. Rev. Drug Discov. *8*, 235–253.

Bell, G.S., Gaitatzis, A., Bell, C.L., Johnson, A.L., and Sander, J.W. (2009). Suicide in people with epilepsy: How great is the risk? Epilepsia *50*, 1933–1942.

Ben-Ari, Y., Lagowska, J., Tremblay, E., and Le Gal La Salle, G. (1979). A new model of focal status epilepticus: intra-amygdaloid application of kainic acid elicits repetitive secondarily generalized convulsive seizures. Brain Res. *163*, 176–179.

Berg, D.A., Su, Y., Jimenez-Cyrus, D., Patel, A., Huang, N., Morizet, D., Lee, S., Shah, R., Ringeling, F.R., Jain, R., et al. (2019). A Common Embryonic Origin of Stem Cells Drives Developmental and Adult Neurogenesis. Cell *177*, 654-668.e15.

Berger, O., Li, G., Han, S.M., Paredes, M., and Pleasure, S.J. (2006). Expression of SDF-1 and CXCR4 during reorganization of the postnatal dentate gyrus. Dev. Neurosci. *29*, 48–58.

Bessman, N.J., Freed, D.M., and Lemmon, M.A. (2014). Putting together structures of epidermal growth factor receptors. Curr. Opin. Struct. Biol. *29*, 95–101.

Del Bigio, M.R. (1999). Proliferative status of cells in adult human dentate gyrus. Microsc. Res. Tech. *45*, 353–358.

Binder, D., and Steinhäuser, C. (2006). Functional changes in astroglial cells in epilepsy. Glia *54*, 358–368.

BIBLIOGRAPHY

"Hippocampal NSCs: from Origin to Pathology"

Biscardi, J.S., Maa, M.C., Tice, D.A., Cox, M.E., Leu, T.H., and Parsons, S.J. (1999). C-Src-mediated phosphorylation of the epidermal growth factor receptor on Tyr845 and Tyr1101 is associated with modulation of receptor function. J. Biol. Chem. *274*, 8335–8343.

Bitanihirwe, B., and Cunningham, M. (2009). Zinc: the brain's dark horse. Synapse *63*, 1029–1049.

Blackstad, T.W. (1956). Commissural connections of the hippocampal region in the rat, with special reference to their mode of termination. J. Comp. Neurol. *105*, 417–537.

Blackstad, T.W. (1958). On the termination of some afferents to the hippocampus and fascia dentata. Cells Tissues Organs *35*, 202–214.

Blackstad, T.W., Brink, K., Hem, J., and June, B. (1970). Distribution of hippocampal mossy fibers in the rat. An experimental study with silver impregnation methods. J. Comp. Neurol. *138*, 433–449.

Blumcke, I., Suter, B., Behle, K., Kuhn, R., Schramm, J., Elger, C.E., and Wiestler, O.D. (2000). Loss of Hilar Mossy Cells in Ammon's Horn Sclerosis. Epilepsia *41*, S174–S180.

Blümcke, I., Schewe, J.C., Normann, S., Brüstle, O., Schramm, J., Elger, C.E., and Wiestler, O.D. (2001). Increase of nestin-immunoreactive neural precursor cells in the dentate gyrus of pediatric patients with early-onset temporal lobe epilepsy. Hippocampus *11*, 311–321.

Blümcke, I., Thom, M., and Wiestler, O.D. (2002). Ammon's horn sclerosis: a maldevelopmental disorder associated with temporal lobe epilepsy. Brain Pathol. *12*, 199–211.

Blümcke, I., Thom, M., Aronica, E., Armstrong, D.D., Bartolomei, F., Bernasconi, A., Bernasconi, N., Bien, C.G., Cendes, F., Coras, R., et al. (2013). International consensus classification of hippocampal sclerosis in temporal lobe epilepsy: A Task Force report from the ILAE Commission on Diagnostic Methods. Epilepsia *54*, 1315–1329.

Boldrini, M., Fulmore, C.A., Tartt, A.N., Simeon, L.R., Pavlova, I., Poposka, V., Rosoklija, G.B., Stankov, A., Arango, V., Dwork, A.J., et al. (2018). Human Hippocampal Neurogenesis Persists throughout Aging. Cell Stem Cell *22*, 589-599.e5.

Bonaguidi, M.A., Wheeler, M.A., Shapiro, J.S., Stadel, R.P., Sun, G.J., Ming, G.L., and Song, H. (2011). In vivo clonal analysis reveals self-renewing and multipotent adult

neural stem cell characteristics. Cell *145*, 1142–1155.

Borrell, V., Del Río, J.A., Alcántara, S., Derer, M., Martínez, A., D'Arcangelo, G., Nakajima, K., Mikoshiba, K., Derer, P., Curran, T., et al. (1999). Reelin regulates the development and synaptogenesis of the layer- specific entorhino-hippocampal connections. J. Neurosci. *19*, 1345–1358.

Bouilleret, V., Ridoux, V., Depaulis, A., Marescaux, C., Nehlig, A., and Le Gal La Salle, G. (1999). Recurrent seizures and hippocampal sclerosis following intrahippocampal kainate injection in adult mice: Electroencephalography, histopathology and synaptic reorganization similar to mesial temporal lobe epilepsy. Neuroscience *89*, 717–729.

Braun, S.M.G., Pilz, G.A., Machado, R.A.C., Moss, J., Becher, B., Toni, N., and Jessberger, S. (2015). Programming Hippocampal Neural Stem/Progenitor Cells into Oligodendrocytes Enhances Remyelination in the Adult Brain after Injury. Cell Rep. *11*, 1679–1685.

Breunig, J.J., Silbereis, J., Vaccarino, F.M., Šestan, N., and Rakic, P. (2007a). Notch regulates cell fate and dendrite morphology of newborn neurons in the postnatal dentate gyrus. Proc. Natl. Acad. Sci. U. S. A. *104*, 20558–20563.

Breunig, J.J., Arellano, J.I., Macklis, J.D., and Rakic, P. (2007b). Everything that Glitters Isn't Gold: A Critical Review of Postnatal Neural Precursor Analyses. Cell Stem Cell *1*, 612–627.

Briellmann, R.S., Kalnins, R.M., Berkovic, S.F., and Jackson, G.D. (2002). Hippocampal pathology in refractory temporal lobe epilepsy: T2-weighted signal change reflects dentate gliosis. Neurology *58*, 265–271.

Brodal, A. (1947). The hippocampus and the sense of smell: A review. Brain *70*, 179–222.

Brown, P., Lam, R., Lakshmanan, J., and Fisher, D. (1990). Transforming growth factor alpha in developing rats. Am J Physiol *Aug*, 256–260.

Brunne, B., Zhao, S., Derouiche, A., Herz, J., Petra, M., Frotscher, M., and Bock, H.H. (2010). Origin, maturation, and astroglial transformation of secondary radial glial cells in the developing dentate gyrus. Glia *58*, 1553–1569.

Brunne, B., Franco, S., Bouché, E., Herz, J., Howell, B.W., Pahle, J., Müller, U., May, P., Frotscher, M., and Bock, H.H. (2013). Role of the postnatal radial glial scaffold for the development of the dentate gyrus as revealed by Reelin signaling mutant mice. Glia *July*, 1347–1363.

Brunne, B., Franco, S., Bouché, E., Herz, J., Howell, B.W., Pahle, J., Müller, U., May, P., Frotscher, M., and Bock, H.H. (2014). the dentate gyrus as revealed by Reelin signaling mutant mice. *61*, 1347–1363.

Bryans, W.A. (1959). Mitotic activity in the brain of the adult rat. Anat. Rec. *133*, 65–73.

Bulchand, S., Grove, E.A., Porter, F.D., and Tole, S. (2001). LIM-homeodomain gene Lhx2 regulates the formation of the cortical hem. Mech. Dev. *100*, 165–175.

Burgoyne, L. (1999). The Mechanisms of Pyknosis: Hypercondensation and death. Exp. Cell Res. *248*, 214–222.

Burrows, R.C., Wancio, D., Levitt, P., and Lillien, L. (1997). Response diversity and the timing of progenitor cell maturation are regulated by developmental changes in EGFR expression in the cortex. Neuron *19*, 251–267.

C

Calof, A.L. (1995). Intrinsic and extrinsic factors regulating vertebrate neurogenesis. Curr. Opin. Neurobiol. *5*, 19–27.

Cameron, H.A., Woolley, C.S., McEwen, B.S., and Gould, E. (1993). Differentiation of newly born neurons and glia in the dentate gyrus of the adult rat. Neuroscience *56*, 337–344.

Caric, D., Raphael, H., Viti, J., Feathers, A., Wancio, D., and Lillien, L. (2001). EGFRs mediate chemotactic migration in the developing telencephalon. Development *128*, 4203–4216.

Carpenter, G. (1983). The biochemistry and physiology of the receptor-kinase for epidermal growth factor. Mol. Cell. Endocrinol. *31*, 1–19.

Carpenter, G. (1999). Factor – independent Signaling Pathways. Cell *146*, 697–702.

Carpenter, G. (2000). EGF receptor transactivation mediated by the proteolytic production of EGF-like agonists. Sci. STKE *2000*, 1–4.

Carpenter, G., King, L., and Cohen, S. (1978). Epidermal growth factor stimulates phosphorylation in membrane preparations in vitro [21]. Nature *276*, 409–410.

Carrasco, J., Penkowa, M., Hadberg, H., Molinero, A., and Hidalgo, J. (2000). Enhanced seizures and hippocampal neurodegeneration following kainic acid-induced seizures in metallothionein-I + II-deficient mice. Eur. J. Neurosci. *12*, 2311–2322.

Carrillo-García, C., Prochnow, S., Simeonova, I.K., Strelau, J., Hölzl-Wenig, G., Mandl,

C., Unsicker, K., von Bohlen und Halbach, O., and Ciccolini, F. (2014). Growth/differentiation factor 15 promotes EGFR signalling, and regulates proliferation and migration in the hippocampus of neonatal and young adult mice. Dev. *141*, 773–783.

Cavalheiro, E. (1995). The pilocarpine model of epilepsy. Ital J Neurol Sci *16*, 33–37.

Cavalheiro, E.A., Riche, D.A., and Le Gal La Salle, G. (1982). Long-term effects of intrahippocampal kainic acid injection in rats: A method for inducing spontaneous recurrent seizures. Electroencephalogr. Clin. Neurophysiol. *53*, 581–589.

Cendes, F., Sakamoto, A.C., Spreafico, R., Bingaman, W., and Becker, A.J. (2014). Epilepsies associated with hippocampal sclerosis. Acta Neuropathol. *128*, 21–37.

Cha, B.H., Akman, C., Silveira, D.C., Liu, X., and Holmes, G.L. (2004). Spontaneous recurrent seizure following status epilepticus enhances dentate gyrus neurogenesis. Brain Dev. *26*, 394–397.

Chauvière, L., Doublet, T., Ghestem, A., Siyoucef, S.S., Wendling, F., Huys, R., Jirsa, V., Bartolomei, F., and Bernard, C. (2012). Changes in interictal spike features precede the onset of temporal lobe epilepsy. Ann. Neurol. *71*, 805–814.

Chawla, M.K., Guzowski, J.F., Ramirez-Amaya, V., Lipa, P., Hoffman, K.L., Marriott, L.K., Worley, P.F., McNaughton, B.L., and Barnes, C.A. (2005). Sparse, environmentally selective expression of Arc RNA in the upper blade of the rodent fascia dentata by brief spatial experience. Hippocampus *15*, 579–586.

Chen, Y.M. (2013). Update of epidermal growth factor receptor-tyrosine kinase inhibitors in non-small-cell lung cancer. J. Chinese Med. Assoc. *76*, 249–257.

Chevaleyre, V., and Siegelbaum, S.A. (2010). Strong CA2 pyramidal neuron synapses define a powerful disynaptic cortico-hippocampal loop. Neuron *66*, 560–572.

Ciaroni, S., Cecchini, T., Ferri, P., Ambrogini, P., Cuppini, R., Lombardelli, G., Peruzzi, G., and Del Grande, P. (2002). Postnatal development of rat dentate gyrus: Effects of methylazoxymethanol administration. Mech. Ageing Dev. *123*, 499–509.

Ciccolini, F., and Svendsen, C.N. (1998). Fibroblast growth factor 2 (FGF-2) promotes acquisition of epidermal growth factor (EGF) responsiveness in mouse striatal precursor cells: Identification of neural precursors responding to both EGF and FGF-2. J. Neurosci. *18*, 7869–7880.

Ciccolini, F., Mandl, C., Hölzl-Wenig, G., Kehlenbach, A., and Hellwig, A. (2005). Prospective isolation of late development multipotent precursors whose migration is

promoted by EGFR. Dev. Biol. *284*, 112–125.

Ciemerych, M.A., Kenney, A.M., Sicinska, E., Kalaszczynska, I., Bronson, R.T., Rowitch, D.H., Gardner, H., and Sicinski, P. (2002). Development of mice expressing a single D-type cyclin. Genes Dev. *16*, 3277–3289.

Cipriani, S., Nardelli, J., Verney, C., Delezoide, A.L., Guimiot, F., Gressens, P., and Adle-Biassette, H. (2016). Dynamic Expression Patterns of Progenitor and Pyramidal Neuron Layer Markers in the Developing Human Hippocampus. Cereb. Cortex *26*, 1255–1271.

Cipriani, S., Journiac, N., Nardelli, J., Verney, C., Delezoide, A.L., Guimiot, F., Gressens, P., and Adle-Biassette, H. (2017). Dynamic Expression Patterns of Progenitor and Neuron Layer Markers in the Developing Human Dentate Gyrus and Fimbria. Cereb. Cortex *27*, 358–372.

Cipriani, S., Ferrer, I., Aronica, E., Kovacs, G.G., Verney, C., Nardelli, J., Khung, S., Delezoide, A.L., Milenkovic, I., Rasika, S., et al. (2018). Hippocampal radial glial subtypes and their neurogenic potential in human fetuses and healthy and Alzheimer's disease adults. Cereb. Cortex *28*, 2458–2478.

Clarke, L., and Van Der Kooy, D. (2011). The adult mouse dentate gyrus contains populations of committed progenitor cells that are distinct from subependymal zone neural stem cells. Stem Cells *29*, 1448–1458.

Clemenson, G.D., Lee, S.W., Deng, W., Barrera, V.R., Iwamoto, K.S., Fanselow, M.S., and Gage, F.H. (2015). Enrichment rescues contextual discrimination deficit associated with immediate shock. Hippocampus *25*, 385–392.

Codega, P., Silva-Vargas, V., Paul, A., Maldonado-Soto, A.R., DeLeo, A.M., Pastrana, E., and Doetsch, F. (2014). Prospective Identification and Purification of Quiescent Adult Neural Stem Cells from Their In Vivo Niche. Neuron *82*, 545–559.

Cole, T.B., Robbins, C.A., Wenzel, H.J., Schwartzkroin, P.A., and Palmiter, R.D. (2000). Seizures and neuronal damage in mice lacking vesicular zinc. Epilepsy Res. *39*, 153–169.

Cooper, J.M., Gadian, D.G., Jentschke, S., Goldman, A., Munoz, M., Pitts, G., Banks, T., Chong, W.K., Hoskote, A., Deanfield, J., et al. (2015). Neonatal hypoxia, hippocampal atrophy, and memory impairment: Evidence of a causal sequence. Cereb. Cortex *25*, 1469–1476.

Coras, R., Siebzehnrubl, F.A., Pauli, E., Huttner, H.B., Njunting, M., Kobow, K.,

Villmann, C., Hahnen, E., Neuhuber, W., Weigel, D., et al. (2010). Low proliferation and differentiation capacities of adult hippocampal stem cells correlate with memory dysfunction in humans. Brain *133*, 3359–3372.

Corotto, F.S., Henegar, J.A., and Maruniak, J.A. (1993). Neurogenesis persists in the subependymal layer of the adult mouse brain. Neurosci. Lett. *149*, 111–114.

Craig, C.G., Tropepe, V., Morshead, C.M., Reynolds, B.A., Weiss, S., and Van Der Kooy, D. (1996). In vivo growth factor expansion of endogenous subependymal neural precursor cell populations in the adult mouse brain. J. Neurosci. *16*, 2649–2658.

Crespel, A., Rigau, V., Coubes, P., Rousset, M.C., De Bock, F., Okano, H., Baldy-Moulinier, M., Bockaert, J., and Lerner-Natoli, M. (2005). Increased number of neural progenitors in human temporal lobe epilepsy. Neurobiol. Dis. *19*, 436–450.

Cuccioli, V., Bueno, C., Belvindrah, R., Lledo, P.M., and Martinez, S. (2015). Attractive action of FGF-signaling contributes to the postnatal developing hippocampus. Hippocampus *25*, 486–499.

Cully, M., You, H., Levine, A.J., and Mak, T.W. (2006). Beyond PTEN mutations: The PI3K pathway as an integrator of multiple inputs during tumorigenesis. Nat. Rev. Cancer *6*, 184–192.

Cunnick, J.M., Dorsey, J.F., Standley, T., Turkson, J., Kraker, A.J., Fry, D.W., Jove, R., and Wu, J. (1998). Role of tyrosine kinase activity of epidermal growth factor receptor in the lysophosphatidic acid-stimulated mitogen-activated protein kinase pathway. J. Biol. Chem. *273*, 14468–14475.

Curia, G., Longo, D., Biagini, G., Jones, R.S.G., and Avoli, M. (2008). The pilocarpine model of temporal lobe epilepsy. J. Neurosci. Methods *172*, 143–157.

D

Dalby, N.O., and Mody, I. (2001). The process of epileptogenesis: A pathophysiological approach. Curr. Opin. Neurol. *14*, 187–192.

Danscher, G. (1981). Histochemical demonstration of heavy metals - A revised version of the sulphide silver method suitable for both light and electronmicroscopy. Histochemistry *71*, 1–16.

Das, G.D., and Altman, J. (1971). Postnatal neurogenesis in the cerebellum of the cat and evaluation of the autoradiograms. Brain *30*, 323–330.

Datson, N.A., Van der Perk, J., De Ronald Kloet, E., and Vreugdenhil, E. (2001). Expression profile 30,000 genes in rat hippocampus using SAGE. Hippocampus *11*, 430–444.

Datson, N.A., Meijer, L., Steenbergen, P.J., Morsink, M.C., Van Der Laan, S., Meijer, O.C., and De Kloet, E.R. (2004). Expression profiling in laser-microdissected hippocampal subregions in rat brain reveals large subregion-specific differences in expression. Eur. J. Neurosci. *20*, 2541–2554.

Daub, H. (1997). Signal characteristics of G protein-transactivated EGF receptor. EMBO J. *16*, 7032–7044.

Daub, H., Weiss, F.U., Wallasch, C., and Ullrich, A. (1996). G-protein-coupled receptors Blot Ab : I- Blot Ab : *379*, 557–560.

David, M., Wong, L., Flavell, R., Thompson, S.A., Wells, A., Larner, A.C., and Johnson, G.R. (1996). STAT Activation by Epidermal Growth Factor (EGF) and Amphiregulin. J. Biol. Chem. *271*, 9185–9188.

Deisseroth, K., Singla, S., Toda, H., Monje, M., Palmer, T.D., and Malenka, R.C. (2004). Excitation-neurogenesis coupling in adult neural stem/progenitor cells. Neuron *42*, 535–552.

Deng, W., Aimone, J.B., and Gage, F.H. (2010). New neurons and new memories: How does adult hippocampal neurogenesis affect learning and memory? Nat. Rev. Neurosci. *11*, 339–350.

Dennis, C. V., Suh, L.S., Rodriguez, M.L., Kril, J.J., and Sutherland, G.T. (2016). Human adult neurogenesis across the ages: An immunohistochemical study. Neuropathol. Appl. Neurobiol. *42*, 621–638.

Dennis, C. V., Suh, L.S., Rodriguez, M.L., Kril, J.J., and Sutherland, G.T. (2017). Response to: Comment on 'Human adult neurogenesis across the ages: An immunohistochemical study.' Neuropathol. Appl. Neurobiol. *43*, 452–454.

Deschênes-Simard, X., Kottakis, F., Meloche, S., and Ferbeyre, G. (2014). ERKs in cancer: Friends or foes? Cancer Res. *74*, 412–419.

Dibble, C.C., and Cantley, L.C. (2015). Regulation of mTORC1 by PI3K signaling. Trends Cell Biol. *25*, 545–555.

Dionne, C.A., Crumley, G., Bellot, F., Kaplow, J.M., Searfoss, G., Ruta, M., Burgess, W.H., Jaye, M., and Schlessinger, J. (1990). Cloning and expression of two distinct high-affinity receptors cross-reacting with acidic and basic fibroblast growth factors.

EMBO J. *9*, 2685–2692.

Donaldson, J., St Pierre, T., Minnich, J., and Barbeau, A. (1971). Seizures in rats associated with divalent cation inhibition of NA + -K + -ATP'ase. Can. J. Biochem. *49*, 1217–1224.

Dorn, M., Lidzba, K., Bevot, A., Goelz, R., Hauser, T.K., and Wilke, M. (2014). Long-term neurobiological consequences of early postnatal hCMV-infection in former preterms: A Functional MRI study. Hum. Brain Mapp. *35*, 2594–2606.

Downward, J. (2003). Targeting RAS signalling pathways in cancer therapy. Nat. Rev. Cancer *3*, 11–22.

Downward, J., Parker, P., and Waterfield, M.D. (1984). Autophosphorylation sites on the epidermal growth factor receptor. Nature *311*, 483–485.

Drew, L.J., Fusi, S., and Hen, R. (2013). Adult neurogenesis in the mammalian hippocampus: Why the dentate gyrus? Learn. Mem. *20*, 710–729.

Duque, A., and Spector, R. (2019). A balanced evaluation of the evidence for adult neurogenesis in humans: implication for neuropsychiatric disorders. Brain Struct. Funct. *224*, 2281–2295.

Dziedzic, B., Prevot, V., Lomniczi, A., Jung, H., Cornea, A., and Ojeda, S.R. (2003). Neuron-to-glia signaling mediated by excitatory amino acid receptors regulates ErbB receptor function in astroglial cells of the neuroendocrine brain. J. Neurosci. *23*, 915–926.

E

Earp, H.S., Dawson, T.L., Li, X., and Yu, H. (1995). Heterodimerization and functional interaction between EGF receptor family members: a new signaling paradigm with implications for breast cancer research. Breast Cancer Res. Treat. *35*, 115–132.

Eckenhoff, M.F., and Rakic, P. (1984). Radial organization of the hippocampal dentate gyrus: A Golgi, ultrastructural, and immunocytochemical analysis in the developing rhesus monkey. J. Comp. Neurol. *223*, 1–21.

Eckenhoff, M.F., and Rakic, P. (1988). Nature and fate of proliferative cells in the hippocampal dentate gyrus during the life span of the rhesus monkey. J. Neurosci. *8*, 2729–2747.

Eguchi, S., Numaguchi, K., Iwasaki, H., Matsumoto, T., Yamakawa, T., Utsunomiya,

H., Motley, E.D., Kawakatsu, H., Owada, K.M., Hirata, Y., et al. (1998). Calcium-dependent epidermal growth factor receptor transactivation mediates the angiotensin II-induced mitogen-activated protein/kinase activation in vascular smooth muscle cells. J. Biol. Chem. *273*, 8890–8896.

Eid, T., Lee, T.S.W., Patrylo, P., and Zaveri, H.P. (2019). Astrocytes and Glutamine Synthetase in Epileptogenesis. J. Neurosci. Res. *97*, 1345–1362.

Ekholm, S. V., and Reed, S.I. (2000). Regulation of G1 cyclin-dependent kinases in the mammalian cell cycle. Curr. Opin. Cell Biol. *12*, 676–684.

Elenius, K., Paul, S., Allison, G., Sun, J., and Klagsbrun, M. (1997). Activation of HER4 by heparin-binding EGF-like growth factor stimulates chemotaxis but not proliferation. EMBO J. *16*, 1268–1278.

Encinas, J.M., and Enikolopov, G. (2008). Identifying and Quantitating Neural Stem and Progenitor Cells in the Adult Brain. Methods Cell Biol. *85*, 243–272.

Encinas, J.M., and Sierra, A. (2012). Neural stem cell deforestation as the main force driving the age-related decline in adult hippocampal neurogenesis. Behav. Brain Res. *227*, 433–439.

Encinas, J.M., Vaahtokari, A., and Enikolopov, G. (2006). Fluoxetine targets early progenitor cells in the adult brain. Proc. Natl. Acad. Sci. U. S. A. *103*, 8233–8238.

Encinas, J.M., Michurina, T. V., Peunova, N., Park, J.H., Tordo, J., Peterson, D.A., Fishell, G., Koulakov, A., and Enikolopov, G. (2011a). Division-coupled astrocytic differentiation and age-related depletion of neural stem cells in the adult hippocampus. Cell Stem Cell *8*, 566–579.

Encinas, J.M., Hamani, C., Lozano, A.M., and Enikolopov, G. (2011b). Neurogenic hippocampal targets of deep brain stimulation. J. Comp. Neurol. *519*, 6–20.

Eriksson, P.S., Perfilieva, E., Björk-Eriksson, T., Alborn, A.M., Nordborg, C., Peterson, D.A., and Gage, F.H. (1998). Neurogenesis in the adult human hippocampus. Nat. Med. *4*, 1313–1317.

Estivill-Torrús, G., Llebrez-Zayas, P., Matas-Rico, E., Santín, L., Pedraza, C., De Diego, I., Del Arco, I., Fernández-Llebrez, P., Chun, J., and De Fonseca, F.R. (2008). Absence of LPA1 signaling results in defective cortical development. Cereb. Cortex *18*, 938–950.

F

Faber-Elman, A., Solomon, A., Abraham, J.A., Marikovsky, M., and Schwartz, M. (1996). Involvement of wound-associated factors in rat brain astrocyte migratory response to axonal injury: In vitro simulation. J. Clin. Invest. *97*, 162–171.

Fahrner, A., Kann, G., Flubacher, A., Heinrich, C., Freiman, T.M., Zentner, J., Frotscher, M., and Haas, C.A. (2007). Granule cell dispersion is not accompanied by enhanced neurogenesis in temporal lobe epilepsy patients. Exp. Neurol. *203*, 320–332.

Falconer, M.A., Serafetinides, E.A., and Corsellis, J.A.N. (1964). Etiology and Pathogenesis of Temporal Lobe Epilepsy. Arch. Neurol. *10*, 233–248.

Fanselow, M.S., and Dong, H.W. (2010). Are the Dorsal and Ventral Hippocampus Functionally Distinct Structures? Neuron *65*, 7–19.

Fazel, S., Wolf, A., Långström, N., Newton, C.R., and Lichtenstein, P. (2013). Premature mortality in epilepsy and the role of psychiatric comorbidity: A total population study. Lancet *382*, 1646–1654.

Ferrer, I., Alcántara, S., Ballabriga, J., Olivé, M., Blanco, R., Rivera, R., Carmona, M., Berruezo, M., Pitarch, S., and Planas, A.M. (1996). Transforming growth factor-α (TGF-α) and epidermal growth factor-receptor (EGF-R) immunoreactivity in normal and pathologic brain. Prog. Neurobiol. *49*, 99–119.

Filippov, V., Kronenberg, G., Pivneva, T., Reuter, K., Steiner, B., Wang, L.P., Yamaguchi, M., Kettenmann, H., and Kempermann, G. (2003). Subpopulation of nestin-expressing progenitor cells in the adult murine hippocampus shows electrophysiological and morphological characteristics of astrocytes. Mol. Cell. Neurosci. *23*, 373–382.

Fisher, R.S. (2015). Redefining epilepsy. Curr. Opin. Neurol. *28*, 130–135.

Fisher, R.S., Van Emde Boas, W., Blume, W., Elger, C., Genton, P., Lee, P., and Engel, J. (2005). Response: Definitions proposed by the International League Against Epilepsy (ILAE) and the International Bureau for Epilepsy (IBE) [4]. Epilepsia *46*, 1701–1702.

Fisher, R.S., Acevedo, C., Arzimanoglou, A., Bogacz, A., Cross, J.H., Elger, C.E., Engel, J., Forsgren, L., French, J.A., Glynn, M., et al. (2014). ILAE Official Report: A practical clinical definition of epilepsy. Epilepsia *55*, 475–482.

Fisher, R.S., Cross, J.H., French, J.A., Higurashi, N., Hirsch, E., Jansen, F.E., Lagae, L., Moshé, S.L., Peltola, J., Roulet Perez, E., et al. (2017). Operational classification of

seizure types by the International League Against Epilepsy: Position Paper of the ILAE Commission for Classification and Terminology. Epilepsia *58*, 522–530.

Flor-García, M., Terreros-Roncal, J., Moreno-Jiménez, E.P., Ávila, J., Rábano, A., and Llorens-Martín, M. (2020). Unraveling human adult hippocampal neurogenesis. Nat. Protoc. 1–26.

Förster, E., Tielsch, A., Saum, B., Weiss, K.H., Johanssen, C., Graus-Porta, D., Müller, U., and Frotscher, M. (2002). Reelin, disabled 1, and β1 integrins are required for the formation of the radial glial scaffold in the hippocampus. Proc. Natl. Acad. Sci. U. S. A. *99*, 13178–13183.

Fox, I.J., and Kornblum, H.I. (2005). Developmental profile of ErbB receptors in murine central nervous system: Implications for functional interactions. J. Neurosci. Res. *79*, 584–597.

Frederickson, C.J. (1989). Neurobiology of Zinc and Zinc-Containing Neurons. Int. Rev. Neurobiol. *31*, 145–238.

Frederickson, C.J., and Danscher, G. (1990). Zinc-containing neurons in hippocampus and related CNS structures. Prog. Brain Res. *83*, 71–84.

Frederickson, C.J., Klitenick, M.A., Manton, W.I., and Kirkpatrick, J.B. (1983). Cytoarchitectonic distribution of zinc in the hippocampus of man and the rat. Brain Res. *273*, 335–339.

Frotscher, M., Haas, C.A., and Förster, E. (2003). Reelin controls granule cell migration in the dentate gyrus by acting on the radial glial scaffold. Cereb. Cortex *13*, 634–640.

Fuentealba, L.C., Rompani, S.B., Parraguez, J.I., Obernier, K., Romero, R., Cepko, C.L., and Alvarez-Buylla, A. (2015). Embryonic origin of postnatal neural stem cells. Cell *161*, 1644–1655.

Fukahori, M., and Itoh, M. (1990). Effects of dietary zinc status on seizure susceptibility and hippocampal zinc content in the El (epilepsy) mouse. Brain Res. *529*, 16–22.

Fukahori, M., Itoh, M., Oomagari, K., and Kawasaki, H. (1988). Zinc content in discrete hippocampal and amygdaloid areas of the epilepsy (El) mouse and normal mice. Brain Res. *455*, 381–384.

De Furtado, M.A., Braga, G.K., Oliveira, J.A.C., Del Vecchio, F., and Garcia-Cairasco, N. (2002). Behavioral, morphologic, and electroencephalographic evaluation of seizures induced by intrahippocampal microinjection of pilocarpine. Epilepsia *43*, 37–39.

Furuta, Y., Piston, D.W., and Hogan, B.L.M. (1997). Bone morphogenetic proteins (BMPs) as regulators of dorsal forebrain development. Development *124*, 2203–2212.

Furutachi, S., Miya, H., Watanabe, T., Kawai, H., Yamasaki, N., Harada, Y., Imayoshi, I., Nelson, M., Nakayama, K.I., Hirabayashi, Y., et al. (2015). Slowly dividing neural progenitors are an embryonic origin of adult neural stem cells. Nat. Neurosci. *18*, 657–665.

G

Gaarskjaer, F.B. (1985). The development of the dentate area and the hippocampal mossy fiber projection of the rat. J. Comp. Neurol. *241*, 154–170.

Gaitatzis, A., Trimble, M.R., and Sander, J.W. (2004). The psychiatric comorbidity of epilepsy. Acta Neurol. Scand. *110*, 207–220.

Galceran, J., Miyashita-Lin, E.M., Devaney, E., Rubenstein, J.L.R., and Grosschedl, R. (2000). Hippocampus development and generation of dentate gyrus granule cells is regulated by LEF1. Development *127*, 469–482.

Galichet, C., Guillemot, F., and Parras, C.M. (2008). Neurogenin 2 has an essential role in development of the dentate gyrus. Development *135*, 2031–2041.

Gall, C. (1993). Seizure-induced changes in neurotrophin expression: implications for epilepsy. Exp Neurol *124*, 150–166.

Gall, C., Lauterborn, J., Bundman, M., Murray, K., and Isackson, P. (1991). Seizures and the regulation of neurotrophic factor and neuropeptide gene expression in brain. Epilepsy Res Suppl *4*, 225–245.

Gall, C.M., Berschauer, R., and Isackson, P.J. (1994). Seizures increase basic fibroblast growth factor mRNA in adult rat forebrain neurons and glia. Mol. Brain Res. *21*, 190–205.

García-Moreno, F., López-Mascaraque, L., and De Carlos, J. (2007). Origins and migratory routes of murine Cajal-Retzius cells. J Comp Neurol *500*, 419–432.

Garcia, P.A., Laxer, K.D., Barbaro, N.M., and Dillon, W.P. (1994). Prognostic Value of Qualitative Magnetic Resonance Imaging Hippocampal Abnormalities in Patients Undergoing Temporal Lobectomy for Medically Refractory Seizures. Epilepsia *35*, 520–524.

de Garengeot, R.C. (1742). Splanchnologie ou, L'anatomie des viscères: avec de

figures originales tirées d'apres les cadavres, suivle d'une dissertation sur l'origine de la chirurgie.

Gastaut, H., and Poirier, F. (1964). Experimental, or "Reflex", Induction of Seizures Report of a Case of Abdominal (Enteric) Epilepsy. Epilepsia *5*, 256–270.

Gazzeri, S. (2018). Nuclear EGFR: a new mode of oncogenic signalling in cancer. Biol Aujourdhui *212*, 27–33.

Gibbons, M.B., Smeal, R.M., Takahashi, D.K., Vargas, J.R., and Wilcox, K.S. (2013). Contributions of astrocytes to epileptogenesis following status epilepticus: Opportunities for preventive therapy? Neurochem. Int. *63*, 660–669.

Gilley, J.A., Yang, C.P., and Kernie, S.G. (2011). Developmental profiling of postnatal dentate gyrus progenitors provides evidence for dynamic cell-autonomous regulation. Hippocampus *21*, 33–47.

Glickstein, S.B., Moore, H., Slowinska, B., Racchumi, J., Suh, M., Chuhma, N., and Ross, M.E. (2007a). Selective cortical interneuron and GABA deficits in cyclin D2-null mice. Development *134*, 4083–4093.

Glickstein, S.B., Alexander, S., and Ross, M.E. (2007b). Differences in cyclin D2 and D1 protein expression distinguish forebrain progenitor subsets. Cereb. Cortex *17*, 632–642.

Glickstein, S.B., Monaghan, J.A., Koeller, H.B., Jones, T.K., and Ross, M.E. (2009). Cyclin D2 is critical for intermediate progenitor cell proliferation in the embryonic cortex. J. Neurosci. *29*, 9614–9624.

Goffin, J.R., and Zbuk, K. (2013). Epidermal growth factor receptor: Pathway, therapies, and pipeline. Clin. Ther. *35*, 1282–1303.

Goffin, K., Nissinen, J., Van Laere, K., and Pitkänen, A. (2007). Cyclicity of spontaneous recurrent seizures in pilocarpine model of temporal lobe epilepsy in rat. Exp. Neurol. *205*, 501–505.

Goldman, S.A., and Nottebohm, F. (1983). Neuronal production , migration , and differentiation in a vocal control nucleus of the adult female canary brain ; E. *80*, 2390–2394.

Golgi, C. (1886). Sulla fina anatomia degli organi centrali di sistema nervoso. V. Sulla anatomia di grande piede d'Hippocampo.

Gomez-Nicola, D., Riecken, K., Fehse, B., and Perry, V.H. (2014a). In-vivo RGB marking and multicolour single-cell tracking in the adult brain. Sci. Rep. *4*, 1–10.

Gomez-Nicola, D., Riecken, K., Fehse, B., and Perry, V.H. (2014b). In-vivo RGB marking and multicolour single-cell tracking in the adult brain. Sci. Rep. *4*, 1–10.

Gómez-Pinilla, F., Knauer, D.J., and Nieto-Sampedro, M. (1988). Epidermal growth factor receptor immunoreactivity in rat brain. Development and cellular localization. Brain Res. *438*, 385–390.

Gómez-Pinilla, F., Vu, L., and Cotman, C. (1995a). Regulation of astrocyte proliferation by FGF-2 and heparan sulfate in vivo. J Neurosci *15*, 2021–2029.

Gómez-Pinilla, F., Van Der Wal, E.A., and Cotman, C.W. (1995b). Possible coordinated gene expressions for FGF receptor, FGF-5, and FGF-2 following seizures. Exp Neurol *133*, 164–174.

Gonçalves, J.T., Schafer, S.T., and Gage, F.H. (2016). Adult Neurogenesis in the Hippocampus: From Stem Cells to Behavior. Cell *167*, 897–914.

Gong, S., Zheng, C., Doughty, M.L., Losos, K., Didkovsky, N., Schambra, U.B., Nowak, N.J., Joyner, A., Leblanc, G., Hatten, M.E., et al. (2003). A gene expression atlas of the central nervous system based on bacterial artificial chromosomes. Nature *425*, 917–925.

Gotoh, N., Tojo, A., Hino, M., Yazaki, Y., and Shibuya, M. (1992). A highly conserved tyrosine residue at codon 845 within the kinase domain is not required for the transforming activity of human epidermal growth factor receptor. Biochem. Biophys. Res. Commun. *186*, 768–774.

Gould, E., and Gross, C.G. (2002). Neurogenesis in adult mammals: Some progress and problems. J. Neurosci. *22*, 619–623.

Gould, E., Cameron, H.A., Daniels, D.C., Woolley, C.S., and McEwen, B.S. (1992). Adrenal hormones suppress cell division in the adult rat dentate gyrus. J. Neurosci. *12*, 3642–3650.

Gould, E., McEwen, B.S., Tanapat, P., Galea, L.A.M., and Fuchs, E. (1997). Neurogenesis in the dentate gyrus of the adult tree shrew is regulated by psychosocial stress and NMDA receptor activation. J. Neurosci. *17*, 2492–2498.

Gould, E., Tanapat, P., Mcewen, B.S., Flügge, G., and Fuchs, E. (1998). Proliferation of granule cell precursors in the dentate gyrus of adult monkeys is diminished by stress. Proc. Natl. Acad. Sci. U. S. A. *95*, 3168–3171.

Gould, E., Beylin, A., Tanapat, P., Reeves, A., and Shors, T.J. (1999a). Learning enhances adult neurogenesis in the hippocampal formation. Nat. Neurosci. *2*, 260–265.

Gould, E., Reeves, A.J., Fallah, M., Tanapat, P., Gross, C.G., and Fuchs, E. (1999b). Hippocampal neurogenesis in adult Old World primates. Proc. Natl. Acad. Sci. U. S. A. *96*, 5263–5267.

Gould, E., Reeves, A.J., Graziano, M.S.A., and Gross, C.G. (1999c). Neurogenesis in the neocortex of adult primates. Science (80-.). *286*, 548–552.

Gratzner et al. (1982). Monoclonal Antibody to 5-Bromo- and 5-Iododeoxyuridine : A New Reagent for Detection of DNA Replication Placental Mononuclear Phagocytes as a Source of Interleukin-1. Science (80-.). *218*, 474–475.

Gray, W.P., and Sundstrom, L.E. (1998). Kainic acid increases the proliferation of granule cell progenitors in the dentate gyrus of the adult rat. Brain Res. *790*, 52–59.

Gross, C.G. (2000). Neurogenesis in the adult brain: Death of a dogma. Nat. Rev. Neurosci. *1*, 67–73.

Grove, E.A., Tole, S., Limon, J., Yip, L.W., and Ragsdale, C.W. (1998). The hem of the embryonic cerebral cortex is defined by the expression of multiple Wnt genes and is compromised in Gli3-deficient mice. Development *125*, 2315–2325.

Gschwind, A., Zwick, E., Prenzel, N., Leserer, M., and Ullrich, A. (2001). Cell communication networks: Epidermal growth factor receptor transactivation as the paradigm for interreceptor signal transmission. Oncogene *20*, 1594–1600.

Gschwind, A., Prenzel, N., and Ullrich, A. (2002). Lysophosphatidic acid-induced squamous cell carcinoma cell proliferation and motility involves epidermal growth factor receptor signal transactivation. Cancer Res. *62*, 6329–6336.

Guentchev, M., and McKay, R.D.G. (2006). Notch controls proliferation and differentiation of stem cells in a dose-dependent manner. Eur. J. Neurosci. *23*, 2289–2296.

H

Hagihara, H., Murano, T., Ohira, K., Miwa, M., Nakamura, K., and Miyakawa, T. (2019). Expression of progenitor cell/immature neuron markers does not present definitive evidence for adult neurogenesis. Mol. Brain *12*, 1–6.

Halassa, M.M., Fellin, T., and Haydon, P.G. (2007). The tripartite synapse: roles for gliotransmission in health and disease. Trends Mol. Med. *13*, 54–63.

Han, Y.G., Spassky, N., Romaguera-Ros, M., Garcia-Verdugo, J.M., Aguilar, A.,

Schneider-Maunoury, S., and Alvarez-Buylla, A. (2008). Hedgehog signaling and primary cilia are required for the formation of adult neural stem cells. Nat. Neurosci. *11*, 277–284.

Hanson, L.R., Fine, J.M., Svitak, A.L., and Faltesek, K.A. (2013). Intranasal administration of CNS therapeutics to awake mice. J. Vis. Exp. 2–7.

Harris, R.C., Chung, E., and Coffey, R.J. (2003). EGF receptor ligands. Exp. Cell Res. *284*, 2–13.

Hattiangady, B., Rao, M.S., and Shetty, A.K. (2004). Chronic temporal lobe epilepsy is associated with severely declined dentate neurogenesis in the adult hippocampus. Neurobiol. Dis. *17*, 473–490.

Häussler, U., Bielefeld, L., Froriep, U.P., Wolfart, J., and Haas, C.A. (2012). Septotemporal position in the hippocampal formation determines epileptic and neurogenic activity in temporal lobe epilepsy. Cereb. Cortex *22*, 26–36.

Haut, S.R. (2006). Seizure clustering. Epilepsy Behav. *8*, 50–55.

Heinrich, C., Nitta, N., Flubacher, A., Müller, M., Fahrner, A., Kirsch, M., Freiman, T., Suzuki, F., Depaulis, A., Frotscher, M., et al. (2006). Reelin deficiency and displacement of mature neurons, but not neurogenesis, underlie the formation of granule cell dispersion in the epileptic hippocampus. J. Neurosci. *26*, 4701–4713.

Heisermann, G.J., and Gill, G.N. (1988). Epidermal growth factor receptor threonine and serine residues phosphorylated in vivo. J. Biol. Chem. *263*, 13152–13158.

Herbst, R.S. (2004). Review of epidermal growth factor receptor biology. Int. J. Radiat. Oncol. Biol. Phys. *59*, S21–S26.

Hermann, A., Maisel, M., Liebau, S., Gerlach, M., Kleger, A., Schwarz, J., Kim, K.S., Antoniadis, G., Lerche, H., and Storch, A. (2006). Mesodermal cell types induce neurogenesis from adult human hippocampal progenitor cells. J. Neurochem. *98*, 629–640.

Hermann, B., Seidenberg, M., Schoenfeld, J., and Davies, K. (1997). Neuropsychological characteristics of the syndrome of mesial temporal lobe epilepsy. Arch Neurol *54*, 369–376.

van den Heuvel, S. (2005). Cell-cycle regulation. Wormbook *Sep*, 1–16.

Hidalgo, J., Belloso, E., Hernandez, J., Gasull, T., and Molinero, A. (1997). Role of Glucocorticoids on Rat Brain Metallothionein-I and -III Response to Stress. Stress *Aug*, 231–240.

Hochgerner, H., Zeisel, A., Lönnerberg, P., and Linnarsson, S. (2018). Conserved properties of dentate gyrus neurogenesis across postnatal development revealed by single-cell RNA sequencing. Nat. Neurosci. *21*, 290–299.

Hodge, R.D., Kowalczyk, T.D., Wolf, S.A., Encinas, J.M., Rippey, C., Enikolopov, G., Kempermann, G., and Hevner, R.F. (2008). Intermediate progenitors in adult hippocampal neurogenesis: Tbr2 expression and coordinate regulation of neuronal output. J. Neurosci. *28*, 3707–3717.

Hodge, R.D., Nelson, B.R., Kahoud, R.J., Yang, R., Mussar, K.E., Reiner, S.L., and Hevner, R.F. (2012). Tbr2 is essential for hippocampal lineage progression from neural stem cells to intermediate progenitors and neurons. J. Neurosci. *32*, 6275–6287.

Hodge, R.D., Garcia, A.J., Elsen, G.E., Nelson, B.R., Mussar, K.E., Reiner, S.L., Ramirez, J.M., and Hevner, R.F. (2013). Tbr2 expression in Cajal-Retzius cells and intermediate neuronal progenitors is required for morphogenesis of the dentate gyrus. J. Neurosci. *33*, 4165–4180.

Holmes, G.L. (2009). The Long-Term Effects of Neonatal Seizures. Clin. Perinatol. *36*, 901–914.

Houser, C.R. (1990). Granule cell dispersion in the dentate gyrus of humans with temporal lobe epilepsy. Brain Res. *535*, 195–204.

Howell, G.A., Welch, M.G., and Frederickson, C.J. (1984). Stimulation-induced uptake and release of zinc in hippocampal slices. Nature *308*, 736–738.

Hsu, D. (2007). The dentate gyrus as a filter or gate: a look back and a look ahead. Prog. Brain Res. *163*, 601–613.

Huard, J.M.T., Forster, C.C., Carter, M.L., Sicinski, P., and Ross, M.E. (1999). Cerebellar histogenesis is disturbed in mice lacking cyclin D2. Development *126*, 1927–1935.

Humphrey, T. (1967). The development of the human hippocampal fissure. J. Anat. *101*, 655–676.

Hunter, T., Ling, N., and Cooper, J. (1984). Protein kinase C phosphorylation of the EGF receptor at a threonine residue close to the cytoplasmic face of the plasma membrane. Nature *311*, 480–483.

Hüttmann, K., Sadgrove, M., Wallraff, A., Hinterkeuser, S., Kirchhoff, F., Steinhäuser, C., and Gray, W.P. (2003). Seizures preferentially stimulate proliferation of radial glia-like astrocytes in the adult dentate gyrus: Functional and immunocytochemical

analysis. Eur. J. Neurosci. *18*, 2769–2778.

I

Iglesias, J.E., Augustinack, J.C., Nguyen, K., Player, C.M., Player, A., Wright, M., Roy, N., and Frosch, M.P. (2015). A computational atlas of the hippocampal formation using ex vivo , ultra-high resolution MRI. Neuroimage 115–137.

Isokawa, M., Levesque, M., Fried, I., and Engel, J. (1997). Glutamate currents in morphologically identified human dentate granule cells in temporal lobe epilepsy. J. Neurophysiol. *77*, 3355–3369.

Ito, H., Morishita, R., Iwamoto, I., and Nagata, K.I. (2014). Establishment of an in vivo electroporation method into postnatal newborn neurons in the dentate gyrus. Hippocampus *24*, 1449–1457.

J

Jarrard, L.E. (1993). On the role of the hippocampus in learning and memory in the rat. Behav. Neural Biol. *60*, 9–26.

Jeha, L., Najm, I., Bingaman, W., Khandwala, F., Widdes-Walsh, P., Morris, H., Dinner, D., Nair, D., Foldvary-Schaeffer, N., Prayson, R., et al. (2006). Predictors of outcome after temporal lobectomy for the treatment of intractable epilepsy. Neurology *66*, 1938–1940.

Jessberger, S., and Parent, J.M. (2015). Epilepsy and adult neurogenesis. Cold Spring Harb. Perspect. Biol. *7*.

Jessberger, S., Römer, B., Babu, H., and Kempermann, G. (2005). Seizures induce proliferation and dispersion of doublecortin-positive hippocampal progenitor cells. Exp. Neurol. *196*, 342–351.

Jessberger, S., Nakashima, K., Clemenson, G.D., Mejia, E., Mathews, E., Ure, K., Ogawa, S., Sinton, C.M., Gage, F.H., and Hsieh, J. (2007). Epigenetic modulation of seizure-induced neurogenesis and cognitive decline. J. Neurosci. *27*, 5967–5975.

Jhaveri, D.J., O'Keeffe, I., Robinson, G.J., Zhao, Q.Y., Zhang, Z.H., Nink, V., Narayanan, R.K., Osborne, G.W., Wray, N.R., and Bartlett, P.F. (2015). Purification of neural precursor cells reveals the presence of distinct, stimulus-specific subpopulations of quiescent precursors in the adult mouse hippocampus. J. Neurosci. *35*, 8132–8144.

Jia, M., Shi, Z., Yan, X., Xu, L., Dong, L., Li, J., Wang, Y., Yang, S., and Yuan, F. (2018). Insulin and heparin-binding epidermal growth factor-like growth factor synergistically promote astrocyte survival and proliferation in serum-free medium. J. Neurosci. Methods *307*, 240–247.

Jia, Y., Jeng, J.M., Sensi, S.L., and Weiss, J.H. (2002). Zn2+ currents are mediated by calcium-permeable AMPA/kainate channels in cultured murine hippocampal neurones. J. Physiol. *543*, 35–48.

Jiang, M., Polepalli, J., Chen, L.Y., Zhang, B., Südhof, T.C., and Malenka, R.C. (2017). Conditional ablation of neuroligin-1 in CA1 pyramidal neurons blocks LTP by a cell-autonomous NMDA receptor-independent mechanism. Mol. Psychiatry *22*, 375–383.

Jin, K., Mao, X.O., Sun, Y., Xie, L., Jin, L., Nishi, E., Klagsbrun, M., and Greenberg, D.A. (2002). Heparin-Binding Epidermal Growth Factor-Like Growth Factor: Hypoxia-Inducible expression in vitro and stimulation of neurogenesis in vitro and in vivo. Processing *22*, 5365–5373.

Johnson, D.E., Lee, P.L., Lu, J., and Williams, L.T. (1990). Diverse forms of a receptor for acidic and basic fibroblast growth factors. Mol. Cell. Biol. *10*, 4728–4736.

Jones, J.T., Akita, R.W., and Sliwkowski, M.X. (1999). Binding specificities and affinities of egf domains for ErbB receptors. FEBS Lett. *447*, 227–231.

Jones, R.B., Gordus, A., Krall, J.A., and MacBeath, G. (2006). A quantitative protein interaction network for the ErbB receptors using protein microarrays. Nature *439*, 168–174.

Jura, N., Shan, Y., Cao, X., Shaw, D.E., and Kuriyan, J. (2009). Structural analysis of the catalytically inactive kinase domain of the human EGF receptor 3. Proc. Natl. Acad. Sci. U. S. A. *106*, 21608–21613.

K

Kägi, J.H.R., and Schäffer, A. (1988). Biochemistry of Metallothionein. Biochemistry *27*, 8509–8515.

Kalamakis, G., Brüne, D., Ravichandran, S., Bolz, J., Fan, W., Ziebell, F., Stiehl, T., Catalá-Martinez, F., Kupke, J., Zhao, S., et al. (2019). Quiescence Modulates Stem Cell Maintenance and Regenerative Capacity in the Aging Brain. Cell *176*, 1407-1419.e14.

Kalluri, H.S.G., Vemuganti, R., and Dempsey, R.J. (2005). Lack of response to

epidermal growth factor in adult neural progenitor cells. Neuroreport *16*, 835–838.

Kambe, T., Tsuji, T., Hashimoto, A., and Itsumura, N. (2015). The physiological, biochemical, and molecular roles of zinc transporters in zinc homeostasis and metabolism. Physiol. Rev. *95*, 749–784.

Kandratavicius, L., Alves Balista, P., Lopes-Aguiar, C., Ruggiero, R.N., Umeoka, E.H., Garcia-Cairasco, N., Bueno-Junior, L.S., and Leite, J.P. (2014). Animal models of epilepsy: Use and limitations. Neuropsychiatr. Dis. Treat. *10*, 1693–1705.

Kaplan, M.S. (1981). Neurogenesis in the 3-month-old rat visual cortex. J. Comp. Neurol. *195*, 323–338.

Kaplan, M.S. (1983). Proliferation of subependymal cells in the adult primate CNS: differential uptake of DNA labelled precursors. J Hirnforsch *24*, 23–33.

Kaplan, M.S., and Bell, D.H. (1983). Neuronal proliferation in the 9-month-old rodent - Radioautographic study of granule cells in the hippocampus. Exp. Brain Res. *52*, 1–5.

Kaplan, M.S., and Bell, D.H. (1984). Mitotic neuroblasts in the 9-day-old and 11-month-old rodent hippocampus. J. Neurosci. *4*, 1429–1441.

Kaplan, M.S., and Hinds, J.W. (1977). Neurogenesis in the adult rat: Electron microscopic analysis of light radioautographs. Science (80-.). *197*, 1092–1094.

KAPLAN, M.S. (1985). Formation and Turnover of Neurons in Young and Senescent Animals: An Electronmicroscopic and Morphometric Analysis. Ann. N. Y. Acad. Sci. *457*, 173–192.

Karunagaran, D., Tzahar, E., Beerli, R.R., Chen, X., Graus-Porta, D., Ratzkin, B.J., Seger, R., Hynes, N.E., and Yarden, Y. (1996). ErbB-2 is a common auxiliary subunit of NDF and EGF receptors: implications for breast cancer. EMBO J. *15*, 254–264.

Kasarskis, E.J., Forrester, T.M., and Slevin, J.T. (1987). Amygdalar kindling is associated with elevated zinc concentration in the cortex and hippocampus of rats. Epilepsy Res. *1*, 227–233.

Keegan, K., Johnson, D.E., Williams, L.T., and Hayman, M.J. (1991). Isolation of an additional member of the fibroblast growth factor receptor family, FGFR-3. Proc. Natl. Acad. Sci. U. S. A. *88*, 1095–1099.

Kempermann, G., Brandon, E.P., and Gage, F.H. (1998). Environmental stimulation of 129/SvJ mice causes increased cell proliferation and neurogenesis in the adult dentate gyrus. Curr. Biol. *8*, 939–944.

Kempermann, G., Jessberger, S., Steiner, B., and Kronenberg, G. (2004). Milestones of neuronal development in the adult hippocampus. Trends Neurosci. *27*, 447–452.

Kempermann, G., Song, H., and Gage, F.H. (2015). Neurogenesis in the adult hippocampus. Cold Spring Harb. Perspect. Biol. *7*.

Kempermann, G., Gage, F.H., Aigner, L., Song, H., Curtis, M.A., Thuret, S., Kuhn, H.G., Jessberger, S., Frankland, P.W., Cameron, H.A., et al. (2018). Human Adult Neurogenesis: Evidence and Remaining Questions. Cell Stem Cell *23*, 25–30.

Kier, E.L., Kim, J.H., Fulbright, R.K., and Bronen, R.A. (1997). Embryology of the human fetal hippocampus: Mr imaging, anatomy, and histology. Am. J. Neuroradiol. *18*, 525–532.

Kim, E., Kim, M., Woo, D.H., Shin, Y., Shin, J., Chang, N., Oh, Y.T., Kim, H., Rheey, J., Nakano, I., et al. (2013). Phosphorylation of EZH2 Activates STAT3 Signaling via STAT3 Methylation and Promotes Tumorigenicity of Glioblastoma Stem-like Cells. Cancer Cell *23*, 839–852.

Kim, E.J., Ables, J.L., Dickel, L.K., Eisch, A.J., and Johnson, J.E. (2011). Ascl1 (Mash1) defines cells with long-term neurogenic potential in subgranular and subventricular zones in adult mouse brain. PLoS One *6*.

Kim, J.H., Jang, B.G., Choi, B.Y., Kwon, L.M., Sohn, M., Song, H.K., and Suh, S.W. (2012). Zinc Chelation Reduces Hippocampal Neurogenesis after Pilocarpine-Induced Seizure. PLoS One *7*, 1–10.

King, C.R., Borrello, I., Bellot, F., Comoglio, P., and Schlessinger, J. (1988). Egf binding to its receptor triggers a rapid tyrosine phosphorylation of the erbB-2 protein in the mammary tumor cell line SK-BR-3. EMBO J. *7*, 1647–1651.

Kippin, T.E., Martens, D.J., and Van Der Kooy, D. (2005). P21 Loss Compromises the Relative Quiescence of Forebrain Stem Cell Proliferation Leading To Exhaustion of Their Proliferation Capacity. Genes Dev. *19*, 756–767.

Knoth, R., Singec, I., Ditter, M., Pantazis, G., Capetian, P., Meyer, R.P., Horvat, V., Volk, B., and Kempermann, G. (2010). Murine features of neurogenesis in the human hippocampus across the lifespan from 0 to 100 years. PLoS One *5*.

Kobow, K., Jeske, I., Hildebrandt, M., Hauke, J., Hahnen, E., Buslei, R., Buchfelder, M., Weigel, D., Stefan, H., Kasper, B., et al. (2009). Increased reelin promoter methylation is associated with granule cell dispersion in human temporal lobe epilepsy. J. Neuropathol. Exp. Neurol. *68*, 356–364.

Kochupurakkal, B.S., Harari, D., Di-Segni, A., Maik-Rachline, G., Lyass, L., Gur, G., Kerber, G., Citri, A., Lavi, S., Eilam, R., et al. (2005). Epigen, the last ligand of ErbB receptors, reveals intricate relationships between affinity and mitogenicity. J. Biol. Chem. *280*, 8503–8512.

Koh, J.Y., Suh, S.W., Gwag, B.J., He, Y.Y., Hsu, C.Y., and Choi, D.W. (1996). The role of zinc in selective neuronal death after transient global cerebral ischemia. Science (80-.). *272*, 1013–1016.

Köhler, C. (1985a). A projection from the deep layers of the entorhinal area to the hippocampal formation in the rat brain. Neurosci. Lett. *56*, 13–19.

Köhler, C. (1985b). Intrinsic projections of the retrohippocampal region in the rat brain. I. The subicular complex. J. Comp. Neurol. *236*, 504–522.

Komada, M., Iguchi, T., Takeda, T., Ishibashi, M., and Sato, M. (2013). Smoothened controls cyclin D2 expression and regulates the generation of intermediate progenitors in the developing cortex. Neurosci. Lett. *547*, 87–91.

Komitova, M., and Eriksson, P.S. (2004). Sox-2 is expressed by neural progenitors and astroglia in the adult rat brain. Neurosci. Lett. *369*, 24–27.

Konoha, K., Kawahara, M., and Sadakane, Y. (2006). Zinc Neurotoxicity and its Role in Neurodegenerative Diseases. J. Heal. Sci. *52*, 1–8.

Kornack, D.R., and Rakic, P. (1999). Continuation of neurogenesis in the hippocampus of the adult macaque monkey. Proc. Natl. Acad. Sci. U. S. A. *96*, 5768–5773.

Kornack, D.R., and Rakic, P. (2001). The generation, migration, and differentiation of olfactory neurons in the adult primate brain. Proc. Natl. Acad. Sci. U. S. A. *98*, 4752–4757.

Kornblum, H.I., Zurcher, S.D., Werb, Z., Derynck, R., and Seroogy, K.B. (1999). Multiple trophic actions of heparin-binding epidermal growth factor (HB-EGF) in the central nervous system. Eur. J. Neurosci. *11*, 3236–3246.

Korr, H. (1980). Proliferation of different cell types in the brain. Adv Anat Embryol Cell Biol *61*, 1–72.

Kosaka, T., and Hama, K. (1986). Three-dimensional structure of astrocytes in the rat dentate gyrus. J. Comp. Neurol. *249*, 242–260.

Kostović, I. (1986). Prenatal development of nucleus basalis complex and related fiber systems in man: A histochemical study. Neuroscience *17*, 1047–1063.

Kostović, I., Seress, L., Mrzljak, L., and Judaš, M. (1989). Early onset of synapse formation in the human hippocampus: A correlation with Nissl-Golgi architectonics in 15- and 16.5-week-old fetuses. Neuroscience *30*, 105–116.

Kovacs, E., Zorn, J.A., Huang, Y., Barros, T., and Kuriyan, J. (2015). A Structural Perspective on the Regulation of the Epidermal Growth Factor Receptor. Annu. Rev. Biochem. *84*, 739–764.

Kowalczyk, A., Filipkowski, R.K., Rylski, M., Wilczynski, G.M., Konopacki, F.A., Jaworski, J., Ciemerych, M.A., Sicinski, P., and Kaczmarek, L. (2004). The critical role of cyclin D2 in adult neurogenesis. J. Cell Biol. *167*, 209–213.

Kozar, K., Ciemerych, M.A., Rebel, V.I., Shigematsu, H., Zagozdzon, A., Sicinska, E., Geng, Y., Yu, Q., Bhattacharya, S., Bronson, R.T., et al. (2004). Mouse development and cell proliferation in the absence of D-cyclins. Cell *118*, 477–491.

Kralic, J.E., Ledergerber, D.A., and Fritschy, J.M. (2005). Disruption of the neurogenic potential of the dentate gyrus in a mouse model of temporal lobe epilepsy with focal seizures. Eur. J. Neurosci. *22*, 1916–1927.

Kraus, M.H., Issing, W., Miki, T., Popescu, N.P., and Aaronson, S.A. (1989). Isolation and characterization of ERBB3, a third member of the ERBB/epidermal growth factor receptor family: Evidence for overexpression in a subset of human mammary tumors. Proc. Natl. Acad. Sci. U. S. A. *86*, 9193–9197.

Kronenberg, G., Reuter, K., Steiner, B., Brandt, M.D., Jessberger, S., Yamaguchi, M., and Kempermann, G. (2003). Subpopulations of Proliferating Cells of the Adult Hippocampus Respond Differently to Physiologic Neurogenic Stimuli. J. Comp. Neurol. *467*, 455–463.

Kruglyakova, E.P., Khovryakov, A. V., Shikhanov, N.P., MacCann, G.M., Vaél', I., Kruglyakov, P.P., and Sosunov, A.A. (2005). Nestin-expressing cells in the human hippocampus. Neurosci. Behav. Physiol. *35*, 891–897.

Kuhn, H.G., Dickinson-Anson, H., and Gage, F.H. (1996). Neurogenesis in the dentate gyrus of the adult rat: Age-related decrease of neuronal progenitor proliferation. J. Neurosci. *16*, 2027–2033.

Kuhn, H.G., Winkler, J., Kempermann, G., Thal, L.J., and Gage, F.H. (1997). Epidermal growth factor and fibroblast growth factor-2 have different effects on neural progenitors in the adult rat brain. J. Neurosci. *17*, 5820–5829.

Kuhn, H.G., Toda, T., and Gage, F.H. (2018). Adult Hippocampal Neurogenesis : A

Coming-of-Age Story. *38*, 10401–10410.

Kuppuswamy, D., Dalton, M., and Pike, L.J. (1993). Serine 1002 is a site of in vivo and in vitro phosphorylation of the epidermal growth factor receptor. J. Biol. Chem. *268*, 19134–19142.

Kuruba, R., and Shetty, A. (2007). Could hippocampal neurogenesis be a future drug target for treating temporal lobe epilepsy? CNS Neurol Disord Drug Targets *6*, 342–357.

Kwan, P., and Brodie, M. (2000). Early identification of refractory epilepsy. N Engl J Med *342*, 314–319.

Kwan, P., and Brodie, M.J. (2006). Refractory epilepsy: Mechanisms and solutions. Expert Rev. Neurother. *6*, 397–406.

L

De La Iglesia, N., Konopka, G., Lim, K.L., Nutt, C.L., Bromberg, J.F., Frank, D.A., Mischel, P.S., Louis, D.N., and Bonni, A. (2008). Deregulation of a STAT3-interleukin 8 signaling pathway promotes human glioblastoma cell proliferation and invasiveness. J. Neurosci. *28*, 5870–5878.

LaFrance, W.C., Kanner, A.M., and Hermann, B. (2008). Chapter 20 Psychiatric Comorbidities in Epilepsy. Int. Rev. Neurobiol. *83*, 347–383.

Lam, E.W.F., Glassford, J., Banerji, L., Thomas, N.S.B., Sicinski, P., and Klaus, G.G.B. (2000). Cyclin D3 compensates for loss of cyclin D2 in mouse D-lymphocytes activated via the antigen receptor and CD40. J. Biol. Chem. *275*, 3479–3484.

de Lanerolle, N.C., and Lee, T.S. (2005). New facets of the neuropathology and molecular profile of human temporal lobe epilepsy. Epilepsy Behav. *7*, 190–203.

de Lanerolle, N.C., Kim, J.H., Robbins, R.J., and Spencer, D.D. (1989). Hippocampal interneuron loss and plasticity in human temporal lobe epilepsy. Brain Res. *495*, 387–395.

Lange, S.C., Neafsey, E.J., and Wyler, A.R. (1980). Neuronal Activity in Chronic Ferric Chloride Epileptic Foci in Cats and Monkey. Epilepsia *21*, 251–254.

Lee, H., and Thuret, S. (2018). Adult Human Hippocampal Neurogenesis: Controversy and Evidence. Trends Mol. Med. *24*, 521–522.

Lee, D.J., Hsu, M.S., Seldin, M.M., Arellano, J.L., and Binder, D.K. (2012). Decreased

expression of the glial water channel aquaporin-4 in the intrahippocampal kainic acid model of epileptogenesis. Exp. Neurol. *235*, 246–255.

Lee, J., Duan, W., Long, J.M., Ingram, D.K., and Mattson, M.P. (2000a). Dietary restriction increases the number of newly generated neural cells, and BDNF expression, in the dentate gyrus of rats. J. Mol. Neurosci. *15*, 99–108.

Lee, J., Auyeung, W.W., and Mattson, M.P. (2003). Interactive Effects of Excitotoxic Injury and Dietary Restriction on Microgliosis and Neurogenesis in the Hippocampus of Adult Mice. NeuroMolecular Med. *4*, 179–195.

Lee, J.C., Vivanco, I., Beroukhim, R., Huang, J.H.Y., Feng, W.L., DeBiasi, R.M., Yoshimoto, K., King, J.C., Nghiemphu, P., Yuza, Y., et al. (2006). Epidermal growth factor receptor activation in glioblastoma through novel missense mutations in the extracellular domain. PLoS Med. *3*, 2264–2273.

Lee, J.Y., Cole, T.B., Palmiter, R.D., and Koh, J.Y. (2000b). Accumulation of zinc in degenerating hippocampal neurons of ZnT3-null mice after seizures: evidence against synaptic vesicle origin. J. Neurosci. *20*, 1–5.

Lee, S.M.K., Tole, S., Grove, E., and McMahon, A.P. (2000c). A local Wnt-3a signal is required for development of the mammalian hippocampus. Development *127*, 457–467.

Lein, E.S., Zhao, X., and Gage, F.H. (2004). Defining a Molecular Atlas of the Hippocampus Using DNA Microarrays and High-Throughput In Situ Hybridization. J. Neurosci. *24*, 3879–3889.

Lein, E.S., Callaway, E.M., Albright, T.D., and Gage, F.H. (2005). Redefining the boundaries of the hippocampal CA2 subfield in the mouse using gene expression and 3-dimensional reconstruction. J. Comp. Neurol. *485*, 1–10.

Lein, E.S., Hawrylycz, M.J., Ao, N., Ayres, M., Bensinger, A., Bernard, A., Boe, A.F., Boguski, M.S., Brockway, K.S., Byrnes, E.J., et al. (2007). Genome-wide atlas of gene expression in the adult mouse brain. Nature *445*, 168–176.

Lemaire, V., Koehl, M., Le Moal, M., and Abrous, D.N. (2000). Prenatal stress produces learning deficits associated with an inhibition of neurogenesis in the hippocampus. Proc. Natl. Acad. Sci. U. S. A. *97*, 11032–11037.

Lendahl, U., Zimmerman, L.B., and McKay, R.D.G. (1990). CNS stem cells express a new class of intermediate filament protein. Cell *60*, 585–595.

Leonardo, E.D., Richardson-Jones, J.W., Sibille, E., Kottman, A., and Hen, R. (2006).

Molecular heterogeneity along the dorsal-ventral axis of the murine hippocampal CA1 field: A microarray analysis of gene expression. Neuroscience *137*, 177–186.

Leutgeb, J.K., Leutgeb, S., Moser, M.B., and Moser, E.I. (2007). Pattern separation in the dentate gyrus and CA3 of the hippocampus. Science (80-.). *315*, 961–966.

Levenson, C.W., and Morris, D. (2011). 22332038.Pdf. 96–100.

Lévesque, M., and Avoli, M. (2013). The kainic acid model of temporal lobe epilepsy. Neurosci. Biobehav. Rev. *37*, 2887–2899.

Lévesque, M., Avoli, M., and Bernard, C. (2016). Animal models of temporal lobe epilepsy following systemic chemoconvulsant administration. J. Neurosci. Methods *260*, 45–52.

Lewis, T.S., Shapiro, P.S., and Ahn, N.G. (1998). Signal transduction through MAP kinase cascades. Adv. Cancer Res. *74*, 137–139.

Li, D., Ambrogio, L., Shimamura, T., Kubo, S., Takahashi, M., Chirieac, L.R., Padera, R.F., Shapiro, G.I., Baum, A., Himmelsbach, F., et al. (2008). BIBW2992, an irreversible EGFR/HER2 inhibitor highly effective in preclinical lung cancer models. Oncogene *27*, 4702–4711.

Li, D., Takeda, N., Jain, R., Manderfield, L.J., Liu, F., Li, L., Anderson, S.A., and Epstein, J.A. (2015). Hopx distinguishes hippocampal from lateral ventricle neural stem cells. Stem Cell Res. *15*, 522–529.

Li, G., Kataoka, H., Coughlin, S.R., and Pleasure, S.J. (2009). Identification of a transient subpial neurogenic zone in the developing dentate gyrus and its regulation by Cxcl12 and reelin signaling. Development *136*, 327–335.

Li, G., Fang, L., Fernández, G., and Pleasure, S.J. (2013). The ventral hippocampus is the embryonic origin for adult neural stem cells in the dentate gyrus. Neuron *78*, 658–672.

Li, Y., Hough, C.J., Suh, S.W., Sarvey, J.M., and Frederickson, C.J. (2001). Rapid translocation of Zn2+ from presynaptic terminals into postsynaptic hippocampal neurons after physiological stimulation. J. Neurophysiol. *86*, 2597–2604.

Li, Z.W., Li, J.J., Wang, L., Zhang, J.P., Wu, J.J., Mao, X.Q., Shi, G.F., Wang, Q., Wang, F., and Zou, J. (2014). Epidermal growth factor receptor inhibitor ameliorates excessive astrogliosis and improves the regeneration microenvironment and functional recovery in adult rats following spinal cord injury. J. Neuroinflammation *11*, 1–16.

Libermann, T., Nusbaum, H., Razon, N., Kris, R., Lax, I., Soreq, H., Whittle, N.,

Waterfield, M., Ullrich, A., and Schlessinger, J. (1985). Am Plification and Overexpression of T H E Egf R Ec Epto R Gene in Primary Hum an. J Cell Sci *3*, 161–172.

Lill, N.L., and Sever, N.I. (2012). Where EGF receptors transmit their signals. Sci. Signal. *5*.

Lin, S.Y., Makino, K., Xia, W., Matin, A., Wen, Y., Kwong, K.Y., Bourguignon, L., and Hung, M.C. (2001). Nuclear localization of EGF receptor and its potential new role as a transcription factor. Nat. Cell Biol. *3*, 802–808.

Lipp, H.P., and Bonfanti, L. (2016). Adult neurogenesis in mammals: Variations and confusions. Brain. Behav. Evol. *87*, 205–221.

Liu, J.Y.W., Matarin, M., Reeves, C., McEvoy, A.W., Miserocchi, A., Thompson, P., Sisodiya, S.M., and Thom, M. (2018). Doublecortin-expressing cell types in temporal lobe epilepsy. Acta Neuropathol. Commun. *6*, 60.

López-García, C., Varea, E., Palop, J.J., Nacher, J., Ramirez, C., Ponsoda, X., and Molowny, A. (2002). Cytochemical techniques for zinc and heavy metals localization in nerve cells. Microsc. Res. Tech. *56*, 318–331.

Lorente de Nó, R. (1934). Studies on the strcuture of the cerebral cortex. II. Continuation of the study of the ammonic system. J Psychol Neurol *46*, 113–177.

Lowenstein, D.H. (1999). Status Epilepticus: An Overview of the Clinical Problem. Epilepsia *40*, s3–s8.

Lucassen, P.J., Fitzsimons, C.P., Salta, E., and Maletic-Savatic, M. (2020). Adult neurogenesis, human after all (again): Classic, optimized, and future approaches. Behav. Brain Res. *381*, 112458.

Lüders, H., Akamatsu, N., Amina, S., Baumgartner, C., Benbadis, S., Bermeo-Ovalle, A., Bleasel, A., Bozorgi, A., Carreño, M., Devereaux, M., et al. (2019). Critique of the 2017 epileptic seizure and epilepsy classifications. Epilepsia *60*, 1032–1039.

Lugert, S., Basak, O., Knuckles, P., Haussler, U., Fabel, K., Götz, M., Haas, C.A., Kempermann, G., Taylor, V., and Giachino, C. (2010). Quiescent and active hippocampal neural stem cells with distinct morphologies respond selectively to physiological and pathological stimuli and aging. Cell Stem Cell *6*, 445–456.

Lukaszewicza, A.I., and Anderson, D.J. (2011). Cyclin D1 promotes neurogenesis in the developing spinal cord in a cell cycle-independent manner. Proc. Natl. Acad. Sci. U. S. A. *108*, 11632–11637.

Lurton, D., El Bahh, B., Sundstrom, L., and Rougier, A. (1998). Granule cell dispersion is correlated with early epileptic events in human temporal lobe epilepsy. J. Neurol. Sci. *154*, 133–136.

Luttrell, L.M., Hawes, B.E., Van Biesen, T., Luttrell, D.K., Lansing, T.J., and Lefkowitz, R.J. (1996). Role of c-Src tyrosine kinase in G protein-coupled receptor- and Gβγ subunit-mediated activation of mitogen-activated protein kinases. J. Biol. Chem. *271*, 19443–19450.

Luzuriaga, J., Pineda, J.R., Irastorza, I., Uribe-Etxebarria, V., García-Gallastegui, P., Encinas, J.M., Chamero, P., Unda, F., and Ibarretxe, G. (2019). BDNF and NT3 reprogram human ectomesenchymal dental pulp stem cells to neurogenic and gliogenic neural crest progenitors cultured in serum-free medium. Cell. Physiol. Biochem. *52*, 1361–1380.

M

Machon, O., Backman, M., Machonova, O., Kozmik, Z., Vacik, T., Andersen, L., and Krauss, S. (2007). A dynamic gradient of Wnt signaling controls initiation of neurogenesis in the mammalian cortex and cellular specification in the hippocampus. Dev. Biol. *311*, 223–237.

Mahar, I., Macisaac, A., Kim, J.J., Qiang, C., Davoli, M.A., Turecki, G., and Mechawar, N. (2016). Effects of neuregulin-1 administration on neurogenesis in the adult mouse hippocampus, and characterization of immature neurons along the septotemporal axis. Sci. Rep. *6*, 1–14.

Malmgren, K., and Thom, M. (2012). Hippocampal sclerosis-Origins and imaging. Epilepsia *53*, 19–33.

Mangale, V.S., Hirokawa, K.E., Satyaki, P.R.V., Gokulchandran, N., Chikbire, S., Subramanian, L., Shetty, A.S., Martynoga, B., Paul, J., Mai, M. V., et al. (2008). Lhx2 selector activity specifies cortical identity and suppresses hippocampal organizer fate. Science (80-.). *319*, 304–309.

Maret, W. (2017). Zinc in cellular regulation: The nature and significance of "zinc signals." Int. J. Mol. Sci. *18*.

Margerison, J.H., and Corsellis, J.A.N. (1966). Epilepsy and the Temporal Lobes. Brain *89*, 499–530.

Margolis, B.L., Lax, I., Kris, R., Dombalagian, M., Honegger, A.M., Howk, R., Givol, D.,

Ullrich, A., and Schlessinger, J. (1989). All autophosphorylation sites of epidermal growth factor (EGF) receptor and HER2/neu are located in their carboxyl-terminal tails. Identification of a novel site in EGF receptor. J. Biol. Chem. *264*, 10667–10671.

Martín-Suárez, S., Valero, J., Muro-García, T., and Encinas, J.M. (2019). Phenotypical and functional heterogeneity of neural stem cells in the aged hippocampus. Aging Cell *18*, 1–14.

Martín-Suárez, S., Abiega, O., Ricobaraza, A., Hernández-Alcoceba, R., and Encinas, J.M. (2020). Alterations of the hippocampal neurogenic niche in a mouse model of dravet syndrome. Front. Cell Dev. Biol. *July*.

Marucci, G. (2017). Commentary on human adult neurogenesis across the ages: An immunohistochemical study. Neuropathol. Appl. Neurobiol. *43*, 450–451.

Maske, H. (1955). Über den topochemischen Nachweis von Zink im Ammonshorn verschiedener Säugetiere. Naturwissenschaften *42*, 424.

Matas-Rico, E., García-Diaz, B., Llebrez-Zayas, P., López-Barroso, D., Santín, L., Pedraza, C., Smith-Fernández, A., Fernández-Llebrez, P., Tellez, T., Redondo, M., et al. (2008). Deletion of lysophosphatidic acid receptor LPA1 reduces neurogenesis in the mouse dentate gyrus. Mol. Cell. Neurosci. *39*, 342–355.

Mathern, G.W., Babb, T.L., Mischel, P.S., Vinters, H. V., Pretorius, J.K., Leite, J.P., and Peacock, W.J. (1996). Childhood generalized and mesial temporal epilepsies demonstrate different amounts and patterns of hippocampal neuron loss and messy fibre synaptic reorganization. Brain *119*, 965–987.

Mathews, E.A., Morgenstern, N.A., Piatti, V.C., Zhao, C., Jessberger, S., Schinder, A.F., and Gage, F.H. (2010). A distinctive layering pattern of mouse dentate granule cells is generated by developmental and adult neurogenesis. J. Comp. Neurol. *518*, 4479–4490.

Mathews, K.J., Allen, K.M., Boerrigter, D., Ball, H., Shannon Weickert, C., and Double, K.L. (2017). Evidence for reduced neurogenesis in the aging human hippocampus despite stable stem cell markers. Aging Cell *16*, 1195–1199.

Matsue, K., Minakawa, S., Kashiwagi, T., Toda, K., Sato, T., Shioda, S., and Seki, T. (2018). Dentate granule progenitor cell properties are rapidly altered soon after birth. Brain Struct. Funct. *223*, 357–369.

Matsushime, H., Ewen, M.E., Strom, D.K., Kato, J.Y., Hanks, S.K., Roussel, M.F., and Sherr, C.J. (1992). Identification and properties of an atypical catalytic subunit

(p34PSK-J3/cdk4) for mammalian D type G1 cyclins. Cell *71*, 323–334.

Matsushime, H., Quelle, D.E., Shurtleff, S.A., Shibuya, M., Sherr, C.J., and Kato, J.Y. (1994). D-type cyclin-dependent kinase activity in mammalian cells. Mol. Cell. Biol. *14*, 2066–2076.

McIntosh, A.M., Kalnins, R.M., Mitchell, L.A., Fabinyi, G.C.A., Briellmann, R.S., and Berkovic, S.F. (2004). Temporal lobectomy: Long-term seizure outcome, late recurrence and risks for seizure recurrence. Brain *127*, 2018–2030.

McKay, R. (1997). Stem cells in the central nervous system. Science (80-.). *276*, 66–71.

McKillop, D., Hutchison, M., Partridge, E.A., Bushby, N., Cooper, C.M.F., Clarkson-Jones, J.A., Herron, W., and Swaisland, H.C. (2004). Metabolic disposition of gefitinib, an epidermal growth factor receptor tyrosine kinase inhibitor, in rat, dog and man. Xenobiotica *34*, 917–934.

McNaughton, N., and Gray, J.A. (2000). Anxiolytic action on the behavioural inhibition system implies multiple types of arousal contribute to anxiety. J. Affect. Disord. *61*, 161–176.

Medina, L., and Abellán, A. (2009). Development and evolution of the pallium. Semin. Cell Dev. Biol. *20*, 698–711.

Meldrum, B.S., Akbar, M.T., and Chapman, A.G. (1999). Glutamate receptors and transporters in genetic and acquired models of epilepsy. Epilepsy Res. *36*, 189–204.

Meloche, S., and Pouysségur, J. (2007). The ERK1/2 mitogen-activated protein kinase pathway as a master regulator of the G1- to S-phase transition. Oncogene *26*, 3227–3239.

Messier, B., Leblond, C.P., and Smart, I. (1958). Presence of DNA synthesis and mitosis in the brain of young adult mice. Exp. Cell Res. *14*, 224–226.

Meyer, G., Socorro, A.C., Garcia, C.G.P., Millan, L.M., Walker, N., and Caput, D. (2004). Developmental roles of p73 in cajal-retzius cells and cortical patterning. J. Neurosci. *24*, 9878–9887.

Meyer, G., González-Arnay, E., Moll, U., Nemajerova, A., Tissir, F., and González-Gómez, M. (2019). Cajal-Retzius neurons are required for the development of the human hippocampal fissure. J. Anat. *235*, 569–589.

Meyerson, M., and Harlow, E. (1994). Identification of G1 kinase activity for cdk6, a novel cyclin D partner. Mol. Cell. Biol. *14*, 2077–2086.

Mignone, J.L., Kukekov, V., Chiang, A.S., Steindler, D., and Enikolopov, G. (2004). Neural Stem and Progenitor Cells in Nestin-GFP Transgenic Mice. J. Comp. Neurol. *469*, 311–324.

Miller, M.W., and Nowakowski, R.S. (1988). Use of bromodeoxyuridine-immunohistochemistry to examine the proliferation, migration and time of origin of cells in the central nervous system. Brain Res. *457*, 44–52.

Minami, A., Sakurada, N., Fuke, S., Kikuchi, K., Nagano, T., Oku, N., and Takeda, A. (2006). Inhibition of presynaptic activity by zinc released from mossy fiber terminals during tetanic stimulation. J. Neurosci. Res. *83*, 167–176.

Mineyeva, O.A., Enikolopov, G., and Koulakov, A.A. (2018). Spatial geometry of stem cell proliferation in the adult hippocampus. Sci. Rep. *8*, 1–12.

Mira, H., Andreu, Z., Suh, H., Chichung Lie, D., Jessberger, S., Consiglio, A., Emeterio, J.S., Hortigüela, R., Marqués-Torrejón, M.Á., Nakashima, K., et al. (2010). Signaling through BMPR-IA regulates quiescence and long-term activity of neural stem cells in the adult hippocampus. Cell Stem Cell *7*, 78–89.

Mitchell, C.L., and Barnes, M.I. (1993). Proconvulsant action of diethyldithiocarbamate in stimulation of the perforant path. Neurotoxicol. Teratol. *15*, 165–171.

Mitchell, C.L., Barnes, M.I., and Grimes, L.M. (1990). Diethyldithiocarbamate and dithizone augment the toxicity of kainic acid. Brain Res. *506*, 327–330.

Mitsuya, K., Nitta, N., and Suzuki, F. (2009). Persistent zinc depletion in the mossy fiber terminals in the intrahippocampal kainate mouse model of mesial temporal lobe epilepsy. Epilepsia *50*, 1979–1990.

Mizuno, D., and Kawahara, M. (2013). The molecular mechanisms of zinc neurotoxicity and the pathogenesis of vascular type senile dementia. Int. J. Mol. Sci. *14*, 22067–22081.

Mody, I., and Miller, J.J. (1985). Levels of hippocampal calcium and zinc following kindling-induced epilepsy. Can. J. Physiol. Pharmacol. *63*, 159–161.

Moe, M.C., Varghese, M., Danilov, A.I., Westerlund, U., Ramm-Pettersen, J., Brundin, L., Svensson, M., Berg-Johnsen, J., and Langmoen, I.A. (2005). Multipotent progenitor cells from the adult human brain: Neurophysiological differentiation to mature neurons. Brain *128*, 2189–2199.

Monuki, E.S., Porter, F.D., and Walsh, C.A. (2001). Patterning of the dorsal telencephalon and cerebral cortex by a roof plate-lhx2 pathway. Neuron *32*, 591–604.

Moreno-Jiménez, E.P., Flor-García, M., Terreros-Roncal, J., Rábano, A., Cafini, F., Pallas-Bazarra, N., Ávila, J., and Llorens-Martín, M. (2019). Adult hippocampal neurogenesis is abundant in neurologically healthy subjects and drops sharply in patients with Alzheimer's disease. Nat. Med. *25*, 554–560.

Morgensztern, D., and McLeod, H.L. (2005). PI3K/Akt/mTOR pathway as a target for cancer therapy. Anticancer. Drugs *16*, 797–803.

Morrison, D.K. (2012). MAP kinase pathways. Cold Spring Harb. Perspect. Biol. *4*, 1–6.

Morton, J.D., Howell, G.A., and Frederickson, C.J. (1990). Effects of Subcutaneous Injections of Zinc Chloride on Seizures Induced by Noise and by Kainic Acid. Epilepsia *31*, 139–144.

Moscovitch, M., Rosenbaum, R.S., Gilboa, A., Addis, D.R., Westmacott, R., Grady, C., McAndrews, M.P., Levine, B., Black, S., Winocur, G., et al. (2005). Functional neuroanatomy of remote episodic, semantic and spatial memory: A unified account based on multiple trace theory. J. Anat. *207*, 35–66.

Moser, E.I., Moser, M.B., and McNaughton, B.L. (2017). Spatial representation in the hippocampal formation: A history. Nat. Neurosci. *20*, 1448–1464.

Muro-García, T., Martín-Suárez, S., Espinosa, N., Valcárcel-Martín, R., Marinas, A., Zaldumbide, L., Galbarriatu, L., Sierra, A., Fuentealba, P., and Encinas, J.M. (2019). Reactive Disruption of the Hippocampal Neurogenic Niche After Induction of Seizures by Injection of Kainic Acid in the Amygdala. Front. Cell Dev. Biol. *7*, 1–14.

Muzio, L., and Mallamaci, A. (2005). Foxg1 confines Cajal-Retzius neuronogenesis and hippocampal morphogenesis to the dorsomedial pallium. J. Neurosci. *25*, 4435–4441.

N

Nakahira, E., and Yuasa, S. (2005). Neuronal generation, migration, and differentiation in the mouse hippocampal primoridium as revealed by enhanced green fluorescent protein gene transfer by means of in utero electroporation. J. Comp. Neurol. *483*, 329–340.

Namba, T., Mochizuki, H., Onodera, M., Mizuno, Y., Namiki, H., and Seki, T. (2005). The fate of neural progenitor cells expressing astrocytic and radial glial markers in the postnatal rat dentate gyrus. Eur. J. Neurosci. *22*, 1928–1941.

Namba, T., Mochizuki, H., Onodera, M., Namiki, H., and Seki, T. (2007). Postnatal neurogenesis in hippocampal slice cultures: early in vitro labeling of neural precursor

cells leads to efficient neuronal production. J Neurosci Res *85*, 1704–1712.

Namba, T., Mochizuki, H., Suzuki, R., Onodera, M., Yamaguchi, M., Namiki, H., Shioda, S., and Seki, T. (2011). Time-lapse imaging reveals symmetric neurogenic cell division of GFAP-expressing progenitors for expansion of postnatal dentate granule neurons. PLoS One *6*.

Namba, T., Shinohara, H., and Seki, T. (2019). Non-radial tortuous migration with cell polarity alterations of newly generated granule neurons in the neonatal rat dentate gyrus. Brain Struct. Funct. *224*, 3247–3262.

Navarro-Quiroga, I., Hernandez-Valdes, M., Lin, S., and Naegele, J. (2006). Postnatal cellular contributions of the hippocampus subventricular zone to the dentate gyrus, corpus callosum, fimbria, and cerebral cortex. J Comp Neurol *497*, 833–845.

Naylor, A.S., Bull, C., Nilsson, M.K.L., Zhu, C., Björk-Eriksson, T., Eriksson, P.S., Blomgren, K., and Kuhn, H.G. (2008). Voluntary running rescues adult hippocampal neurogenesis after irradiation of the young mouse brain. Proc. Natl. Acad. Sci. U. S. A. *105*, 14632–14637.

Nelson, B.R., Hodge, R.D., Daza, R.A., Tripathi, P.P., Arnold, S.J., Millen, K.J., and Hevner, R.F. (2020). Intermediate progenitors support migration of neural stem cells into dentate gyrus outer neurogenic niches. Elife *9*, 1–30.

Ngugi, A.K., Bottomley, C., Kleinschmidt, I., Sander, J.W., and Newton, C.R. (2010). Estimation of the burden of active and life-time epilepsy: A meta-analytic approach. Epilepsia *51*, 883–890.

Nicholson, R.I., Gee, J.M.W., and Harper, M.E. (2001). EGFR and cancer prognosis. Eur. J. Cancer *37*, 9.

Nicola, Z., Fabel, K., and Kempermann, G. (2015). Development of the adult neurogenic niche in the hippocampus of mice. Front. Neuroanat. *9*, 1–13.

Nieto-Sampedro, M., Gómez-Pinilla, F., Knauer, D.J., and Broderick, J.T. (1988). Epidermal growth factor receptor immunoreactivity in rat brain astrocytes. Response to injury. Neurosci. Lett. *91*, 276–282.

Nilsson, M., Perfilieva, E., Johansson, U., Orwar, O., and Eriksson, P.S. (1999). Enriched environment increases neurogenesis in the adult rat dentate gyrus and improves spatial memory. J. Neurobiol. *39*, 569–578.

Noble, A.J., Robinson, A., and Marson, A.G. (2017). A disease, disorder, illness or condition: How to label epilepsy? Acta Neurol. Scand. *136*, 536–540.

Noguchi, H., Castillo, J.G., Nakashima, K., and Pleasure, S.J. (2019). Suppressor of fused controls perinatal expansion and quiescence of future dentate adult neural stem cells. Elife *8*, 1–21.

Nottebohm, F. (2004). The road we travelled: Discovery, choreography, and significance of brain replaceable neurons. Ann. N. Y. Acad. Sci. *1016*, 628–658.

Nowakowski, R.S. (2000). New Neurons: Extraordinary Evidence or Extraordinary Conclusion? Science (80-.). *288*, 771a – 771.

Nowakowski, R.S., Lewin, S.B., and Miller, M.W. (1989). Bromodeoxyuridine immunohistochemical determination of the lengths of the cell cycle and the DNA-synthetic phase for an anatomically defined population. J. Neurocytol. *18*, 311–318.

O

Oberheim, N.A., Tian, G.F., Han, X., Peng, W., Takano, T., Ransom, B., and Nedergaard, M. (2008). Loss of astrocytic domain organization in the epileptic brain. J. Neurosci. *28*, 3264–3276.

Oh, A., Thurman, D.J., and Kim, H. (2019). Independent role of neonatal seizures in subsequent neurological outcomes: a population-based study. Dev. Med. Child Neurol. *61*, 661–666.

Okano, H.J., Pfaff, D.W., and Gibbs, R.B. (1996). Expression of EGFR-, p75NGFR-, and PSTAIR (cdc2)-Like immunoreactivity by proliferating cells in the adult rat hippocampal formation and forebrain? Dev. Neurosci. *18*, 199–209.

Olayioye, M.A. (2000). NEW EMBO MEMBERS' REVIEW: The ErbB signaling network: receptor heterodimerization in development and cancer. EMBO J. *19*, 3159–3167.

Opanashuk, L.A., Mark, R.J., Porter, J., Damm, D., Mattson, M.P., and Seroogy, K.B. (1999). Heparin-binding epidermal growth factor-like growth factor in hippocampus: Modulation of expression by seizures and anti-excitotoxic action. J. Neurosci. *19*, 133–146.

Ortega-Martínez, S., and Trejo, J.L. (2015). The postnatal origin of adult neural stem cells and the effects of glucocorticoids on their genesis. Behav. Brain Res. *279*, 166–176.

Overstreet-Wadiche, L.S., Bromberg, D.A., Bensen, A.S.L., and Westbrook, G.L. (2006). Seizures accelerate functional integration of adult-generated granule cells. J. Neurosci. *26*, 4095–4103.

P

Palmer, T.D., Ray, J., and Gage, F.H. (1995). FGF-2-responsive neuronal progenitors reside in proliferative and quiescent regions of the adult rodent brain. Mol. Cell. Neurosci. *6*, 474–486.

Palmer, T.D., Takahashi, J., and Gage, F.H. (1997). The adult rat hippocampus contains primordial neural stem cells. Mol. Cell. Neurosci. *8*, 389–404.

Palmer, T.D., Schwartz, P.H., Taupin, P., Kaspar, B., Stein, S.A., and Gage, F.H. (2001). Progenitor cells from human brain after death. Nature *411*, 42–43.

Paoletti, P., Vergnano, A.M., Barbour, B., and Casado, M. (2009). Zinc at glutamatergic synapses. Neuroscience *158*, 126–136.

Pardee, B.A. (1989). G1 Events and Regulation of Cell. Science (80-.). *246*, 603–608.

Paredes, M.F., Sorrells, S.F., Cebrian-Silla, A., Sandoval, K., Qi, D., Kelley, K.W., James, D., Mayer, S., Chang, J., Auguste, K.I., et al. (2018). Does Adult Neurogenesis Persist in the Human Hippocampus? Cell Stem Cell *23*, 780–781.

Parent, J.M., Yu, T.W., Leibowitz, R.T., Geschwind, D.H., Sloviter, R.S., and Lowenstein, D.H. (1997). Dentate granule cell neurogenesis is increased by seizures and contributes to aberrant network reorganization in the adult rat hippocampus. J. Neurosci. *17*, 3727–3738.

Parent, J.M., Elliott, R.C., Pleasure, S.J., Barbaro, N.M., and Lowenstein, D.H. (2006). Aberrant seizure-induced neurogenesis in experimental temporal lobe epilepsy. Ann. Neurol. *59*, 81–91.

Park, J.A., and Jae-Young, K. (1999). Induction of an immediate early gene egr-1 by zinc through extracellular signal-regulated kinase activation in cortical culture: Its role in zinc- induced neuronal death. J. Neurochem. *73*, 450–456.

Park, O.K., Schaefer, T.S., and Nathans, D. (1996). In vitro activation of Stat3 by epidermal growth factor receptor kinase. Proc. Natl. Acad. Sci. U. S. A. *93*, 13704–13708.

Partanen, J., Mäkelä, T.P., Eerola, E., Korhonen, J., Hirvonen, H., Claesson-Welsh, L., and Alitalo, K. (1991). FGFR-4, a novel acidic fibroblast growth factor receptor with a distinct expression pattern. EMBO J. *10*, 1347–1354.

Pastrana, E., Cheng, L.C., and Doetsch, F. (2009). Simultaneous prospective purification of adult subventricular zone neural stem cells and their progeny. Proc. Natl. Acad. Sci. U. S. A. *106*, 6387–6392.

Peavy, R.D., Chang, M.S.S., Sanders-Bush, E., and Jeffrey Conn, P. (2001). Metabotropic glutamate receptor 5-induced phosphorylation of extracellular signal-regulated kinase in astrocytes depends on transactivation of the epidermal growth factor receptor. J. Neurosci. *21*, 9619–9628.

Pecháň, P.A., Chowdhury, K., Gerdes, W., and Seifert, W. (1993). Glutamate induces the growth factors NGF, bFGF, the receptor FGF-R1 and c-fos mRNA expression in rat astrocyte culture. Neurosci. Lett. *153*, 111–114.

Pedersen, M.W., Pedersen, N., Ottesen, L.H., and Poulsen, H.S. (2005). Differential response to gefitinib of cells expressing normal EGFR and the mutant EGFRvIII. Br. J. Cancer *93*, 915–923.

Pei, Y., Zhao, D., Huang, J., and Cao, L. (1983). Zinc-Induced Seizures: A New Experimental Model of Epilepsy. Epilepsia *24*, 169–176.

Pencea, V., Bingaman, K.D., Freedman, L.J., and Luskin, M.B. (2001). Neurogenesis in the subventricular zone and rostral migratory stream of the neonatal and adult primate forebrain. Exp. Neurol. *172*, 1–16.

Petrik, D., and Encinas, J.M. (2019). Perspective: Of mice and Men – How widespread is adult neurogenesis? Front. Neurosci. *13*, 1–6.

Pilz, G.A., Bottes, S., Betizeau, M., Jörg, D.J., Carta, S., Simons, B.D., Helmchen, F., and Jessberger, S. (2018). Live imaging of neurogenesis in the adult mouse hippocampus. Science (80-.). *359*, 658–662.

Pineda, J.R., Daynac, M., Chicheportiche, A., Cebrian-Silla, A., Sii Felice, K., Garcia-Verdugo, J.M., Boussin, F.D., and Mouthon, M.A. (2013). Vascular-derived TGF-β increases in the stem cell niche and perturbs neurogenesis during aging and following irradiation in the adult mouse brain. EMBO Mol. Med. *5*, 548–562.

Pinkas-Kramarski, R., Soussan, L., Waterman, H., Levkowitz, G., Alroy, I., Klapper, L., Lavi, S., Seger, R., Ratzkin, B.J., Sela, M., et al. (1996). Diversification of Neu differentiation factor and epidermal growth factor signaling by combinatorial receptor interactions. EMBO J. *15*, 2452–2467.

Planas, A.M., Justicia, C., Soriano, M.A., and Ferrer, I. (1998). Epidermal growth factor receptor in proliferating reactive glia following transient focal ischemia in the rat brain. Glia *23*, 120–129.

Pleasure, S.J., Collins, A.E., and Lowenstein, D.H. (2000a). Unique expression patterns of cell fate molecules delineate sequential stages of dentate gyrus

development. J. Neurosci. *20*, 6095–6105.

Pleasure, S.J., Anderson, S., Hevner, R., Bagri, A., Marin, O., Lowenstein, D.H., and Rubenstein, J.L.R. (2000b). Cell migration from the ganglionic eminences is required for the development of hippocampal GABAergic interneurons. Neuron *28*, 727–740.

Plowman, G.D., Whitney, G.S., Neubauer, M.G., Green, J.M., McDonald, V.L., Todaro, G.J., and Shoyab, M. (1990). Molecular cloning and expression of an additional epidermal growth factor receptor-related gene. Proc. Natl. Acad. Sci. U. S. A. *87*, 4905–4909.

Poppenk, J., Evensmoen, H.R., Moscovitch, M., and Nadel, L. (2013). Long-axis specialization of the human hippocampus. Trends Cogn. Sci. *17*, 230–240.

Van Praag, H., Kempermann, G., and Gage, F.H. (1999). Running increases cell proliferation and neurogenesis in the adult mouse dentate gyrus. Nat. Neurosci. *2*, 266–270.

Van Praag, H., Schinder, A.F., Christie, B.R., Toni, N., Palmer, T.D., and Gage, F.H. (2002). Functional neurogenesis in the adult hippocampus. Nature *415*, 1030–1034.

Prenzel, N., Zwick, E., Daub, H., Leserer, M., Abraham, R., Wallasch, C., and Ullrich, A. (1999). EGF receptor transactivation by G-protein-coupled receptors requires metalloproteinase cleavage of proHB-EGF. Nature *402*, 884–888.

Priego, N., Zhu, L., Monteiro, C., Mulders, M., Wasilewski, D., Bindeman, W., Doglio, L., Martínez, L., Martínez-Saez, E., Cajal, S.R.Y., et al. (2018). STAT3 labels a subpopulation of reactive astrocytes required for brain metastasis article. Nat. Med. *24*, 1024–1035.

Puelles, L. (2001). Thoughts on the development, structure and evolution of the mammalian and avian telencephalic pallium. Philos. Trans. R. Soc. B Biol. Sci. *356*, 1583–1598.

Puschmann, T.B., Zandén, C., Lebkuechner, I., Philippot, C., De Pablo, Y., Liu, J., and Pekny, M. (2014). HB-EGF affects astrocyte morphology, proliferation, differentiation, and the expression of intermediate filament proteins. J. Neurochem. *128*, 878–889.

Q

Qian, J., and Noebels, J.L. (2005). Visualization of transmitter release with zinc fluorescence detection at the mouse hippocampal mossy fibre synapse. J. Physiol. *566*, 747–758.

Qu, W. sheng, Tian, D. shi, Guo, Z. bao, Fang, J., Zhang, Q., Yu, Z. yuan, Xie, M. jie, Zhang, H. qiu, Lü, J. gao, and Wang, W. (2012). Inhibition of EGFR/MAPK signaling reduces microglial inflammatory response and the associated secondary damage in rats after spinal cord injury. J. Neuroinflammation *9*, 1–14.

Quinta-Ferreira, M.E., and Matias, C.M. (2004). Hippocampal mossy fiber calcium transients are maintained during long-term potentiation and are inhibited by endogenous zinc. Brain Res. *1004*, 52–60.

Quirico-Santos, T., Meira, I.D.A., Gomes, A.C., Pereira, V.C., Pinto, M., Monteiro, M., Souza, J.M., and Alves-Leon, S. V. (2013). Resection of the epileptogenic lesion abolishes seizures and reduces inflammatory cytokines of patients with temporal lobe epilepsy. J. Neuroimmunol. *254*, 125–130.

R

Rakhade, S.N., and Jensen, F.E. (2009). Epileptogenesis in the immature brain: Emerging mechanisms. Nat. Rev. Neurol. *5*, 380–391.

Rakic, P. (1985). Limits of neurogenesis in primates. Science (80-.). *227*, 1054–1056.

Rakic, P., and Yakovlev, P.I. (1968). Development of the corpus callosum and cavum septi in man. J. Comp. Neurol. *132*, 45–72.

RAKIC, P. (1985). DNA Synthesis and Cell Division in the Adult Primate Brain. Ann. N. Y. Acad. Sci. *457*, 193–211.

Ramón y Cajal, S. (1893). Estructura del asta de Ammon. Anal Soc. Español Hist. Nat. *22*.

Ramón y Cajal, S. (1911). Histologie du système nerveux de l'homme et des vertébrés.

Rapraeger, A.C., Krufka, A., and Olwin, B.B. (1991). Requirement of heparan sulfate for bFGF-mediated fibroblast growth and myoblast differentiation. Science (80-.). *252*, 1705–1708.

Rassendren, F., and Audinat, E. (2016). Purinergic signaling in epilepsy. J. Neurosci. Res. *94*, 781–793.

Rees, S., and Inder, T. (2005). Fetal and neonatal origins of altered brain development. Early Hum. Dev. *81*, 753–761.

Reynolds, B.A., and Weiss, S. (1992). Generation of neurons and astrocytes from isolated cells of the adult mammalian central nervous system. Science (80-.). *255*,

1707–1710.

Reynolds, B.A., Tetzlaff, W., and Weiss, S. (1992). A multipotent EGF-responsive striatal embryonic progenitor cell produces neurons and astrocytes. J. Neurosci. *12*, 4565–4574.

Richards, L.J., Kilpatrick, T.J., and Bartlett, P.F. (1992). De novo generation of neuronal cells from the adult mouse brain. Proc. Natl. Acad. Sci. U. S. A. *89*, 8591–8595.

Rickmann, M., Amaral, D.G., and Cowan, W.M. (1987). Organization of radial glial cells during the development of the rat dentate gyrus. J. Comp. Neurol. *264*, 449–479.

Riese, D.J., and Stern, D.F. (1998). Specificity within the EGF family/ErbB receptor family signaling network. BioEssays *20*, 41–48.

Río, C., Pérez-Cerdá, F., Matute, C., and Nieto-Sampedro, M. (1995). Preparation of a monoclonal antibody to a glycidic epitope of the epidermal growth factor receptor that recognizes inhibitors of astrocyte proliferation and reactive microglia. J. Neurosci. Res. *40*, 776–786.

Del Rio, J.A. Del, Heimricht, B., Borrell, V., Forstert, E., Drakewt, A., Alcantara, S., Nakajima, K., Miyata, T., Ogawa, M., Mikoshiba, K., et al. (1997). A role for Cajal-Retzius cells and reelin in the development of hippocampal connections. Nature *385*, 70–74.

Del Río, J.A., Martinez, A., Fonseca, M., Auladell, C., and Soriano, E. (1995). Glutamate-like immunoreactivity and fate of cajal-retzius cells in the murine cortex as identified with calretinin antibody. Cereb. Cortex *5*, 13–21.

Del Río, J.A., Heimrich, B., Supèr, H., Borrell, V., Frotscher, M., and Soriano, E. (1996). Differential survival of Cajal-Retzius cells in organotypic cultures of hippocampus and neocortex. J. Neurosci. *16*, 6896–6907.

Riva, M.A., Donati, E., Tascedda, F., Zolli, M., and Racagni, G. (1994). Short- and long-term induction of basic fibroblast growth factor gene expression in rat central nervous system following kainate injection. Neuroscience *59*, 55–65.

Robson, J.P., Wagner, B., Glitzner, E., Heppner, F.L., Steinkellner, T., Khan, D., Petritsch, C., Pollak, D.D., Sitte, H.H., and Sibilia, M. (2018). Impaired neural stem cell expansion and hypersensitivity to epileptic seizures in mice lacking the EGFR in the brain. FEBS J. *285*, 3175–3196.

Rodriguez, A., Ehlenberger, D.B., Hof, P.R., and Wearne, S.L. (2006). Rayburst

sampling, an algorithm for automated three-dimensional shape analysis from laser scanning microscopy images. Nat. Protoc. *1*, 2152–2161.

Roepstorff, K., Grandal, M.V., Henriksen, L., Knudsen, S.L.J., Lerdrup, M., Grøvdal, L., Willumsen, B.M., and Van Deurs, B. (2009). Differential effects of EGFR ligands on endocytic sorting of the receptor. Traffic *10*, 1115–1127.

Rogawski, M.A., and Löscher, W. (2004). The neurobiology of antiepileptic drugs. Nat. Rev. Neurosci. *5*, 553–564.

Ross, M.E., Carter, M.L., and Lee, J.H. (1996). MN20, a D2 cyclin, is transiently expressed in selected neural populations during embryogenesis. J. Neurosci. *16*, 210–219.

Roy, N.S., Wang, S., Jiang, L., Kang, J., Benraiss, A., Harrison-Restelli, C., Fraser, R.A.R., Couldwell, W.T., Kawaguchi, A., Okano, H., et al. (2000). In vitro neurogenesis by progenitor cells isolated from the adult human hippocampus. Nat. Med. *6*, 271–277.

S

Salomon, D.S., Brandt, R., Ciardiello, F., and Normanno, N. (1995). Epidermal growth factor-related peptides and their receptors in human malignancies. Crit. Rev. Oncol. Hematol. *19*, 183–232.

Samet, J.M., Dewar, B.J., Wu, W., and Graves, L.M. (2003). Mechanisms of Zn2+-induced signal initiation through the epidermal growth factor receptor. Toxicol. Appl. Pharmacol. *191*, 86–93.

Sanderson, M., Dempsey, P., and Dunbar, A. (2006). Control of ErbB signaling through metalloprotease mediated ectodomain shedding of EGF-like factors. Growth Factors *24*.

Sandstead, H.H. (2012). Subclinical zinc deficiency impairs human brain function. J. Trace Elem. Med. Biol. *26*, 70–73.

Sandstead, H.H., Frederickson, C.J., and Penland, J.G. (2000). History of Zinc as Related to Brain Function. J. Nutr. *130*, 496S-502S.

Sano, K., and Malamud, N. (1953). Clinical significance of sclerosis of the cornu ammonis: ictal psychic phenomena. AMA Arch Neurol Psychiatry *70*, 40–53.

Sasaki, H., Shimizu, S., Okuda, K., Kawano, O., Yukiue, H., Yano, M., and Fujii, Y. (2009). Epidermal growth factor receptor gene amplification in surgical resected

Japanese lung cancer. Lung Cancer *64*, 295–300.

Sato, K.I., Sato, A., Aoto, M., and Fukami, Y. (1995). c-SRC phosphorylates epidermal growth factor receptor on tyrosine 845. Biochem. Biophys. Res. Commun. *215*, 1078–1087.

Savage, N. (2014). Epidemiology: The complexities of epilepsy. Nature *511*, S2-3.

Scharfman, H.E., Goodman, J.H., and Sollas, A.L. (2000). Granule-like neurons at the hilar/CA3 border after status epilepticus and their synchrony with area CA3 pyramidal cells: Functional implications of seizure-induced neurogenesis. J. Neurosci. *20*, 6144–6158.

Scheffer, I.E., Berkovic, S., Capovilla, G., Connolly, M.B., French, J., Guilhoto, L., Hirsch, E., Jain, S., Mathern, G.W., Moshé, S.L., et al. (2017). ILAE classification of the epilepsies: Position paper of the ILAE Commission for Classification and Terminology. Epilepsia *58*, 512–521.

Schlessinger, A.R., Cowan, W.M., and Gottlieb, D.I. (1975). An autoradiographic study of the time of origin and the pattern of granule cell migration in the dentate gyrus of the rat. J. Comp. Neurol. *159*, 149–175.

Schouten, M., Bielefeld, P., Garcia-Corzo, L., Passchier, E.M.J., Gradari, S., Jungenitz, T., Pons-Espinal, M., Gebara, E., Martín-Suárez, S., Lucassen, P.J., et al. (2019). Circadian glucocorticoid oscillations preserve a population of adult hippocampal neural stem cells in the aging brain. Mol. Psychiatry.

Schuele, S.U., and Lüders, H.O. (2008). Intractable epilepsy: management and therapeutic alternatives. Lancet Neurol. *7*, 514–524.

Schunemann, D.P., Grivicich, I., Regner, A., Leal, L.F., De Araújo, D.R., Jotz, G.P., Fedrigo, C.A., Simon, D., and Da Rocha, A.B. (2010). Glutamate promotes cell growth by EGFR signaling on U-87MG human glioblastoma cell line. Pathol. Oncol. Res. *16*, 285–293.

Scoville, W.B., and Milner, B. (2000). Loss of recent memory after bilateral hippocampal lesions. 1957. J. Neuropsychiatry Clin. Neurosci. *12*, 103–113.

Seaberg, R.M., and Van der Kooy, D. (2002). Adult rodent neurogenic regions: The ventricular subependyma contains neural stem cells, but the dentate gyrus contains restricted progenitors. J. Neurosci. *22*, 1784–1793.

Seaberg, R.M., and Van Der Kooy, D. (2003). Stem and progenitor cells: The premature desertion of rigorous definitions. Trends Neurosci. *26*, 125–131.

Segi-Nishida, E., Warner-Schmidt, J.L., and Duman, R.S. (2008). Electroconvulsive seizure and VEGF increase the proliferation of neural stem-like cells in rat hippocampus. Proc. Natl. Acad. Sci. U. S. A. *105*, 11352–11357.

Seinfield, S., Goodkin, H., and Shinnar, S. (2016). Status Epilepticus. Cold Spring Harb Perspect Med *6*.

Seki, T., and Arai, Y. (1993). Highly polysialylated neural cell adhesion molecule (NCAM-H) is expressed by newly generated granule cells in the dentate gyrus of the adult rat. J. Neurosci. *13*, 2351–2358.

Seki, T., and Arai, Y. (1995). Age-related production of new granule cells in the adult dentate gyrus. Neuroreport *6*, 2479–2482.

Seki, T., Sato, T., Toda, K., Osumi, N., Imura, T., and Shioda, S. (2014). Distinctive population of Gfap-expressing neural progenitors arising around the dentate notch migrate and form the granule cell layer in the developing hippocampus. J. Comp. Neurol. *522*, 261–283.

Seki, T., Hori, T., Miyata, H., Maehara, M., and Namba, T. (2019). Analysis of proliferating neuronal progenitors and immature neurons in the human hippocampus surgically removed from control and epileptic patients. Sci. Rep. *9*, 1–14.

Semba, K., Toyoshima, K., and Yamamoto, T. (1985). c-erbB-1/epidermal growth factor-receptor. *82*, 6497–6501.

Seress, L. (1988). Interspecies comparison of the hippocampal formation shows increased emphasis on the regio superior in the Ammon's horn of the human brain. J Hirnforsch *29*, 335–340.

Seress, L., Gulyás, A.I., and Freund, T.F. (1992). Pyramidal neurons are immunoreactive for calbindin D28k in the CA1 subfield of the human hippocampus. Neurosci. Lett. *138*, 257–260.

Seress, L., Ábrahám, H., Tornóczky, T., and Kosztolányi, G. (2001). Cell formation in the human hippocampal formation from mid-gestation to the late postnatal period. Neuroscience *105*, 831–843.

Seri, B., García-Verdugo, J.M., McEwen, B.S., and Alvarez-Buylla, A. (2001). Astrocytes give rise to new neurons in the adult mammalian hippocampus. J. Neurosci. *21*, 7153–7160.

Seri, B., García-Verdugo, J.M., Collado-Morente, L., McEwen, B.S., and Alvarez-Buylla, A. (2004). Cell types, lineage, and architecture of the germinal zone in the adult

dentate gyrus. J. Comp. Neurol. *478*, 359–378.

Sharma, A.K., Reams, R.Y., Jordan, W.H., Miller, M.A., Thacker, H.L., and Snyder, P.W. (2007a). Mesial temporal lobe epilepsy: Pathogenesis, induced rodent models and lesions. Toxicol. Pathol. *35*, 984–999.

Sharma, S. V., Bell, D.W., Settleman, J., and Haber, D.A. (2007b). Epidermal growth factor receptor mutations in lung cancer. Nat. Rev. Cancer *7*, 169–181.

Sherr, C.J. (1995). Mammalian G1 cyclins and cell cycle progression. Proc. Assoc. Am. Physicians *107*, 181–186.

Sherr, C.J., and Roberts, J.M. (2004). Living with or without cyclins and cyclin-dependent kinases. Genes Dev. *18*, 2699–2711.

Shimogori, T., Banuchi, V., Ng, H.Y., Strauss, J.B., and Grove, E.A. (2004). Embryonic signaling centers expressing BMP, WNT and FGF proteins interact to pattern the cerebral cortex. Development *131*, 5639–5647.

Shin, J., Berg, D.A., Zhu, Y., Shin, J.Y., Song, J., Bonaguidi, M.A., Enikolopov, G., Nauen, D.W., Christian, K.M., Ming, G.L., et al. (2015). Single-Cell RNA-Seq with Waterfall Reveals Molecular Cascades underlying Adult Neurogenesis. Cell Stem Cell *17*, 360–372.

Shipley, M.T. (1975). The topographical and laminar organization of the presubiculum's projection to the ipsi??? and contralateral entorhinal cortex in the guinea pig. J. Comp. Neurol. *160*, 127–145.

Shoelson, S.E. (1997). SH2 and PTB domain interactions in tyrosine kinase signal transduction. Curr. Opin. Chem. Biol. *1*, 227–234.

Shors, T.J., Miesegaes, G., Beylin, A., Zhao, M., Rydel, T., and Gould, E. (2001). Erratum: Neurogenesis in the adult is involved in the formation of trace memories (Nature (2001) 410 (372-376)). Nature *414*, 938.

Sibbe, M., Förster, E., Basak, O., Taylor, V., and Frotscher, M. (2009). Reelin and Notch1 cooperate in the development of the dentate gyrus. J. Neurosci. *29*, 8578–8585.

Sibilia, M., Steinbach, J.P., Stingl, L., Aguzzi, A., and Wagner, E.F. (1998). A strain-independent postnatal neurodegeneration in mice lacking the EGF receptor. EMBO J. *17*, 719–731.

Sicinski, P., Donaher, J.L., Geng, Y., Parker, S.B., Gardner, H., Park, M.Y., Robker, R.L., Richards, J.A.S., McGinnis, L.K., Biggers, J.D., et al. (1996). Cyclin D2 is an FSH-

responsive gene involved in gonadal cell proliferation and oncogenesis. Nature *384*, 470–474.

Sierra, A., Encinas, J.M., Deudero, J.J.P., Chancey, J.H., Enikolopov, G., Overstreet-Wadiche, L.S., Tsirka, S.E., and Maletic-Savatic, M. (2010). Microglia shape adult hippocampal neurogenesis through apoptosis-coupled phagocytosis. Cell Stem Cell *7*, 483–495.

Sierra, A., Beccari, S., Diaz-Aparicio, I., Encinas, J.M., Comeau, S., and Tremblay, M.È. (2014). Surveillance, phagocytosis, and inflammation: How never-resting microglia influence adult hippocampal neurogenesis. Neural Plast. *2014*.

Sierra, A., Martín-Suárez, S., Valcárcel-Martín, R., Pascual-Brazo, J., Aelvoet, S.A., Abiega, O., Deudero, J.J., Brewster, A.L., Bernales, I., Anderson, A.E., et al. (2015). Neuronal hyperactivity accelerates depletion of neural stem cells and impairs hippocampal neurogenesis. Cell Stem Cell *16*, 488–503.

Sievers, J., Hartmann, D., Pehlemann, F.W., and Berry, M. (1992). Development of astroglial cells in the proliferative matrices, the granule cell layer, and the hippocampal fissure of the hamster dentate gyrus. J. Comp. Neurol. *320*, 1–32.

Silvestre, F., Fissore, R.A., Tosti, E., and Boni, R. (2012). [Ca2+]i rise at in vitro maturation in bovine cumulus-oocyte complexes. Mol. Reprod. Dev. *79*, 369–379.

Simpson, D.L., Morrison, R., de Vellis, J., and Herschman, H.R. (1982). Epidermal growth factor binding and mitogenic activity on purified populations of cells from the central nervous system. J. Neurosci. Res. *8*, 453–462.

Sindreu, C.B., Varoqui, H., Erickson, J.D., and Pérez-Clausell, J. (2003). Boutons containing vesicular zinc define a subpopulation of synapses with low AMPAR content in rat hippocampus. Cereb. Cortex *13*, 823–829.

Singh, D., Attri, B., Gill, R., and Bariwal, J. (2016). Review On EGFR Inhibitors: Critical Updates. Mini-Reviews Med. Chem. *16*, 1–1.

Slomianka, L. (1992). Neurons of origin of zinc-containing pathways and the distribution of zinc-containing boutons in the hippocampal region of the rat. Neuroscience *48*, 325–352.

Sloviter, R.S., and Lømo, T. (2012). Updating the lamellar hypothesis of hippocampal organization. Front. Neural Circuits *6*, 1–16.

Smart, I., and Leblond, C.P. (1961). Evidence for division and transformations of neuroglia cells in the mouse brain, as derived from radioautography after injection of

thymidine-H3. J. Comp. Neurol. *116*, 349–367.

Snyder, J.S., and Drew, M.R. (2020). Functional Neurogenesis Over the Years. Behav. Brain Res. *382*, 112470.

Sofroniew, M. V. (2009). Molecular dissection of reactive astrogliosis and glial scar formation. Trends Neurosci. *32*, 638–647.

Sommer, W. (1880). Erkrankung des Ammonshorns als aetiologisches Moment der Epilepsie. Arch. Psychiatr. Nervenkr. *10*, 631–675.

Song, J., Zhong, C., Bonaguidi, M.A., Sun, G.J., Hsu, D., Gu, Y., Meletis, K., Huang, Z.J., Ge, S., Enikolopov, G., et al. (2012). Neuronal circuitry mechanism regulating adult quiescent neural stem-cell fate decision. Nature *489*, 150–154.

Soriano, E., Del Río, J.A., Martínez, A., and Supèr, H. (1994). Organization of the embryonic and early postnatal murine hippocampus. I. Immunocytochemical characterization of neuronal populations in the subplate and marginal zone. J. Comp. Neurol. *342*, 571–595.

Sorrells, S.F., Paredes, M.F., Cebrian-Silla, A., Sandoval, K., Qi, D., Kelley, K.W., James, D., Mayer, S., Chang, J., Auguste, K.I., et al. (2018). Human hippocampal neurogenesis drops sharply in children to undetectable levels in adults. Nature *555*, 377–381.

Spalding, K.L., Bergmann, O., Alkass, K., Bernard, S., Salehpour, M., Huttner, H.B., Boström, E., Westerlund, I., Vial, C., Buchholz, B.A., et al. (2013). Dynamics of hippocampal neurogenesis in adult humans. Cell *153*, 1219.

Spielmeyer, W. (1927). Die Pathogenese des epileptischen Krampfes - Histopathologischer Teil. Zeitschrift Für Die Gesamte Neurol. Und Psychiatr. *109*, 501–520.

Stanfield, B.B., and Cowan, W.M. (1979). The development of the hippocampus and dentate gyrus in normal and reeler mice. J. Comp. Neurol. *185*, 423–459.

Stanfield, B.B., and Trice, J.E. (1988). Evidence that granule cells generated in the dentate gyrus of adult rats extend axonal projections. Exp. Brain Res. *72*, 399–406.

Stark, K.L., McMahon, J.A., and McMahon, A.P. (1991). FGFR-4, a new member of the fibroblast growth factor receptor family, expressed in the definitive endoderm and skeletal muscle lineages of the mouse. Development *113*, 641–651.

Stern, D.F., and Kamps, M.P. (1988). EGF-stimulated tyrosine phosphorylation of p185neu: a potential model for receptor interactions. EMBO J. *7*, 995–1001.

Steve, T.A., Jirsch, J.D., and Gross, D.W. (2014). Quantification of subfield pathology in hippocampal sclerosis: A systematic review and meta-analysis. Epilepsy Res. *108*, 1279–1285.

Steward, O., and Scoville, S.A. (1976). Cells of origin of entorhinal cortical afferents to the hippocampus and fascia dentata of the rat. J. Comp. Neurol. *169*, 347–370.

Stover, D.R., Becker, M., Liebetanz, J., and Lydon, N.B. (1995). Src phosphorylation of the epidermal growth factor receptor at novel sites mediates receptor interaction with Src and P85α. J. Biol. Chem. *270*, 15591–15597.

Strange, B.A., and Dolan, R.J. (1999). Functional segregation within the human hippocampus. Mol. Psychiatry *4*, 508–511.

Strange, B.A., Witter, M.P., Lein, E.S., and Moser, E.I. (2014). Functional organization of the hippocampal longitudinal axis. Nat. Rev. Neurosci. *15*, 655–669.

Sugiura, S., Kitagawa, K., Tanaka, S., Todo, K., Omura-Matsuoka, E., Sasaki, T., Mabuchi, T., Matsushita, K., Yagita, Y., and Hori, M. (2005). Adenovirus-mediated gene transfer of heparin-binding epidermal growth factor-like growth factor enhances neurogenesis and angiogenesis after focal cerebral ischemia in rats. Stroke *36*, 859–864.

Sugiyama, T., Osumi, N., and Katsuyama, Y. (2013). The germinal matrices in the developing dentate gyrus are composed of neuronal progenitors at distinct differentiation stages. Dev. Dyn. *242*, 1442–1453.

Sun, G.J., Zhou, Y., Ito, S., Bonaguidi, M.A., Stein-O'brien, G., Kawasaki, N.K., Modak, N., Zhu, Y., Ming, G.L., and Song, H. (2015). Latent tri-lineage potential of adult hippocampal neural stem cells revealed by Nf1 inactivation. Nat. Neurosci. *18*, 1722–1724.

Sun, Y., Goderie, S.K., and Temple, S. (2005). Asymmetric distribution of EGFR receptor during mitosis generates diverse CNS progenitor cells. Neuron *45*, 873–886.

Sutula, T., Cascino, G., Cavazos, J., Parada, I., and Ramirez, L. (1989). Mossy fiber synaptic reorganization in the epileptic human temporal lobe. Ann. Neurol. *26*, 321–330.

T

Takahashi, D.K., Vargas, J.R., and Wilcox, K.S. (2010). Increased coupling and altered glutamate transport currents in astrocytes following kainic-acid-induced status

epilepticus. Neurobiol. Dis. *40*, 573–585.

Takeda, A., and Tamano, H. (2009). Insight into zinc signaling from dietary zinc deficiency. Brain Res. Rev. *62*, 33–44.

Takeda, A., Minami, A., Seki, Y., and Oku, N. (2003). Inhibitory function of zinc against excitation of hippocampal glutamatergic neurons. Epilepsy Res. *57*, 169–174.

Takeda, A., Minami, A., Seki, Y., and Oku, N. (2004). Differential Effects of Zinc on Glutamatergic and GABAergic Neurotransmitter Systems in the Hippocampus. J. Neurosci. Res. *75*, 225–229.

Takeda, A., Nakajima, S., Fuke, S., Sakurada, N., Minami, A., and Oku, N. (2006). Zinc release from Schaffer collaterals and its significance. Brain Res. Bull. *68*, 442–447.

Takiguchi-Hayashi, K., Sekiguchi, M., Ashigaki, S., Takamatsu, M., Hasegawa, H., Suzuki-Migishima, R., Yokoyama, M., Nakanishi, S., and Tanabe, Y. (2004). Generation of Reelin-Positive Marginal Zone Cells from the Caudomedial Wall of Telencephalic Vesicles. J. Neurosci. *24*, 2286–2295.

Tanapat, P., Hastings, N.B., Rydel, T.A., Galea, L.A.M., and Gould, E. (2013). Exposure to fox odor inhibits cell proliferation in the hippocampus of adult rats via an adrenal hormone- dependent mechanism. Sci. Ment. Heal. Stress Brain *9*, 110–118.

Tanguay, D.A., and Chiles, T.C. (1996). Regulation of the catalytic subunit (p34PSK-J3/cdk4) for the major D-type cyclin in mature B lymphocytes. J Immunol *Jan*, 539–548.

Tao, Y., Black, I.B., and DiCicco-Bloom, E. (1996). Neurogenesis in neonatal rat brain is regulated by peripheral injection of basic fibroblast growth factor (bFGF). J. Comp. Neurol. *376*, 653–663.

Tartt, A.N., Fulmore, C.A., Liu, Y., Rosoklija, G.B., Dwork, A.J., Arango, V., Hen, R., Mann, J.J., and Boldrini, M. (2018). Considerations for Assessing the Extent of Hippocampal Neurogenesis in the Adult and Aging Human Brain. Cell Stem Cell *23*, 782–783.

Thom, M. (2014). Review: Hippocampal sclerosis in epilepsy: A neuropathology review. Neuropathol. Appl. Neurobiol. *40*, 520–543.

Thom, M., Sisodiya, S.M., Beckett, A., Martinian, L., Lin, W.R., Harkness, W., Mitchell, T.N., Craig, J., Duncan, J., and Scaravilli, F. (2002). Cytoarchitectural abnormalities in hippocampal sclerosis. J. Neuropathol. Exp. Neurol. *61*, 510–519.

Thomas, S.M., and Brugge, J.S. (1997). Cellular Functions Regulated By Src Family

Kinases. Annu. Rev. Cell Dev. Biol. *13*, 513–609.

Thompson, C.L., Pathak, S.D., Jeromin, A., Ng, L.L., MacPherson, C.R., Mortrud, M.T., Cusick, A., Riley, Z.L., Sunkin, S.M., Bernard, A., et al. (2008). Genomic Anatomy of the Hippocampus. Neuron *60*, 1010–1021.

Tian, G.F., Azmi, H., Takano, T., Xu, Q., Peng, W., Lin, J., Oberheim, N.A., Lou, N., Wang, X., Zielke, H.R., et al. (2005). An astrocytic basis of epilepsy. Nat. Med. *11*, 973–981.

Tice, D.A., Biscardi, J.S., Nickles, A.L., and Parsons, S.J. (1999). Mechanism of biological synergy between cellular Src and epidermal growth factor receptor. Proc. Natl. Acad. Sci. U. S. A. *96*, 1415–1420.

Tobin, M.K., Musaraca, K., Disouky, A., Shetti, A., Bheri, A., Honer, W.G., Kim, N., Dawe, R.J., Bennett, D.A., Arfanakis, K., et al. (2019). Human Hippocampal Neurogenesis Persists in Aged Adults and Alzheimer's Disease Patients. Cell Stem Cell *24*, 974-982.e3.

Tozuka, Y., Fukuda, S., Namba, T., Seki, T., and Hisatsune, T. (2005). GABAergic excitation promotes neuronal differentiation in adult hippocampal progenitor cells. Neuron *47*, 803–815.

Treves, A., Tashiro, A., Witter, M.E., and Moser, E.I. (2008). What is the mammalian dentate gyrus good for? Neuroscience *154*, 1155–1172.

Tropepe, V., Sibilia, M., Ciruna, B.G., Rossant, J., Wagner, E.F., and Van Der Kooy, D. (1999). Distinct neural stem cells proliferate in response to EGF and FGF in the developing mouse telencephalon. Dev. Biol. *208*, 166–188.

Tsunekawa, Y., Britto, J.M., Takahashi, M., Polleux, F., Tan, S.S., and Osumi, N. (2012). Cyclin D2 in the basal process of neural progenitors is linked to non-equivalent cell fates. EMBO J. *31*, 1879–1892.

Tucker, M.S., Khan, I., Fuchs-Young, R., Price, S., Steininger, T.L., Greene, G., Wainer, B.H., and Rosner, M.R. (1993). Localization of immunoreactive epidermal growth factor receptor in neonatal and adult rat hippocampus. Brain Res. *631*, 65–71.

Turski, W.A., Czuczwar, S.J., Kleinrok, Z., and Turski, L. (1983). Cholinomimetics produce seizures and brain damage in rats. Experientia *39*, 1408–1411.

Tzahar, E., Waterman, H., Chen, X., Levkowitz, G., Karunagaran, D., Lavi, S., Ratzkin, B.J., and Yarden, Y. (1996). A hierarchical network of interreceptor interactions determines signal transduction by Neu differentiation factor/neuregulin and epidermal

growth factor. Mol. Cell. Biol. *16*, 5276–5287.

U

Ullrich, A., Coussens, L., Hayflick, J.S., Dull, T.J., Gray, A., Tam, A.W., Lee, J., Yarden, Y., Libermann, T.A., Schlessinger, J., et al. (1984). Human epidermal growth factor receptor cDNA sequence and aberrant expression of the amplified gene in A431 epidermoid carcinoma cells. Nature *309*, 418–425.

Urbán, N., Van Den Berg, D.L.C., Forget, A., Andersen, J., Demmers, J.A.A., Hunt, C., Ayrault, O., and Guillemot, F. (2016). Return to Quiescence of mouse neural stem cells by degradation of a proactivation protein. Science (80-.). *353*, 292–295.

V

Valcárcel-Martín, R., Martín-Suárez, S., Muro-García, T., Pastor-Alonso, O., Rodríguez de Fonseca, F., Estivill-Torrús, G., and Encinas, J.M. (2020). Lysophosphatidic acid receptor 1 specifically labels seizure-induced hippocampal reactive neural stem cells and controls their division. Front. Neurosci. - Neurogenes. *August*.

Vargas, J.R., Takahashi, D.K., Thomson, K.E., and Wilcox, K.S. (2013). The expression of kainate receptor subunits in hippocampal astrocytes after experimentally induced status epilepticus. J. Neuropathol. Exp. Neurol. *72*, 919–932.

Vašák, M., and Hasler, D.W. (2000). Metallothioneins: New functional and structural insights. Curr. Opin. Chem. Biol. *4*, 177–183.

Verwer, R.W.H., Sluiter, A.A., Balesar, R.A., Baayen, J.C., Noske, D.P., Dirven, C.M.F., Wouda, J., Van Dam, A.M., Lucassen, P.J., and Swaab, D.F. (2007). Mature astrocytes in the adult human neocortex express the early neuronal marker doublecortin. Brain *130*, 3321–3335.

Verwer, R.W.H., Sluiter, A.A., Balesar, R.A., Baaijen, J.C., De Witt Hamer, P.C., Speijer, D., Li, Y., and Swaab, D.F. (2015). Injury Response of Resected Human Brain Tissue in Vitro. Brain Pathol. *25*, 454–468.

Viti, J., Feathers, A., Phillips, J., and Lillien, L. (2003). Epidermal growth factor receptors control competence to interpret leukemia inhibitory factor as an astrocyte inducer in developing cortex. J. Neurosci. *23*, 3385–3393.

Vivanco, I., Ian Robins, H., Rohle, D., Campos, C., Grommes, C., Nghiemphu, P.L.,

Kubek, S., Oldrini, B., Chheda, M.G., Yannuzzi, N., et al. (2012). Differential sensitivity of glioma- versus lung cancer-specific EGFR mutations to EGFR kinase inhibitors. Cancer Discov. *2*, 458–471.

Vivar, C., and van Praag, H. (2013). Functional circuits of new neurons in the dentate gyrus. Front. Neural Circuits *7*, 1–13.

Vivar, C., Peterson, B.D., and van Praag, H. (2016). Running rewires the neuronal network of adult-born dentate granule cells. Neuroimage *131*, 29–41.

Vogel, J.W., La Joie, R., Grothe, M.J., Diaz-Papkovich, A., Doyle, A., Vachon-Presseau, E., Lepage, C., Vos de Wael, R., Thomas, R.A., Iturria-Medina, Y., et al. (2020). A molecular gradient along the longitudinal axis of the human hippocampus informs large-scale behavioral systems. Nat. Commun. *11*, 1–17.

W

Wada, T., Qian, X., and Greene, M.I. (1990). Intermolecular association of the p185neu protein and EGF receptor modulates EGF receptor function. Cell *61*, 1339–1347.

Wagner, B., Natarajan, A., Grünaug, S., Kroismayr, R., Wagner, E.F., and Sibilia, M. (2006). Neuronal survival depends on EGFR signaling in cortical but not midbrain astrocytes. EMBO J. *25*, 752–762.

Wagner, J.P., Black, I.B., and DiCicco-Bloom, E. (1999). Stimulation of neonatal and adult brain neurogenesis by subcutaneous injection of basic fibroblast growth factor. J. Neurosci. *19*, 6006–6016.

Wakeling, A.E., Guy, S.P., Woodburn, J.R., Ashton, S.E., Curry, B.J., Barker, A.J., and Gibson, K.H. (2002). ZD1839 (Iressa): An orally active inhibitor of epidermal growth factor signaling with potential for cancer therapy. Cancer Res. *62*, 5749–5754.

Van Der Wal, E.A., Gómez-Pinilla, F., and Cotman, C.W. (1994). Seizure-associated induction of basic fibroblast growth factor and its receptor in the rat brain. Neuroscience *60*, 311–323.

Walker, T.L., Overall, R.W., Vogler, S., Sykes, A.M., Ruhwald, S., Lasse, D., Ichwan, M., Fabel, K., and Kempermann, G. (2016). Lysophosphatidic Acid Receptor Is a Functional Marker of Adult Hippocampal Precursor Cells. Stem Cell Reports *6*, 552–565.

Walton, G.M., Chen, W.S., Rosenfeld, M.G., and Gill, G.N. (1990). Analysis of deletions of the carboxyl terminus of the epidermal growth factor receptor reveals self-

phosphorylation at tyrosine 992 and enhanced in vivo tyrosine phosphorylation of cell substrates. J. Biol. Chem. *265*, 1750–1754.

Wang, S., Brunne, B., Zhao, S., Chai, X., Li, J., Lau, J., Failla, A.V., Zobiak, B., Sibbe, M., Westbrook, G.L., et al. (2018). Trajectory analysis unveils Reelin's role in the directed migration of granule cells in the dentate gyrus. J. Neurosci. *38*, 137–148.

Wang, S., Lévesque, M., and Avoli, M. (2019). Transition from status epilepticus to interictal spiking in a rodent model of mesial temporal epilepsy. Epilepsy Res. *152*, 73–76.

Watanabe, M., Oizumi, S., Kiuchi, S., Yamada, N., Yokouchi, H., Fukumoto, S., and Harada, M. (2018). The effectiveness of afatinib in a patient with advanced lung adenocarcinoma harboring rare G719X and S768I mutations. Intern. Med. *57*, 993–996.

Watt, F.M., and Hogan, B.L.M. (2000). Out of eden: Stem cells and their niches. Science (80-.). *287*, 1427–1430.

Weber, K., Thomaschewski, M., Benten, D., and Fehse, B. (2012). RGB marking with lentiviral vectors for multicolor clonal cell tracking. Nat. Protoc. *7*, 839–849.

Weiss, S., Reynolds, B.A., Vescovi, A.L., Morshead, C., Craig, C.G., and Van Der Kooy, D. (1996). Is there a neural stem cell in the mammalian forebrain? Trends Neurosci. *19*, 387–393.

Werner, M.H., Nanney, L.B., Stoscheck, C.M., and King, L.E. (1988). Localization of immunoreactive epidermal growth factor receptors in human nervous system. J. Histochem. Cytochem. *36*, 81–86.

West, M.J. (1990). Understanding the Brain Through the Hippocampus the Hippocampal Region as a Model for Studying Brain Structure and Function. Prog. Brain Res. *83*, 13–36.

White, A., Williams, P.A., Hellier, J.L., Clark, S., Dudek, F.E., and Staley, K.J. (2010). EEG spike activity precedes epilepsy after kainate-induced status epilepticus. Epilepsia *51*, 371–383.

Wiebe, S. (2000). Epidemiology of Temporal Lobe Epilepsy. Can. J. Neurol. Sci. *27*, S6–S10.

Wieser, H.-J. (2004). ILAE Commission Report. Mesial temporal lobe epilepsy with hippocampal sclerosis. Epilepsia *45*, 695–714.

Wilcox, K.S., Gee, J.M., Gibbons, M.B., Tvrdik, P., and White, J.A. (2015). Altered

structure and function of astrocytes following status epilepticus. Epilepsy Behav. *49*, 17–19.

Wilhelmsson, U., Bushong, E.A., Price, D.L., Smarr, B.L., Phung, V., Terada, M., Ellisman, M.H., and Pekny, M. (2006). Redefining the concept of reactive astrocytes as cells that remain within their unique domains upon reaction to injury. Proc. Natl. Acad. Sci. U. S. A. *103*, 17513–17518.

Williams, P.A., White, A.M., Clark, S., Ferraro, D.J., Swiercz, W., Staley, K.J., and Dudek, F.E. (2009). Development of spontaneous recurrent seizures after kainate-induced status epilepticus. J. Neurosci. *29*, 2103–2112.

Williamson, P.D., French, J.A., Thadani, V.M., Kim, J.H., Novelly, R.A., Spencer, S.S., Spencer, D.D., and Mattson, R.H. (1993). Characteristics of medial temporal lobe epilepsy: II. Interictal and ictal scalp electroencephalography, neuropsychological testing, neuroimaging, surgical results, and pathology. Ann. Neurol. *34*, 781–787.

Willmarth, N.E., and Ethier, S.P. (2006). Autocrine and juxtacrine effects of amphiregulin on the proliferative, invasive, and migratory properties of normal and neoplastic human mammary epithelial cells. J. Biol. Chem. *281*, 37728–37737.

Willmore, L.J., Sypert, G.W., Munson, J.B., and Hurd, R.W. (2020). Chronic focal epileptiform discharges induced by injection of iron into rat and cat cortex. *200*, 1501–1503.

Wilson, K.J., Gilmore, J., Foley, J., Lemmon, M., and Riese II, D. (2009). Functional selectivity of EGF family peptide growth factors: Implications for cancer. Pharmacol. Ther. *122*, 1–8.

Wilson, K.J., Mill, C., Lambert, S., Buchman, J., Wilson, T.R., Hernandez-Gordillo, V., Gallo, R.M., Ades, L.M.C., Settleman, J., and Riese, D.J. (2012). EGFR ligands exhibit functional differences in models of paracrine and autocrine signaling. Growth Factors *30*, 107–116.

Wu, W., Graves, L.M., Gill, G.N., Parsons, S.J., and Samet, J.M. (2002). Src-dependent phosphorylation of the epidermal growth factor receptor on tyrosine 845 is required for zinc-induced Ras activation. J. Biol. Chem. *277*, 24252–24257.

Wu, W., Samet, J.M., Silbajoris, R., Dailey, L.A., Sheppard, D., Bromberg, P.A., and Graves, L.M. (2004). Heparin-binding epidermal growth factor cleavage mediates zinc-induced epidermal growth factor receptor phosphorylation. Am. J. Respir. Cell Mol. Biol. *30*, 540–547.

X

Xu, W., Morishita, W., Buckmaster, P.S., Pang, Z.P., Malenka, R.C., and Südhof, T.C. (2012). Distinct Neuronal Coding Schemes in Memory Revealed by Selective Erasure of Fast Synchronous Synaptic Transmission. Neuron *73*, 990–1001.

Y

Yamaguchi, M., Saito, H., Suzuki, M., and Mori, K. (2000). Visualization of neurogenesis in the central nervous system using nestin promoter-GFP transgenic mice. Neuroreport *11*, 1991–1996.

Yamashita, N., Kondo, M., Zhao, S., Li, W., Koike, K., Nemoto, K., and Kanno, Y. (2017). Picrasidine G decreases viability of MDA-MB 468 EGFR-overexpressing triple-negative breast cancer cells through inhibition of EGFR/STAT3 signaling pathway. Bioorganic Med. Chem. Lett. *27*, 2608–2612.

Yang, J.C.H., Sequist, L. V., Geater, S.L., Tsai, C.M., Mok, T.S.K., Schuler, M., Yamamoto, N., Yu, C.J., Ou, S.H.I., Zhou, C., et al. (2015). Clinical activity of afatinib in patients with advanced non-small-cell lung cancer harbouring uncommon EGFR mutations: A combined post-hoc analysis of LUX-Lung 2, LUX-Lung 3, and LUX-Lung 6. Lancet Oncol. *16*, 830–838.

Yang, P., Zhang, J., Shi, H., Zhang, J., Xu, X., Xiao, X., and Liu, Y. (2014). Developmental profile of neurogenesis in prenatal human hippocampus: An immunohistochemical study. Int. J. Dev. Neurosci. *38*, 1–9.

Yarden, Y., and Sliwkowski, M.X. (2001). Untangling the ErbB signalling network. Nat. Rev. Mol. Cell Biol. *2*, 127–137.

Yokose, J., Ishizuka, T., Yoshida, T., Aoki, J., Koyanagi, Y., and Yawo, H. (2011). Lineage analysis of newly generated neurons in organotypic culture of rat hippocampus. Neurosci. Res. *69*, 223–233.

Yoshida, M., Assimacopoulos, S., Jones, K.R., and Grove, E.A. (2006). Massive loss of Cajal-Retzius cells does not disrupt neocortical layer order. Development *133*, 537–545.

Youssef, M., Krish, V.S., Kirshenbaum, G.S., Atsak, P., Tamara, J., Lieberman, S.R., Leonardo, E.D., and Dranovsky, A. (2019). Sufficient To Reduce Adult Hippocampal Neurogenesis. *28*, 586–601.

Yu, K.K., Dong, S.L., Sang, K.L., Kim, S.K., Chun, K.C., Ki, H.C., Ki, Y.C., Chung, J.K., and Myung, C.L. (2003). Differential features of metabolic abnormalities between medial and lateral temporal lobe epilepsy: Quantitative analysis of 18 F-FDG PET using SPM. J. Nucl. Med. *44*, 1006–1012.

Yuasa, S. (2001). Development of astrocytes in the mouse hippocampus as tracked by tenascin-C gene expression. Arch. Histol. Cytol. *64*, 149–158.

Z

Zhang, L., Blomgren, K., Kuhn, H.G., and Cooper-Kuhn, C.M. (2009). Effects of postnatal thyroid hormone deficiency on neurogenesis in the juvenile and adult rat. Neurobiol. Dis. *34*, 366–374.

Zhang, Y., Chen, K., Sloan, S.A., Bennett, M.L., Scholze, A.R., O'Keeffe, S., Phatnani, H.P., Guarnieri, P., Caneda, C., Ruderisch, N., et al. (2014). An RNA-sequencing transcriptome and splicing database of glia, neurons, and vascular cells of the cerebral cortex. J. Neurosci. *34*, 11929–11947.

Zhao, C., Teng, E.M., Summers, R.G., Ming, G.L., and Gage, F.H. (2006a). Distinct morphological stages of dentate granule neuron maturation in the adult mouse hippocampus. J. Neurosci. *26*, 3–11.

Zhao, C., Guan, W., and Pleasure, S.J. (2006b). A transgenic marker mouse line labels Cajal-Retzius cells from the cortical hem and thalamocortical axons. Brain Res. *1077*, 48–53.

Zhao, S., Chai, X., Förster, E., and Frotscher, M. (2004). Reelin is a potential signal for the lamination of dentate granule cells. Development *131*, 5117–5125.

Zhao, X., Lein, E.S., He, A., Smith, S.C., Aston, C., and Gage, F.H. (2001). Transcriptional profiling reveals strict boundaries between hippocampal subregions. J. Comp. Neurol. *441*, 187–196.

Zhong, Z., Wen, Z., and Darnell, J.E. (1994). Stat3: A STAT family member activated by tyrosine phosphorylation in response to epidermal growth factor and interleukin-6. Science (80-.). *264*, 95–98.

Zhou, C.J., Zhao, C., and Pleasure, S.J. (2004). Wnt Signaling Mutants Have Decreased Dentate Granule Cell Production and Radial Glial Scaffolding Abnormalities. J. Neurosci. *24*, 121–126.

Zhou, Y., James, I., and Besner, G.E. (2012). Heparin-binding epidermal growth factor-

like growth factor promotes murine enteric nervous system development and enteric neural crest cell migration. J. Pediatr. Surg. *47*, 1865–1873.

Ziebell, F., Dehler, S., Martin-Villalba, A., and Marciniak-Czochra, A. (2018). Revealing age-related changes of adult hippocampal neurogenesis using mathematical models. Dev. *145*, 1–12.

Zulkifli, A.A., Tan, F.H., Putoczki, T.L., Stylli, S.S., and Luwor, R.B. (2017). STAT3 signaling mediates tumour resistance to EGFR targeted therapeutics. Mol. Cell. Endocrinol. *451*, 15–23.

eman ta zabal zazu

Universidad del País Vasco

Euskal Herriko Unibertsitatea

Hipokanpoko Zelula Ama Neuralak: Garapenetik Patologiara

Hipokanpoko zelula ama neural helduen jaio ondorengo tokiko sorrera eta hazkuntza faktore epidermal hartzailearen blokeoa lobulu tenporaleko epilepsian neurogenesia babesteko

PhD gradurako hautesle den doktoretza-tesia

Oier Pastor Alonso

-k aurkeztua

2020

Zuzendariak:

Dr. Juan Manuel Encinas Pérez

Dr. José Ramón Pineda Martí

(c)2020 OIER PASTOR ALONSO

EDUKI TAULA

EDUKI TAULA

1. LABURDUREN LISTA 3

2. LABURPENA 9

3. SARRERA 15

3.1. Hipokanpoko formazioa (Ingelesetik hippocampal formation, HPF): Burmuineko itsas zaldia 15

3.2. Neurona sorrera burmuin helduan 16

3.3. Urjauzi neurogeniko hipokanpala 17

3.4. NSC helduen jatorria 19

3.4.1. NSC helduen jatorria jaio aurretik 19

3.4.2. dNSC vs NSC helduak 22

3.5. Giza neurogenesi heldua: Izan ala ez izan 23

3.6. Lobulu tenporal medialeko epilepsia (ingelesetik medial temporal lobe epilepsy, MTLE) eta NSCak 25

3.6.1. MTLE-HSan mekanismo posibleak 27

3.6.2. Hazkuntza faktore epidermal hartzailea (ingelesetik epidermal growth factor receptor, EGFR) 28

3.6.3. Zink (Zn^{+2}) parte hartzaile bezala KAren osteko EGFRren aktibazioan 29

3.6.4 EGFR seinalizazioa blokeatuz 30

EDUKI TAULA

Hipokanpoko NSCak: Garapenetik Patologiara

5. MATERIALAK ETA METODOAK 41

5.1. Animaliak 41

5.2. Giza Laginak 42

5.3. Injekzio intrahipokanpal estereotaxikoak 42

5.3.1. Jaio ondorengo SFFV-RV infekzioak 42

5.3.2. Injekzio intrahipokanpal estereotaxikoak helduetan 43

5.4. Tratamenduak 44

5.4.1. EGFRaren inhibitzaile Gefitinibaren sudurretiko administrazioa 44

5.4.2. TPEN Zn^{+2} isolatzailearen azal-azpiko administrazioa 44

5.4.3. BrdU administrazioa 45

5.5. Hazkuntza zelularrak 45

5.6. RNA erauzketa eta uneko polimerasa kate erreakzio kuantitatiboa (Ingelesetik real time- quantitative polymerase chain reaction, RT-qPCR) 46

5.6.1 RNA erauzketa eta alderantzizko transkripzioa 46

5.6.2 RT-qPCR 47

5.7. IHC 48

5.7.1. Sagu burmuin ehuna 48

5.7.2. Hazkuntza zelularrak 49

5.7.3. Giza ehuna 50

5.8. WB 54

5.9. ELISA 56

5.10. Danscher tindaketa 57

5.11. Irudien analisia 57

5.11.1. Zelula populazioen analisi kuantitatiboa 57

5.11.2. NSCen analisi morfologikoa: SHOLL analisia 59

5.12. Analisi estatistikoa 59

6. EMAITZAK 64

6.1. cD2 ezinbestekoa da NSC helduen populazioa sortu dadin 64

6.1.1. cD2ren absentzian, NSC helduen populazioa ez da sortzen 64

6.1.2. *cD2*ren gabezian heriotza zelularra ez zen areagotu 71

6.2. NSC helduen populazioaren jaio ondorengo sorkuntza 72

6.2.1. *In vivo* infekzio erretrobiralak NSC helduen jatorri espaziala identifikatzeko 73

6.2.2. NSC helduen populazioaren sorkuntzan soilik DG barruko aitzindariek egiten zuten ekarpena 77

6.2.3. DMSko sortzaileek DGrenganako ekarpen espazial dibergentea egiten zuten 82

6.3. LPA_1 NSC helduen markatzaile diferentzial bezala 84

6.3.1. NSCek jaio ondorengo aroan zehar bereganatu zuten LPA_1 espresioa 84

6.3.2. LPA_1 espezifikotasuna jaio ostetik helduarora aldatzen da 86

6.4. Haurdunaldiaren erdirako giza DGaren garapena ia amaiturik dago 87

6.4.1. DMSa presente zegoen giza garapen goiztiarrean (GW14) 87

6.4.2. Patroi espazial diferentzialak DGaren garapenean zehar 89

6.4.3. GW30rako DGaren formazioa GCLra mugatua dago 91

6.4.4. Jaio ondoren eta gutxira RGC aldamio batek DGan presente zirauen 92

EDUKI TAULA

Hipokanpoko NSCak: Garapenetik Patologiara

6.5. FGFR ibilbideak eta MTLE egoeran HPFak ematen duen erantzun goiztiarrak ez dute loturarik 94

6.6. EGFRek gune neurogenikoak MTLE indukzioaren ostean duen hasierako erantzunean parte hartzen du 97

6.6.1. MTLEren indukzioaren ostean, EGFR seinalizazio ibilbidearen aktibazio eta areagotzea jazoera azkarrak izan ziren 97

6.6.2. EGFRk NSPC hipokanpalen ugaritze jardueran parte hartzen zuen 101

6.6.3. EGFRren blokeo farmakologikoak MTLE osteko NSCen erantzun patologikoaren hobetzea ekarri zuen 107

6.7. Zn^{+2}aren rola MTLE egoeran NSCen aktibazioan eta React-NSC indukzioan 113

6.7.1. MTLE egoeran Zn^{+2} areagotu egin zen gune neurogenikoan 113

6.7.2. Zn^{+2}ak dosiaren araberako ugaritzea sustatu zuen NSPCetan..... 116

6.7.3. Zn^{+2} administrazio intrahipokanpalak MTLEak gune neurogenikoan eragiten dituen alterazioen antzekoak sortu zituen 117

6.7.4. Zn^{+2}ak NSCengan duen efektuan EGFR bitartekari izan zitekeen..... 121

6.7.5. Zn^{+2} kelazioak MTLE egoeran heriotza zelularra areagotu zuen GCLean 125

6.8. KA administrazioaren ostean HB-EGF DGan masiboki askatua izan zen 126

7. ONDORIOAK 134

8. BIBLIOGRAFIA 138

1. LABURDUREN LISTA

1. LABURDUREN LISTA

AHN	Hipokanpoko neurogenesi heldua
ANOVA	Bariantza analisia
ANP	Neurona sortzaile anplifikadoreak
AP	Aurretik atzera
ATP	Adenosina trifosfatoa
BBB	Muga hematoentzefalikoa
BDNF	Garunetik eratorritako faktore neurotrofikoa
BLBP	Garun lipido atxikitzaile proteina
BrdU	5-bromo-2'-deoxiuridina
BSA	Behi serum albumina
CA	Cornu ammonis
cD	D ziklina
CNS	Nerbio-sistema zentrala
CR	Cajal retzius
CTRL	Kontrol
CX	Kortex
D	Bizkarraldea
DCX	Doblekortina
DG	Hortzdun zirkunboluzioa
dHPF	Bizkarraldeko hipokanpoko formazioa
DMS	Horzdun migrazio-korrontea
DNA	Azido desoxirribonukleikoa
DNe	Horzdun neuroepitelioa
dNSC	Garapen zelula ama neurala
DV	Bizkarraldetik sabelaldera
EC	Kortex entorrinala
EGF	Hazkuntza faktore epidermala
EGFP	Proteina fluoreszente berde aberastua
EGFR	Hazkuntza faktore epidermal hartzailea
EM	Mikroskopia elektronikoa
FDJ	Fimbrio-hortzdun lotunea
FGF	Hazkuntza faktore fibroblastikoa
FGFR	Hazkuntza faktore fibroblastiko hartzailea

LABURDUREN LISTA

Hipokanpoko NSCak: Garapenetik Patologiara

FI	Fimbria
GC	Zelula granular
GCD	Zelula granular dispertsioa
GCL	Zelula granular geruza
GFP	Proteina fluoreszente berdea
GFAP	Proteina azidiko fibratzaile gliala
GW	Haurdunaldi astea
hAHN	Giza hipokanpoko neurogenesi heldua
HATA	Hipokanpo-amigdala trantsizio eremua
HB-EGF	Heparinari loturiko hazkuntza faktore epidermala
HCL	Azido klorhidrikoa
HF	Hipokanpoko arrakala
HH	Kirikiño
HNe	Hipokanpoko neuroepitelioa
HOPX	Homeodomeinu proteina kutxa
HP	Hipokanpoa
HS	Hipokanpoko esklerosia
HPF	Hipokanpoko formazioa
IHC	Inmunohistokimika
KA	Azido kainikoa
L	Laterala
LL	Albotik albora
LPA	Azido lisofosfatidikoa
LPA_1	Azido lisofosfatidikoaren 1 hartzailea
LV	Bentrikulu laterala
M	Mediala
mRNA	Azido ribonukleiko mezularia
MT	Metalotioneina
MTLE	Lobulu tenporal medialeko epilepsia
MF	Goroldio zuntza
ML	Geruza molekularra
NB	Neuroblasto
NSC	Zelula ama neurala
NSPC	Zelula ama neural eta sortzaileak
P*x*	Jaio ondorengo eguna
PBS	Fosfato tanpoi soluzio isotonikoa

PFA	Paraformaldehidoa
REACT-NSC	Zelula ama neural erreaktiboa
RGC	Zelula glial erradiala
ROI	Interes gunea
RT-qPCR	Uneko polimerasa kate erreakzio kuantitatiboa
SAL	Disoluzio isotonikoa
SC	Zelula ama
ScRNA-seq	Zelula bakarreko azido ribonukleiko-sekuentziazioa
SEM	Errore estandarraren batez bestekoa
SFFV-RV	Bare gunean eraturiko birus gamma-erretrobirusa
SHH	Sonic kirikiñoa
SGZ	Gune azpigranularra
SOX2	Y kutxa 2 sexu determinatzaile eremua
SPZ	Gune azpipiala
SVZ	Gune azpibentrikularra
TBR	T-kutxa garun proteina
TLE	Lobulu tenporaleko epilepsia
TKI	Tirosina kinasa inhibitzaileak
UCSF	University of California, San Francisco
UPV/EHU	Euskal Herriko Unibertsitatea
V	Sabelaldea
VEGF	Hazkuntza faktore endotelial baskularra
vHPF	Sabelaldeko hipokanpoko formazioa
VZ	Gune bentrikularra
WB	Western blot
WT	Mota basatia
Zn^{+2}	Zink

2. LABURPENA

2. LABURPENA

Ugaztun gehienen burmuina neurona berriak sortzeko gai da bizitza osoan zehar, jaio ondorengo aroa eta helduaroa barne, neurogenesi heldua bezala ezagutzen den prozesu baten bitartez. Gaur egun ongi jakina da prozesu neurogeniko heldu osoa zelula ama neural (ingelesetik neural stem cell; NSC) helduetan oinarritzen dela. Zelula hauetatik jaiotzen dira aurretiaz ezarritako zirkuituetan integratuko diren neurona berriak, behintzat burmuinaren bi zonaldetan; bentrikulu lateraletan aurkitzen den gune azpibentrikularrean (ingelesetik subventricular zone; SVZ) eta hipokanpoko formazioko (ingelesetik hippocampal formation; HPF) horzdun zirkunboluzioan (ingelesetik dentate gyrus; DG) aurkitzen den gune azpigranularrean (ingelesetik subgranular zone, SGZ). Azken honetan jazotzen dena hipokanpoko neurogenesi heldu (ingelesetik adult hippocampal neurogenesis, AHN) bezala ezagutzen da, tesi honetan jorratuko duguna.

Saguetan, SGZko ahalmen neurogenikoa denborarekin murriztu egiten dela deskribatu da. Adinarekin erlazionaturik dagoen AHNaren murrizketa hau NSCen agortzeagatik jazotzen dela proposatu da, neurona aurrekariak sortzeko ziklo zelularrean barneratzen diren (bestela esanda, aktibatuak izaten diren) NSCek prozesuaren ostean pairatzen duten diferentziazio astrozitiko edo neuronalaren ondorioz. Gainera, nahiz eta SGZ helduan NSCen auto-errepikapena posiblea dela deskribatu den ez da NSC populazioaren agorpen progresiboari aurre egiteko gai. Honela, norbanakoaren ahalmen neurogenikoa hasierako NSC kopuruak baldintzatzen du. Honen harira, NSCen jatorria ondo ezagutzen ez den arren, hauek zein AHNa jaio aurreko hipokanpoaren garapeneko hondakin bat direla da zabalduen dagoen ikuspegia.

Gizakietan, AHNaren benetako jazoera eta hedadura historikoki debate beroak sorrarazi dituen gaia izan da. Duela gutxi, debatea berpiztua izan zen umezarotik aurrera AHNaren gabezia argitaratu zuen ikerlan baten ondorioz. Hala ere, beste autore batzuek doblekortina (ingelesetik doublecortin, DCX) espresatzen duten zelulen presentzia adierazi izan dute DG helduko SGZan, AHNaren izatea ondorioztatuz. Gaurdaino, bi ikuspegi kontrajarriek eztabaidapean diraute.

Tesi honen lehengo zatian, NSC helduen garapeneko jatorriari helduko diogu. Honetarako, DGaren jaio ondorengo garapena ziklina D2rik (ingelesetik cyclin D2, cD2) gabeko sagu transgeniko lerro batean ikertu genuen, zeina NSCak behar bezala

ikusaraztea ahalbidetzen duen Nestin-proteina fluoreszente berde (ingelesetik green fluorescente protein, GFP) sagu transgeniko batekin gurutzatua izan zen. Jaio ondorengo burmuineko eremu ezberdinetan ugaritzen zeuden zelulak markatu eta haien leinuaren jarraipena egiteko, eremu espezifikoetara zuzenduriko infekzio retrobiralak erabili genituen. Emaitzek adierazten dutenez, NSC helduen populazioa tokian sortzen da DGan jaio ondorengo lehen 2-7 egunen artean eta cD2ren menpeko prozesu baten bitartez. Aurkikuntza honek NSC helduek garapeneko sortzaileengandik ezberdina den populazio bat osatzen dutela iradokitzen du, jaio ondoren sortuak izanda era independente batean. Hala, jaio ondorengo eta helduaroan zehar ematen den AHNa ez da jaio aurreko garapenaren hondakin soil bat. Emaitza hauek babestuz, garapeneko NSCek aurkezten ez duten biomarkatzaile baten espresio diferentziala aurkitu genuen. Azido lisofosfatidiko 1 hartzailea (ingelesetik lysophosphatidic acid receptor 1, LPA_1)-areagoturiko proteina fluoreszente berdea (ingelesetik enhanced green fluorescent protein, EGFP) sagu transgenikoa erabiliz, LPA_1 NSCetan jaio ondorengo 10-14 egunetatik (ingelesetik postnatal, P10-P14) aurrera espresatua izaten hasten dela ikusi genuen, hortik aurrera bere espresioak hipokanpoko NSCetan dirauelarik.

Esan bezala, AHNaren existentzia gizakietan azkenaldian eztabaida beroa sortu duen gaia izan da guztiz kontrajarriak diren emaitzak argitaratu direlarik. Arazoari garapen ikuspegi batetik helduz, giza eta sagu garapen prozesuek dinamika tenporal ezberdinak jarraitu litzaketela deskribatu genuen, nahiz eta formazio patroi antzekoak konpartitu. Nagusiki, jaio ondorengoa den sagu DGaren garapenaren aurrean, gizakietan prozesu hau ia guztiz amaiturik dago haurdunaldi erdirako. Nolanahi ere, zelula glial erradial (ingelesetik erradial glial cell, RGC) populazioak oraindik presente daude jaio eta gutxira. Hala, giza DGan jaio ondorengo garai goiztiarrean NSC populazio baten existentzia (duen hedadura tenporala kontuan hartu barik) garrantzia handikoa izan litzake patologia egoeretan.

Hipokanpoko gune neurogenikoaren galerak, eteteak edo alterazioak zonalde honekin erlazionaturiko ariketa kognitibo guztien gaitza dakar, hala nola ikaskuntza, memoria, patroi separazioa, antsietatea, etab. Izan ere, AHNaren alterazio patologikoa erlazionatua izan da gaitz neurodegeneratibo ezberdinekin, adibidez epilepsia, Parkinson, Alzheimer eta Huntington gaixotasunak eta dementzia, patologia guzti hauetan gutxienez sintomen parte bat potentzialki eraginda edo bultzatuak izan litezkeelarik AHN alteratu edo murriztu batengatik. Izan ere, nire laborategi hartzaileak duela gutxi erakutsi du konbultsioek sustaturiko hiperaktibitate neuronalak NSCak NSC

erreaktibo (ingelesetik reactive NSC, React-NSC) bihurtzera bultzatzen dituela, euren propietate morfologiko eta mitotikoak errotik aldatuz eta azkenera astrozito erreaktiboak sortuz, neurogenesiaren kaltean.

Tesiaren bigarren partean, lobulu tenporal medialaren epilepsia (ingelesetik mesial temporal lobe epilepsy, MTLE) aztertu genuen azido kainiko (ingelesetik kainic acid, KA) injekzio bakarra HPFan gauzatuz. Ondoren, hazkuntza faktore epidermal hartzailearen (ingelesetik epidermal growth factor receptor, EGFR) seinalizazio ibilbideak konbultsio ostean gune neurogenikoan duen erantzun patologikoaren hasieran duen rola aztertu genuen. Konbultsioak jazo eta gutxira, EGFR NSCetan areagotu egiten dela eta EGFRren inhibitzaile itzulgarria den Gefitinib (gliomaren tratamendurako erabiltzen dena) MTLE indukzioaren ondoren erabiliz, ugaritze jarduera masiboa eta React-NSC indukzioa murrizturik zeudela erakutsi genuen, prozesu honetan EGFR ibilbideak rol nagusi bat jokatzen duela iradokiz. Gainera, garrantzitsua da neurogenesia, DCX espresatzen zuten neurona heldugabeen presentzia bezala ulertuz, babestu egiten zela Gefitinib jaso zuten MTLE saguetan. Are gehiago, konbultsio ostean gertatzen den zink (Zn^{+2}) askapenaren areagotzeak React-NSC indukzioan parte hartzen duela ere demostratu dugu, bai EGFRren estimulazio zuzenaren bitartez zein zelula mintzera loturik dagoen heparinari loturiko-hazkuntza faktore epidermalaren (ingelesetik heparin binding-epidermal growth factor, HB-EGF) mozketa bultzatuz, azken hau EGFRren estekatzaile natural bat izanik, KA administrazioaren osteko lehen hiru egunetan masiboki askatua izaten dena.

3. SARRERA

3. SARRERA

3.1. Hipokanpoko formazioa (Ingelesetik hippocampal formation, HPF): Burmuineko itsas zaldia

1587a zen Giulio Cesare Arantius anatomistak itsas zaldiaren antza handia hartzen zuen estruktura bat aurkitu zuenean giza burmuinaren lobulu tenporal medialaren barnealde sakonean. Antzekotasuna onartuz, itsas izaki honen greziar hitza hartu zuen estruktura izendatzeko: "*Hippocampus*" (HP) (Arantius, 1587). Ordutik, estruktura arkikortikal honek hainbat ikertzaileren interesa piztu du, zeinek bere ezaugarri morfologiko eta funtzionalak argitzeko lan egin duten. Gaur egun, HP terminoak "*cornu ammonis"* (CA) edo "*ammon's horn*" izenak ere hartu izan dituen estruktura bat adierazten du. Izen hauek estrukturak ahari adar batekiko duen antzaren eraginez eman zitzaizkion eta baita Amun Knepth jainkosaren ondotik, honen sinboloa ahari bat izanik (de Garengeot, 1742). Era xelebrean, CA izendapena mantendu egin zen harrezkero HParen azpieremuak definitzeko (CA1, CA2, CA3 and CA4) **(S1 A Figura)**.

HPa burmuineko beste eremu batzuekin konektaturik dago, guztiek batera HPFa osatzen dutelarik, Golgik lehenbizikoz errepresentatu (Golgi, 1886) eta Santiago Ramón y Cajalek eta bere ikasle Raphael Lorente de Nók osotasunean deskribatu zutena (Lorente de Nó, 1934; Ramón y Cajal, 1893, 1911). Haien ikerlanetan oinarriturik, egun badakigu HPFa HPak baino estruktura gehiagok osatzen dutela, hala nola subikuluma, presubikuluma, parasubikuluma, kortex entorrinala (ingelesetik entorhinal cortex, EC), albeoloa, hipokanpoko arrakala (ingelesetik hippocampal fissure, HF), buztan hipokanpala, HP-amigdala trantsizio eremua (ingelesetik HP-amygdala transition area, HATA) eta baita ere horzdun zirkunboluzioa (ingelesetik dentate gyrus, DG) (Iglesias et al., 2015) **(S1 A Figure)**. Estruktura hauek, nahiz eta tamainan ezberdinak, ugaztun guztietan daude presente sagutik gizakira **(S1 B Figura)**.

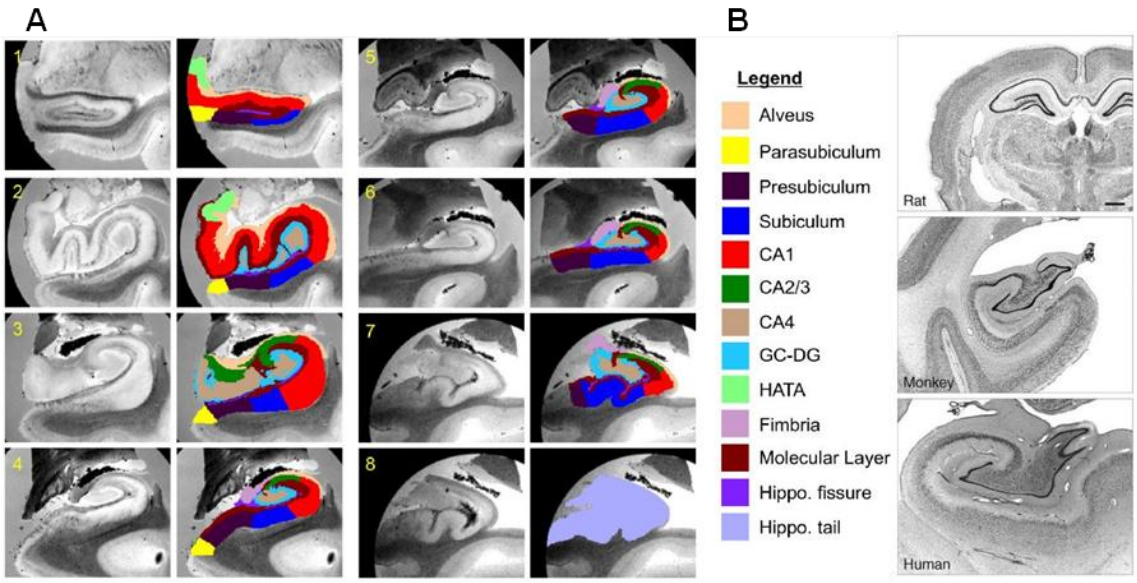

S1 Figura. A) HPFko azpieremu ezberdinak. **B)** Arratoiaren, tximinoaren eta gizakiaren HPFa (Iglesias et al., 2015 eta Savage et al., 2013 artikuluetatik eraldatua).

3.2. Neurona sorrera burmuin helduan

90. hamarkadan, 5-bromo-2'-deoxiuridina (BrdU) arrakasta osoz erabili zen saguetan neurogenesi helduaren existentzia demostratzeko bai bentrikulu lateralaren (ingelesetik lateral ventricle, LV) gune azpibentrikularrean (ingelesetik subventricular zone, SVZ) zein DGko gune azpigranularrean (ingelesetik subgranular zone, SGZ) (Cameron et al., 1993; Kuhn et al., 1996; Seki and Arai, 1993) **(S2 Figura)**. Are garrantzitsuago, hamarkadaren amaiera aldera Elizabeth Gould eta bere kideek hainbat ikerlan argitaratu zituzten BrdU erabiliz eta neurogenesi hipokanpal helduaren (ingelesetik adult hippocampal neurogenesis, AHN) existentzia erakutsiz zuhaitz basakuetan, mundu zaharreko tximinoetan (Gould et al., 1997, 1999a, 1999b) eta makakoen SVZan (Gould et al., 1999c). Aurkikuntza hauek beste autore batzuek babestu zituzten hurrengo urteetan zehar (Kornack and Rakic, 1999, 2001; Pencea et al., 2001), mundu zaharreko tximinoetan AHNa saguetan baino hamar aldiz baxuagoa zela adierazi zuten arren (Kornack and Rakic, 1999). Hala, hurrengo urteetan BrdUaren erabilera eta interpretazio egokiak sorrarazitako iritzia ezegonkorra izanagatik (Nowakowski, 2000), Joseph Altmanen lehenengo aurkikuntzetatik 50 urtera (Altman and Das, 1965) neurogenesi helduaren kontzeptua guztiz onartua eta biziki ikertua izan zen.

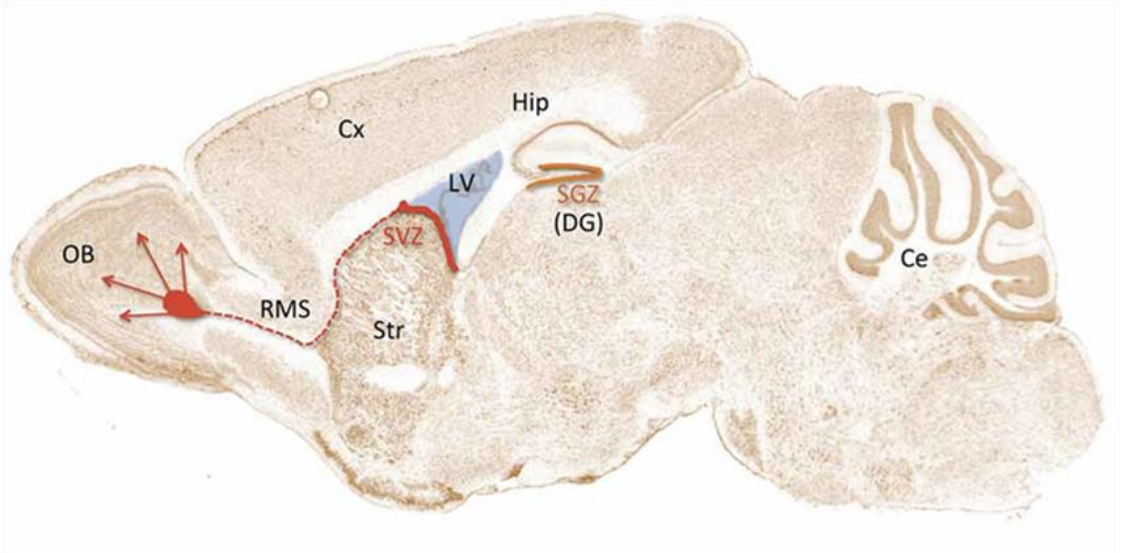

S2 Figura. Gune neurogeniko helduak LVko SVZan eta hipokanpoko DGko SGZan.

3.3. Urjauzi neurogeniko hipokanpala

DG helduan, proteina azidiko fibratzaile gliala (ingelesetik glial fibrillary acid protein, GFAP) espresatzen zuten zelula glial erradialak (ingelesetik erradial glial cells, RGCs) zatitzeko kapazak zirela aurkitu zen (Kosaka and Hama, 1986; Rickmann et al., 1987), nahiz eta ugaritze aktibitate hau gliogenesiarekin erlazionatu zen hasiera batean (Cameron et al., 1993; Kaplan and Bell, 1984). Nolanahi ere, handik urte batzuetara Arturo Álvarez-Buylla eta bere kideek lehenengoz deskribatu zuten, BrdUaren erabileraren bitartez zelula mitotikoen jarraipena eginez, GFAP positiboak ziren astrozito erradialak zelula ama (ingelesetik stem cell, SC) bezala aritzen zirela eta neurona jaioberriak ematen zituztela DG helduko SGZan (Seri et al., 2001).

Gutxira, bitarteko zelula ama neuroektodermalen markatzaile (ingelesetik neuroectodermal stem cell intermediate marker, Nestin) SC neuroepitelialen markatzailearen espresioan oinarriturik zelula ama neuralak (ingelesetik neural stem cells, NSCs) ikusaraztea ahalbidetzen zuten sagu transgeniko anduiak garatu ziren (Lendahl et al., 1990). Sagu transgeniko berri hauen bitartez SGZko astrozito erradial haiek hobeto karakterizatu ahal izan ziren. Honela, urjauzi neurogeniko helduaren lehenengo urratsa diren astrozito erradialak mota-1 zelulak deitarazi ziren (Filippov et al., 2003; Kronenberg et al., 2003). Morfologia karakteristiko bat adierazten zuten zelula bezala identifikatuak izan ziren, soma SGZan kokaturik eta prozesu bat geruza molekularrerantza (ingelesetik molecular layer, ML) luzaturik zituztelarik, azken hau zelula granular geruzaren (ingelesetik granule cell layer, GCL) kanpoaldera iritsi bezain pronto arbolaztatzen zelarik, brokoliaren itxurako koro bat osatuz (Filippov et al., 2003;

Mignone et al., 2004) **(S3 A Figura)**. GFAPaz eta Nestinaz gain, beste markatzaile batzuen espresioa erakusten dutela deskribatu da, hala nola Vimentin, garun lipido atxikitzaile proteina (ingelesetik brain lipid-binding protein, BLBP) eta Y kutxa 2 sexu determinatzaile eremua (ingelesetik sex determining region Y box 2, Sox2), astrozito helduen markatzaile den S100β-ren gabezia bezala (Encinas and Enikolopov, 2008; Filippov et al., 2003; Gould et al., 1992; Yamaguchi et al., 2000). Zelula hauek sortzaile neural iraunkor bezala deskribatu izan dira baita ere, populazio mailan orokorrean iraunkorrak direnetik, %2-5a bakarrik sartuta mitosian edozein une aleatoriotan (Encinas et al., 2011). Sortzaile terminoa nahiago izan zen baita momentu hartan neuronak bakarrik ematen zituztela uste zelako eta ez beste edozein zelula mota, beraz SC definizioarekin bat etorri ezinik. Gaur egun, era orokorrean onartuak daude *bona fide* NSC bezala (eta hala izendatuko ditugu hemendik aurrera) multipotentzialak direnetik, bere burua berritzeko gai izanda baita ere.

Zientzia komunitateak duela askotik heldu dio NSCek zatitzeko erabiltzen dituzten mekanismo eta dinamikak ikertzeari, SGZan jazotzen diren zelula zatiketa patroiak argitzeko asmoz. Leinuaren jarraipen induziblea BrdU markapenarekin konbinatuz eta beranduago *in vivo* bi-fotoi irudikapenarekin, erreportatu da behin aktibatuta NSCak batez-beste hiru aldiz ugaritzen direla (gehienetan era asimetrikoan) (Encinas et al., 2011; Pilz et al., 2018), beren buruaren kopia bat eta zelula alaba borobildu bat sortuz, azken honek GFAP eta Vimentin espresiorik ez dutelarik (Encinas et al., 2006; Kempermann et al., 2004; Kronenberg et al., 2003; Seki et al., 2007). Sortzaile hauen patua neurogenikoa den bitartean, aktibaturiko NSCak astrozitoetan diferentziatzen amaitzen dute, horrela euren kapazitate neurogenikoa galduz (Encinas et al., 2011) **(S3 B Figura)**.

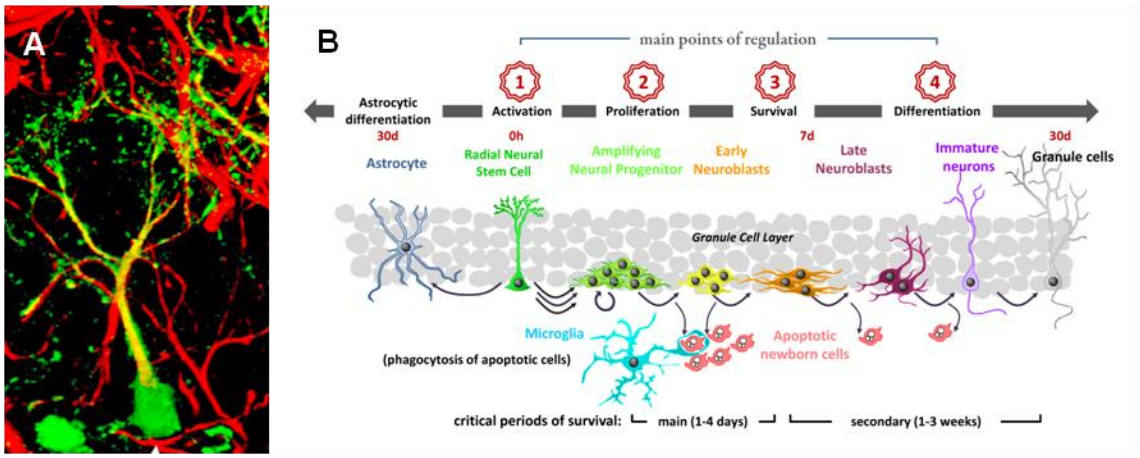

← **Aurreko orrialdean. S3 Figura. A)** Nestin (berdez) eta GFAP (gorriz) espresatzen duen NSC bat, soma SGZan kokaturik eta prozesua MLrantza luzaturik duelarik, bertan brokoli antzeko koro bat osatuz. **B)** Urjauzi neurogeniko hipokanpala. NSCek, morfologia erradialarekin, gehienbat iraunkorrak dira, baina behin aktibatzen direlarik hainbat aldiz ugaritzen dira, era asimetrikoan beren buruaren kopia bat eta neurona sortzaile anplifikadore (ingelesetik amplifying neural progenitor, ANP) bat sortuz, zeina apoptosi prozesu baten bitartez hil edo neurona granular heldu batean diferentziatzen den (Encinas et al., 2011 eta Encinas and Sierra 2012 artikuluetatik eraldatua).

Kontuan harturik NSC aktiboen proportzioa aldakaitz mantentzen dela denboran zehar, NSCen agorpen jarraitu eta esponentziala da adinarekin datorren AHNaren murriztea eragiten duen faktore printzipala (Encinas and Sierra, 2012; Encinas et al., 2011) **(S4 Figura)**. Nahiz eta NSCak potentzialki gai diren beren buruaren kopiak emateko, ahalmen hau ez da nahikoa adinarekin gertatzen den NSCen galera ekiditeko populazio mailan (Bonaguidi et al., 2011; Encinas et al., 2011; Pilz et al., 2018). Denak batera, dinamika hauek NSCen hasierako kopuruaren garrantzia iradokitzen dute, honek norbanako batek bizitza osoa zehar izango duen kapazitate neurogenikoa determinatzen duenetik. Honela, berebizikoa da zelai honetan azken hamarkadetan egon den galdera baten gainean argia igortzea. Noiz eta nola sortzen dira hipokanpoko NSC helduak?

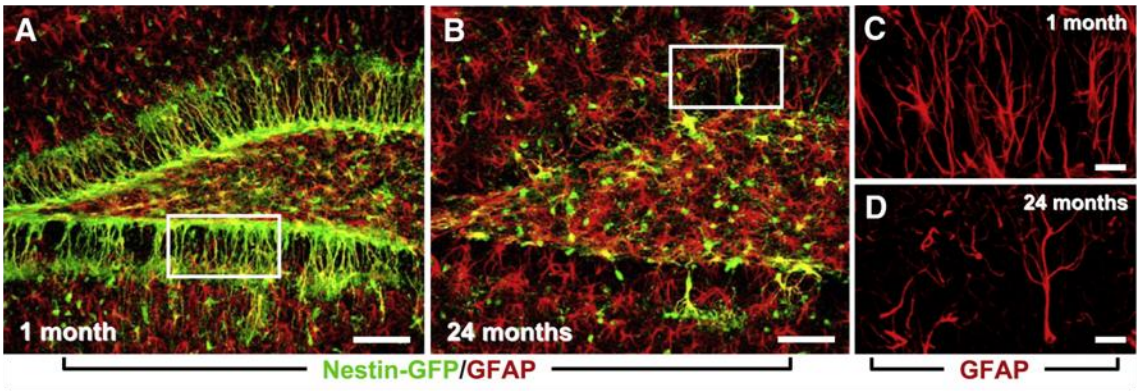

S4 Figura. NSC populazioaren agorpena adinarekin. **A)** DG gazte bat NSCz beterik SGZ osoan zehar. **B)** DG edadetu bat non bakarrik NSC bakan batzuk geratzen diren. **C-D)** Sagu gazteen (C) eta edadetuen (D) GCLaren hurbileko konfokal irudiak (Encinas et al., 2011 artikulutik hartua).

3.4. NSC helduen jatorria

3.4.1. NSC helduen jatorria jaio aurretik

DGak SVZarenekotik ezberdintasun azpimarragarriak dituen gune neurogeniko bat du. Hala, bentrikulutik urrun aurkitzen da. Izan ere, DGko SGZa bere jaio aurretiko hozi-gunetik guztiz banandua mantentzen da (Altman and Bayer, 1990). DGaren garapena deskribatua izaten hasi zenean, argitaratua izan zen hipokanpoko NSC

helduak garapenean zehar horzdun neuroepitelioan (ingelesetik dentate neuroepithelium, DNe) kokatuak zeuden aurrekariengandik sortuak zirela, bai translokazio zuzenaren bitartez (Eckenhoff and Rakic, 1984) edo DGa osatzeko sortzen diren migrazio prozesu ezberdinen bitartez, hala nola horzdun migrazio korrontea (ingelesetik dentate migrazio stream, DMS)(Altman and Bayer, 1990), jaio ondoren DGko SGZan kokaturik amaitzen duten arte (Nicola et al., 2015; Sugiyama et al., 2013). Hala, NSC helduak eta AHNa jaio aurretiko HPFaren garapenaren hondakin bat direla orokorki onartu den ikuspegia izan da, Gage eta kolaboratzaileek adierazi bezala (Gonçalves et al., 2016).

Ikuspegi hau babestuz, markatzaile ezberdinak eta sagu transgenikoak erabiliz hainbat ikerlanek ustezko garapeneko NSCak (ingelesetik developmental NSCs, dNSCs) DNetik SGZra migratzen identifikatu dituzte: Nestin, eomesodermin bitarteko aurrekarien markatzaileak, T-kutxa garun protein 2 bezala ezagutua (ingelesetik T-box brain protein 2, Tbr2) (Hodge et al., 2008, 2012) eta neurogenina-2 (ingelesetik neurogenin-2, Ngn2) DG-aren jaio aurretiko garapenean sortzen diren hozi-matrizeetan aurrekari neuronalak markatzen dituztela deskribatu izan da (Galichet et al., 2008; Hodge et al., 2013; Li et al., 2009). Ildo honetatik, Samuel Pleasure eta kideek iradoki egin zuten sortzaile hauetako batzuk DNetik migratzen dutela, euren diferentziatu gabeko egoera mantenduz seinale neurogenikoen inhibizioari esker, SGZra jaio ondorengo aroan iristen diren arte, bertan mantenduz helduaroan zehar (Pleasure et al., 2000). Are gehiago, deskribatu egin zuten dNSCek HFaren eta fimbrio-horzdun lotunearen (ingelesetik fimbrio-dentate junction, FDJ) arteko gune neurogeniko iragankor batean egoten direla, gune azpipialean (ingelesetik subpial zone, SPZ), gutxienez aste batez SGZan ezarri baino lehen (Li et al., 2009) **(Figure S5)**.

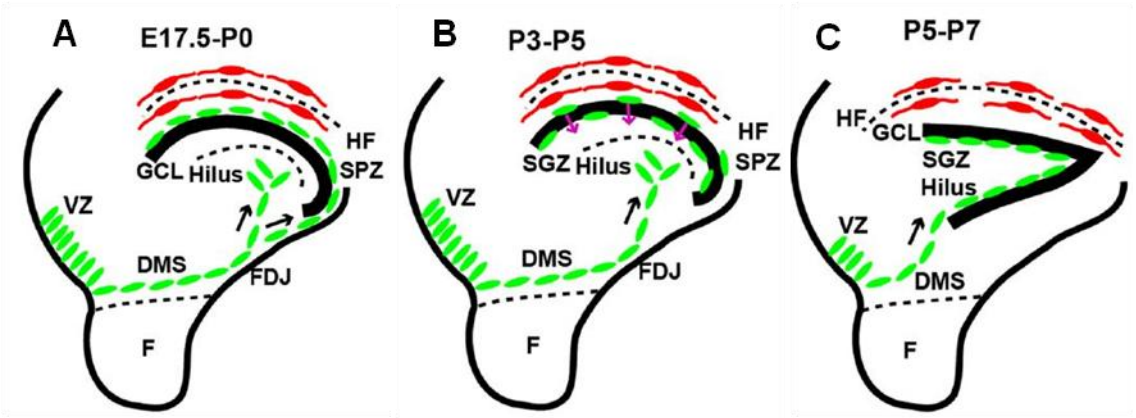

S5 Figura. A-C) HFean zehar SPZan kokaturiko Cajal-Retzius (CR) zelulek gidaturik, NSC helduen aurrekariek DNetik DGra migratzen dute SGZan zehar kokatu egiten diren arte, NSC helduen populazioa eratuz (Hodge et al., 2013 artikulutik eraldatua).

Homeodomeinu protein kutxa (ingelesetik homeodomain protein box, Hopx) DGko NSC helduetan espresatua da eta SVZko NSCetatik desberdintzen ditu (Shin et al., 2015). Baita, Hopx-ek AHNaren gainean rol bat jokatzen duela iradoki egin da Notch seinalizazioarekin jazotzen den interakzioaren bitartez (Li et al., 2015). Duela gutxi, Daniel Berg eta kolaboratzaileek Hopx positiboak diren dNSCek DNetik SGZra migratzen dutela deskribatu dute, DGaren formazioari ekarpena eginez jaio aurretiko eta jaio ondorengo etapetan zehar, gerora iraunkor bihurtu eta NSC helduen populazioa eratzeko. Are gehiago, aldarrikatzen dute Hopx positibo diren sortzaileek zelula granularrak (ingelesetik granule cell, GC) bakarrik sortzen dituztela, leinu neuronal honenganako duten joera espezifikoa azpimarratuz. Emaitza hauetan oinarrituz, AHNa jaio aurretiko eta ondorengo garapenaren bizitza osoko hedapena besterik ez dela babesten dute, “jarraipen” modelo bat defendatuz non Hopx positibo diren sortzaileek GCak sortzen dituzten bizitza osoan zehar, garapenetik helduarora (Berg et al., 2019).

NSC helduen jatorri espazialari erreparatuz, sortzaileen korronte migratzaile tenporal-septal berri bat adierazi zuen Samuel Pleasure eta kideen lana erronka bezala iritsi zen ikerkuntza zelaira. Autore hauen arabera NSC helduen aurrekariek sabelaldeko DGtik hurbil dagoen gune bentrikularretik (ingelesetik ventricular zone, VZ) bizkarraldeko DGra bidean migratzen dute jaio aurretiko eta jaio ondoko etapan, SGZan ezartzen direlarik jaio ondorengo lehen asteetan. Sonic kirikiñoaren (ingelesetik sonic hedgehog, Shh) gabeziak edo bere erregulatzaileetan okerren presentziak ekartzen duen NSC helduen populazioaren formazio okerrak adierazten duen bezala, aurrekariek seinalizazio ibilbide honen menpeko eran migratzen dute (Li et al., 2013). Shh seinalizazio ibilbidea kirikiño (ingelesetik hedgehog, Hh) familiako kide ezagun bat da eta neokortexaren hazkuntzan zein garapenean RGC eta sortzaileen hedapenean inplikatua dagoela demostratu izan da. Edonola ere, Samuel Pleasure eta bere kideen lanak seinalizazio ibilbide hau hipokanpoaren bazterrera ekarri zuen. Izan ere, ikerkuntza zelaian zegoen ikuspegi orokorra kontrajarri zuten DNeak GCLaren kanpoko geruzari, lehenbizi sortzen denari, bakarrik egiten diola ekarpena iradokiz. Ostera, barnealdeko GCLa eta NSC helduen populazioa sabelaldeko DGtik migratzen duten dNSCek sortuko lukete, Shh-ren menpeko era batean. Hala, deskribaturiko bi migrazio korronteak jaio ondoan FDJan konektatzen direla azaltzen duen modelo bat

proposatu zuten, NSC helduen jatorri espazial bat baino gehiagoren aukerari atea zabalduz (Li et al., 2013).

3.4.2. dNSC vs NSC helduak

DG helduko NSCen jatorriaren inguruan argia igortzeak ikerkuntza zelaian gertatzen den galdera nagusietako bati erantzuna ematera hurbiltzea ahalbidetuko du: AHNa DGaren sorrera dakarren garapeneko neurogenesiaren hondakin bat da edo ostera aparteko fenomeno biologiko bezala eraikia den prozesu independente bat da? Galdera honi heltzea AHNaren funtzioak ulertzeko nahitaezkoa izan daiteke, hala nola bere rola hainbat egoera normal zein patologikotan zein den argitzeko.

Bizitza osoan zehar bentrikulutik kanpo neurona berriak emateko kapaza den estruktura berri baten jaio ondorengo agerpenak autore batzuk garapeneko neurogenesiaren eta neurogenesi helduaren arteko ezberdintasunak azpimarratzera eraman ditu (Nicola et al., 2015). Nolanahi ere, SGZa DGa osatzeko prozesuan jazotzen diren prozesu eta estruktura iragankor desberdinen helmuga izanik, gaur egungo ikuspegi orokorra AHNa DGaren formazioan ematen den azken urratsaren hedapena dela da. Beste hitz batzuetan esanda, garapeneko neurogenesiaren programaren jarraipen bat (Berg et al., 2019; Matsue et al., 2018; Nicola et al., 2015; Seki et al., 2014).

Duela gutxi argitaraturiko lan batek, zelula bakarreko azido ribonukleiko-sekuentziazio (ingelesetik single cell RNA-sequencing, scRNA-seq) teknologia erabiliz, prozesu neurogenikoak bai garapenean zein helduaroan ibilbide molekular antzekoak jarraitzen dituela deskribatu zuen. Hala, ANPak, neuroblastoak (ingelesetik neuroblast, NB) eta neurona heldugabeak molekularki oso antzekoak dira jaio aurretik, jaio ondoan eta helduaroan (Hochgerner et al., 2018). Emaitza hauek AHNa garapeneko hondakin bat dela defendatzeko erabiliak izan dira (Berg et al., 2019). Hala ere, Sten Linnarson eta kideek jaio aurreko etapetatik jaio ondorengo/helduaro adinera bitartean NSCek pairatzen dituzten propietate molekularren aldaketak identifikatu zituzten baita ere. Autoreen arabera, dNSCek aldaketa molekularrak jasaten dituzte (iraunkortasun handiagoa eta markatzaile espresioan aldaketak) SGZan kokatzen diren momentuan, aurreko dNSCengandik argi eta garbi desberdintzen den zelula populazio bat osatuz (Hochgerner et al., 2018). Ildo honetan, Jennifer Gilley eta bere taldeak jaio ondorengo aro goiztiarretik helduarora bitartean aldaketa zelular autonomoak bistaratu zituen saguetan, bi adinetan transkripzio perfil ezberdinak antzemanez (Gilley et al., 2011).

Dena batera hartuta, emaitza hauek garapeneko neurogenesia eta neurogenesi heldua prozesu ezberdinak direla pentsatzera eraman gintuen, behintzat NSCeei dagokienez.

3.5. Giza neurogenesi heldua: Izan ala ez izan

Saguetan bezala, giza DGa hipokanpoan osatzen den azken estruktura da eta GCak GCLera gehituak izaten dira 30. haurdunaldi astetik (ingelesetik gestational week, GW30) aurrera eta gutxienez jaio ondorengo aro goiztiarrera bitartean (Arnold and Trojanowski, 1996; Humphrey, 1967; Seress et al., 2001), garai honetan Nestin espresatzen duten zelulek hilusa eta GCLa populatzen dutelarik oraindik ere (Cipriani et al., 2018; Sorrells et al., 2018). Hala, NB migrazioaren azken olatuak GCL bidean jaio ondorengo lehenengo zortzi hilabeteetan gertatzen dira (Seress, 1988; Seress et al., 1992). Nolanahi ere, GCL haurdunaldi erdirako ia guztiz osatua geratzen dela kontsideratzen da, ugaritzea haurdunaldiaren bigarren erdian eta jaio ondoren oso murriztua agertzen delarik (Arnold and Trojanowski, 1996; Humphrey, 1967; Seress et al., 2001; Sorrells et al., 2018). Jaio ondorengoko gune neurogeniko baten existentziak zientzialarien kuriositatea piztu izan du beti eta autore asko saiatu dira jaio ondorengo giza AHNaren (ingelesetik human AHN, hAHN) hedapena argitzen, bere potentzial terapeutikoaren inplikazioak erakarrita.

Duela gutxi, hAHNa itxuraz errotuta eta ia zalantza guztietatik at zirudienean, duela gutxi argitaraturiko ikerlan berriek halako prozesu baten gabezia aldarrikatu dute, komunitate zientifikoa nahasiz eta galdera berriak plazaratuz. Hauetatik lehenengoa inmunohistokimika (ingelesetik immunohistochemistry, IHC) emaitzetan oinarriturik etorri zen, 3 urtetatik aurrera giza DGan ugaritzen den zelula mota bakarra mikroglia dela adieraziz (Dennis et al., 2017). Emaitza hauekin eztabaida eta sinesgaiztasuna sortu zen neurogenesi helduaren plazan (Dennis et al., 2017; Marucci, 2017), nahiz eta komunitatea ez zen benetan aztoratu Arturo Álvarez-Buylla eta bere kideen lana agertu zen arte. Autore hauek jaio aurreko, jaio ondoko eta helduaroko laginetan argi eta mikroskopia elektroniko (ingelesetik electron microscopy, EM) irudiak aztertuz, DCX zelula positiboetan murrizte bortitza deskribatu zuten jaio aurretiko arotik jaio osteko lehenengo urteetara, DCX zelula positiboen kopuru arbuiagarriak aurkituz zazpi eta 13 urteetako laginetan (Sorrells et al., 2018) **(S6 A Figura)**. Halaber, Sorrells eta bere taldeak bizitzaren bederatzigarren hamarkadaz geroztik hAHNaren gabezia aldarrikatu ondoren eta gutxira, artikulu berri batek bereganatu zuen komunitatearen aditasuna. Euren lana DCX eta kalretinina (neurona heldugabeen beste markatzaile bat) espresioan oinarritu zuten eta neurona jaioberrien presentzia aldarrikatu zuten

metodologikoki oso zaindua zen lan batekin, zeinetan finkapen protokoloak oso zorrozki kontrolatuak izan ziren (Moreno-Jiménez et al., 2019) **(S6 B Figura)**.

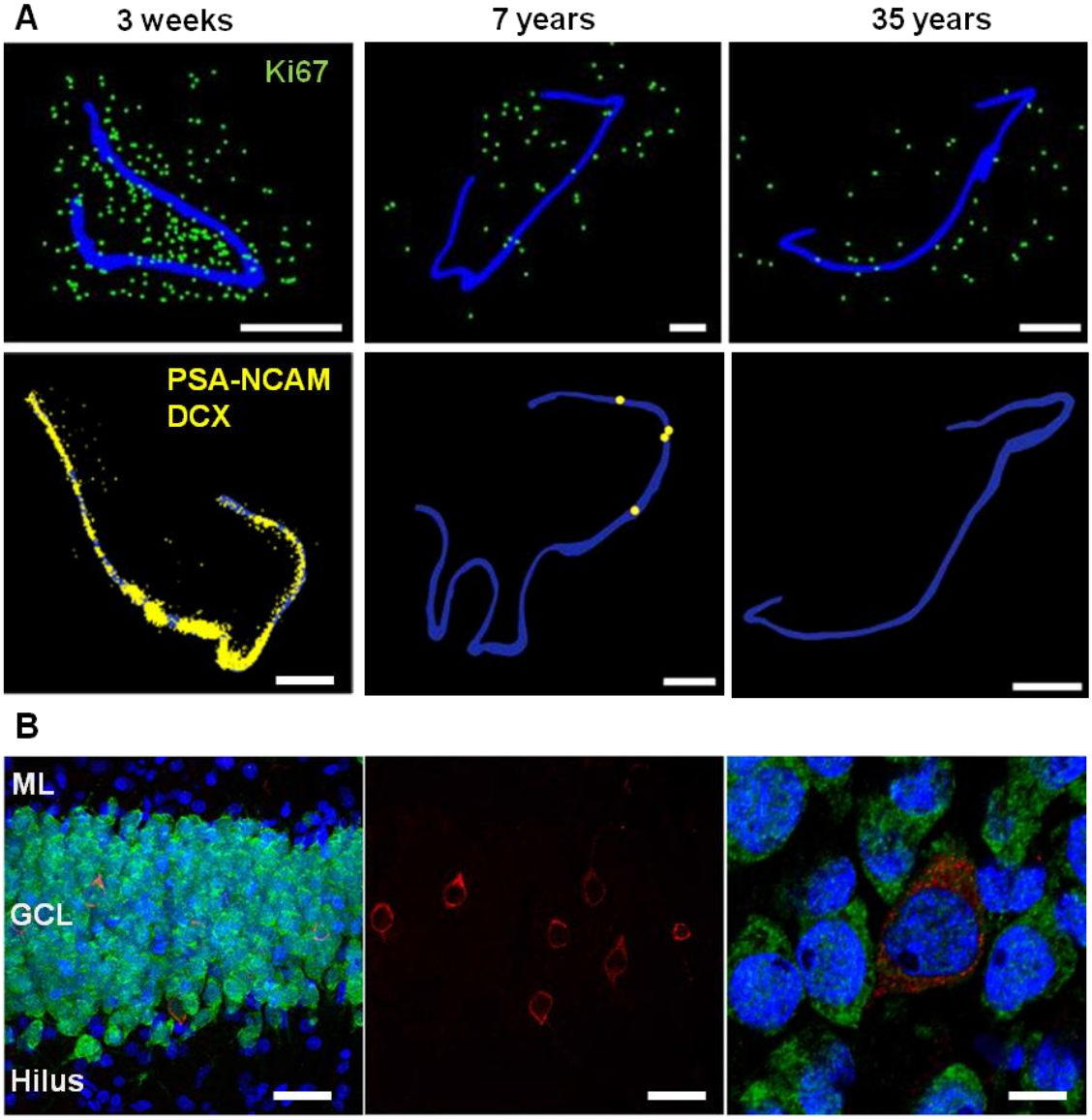

S6 Figura. A) Ugaritze fasean aurkitzen diren zelulen eta neurona heldugabeen murriztea haurtzarotik helduarora bitartean, gizakietan neurogenesi helduaren gabezia iradokiz, Sorrells et al.-ek (2018) adierazi bezala. **B)** DCX espresatzen duten zelulen presentzia (gorriz) gizaki helduen GCLean (47-83 urte), DAPI (urdinez) eta NeuN (berdez) tindaketekin gainjarriz. Emaitza hauek GCLean neurona heldugabeen presentzia iradokitzen dute, Moreno-Jiménez et al-ek (2019) adierazi bezala (Sorrells et al., 2018 eta Moreno-Jiménez et al., 2019 artikuluetatik eraldatua). *GCL: Zelula granular geruza. ML: Geruza molekularra.*

Eztabaida guzti honen arren, jaio ondorengo etapa goiztiarrean neurogenesia giza DGan oraindik jazotzen denaren gainean adostasuna dago komunitatean (Cipriani et al., 2018; Knoth et al., 2010; Sorrells et al., 2018). Gainera, helduaroan ez bezala,

bizitzaren lehenengo urteetan jasandako estres sozialak edo kimikoak garunaren funtzioan efektu iraunkorrak sorrarazten dituztela erakutsi da, potentzialki hipokanpoko disfuntzioa ere barne (Cooper et al., 2015; Dorn et al., 2014; Rees and Inder, 2005). Honek jaioberri etapan leiho iragankor baten existentzia iradokitzen du zeinetan edozein eragin patologikok efektu itzulezinak sortu litzakeen oraindik osatu barik dagoen HPF batean. Izan ere, helduaroko egoera epileptikoetan ikusiriko emaitzak kontrajarriz (Fahrner et al., 2007; Seki et al., 2019), hasiera goiztiarreko lobulu tenporaleko epilepsia (ingelesetik temporal lobe epilepsy, TLE) zuten paziente pediatrikoetan areagotutako neurogenesia adierazten zuten frogak aurkeztu ziren (Blümcke et al., 2001), ziurrenik jaio aurreko garapen fetaletik geratzen diren Nestin espresatzen duten zelula astroglialetatik eratorria (Cipriani et al., 2018; Kruglyakova et al., 2005; Sorrells et al., 2018).

TLEn, hAHNaren areagotze eza demostratu den arren (Fahrner et al., 2007; Seki et al., 2019), neuronen eta astroglia populazioen erreorganizazioa erakutsi da (Crespel et al., 2005; Liu et al., 2018; Verwer et al., 2015). Izan ere, sagu modeloetan adierazi egin da NSCek era aktiboan ekarpena egiten diotela konbultsio osteko gliosiari (Muro-García et al., 2019; Sierra et al., 2015). Guzti honek giza DGaren formazioaren gainean argia igortzeak duen garrantzia adierazten du, neurona eta glia populazio ezberdinak hasieratik zelan antolatzen diren osoki ezagutuz, gune neurogeniko helduak duen ahalmen neurogenikoaz aparte. Era berean, hipokanpoaren funtzionalitatearekin estu loturik dauden mekanismo patologikoak ulertzeak, hala nola TLEa, eta DGko zelula populazio ezberdinetan eragiten duten efektua ikertzeak estruktura honi lotutako ezaugarriak deskubritzen lagunduko du.

3.6. Lobulu tenporal medialeko epilepsia (ingelesetik medial temporal lobe epilepsy, MTLE) eta NSCak

Konbultsioak probokatu eta jarduera neuronala areagotu egin den sagu modeloetan hipokanpoko NSC helduak aktibatuak izaten direla erakutsi egin da (Gray and Sundstrom, 1998; Hüttmann et al., 2003; Lugert et al., 2010; Segi-Nishida et al., 2008; Sierra et al., 2015). Izan ere, proposatua izan da jarduera neuronala eta NSCen aktibazioa erlazionaturik daudela, lehenak bigarrena eragiten duelarik (Deisseroth et al., 2004). Hala ere, argitaratua izan da konbultsio epileptiko kronikoek AHNa gaitzesten dutela estimulatu beharrean (Hattiangady et al., 2004; Heinrich et al., 2006; Kralic et al., 2005; Sierra et al., 2015). Arratoietan bai azido kainiko (ingelesetik kainic acid, KA) injekzio intrahipokanpalak zein intraperitonealak, sortzaileen ugaritzean hasierako areagotze baten ostean, neurogenesiaren desagerpena probokatzen dute

epe luzera (Hattiangady et al., 2004). Horrez gain, animali epileptiko kronikoetan Sox2 edo Vimentin positiboak diren NSCak geratzen ez direnez, ahalmen neurogenikoaren murriztea gune neurogenikoaren aldaketagatik azaldua izan da, zeina NSCenganako aurkako ingurugiroa bilakatzen den (Kuruba and Shetty, 2007).

KA intrahipokanpalki injektatua izaten den sagu modeloetan MTLE eta hipokanpoko esklerosiaren (ingelesetik hippocampal sclerosis, HS) ezaugarriak errepikatuak izaten dira: 1) Lesioaren osteko jarduera mitotikoa ez da neurogenikoa, aurretik aurkeztutako mikrogliosiari eta astrogliosiari ekarpena eginez (Heinrich et al., 2006; Kralic et al., 2005; Lee et al., 2003). 2) Etendako gune neurogeniko batean neurona jaioberrien produkzioa nabarmen murriztu egiten da, orduan “NSCen iraunkortasunaren indukzioa” bezala azaldu zena (Kralic et al., 2005). 3) Gure laborategiaren aurretiazko ikerlanetan, Juan Manuel Encinas eta kideek modelo intrahipokanpala aplikatu zuten Nestin-GFP sagu transgeniko konstitutibo eta induzibleak erabiliz, NSCen aktibazio masiboa eta euren programa neurogenikoaren aldaketa bortitza berretsiz. HPFa eta ondoko eremuei eragiten dien konbultsioen ostean, NSCek aldaketa dramatikoa pairatzen dute euren morfologian, fenotipo erreaktiboa bereganatuz (hipertrofikoa eta poliadartua) eta egoera neurogeniko batetik gliogeniko batera aldatuz. Hala, zelula ama neural erreaktiboek (ingelesetik reactive neural stem cell, React-NSC) simetrikoki zatitzeko joera aurkezten dute, bere buruaren kopia gehiago sortuz, zeinak azkenean astrozito erreaktiboetan diferentziatzen diren zatiketa edo transformazio zuzenaren bitartez. Honela, NSCen transformazioak React-NSCetan hipokanpoko gliosi erreaktiboari ekarpena egiten dio eta neurogenesia gaitzesten du epe luzera (Muro-García et al., 2019; Sierra et al., 2015; Valcárcel-Martín et al., 2020) **(S7 Figura)**.

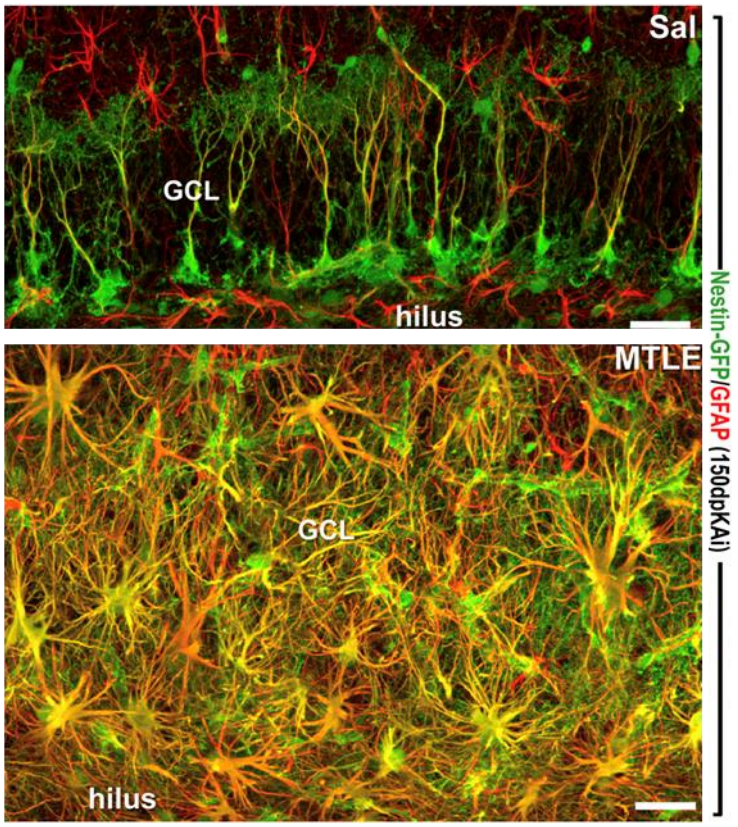

S7 Figura. KA injekzioak eragindako MTLEtik 150 egunera, gune neurogeniko hipokanpala guztiz etenda suertatzen da. NSCak masiboki aktibatuak dira, React-NSCak sortuz eta gliosi erreaktiboari ekarpena eginez (Sierra et al., 2015 artikulutik eraldatua).

NSC erreserbaren eteteak epilepsia kronikoaren ondorio patologikoei dakarkien ekarpen potentzialaren arren, alterazio hauek eragiten dituen mekanismoak ezezagun dirau. Hazkuntza faktoreak luzaroan ezagunak izan dira neurona jaioberrien formazioa erregulatzeko daukaten kapazitatearengatik, SC eta sortzaile ugaritzea, diferentziazioa eta biziraupena modulatuz (Calof, 1995). Are gehiago, konbultsioek eragindako faktore trofikoen espresioak, hala nola garunetik eratorritako faktore neurotrofikoa (ingelesetik brain-derived neurotrophic factor (BDNF), hazkuntza faktore endothelial baskularra (ingelesetik vascular endothelial growth factor, VEGF) eta beste batzuek zeharka NSCen ugaritzea eragin lezakete (Gall, 1993; Gall et al., 1991).

3.6.1. MTLE-HSan mekanismo posibleak

Aspaldian erakutsi zen hazkuntza faktore epidermala (ingelesetik epidermal growth factor, EGF) hazitako astrozitoetan mitogenikoa dena (Simpson et al., 1982). Geroago, biak EGF eta hazkuntza faktore fibroblastikoa 2 (ingelesetik fibroblast growth factor 2, FGF2) hazitako SC eta sortzaileetan ugaritzea estimulatzen zutela erakutsi zen (Reynolds et al., 1992; Tropepe et al., 1999) eta zenbait ikerlanek bi faktoreen

efektu mitogenikoa seinalatu zuten sagu garun heldutik eratorritako NSCak erabiliz (Kuhn et al., 1997; Palmer et al., 1995). Garrantzitsua da baita ere nola EGFk NSCen hedapena eragiten duen SVZan *in vivo* injektatua izan eta gero (Craig et al., 1996). Denak batera harturik, emaitza hauek faktore hauen eta euren seinalizazio ibilbidearen rol posible bat iradokitzen dute NSCen eta astrozitoen aktibazioan, beraz epilepsiaren testuinguruan kontuan hartzeko zerbait izanik.

3.6.2. Hazkuntza faktore epidermal hartzailea (ingelesetik epidermal growth factor receptor, EGFR)

EGFR (HER edo ErbB1 bezala ezagutua baita) ErbB familiako lehen hartzailea da, zeina EGFRrekin erlazionaturik dauden hiru mintz-bitarteko hartzaile gehiagoz osatua dagoen: ErbB2 (Semba et al., 1985), ErbB3 (Kraus et al., 1989; Plowman et al., 1990) eta ErbB4 (Plowman 1993). EGFR 1978an deskubritua izan zen Graham Carpenter eta bere taldearengatik. Zelularik gabeko mintz prestakuntza bat erabilita, lehen aldiz erakutsi zuten tirosina kinasa hartzaile bat, zeinari EGF batzen zitzaion barneko eta kanpoko proteinen fosforilazioa eraginez (Carpenter et al., 1978). Beranduago, hartzailearen amino azido sekuentzia osoa aurkeztu zen, bere rol zelular zein seinalizazio ibilbidean sakontzeko bidea irekiz (Ullrich et al., 1984).

ErbB hartzaile kinasa bakoitza kate bakarreko mintz-bitarteko polipeptido proteinak dira, hiru domeinu ezberdin dituztenak: 1) zisteina-aberatsa den zelulaz kanpoko domeinu bat, hartzailearen aktibazioa eragingo duten estekatzaileentzako lotura leku bezala jarduten duena, 2) mintz-bitarteko domeinu bat estekatzailearen estimulazioaren ondoren hartzaileen arteko dimerizazioan parte hartzen duena eta 3) tirosina kinasa zitoplasmatiko domeinu handi bat tirosina hondakinak proteina sustratoetan fosforilatzen dituena, dagokion seinalizazio ibilbidea piztuz, emaitza zelular konkretu bat eragiten amaituko duena (Bessman et al., 2014; Herbst, 2004; Riese and Stern, 1998; Yarden and Sliwkowski, 2001) **(S8 Figura)**.

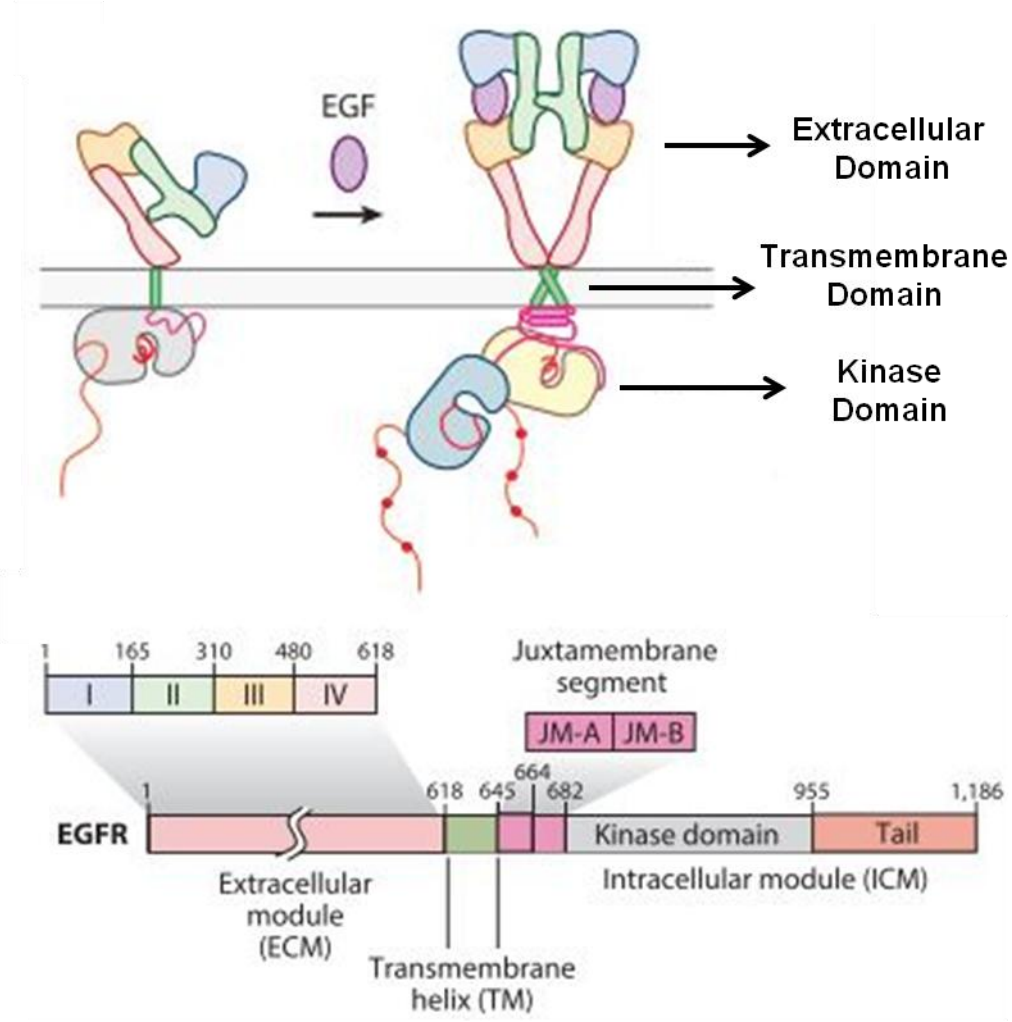

S8 Figura. EGFRren estruktura estekatzaile batekiko loturaren aurretik eta ondoren. zelulaz kanpoko modulua osatzen duten lau domeinu ezberdinek dimero bat osatzen dute estekatzaileari lotu eta mintz-bitarteko domeinuaren eta juxtamintz domeinuaren bitartez tirosina kinasa domeinuaren aktibazioa eragiteko (zelulaz barneko domeinua) ur-beherako seinalizazio ibilbide ezberdinak aktibatuz (Kovacs et al., 2015 artikulutik eraldatua).

3.6.3. Zink (Zn^{+2}) parte hartzaile bezala KAren osteko EGFRren aktibazioan

Ioi metalen artean, Zn^{+2} aski ezaguna da jaiotzaren aurretiko eta ondorengo garaietan garunaren garapenean eta garun helduaren funtzionamendu aproposean kritikoa izateagatik, prozesu neurogenikoaren modulazioa barne (Levenson and Morris, 2011; Sandstead, 2012; Sandstead et al., 2000). Gutxi gora behera garunean dagoen Zn^{+2}aren %80a bere biltegiratze lanetan aritzen diren metalotioneinak (ingelesetik metallothionein, MT) bezalako metaloproteinetan existitzen da, beste %20a neurona glutamatergiko azpiklase baten besikula aurresinaptikoetan dagoelarik. Azken honek seinalizazio faktore lanak egiten ditu zelulaz barneko konpartimentu zitosolikoetan zein zelulaz kanpoko konpartimentuetan (Frederickson, 1989; Frederickson and Danscher,

1990; Kambe et al., 2015; Maret, 2017; Takeda and Tamano, 2009) **(S9 A Figura)**. Zn^{+2} sinaptiko hau histokimikoki erreaktiboa da eta Danscherren zilar-sulfido tindaketa metodoaren bitartez azaleratu daiteke (Danscher, 1981).

Helmut Maskek ausaz eginiko aurkikuntzaz geroztik jakin izan dugu HPFan dagoen Zn^{+2} presentzia garuneko handienetakoa dena (Maske, 1955). Zn^{+2} gehiena HPFaren eremu ezberdinetan sakabanaturik aurkitu daiteke, subikuluma eta ECa barne (Frederickson et al., 1983; Slomianka, 1992). Zn^{+2} hipokanpalaren %10 inguru eta Zn^{+2} sinaptikoaren gehiengoa hiluseko goroldio zuntzen (ingelesetik mossy fiber, MF) botoi erraldoietan aurki daiteke, besikula aurresinaptikoetan (Frederickson et al., 1983; Sindreu et al., 2003). Baita, Schaffer kolateralen erdiek besikula aurresinaptikoetan Zn^{+2}a dutela erakutsi da (Sindreu et al., 2003) **(S9 B Figura).**

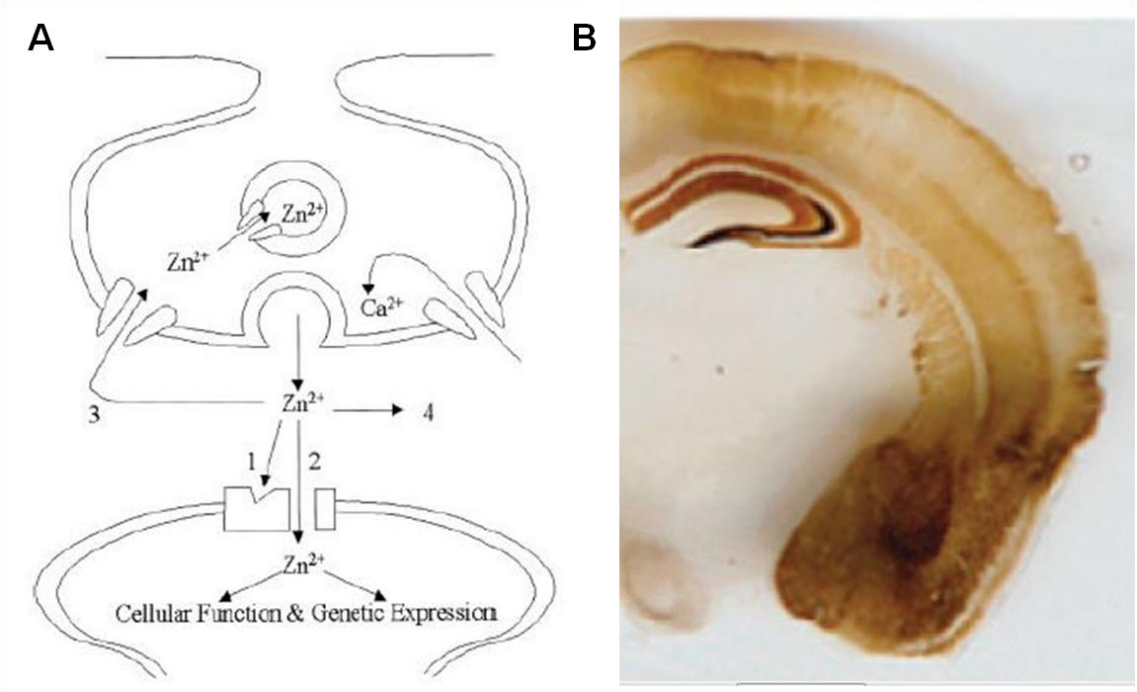

S9 Figura. A) Behin Zn^{+2} arraila sinaptikoan askatua denean, neurona postsinaptikoa modulatu dezake bai zuzenean (1) edo hartzaile bati lotzearen bitartez (2). Hala nola, zelula aurresinaptikoak berreskuratu lezake (3) edo zelulaz kanpoko espazioan askatua izan (4). **B)** Zn^{+2} sinaptikoa batez ere HPFan askatua izaten da, bereziki MFtan, eta baita amigdalan (Takeda et al, 2013 eta Burdette et al., 2000 artikuluetatik eraldatua).

3.6.4 EGFR seinalizazioa blokeatuz

EGFRaren inhibizioa orno-muinaren gliosi erreaktiboa murrizteko estrategia egokia dela erakutsi da (Li et al., 2014; Qu et al., 2012). Are gehiago, EGFR oso inplikatua izanik kantzer gaixotasun ezberdinen eboluzioan (Arteaga, 2011; Nicholson

et al., 2001; Salomon et al., 1995; Sasaki et al., 2009; Sharma et al., 2007), EGFR jomuga duten estrategia ezberdinak garatu dira. Estrategia hauetatik, antigorputz monoklonalak eta tirosina kinasa inhibitzaileak (ingelesetik tyrosine kinase inhibitors, TKI) aurreratuen daudenak dira, biak EGFRren ur-beherako seinalizazio transdukzioaren blokeo efektiboa eragiten dutenak. Estrategia bien artean, TKIak izan dira ikertuenak (Chen, 2013).

Gefitinib (ZD1839) tumoreen ugaritzea murrizteko helburuarekin onarturiko EGFR jomuga zuen molekula txikiko lehen TKIa izan zen. EGFRri lotzen zaio era itzulgarrian adenosina trifosfato (ingelesetik adenosine triphosphate, ATP) lotura lekuan seinalizazio ibilbidearen aktibatzaile bezala jarduten duen tirosina kinasaren barruan. Albo-efektuak leunetik moderatura doaz, dosiaren menpekoak diren azal narritadura eta diarrea barne (Wakeling et al., 2002). Aldi berean, Afatinib, EGFRren inhibitzaile itzulezin bat duela gutxi onartua eta klinikoki saiatua izan da (Watanabe et al., 2018; Yang et al., 2015). Hemen, Gefitiniben eta Afatiniben erabilerak MTLE-HSaren ondorio patologikoak murriztu litzakeela iradokitzen dugu, bereziki NSCen aktibazio masiboari eta gliosi erreaktiboari dagozkionak.

4. HIPOTESIAK ETA HELBURUAK

4. HIPOTESIAK ETA HELBURUAK

NSC hipokanpalak urjauzi neurogeniko helduaren lehenengo urratsa dira, neurona berrien iturri ez berriztagarria izanda ugaztun gehienen bizitza osoan zehar. Honela, NSC populazioaren hasierako tamainak norbanakoak bere bizitza guztian izango duen ahalmen neurogenikoa mugatzen du. Are gehiago, behin NSC populazioa sortzen denean, epilepsia bezalako egoera patofisiologikoek NSCen propietateak eraldatu ditzakete, neurogenesia biziki eraginez. Premisa hauetan eta gure atariko emaitzetan oinarrituz hurrengo hipotesiak azaleratzen ditugu:

1. NSC helduak *de novo* sortuak izaten dira DGaren garapenaren jaio ondorengo etapa goiztiarrean
2. NSC helduak tokian sortuak izaten dira jaio ondorengo DGan
3. NSC helduen sorrerak jaio ondorengo DGan cD2ren espresioa eskatzen du.
4. Hazkuntza faktore fibroblastiko hartzailea (ingelesetik fibroblast growth factor receptor, FGFR) eta EGFR seinalizazio bideen espresio eta jarduera igo egiten da konbultsio ostean, rol garrantzitsua jokatuz aktibazio masiboan eta React-NSC indukzioan.
5. Gefitiniben bidezko EGFRren inhibizio eraginkorrak konbultsio osteko aktibazio masiboa eta React-NSC indukzioa ekiditen ditu.
6. Konbultsio osteko Zn^{+2} askapen masiboak EGFRren bitartezko aktibazioa eta React-NSC indukzioa sustatzen ditu.
7. Konbultsio osteko HB-EGF askapen masiboak EGFRren bitartezko aktibazioa eta React-NSC indukzioa sustatzen ditu.
8.

1. Helburu orokorra: Saguetan ikertu NSC helduen garapena eta formazioa.

1.1. Helburua. Aztertu cD2ren rola NSC helduen populazioaren jaio ondorengo formazioan. Helburu honetarako sagu transgeniko bikoitz bat erabiliko dugu, cD2rik gabeko sagu baten (*cD2*KO) eta Nestin-GFP sagu baten gurutzaketatik ateratzen dena. Era konparatibo batean aztertuko ditugu (WT vs. *cD2*KO) NSCen garapena (kopurua eta dibisio dinamikak) eta heriotza zelularra GCL+SGZ zonaldean

jaio ondorengo denbora-puntu ezberdinetan zehar mikroskopia konfokalean oinarrituriko irudi analisi kuantitatiboaren bitartez.

1.2. Helburua. Aztertu eremu ezberdinetako (DMS eta DG) jaio ondorengo zelula ama neural eta sortzaile (ingelesetik neural stem and progenitor cells, NSPC) goiztiarrek NSC helduen populazioari egiten dioten kontribuzioa. Helburu honetarako, eremu espezifikoetan (DMS eta DG) jaio ondorengo etapa goiztiarrean infekzio erretrobiralen bidezko zelula markaketa egiteko metodo bat garatu eta balioztatuko dugu. Markaturiko zelulen leinuaren identitatea aztertuko dugu mikroskopia konfokalean oinarrituriko irudi analisi kuantitatiboaren bitartez.

1.3. Helburua. Karakterizatu LPA_1en espresioa dNSC zein NSC helduetan DGan. Helburu honetarako sagu modelo transgeniko bat erabiliko dugu zeinetan areagoturiko proteina fluoreszente berdea (ingelesetik enhanced green fluorescent protein, EGFP) espresioa LPA_1 espresioak gidatzen duen. LPA_1-EGFPren espresioa aztertuko dugu DGan eta espezifikoki NSCetan jaio ondorengo denbora-puntu ezberdinetan mikroskopia konfokalean oinarrituriko irudi analisi kuantitatiboaren bitartez.

2. Helburu orokorra: Ikertu gune neurogeniko hipokanpalaren garapena gizakietan.

2.1. Helburua. Aztertu dNSC populazio ezberdinak giza HPFaren garapenean zehar eta sagu datuekin konparatu. Helburu honetarako, IHCa gauzatuko dugu haurdunaldiko eta jaio ondorengo etapa goiztiarreko giza laginetan eta DGa sortuko duten sortzaile matrize ezberdinak ikertuko ditugu mikroskopia konfokalean oinarrituriko irudi analisi kuantitatiboaren bitartez.

3. Helburu orokorra: Ikertu React-NSC indukzio mekanismoak MTLEn.

3.1. Helburua. Ikertu MTLEren indukzioa eta berehala ematen den hipokanpoaren erantzunean FGFRk duen inplikazio potentziala. Helburu honetarako, uneko polimerasa kate erreakzio kuantitatiboa (ingelesetik real time-quantitative polymerase chain reaction, RT-qPCR) eta western blot (WB) bitartez

FGFR azido ribonukleiko mezularia (ingelesetik messenger ribonucleic acid, mRNA) eta proteina nibelak neurtuko ditugu MTLE modelo bezala KA injekzio intrahipokanpala gauzatu eta denbora-tarte ezberdinetara.

3.2. Helburua. Ikertu EGFR seinalizazio ibilbideak MTLEn duen inplikazio potentziala. Helburu honetarako RT-qPCR eta WB bitartez EGFR eta bere ur beherako seinalizazio ibilbide diren Akt, ERK1/2 eta STAT3 mRNA eta proteina nibelak neurtuko ditugu MTLEren indukzioa eta denbora-tarte ezberdinetara. EGFRren espresioa aztertuko dugu baita Nestin-GFP saguetan eta Nestin-GFP saguetatik eratorritako neuroesferetan, IHC eta mikroskopia konfokalean oinarrituriko irudi analisi kuantitatiboaren bitartez.

3.3. Helburua. Ebaluatu Gefitiniben eraginkortasuna EGFRren seinalizazio ibilbidea blokeatzeko *in vitro* NSPCtan. Helburu honetarako NSPCak hazi eta EGFRren inhibitzaile Gefitinibek euren ugaritze kapazitatean duen eragina ebaluatuko dugu. WB eta mikroskopia konfokalean oinarrituriko irudi analisi kuantitatiboaren bitartez Gefitinibek EGFR seinalizazio ibilbidean duen eraginkortasuna determinatuko dugu eta NSPCen ugaritze kapazitatean duen efektua BrdU bereganatzearen bidez neurtuko dugu.

3.4. Helburua. Aztertu Gefitiniben efektua *in vivo* NSC eta neurogenesiaren gainean MTLEn. Helburu honetarako, Gefitinib administratuko diegu sagu helduei KA injekzio intrahipokanpalaren bitartez MTLEa induzitu eta lehenengo hiru egunetan zehar. Tratamenduaren ostean, NSCen kopuru, aktibazio eta konplexutasun morfologikoa ebaluatuko ditugu. Gainera, NBen presentzia SGZ+GCL zonaldean mikroskopia konfokalean oinarrituriko irudi analisi kuantitatiboaren bitartez.

3.5. Helburua. Ebaluatu Zn^{+2}ak MTLE egoeran duen akzio potentziala NSCengan. Helburu honetarako lehenik Zn^{+2} eta MT kopurua ebaluatuko ditugu HPFan Danscher tindaketa eta RT-qPCR tekniken bitartez MTLEa induzitu eta gutxira. Zn^{+2} administrazioaren efektua ikertuko dugu *in vitro* NSPCetan eta *in vivo* DGko NSCetan mikroskopia konfokalean oinarrituriko irudi analisi kuantitatiboaren bitartez.

3.6. Helburua. Determinatu Zn^{+2}aren efektu potentziala EGFRren bidezko React-NSC indukzioa sustatzeko. Helburu honetarako, pare bat EGFR tirosina lekuren fosforilazioa determinatuko dugu (Y845 eta Y1068) WB bidez *in vitro* hazitako NSPCei egindako Zn^{+2} administrazioaren ondoren. Baita ere, *in vivo* ebaluatuko dugu mikroskopia konfokalean oinarrituriko irudi analisi kuantitatiboaren bitartez Zn^{+2} bidezko

SGZan potentzialki sorturiko ugaritzea Gefitinib administrazioak murrizteko duen ahalmena.

3.7. Helburua. Ebaluatu Zn^{+2} kelazioaren efektua NSC eta neurogenesian MTLEn. Helburu honetarako Zn^{+2} kelatzailea den TPEN erabiliko dugu, sagu helduetan MTLEa induzitu eta lehenengo zazpi egunetan zehar administratuz eta zelula granular dispertsioa (ingelesetik granule cell dispersion, GCD) eta heriotza zelularraren babes potentziala ebaluatuko ditugu mikroskopia konfokalean oinarrituriko irudi analisi kuantitatiboaren bitartez.

3.8. Helburua. Ebaluatu HB-EGF EGFRren aktibazioa sustatzen duen mekanismo posible bezala MTLEn. Helburu honetarako Entzimari loturiko saiakera inmunosorbentea (ingelesetik Enzyme-linked immunosorbent assay (ELISA)) erabiliz kuantifikatu dugu *in vivo* MTLE indukzioaren osteko lehenengo hiru egunetan eta *in vitro* ugaritze kondizioetan mantendutako NSPCetan askaturiko HB-EGF kopurua. IHCra ere joko dugu KA injekzio intrahipokanpalaren ostean DGaren barruan HB-EGF distribuzioa ebaluatzeko eta WBra EGFR seinalizazio ibilbidearen aktibazioa neurtzeko NSPCtan eginiko HB-EGF administrazioaren ostean.

5. MATERIALAK ETA METODOAK

5. MATERIALAK ETA METODOAK

5.1. Animaliak

Ikerlan honetan erabilitako animalia guztiek janaria eta ura *ad libitum* izan dute eskuragarri, tenperatura (19-22°C) eta hezetasun (%40-50) konstantea zuen gela batean mantendu direlarik, 12:12 orduko argi/iluntasun zikloetan. Prozedura guztiak Euskal Herriko Unibertsitateko (UPV/EHU) Komite Etikoarengandik eta Bizkaiko Foru Aldundiarengandik onartuak izan dira M20/2015/236 protokolopean, 2010/63/UE direktiba europearra eta NIH jarraibideak segituz.

Nestin-GFP sagu transgenikoak Grigori Enikolopoven laborategian sortuak izan dira (Cold Spring Harbor, NY, USA), honek adeitasun osoz anduia gure laborategiari eman ziolarik. Nestin-GFP saguak aldez aurretik erabat karakterizatuak izan dira (Mignone et al., 2004).

LPA_1-EGFP sagu transgenikoak Howard Hughes Institutu Medikoko (The Rockefeller University, NY, USA) GENSAT proiektuan sortuak izan dira, gure laborategira Dresden Terapia Erregeneratzaileentzako Zentruko (Technische Universität Dresden, Dresden, Germany) Gerd Kempermannek adeitasun osoz helarazita. LPA_1-EGFPren espresioaren karakterizazioa NSC helduetan beste ikerlan batzuetan egina izan da (Valcárcel-Martín et al., 2020; Walker et al., 2016).

Bi sagu anduiak C57BL/6 saguekin gurutzatuak izan ziren gutxienez 10 belaunaldiz, aldagarritasun genetikoa homogeneizatzeko xedez. Nestin-GFP saguak DGko gune neurogenikoaren jaio ondorengo karakterizazioa, bare gunean eraturiko virus gamma-erretrobirus (ingelesetik spleen-focus forming virus gamma-retrovirus, SFFV-RV) injekzioak eta MTLEko esperimentuak egiteko erabili ziren. LPA1-EGFP saguak garapen ikerlanetan erabiliak izan ziren.

cD2k jaio ondorengo DGaren garapenean duen rola karakterizatzea helburu, *ccnd2* gabeko saguak, *cD2*KO izendatuak, Nestin-GFP sagu mota ezberdin batekin (Yamaguchi et al., 2000) gurutzatuak izan ziren Anja Urbachen laborategian (Universitätsklinikum Jena, Jena, Germany). Lehenengo hazkuntzaren ondorengoak euren artean gurutzatuak izan ziren *cD2*KO edo WT homozigoto eta Nestin-GFP saguak lortzeko. Azken hauen burmuinak jaio ondorengoko garapenaren adin

ezberdinetan (P0, P7, P14 and P28) finkatuak izan ziren, ostean gure laborategira bidaliak izateko guk analisi histologikoa egin genezan.

5.2. Giza Laginak

Haurdunaldiko eta jaio ondorengo *post-mortem* kontrol laginak Mercedes Paredesen eskutik batuak izan ziren gurasoen baimen idatzia jaso ostean eta University of California, San Franciscoko (UCSF) erregulazio etiko legal eta instituzionalen behaketa zorrotzean. Protokoloak Human Gamete, Embryo eta Stem Cell Research Comittearengandik onartuak izan ziren, UCSFen. Aurretik deskribatu bezala (Sorrells et al., 2018), lobulu tenporaleko lagin guztiak konplexu amigdaloidetik LVaren azpiko adarraren atzeko amaierararte moztuak izan ziren gutxi gora behera 1.5 zm-ko blokeetan, %4 paraformaldehidoan (ingelesetik paraformaldehyde, PFA)(Sigma-Aldrich, #441244) finkatuak beste bi egunez, kriobabestuak %30ko sukrosa soluzioan eta azkenik murgiltze medioan (OCT) izoztuak, analisi histologikoak aurrera eraman arte.

5.3. Injekzio intrahipokanpal estereotaxikoak

5.3.1. Jaio ondorengo SFFV-RV infekzioak

Injekzio intrahipokanpalak burutzeko metodo bat optimizatu genuen gure baldintzei egokituz: 1) HPFaren bi zonalde ezberdinetan injektatzeko beharra (DG eta DMS) eta 2) zonalde hauek jaio ondorengo garapenean zehar jasotzen duten tamaina aldaketarekiko adaptazioa. Hau lortzeko aurretiaz publikaturiko sagu jaioberrietan eginiko injekzio intrahipokanpalen saiakeretan erabilitako koordenada ezberdinak frogatu genituen (Jiang et al., 2017; Xu et al., 2012).

Jaio ondorengo sortzaileen leinua denboran zehar jarraitzeko mCerulean eta mCherry espresioa zuten SFFV-RVak erabili genituen, zeinak adeitasun osoz Diego Gómez-Nicolak (University of Southampton, UK) helarazi zizkigun (Gomez-Nicola et al., 2014; Weber et al., 2012). P2 eta P5 adineko saguak hipotermia bidez anestesiatuak izan ziren, animaliak bi minutuz izotz kubo batean jarriz, segituan aparatu estereotaxikoan jarritako plataforma batean kokatuak zirela. Zuntzezko argi optiko baten laguntzaz, Lambda lokalizatua izan zen saguaren burua transiluminatuz, ondoren injektatzeko erreferentzia gisa erabiliz. Injekzioa burutzeko beirazko mikrokapilare bat erabili zen, hurrengo koordenatuetan: DGrako, -1 mm aurretik atzera (ingelesetik anteroposterior, AP), ± 1.2 mm albotik albora (ingelesetik laterolateral, LL), -1.7 mm bizkarraldetik sabelaldera (ingelesetik dorsoventral, DV); DMSrako, -0.9 mm

AP, ±1.4 mm LL, -1.7 mm DV. Mikrokapilarea azala zeharkatuz izan zen barneratua zegokion injekzio tokian, SFFV-RVaren 0.3 µl injektatuz 0.3 µl/min-ko jario ratioan. Ebakuntza amaitu eta berehala saguak ur berozko bainu batean jarriak izan ziren lehenbizi eta manta termiko batean ondoren, arnasketa, azalaren kolorea eta aktibitate lokomotorea normalera itzuli arte. Azkenik, amaren berronarpena ahalbidetzeko xedez, amaren beraren gorotz, azpi eta urez osaturiko nahaste batekin blaituak ziren hazkuntza kaiolara itzuli baino lehen. Amaren estresa ahal bezain beste gutxiesteko, prozedura osoa kume bakoitzeko 10 minutu baino gutxiagoan burutzen zen. Kume bat ere ez zen amarengandik ukatua edo kaltetua izan. Aldiz, nahiz eta heriotza tasa oso txikia izan, anestesiatik errekuperatzea lortu ez zuten kume guztiak P5 adin taldekoak izan ziren, adin honetan hipotermiarekiko minberatasun handiagoa iradokiz.

Inplementaturiko metodoak birus partikulak proposatutako gune anatomikoetan zabaltzea ahalbidetzen du, injekzioaren prezisioa %100 ez bada ere, erabilitako adinetan suertatzen diren animalien arteko tamaina diferentzien eta muga metodologikoen poderioz. Hala, kontuan harturik helburu bezala hartutako bi guneen tamaina txikia eta elkarren arteko gertutasuna, *a posteriori* irizpideak erabili genituen injektaturiko animaliak talde zuzenean egokitzeko; injekzio bat “DG” taldean sailkatzeko, DMSan SFFV-RVak markatutako zelula bakar bat ere ez egotea ziurtatu genuen. Gainera, mikrokapilarearen ibilbidea ikusi zitekeen kasu askotan, injekzio motaren identifikazioa erraztuz. Bestalde, injekzioak “DMS” taldean sailkatzeko, SFFV-RV zelula positiboen presentzia finbriaren gainaldetik korronte osoan zehar, injekzio lekutik DGerantz, beharrezkoa zen. Soilik meningeetara iritsitako injekzio motak “DMS” injekzio motengandik ezberdindu genituen euren kokapena, DGaren azpiko adarraren azpialdetik korronte bat osatuz, eta SFFV-RV-positibo ziren zelulen morfologia luzea kontuan hartuz.

5.3.2. Injekzio intrahipokanpal estereotaxikoak helduetan

KA injekzio intrahipokanpalak aurretiaz deskribatu bezala burutu ziren (Sierra et al., 2015). Laburbilduz, animaliak intraperitonealki lokartuak izan ziren ketamina (75 mg/kg; Ketamine, #581140) eta medetomidina (1 mg/kg; Sedastart, Pfizer) nahasten zituen anestesiarekin eta buprenorfina (1 mg/kg; Buprecare, Animalcare Lted., #582039) analgesikoaren azal-azpiko injekzio bakarra jaso zuten. Saguak anestesia sakonean murgilduak zeudena ziurtatu genuen arnasketa erlaxatu eta erregularraren presentzia kontrolatuz eta buztan/hatzaparrean atximurka egin ondoko erantzun eza egiaztatuz. Ondoren, buru gaineko ilea moztu eta sagua aparatu estereotaxikoan ipini eta gero ur oxigenatua aplikatzen zitzaion garezurretik banantzeko mozketa

kirurgikoaren aurretik azala garbitu eta desinfektatzeko. Koordenada estereotaxikoak Bregma erreferentzia puntutik hartuak izan ziren. Hipokanpoa aurkitzen den zonaldean injektatzeko hurrengo koordenadak jarraitu ziren: -1.8 mm AP, -1.6 mm LL eta -1.9 mm DV. Finkaturiko posiziora heltzea helburu, garezurra zulatua izan zen 0.6 mm-ko abiadura handiko zulagailu mikromotore bat erabiliz.

Status epilepticusa sorrarazteko 20 mM-ko KA (Sigma-Aldrich, #K0250/K3375) soluzio bateko 50 nl administratu ziren olio mineralez beteriko beirazko mikrokapilare bati loturiko nanoinjektore (Nanoject II, Drummond Scientific, #3-000-205A) bat erabiliz, aurretiaz deskribatu bezala (Sierra et al., 2015). Zn^{+2}aren rola gune neurogenikoan zein den ebaluatzeko, 5, 20 eta 30 nM administratu genituen Hamilton mikroxiringa (Hamilton, #84250) bati konektatutako altzairu herdoilgaitzez eginiko kanula bat erabiliz (kanpoko diametroa, 0.28 mm). EGFRaren inhibitzaile Afatinib bimaleatua (Selleck Chemicals, #S7810) 70 µM-ko kontzentraziora diluitua izan zen disoluzio isotonikoan eta intrahipokanpalki injektatu zen KA injekzioaren aurretik. Kasu bakoitzean, %0.9ko NaCl esterilezko soluzioa erabili zen kontrol animalia taldea osatzeko. Kanula 5 minutuz injekzio puntuan geldirik mantendu zen kanularen ibilbidean errefluxurik gera ez zedin eta ondoren saguaren garezurraren gainaldeko azala josia izan zen, azkenik animaliak manta termiko batean lagaz anestesiaren efektuak igaro arte.

5.4. Tratamenduak

5.4.1. EGFRaren inhibitzaile Gefitinibaren sudurretiko administrazioa

10 mg/Kg Gefitinib (Selleck Chemicals, #S1025) %0.5 metilzelulosarekin eta %0.2 Tween 80rekin diluituak izan ziren ekoizlearen argibideei jarraituz eta sudurretik administratu estereotaxia amaitu eta berehala hasita, egunean birritan lehenengo hiru egunetan zehar, aurretiaz deskribatu den bezala (Hanson et al., 2013; Pineda et al., 2013). Soluzioaren 10 µl eskumako sudurzuloan administratu ziren pipeta punta bat erabiliz eta sagua aurretiaz deskribatu den bezala helduz (Hanson et al., 2013). Saguak soluzio tantarik arnasaldi batez kanporatu ez zezan, administrazioa hainbat serietan egin zen, administrazio bakoitzeko segundo gutxi batzuk itxaronez animalia immobilizaturik mantentzen zelarik. Pipeta punta berriak erabili ziren animalia bakoitzeko, gehiegizko dosiak ekiditea helburu.

5.4.2. TPEN Zn^{+2} isolatzailearen azal-azpiko administrazioa

Zelulaz kanpoko Zn^{+2}a isolatzeko, TPEN soluzioa fresko prestatu zen %10 etanolean (10% etil alkola disoluzio isotoniko fisiologiko normalean, Merck, #616394)

eta azal-azpitik injektatu zen animalien lepondoan egunean birritan, 5 mg/kg-ko kontzentrazioan, aurretiaz deskribatu bezala (Kim et al., 2012). Administrazioa aste oso batez burutu zen KAaren injekzio intrahipokanpalaren ostean. Kontrol animaliek %10 etanoleko bolumen baliokide bat jaso zuten administrazio bakoitzeko.

5.4.3. BrdU administrazioa

BrdUa (Sigma, #B5002-1G) disoluzio isotonikoan disolbatua eta intraperitonealki administratua izan zen 150 mg/kg-tan, hiru aldiz, hiru orduko tarteak utziz. KA edo Zn^{+2} injekzioaren ostean hiru egunetara eta Zn^{+2} injekzioaren ostean zazpi egunetara egindako analisietan, BrdUa animaliak sakrifikatu baino 24 ordu aurretik eman zen momentu horretan ugaritzen ari ziren zelulak markatzeko asmoz. KA edo Zn^{+2} injekzioaren ostean 14 egunera eginiko analisietan, BrdUa Gefitinib tratamendua amaitu eta berehala eman zen (KA/Zn^{+2} osteko hirugarren eguna), tratamendua amaitu bezain laster zatitzen ari ziren zelulen patua aztertzeko asmoz. *In vitro* esperimentuetan, 10 µM-ko BrdU pultsu bat gauzatu zen ordu batez, zelulak finkatu baino lehen, ugaritzen ari ziren zelulak markatzeko asmoz.

5.5. Hazkuntza zelularrak

NSPCen hazkutzak HPFarentzako eta SVZarentzako aurretiaz deskribaturiko protokolo bat egokituz lortu ziren (Jhaveri et al., 2015; Pineda et al., 2013) non papaina eta azido desoxirribonukleikoasa (ingelesetik desoxyribonucleic acid, DNA) nahasten dituen soluzio entzimatiko bat (20.000 U; 195 U/µl) aurretiaz berotu eta ondoren (37ºC and 5% CO_2) Ovomucoid erabiliz DMEM/F-12 medioaren ordez jarduera entzimatikoa oztopatzeko. Laburki, hipokanpoak bai C57BL/6 edo Nestin-GFP saguetatik erauziak izan ziren, elkartu eta izotzean hoztutako fosfato tanpoi soluzio isotoniko (Ingelesetik phosphate buffered saline, PBS) -Glukosa %30n ipiniak izan ziren, ondoren gutxi gora behera 2 mm-ko zati txikietan moztuak izateko. Ostean, lagina 15 ml-ko hodian jarri, kontaminazio arriskua murrizteko garbitu eta aurretiaz beroturiko soluzio entzimatikoarekin inkubatua izan zen, 37ºCtan 15 minutuz. Lagina bost minuturo mekanikoki agitatua izan zen ehunaren metaketa ekiditeko asmoz.

Gero, gainjalkina alde batera utzi eta erreakzio entzimatikoa oztopatua izan zen papainaren inhibitzaile den 950 µl Ovomucoid erabiliz. Horrenbestez, zelulak pipeta punta batekin disoziazio mekanikoaren bitartez disgregatuak izan ziren. Ondorioz, geraturiko zelula suspentsioa 15 ml-ko hodietan filtratua izan zen, segidan zelulak 10 minutuz 200 Gtan zentrifugatu. Zelula alea berriro nahasia izan zen bolumen totalaren %10 ugaritze osagarriarekin (Stem Cell Technologies, #05702), %2 B27rekin, %0.24

Heparinarekin (Stem Cell Technologies, #07980), %0.8 EGFrekin eta %0.2 FGFrekin (Peprotech, #P01132 eta #P15655) aberasturiko 500 µl Neurocult ugaritze medioan eta Neurocult medio aberastuko 5 ml-rekin beteriko T25ko flaskoetan kokatua izan zen. Zelulak kondizio estandarretan mantenduak izan ziren %5 CO_2 duen 37 ºCko inkubagailu heze batean.

NSPC hazkuntzak 7 egunetik behin pasatuak izan ziren disgregazio entzimatikoaren bitartez, Akutasa (Stem Cell Technologies, #7920) erabiliz aurretiaz deskribatu bezala (Pineda et al., 2013), 100 U/ml penizilinaren eta 150 µg/ml streptomizinaren (Gibco, #15140 eta #15122) presentzian. Populazioaren heterogeneitiatea kontserbatu eta zelula hautaketa arazoak ekiditeko NSPC hazkuntzak gehienez 4 aldiz pasatu ziren. IHC saiakeretan NSPCak lamininarekin gainjantzitako 12 mm-ko estalkietan (Sigma, #L2020) ereinak izan ziren, aurretiaz deskribatu bezala (Silvestre et al., 2012). Kontrol eta KA egoeretan WB bidezko seinalizazio zelularraren ebaluaketa egiteko, kondizioko 400.000 NSPC erabili ziren. Ugaritze/inhibitze saiakeretan, NSPC kopurua putzuko 25.000 zelulara murriztua izan zen dentsitate zelularra gutxitu eta zelulen arteko kontaktuaren ondorioz suertaturiko ugaritzearen inhibizioa murrizteko asmoz. Zn^{+2}ak eta honen inhibizioak (Gefitiniba erabiliz) EGFR seinalizazio bidearengan duen efektua neurtzeko asmoz, zelulak garbituak eta bi orduz hazkunde faktorerik gabeko hazkuntza medioan inkubatuak izan ziren EGFR seinalizazio bidea itzaltzea xede. Ondoren, zelulei 2 µM Gefitinibekin aurreinkubatuak izan ziren eta/edo bi orduz estimulatuak bai 200 µM Zn^{+2}kin, bai 100 ng/ml edo 20 ng/ml EGFrekin

5.6. RNA erauzketa eta uneko polimerasa kate erreakzio kuantitatiboa (Ingelesetik real time- quantitative polymerase chain reaction, RT-qPCR)

5.6.1 RNA erauzketa eta alderantzizko transkripzioa

Denbora-puntu ezberdinetan eratorritako hipokanpoak (0, 1.5, 12, 24 eta 72 ordu KA injekzioaren ostean) berehala izoztuak izan ziren RLT tanpoiarekin. RNA totalaren erauzketa eta DNA soberakinak eliminatzeko DNAsa tratamenduak ekoizlearen irizpideak jarraituta burutu ziren (Qiagen). RNA kantitatea Nanodrop 2000 erabiliz neurtu zen. Ondoren, ausazko hexameroak eta Superscript III alderantzizko transkriptasa kita (Invitrogen, #10432122) erabiliz 1,5 µg RNA erretrotranskribatuak izan ziren, ekoizlearen irizpideen arabera Veriti ziklatzaile termikoa erabiliz (Applied Biosystems, #4375305).

5.6.2 RT-qPCR

RT-qPCRa BioRad CFX96 baten gauzatu zen (California, USA) eta osagarriaren anplifikaziorako Power SybrGreen (BioRad, #1708880) eta **1. Taulan** erakutsitako primerrak erabiliz. Protokoloa hurrengoa izan zen: 3 min 95ºC-tan desnaturalizaziorako, 10 segundoko 45 ziklo 95ºCtan sendotzeko eta 30 segundo 60ºCtan. Lagin bakoitza GAPDHen eta HPRTen barne espresioa kontuan hartuz normalizatua izan zen. Erreakzio bakoitza gutxienez birritan gauzatu zen, bikoizturik.

GENEA	GENE BANKUA	ANPLIKON TAMAINA	SEKUENTZIA
HPRT	NM_013556.2	150	Fwd:5'-GTTGGGCTTACCTCACTGCT-3' Rev:5'-TCATCGCTAATCACGACGCT-3'
GAPDH	NM_001289726.1	153	Fwd:5'-CCAGTATGACTCCACTCACG-3' Rev:5'-GACTCCACGACATACTCAGC-3'
EGFR	NM_007912.4	165	Fwd:5'-GCCAACTGTACCTATGGATGT-3' Rev:5'-GGCCCAGAGGATTTGGAAGAA-3'
FGFR1	NM_001079908.2	88	Fwd:5'-CCAAACCCTGTAGCTCCCTA-3' Rev:5'-TGAACTTCACCGTCTTGGCA-3'
FGFR2	NM_010207.2	105	Fwd:5'-CCGAATGAAGACCACGACCA-3' Rev:5 -TCGGCCGAAACTGTTACCTG-3'
MTH1	NM_013602.3	86	Fwd:5'-TCACCACGACTTCAACGTCC-3' Rev:5'-CAGTTGGGGTCCATTCCGAG-3'
MTH2	NM_008630.2	133	Fwd:5'-GCATCTGCAAAGAGGCTTCC-3' Rev:5'-AGTTGTGGAGAACGAGTCAGG-3'
MTH3	NM_013603.2	77	Fwd:5'-GCTGCTGGACTGGATATGGA-3' Rev:5'-TTGCATTTGTCCGAGCAGGT-3'

1. Taula. RT-qPCRean erabilitako primer lista.

5.7. IHC

5.7.1. Sagu burmuin ehuna

IHCa aurretiaz deskribatu den bezala burutu zen sagu transgenikoentzako optimizaturiko metodoak erabiliz (Encinas and Enikolopov, 2008; Encinas et al., 2011). Labur, animaliak bihotzetik perfusatuak izan ziren lehenik 30 ml PBS 1X eta ondoren %4 PFA PBSn (Ph 7.4) erabiliz. Gero, burmuinak atera eta hiru orduz gehiago

finkatzen uzten ziren, PFA soluzio berean eta giro tenperaturan, PBS- %0.2 sodio azide soluzio batera aldatuak izan baino lehen, non 4 ºCtan gordeak izaten ziren. 50 µm lodi ziren sekzio sagitalak moztuak izan ziren era serialean Leica VT 1200S bibrazio xafla mikrotomo (Leica Microsystems GmbH, Wetzlar, Germany) bat erabiliz. Jaio ondorengo SFFV-RV esperimentuetan, 70 µm lodi ziren sekzio koronalak moztu ziren era serialean, SFFV-RV infekzioen hedadura zuzen eta egoki ikustea ahalbidetzeko. IHC esperimentuetan, sekzioak blokeo eta permeabilizazio soluzioetan inkubatuak izaten ziren (PBSa %0.25 Triton-X100-arekin eta %3 behi serum albumina (Ingelesetik bovin serum albumin, BSA)) hiru orduz giro tenperaturan, ondoren gau osoan zehar antigorputz primarioarekin inkubatuak izateko (soluzio berean diluituak) 4ºCtan. Inkubazioaren ostean, antigorputz primarioa kendu eta sekzioak PBSa erabiliz garbitzen ziren hiru aldiz 10 minutuz. Ostean, sekzioak blokeo eta permeabilizazio soluzioan diluituriko fluorokromo bati itsatsitako antigorputz sekundarioekin inkubatzen ziren 3 orduz giro tenperaturan. Azkenik, PBS erabiliz garbitu eta sekzioak gelatinaz gainjantzitako laminatan kokatuak ziren DakoCytomation kokatze medio fluoreszentea erabiliz (DakoCytomation, #S302380). BrdU eta Nestin erabilpena eskatzen zuten esperimentuetan, sekzioak 2M azido klorihidrikoarekin (Ingelesetik chlrohydric acid, HCL) tratatuak izan ziren 37ºC-tan 20 minutuz eta segituan 0.1M tetraboratoarekin inkubatu giro tenperaturan 10 minutuz tindaketa hasi baino lehen. Ondoren, sekzioak PBS erabiliz garbitu eta tindaketak lehenago deskribatu bezala jarraitu zen. Nestin-GFP eta LPA_1- EGFP animalia transgenikoen GFP seinalea, SFFV-RVen mCerulean seinalea bezalaxe, GFParen kontrako antigorputz bat erabiliz detektatu zen seinalearen areagotze eta irudikapen hobea lortzeko. Era berean, SFFV-RVen mCherry seinalea DsRedaren kontrako antigorputz batekin detektatu zen seinalearen areagotze eta irudikapen hobea lortzeko. Antigorputz primario eta sekundarioen lista osoa **2. eta 3. Tauletan** aurki daiteke.

5.7.2. Hazkuntza zelularrak

Tratamendu bakoitzaren ondoren, hazkuntza zelularrak finkatuak izan ziren PBS-%4 sukrosan disolbaturiko %4 PFA erabiliz. Gero, permeabilizatu zitezen, zeluladun estalkiak PBS-%0.3 Triton-X100 eta %1 BSArekin inkubatuak izan ziren hiru minutuz giro tenperaturan eta %0.2 Triton-X100 eta %3 BSA PBSan diluituriko antigorputz primarioekin inkubatuak gau osoan zehar 4ºCtan. Ostean, PBS erabiliz garbituak izan ziren hiru aldiz eta antigorputz sekundarioekin inkubatuak bi orduz giro tenperaturan, DAPI ere bazuen soluzioan. Azkenik, estalkiak beirazko laminetan buruz behera kokatuak izan ziren DakoCytomation kokatze medio fluoreszentea erabiliz.

BrdU esperimentuentzako, tindaketa baino lehenago zelulak 2M HCl erabiliz bost minutuz 37ºCtan tratatuak eta segituan 10 minutuz inkubatuak izan ziren giro tenperaturan 0.1M tetraboratoa erabiliz. Ondoren, sekzioak PBS bidez garbitu eta tindaketak lehenago deskribatu bezala jarraitu zuen. Antigorputzen lista osoa **2. eta 3. Tauletan** aurki daiteke.

5.7.3. Giza ehuna

Giza garuneko ehun blokeak 30 µm-ko lodierarekin moztuak izan ziren kriostato bat erabiliz, ondoren zuzenean aurreizoztutako (-20ºC) Superfrost beirazko laminetan (sekzio bat lamina bakoitzeko) atxiki eta erabili arte -80ºCtan gordez. Kasu bakoitzean, gutxienez hiru sekzio kresil bioleta tindaketaren bitartez koloreztatuak izan ziren laginaren orientazioa eta mugarri anatomikoak konfirmatzeko. IHCa aurretiaz deskribatuko protokoloa jarraituz burutu zen (Sorrells et al., 2018).

IHCa baino lehen, izoztutako laminak giro tenperaturan orekatzen ziren hiru orduz, 65ºCtan 30 minutuz labean sartu baino lehen. %0.05 Triton-X100 PBSa (TNT tanpoia) erabiliz laminak berriro hidratatu eta gero, %4 PFA erabiliz finkatuak izan ziren 45 minutuz. Laminak TNTa eta ur destilatua erabiliz garbituak izan ziren eta ondoren barruko peroxidasa seinalea itzalia izan zen PBS-%1 H_2O_2ko soluzioa erabiliz 30 minutuz. Antigenoaren berreskurapena behar zuten epitopoen kasuan **(4. Taula)**, 10mM sodio zitrato tanpoi batekin inkubazio gehigarri bat egin zen, pH 6.0 95ºCtan 10 minutuz, eta gero laminak giro tenperaturan hozten utzi ziren. Horren ostean, laminak TNTarekin garbituak izan ziren 10 minutuz hiru aldiz eta berriro PBS-%1 H_2O_2an jarriak ordubete eta 30 minutuz barne peroxidasa seinalearen itzaltzea ziurtatzeko asmoz. Lotura ez zehatzak 0.1 M Tris-HCl, pH 7.5, 0.15 M NaCl, %0.5 PerkinElmereko blokeo erreaktiboarekin blokeatuak izan ziren (TNB soluzioa) ordubetez eta laminak TNBn diluituriko antigorputz primarioekin inkubatuak izan ziren **(4. Taula)**.

Gau osoko inkubazioaren ondoren, laminak TNT erabiliz 10 minutuz hiru aldiz garbituak eta TNBn diluituriko antigorputz sekundarioekin inkubatuak izan ziren. Alexa seinale indartsuenentzako zuzenean akoplaturiko antigorputz sekundarioak erabili ziren. Seinalerik ahulenentzako, Tiramida seinale anplifikazio kitarekin (PerkinElmer) tindaketa intentsitatearen handitze bat gauzatu zen. Labur, biotindaturiko antigorputz sekundarioak (Jackson Immunoresearch Laboratories) 2.5 orduz inkubatuak izan ziren giro tenperaturan. Ondoren, streptabidina peroxidasarekiko (TNB-n 1:200ean diluiturik) lotura 30 minutuz ahalbidetua izan zen. Azkenik, tiramida soluzio bat fluoroforo

konjugatuekin 5 minutuz inkubatua izan zen, azkenik erreakzioa bukatutzat emateko “Reaction Stop Reagent” erabiliz.

IHC protokoloa antigorputz ezberdinentzako sekuentziak jarraituz gauzatu zen, antigorputz primarioetatik indartsuena eta zegokion antigorputz sekundarioa lehenbizi inkubatuz. Honela, tiramida soluzioaren inkubazioaren ostean, laminak beste 30 minutuz finkatuak eta %3 H_2O_2 PBSn inkubatuak izan ziren, protokoloa berriz ere hasteko gainontzeko antigorputz primarioentzako. Azkenik, behin antigorputz guztiak inkubaturik, sekzioak TNTn zeharo garbituak, deshidratatuak, laminetan kokatuak eta estalduak izan ziren.

IHC-RAKO ANTIGORPUTZ PRIMARIOAK		
ANTIGORPUTZA	**KONPAINIA**	**DILUZIOA**
Chicken anti-GFP	Aves Laboratories #GFP-1020	1:1000
Rabbit anti-NeuN	Abcam #ab177487	1:500
Rabbit anti-Ki67	Vector Laboratories #ab16667	1:750
Rabbit anti-GFAP	Dako #Z0334	1:1000
Rat anti-BrdU	AbD Serotech #MCA2060GA	1:1000
Goat anti- DCX	St. cruz Biotech. #sc-8067	1:750
Chicken anti-Nestin	Aves Laboratories #NES	1:1000
Rabbit anti-GFP	Abcam #ab6556	1:1000
Goat anti-GFAP	Abcam #ab53554	1:1000
Rabbit anti-BLBP	Abcam #ab32423	1:1000
Rabbit anti DsRed	Abcam #MA5-15257	1:2000
Rabbit anti-EGFR	Abcam #ab131498	1:1000
Rabbit anti-FGFR	Cell Signaling #34725	1:200
Rabbit anti-HB-EGF	Cell Signaling #85672	1:400

2. Taula. Sagu ehunean eta hazkuntza zelularretan erabilitako antigorputz primarioak.

IHC-RAKO ANTIGORPUTZ SEKUNDARIOAK		
ANTIGORPUTZA	**KONPAINIA**	**DILUZIOA**
AlexaFluor 488 goat anti-chicken	Molecular Probes #A11039	1:500
Alexa Fluor 568 donkey anti-chicken	Invitrogen #A11042	1:500
AlexaFluor 680 goat anti-rabbit	Molecular Probes #111605003	1:500
Alexa Fluor 488 Donkey anti-rabbit	Invitrogen #A21206	1:500
Alexa Fluor 568 Donkey anti-rabbit	Invitrogen #A10042	1:500
AlexaFluor 594 goat anti-rat	Molecular Probes #112295167	1:500
Alexa Fluor 568 Donkey anti-goat	Invitrogen #A11057	1:500
Alexa Fluor 680 Donkey anti-goat	Invitrogen #21084	1:500
DAPI	Sigma #32670	1:1000

3. Taula. Sagu ehunean eta hazkuntza zelularretan erabilitako antigorputz sekundarioak.

IHC-RAKO ANTIGORPUTZ PRIMARIOAK		
ANTIGORPUTZA	**KONPAINIA**	**DILUZIOA**
Rabbit anti-Tbr2	Abcam Inc #ab23345	1:1000
Chicken anti-GFAP	Abcam #ab134436	1:750
Rabbit anti-Ki67	BD Pharmigen #550609	1:200
Rabbit anti-Hopx	Sigma-Aldrich #HPA030180	1:200
Rabbit anti- S100B	Sigma-Aldrich #HPA015768	1:750
Mouse anti-Nestin	Covance #AB291466	1:250
Mouse anti-Vimentin	Sigma-Aldrich #V2258	1:1000

4. Taula. Giza ehunean erabilitako antigorputz primarioak.

5.8. WB

Esperimentuaren arabera, hipokanpo ehuna edo hazitako NSPCak adierazitako denboretan bilduak izan ziren RIPA tanpoia proteasa inhibitzaile koktelarekin eta fosfatasa inhibitzaileekin nahasturik erabiliz. Lagin bakoitza -80ºCtan gordea izan zen erabili arte. Esperimentu egunean, laginak homogeneizatuak eta 10 minutuz 14000 rpm-tan zentrifugatuak izan ziren. Proteina gainjalkina (20 µg) %10 Tris-Glizina geletan kargatua eta nitrozelulosa mintz batera (Life technologies, #88018) transferitua izan zen. Ponceau tindaketa (Sigma-Aldrich, #P7170) mintzetan gauzatu zen proteinaren eta bandaren migrazio zuzena egiaztatzeko asmoz. Gure intereseko proteinak tindatzeko, mintzak %5 gantzik gabeko lehorturiko esnea TBS-Tn (150mM NaCl, 20 mM Tris-HCl, pH 7.5, %0.05 Tween 20) blokeatuak izan ziren ordubetez, ondoren antigorputz primarioekin **(5. Taula)** bi orduz inkubatuak izateko. TBS-Tn hiru garbiketa

egin ostean, mintzak antigorputz sekundarioekin **(6. Taula)** inkubatuak izan ziren beste ordubetez eta ECL Supersignal (Thermo Fisher, #34095) WB analisi sistemaren bitartez irudikatuak.

WB-ERAKO ANTIGORPUTZ PRIMARIOAK		
ANTIGORPUTZA	**KONPAINIA**	**DILUZIOA**
Rabbit anti- ß-actin	Cell Signaling #4970	1:1000
Mouse anti-EGFR	Abcam #ab8465	1:1000
Rabbit anti-AKT	Cell signaling #9272	1:1000
Rabbit anti-ERK	Cell signaling #9102	1:1000
Rabbit anti-STAT3	Cell signaling #12640	1:2000
Rabbit anti-FGFR	Cell signaling #9740	1:1000
Rabbit anti- MT1/2	Thermo Fisher #MA1-25479	1:1000
Rabbit anti-pEGFR (Y1068)	Cell Signaling #2234	1:1000
Rabbit anti-pEGFR (Y845)	Cell Signaling #2231	1:1000
Rabbit anti-pAKT (Ser473)	Cell Signaling #3787	1:1000
Rabbit anti-pERK (Tyr 202/204)	Cell Signaling #9101	1:2000
Rabbit anti-pSTAT3 (Tyr 705)	Cell Signaling #9145	1:1000

5. Taula. WBerako erabilitako antigorputz primarioak.

WB-ERAKO ANTIGORPUTZ SEKUNDARIOAK		
ANTIGORPUTZA	**KONPAINIA**	**DILUZIOA**
HRP-conjugated anti-rabbit	Life technologies #65-6120	1:1000
HRP-conjugated anti-mouse	Life technologies #62-6520	1:1000

6. Taula. WBerako erabilitako antigorputz sekundarioak.

5.9. ELISA

NSPCtan edo KAra esposaturiko garun ehunean HB-EGF maila neurtzeko xedez, “R&D DuoSet Immunoassay” erabili genuen, aurretiaz deskribaturik bezala (Luzuriaga et al., 2019). Bai zelula alea zein garun ehuna Hepes 25 mM, 5 $MgCl_2$ 5 mM EGTA 1 mM, EDTA 1.3 mM, PMSF 1 mM eta proteasa eta fosfatasa koktel inhibitzaileak zituen tanpoia erabiliz lisatuak izan ziren (Thermo Fisher, #88665 eta #78420).

Hazkuntza zelularren kasuan, 96 putzuko plaka batean hazkuntza faktorerik gabeko150 µl kultibo medio erabiliz 250.000 zelula hazi ziren. Medioa, zelulak barne, plakan jarri eta 72 ordura bildua izan zen. 4ºCtan, 14.000 rpm-tan 10 minutuz zentrifugatu ostean, ondorengo analisiak egiteko lisaturiko zelula alearen eta/edo gainjalkinaren 100 µl erreaktibo diluentean 1:1 diluituak izan ziren. Baldintza paralelotan, 72 orduko kultiboaren segidan, zelula kopurua Bio-Rad TC20 zelula kontatzaile automatizatua erabiliz zenbatua izan zen, era berean zelula hilak markatu eta baztertzeko asmoz trypan urdina erabiliz. Hala, esperimentu amaieran zelula bakoitzeko HB-EGF kopurua kalkulatu genuen.

Garun ehunean zegoen HB-EGF kopuruaren analisirako, saguak CO_2 kamera baten 0, 1.5, 12, 24 eta 72 ordu KA edo disoluzio isotoniko administrazioa eta gero (n=4 kondizioko) sakon anestesiatuak izan ziren. Euren hipokanpoak izotzean erauziak eta laster izotz lehorraren bitartez izoztuak izan ziren. Laginak lisis tanpoian homogenizatuak eta segituan zentrifugatuak izan ziren (20 minutu 14000 rpm-tan 4ºCtan). Gainjalkinak bildu eta proteina kopuru totala BCA proteina saiakera kita (Pierce, #23227) erabiliz neurtua izan zen. 1:1 erlazioan disolbaturik erreaktibo diluente tanpoian 100 µg proteina kargatu ziren puntu bakoitzerako.

Biak *in vitro* eta *in vivo* kuantifikazioak hurrengo lau parametro logistikoak erabiliz burutuak izan ziren:

$$y = d + \frac{a - d}{1 + \left(\frac{x}{c}\right)^b}$$

Non *x* eta *y* aldagai aske eta mendekoak ziren, *a* eta *d* neurturiko balio minimo eta maximoak ziren, *c* inflexio puntua zen, *a* eta *d* erdibidea eta *b* kurban Hillen aldapa zen (Kurbaren malda *c* puntuan).

In vitro analisietan balioak normalizatuak eta HB-EGF pg/ml bezala aurkeztuak izan ziren eta *in vivo* analisietan balioak HB-EGF pg ehun proteina µg-ko bezala kalkulatuak izan ziren.

5.10. Danscher tindaketa

Danscher metodo autometalografiko ez zuzena egiteko, 20 mg/Kg sodio selenito %4 PFA- %0.5 Glutaraldehido perfusioa baino 30 minutu lehenago intraperitonealki injektatuak izan ziren eta ehuna 50 µm-ko sekzio serialetan prozesatua izan zen. Tindaketa aurretiaz deskribatu izan den bezala burutua izan zen (López-García et al., 2002). Granuloen tamaina eta kuantifikazioa GFP zelula eremuaren interes gunea (ingelesetik region of interest, ROI) determinatuz eta ImageJ softwarea erabiliz eraman zen aurrera (15-20 zelula kondizioko).

5.11. Irudien analisia

Fluoreszentzia IHC irudien gehiengoa Leica SP8 laser eskaner mikroskopio konfokal baten 40X olio-murgilketa objektiboa erabiliz bilduak izan ziren. DGaren area totalen kuantifikaziorako 10X objektiboa erabili zen sekzio bakoitzean DGa guztiz irudikatzeko asmotan. Garapeneko DGaren irudiak hartzeko, non DMS irudikaturik agertzen den, eta baita giza ehunean eginiko irudi guztientzako ere, “3DHistech panoramic digital slidescanner” izenekoa erabili zen. Fluorokromo bakoitzaren seinalea sekuentzietan bildua izan zen eta argitasuna, kontrastea eta atzealdea irudi osoan berdin orekatuak izan ziren Leica LAS X Life Science mikroskopio konfokalaren softwarea erabiliz.

5.11.1. Zelula populazioen analisi kuantitatiboa

Zelula populazioen analisi kuantitatiboa moldaturiko zatitzaile optiko sekzio eskema bat erabiliz *in vivo* diseinuan oinarritutako estereologia erabiliz gauzatu zen,

aurretiaz deskribaturiko eran (Encinas and Enikolopov, 2008; Encinas et al., 2006, 2011).

Zelula dentsitateentzako, kuantifikazioak kondizioen artean z-pilaketa tamaina berdinak mantenduz gauzatu zen. Kuantifikaturiko arean balioak SGZ+GCL bolumenera normalizatuak izan ziren. Zenbaketa totalentzako, DGaren area guztia serie bakoitzeko sekzio guztietan zehaztua izan zen, lortutako balioa ondoren GCLaren zabalerarengandik biderkatua izateko, zeina gutxienez sekzio bakoitzaren hiru puntu ezberdinetan kalkulatua izan zen. DG osoaren bolumena lortzeko lortutako balioa bost aldiz biderkatua izan zen.

P14 baino lehenagoko jaio ondorengo esperimentuetan, non NSCak ez diren oraindik helduak (Brunne et al., 2013; Nicola et al., 2015), zelulak dNSC bezala kuantifikatuak izan ziren euren soma GCL barruan zutenean, hala nola hurrengo irizpideak betetzen zituztenean: Ondo deskribaturiko NSC markatzaile Nestin-GFPren eta GFAPren espresioa (Encinas and Enikolopov, 2008; Kronenberg et al., 2003; Seri et al., 2001) eta MLarengana luzaturiko prozesu ererradialaren presentzia. P14 geroztik, NSCak aurretiaz deskribaturiko irizpideak jarraituz zenbatu ziren (Encinas and Enikolopov, 2008; Kronenberg et al., 2003). Ugaritze fasean aurkitzen ziren zelulak identifikatzeko, Ki67 ziklo zelular markatzailea erabili zen. Markatzaile honentzat positiboak ziren eta lehenago deskribaturiko irizpideak betetzen zituzten NSCak ugaritze fasean sarturiko dNSC/NSC bezala zenbatu ziren. DG sekzioren GCLean1024x1024 marko tamainazko 3-4 z-pilaketa ausaz aukeratu ziren 3-5 (animaliaren adinaren arabera). Ehun helduko sekzioetan, hipokanpo sekzio bakoitzeko 3-4 z-pilaketa DGan ausaz kokaturiko eremuetan batu ziren eta serie bakoitzeko 4-6 sekzio analizatu ziren, esperimentuaren arabera. Hazkuntza zelularretan, lagin eta kondizio bakoitzeko estalkiaren ausazko eremuetan 4 µm-lodiko 5 z-pilaketa bildu ziren.

SFFV-RV infekzioak erabili ziren esperimentuetan, kondizio bakoitzeko GCLean infektaturiko zelula guztiak kuantifikatu genituen. Halaber, infektaturiko eremuan zeuden NSC zenbakia kuantifikatu genuen (zelula SFFV-RV-positiboak zituen eremua), kondizio bakoitzean SFFV-RVarekin infektaturiko NSC portzentajea lortzeko asmoz.

Zelula heriotza neurtzeko, zelula apoptotikoak morfologia nuklear anormala zuten zelula bezala definituak izan ziren (piknotikoak/karriorektikoak). MTLE

esperimentuetan, GCDa DAPIrekin eta NeuNrekin tindatutako sekzioetan neurtua izan zen.

KA administrazio osteko EGFR espresioaren analisietan, ImageJrentzako kode irekiko plugin bat erabili zen. Labur, EGFRk okupaturiko pixelen area neurtua izan zen. Kondizio guztientzako zarata-tolerantzia berbera erabiliz area "find-maxima" aukerarekin kuantifikatu zen, EGFRk okupaturiko area totala lortuz.

NSPCen ugaritzea BrdU barneraketa kontutan hartuz neurtu zen. BrdU-positiboak ziren NSPCen proportzio erlatiboak kondizio eta estalki bakoitzeko zelula kopuru totalarekin (DAPI tindaketa) konparatu zen. Kondizio guztietako ugaritze kopurua kontrol kondizioko ugaritze kopuru basalarekin konparatua izan zen.

5.11.2. NSCen analisi morfologikoa: SHOLL analisia

3D konfokal argazkiak esportatuak izan ziren eta zelula morfologia NeuronStudio 0.9.92 softwarea erabiliz analizatua izan zen (Computational Neurobiology and Imaging Center Mount Sinai School of Medicine, New York, NY)(Rodriguez et al., 2006). Zelula guztiak batzeko asmoz emaitzak Excelera esportatuak izan ziren eta analisi estatistiko eta errepresentazio grafikoak egiteko GraphPad Prism v5 erabili zen.

5.12. Analisi estatistikoa

Analisi estatistikoak egiteko SigmaPlot (San Jose, CA, USA) erabili zen, analisi morfologikoen kasuan salbu, zeinetan GraphPad Prism v5 erabili zen. Talde biren arteko analisiak egiteko Studenten t testa erabili zen, datuak parametrikoak ez ziren kasuetan U-Mann Whitneyra joz. Bi talde baino gehiagoren presentzian, faktore bakoitzaren efektu jenerala ikusarazteko asmoz talde guztien bide bakarreko bariantza analisia (ingelesetik analysis of variance, ANOVA) testa erabili zen. Era berean, datuak parametrikoak suertatu ez ziren kasuetan Kruskal-Wallis testa erabili zen. Faktoreen arteko interakzioa detektatzeko, bide bikoitzeko ANOVA erabili zen. Kasu guztietan, *post-hoc* test bezala faktore bakoitzeko taldeen arteko esangura determinatzeko binakako konparazio anizkoitzak (Holm-Sidak, Dunn or Student-Newman-Keuls test) erabili ziren eta kontrol taldearekin alderatuz faktore bakoitzaren esangura determinatzeko kontrol taldearekiko konparaketak (Holm-Sidak, Dunn, Dunnet or Tukey test). ANOVA baldintzekin (normaltasun eta homozedastizitatea) betetzeko behar zuten kasuetan datuen transformazio logaritmikoa gauzatu zen. $p<0.05$ estatistikoki esanguratsu bezala ulertu zen. Emaitzak batez besteko ± errore

estandarraren batez bestekoa (ingelesetik standard error mean, SEM) bezala aurkeztuak izan ziren. Esperimentu independente zenbakia dagokion sekzioan aurkezten da.

6. EMAITZAK

6. EMAITZAK

6.1. cD2 ezinbestekoa da NSC helduen populazioa sortu dadin

Jaio ondorengo ugaritzeak NSC helduen sorkuntzan duen papera ikertzeko xedez, DGaren garapena *cD2*ren presentzian (WT) zein absentzian (*cD2*KO) aztertu genuen; ziklo zelularrean G1 fasetik S fasera bideko trantsizioan parte hartzen duen faktore garrantzitsu bat (Matsushime et al., 1992; Meyerson and Harlow, 1994; Sherr, 1995). *cD2*KO saguek AHN maila arbuiagarria aurkezten dutela deskribatu izan da (Ansorg et al., 2012), nahiz eta oraindik hau NSC helduen kapazitate neurogenikoaren gaitz baten poderioz den edo ostera, NSC populazioaren formakuntzan jaio ondoren suertaturiko akats baten poderioz ezezaguna den. Hemen, Nestin-GFP/*cD2*KO eta Nestin-GFP/WT sagu mutanteetan jaio ondorengo bost denbora puntu ezberdinetan (P0, P7, P10, P14 and P28) NSCak irudikatu genituen **(R1-R3 Figurak)**, NSC bezala definituz GCLean kokaturiko, Nestin-GFP eta GFAP espresatzen zuten eta MLrantza prozesu erradial bat luzatzen zuten zelula haiek.

6.1.1. cD2ren absentzian, NSC helduen populazioa ez da sortzen

DGaren enbrioi aroko garapena, jaio ondorengo aro goiztiarra iristen den arte, antzekoa da WT eta *cD2*KO saguetan (Kowalczyk et al., 2004). Halere, azken hauetan ugaritze orokorra GCLean P7tik aurrera gutxitu egiten da eta AHNa oso urria da (Ansorg et al., 2012). Honela, geure buruari galdetu genion AHNren absentzia NSCen ahalmen neurogenikoaren gaitzaren ondorioa edo euren formazioan/establezimenduan gertaturiko akatsen baten efektua ote zen. Hemen, *cD2*KO eta WT saguetan estereologia, espresio markatzaile zorrotzak eta NSCak definitzeko irizpide morfologikoak (Nestin eta GFAP espresioa, GCLean kokaturiko soma, MLrentzat luzaturiko prozesua eta brokoli formako koroa) erabiliz, GCLean presente zeuden NSCen zenbaki eta ugaritze dinamikak (Ki67 espresioa baliatuz) aztertu genituen jaio ondorengo adin ezberdinetan (P0, P7, P10, P14 and P28) **(R1-R3 Figurak)**. Era berean, DAPI erabiliz GCLaren bolumena neurtu genuen. Gutxienez jaio ondorengo etapak iraun bitartean dNSC eta NSC helduen arteko bereizketa argi ez dagoenez (beranduago helduko diogun gaia izanik) eta NSC helduen populazioaren sorkuntza momentu zehatzak ezezagun darraionez, bi NSC moten arteko bereizketa egiteko irizpide tenporalak erabili genituen. Populazio mailan, NSCak heldu bezala onartzen

dira P14tik aurrera (Nicola et al., 2015) eta honegatik, GCLeko NSCak dNSC bezala identifikatu genituen P14ren aurretik eta NSC heldu bezala ondoren.

Gure emaitzek adierazi zutenez, bi kondizioak konparatuta P0n dNSCen morfologia antzekoa zen, GCLean kokaturiko dNSC zenbakia eta GCL bolumena bezalaxe **(R1 A-F Figurak)**. Hala ere, antzekotasun hauek P7ra iritsitakoan aldatu egin ziren. *cD2* gabe, GCL txikiago bat argi ikus zitekeen, dNSCak era esanguratsuan gutxituak zeuden WT saguekin alderatuz eta morfologia arraroa erakusten zuten, prozesu laburragoarekin **(R1 I-N Figurak)**. Ziklo zelularraren markatzailea den Ki67 erabiliz, dNSCtan zelula dibisioa gaitzesturik ba ote zegoen ere ebaluatu genuen, adin-puntu bakoitzean ugaritzen zebiltzan zelulak kuantifikatuz. *cD2*KO saguetan ugaritze prozesuan mantentzen zen zelulen kopuru totala eta proportzioa ez zen diferentea ez P0n ezta P7n ere ez, nahiz eta P7n ugaritze prozesuan zeuden dNSCen gutxitze bat agertzeko tendentzia zegoen **(R1 G-H;O-P Figurak)**.

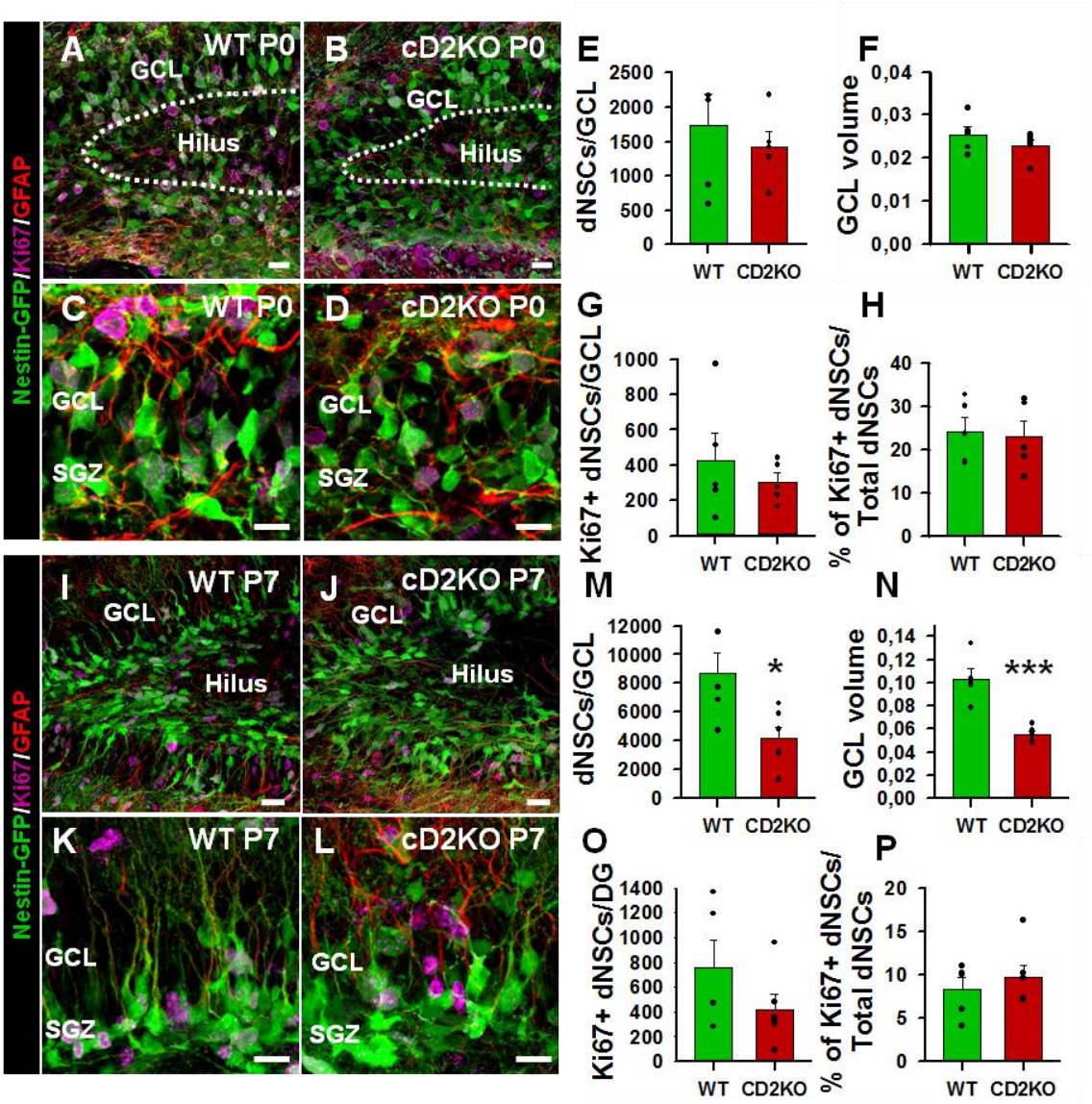

R1 Figura. *cD2*KO saguetan, jaio ondorengo lehenengo asteetan dNSCak ez ziren era egokian areagotzen. A-D) dNSCen eta ugaritze prozesuan zeuden zelulen (Ki67) (Nestin-GFP /GFAP) konfokal irudi errepresentatiboak WT eta *cD2*KO saguen DGan P0n. **E)** WT eta *cD2*KO saguen GCLean P0n eginiko dNSC kopuru totalaren kuantifikazioa. **F)** WT eta *cD2*KO saguetan P0n eginiko GCL bolumenaren kuantifikazioa. **G)** WT eta *cD2*KO saguen GCLean P0n eginiko ugaritze prozesuan zeuden dNSC kopuru totalaren kuantifikazioa. **H)** WT eta *cD2*KO saguen GCLean P0n eginiko ugaritze prozesuan zeuden dNSC portzentaiaren kuantifikazioa. **I-L)** dNSCen (Nestin-GFP /GFAP) eta ugaritze prozesuan zeuden zelulen (Ki67) konfokal irudi errepresentatiboak WT eta *cD2*KO saguen DGan P7n. **M)** WT eta *cD2*KO saguen GCLean P7n eginiko dNSC kopuru totalaren kuantifikazioa. **N)** WT eta *cD2*KO saguetan P7n eginiko GCL bolumenaren kuantifikazioa. **O)** WT eta *cD2*KO saguen GCLean P7n eginiko ugaritze prozesuan zeuden dNSC kopuru totalaren kuantifikazioa. **P)** WT eta *cD2*KO saguen GCLean P7n eginiko ugaritze prozesuan zeuden dNSC portzentajearen kuantifikazioa. *GCL: Zelula granular geruza. SGZ: Gune azpigranularra. Eskala barrak 10 µm-koak dira. *p<0.05 eta ***p<0.001 Student 's t-test. Barrek batez bestekoa ± errore estandarra erakusten dute. Puntuek datu indibidualak erakusten dituzte.*

P14n, hipokanpoko gune neurogenikoa jada heldu kontsideratzen denean (Nicola et al., 2015), *cD2*KO saguetan NSCak morfolokoki ezberdinak ziren **(R2 A-D Figura)** eta WT saguekin alderatuta kopurua era esanguratsuan gutxitua zegoen **(R2 E Figura)**. Era berean, *cD2*ren faltan GCL bolumena askoz ere txikiagoa zen **(R2 F Figura)** eta ugaritze fasean zeuden NSCen zenbakia ere era esanguratsuan murriztua zegoen **(R2 G Figura)**, nahiz eta NSC guztien artean ugaritze prozesuan zeuden NSCen portzentaia aldakaitz aurkezten zen **(R2 H Figura)**. Are gehiago, P14n ikusiriko diferentziak P28n areagotu egin ziren; *cD2*KO saguetan geratzen ziren NSC bakanak morfologikoki aberranteak ziren **(R2 I-L Figura)**, NSC kopurua 3 aldiz baino gehiago murrizturik zegoen eta GCL bolumena %50 txikiagoa zen **(R2 M-N Figura)**. Baita, P28n NSC ugaritzea nabari gaitzetsia zegoen, ugaritze prozesuan zeuden NSC kopuru eta portzentaje arbuiagarriarekin **(R2 O-P Figura)**.

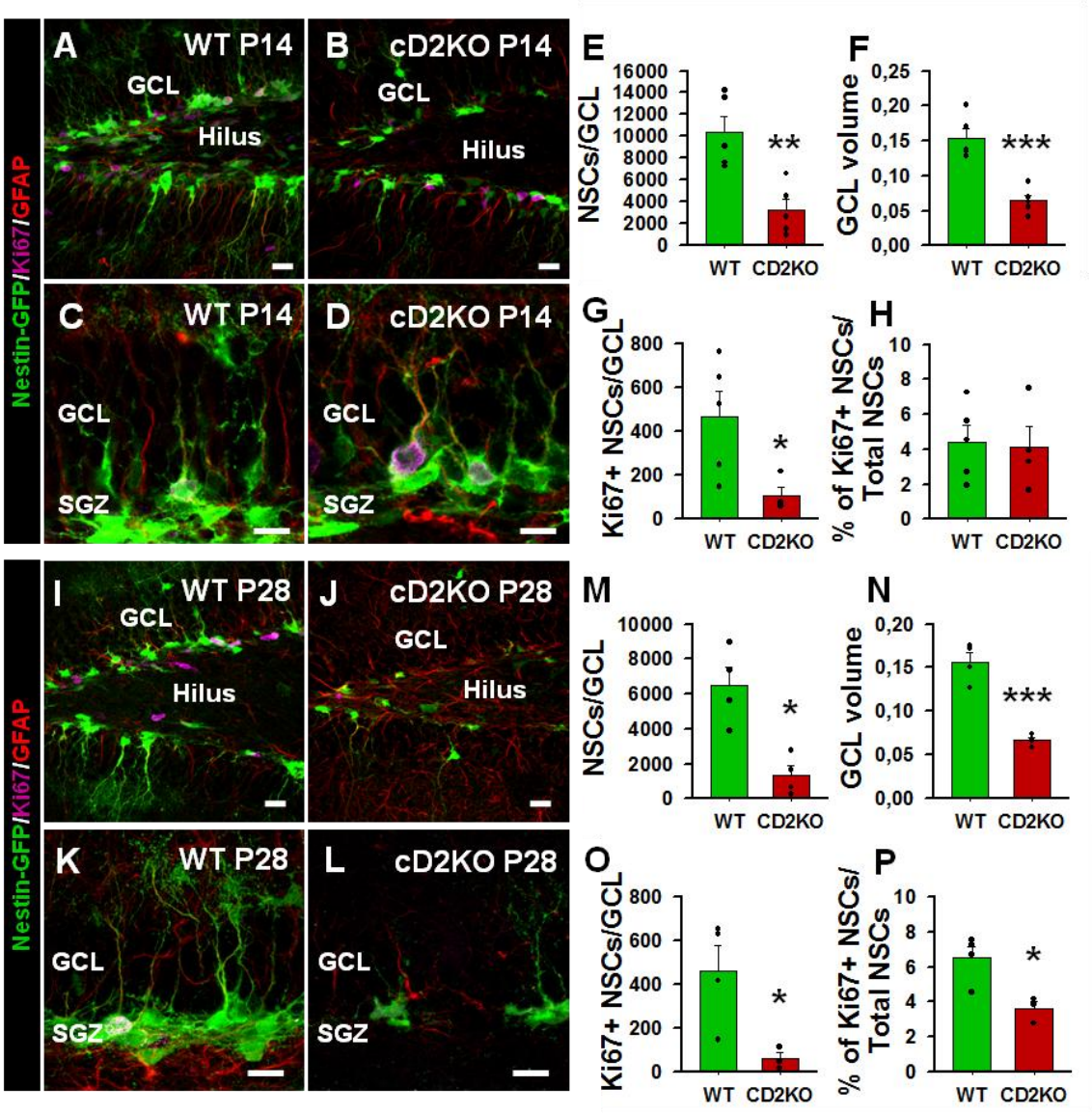

R2 Figura. *cD2ren* gabezian, NSC helduen populazioa ez da guztiz sortzen, P28 bezain goiz agortzen delarik. A-D) NSCen (Nestin-GFP /GFAP) eta ugaritze prozesuan zeuden zelulen (Ki67) konfokal irudi errepresentatiboak WT eta *cD2*KO saguen DGan P14n. **E)** WT eta *cD2*KO saguen GCLean P14n eginiko NSC kopuru totalaren kuantifikazioa. **F)** WT eta *cD2*KO saguetan P14n eginiko GCL bolumenaren kuantifikazioa. **G)** WT eta *cD2*KO saguen GCLean P14n eginiko ugaritze prozesuan zeuden NSC kopuru totalaren kuantifikazioa. **H)** WT eta *cD2*KO saguen GCLean P14n eginiko ugaritze prozesuan zeuden NSC portzentajearen kuantifikazioa. **I-L)** NSCen (Nestin-GFP /GFAP) eta ugaritze prozesuan zeuden zelulen (Ki67) konfokal irudi errepresentatiboak WT eta *cD2*KO saguen DGan P28n. **M)** WT eta *cD2*KO saguen GCLean P28n eginiko NSC kopuru totalaren kuantifikazioa. **N)** WT eta *cD2*KO saguetan P28n eginiko GCL bolumenaren kuantifikazioa. **O)** WT eta *cD2*KO saguen GCLean P28n eginiko ugaritze prozesuan zeuden NSC kopuru totalaren kuantifikazioa. **P)** WT eta *cD2*KO saguen GCLean P28n eginiko ugaritze prozesuan zeuden NSC portzentajearen kuantifikazioa. *GCL: Zelula granular geruza. SGZ: Gune azpigranularra. Eskala barrak 10 µm-koak dira.*p<0.05, **p<0.001 eta ***p<0.001 Student's t-test. Barrek batez bestekoa ± errore estandarra erakusten dute. Puntuek datu indibidualak erakusten dituzte.*

Laburbilduz, *cD2*ren gabezian DGa ez zen era egokian sortu eta dNSCak ez ziren P0-P14 artean zegokien bezala hedatu **(R3 A-F; I-J Figura)**. Horrenbestez, P14 geroztik *cD2*KO saguen DGak franko NSC gutxiago biltzen zituen, populazioaren ia agorpen osoa ekarriz P28 bezain pronto **(R3 G-I Figura)**. Gainera, *cD2*KO animalietan P7tik aurrera NSCen ugaritze fasean gutxiago sartzeko tendentzia ikusi zen, P28n estatistikoki esanguratsua izanik **(R3 K Figura)**. Halere, dibisioan zeuden NSCen portzentajea P28 arte aldatu barik mantendu zen, nahiz eta adin honetan *cD2*KO saguetan dibisioan zeuden NSC gutxiago egoteko tendentzia ikusi zen **(R3 L Figura)**. Hala, *cD2*KO saguetan ikusitako NSC populazioaren murriztea dNSCek jaio ondorengo etapan dituzten dinamika aberranteen ondorio bat izan litzake (zelula biziraupen eta apoptosiarekin erlazionatuak), zeinek NSCen sorkuntza egokia ekidingo luketen.

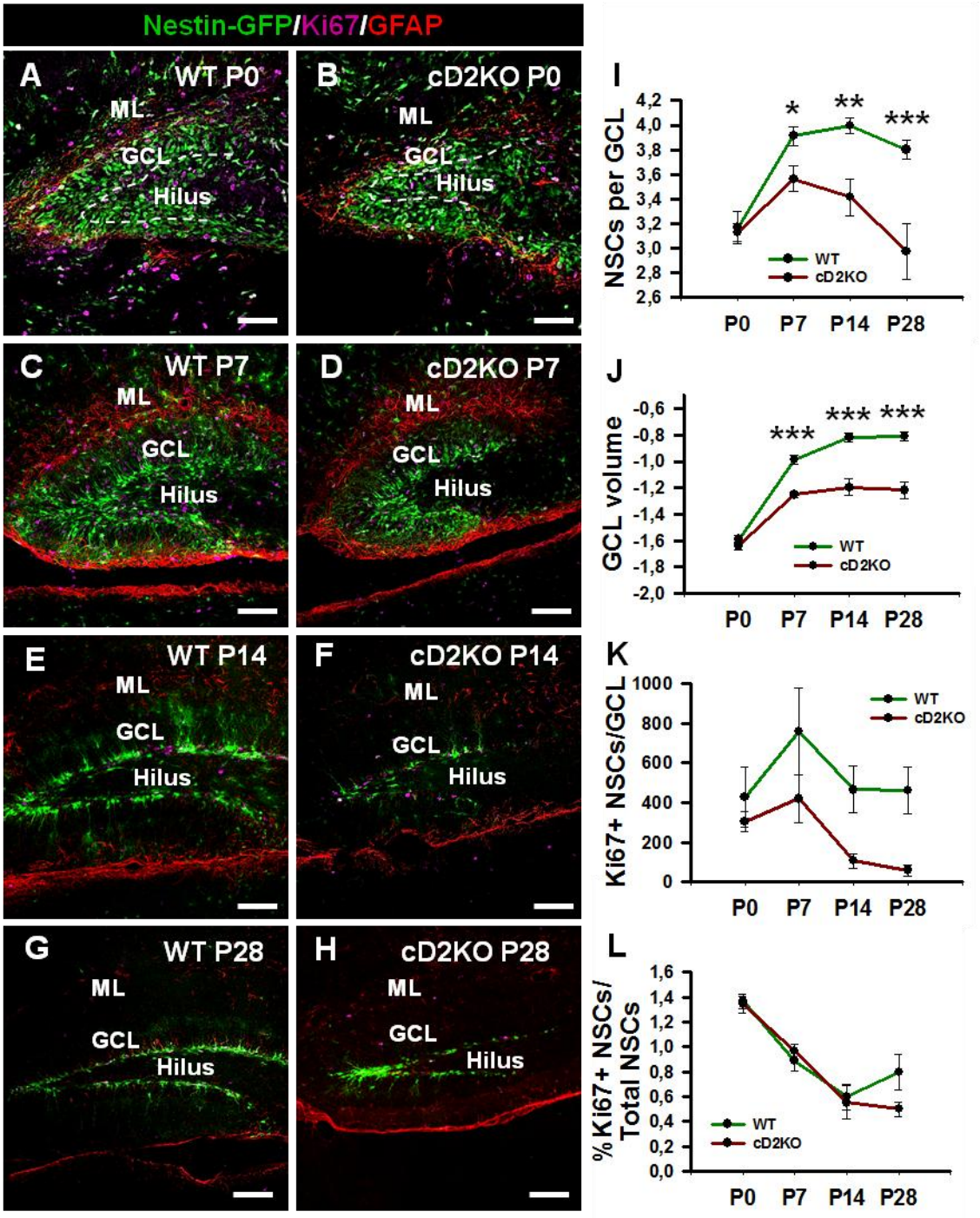

R3 Figura. *cD2* gabeko saguetan NSC populazioa ez da guztiz sortzen jaio ondorengo lehen bi asteetan zehar. A-D) NSCen (Nestin-GFP /GFAP) eta ugaritze prozesuan zeuden zelulen (Ki67) konfokal irudi errepresentatiboak WT eta *cD2*KO saguen DGan P0tik P28ra. **E)** WT eta *cD2*KO saguen GCLean eginiko NSC kopuru totalaren kuantifikazioa P0tik P28ra. **F)** WT eta *cD2*KO saguetan eginiko GCL bolumenaren kuantifikazioa P0tik P28ra. **G)** WT eta *cD2*KO saguen GCLean eginiko ugaritze prozesuan zeuden NSC kopuru totalaren kuantifikazioa P0tik P28ra. **H)** WT eta *cD2*KO saguen GCLean eginiko ugaritze prozesuan zeuden NSC portzentajearen kuantifikazioa P0tik P28ra. *GCL: Zelula granular geruza. SGZ: Gune azpigranularra. Eskala barrak 10 µm-koak dira. *p<0.05, **p<0.01 eta ***p<0.001. Bide bikoitzeko ANOVA Holm-Sidak post-hoc testaren bidezko binakako konparazio anizkoitzez jarraitua.*

Puntuek batez bestekoa ± errore estandarra erakusten dute. Normaltasun eta homozedastizitatearekin betetzeko datu guztiak Log_{10}era transformatuak izan ziren.

6.1.2. *cD2*ren gabezian heriotza zelularra ez zen areagotu

Ondoren *cD2*KO saguetan jaio ondoren ematen den NSC populazioaren sorkuntza murriztua dNSCetan emandako heriotza zelularraren areagotze baten ondorioz gerta ote zitekeen ikertu genuen. Heriotza zelularra ebaluatzeko, GCLean adin-puntu bakoitzean (P0, P7, P14, P28) nukleo piknotikoen dentsitatea kuantifikatu genuen **(R4 E-F Figura)**, piknosiak nekrosia edo apoptosia pairatzen ari diren kromatinaren kondentsazio itzulezina adierazten duelarik (Burgoyne, 1999). Emaitzek nukleo piknotikoen alteraziorik eza erakutsi zuten P0 eta P7 adin-puntuetan **(R4 F Figura)**. Halere, P14 geroztik *cD2*KO saguetan nukleo piknotiko gutxiago ageri ziren **(R4 A-D; F Figura)**, NSC eta neurogenesi gutxiago egoteak azaldu lezakeena. Horrela, *cD2*ren gabezian dNSCek WTean ematen diren dinamika apoptotiko berak jarraituz burutu zuten euren garapena, P14 eta gero heroitza zelularra gutxitzen den arren, murriztutako gune neurogeniko eta ugaritze kapazitatearekin bat etorriz.

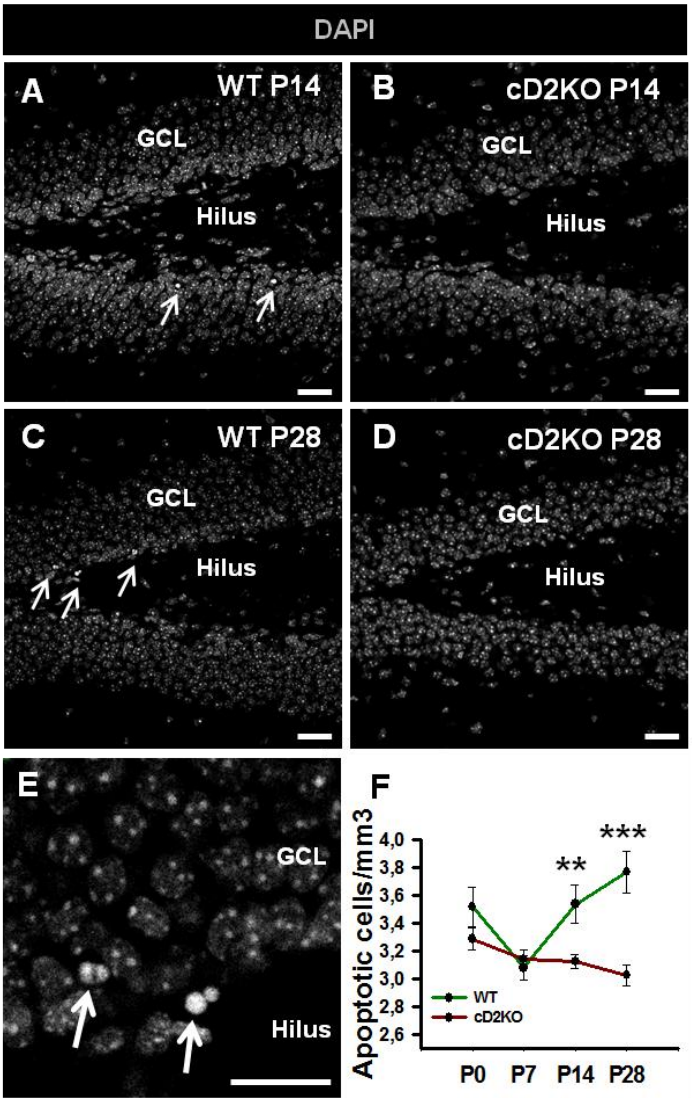

R4 Figura. Gune neurogenikoaren formazioa osatu artean *cD2ren* gabeziak ez ditu dinamika apoptotikoak alteratzen. A-D) Irudi konfokal errepresentatiboak WT eta *cD2*KO saguen GCLa erakutsiz P14n. Geziek zelula apoptotikoak adierazten dituzte WT sagu batean. **E)** Zelula apoptotiko baten konfokal irudi errepresentatiboa. **F)** Jaio ondorengo DGaren formazioan zehar adin desberdinetan (P0, P7, P14, P28) eginiko heriotza zelular dentsitatearen kuantifikazioa. *GCL: Zelula granular geruza. Eskala barrak 10 µm-koak dira A-Dn eta 5 µm-koak E-n. **p<0.01 eta ***p<0.001. Bide bikoitzeko ANOVA Holm-Sidak post-hoc testaren bidezko binakako konparazio anizkoitzez jarraitua. Puntuek batez bestekoa ± errore estandarra erakusten dute. Ikusarazte eta estatistika errazteko, datu guztiak log10 eskala batean irudikatuak agertzen dira. Normaltasun eta homozedastizitatearekin betetzeko datu guztiak Log$_{10}$era transformatuak izan ziren.*

6.2. NSC helduen populazioaren jaio ondorengo sorkuntza

Gure aurreko emaitzek NSC helduen erreserba sor zedin jaio ondorengo ugaritzea ezinbestekoa zela erakutsi zuten, *cD2*ren menpekoa zen prozesu batean. Hori bakarrik ez eta DGaren formazio etapan, jaio ondorengo periodoa barne, HPFko hainbat eremutan aldi baterako gune neurogeniko/gliogeniko anitz sortu egiten dira (Hodge et al., 2013; Li et al., 2013). Aldi baterako gune neurogeniko/gliogenikoetako bat DMSa da, enbrioi garapen goiztiarrean sortzen den korronte migratzaile bat, DNetik DGra doazen dNSCez eta sortzailez osatua. Nabarmen, jaio ondorengo etapa goiztiarrean zehar DMSa aktibo mantentzen da (Hodge et al., 2013; Li et al., 2013; Nakahira and Yuasa, 2005; Sugiyama et al., 2013). Hau kontuan harturik, HPFko bi leku desberdin hauetan kokaturiko aitzindariek, hau da DG barrualdean kokatuta daundenek eta DMStik datozenek (Altman and Bayer, 1990; Berg et al., 2019; Hodge

et al., 2013; Sugiyama et al., 2013), DGaren formazioari egiten dioten ekarpena ikertu genuen, jaio ondorengo etapan kontzentratuz.

6.2.1. *In vivo* infekzio erretrobiralak NSC helduen jatorri espaziala identifikatzeko

DGaren barruan edo DMSean kokaturiko sortzaileak era diferentzialean markatzeko asmoz, injekzio erretrobiralak erabili genituen, mitosi fasean dauden zelulek soilik barneratzen dituztenak (Weber et al., 2012). SFFV-RVen difusio eta efizientzia eta gure injekzioen zehaztasuna frogatzeko asmoz, P2 eta P5 adinetan SFFV-RVmCherry bektore baten injekzio intrahipokanpalaren bitartez *in vivo* infektatu genituen saguak eta SFFV-RVarekin infektaturiko zelulen kokapena aztertu hortik gutxira (2 egun injekzioaren ondoren) **(R5 A Figura)**.

Bi injekzio paradigma ezberdin antolatu genituen. Lehenik, DGaren barnealdean injektatu genuen soilik hilus eta GCLean zeuden sortzaileak tindatzea bilatuz. Honek tindaketa DMStik baztertua zeuden injekzioak suertatu zituen **(R5 B-C Figura)**. Bigarren paradigman DGaren kanpoaldean injektatu genuen, DMSan zehazki. Injekzio mota hauekin DMSan ezarrita zeuden sortzaileak tindatu genituen DGaren barnealdeko sortzaile bakar bat ere ez infektatu barik **(Figure R5 D-E)**. Honela, bi injekzio paradigma hauek HPFko bi eremu desberdinetan kokaturiko sortzaileen leinua era independentean jarraitzeko eraginkorrak zirela frogatu genuen.

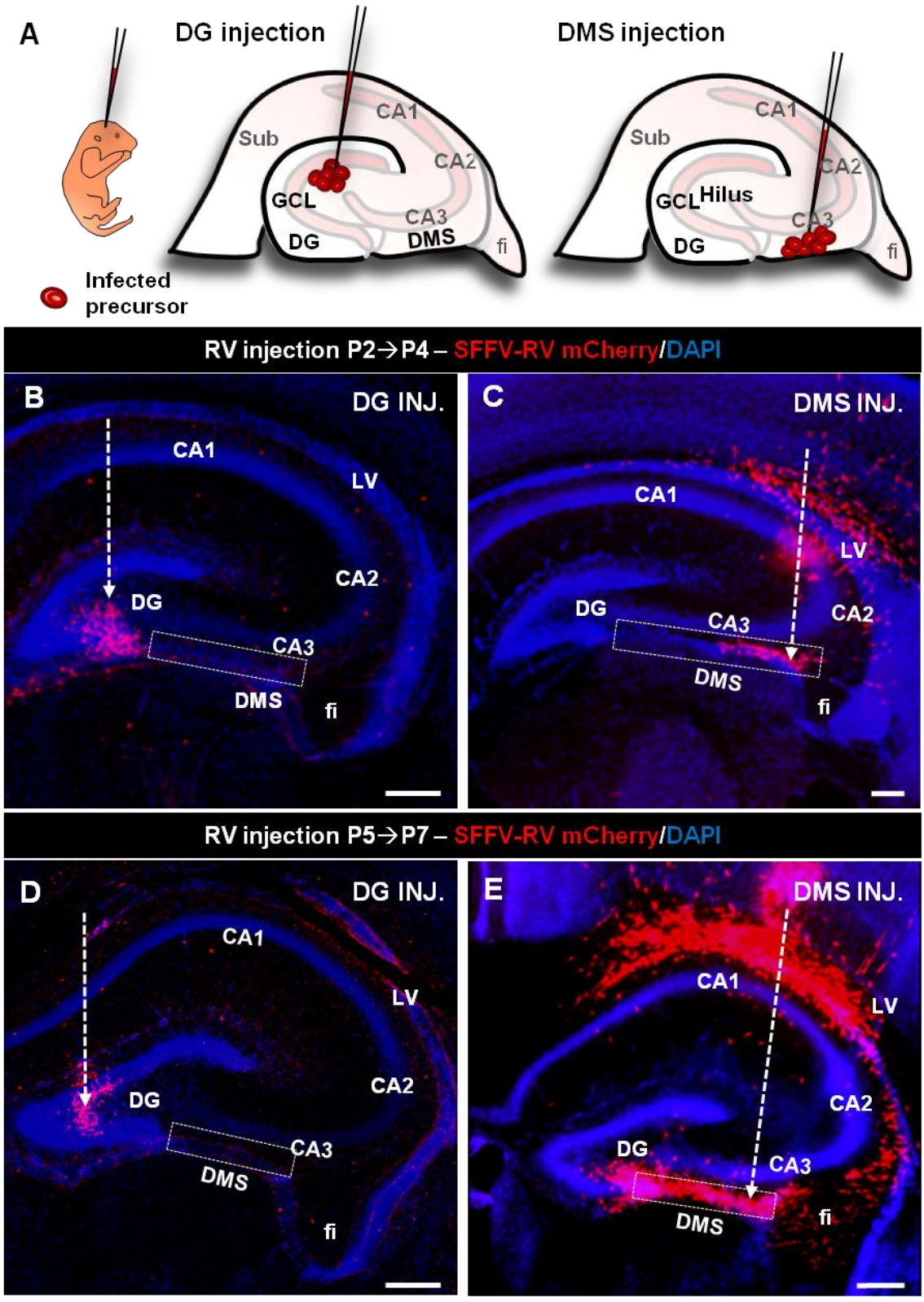
A
DG injection
DMS injection
CA1
Sub
CA2
GCL
Hilus
CA3
DG
DMS
fi
Infected precursor
RV injection P2→P4 – SFFV-RV mCherry/DAPI
B
DG INJ.
LV
C
DMS INJ.
RV injection P5→P7 – SFFV-RV mCherry/DAPI
D
E

← Aurreko orrialdean. R5 Figura. Jaio ondorengo SFFV-RV infekzioak HPFko populazio ezberdinak espazialki markatzeko erreminta gisa. A) Paradigma esperimentalaren eskema. **B-E)** Lamina-eskaner fluoreszente irudiak SFFV-RV infekzio espazial desberdinak erakutsiz. Kumeak P2 adinean injektatuak izan ziren bai DG barruan (A) zein DMSan (B) eta inkezioaren lekua P4n ebaluatua izan zen. **C-D)** Lamina-eskaner fluoreszente irudiak SFFV-RV infekzio espazial desberdinak erakutsiz. Kumeak P5 adinean injektatuak izan ziren bai DG barruan (A) zein DMSan (B) eta inkezioaren lekua P7n ebaluatua izan zen. Karratuak DMSa zehazten du eta geziak injekzio bidea. Bi adinetan, infektaturiko zelulak ez ziren inoiz aldi berean eremu bietan (DG eta DMSa) ikusi, injekzioak bata bestearen esklusiboak zirela adieraziz. *CA: Cornu ammonis. DG: Hortzdun zirkunboluzioa. DMS: Hortzdun migrazio korrontea. fi: fimbria. GCL: Zelula granular geruza. LV: Bentrikulu laterala. Eskala barrak 10 µm-koak dira.*

Bi paradigma hauen zelularen leinuaren jarraipen ahalmena haratago demostratzeko xedez, P2 adinean aldi berean bi injekzioak gauzatzea eta injekzio bakoitza gene erreportari fluoreszenteek kodetutako SFFV-RV ezberdinekin desberdintzea erabaki genuen. SFFV-RV-mCherry bektore bat DMSean eta SFFV-RV-mCerulean bektore bat DGan injektatu genituen, honela eremu bakoitzetik eratorritako leinuaren ezberdintzea ahalbidetuz **(R6 A Figura)**. P14an ebaluatu genuen infektaturiko sortzaileen leinua, garai hau izanik NSC helduak SGZan ezartzen diren garaia (Nicola et al., 2015), bi injekzioak diferente eta independenteak zirela ikusaraziz. Injekzioen kokapen ezberdinak (DGa eta DMSa) independenteki tindaturiko zelula populazioak ikusaraztea ekarri zuen, nahiz eta bi populazioek GCLean ezarririk amaitu. Are gehiago, DG injekzioetatik eratorriko zelulak ardatz rostrokaudalera mugatuago agertzen ziren bitartean, DMS injekzio modeloan infektaturiko zelulak HPFaren eremu dorsaletatik kaudaletara ikus zitezkeen **(R6 B-E Figura)**.

Hipokanpoko NSCak: Garapenetik Patologiara

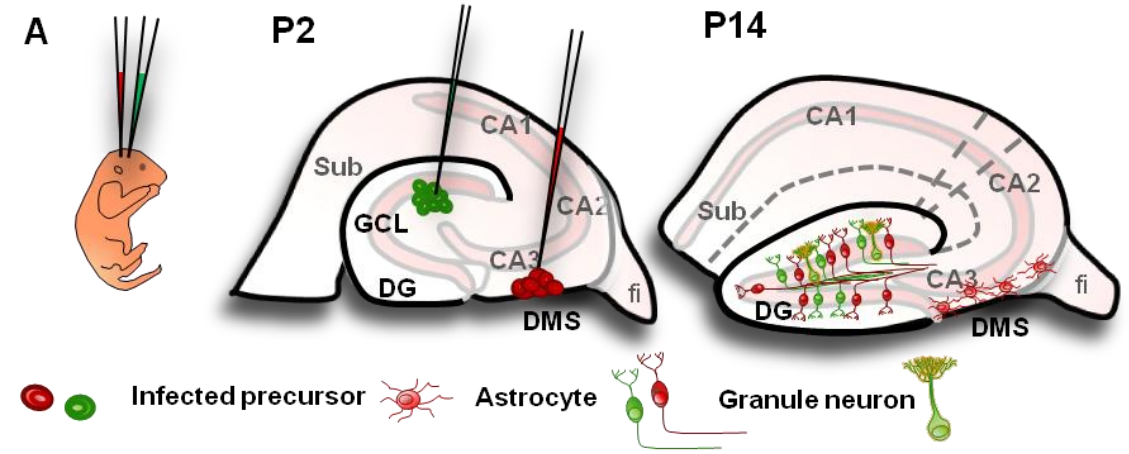

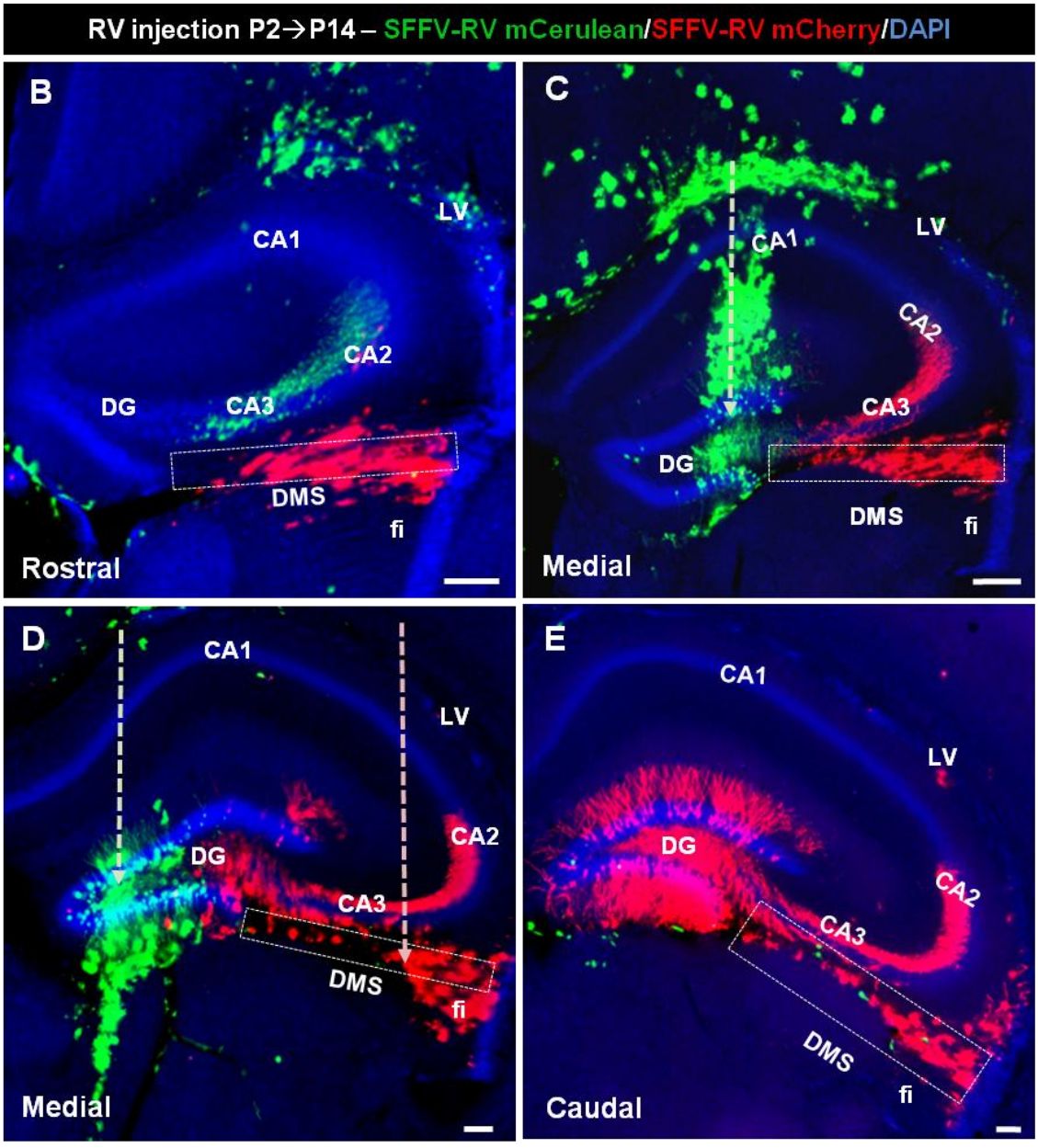

← Aurreko orrialdean. R6 Figura. Jaio ondorengo SFFV-RV infekzioek selektiboki tindatu zituzten injekzio tokiko sortzaileak, beste eremuarekin gainjarri barik. A) Paradigma esperimentalaren eskema. **B-E)** Lamina-eskaner fluoreszente irudiak SFFV-RV animali berean eginiko infekzio espazial desberdinak erakutsiz. Irudiak ardatz rostro-kaudalean zehar erakusten dira infekzioaren extensioaren era adierazgarri batean. Kumeak P2n injektatuak izan ziren DGaren barnealdean (berdez) edo DMSan (gorriz) eta injekzio lekua P14n ebaluatua izan zen. Karratuak DMSa zehazten du eta geziak injekzio bidea. Eremu ezberdinetatik eratorritako zelulak ez ziren inoiz gainjarririk agertu, nahiz eta zelula gehiengoaren helmuga GCLa zen bi injekzio mota kasuetan. Honek injekzioak elkarren artean esklusiboak zirela adierazi zuen. *CA: Cornu ammonis. DG: Hortzdun zirkunboluzioa. DMS: Hortzdun migrazio korrontea. fi: fimbria. GCL: Zelula granular geruza. LV: Bentrikulu laterala. Eskala barrak 10 µm-koak dira.*

6.2.2. NSC helduen populazioaren sorkuntzan soilik DG barruko aitzindariek egiten zuten ekarpena

Behin metodoa antolaturik, NSC helduen populazioaren jatorri espaziala identifikatzeko asmoz P2 eta P5 adinetan sortzaile hipokanpalen leinu osoa ikertu genuen. Horretarako, SFFV-RV-mCherry bektorea erabili genuen. Bi adinetan, DG injekzioean ostean DGa bera SFFV-RVarekin infektaturiko zelulez betea agertu zen maila medial eta medial-kaudaletan, zeinetan injekzioa gauzatua izan zen. Itxaron bezala, DMSan ez zen infektaturiko zelularik aurkitu **(R7 A Figura)**. Era berean, infektaturiko zelulen artean, gehienak neurona bezala identifikatu genituen, haien morfologia eta NSC/astrozito markatzaileen gabezia kontuan hartuz. GC hauen axoiak ikusi genituen DG rostralera iritsiz eremu hilarrean zehar **(R7 A Figura)**. Bestalde, DMS injekzioen ostean tindaturiko leinua DGaren eremu medial eta kaudaletan GCL osoan zehar ikusi zitekeen, neurona propietateak agertuz, euren axoiek DGaren parte rostralera iristen zirelarik. Horrez gain, injekzio mota hauetan DMSa maila rostraletik kaudalera SFFV-RV-mCherryarekin infektaturiko zelulaz betea agertu zen, beharbada jaio ondoren dibiditutako dNSCen diferentziazio glialaren ondorioz **(R7 B Figura)**.

P2n egindako DG injekzioen ostean, zelulak GCL osoan zehar banatuak zeuden, SGZa barne, DMSan injektaturiko zelulak GCLaren goialdera mugatuak zeudelarik, SGZa guztiz libre utzirik. Are gehiago, SFFV-RV-mCherry tindaturiko sortzaileek patu ezberdinak zituzten injekzio modeloaren arabera. DG infekzioetan, infektaturiko zelulen gehiengoa neuronak ziren (neurona morfologia dendrita eta axoiekin eta Nestin-GFP eta GFAP markatzaileen gabezia), baina bai SFFV-RV-mCherry zelula positibo guztien artean bai NSC guztien artean kuantifikatuta, SFFV-RV-mCherry zelula positiboen %4-5a NSC helduak suertatu ziren, euren Nestin-GFP eta GFAP espresioarengatik, morfologia erradialarengatik eta SGZan kokaturiko somarengatik identifikatuak. Kontrara, SFFV-RV-mCherryak infektaturiko NSC zenbakia arbuiagarria izan zen DMSan **(R7 C-F Figura; R9 Figura)**.

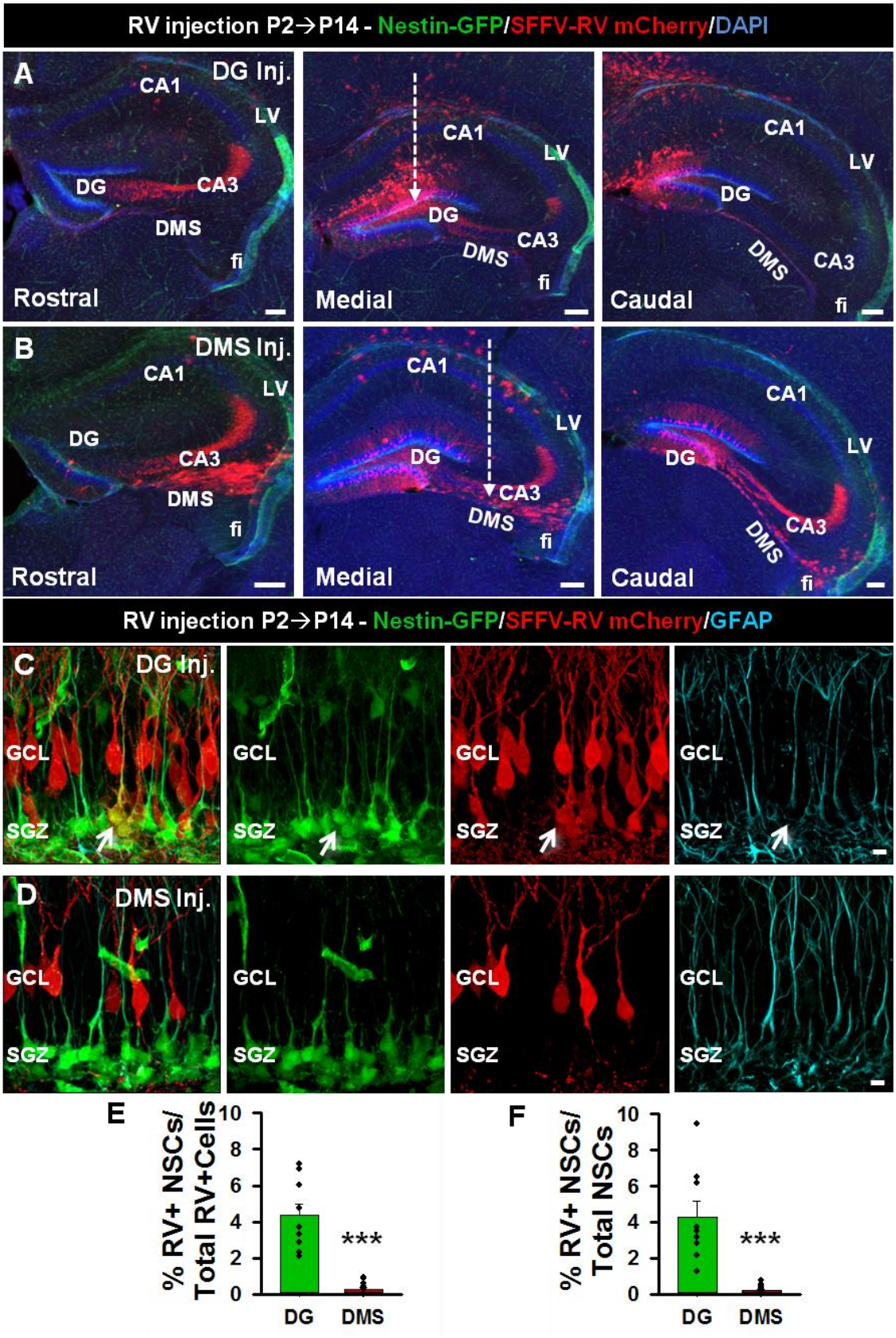
RV injection P2→P14 - Nestin-GFP/SFFV-RV mCherry/DAPI
A
DG Inj.
CA1
LV
DG
CA3
DMS
fi
Rostral
Medial
Caudal
B
DMS Inj.
RV injection P2→P14 - Nestin-GFP/SFFV-RV mCherry/GFAP
C
D
GCL
SGZ
E
F
% RV+ NSCs/ Total RV+Cells
% RV+ NSCs/ Total NSCs
***
DG
DMS

← Aurreko orrialdean. R7 Figura. Jaio ondorengo etapa goiztiarrean NSC helduen aitzindarien gehiengo haundia DGaren barruan kokatua zegoen. A-B) Lamina-eskaner fluoreszente irudiak SFFV-RV infekzio espazial desberdinak erakutsiz. Kumeak P2 adinean injektatuak izan ziren bai DG barruan (A) zein DMSan (B) eta injekzioaren lekua P14n ebaluatua izan zen. Geziak injekzio bidea adierazten du. **C-D)** Irudi konfokalak GCLean kokaturiko SFFV-RVaz infektaturiko zelulen morfologia eta markatzaile espresioa (Nestin-GFP eta GFAP) adieraziz. Geziek SFFV-RVak infektaturiko NSC bat adierazten dute. **E)** SFFV-RV NSC positiboen portzentajearen kuantifikazioa SFFV-RV zelula guztien artean. **F)** SFFV-RV NSC positiboen portzentajearen kuantifikazioa NSC guztien artean. *CA: Cornu ammonis. DG: Hortzdun zirkunboluzioa. DMS: Hortzdun migrazio korrontea. fi: fimbria. GCL: Zelula granular geruza. LV: Bentrikulu laterala. Eskala barrak 200 µm-koak dira A-Bn eta 10 µm-koak C-Dn. Scale bars are 200 µm in A-B and 10 µm in C-D. ***p<0.005. Student's t-test. Barrek batez-bestekoa ± errore estandarra erakusten dute. Puntuek datu indibidualak erakusten dituzte.*

Ikusitako eremuaren menpeko diferentziak mantenduak izan ziren P5n. Adin honetan sortzaileak DGaren barnealdean infektatuak izan zirenean, SFFV-RV-mCherry zelula positiboak GCLaren behealdera mugatuak eta SGZan zehar kokatuak aurkitu ziren **(R8 A-D Figura)**. Lehenago bezala, zelula gehienak neurona bezala identifikatuak izan ziren. Garrantzia handiz, SFFV-RV-mCherry zelula positiboen %3-4a NSCak ziren **(R8 E Figura; R9 Figura)**, NSC populazioaren %2a izanik **(R8 F Figura; R9 Figura)**. Beste alde batetik, P2an ikusitako patroi berbera erakutsiz, aitzindariak P14n DMSan markatuak zirenean GCLean kokaturiko SFFV-RV-mCherry zelula positiboen gehiengo handia neuronak ziren, euren dendrita, axoi eta Nestin-GFP eta GFAP markatzaileen gabezia kontuan hartuta **(R8 C-F Figura)**. *In vivo* patuaren jarraipen ikerketa hauek NSC populazio heldua jaio ondorengo aro goiztiarrean zuzenean sortua izan zela irmo iradoki zuten, esklusiboki DG barruan kokaturiko dNSC/sortzaile zelulengandik, nahiz eta DGaren formazio neuronalera ekarpena egiten zuten DMStik zetozen sortzaileak bazeuden baita. *cD2* datuekin batera postulatu genezakeen DGan kokaturiko dNSC/sortzaile zelula populazio batek NSC populazio heldua zuzenean DGan bertan *cD2*-ren menpeko mitosiaren bitartez sortu zuela. Hala, gure konklusioa izan zen NSC helduek dNSCengandik desberdintzen den populazioa osatzen dutela eta beraz, AHNa ez dela garapenean zehar ematen den neurogenesiaren hondakin bat baizik eta fenomeno berri eta ezberdin bat.

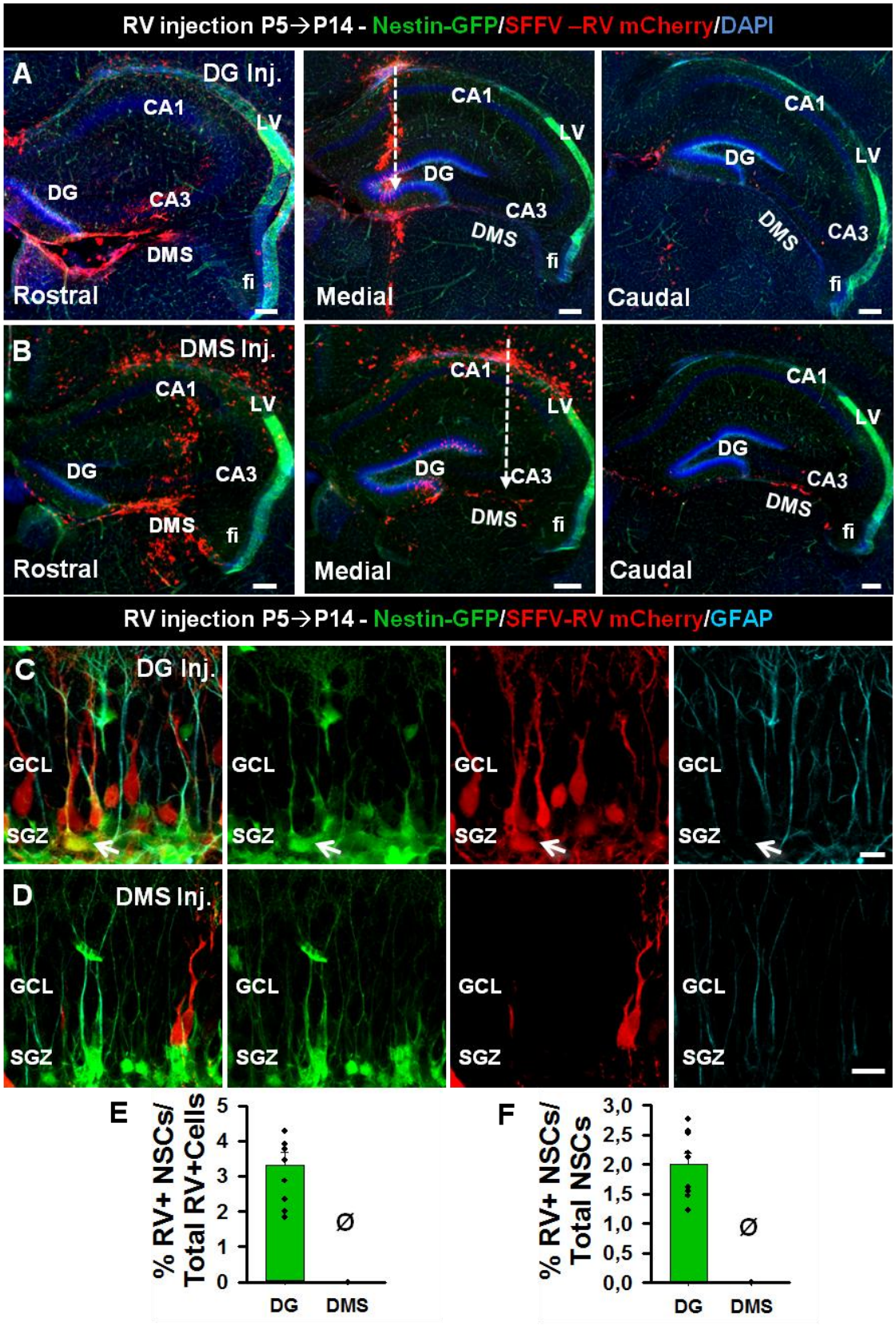
RV injection P5→P14 - Nestin-GFP/SFFV –RV mCherry/DAPI
A
DG Inj.
CA1
LV
DG
CA3
DMS
fi
Rostral
Medial
Caudal
B
DMS Inj.
RV injection P5→P14 - Nestin-GFP/SFFV-RV mCherry/GFAP
C
D
GCL
SGZ
E
% RV+ NSCs/ Total RV+Cells
F
% RV+ NSCs/ Total NSCs
Ø

← Aurreko orrialdean. R8 Figura. Jaio ondorengo lehen astearen amaiera aldera NSC helduen aitzindari guztiak DG barruan kokaturik zeuden. A-B) Lamina-eskaner fluoreszente irudiak SFFV-RV infekzio espazial desberdinak erakutsiz. Kumeak P5 adinean injektatuak izan ziren bai DG barruan (A) zein DMSan (B) eta inkezioaren lekua P14n ebaluatua izan zen. Geziak injekzio bidea adierazten du. **C-D)** Irudi konfokalak GCLean kokaturiko SFFV-RVaz infektaturiko zelulen morfologia eta markatzaile espresioa (Nestin-GFP eta GFAP) adieraziz. Geziek SFFV-RVak infektaturiko NSC bat adierazten dute. **E)** SFFV-RV NSC positiboen portzentajearen kuantifikazioa SFFV-RV zelula guztien artean. **F)** SFFV-RV NSC positiboen portzentajearen kuantifikazioa NSC guztien artean. *CA: Cornu ammonis. DG: Hortzdun zirkunboluzioa. DMS: Hortzdun migrazio korrontea. fi: fimbria. GCL: Zelula granular geruza. LV: Bentrikulu laterala. Eskala barrak 200 µm-koak dira A-Bn eta 10 µm-koak C-Dn. Scale bars are 200 µm in A-B and 10 µm in C-D. Barrek batez bestekoa ± errore estandarra erakusten dute. Puntuek datu indibidualak erakusten dituzte.*

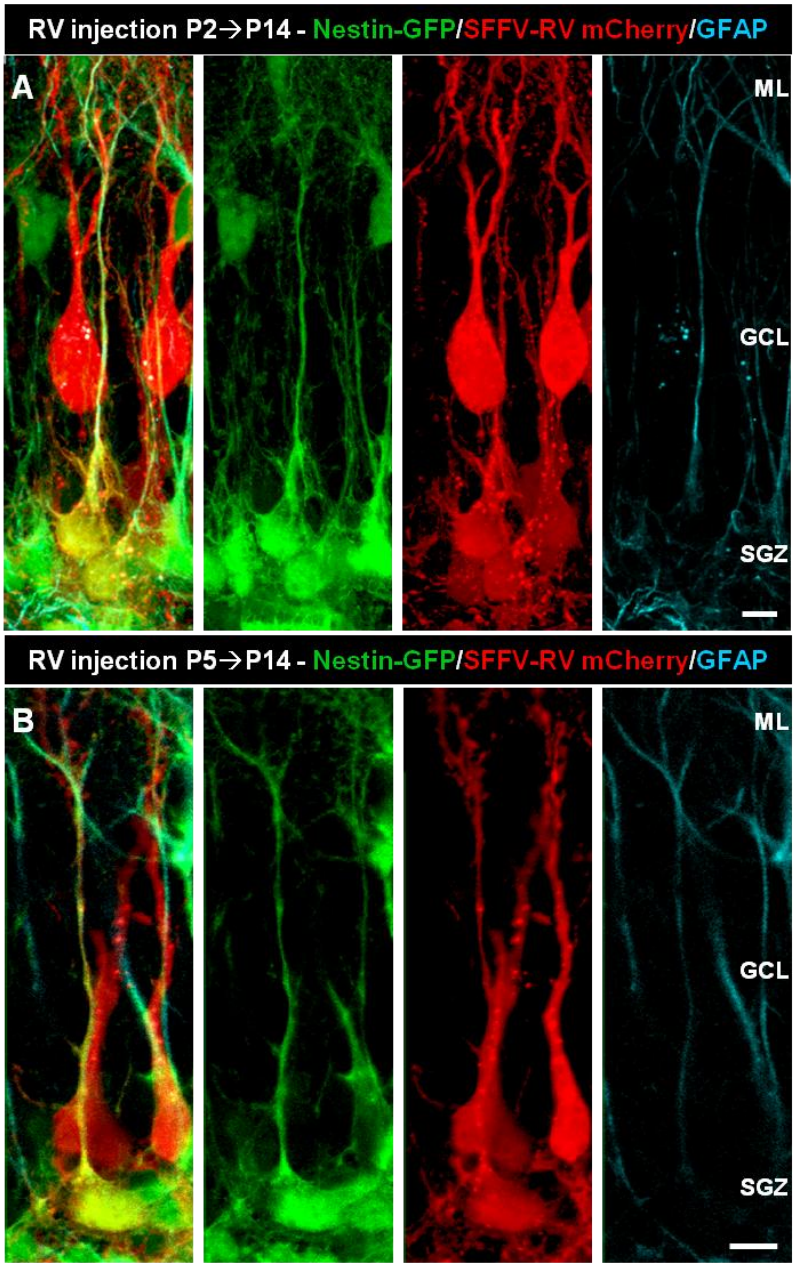

R9 Figura. SFFV-RVak eraginkortasunez markatu zituen NSCak DGaren barnean injektatzerakoan. A-B) Irudi konfokalak SFFV-RVarekin markaturiko NSCak erakutsiz GCLan. SFFV-RVa P2 edo P5 adinetan injektatuz, Nestin-GFP eta GFAP espresioa erakutsi zuten hainbat zelula ikusarazi ziren. SGZan kokaturiko soma, MLrenganako prozesu luzatua eta MLean zabaltzen zen brokoli formako koroa argitasunez ikusi zitezkeen. *GCL: Zelula granular geruza. ML: Geruza molekularra. SGZ: Gune azpigranularra. Eskala barrak 10 µm-koak dira.*

6.2.3. DMSko sortzaileek DGrenganako ekarpen espazial dibergentea egiten zuten

Hala, NSC helduak emango dituzten aitzindariak badaude DG barruan kokatuak jaio ondorengo aro goiztiarrean. Nolanahi, DMSa aktibo mantendu zen jaio ondorengo etapa honetan zehar. Hargatik DMSko sortzaileek GCLra egiten duten

ekarpena ikertzera pasatu ginen. SFFV-RV-mCherrya erabiliz P2 eta P5 adinetan DMSan injekzio erretrobiralak gauzatuz, P14n dibisioan sarturiko zelulen patu espazial diferentzial preferentzia aztertu genuen.

Bi adinetan neurona itxurako zelulak dentsitate handiagoan DGaren beso bentralean multzokatuak zeuden, beso dorsalean baino. SFFV-RVarekin infektaturiko zelulak gehienbat beso bentraleko bazterrean pilaturik aurkitzen ziren, sakabanatutako zelulak gainontzeko GCLean zehar ikusarazi zitezkeen bitartean **(R10 A-B Figura)**. Hori gutxi balitz, beso bentraleko eta beso dorsaleko SFFV-RV zelula positiboek euren morfologian diferentziak aurkezten zituzten. Beso bentralekoak SGZaren eta MLaren artean kokaturik agertzen ziren eta gehiengoak prozesu apikal labur bat zuen, zeinetik dendritak berehala MLean zehar hedatzen ziren. Alderantziz, beso dorsalekoak sarri GCLaren behealdean kokatuak ageri ziren, prozesu luzeekin, zeinetatik dendritak MLean zehar hedatzen ziren **(R10 A-B Figura).**

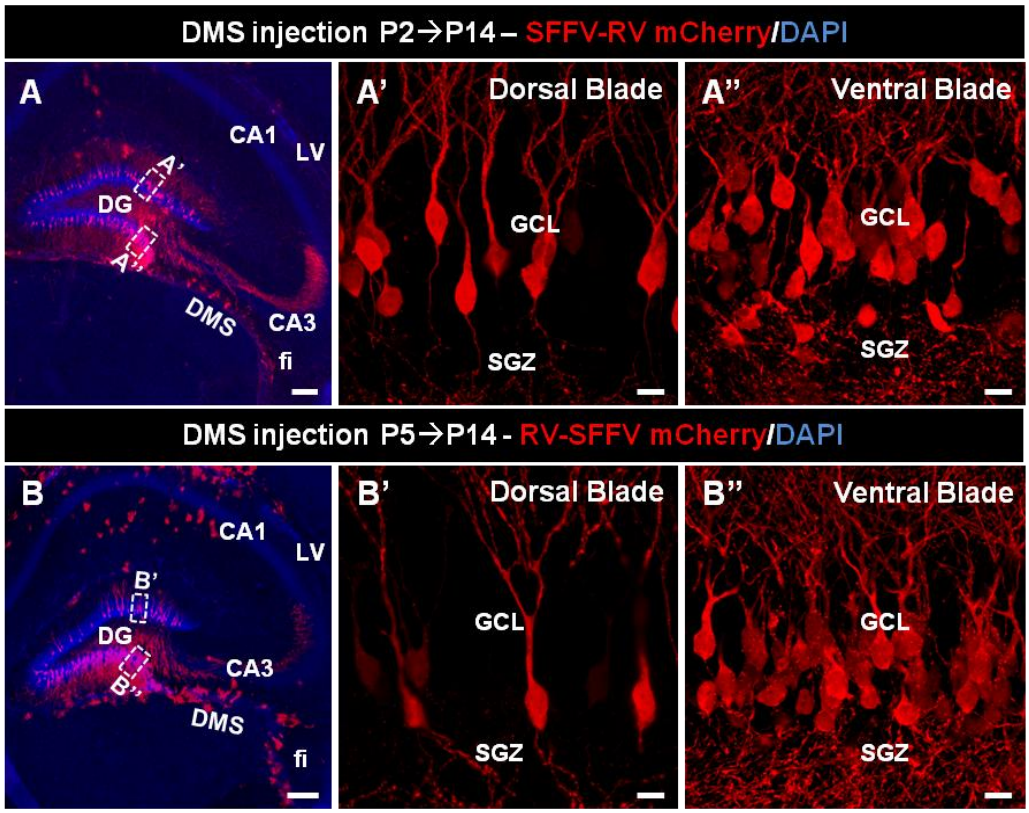

R10 Figura. DMSko sortzaileek DGarenganako ekarpen espazial dibergentea egiten zuten. A-B) Lamina-eskaner fluoreszente irudiak P2 eta P5 adinetan SFFV-RVarekin infektaturiko DMSko aitzindarien leinuak P14n duen distribuzio espaziala erakutsiz. Neuronak ikusarazi zitezkeen GCL guztian zehar. Nolanahi ere, beso dorsalean banakako, ongi separaturiko zelulek populatzen zutelarik GCLa (A', B'), beso bentrala zelula multzoz beterik ageri zen (A'', B''). *CA: Cornu ammonis. DG: Hortzdun zirkunboluzioa.*

DMS: Hortzdun migrazio korrontea. GCL: Zelula granular geruza. LV: Bentrikulu laterala. SGZ: Gune azpigranularra. Eskala barra 10 µm-koa da.

6.3. LPA_1 NSC helduen markatzaile diferentzial bezala

Aurretiaz ezarri izan dugu jaio ondorengo aro goiztiarrean zehar dNSCak *cD2*ren menpeko prozesu bat jarraituz DGaren barruan ugaritu egiten direla. Hala, teorizatu genuen NSC helduek DGan populazio berri independente bat osatzen zutela. Hala ere, NSCen garapen dinamikak ikertzerakoan topatzen den arazo nagusietako bat dNSC eta NSC helduen arteko ezberdintzerako markatzaile gabezia da. Berriki, LPA_1 hipokanpoko NSC helduen markatzaile selektibo bezala aurkeztu izan da (Walker et al., 2016). LPA_1ek AHN eta garapen kortikalaren modulatzaile bezala jokatzen duenetik (Estivill-Torrús et al., 2008; Matas-Rico et al., 2008), bere espresioa LPA_1-EGFP sagu transgenikoa erabiliz jaio ondorengo aroan ikertzea proposatu genuen (Gong et al., 2003).

6.3.1. NSCek jaio ondorengo aroan zehar bereganatu zuten LPA_1 espresioa

Jaio ondorengo bost adin ezberdinetan (P4, P7, P10, P14 and P21) DGa eta gune neurogenikoa aztertu genituen. P4n LPA_1-EGFP espresioa hilusean zehar zabal hedatua zegoen, GCLean arbuiagarria zen bitartean. Beranduago P7n, LPA_1-EGFP espresioa hilus eremutik GCLrantza aldatzen hasi zen. P14 aldera, aldaketa guztiz nabarmena zen eta LPA_1-EGFP espresioa SGZra mugatua ageri zen **(R11 A Figura)**. Era interesgarrian, P4n GCLean LPA_1-EGFP espresiorik ez zegoenez, Nestin espresioa zuten eta era erradialen orientaturiko dNSCtako batek ere ez zuen LPA_1-EGFP espresioa agertzen. Hala ere, P7 geroztik, dNSC batzuk LPA_1-EGFP bereganatzen hasi ziren. Azpimarragarria da behin NSC populazioa heldu bilakatzen denean (Nicola et al., 2015), ia NSC guztiek aurkezten zutela LPA_1-EGFP espresioa **(R11 B Figura)**. Emaitza hauek LPA_1 NSCek garapenetik helduarora egiten duten trantsizioa ezberdintzeko markatzaile baliagarria izan litekeela iradoki zuten.

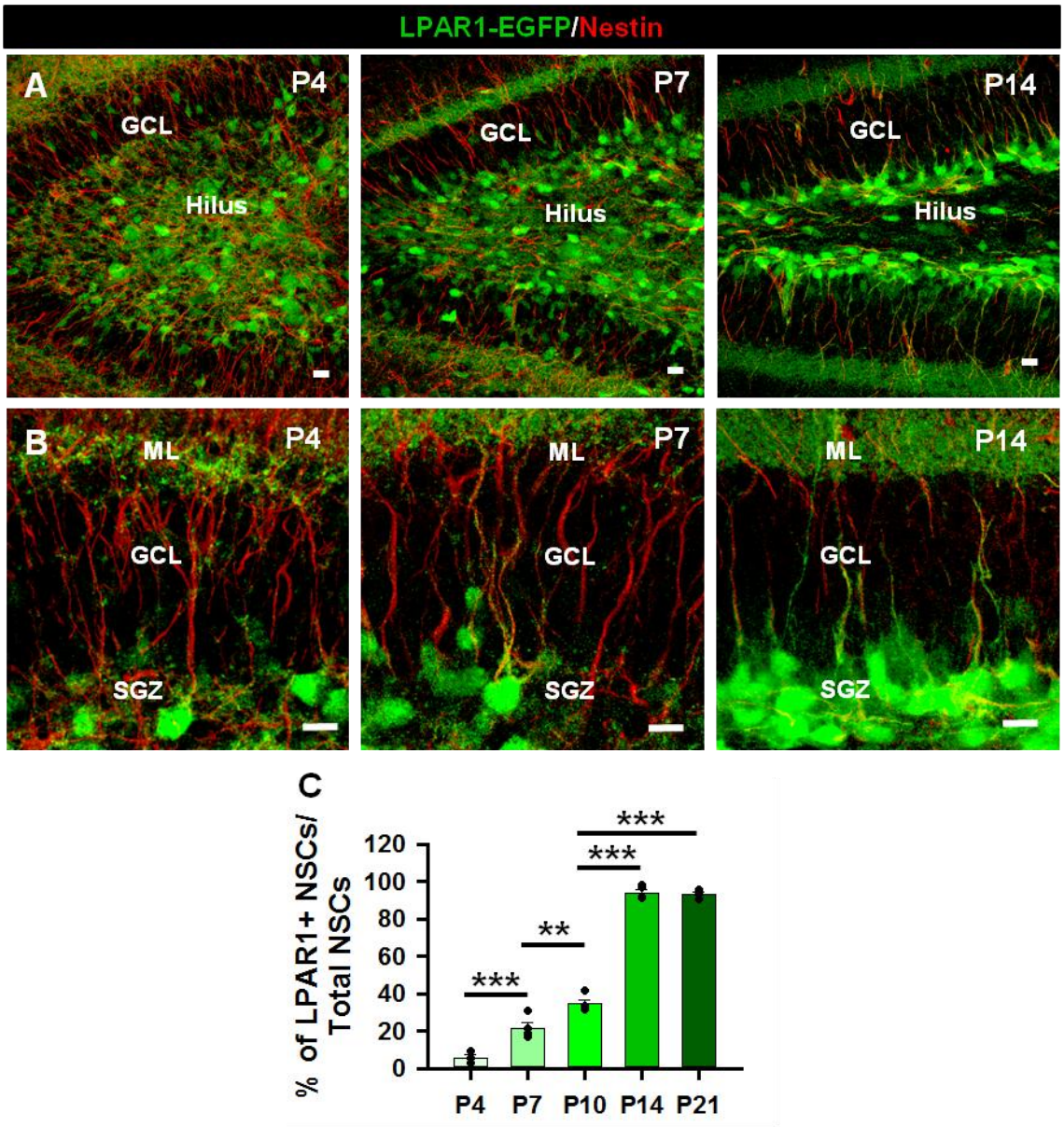

R11 Figura. LPA_1-EGFP espresioak diferentzialki ezberdintzen ditu dNSCak NSC helduengandik. A-B) Konfikal irudi errepresentatiboak LPA_1-EGFP espresioa erakutsiz DGan (A) eta GCLean (B) P4n, P7n eta P14n. dNSCen gehiengoa LPA_1-EGFP negatiboak ziren bitartean, P14n ia NSC helduen populazio osoak LPA_1-EGFP espresatzen zuen. **C)** P4, P7 eta P14 adinetan LPA_1-EGFP espresioa zuten dNSC/NSCen portzentajearen kuantifikazioa (Nestin-positibo, era erradialean bideraturiko zelula bezala definiturik). Garapen arotik P14ra bitartean LPA_1-EGFP espresioa zuten NSCetan hazkuntza esanguratsua ikusarazi zen. *GCL: Zelula granular geruza. ML: Geruza molekularra. SGZ: Gune azpigranularra. Eskala barrak 10 µm-koak dira. **p<0.005, ***p<0.001. Bide bakarreko ANOVA Holm-Sidak post-hoc testaren bidezko binakako konparazio anizkoitzez jarraitua. Barrek batez bestekoa ± errore estandarra erakusten dute.Puntuek datu indibidualak erakusten dituzte.*

6.3.2. LPA_1 espezifikotasuna jaio ostetik helduarora aldatzen da

Ondoren hilusean kokaturiko LPA_1-EGFP espresatzen zuten zelulen natura ebaluatu genuen, neuronak izan zitezkeelakoan euren morfologiari so eginik . Hain zuzen ere, emaitzek LPA_1-EGFPren espresioaren zelula espezifikotasunean aldaketa bat jasotzen zela erakutsi zuten. P4-P7 bitartean, hiluseko LPA_1-EGFP zelulen gehiengoa neurona helduen markatzailea den NeuNrentzako positiboak ziren **(R12 A-B Figura)**. Hortik aurrera aldiz, NSCak LPA_1-EGFP espresatzen hasten diren aldiarekin bat etorriz, LPA_1-EGFP espresatzen zuten zelulen ehuneko txiki bat soilik zen NeuN-positiboa **(R12 C-D Figura)**.

Guzti hau kontuan izanik, emaitza hauek jaio ondorengo aro goiztiarretik (P4-P7) gune neurogenikoaren formazio amaiera bitartean LPA_1-EGFP espresioan jazotzen den aldaera espazial eta zelular baten erakusle dira. Jaio ondorengo garapen goiztiarrean espresioa nagusiki neuronala den arren, NSCetara mugatzen da P14tik aurrera. Honela, LPA_1 dNSC eta NSC helduen artean ezberdintzeko baliabide bezala iradokitzen dugu, beharbada bien arteko igarotze honetan rolen bat jokatuz. Era berean, emaitza hauek NSC helduek dNSCenganik osoki ezberdina den populazio bat osatzen duten ideia babesten dute.

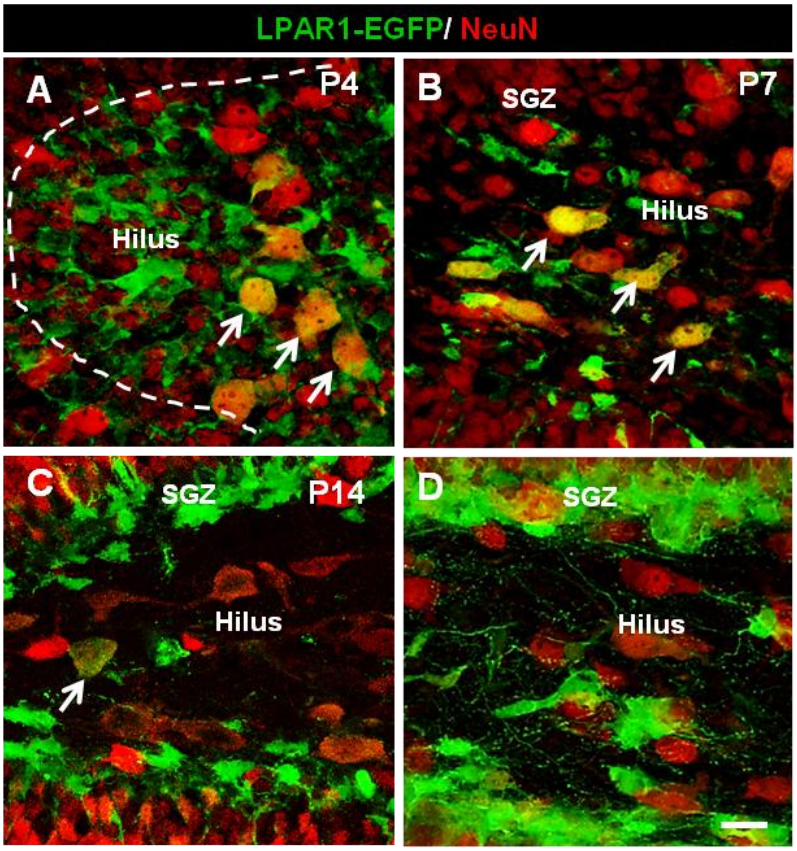

← Aurreko orrialdean. R12 Figura. Jaio ondorengo aro goiztiarrean DGan LPA_1-EGFPren espresioak aldaera bat izan zuen. A-D) Irudi konfokal errepresentatiboak jaio ondorengo adin ezberdinetan hilusean LPA_1-EGFP eta NeuN espresatzen zuten zelulak erakutsiz. Jaio ondorengo adin goiztiarretan bi markatzaileak espresatzen zituzten zelula handiak ageri ziren arren, apurka LPA_1-EGFP espresioa galtzen joan ziren. Gida-marrak SGZa zehazten du. Geziek LPA_1-EGFP eta NeuN, biak, ko-espresatzen zituzten zelula haiek adierazten ditu. *Eskala barrak 10 µm-koak dira.*

6.4. Haurdunaldiaren erdirako giza DGaren garapena ia amaiturik dago

Gure aurreko emaitzek adierazten zutenez, DGan jaio ondorengo aroan zehar NSC populazio independente bat sortzen da, zeinak saguaren bizitza osoan zehar neuronak emango dituen eta DGko eta HPFko beste eremu batzuen formazioan parte hartzen duten dNSCetatik desberdina den. Gure hurrengo pausua, hala, aurkikuntza hauek gizakira zelan aplikatu zitezkeen ikertzea izan zen. AHNaren existentziak eztabaidagarri darraien testuinguru batean (Moreno-Jiménez et al., 2019; Sorrells et al., 2018), AHNak gizakietan duen hedadura esploratzeko DGaren eta honen gune neurogenikoaren formazio patroien inguruan argia igortzea aberasgarria izango litzake.

6.4.1. DMSa presente zegoen giza garapen goiztiarrean (GW14)

Mercedes Paredesekin kolaborazioan, UCSFetik, nork adeitasun osoz giza ehuna erabiltzea ahalbidetu zigun, giza DGaren garapena eta espezifikoki dNSCen populazio ezberdinen potentziala karakterizatzeari ekin genion. Aurretiko lanek ugaritze prozesuan zeuden sortzaile eta RGC neurogenikoak GW14an DMSa eratuz erakutsi izan dituzte (Cipriani et al., 2017, 2018; Sorrells et al., 2018). Are gehiago, hau da neurogenesiak bere goia erdiesten duen enbrioi garapenaren garaia (Yang et al., 2014). Hemen, HPFa haratago karakterizatu genuen adin honetan, RGC eta sortzaile markatzaileak erabiliz. Adin honetan bizkarraldeko hipokanpoko formazioa (ingelesetik dorsal hippocampal formation, dHPF) eta sabelaldeko hipokanpoko formazioa (ingelesetik ventral hippocampal formazioa, vHPF) behagarriak izanagatik, sabelaldeko gunea da HPF helduan eboluzionatzen duena eta beraz, geure analisia oinarritu genuen gunea **(R13 A Figura)**. Gainjarri egiten ziren Nestin eta GFAP positiboak ziren zuntzak DNetik DGra luzatzen ziren, DMSan zehar RGC aldamio bat sortuz. Nestin espresatzen zuten zelulak DG barruan ere bazeuden, nagusiki kanpoko beso inguruan eta HFaz gertu zegoen ML populatzen **(R13 B Figura)**. Horrez gain, GFAP espresatzen zuten zelulek HOPXen espresioa ere agertzen zuten, zeinen tindaketak DGa FDJtik erdiesten zuen, GCLa HOPX barik ageri zen arren **(R13 C Figura)**. Saguetan, HOPX haurdunaldi garaitik helduarora GCen aurrekarien markatzaile bezala

iradoki izan da (Berg et al., 2019) eta gure emaitzek gizakietan antzeko HOPX populazio baten existentzia planteatzeko aukera ireki zuten.

Sagu helduetan S100ßk astrozito helduak markatzen ditu, nahiz eta saguaren jaio ondorengo DGaren garapenean neurona aurrekarien markatzaile bezala ere izan den proposatua (Namba et al., 2005). Hemen, S100ß positiboak ziren zelulak DMS osoan zehar ikusi genituen, Tbr2 positiboak ziren sortzaile intermedioetatik hurbil **(R13 D Figura)**. Ugaritze prozesuan zeuden zelulei erreparatuta, Ki67 markatzaile mitotikoa erabiliz, HPF osoan zehar sakabanatuak agertzen ziren, Ki67 positibo zelulen presentzia sendo bat FDJ inguruan hilusera bidean ikusi zitekeen arren **(R13 E Figura)**.

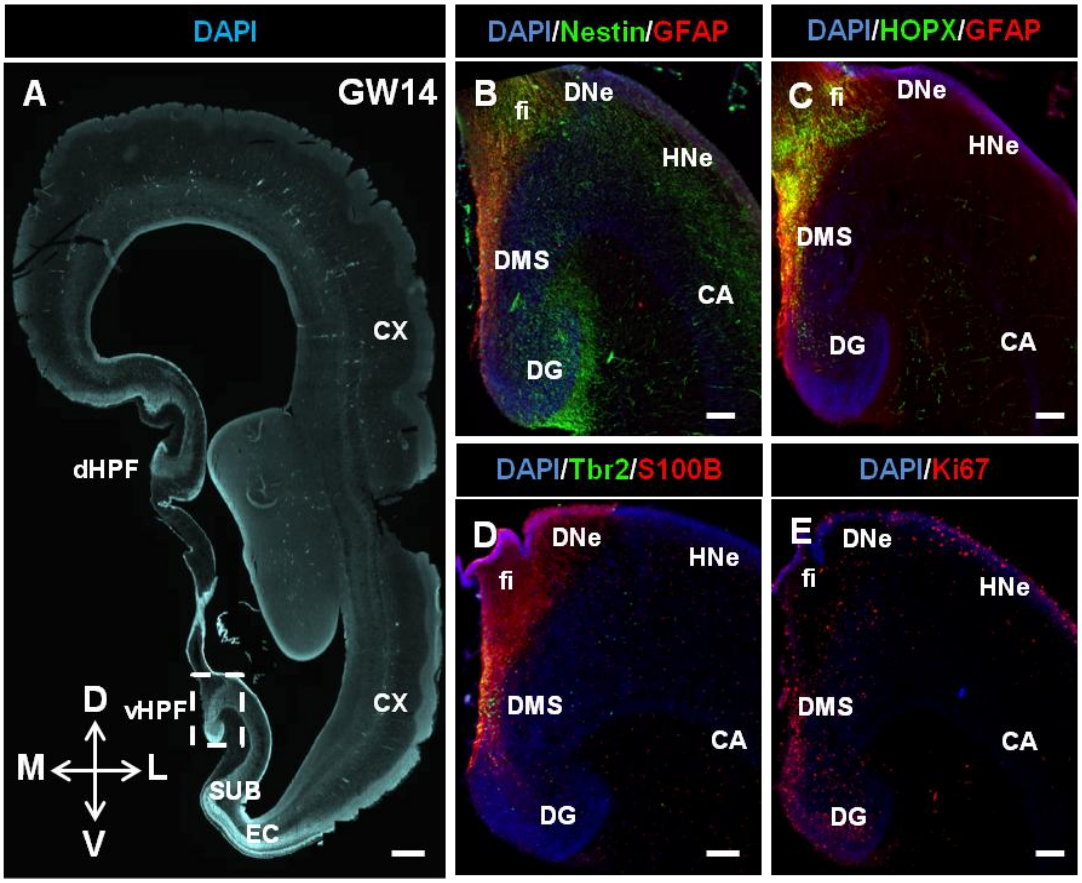

R13 Figura. RGC eta sortzaileek DMSa eratzen zuten giza HPFaren garapen goiztiarrean. A) Lamina-eskaner fluoreszente irudiak GW14 adineko garun baten hemisferioa erakutsiz. Gida-karratuak vHPFa adierazten du. **B)** Nestin (berdez) eta GFAP (gorriz) espresatzen zuten zelulak HPFan GW14n. GFAP espresatzen zuten zuntzak presente zeuden DMSan zehar, Nestin espresatzen zuten zelulak DGaren sortzeke dagoen MLan ere ikusarazi zitezkeen bitartean. **C)** Era berean, HOPX espresatzen zuten zelulak DMSa populatzen ageri ziren baita ere, hein handi batean GFAP positiboak ziren zuntzekin gainjarriz. **D)** S100β eta Tbr2 espresatzen zuten zelulak ere eremu honetan zehar aurki zitezkeen. **E)** Ki67 zelula positiboak DNetik DGra bidean sakabanatuak ageri ziren. *CA: Cornu ammonis. Cx: Kortex. D:*

Bizkarraldea. DG: Horzdun zirkunboluzioa. dHPF: Bizkarraldeko formazio hipokanpala. DMS: Horzdun migrazio korrontea. DNe: Horzdun neuroepitelioa. EC: Kortex entorrinala fi: fimbria. GCL: Zelula granular geruza. HNe: Hipokanpoko neuroepitelioa. L: Laterala. M: Mediala. SUB: Subiculum. V: Sabelaldea. vHPF: Sabelaldeko formazio hipokanpala. Eskala barrak 500 µm-koak An eta 100 µm-koak B-En dira.

6.4.2. Patroi espazial diferentzialak DGaren garapenean zehar

Ondoren, HPFko aurrekoz atzerako ardatzean zehar sortzaile eta ugaritze markatzaileen distribuzioa deskribatzeari ekin genion. Era nabarmenean, aurreko HPFan Ki67 zelula positiboen gehiengoa DNe-ari eta HNe-ari elkarturik ageri zen, DMSa eta DGa nukleo bakar batzuek populatzen zituztelarik **(R14 A Figura)**. Hala ere, posizio medialagoetan Ki67 espresatzen zuten nukleoak DMS eta hilus inguruan kontzentratuagoak zeuden, nahiz eta batzuk DNe-an aurki zitezkeen **(R14 B Figura)**. Tendentzia hau nabariagoa bihurtu zen atzeragoko posizioetan non Ki67 espresatzen zuten zelulen gehiengoa DGra mugaturik zegoen, bereziki DMSak DGarekin konektatzen duen barruko besoaren muturrean, baina GCLtik sakabanatuak eta kanpoko besora iritsiz baita ere **(R14 C Figura)**. HPFaren aurreko eta atzeko eremuen arteko espresio zelularraren patroi diferentzialak ez ziren ugaritze prozesuan zeuden zeluletara mugatu, HOPX zelula positiboak era berdintsuan sakabanaturik ageri zirelarik. Aurreko posizioetan DNe-ra loturik eta euren prozesuak DMSan zehar eta fimbriaren gainetik luzatuz ageri ziren **(R14 D Figura)**, atzeko posizioetan DGaren barruan hilusera ia guztiz mugaturik ikusarazi zitezkeen bitartean **(R14 E Figura)**. Aitzitik, GFAP espresatzen zuten zelulak DMSra mugatuak ageri ziren aurreko eta atzeko maila ezberdinetan **(R14 D-E Figura)**.

Hau dena kontuan harturik, GW14n ikusiriko zelulen espresio patroiek sortzaileen distribuzioa enbrioi garaian eta jaio ondorengo aro goiztiarrean saguetan ikusi daitekeenaren antzekoa dela iradoki zuten. Nolanahi ere, zelula populazio heterogeneoak ikusarazi zitezkeen kokapen espazialaren arabera, (DG barruan edo kanpoan) eta markatzaile espresioaren arabera. Honen ostean, populazio hauen garapena aztertu nahi izan genuen beranduagoko etapetan, haurdunaldi erdia eta gero.

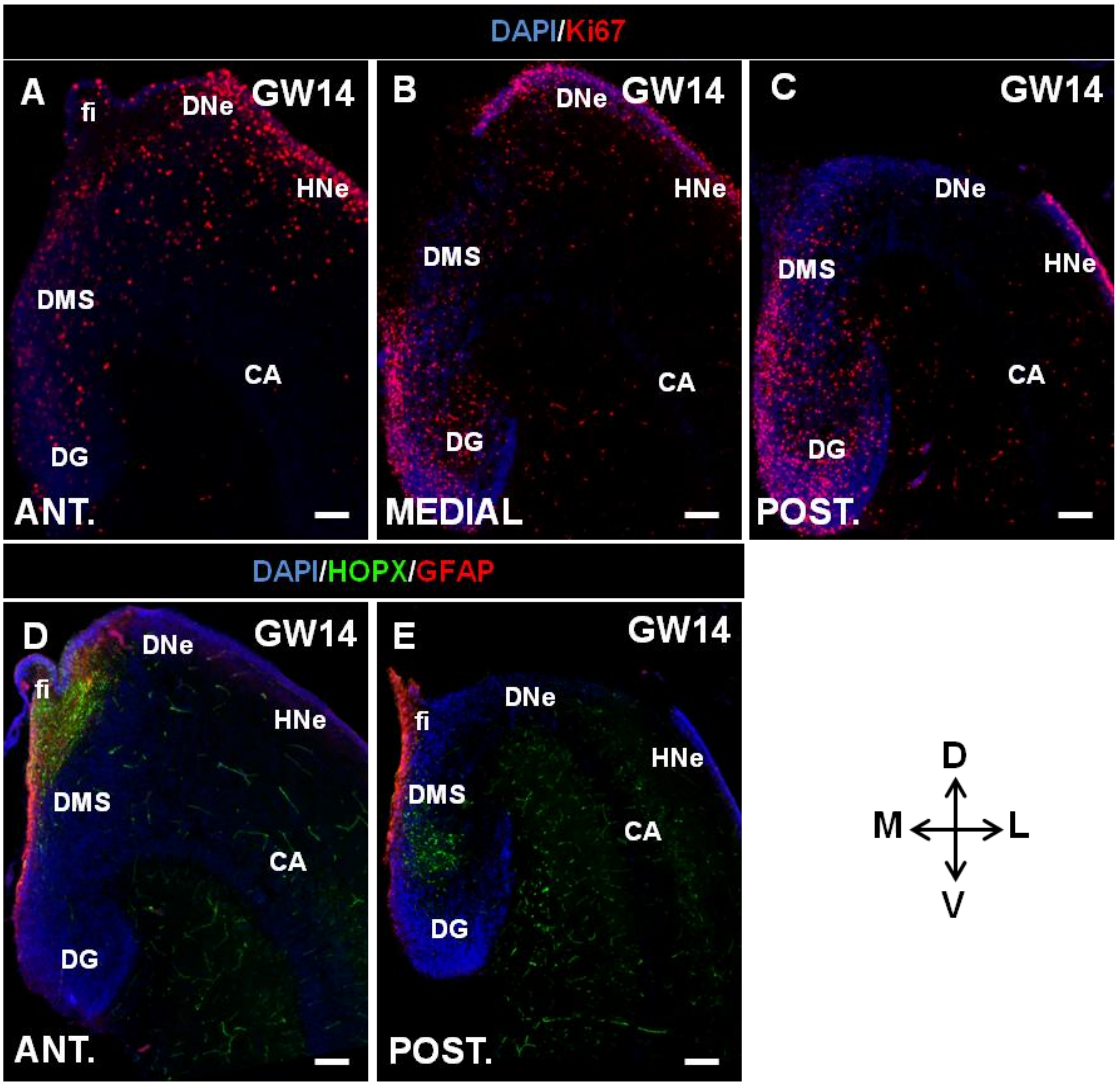

R14 Figura. Espresio patroi diferentzialak garapen goiztiarrean aurrekoz atzerako ardatzean zehar. A-C) Lamina-eskaner fluoreszente irudiak ugaritze prozesuan zeuden zelulak (Ki67) aurrekoz atzerako ardatzean zehar maila ezberdinetan erakutsiz (esker eskuin, aurretik atzera). Aurreko partean, Ki67 espresatzen zuten zelulak gehienbat DNe eta HNe inguruan kokaturik ageri ziren, atzeragoko parteetan DMS eta DG ingurura aldatzen zirelarik. **D-E)** HOPX espresatzen zuten zelulek patroi berbera jarraitu zuten. Aurreko parteetan DNe-ra eta DMSra mugatzen ziren baina atzeragoko parteetan DGaren barruan agertzen ziren. Aitzitik, GFAP espresioak ardatz osoan zehar patroi berdina mantentzen zuen, DMSra mugaturik. *CA: Cornu ammonis. D: Dorsal. DG: Dentate gyrus. DMS: Dentate migratory stream. DNe: Dentate neuroepithelium. fi: fimbria. GCL: Granule cell layer. HNe: Hippocampal neuroepithelium L: Lateral. M: Medial. V: Ventral. Scale bars are 100 µm.CA: Cornu ammonis. D: Bizkarraldea. DG: Horzdun zirkunboluzioa. dHPF: Bizkarraldeko formazio hipokanpala. DMS: Horzdun migrazio korrontea. DNe: Horzdun neuroepitelioa. EC: Kortex entorrinala fi: fimbria. GCL: Zelula granular geruza. HNe: Neuroepitelio hipokanpala. L: Laterala. M: Mediala. SUB: Subiculum. V: Ventral. vHPF: Sabelaldeko formazio hipokanpala. Eskala barrak 500 µm-koak A-n eta 100 µm-koak B-E-n dira.*

6.4.3. GW30rako DGaren formazioa GCLra mugatua dago

Haurdunaldi erdi eta berantiarrean zehar DG formazioan sortzaileek duten bilakaera ikertzeko asmoz, GW30 adineko enbrioiak aztertzera pasa ginen. Adin honetan, dHPFa ikusarazi daiteke, nahiz eta vHPFa baino txikiagoa izan. Azken hau aurretiaz deskribaturiko patroiak jarraituz tolesturik agertzen da (Humphrey, 1967) **(R15 A Figura)**. GW14n eginiko behaketen aurrean, adin honetan Nestin espresatzen duten zelulak hilusa populatzen agertzen dira, euren zuntzak GCLra eta MLra luzatuz. Era nabarmenean, GW30an oraindik ere zuntzak ikusarazi zitezkeen norabide horizontalean DNe-an zehar, fimbriaren gainetik eta DMSa zeharkatuz **(R15 B Figura)**. HOPX tindaketa HPF osoan zehar agertzen zen, GW14rekin alderatuz markatzailearen espresio zelular zabal eta ez espezifikoa iradokiz. DGan, HOPX espresatzen zuten zelulak euren prozesuak ML aldera luzatuz hilusean kokaturik agertzen ziren, Nestin espresatzen zuten zelulen antzera. Xelebrea nola DGaren barruko besoak HOPX espresatzen zuen zelularik ez zuen agertzen, kanpoko besoa guztiz beterik zegoelarik. Bestalde, DMSan zehar GFAP espresio indartsua ikusi zitekeen **(R15 C Figura)**. Hala, DMSaren amaierarekin lotzen den DGaren barruko besoan S100βren espresio indartsua presente zegoen **(R15 D Figura)**, HOPX espresioak jarraitzen zuen antzeko patroia segituz **(R15 C Figura)**. S100βren espresioak GCLean zehar patroi diferentziala agertzen zuen, zelulak kanpoko besoan kokaturik ageriz barruko besoan baino maizago **(R15 D Figura)**. Tbr2 espresatzen zuten sortzaile eta ugaritze prozesuan aurkitzen ziren zelulak hilusera mugaturik zeuden, GCLaren azpian geruza bat osatuz **(R15 D-E Figura)**, GW30rako DG formazioa hein handi batean amaiturik dagoena adieraziz, saguaren DGaren garapeneko jaio ondorengo aro berantiarraren antza handia hartuz.

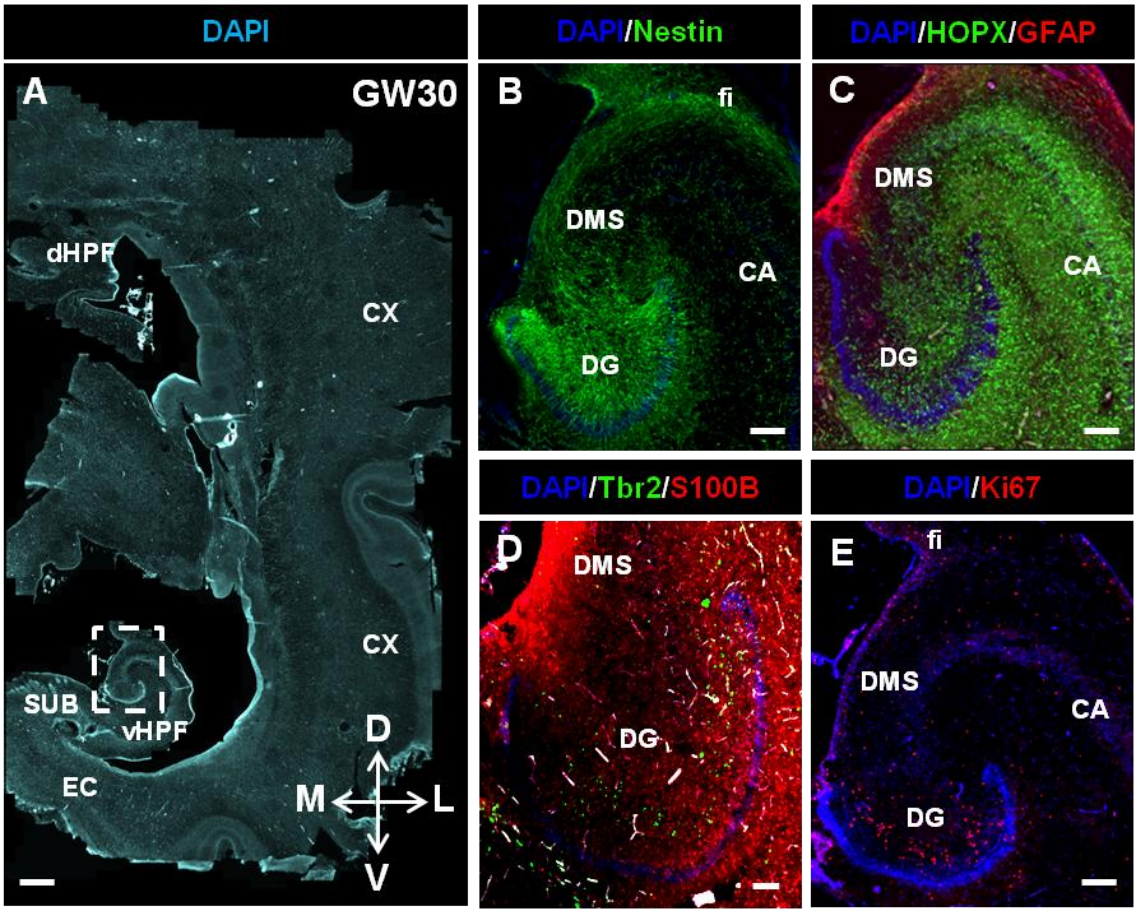

R15 Figura. GW30rako RGC eta sortzaileak hilusera mugatuak daude. A) Lamina-eskaner fluoreszente irudiak GW30 adineko garun baten hemisferioa erakutsiz. Gida-karratuak vHPFa adierazten du. **B)** GW30n Nestin espresatzen zuten zelulak DGaren barruan ageri ziren, kanporantz zabalduz. Hilusa GCLarenganako bidean gurutzatzen zuen aldamio bat eratzen zuten. **C)** GFAP espresioa zuten zuntzak DMSan zehar ageri ziren, HOPX espresatzen zuten zelulak HPF osoan zehar zeudelarik, DGa barne, non Nestin zuntzek sortzen zuten aldamioaren antzekoa osatzen zuten. **D)** S100β zelula positiboak GCLean eta MLean zehar sakabanaturik zeuden, nahiz eta DGaren kanpoko besoan espresioa askoz indartsuagoa zen barrukoan baino. Aitzitik, GCL azpialdean Tbr2 bitarteko sortzaileen markatzailearentzako positiboak ziren zelulek geruza zabal bat osatzen zuten. **E)** Era berean, ugaritze prozesuan aurkitzen ziren zelulak hilusera mugatuak zeuden orain, GCLaren azpialdean geruza bat osatuz. *CA: Cornu ammonis. Cx: Kortex. D: Bizkarraldea. DG: Horzdun zirkunboluzioa. dHPF: Bizkarraldeko formazio hipokanpala. DMS: Horzdun migrazio korrontea. EC: Kortex entorrinala. fi: fimbria. GCL: Zelula granular geruza. L: Laterala. M: Mediala. SUB: Subiculum. V: Sabelaldea. vHPF: Sabelaldeko formazio hipokanpala. Eskala barrak 500 µm-koak An eta 100 µm-koak B-En dira.*

6.4.4. Jaio ondoren eta gutxira RGC aldamio batek DGan presente zirauen

Nahiz eta HPFaren formazioa ia amaiturik dagoen jaio aurretik, helduaroan izango duen itxura jada aurkeztuz **(R16 A Figura)**, NBen azken korronte migratzaileak jaio ondorengo lehen urteetan iristen dira GCLra, euren sinapsiak ezarriz eta zirkuitu hipokanpala osatuz (Cipriani et al., 2018; Seress et al., 2001; Sorrells et al., 2018).

Jaiotzetik hilabete batera, RGCek hilusa populatu zuten GCLaren azpialdean, euren prozesuek GCLa MLrentza zeharkatzen zutelarik. Interesgarria da Vimentin tindaketa GCL osoan zehar banaturik ikusi daitekeen era berean, Nestin espresioa DGaren barruko besora mugaturik zegoela, adin honetan geratzen den RGC populazioaren heterogeneitatea iradokiz **(R16 B-C Figura)**. Baita ere, ugaritze prozesuan aurkitzen ziren zelula apurrak hilusean zehar sakabanaturik agertzen ziren, nahiz eta ez zuten SGZ hautemangarririk eratzen saguetan egiten duten antzera **(R16 D Figura)**, aurretiaz Arturo Alvarez-Buylla eta bere kideek azaldu izan duten bezala (Sorrells et al., 2018). Hau guztia kontuan harturik, emaitzek RGC populazioa heterogeneoa dela adierazten dute, jaiotzaren ondoren DGan mantentzen diren azpipopulazioekin, ugaritze prozesuan dauden zelulak gehienbat hilusean ageri ziren arren.

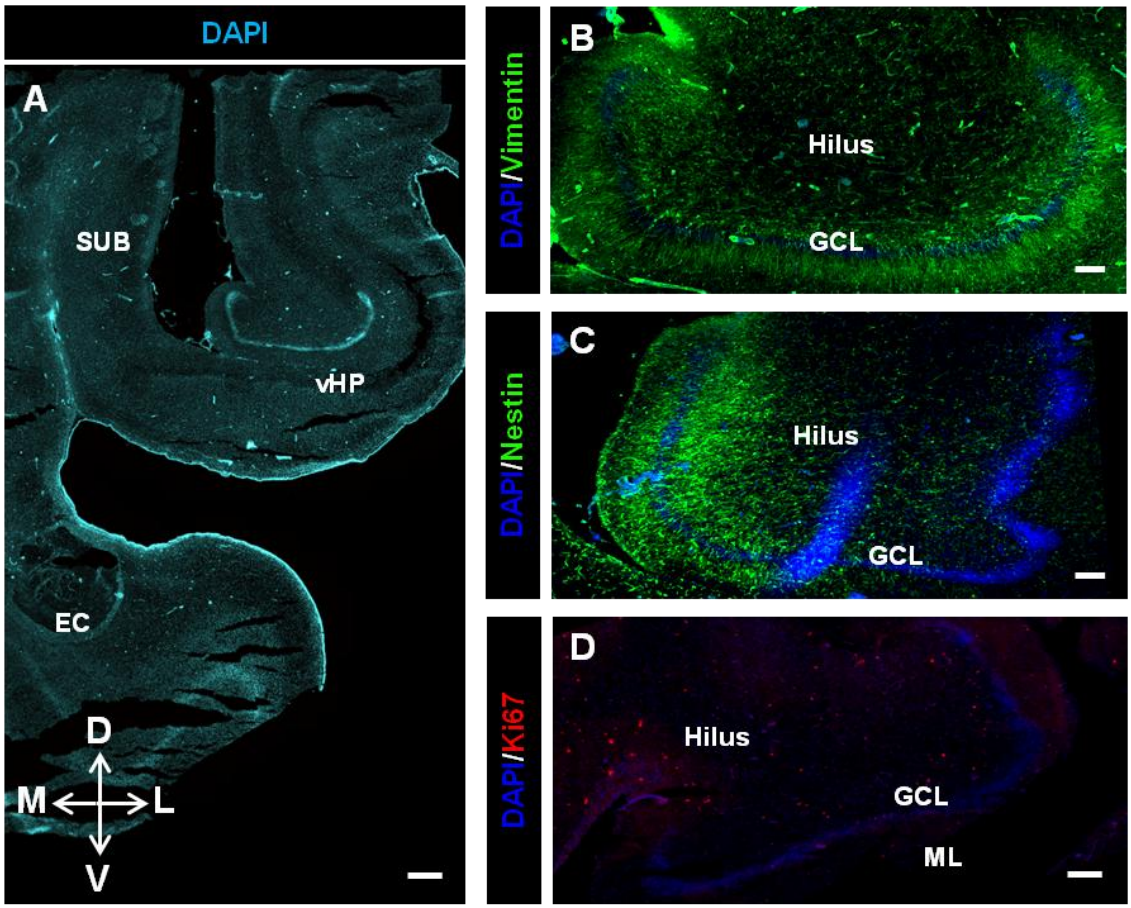

R16 Figura. Jaiotzetik gutxira, RGC eta ugaritze prozesuan zeuden zelulak oraindik ere DGan presente zeuden. A) Lamina-eskaner fluoreszente irudiak hilabete bateko garun baten HPFa erakutsiz. **B-C)** Vimentin eta Nestin zelula positiboa DGan jaio eta hilabete batera. Bi markatzaileak aurkezten zituzten zuntzak ageri ziren GCLa zeharkatuz, hilusetik MLra. **D)** Ugaritze prozesuari begira, DG barruan Ki67 zelula positiboak ikusarazi genituen, nahiz eta gehienbat hilusean ageri ziren, GCLean beharrean. *D: Bizkarraldea. DG: Horzdun zirkunboluzioa. EC: Kortex entorrinala. GCL: Zelula granular geruza. L:*

Laterala. M: Mediala. SUB: Subiculum. V: Sabelaldea. vHPF: Sabelaldeko formazio hipokanpala. Eskala barrak 500 µm-koak An eta 50 µm-koak B-Dn dira.

Tesi honen lehenengo atalean lorturiko emaitzek adierazten dutenez, saguetan hipokanpoko NSC helduak DGaren formazioan parte hartzen duten dNSCengandik desberdintzen den populazio independente bat dira. Halaber, NSC helduen formazioa hain zuzen jaio ondoren DG barruan jazotzen da. Bestetik, gizakietan jaio aurretik ugaritzea DGra mugatzen da, GCLko gune neurogenikoaren formazioa amaiturik legokeela iradokiz. NSC eta neurogenesiaren izatearen inguruan sortu berri den eztabaida alde batera utziz (Moreno-Jiménez et al., 2019; Sorrells et al., 2018), NSC markatzaileak adierazten dituzten RGCen existentziak ez du zalantza izpirik uzten (Blümcke et al., 2001; Cipriani et al., 2018; Sorrells et al., 2018) **(R16 Figura)**. Izan ere, konbultsio infantilen ondoren Nestin zelula positiboak areagotzen direla deskribatu izan da, estimulu patologikoetan zelula hauen paper posible bat iradokiz. Saguetan, konbultsioen ostean hipokanpoko zelula helduak masiboki aktibatuak izaten dira, erreaktibo bihurtuz (Muro-García et al., 2019; Sierra et al., 2015), nahiz eta emaitza honetara eramaten duen mekanismoak ezezagun dirauen. Hemen, MTLE sagu modelo bat erabiliz zeinetan konbultsioak KA injekzio intrahipokanpal baten bitartez eragiten diren (Bouilleret et al., 1999; Sierra et al., 2015), NSCen erantzun goiztiarrean jardun dezaketen bi posible hartzaile ikertu genituen (FGFR eta EGFR).

6.5. FGFR ibilbideak eta MTLE egoeran HPFak ematen duen erantzun goiztiarrak ez dute loturarik

FGFR seinalizazio ibilbidea, batez ere FGF2ra erantzuten duen FGFR1en bitartez, hazitako NSPC eta astrozitoen jarduera mitotikoaren modulatzaile dela demostratu izan da (Reynolds and Weiss, 1992; Tropepe et al., 1999). Izan ere, KA injekzio intraperitonealaren ostean FGF2ren eta bere hartzaile FGFR1en areagotzea ikusi izan da, bereziki zelula glial erreaktiboetan (Van Der Wal et al., 1994; Gómez-Pinilla et al., 1995). Honela, gure ustez FGFR seinalizazio ibilbideak, eta bereziki FGFR1ek, rol garrantzitsu bat joka lezakete MTLE sagu modeloetan erantzun azkar bezala NSCek pairatzen duten aktibazio eta React-NSC transformazioan (Muro-García et al., 2019; Sierra et al., 2015).

Hemen, ongi karakterizatua dagoen MTLE sagu modelo batean FGFR1en espresioa neurtzea izan dugu helburu (Bouilleret et al., 1999; Sierra et al., 2015). Horretarako, bai KA (MTLE group) zein disoluzio isotoniko (kontrol talde bezala) 1 nM intrahipokanpalki sagu helduetan administratu ziren eta euren hipokanpoak

injekzioaren ostean denbora ezberdinetan batuak izan ziren **(R17 A Figura)**. Espero genuenaren kontrara, KA injekzioaren osteko lehen 72 h-etan zehar FGFR1k ez zuen mRNA edo proteina mailan aldaketarik pairatu, RT-qPCR eta WB bidez neurturik, hurrenez hurren **(R17 B-C Figura)**. FGFR1az gain, FGFR2ren mRNA maila ere neurtu genuen, FGF2rekiko afinitate handiko beste hartzailea (Dionne et al., 1990; Johnson et al., 1990), KA administrazioaren osteko lehen 72 h-etan aldaketarik ikusi barik ezta ere **(R17 C Figura)**. HPF osoaren analisiak DGan gertatu litezkeen FGFR1en alterazio espezifikoak ezkutatu zitzakeenaren beldurrez, IHC bitartez FGFR1en espresioa ehunean neurtzera pasatu ginen, KA injekzioaren ostean 24 h-tara. Gune neurogenikoan eman zitezkeen FGFR1en alterazio posibleak ikusarazteko 24 h denbora tarterik hoberena izatea kontsideratu genuen, KA administrazioaren osteko ugaritzea areagotzen hasten baita 24 h-tara eta 72 h-tan goia jotzen du (Sierra et al., 2015). Hala, ondorengo erantzun osoa probokatzeko FGFR1ek 24 h-tarako areagotua egon behar litzatekeela kontsideratu genuen. Haatik, ez genuen diferentziarik antzeman kontrol eta KA animalien artean **(R17 D Figura)**, FGFR seinalizazio ibilbideak MTLEren indukzioaren ostean gertatzen den erantzun azkarrarekin zerikusirik ez duela adieraziz.

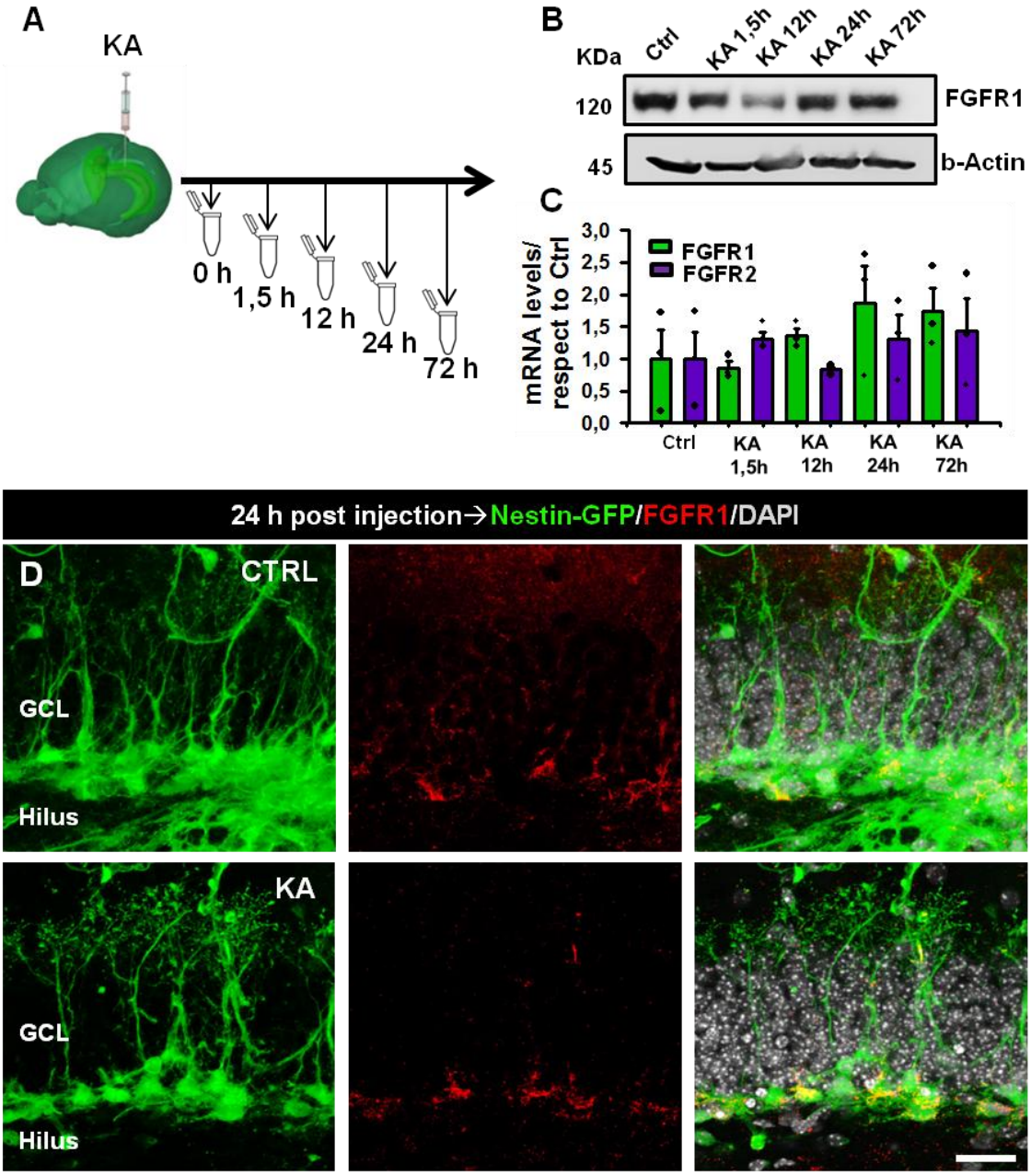

R17 Figura. KA administrazioaren ostean FGFR maila ez zen aldatu. A) KA injekzioaren osteko hipokanpo bilketarako jarraituriko denbora-eskalaren eskema. **B)** WBak erakutsi bezala, KA injekzioaren osteko lehen 72 h-tan FGFR1 proteina maila ez zen aldatu. **C)** RT-qPCR analisiak FGFR1 eta FGFR2 mRNA mailan, KA injekzioaren lehen 72 h-tan, aldaketarik ez zegoela erakutsi zuen. **D)** Irudi konfokal errepresentatiboak KA edo disoluzio isotoniko (kontrol) injekzioaren ostean GCLa eta Nestin-GFP espresatzen zuten zelulak erakutsiz. KA injekzioa eta 24 h-ra ez zen FGFR1 espresioaren aldaketarik antzeman. *CTRL: Kontrol. GCL: Zelula granular geruza. KA: Azido kainikoa. Eskala barrak 20 µm-koak dira. Diferentzia estatistikorik ez zegoen (C)n bide bakarreko ANOVAk kontrol taldearen aurkako Holm-Sidak post-hoc testak jarraiturik adierazi bezala. Barrek batez-bestekoa ± errore estandarra erakusten dute. Puntuek datu indibidualak erakusten dituzte.*

6.6. EGFRek gune neurogenikoak MTLE indukzioaren ostean duen hasierako erantzunean parte hartzen du

Honela, aurreko emaitzek FGFR gune neurogenikoak eta NSCek konbultsioen ostean duten erantzunaren erregulatzaile bezala albo batera uzten dute. Hortaz, hurrengo hautagaia ikertzera jo genuen, EGFR seinalizazio ibilbidea, NSPCen ugaritzean ere parte hartzen duena (Reynolds and Weiss, 1992; Tropepe et al., 1999), haren espresio nuklearra ugaritze prozesuan sakon murgilduriko zelulekin zuzenean erlazionatuta egonik (Lin et al., 2001). EGFR astrozitoentzako agente mitogeniko indartsua dela demostratu izan da (Simpson et al., 1982) eta glioblastomaren garapenarekin oso erlazionaturik dago (Lee et al., 2006; Libermann et al., 1985; Vivanco et al., 2012). Are gehiago, bai arratoi zein gizakietan EGFR areagotu egiten da zauri fokalen modelo ezberdinetan (Ferrer et al., 1996; Nieto-Sampedro et al., 1988; Río et al., 1995). Garrantzitsuago, ErbB familiaren espresioak (EGFR parte delarik) KAren administrazioaren ostean HPFan gora egiten du (Sierra et al., 2015). Hala ere, EGFRren konbultsioen osteko inplikazio espezifikoa ez da oraindik ezagutzen eta honela, MTLE sagu modeloan EGFRren alterazio posibleak ebaluatzeari ekin genion.

6.6.1. MTLEren indukzioaren ostean, EGFR seinalizazio ibilbidearen aktibazio eta areagotzea jazoera azkarrak izan ziren

Aurretik erabilitako paradigma berdina erabiliz EGFRren espresioa ebaluatzeari ekin genion; KAa edo disoluzio isotonikoa (kontrol taldea) intrahipokanpalki administratu genituen eta ondoren denbora-eskala bat jarraituz hipokanpoak bildu genituen (1,5 h, 12 h, 24 h eta 72 h) **(R18 A Figura)**. RT-qPCR analisiaren bitartez EGFR mRNA maila neurtu genuen, 1,5 h, 24 h eta 72 h KA administrazioaren ostean 2-3 aldiko areagotzea ikusaraziz **(R18 B Figura)**. Hurren, KA administrazioaren ostean EGFR maila areagotua ageri zenez, WB bidez EGFR seinalizazio bidearen aktibazioa neurtzera jo genuen. Y845 EGFR fosforilazio hondakinaren maila neurtu genuen, zeina EGFR bitartezko mitogenesiarekin erlazionatua dagoen (Biscardi et al., 1999; Sato et al., 1995; Tice et al., 1999). Emaitzek EGFR totalaren artean fosforilatutako Y845 EGFR proportzioaren areagotzea azaldu zuten, estatistikoki esanguratsua bilakatuz 24 h-ko denbora puntua eta gero **(R18 C-D Figura)**.

Y845 EGFRren fosforilazioak hainbat ur beherako seinalizazio ibilbide aktibatzen ditu, STAT3, Akt eta ERK1/2 barne, zeinek erreaktibotasun glialean, zelula biziraupenean, apoptosian eta ugaritze zelularrean parte hartzen duten (Goffin and Zbuk, 2013; Lill and Sever, 2012; Meloche and Pouysségur, 2007; Priego et al., 2018).

Geure analisiek KA administratu eta 12 h-ra STAT3ren kopuru totalaren artean maila fosforilatuen (aktibatuen) areagotzea demostratu zuten, hortik aurrera murriztu egiten delarik **(R18 C-E Figura)**. Akt seinalizazio ibilbideari erreparatuz, Akt totalaren artean fosforilaturiko Akt proportzioa era esanguratsuan areagotua zegoen KA administratu eta 24 h-tik aurrera **(R18 C-F Figura)**. Era berean, fosforilaturiko ERK1/2a ere areagotua ageri zen KA asministratu eta 1,5 h-ra eta areagotze honek goraka jarraitu zuen aztertutako azken denbora punturaino (72 h KAren ostean). Garrantzitsua da esatea aldaketa hauek proteina kopuru totalaren kontingente direla, zeina era ezberdinetan aldatu daitekeen. Izan ere, WBak EGFRk eta STAT3k areagotzeko tendentzia zutela erakutsi zuen, Akt-k eta ERK1/2k gutxitzeko tendentzia agertu zuten artean **(R18 C Figura)**. Edozein kasutan, MTLE induzitu eta gutxira EGFRren espresioa HPFan ez zen bakarrik areagotu, baizik eta gutxienez bere Y845 fosforilazio lekuan oso fosforilatua gertatu zen. Are gehiago, KA administratu eta gutxira EGFRren hainbat ur beherako seinalizazio ibilbide (STAT3, Akt eta ERK1/2) fosforilatuak izan ziren, konbultsio ostean jazotzen den erantzun hipokanpalean seinalizazio ibilbide honek rol inportante bat joka lezakeela iradokiz.

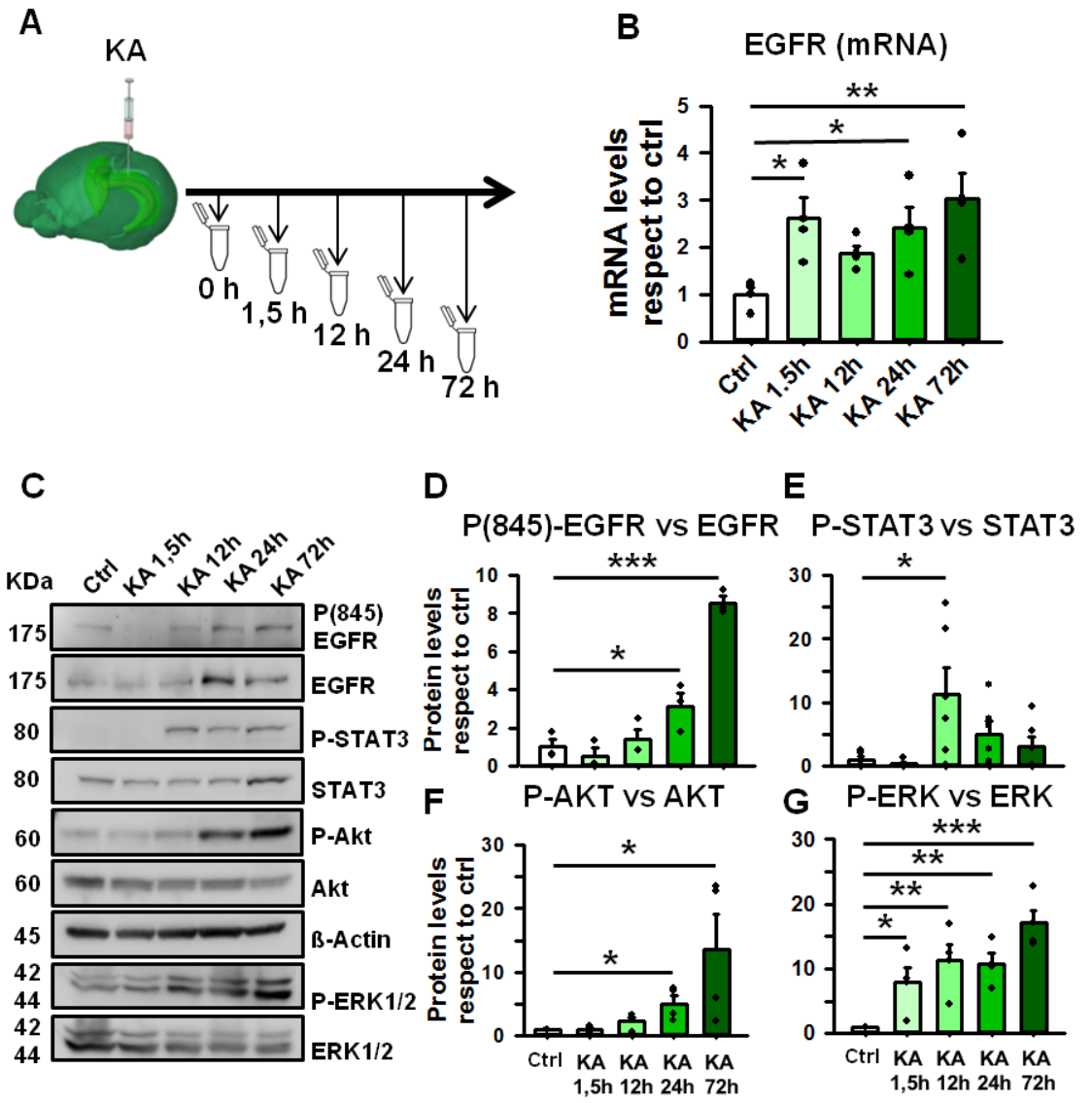

R18 Figura. EGFR seinalizazio ibilbidearen aktibazioa eta espresio areagotzea MTLE osteko gertakizun azkarrak izan ziren. A) KA injekzioaren osteko hipokanpo bilketarako jarraituriko denbora-eskalaren eskema. **B)** KA administratu eta denbora-tarte ezberdinetan RT-qPCRak EGFRren mRNA mailaren areagotzea erakutsi zuen. **C)** KA administratu eta denbora-tarte ezberdinetan WBak aldaketak erakutsi zituen EGFR, Y845 EGFR, STAT3, Akt eta ERK1/2 proteina kopuruan eta fosforilazio mailan. **D-G)** Fosforilaturiko isoformen kuantifikazioa proteina kopuru totalarekin alderatuta EGFRan eta bere ur beherako seinalizazio ibilbide diren STAT3an, Aktan eta ERK1/2an. Grafiko bakoitzeko datuak normalizatuak izan ziren kontrol taldearen batez bestekoa 1 ± errore estandarra bezala hartuta. **p<0.05*, ***p<0.01 eta ***p<0.001. Bide bakarreko ANOVA Holm-Sidak post hoc testaren bidezko kontrol taldearen aurkako konparazio anizkoitzez jarraitua (A)n, (D)n eta (G)n. Kruskal Wallis Dunnet post hoc testaren bidezko kontrol taldearen aurkako konparazio anizkoitzez jarraitua (E)n eta (F)n. Barrek batez bestekoa ± errore estandarra erakusten dute.Puntuek datu indibidualak erakusten dituzte.*

Behin konfirmaturik KAaren bitartez MTLEa induzitu eta berehala HPFan EGFRren espresioa areagoturik ageri zela eta bere hainbat ur beherako seinalizazio

ibilbide (STAT3, Akt eta ERK1/2) aktibaturik ageri zirela, gure hurrengo hipotesia EGFRa espezifikoki NSCetan areagotua egon beharko lukeela izan zen, euren aktibazio masibo eta transformazio erreaktiboan paper bat jokatuz. Hau aztertzeko, Nestin-GFP sagu transgenikoetan bai KA edo disoluzio isotoniko (kontrol taldea) injekzio intrahipokanpalak gauzatu genituen eta 24 h geroago EGFR espresioa gune neurogenikoan neurtu genuen. Horretarako, IHC eta mikroskopia konfokala konbinatu genituen, EGFR pixel positiboek Nestin-GFP espresatzen zuten zelulekin zuten gainjarpena neurtuz.

Kontrol egoeretan, EGFR espresioa Nestin-GFP espresatzen zuten zelula kopuru murriztu batera estuki mugaturik ageri zen, hain zuzen ere RGC antzerako NSC helduak eta ANPak. Kontraste zorrotzean, KA eman eta 24 h-ra gune neurogenikoan eta Nestin-GFP espresatzen zuten zeluletan EGFR espresioa era esanguratsuan areagotu zen **(R19 A Figura)**. Izan ere, KAren ostean EGFR positiboak ziren pixel kopuruaren kuantifikazioak GCLean gora egiteko tendentzia **(R19 B Figura)** eta hilusean areagotze esanguratsua ageri zituen **(R19 C Figura)**. Are garrantzitsuago, KAren ostean EGFRren gainjarpena Nestin-GFP espresatzen zuten NSCekin, irizpide morfologikoen bitartez identifikatuak (Mignone et al., 2004), %450 batean areagotua ageri zen **(R19 D Figura)**, konbultsio osteko erantzunean NSCek ematen duten erantzunean hartzaile honek rol bat jokatzen duela biziki iradokiz.

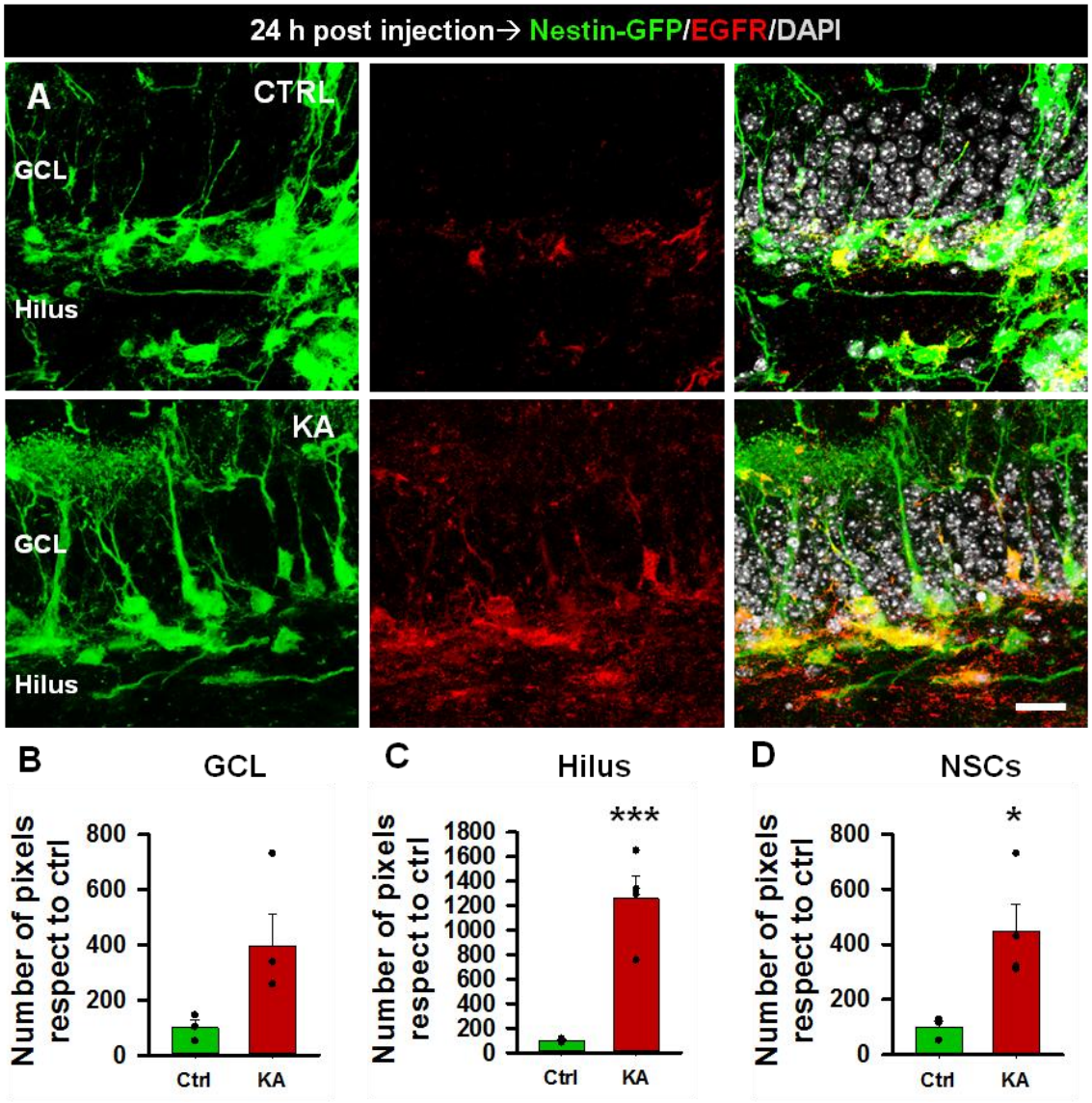

R19 Figura. KA administrazioaren ostean gune neurogenikoan eta NSCetan EGFR areagotu egin zen. A) Irudi konfokal errepresentatiboak KA edo disoluzio isotoniko (kontrol) injekzioen ondoren. **B-D)** DGko eremu ezberdinetan (GCL eta hilusa) EGFR espresioaren (pixeletan) eta NSCekiko gainjarpenaren kuantifikazioak. Grafiko bakoitzeko datuak normalizatuak izan ziren kontrol taldearen batez bestekoa 100 ± errore estandarra bezala hartuta. *GCL: Zelula granular geruza. KA: Azido kainikoa. SAL: Disoluzio isotonikoa. Eskala barrak 20 µm-koak dira.* *p<0.05 eta ***p<0.001. *Mann Whitney testa (B)n eta Student's t testa (C)n eta (D)n. Barrek batez-bestekoa ± errore estandarra erakusten dute.Puntuek datu indibidualak erakusten dituzte.*

6.6.2. EGFRk NSPC hipokanpalen ugaritze jardueran parte hartzen zuen

Lorturiko emaitzek konbultsioen ondoren EGFRak NSCengan izan lezakeen akzio potentzial bat erakusten dute, gune neurogenikoan eta NSCetan KA administratu ostean ematen den hartzailearen areagotzea kontuan harturik. Honela, hartzailearen

rola argitzea bilatuz NSPC hipokanpalak *in vitro* isolatu eta aberastera pasatu ginen, aurretiaz optimizaturiko metodoak moldatuz (Pineda et al., 2013). Planteamendu honek EGFRren presentzia egiaztatu eta honen seinalizazioa kanpoko gune seinaleen interferentzia barik (ioiak, molekulak edota zirkuituaren jarduera elektrikoa) modulatzea ahalbidetu zuen.

Espero zen bezala, 2 hilabete heldu ziren saguetatik NSPCak isolatu, hazi eta astebetera EGFR zelula guztietan presente zegoela egiaztatu genuen **(R20 A Figura)**. Hortaz, behin artifizialki ugaritzera bultzatutako NSPCetan EGFRren presentzia demostratuta, euren ugaritze ahalmenean EGFRren inhibizioak izan zezakeen efektua ebaluatzeari ekin genion. NSPCak ugaritze prozesu jarraituan izanik, EGF estimulazioaren bitartez EGFR seinalizazioa aktibaturik zelarik, EGFRren inhibizio farmakologikoaren efektua ebaluatu genuen bere inhibitzaile itzulgarria den Gefitinib erabiliz, zeinak EGFRren tirosina leku guztietako fosforilazioa blokeatzen duen (Pedersen et al., 2005). Kasu honetan, Gefitinibek EGFRrengan duen efektua zentzu global batean ulertzeko helburuarekin, ez genuen soilik Y845 fosforilazio lekua aztertu, aurretik egin bezala, baizik eta Y1068 autofosforilazio lekua ere, zeina aski ezaguna den EGFRren bitartezko zelula ugaritzea kontrolatzeagatik (Downward et al., 1984). Haratago joanik, zelula ugaritzearekin zuzenean loturik dagoen EGFRren ur beherako seinalizazio ibilbidea denetik, ERK1/2 fosforilazioa ere aztertu genuen (Meloche and Pouysségur, 2007). WB bitartez emaitzek erakutsi zutenez, haziriko NSPCetan ordubetez Gefitinib 2 µM gehitzeak EGFRren Y845 eta Y1068 hondakinen fosforilazioa era eraginkorrean murrizten du eta baita ERK1/2ren fosforilazioa baita **(Figure R20 B-E)**. Honela, Gefitinibek NSPCengan duen efektua demostratu zen eta *in vivo* konbultsio ostean gertatzen den NSCen aktibazio masiboa eta React-NSC indukzioa alderantzikatzeko alternatiba terapeutiko potentzial bezala aurkeztu zen.

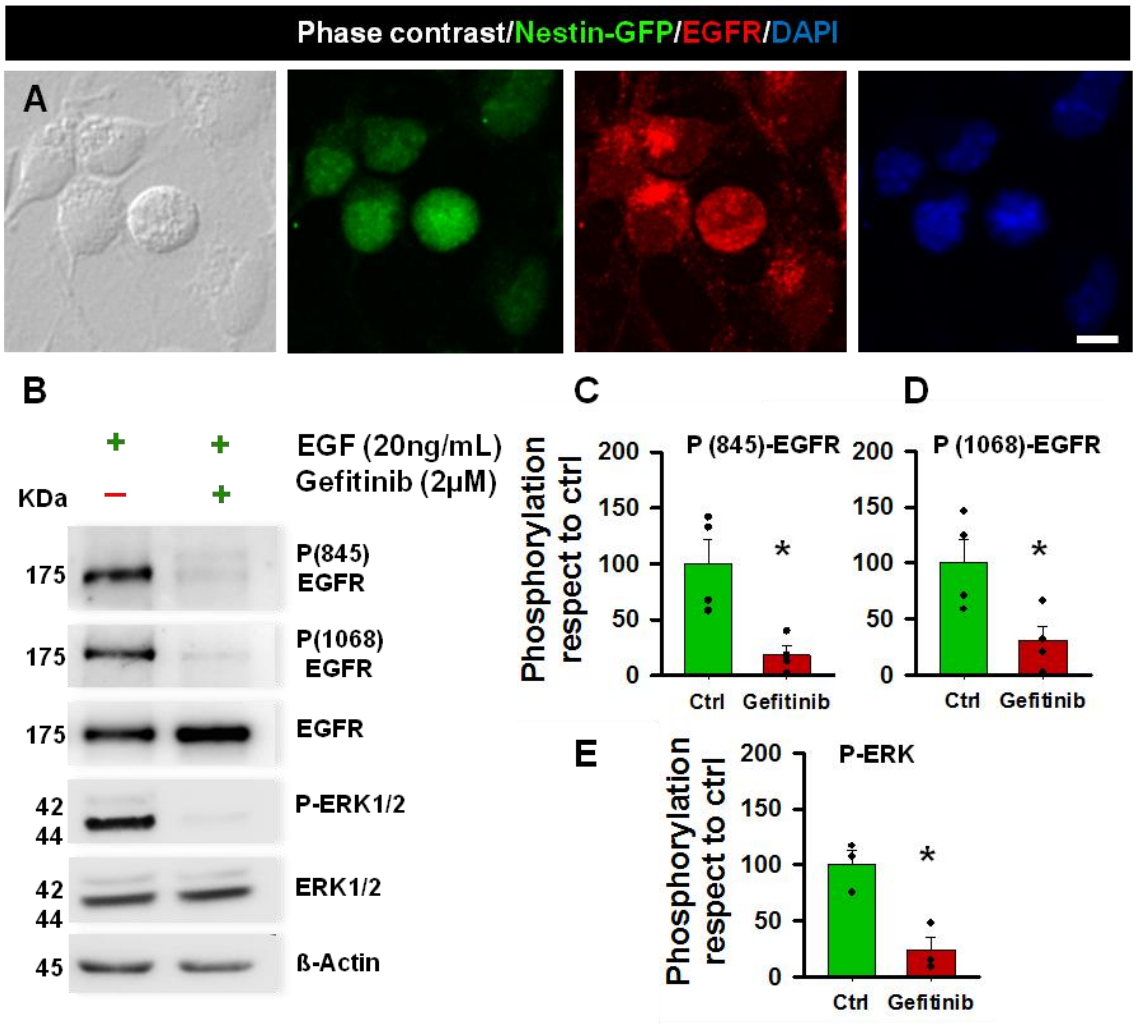

R20 Figura. ***In vitro*** **haziriko DGko NSPCetan Gefitinibek era eraginkorrean itzaltzen du EGFR seinalizazioa. A)** Irudi konfokal errepresentatiboak Nestin-GFP espresatzen duten haziriko NSPCetan EGFR espresioa erakutsiz. **B)** WB irudi errepresentatiboak EGFR eta ERK1/2 eta hauen aktibazioa EGFrekin eta FGFrekin estimulaturiko NSPCetan, baita EGFRren inhibitzaile den Gefitinibekin ere. **C-E)** Fosforilaturiko isoformen kuantifikazioa proteina kopuru totalarekin alderatuta EGFRrentzako (Y845 eta Y1068) eta honen ur beherako seinalizazio ibilbidea den ERK1/2rentzako. Grafiko bakoitzeko datuak normalizatuak izan ziren kontrol taldearen batez bestekoa 100 ± errore estandarra bezala hartuta. *Eskala barrak 20 µm-koak dira. *p<0.05. Mann Whitney testa (C)n. Student's t testa (D)n eta (E)n. Barrek batez bestekoa ± errore estandarra erakusten dute.Puntuek datu indibidualak erakusten dituzte.*

Gure emaitzek orain arte adierazi zutenez, *in vitro* hazitako NSPC hipokanpaletan EGFR presente ageri zen eta Gefitinib bere seinalizazio aktibitatea eteteko kapaza zen. Ondoren, EGFRek NSPCen ugaritze jardueran izan lezakeen rol potentzialaren gainean argia igortzea jarri genuen helburu. EGFR SVZan aktibaturiko NSCetan presente ageri dela demostratu egin da (Codega et al., 2014; Pastrana et al., 2009), baina honek NSC hipokanpaletan duen rolak ezezagun dirau. Honela, gure *in*

vitro paradigma esperimentalarekin segituz, lehenbizi EGFRren espresioa NSPC mitotiko eta ez-mitotikoetan neurtu genuen, ondoren BrdU erabiliz ugaritze prozesuan zeuden NSPCen proportzioa neurtuz Gefitinibek euren gainean duen efektu funtzionala ikertzeko. Emaitzen arabera, mitosian zeuden NSPCetan EGFR espresioa areagotu egiten zen ,interfasean zeudenekin alderatuta, azken hauek DAPI tindaketaren disposizio kromosomikoaren bidez identifikatu zirelarik **(R21 A-C Figura)**. Are gehiago, BrdUa finkatu baino ordubete lehenago bereganatzen zuten zelulak 2 µM Gefitiniben presentzian%37 batean gutxitu egiten ziren, ibilgailuaren (DMSO) presentzian zeudenekin alderaturik **(R21 D-E Figura)**, NSPCen ugaritzerako EGFRren garrantzia esentziala eta Gefitiniben bitartezko blokeo eraginkorra konfirmatuz.

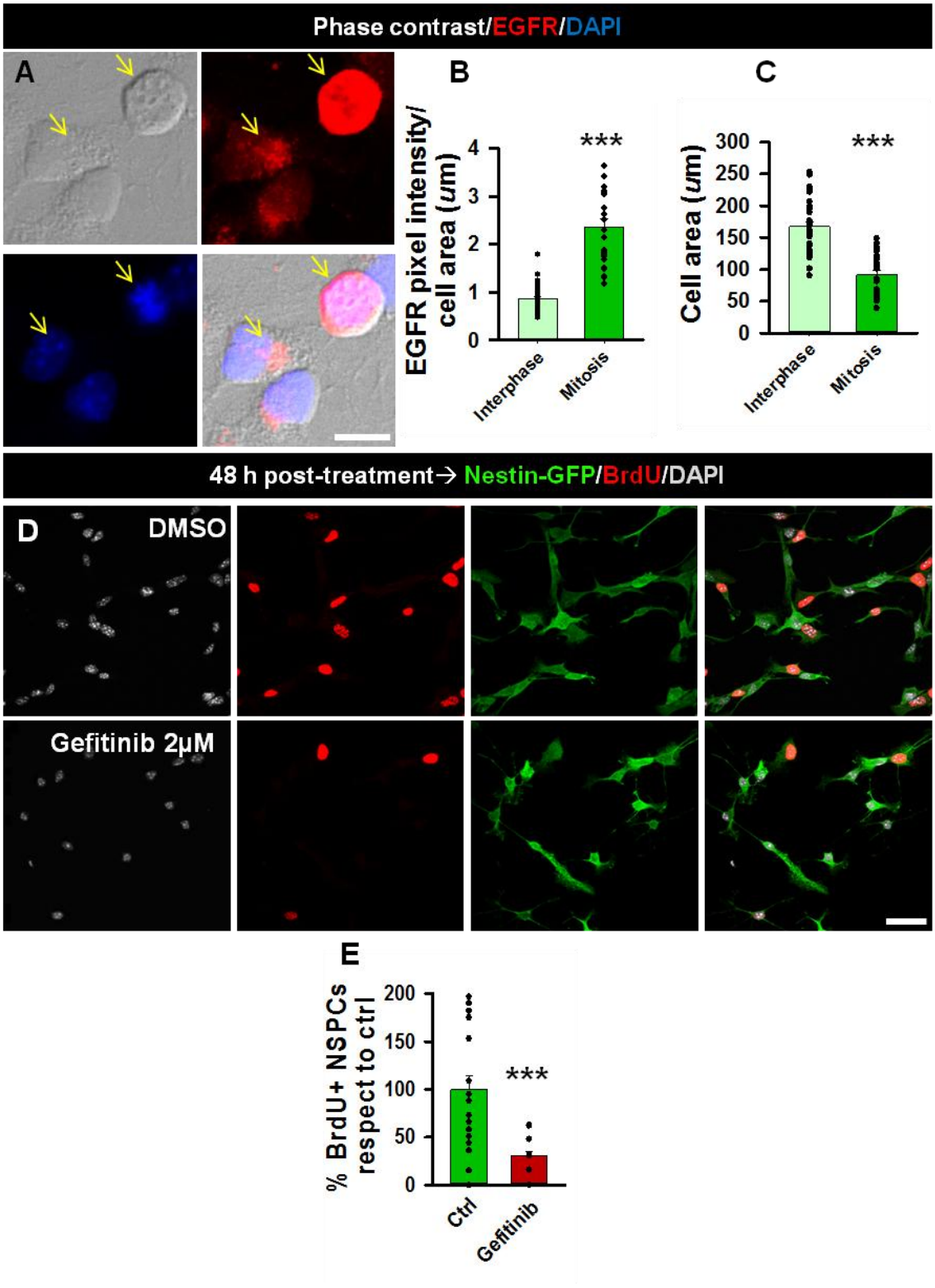

R21 Figura. DGtik eratorritako NSPCen EGFRren bitartezko ugaritze jarduera gutxitu egiten zen Gefitiniben presentzian. A) Irudi konfokal errepresentatiboak NSPC mitotiko eta ez-mitotikoak erakutsiz (DAPI erabiliz disposizio kromosomikoaren bitartez identifikatuz), NSPC mitotikoetan EGFR intentsitate handiagoa dagoelarik. Geziek zelulen kokapena adierazten dute. **B-C)** Zelulen arean eginiko EGFR intentsitate kuantifikazioak (B) eta zelulen area totala NSPC mitotiko eta ez-mitotikoetan (C). **D)** Irudi

konfokal errepresentatiboak Gefitinib bitartez trataturiko zeluletan ugaritze fasean aurkitzen ziren zelulen (BrdU bereganatzeak adierazi bezala) murriztea erakutsiz, DMSOrekin trataturiko kontrol NSPCekin alderatuz. **E)** Kontrol taldearekin (DMSOrekin trataturiko NSPCak) alderatuz Gefitiniben presentzian BrdU positiboak ziren NSPCetan gertatzen zen gutxitzea erakusten duen kuantifikazioa. Grafiko bakoitzeko datuak normalizatuak izan ziren kontrol taldearen batez bestekoa 100 ± errore estandarra bezala hartuta. *Eskala barra 20 µm-koa da. ***p<0.001. Mann Whitney (B)n eta (E)n. Student's t testa (C)n. Barrek batez bestekoa ± errore estandarra erakusten dute.Puntuek datu indibidualak erakusten dituzte.*

Gefitinib, EGFRren inhibitzaile itzulgarria, NSPCtan ugaritzea eraginkorki murrizteko kapaza izanik, Afatinib EGFRren inhibitzaile ez itzulgarriak efektu handiagoa izan ote zezakeen probatzea erabaki genuen. Afatinibek EGFRren kinasa jarduera eraginkorki erreprimitzen du eta tumore pazienteek inhibitzaile itzulgarriekiko kinasa domeinuaren mutazioen ondorioz duten erresistentziari aurre egiteko diseinatua izan zen (Li et al., 2008). Gefitinib erabiliz lorturiko emaitzen kontrara, 2µM Afatinib inhibitzaileak heriotza zelular masiboa eragin zuen 48 h-tan, NSPC ia guztien galerak, geratu zirenen morfologia boroboilduarekin, tamaina txikiarekin eta DNA nuklear kondentsatuarekin batera adierazten zuenez **(R22 A Figura)**. Izan ere, kuantifikazioak BrdU zelula positiboen murriztea erakutsi zuen Afatiniben presentzian, nahiz eta jazoriko heriotza zelular maila altuaren ondorioz Afatinibek mitosiaren gainean duen efektuari buruzko konklusio sendorik ezin den irudikatu **(R22 B Figura)**.

Hala, lorturiko emaitzetan oinarriturik, *in vivo* MTLE esperimentalean EGFR inhibitzeko eta inhibizo honek gune neurogenikoaren gainean duen efektua ebaluatzeko Gefitinib hautagai apropos bezala ikusi genuen. Afatinib erabilita *in vitro* lorturiko aurkako efektuek bere erabilera estrategia terapeutiko bezala burutik kentzea ekarri zuten.

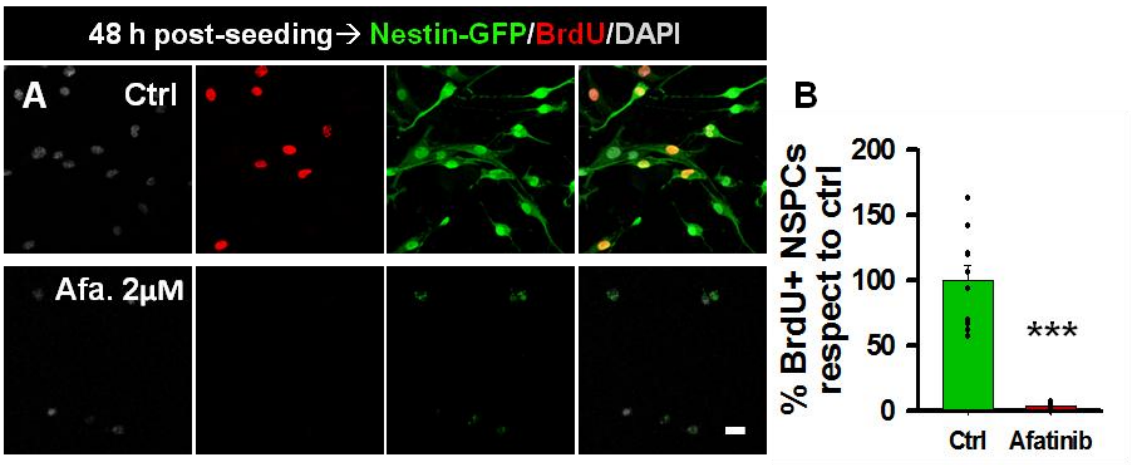

← Aurreko orrialdean. R22 Figura. Afatiniben bidezko EGFRren blokeo itzulezinak NSPCen heriotza zelularra eragin zuen. A) Konfokal irudi errepresentatiboak Afatinibek NSPCetan duen efektu suntsitzailea erakutsiz, zelula galera masiboa ekarriz. **B)** Afatinibekin tratatutako zeluletan eman zen BrdU zelula positiboen galera erakusten duen kuantifikazioa, kontrol kondizioarekin konparatuz. Grafiko bakoitzeko datuak normalizatuak izan ziren kontrol taldearen batez bestekoa 100 ± errore estandarra bezala hartuta. *Eskala barra 20 µm-koa da. ***p<0.001. Mann Whitney. Barrek batez bestekoa ± errore estandarra erakusten dute. Puntuek datu indibidualak erakusten dituzte.*

6.6.3. EGFRren blokeo farmakologikoak MTLE osteko NSCen erantzun patologikoaren hobetzea ekarri zuen

KA administrazio hipokanpalaren ostean EGFR inhibitzeak gune neurogenikoan eta NSCetan duen efektua ebaluatzeko Gefitinib erabiliz jarraitzea erabaki genuen, Afatinibek probokatutako heriotz zelular masiboa kontuan izanik. Injekzio zuzenak sor zezakeen lesioa ekiditeko (KA soila injektatzean baino bolumen handiagoa baitzen); gizakietan aplikazio potentziala errazteko eta Gefitinibak muga hematoentzefalikoa (ingelesetik blood brain barrier, BBB) zeharkatzen ez duelako sudurreko administrazioa erabili genuen (Chen, 2013; McKillop et al., 2004). Sudurreko bidea erabilia izan da beste droga antiepileptiko batzuen administraziorako, hortaz bere eraginkortasuna frogatuz (Barakat et al., 2006).

Aurretiaz eginiko ikerlanek adierazi dutenez KA injekzio intrahipokanpalaren osteko ugaritzea goiz areagotzen da (24 h) eta bere goia jotzen du 72 h-tan (Sierra et al., 2015). Nahiz eta Gefitinib dosi bakar batek ugaritzea 72 orduz murriztu dezakeela argitaratu izan den (Pedersen et al., 2005), guk 12 orduro administratu genuen MTLE eragin eta berehala, ugaritzeak goia jotzen duenean bere efektua maximizatzeko asmoz (Sierra et al., 2015) **(R23 A Figura)**. Espero zen bezala, emaitzek KA ostean 72 ordura Gefitiniba jaso zuten animalietan ugaritzea zeharo murriztua zegoela (hilus eta GCL+SGZ) adierazi zuten, kontrol taldearekin alderatuz, zeinak DMSO intranasalarekin soilik tratatuak izan ziren **(R23 B Figura)**. Are gehiago, gune neurogenikoaren analisi espezifikoak erakutsi bezala KA ostean Gefitiniba jaso zuten animalietan SGZan kokaturiko Ki67 zelula positiboen dentsitatea eta Ki67 positiboak ziren NSCen portzentaia era esanguratsuan murrizturik zeuden **(R23 C and R23 D Figura)**. Emaitza honek EGFRak konbultsio osteko gune neurogenikoan jazotzen den NSCen aktibazio masiboan eta ugaritze orokorrean parte hartzen duela eta are gehiago, Gefitiniben bidezko bere blokeoa alternatiba bat izan daitekeela NSCn populazioa kontserbatu eta neurogenesia epe erdi-luzera mantentzeko adierazten zuten.

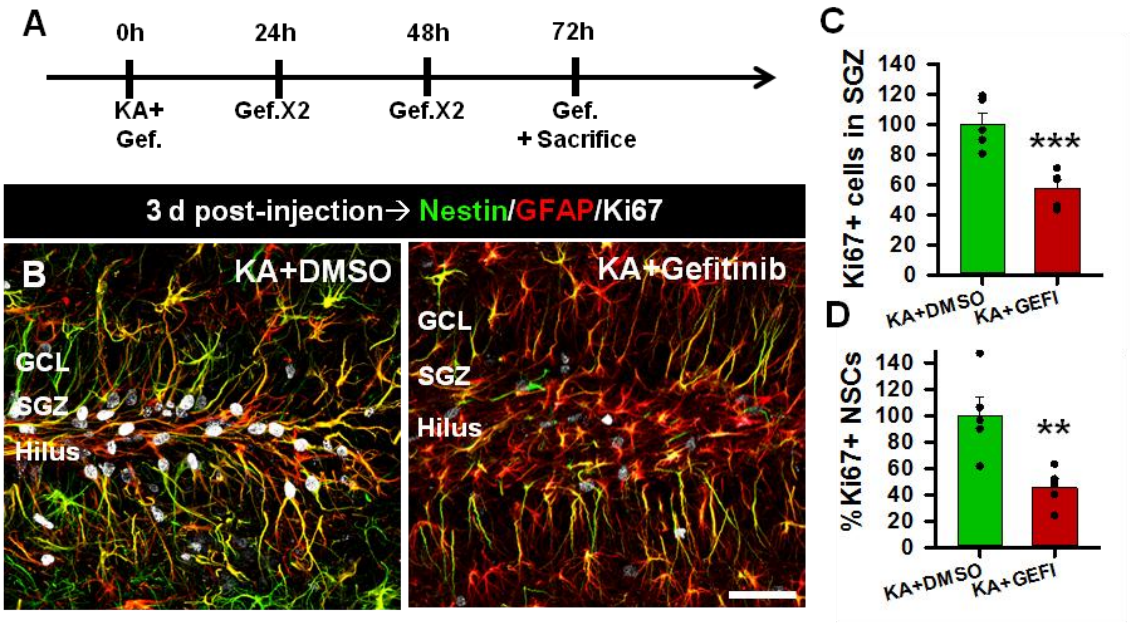

R23 Figura. Gefitiniben administrazioak KA ostean gune neurogenikoan eta NSCetan ematen den ugaritzea murrizten du. A) Paradigma esperimentalaren eskema. KA intrahipokanpalaren administrazioaren ondoren, Gefitinib edo DMSO (CTRL) administratu ziren 12 orduro KA osteko 72 h-tara sakrifizioa egin zen arte. **B)** Irudi konfokal errepresentatiboak KA administrazioaren ondoren DMSO (CTRL) edo Gefitinibarekin trataturiko animalietan DGa erakutsiz. **C-D)** Kuantifikazioak SGZan Ki67 zelula positiboen dentsitatea erakutsiz (C) eta Ki67 positiboak ziren NSCen portzentaia erakutsiz (D) bai KA+CTRL zein KA+Gefitinib taldeetan. Grafiko bakoitzeko datuak normalizatuak izan ziren KA+CTRL taldearen batez bestekoa 100 ± errore estandarra bezala hartuta. *CTRL: Kontrol. GCL: Zelula granular geruza. GEFI: Gefitinib. KA: Azido kainikoa. SGZ: Gune azpigranularra. Eskala barra 20 µm-koa da. **p>0.01, ***p<0.001. Student's t testa. Barrek batez bestekoa ± errore estandarra erakusten dute. Puntuek datu indibidualak erakusten dituzte.*

SGZan emandako ugaritze orokorra eta NSCen aktibazio goiztiarra MTLEa eragin eta berehala Gefitinib emandakoan eragotzita, Gefitinib tratamenduak NSCak epe erdira babesteko balioko lukeen galdetu genion geure buruari, gunearen ahalmen neurogenikoaren galera dakarren React-NSC indukzioa ekidinez (Muro-García et al., 2019; Sierra et al., 2015; Valcárcel-Martín et al., 2020). Honela, DMSO edo Gefitinib bidezko tratamenduak errepikatu genituen KA edo disoluzio isotoniko (kontrol taldea) administrazioaren osteko lehen 72 h-tan zehar, baina oraingoan Nestin-GFP saguak KA eman eta 14 egunera izan ziren sakrifikatuak **(R24 A Figura)**.

MTLE modeloan, bi eragin nagusienetarikoak GCDa eta berriki sorturiko DCX positibo zelula heldugabeen produkziorik eza dira (Muro-García et al., 2019; Sierra et al., 2015). Hemen, KArekin injektaturiko eta DMSOrekin trataturiko animalietan (KA+CTRL) DCX espresatzen zuten zelulen koporu totala 4 aldiz murriztua zegoela

aurkitu genuen, DMSOrekin trataturiko kontrol animaliekin alderatuz (CTRL+CTRL). Interesgarria da zelan KArekin injektaturiko eta Gefitinibekin trataturiko animalietan (KA+GEFI) DCX espresatzen zuten zelulen kopurua kontrol mailara berreskuratu zen, gogor iradokiz Gefitiniben bidezko EGFRren inhibizioa konbultsio osteko epe erdira gune hipokanpalaren ahalmen neurogenikoa babesteko gai dela. Kontrol kondizioetan Gune neurogenikoan zuen efektuaren kontrol neurri modura, Gefitinib animaliak disoluzio isotonikoarekin injektatu ostean administratu genuen (CTRL+GEFI). Kasu honetan, DCX espresatzen zuten zelulen kopurua ez zen disoluzio isotonikoarekin injekatataturiko eta DMSOrekin trataturiko animalietan (CTRL+CTRL) zenaren ezberdina, Gefitiniben bitartez emandako EGFRren inhibizioak neurogenesian eraginik ez duela iradokiz **(R24 B-C Figura)**. GCDa ere ebaluatu genuen (DAPI tindaketaren bidez bere lodiera neurtuz, hilusetik MLra) kontrol eta KArekin injektaturiko animalietan DMSO edo Gefitinib tratamenduen ondoren. Emaitzek erakutsi zutenez, animaliak KArekin injektaturik zeudenean (KA+CTRL) GCDa ageri zen, disoluzio isotonikoarekin injektaturiko kontrol animaliekin alderatuz (CTRL+CTRL). Aurretik DCX espresatzen zuten zelulekin ikusiriko tendentzia bera jarraituz, KArekin injektaturiko animaliak Gefitinibekin tratatuak zirenean (KA+GEFI) GCDa kontrol mailara itzularazten zen **(R24 B-D Figura)**. Espero bezala, DMSO (CTRL+CTRL) zein Gefitinibekin (CTRL+GEFI) tratatuak izan, disoluzio isotonikoarekin injektaturiko animalietan GCDa berdina zen. Beraz, KA administrazioaren ostean Gefitinib bitartezko EGFR inhibizioa gune neurogenikoa babesteko kapaza zela ondorioztatu genuen, gutxienez DCX espresioa zuten zelulen kopuruari eta GCDari dagokionez. Are gehiago, Gefitinib bitartez trataturiko KArekin injektaturiko animalietan React-NSCen indukzioak murriztua ematen zuen DMSOrekin trataturikoekin alderatuz **(R24 B Figura)**, EGFRak React-NSC indukzioan parte hartzen ote duen, hala nola bere inhibizioak Gefitinib erabiliz epe erdira babestu zituzkeen geure buruari galdetzera eraman gintuena.

Hipokanpoko NSCak: Garapenetik Patologiara

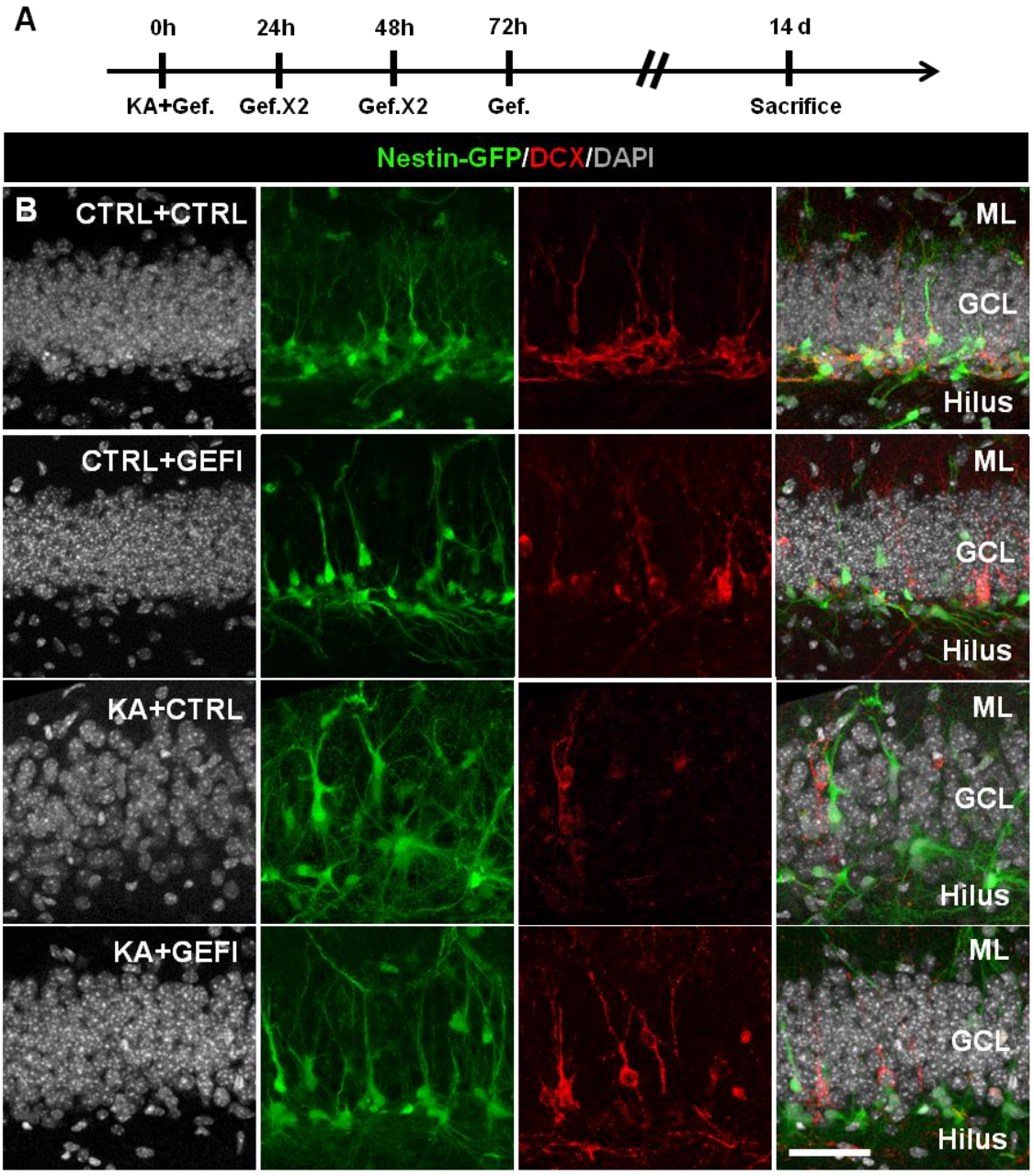

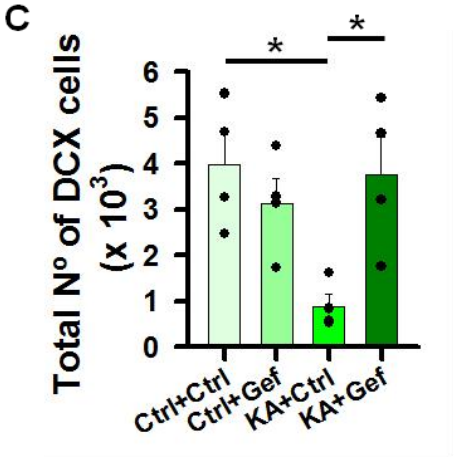

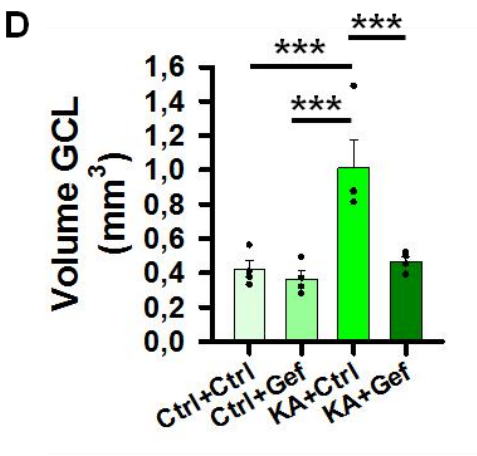

← Aurreko orrialdean. R24 Figura. Gefitiniben administrazioak gune neurogenikoa babestu zuen KA administratu eta 14 egunera. A) Paradigma experimentalaren eskema. Disoluzio isotoniko (kontrol taldea) edo KAren administrazio hipokanpalaren ostean, Gefitinib edo bere ibilgailua (DMSO) 12 h-ro administratuak izan ziren KA eman eta 14 egunera animaliak sakrifikatuak izan ziren arte. Honela, lau talde ezberdin osatu ziren (CTRL+CTRL; CTRL+GEFI; KA+CTRL; KA+GEFI). **B)** Irudi konfokal errepresentatiboak DGa erakutsiz DMSO edo Gefitinib administrazioen ostean disoluzio isotonikoarekin edo KArekin injektaturiko animalietan. **C-D)** Talde bakoitzaren GCLean egindako DCX espresatzen zuten zelula kopuruaren kuantifikazioak (C) eta GCDaren (DAPIren bitartez neurtua) kuantifikazioa (D). *CTRL: Kontrol. GCL: Zelula granular geruza. GEFI: Gefitinib. KA: Azido kainikoa. ML: Geruza molekularra. SGZ: Gune azpigranularra. Eskala barra 20 µm-koa da. *p<0.05, ***p<0.001. Bide bakarreko ANOVA Holm-Sidak post-hoc testaren bidezko binakako konparazio anizkoitzez jarraitua (C)n eta Kruskal-Wallis Student-Newman-Keuls post-hoc testaren bidezko binakako konparazio anizkoitzez jarraitua (D)n. Barrek batez bestekoa ± errore estandarra erakusten dute. Puntuek datu indibidualak erakusten dituzte.*

Ondoren KA administrazioaren osteko React-NSC indukzioan zentratu ginen, hau atzera botatzeko Gefitinibek eduki lezakeen efektua ebaluatuz. Aurretik jarraitutako paradigma berdina jarraitu genuen, intrahipokanpalki KA edo disoluzio isotonikoa injektatuz eta ondorengo egunetan animaliak DMSO edo Gefitinib bitartez sudurretik tratatuz, lau talde ezberdin eratuz (CTRL+CTRL; CTRL+GEFI; KA+CTRL; KA+GEFI). NSCak epe erdira ebaluatzeko asmoz, animaliak injekzio intrahipokanpalak gauzatu eta 14 egunera sakrifikatu genituen **(R25 A Figura)**. Astrozito erreaktiboen ezaugarrietako bat euren morfologia hipertrofiatua da, handituriko soma eta lodituriko prozesuekin (Sofroniew, 2009). Konbultsio ostean NSCek antzeko aldaketak pairatzen dituztela deskribatua izan da baita ere, React-NSCen ezaugarria izanik (Muro-García et al., 2019; Sierra et al., 2015). Hala, aldaketa morfologikoak neurtzeko asmoz 3D Sholl analisira jo genuen (Rodriguez et al., 2006), Nestin-GFP saguetan NSCen prozesuaren luzeera, gurutzebide puntuak eta bolumena neurtuz.

KAren administrazio hipokanpalak, Gefitinibaren ibilgailu den DMSOren sudurreko administrazioaz jarraitua (KA+CTRL), NSCetan prozesu luzeeraren, bolumenaren eta gurutzebide puntuen areagotzea eragin zuen, kontrol taldearekin alderatuz (CTRL+CTRL) **(R25 B-E Figura)**. Aurretik gune neurogenikoaren ebaluaketa orokorra egiterakoan erakutsi bezala (GCDa eta DCX espresatzen zuten zelulen kopurua), Gefitinibaren administrazioarekin KAren administrazioak eragindako Nestin-GFP espresatzen zuten NSCen morfologia erreaktiboa atzera bota zen (KA+GEFI). Aipagarria da nola KA+GEFI taldeak aukeratutako irizpide morfologikoetan CTRL+CTRL eta CTRL+GEFI taldeekin diferentziarik erakutsi ez bazuen ere, euren brokoli itxurako koroa galdua zutela ikusi zitekeen, React-NSCen beste ezaugarrietako bat. Nolanahi ere, EGFRk React-NSCen indukzioan parte hartzen duela ondorioztatu

genuen, hala nola bere Gefitiniben bitartezko inhibizioak NSCen morfologia normala epe erdira (14 egun) kontserbatu zezakeela **(R25 B-E Figura)**. Bestalde, disoluzio isotonikoarekin injektaturiko animalietan Gefitinib administrazioak (CTRL+GEFI) NSCetan aldaketak eragin zituen baita ere, kontrol taldearekin alderatuz (CTRL+CTRL) euren bolumena eta gurutzebide puntuak murriztuz **(R25 D-E Figura)**.

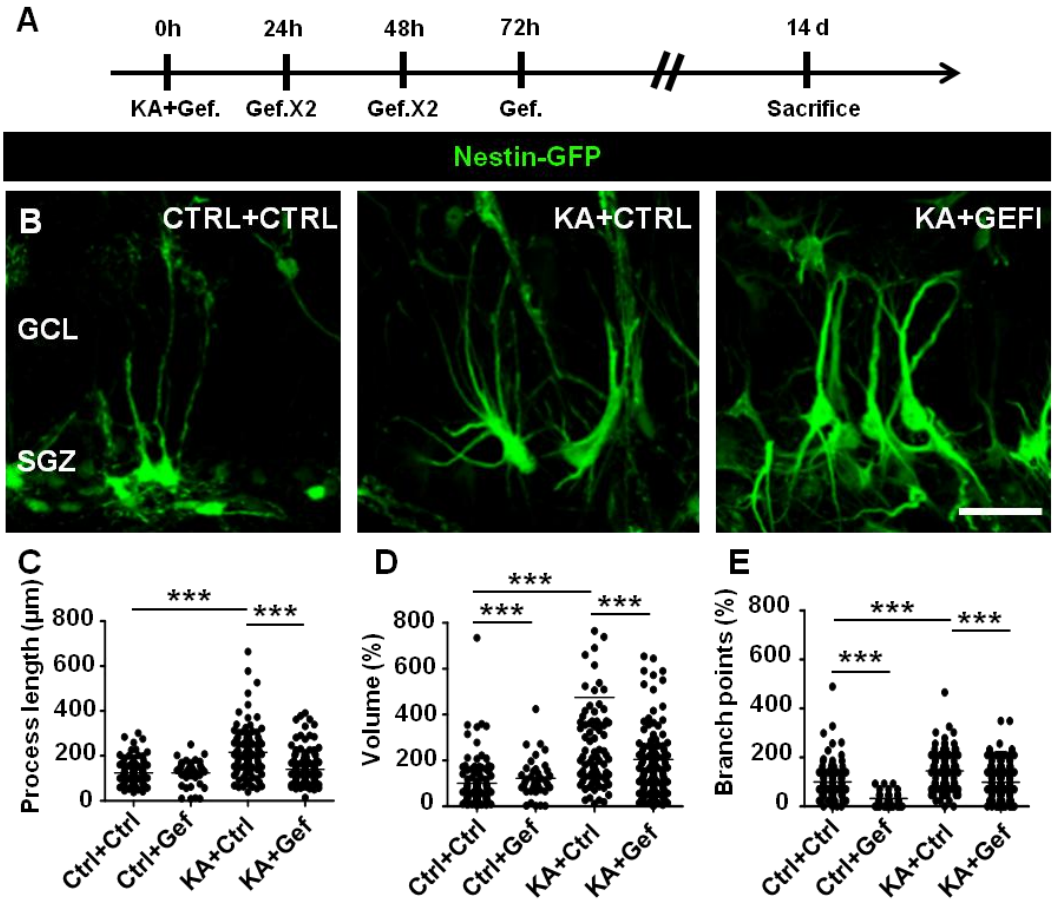

R25 Figura. Gefitinib administrazioak KA administrazioaren ondorioz eragindako React-NSC transformazioa epe erdira murrizten du. A) Paradigma esperimentalaren eskema. Disoluzio isotoniko (kontrol taldea) edo KA administrazio hipokanpalaren ostean, animaliak KA eman eta 14 egunera sakrifikatuak izan ziren arte Gefitinibarekin edo bere ibilgailuarekin (DMSO) 12 orduro administratuak izan ziren. Honela, lau talde ezberdin osatu ziren (CTRL+CTRL; CTRL+GEFI; KA+CTRL; KA+GEFI). **B)** Irudi konfokal errepresentatiboak talde bakoitzeko Nestin-GFP espresioa zuten zelulen morfologia erakutsiz. **C-E)** 3D Sholl analisiaren bidez eginiko kuantifikazioak talde bakoitzean Nestin-GFP espresioa zuten NSCen prozesu luzeera (C), bolumena (D) eta gurutzebide puntuak (E) erakutsiz. Grafiko bakoitzeko datuak normalizatuak izan ziren CTRL+CTRL taldearen batez bestekoa 100 ± errore estandarra bezala hartuta. *CTRL: kontrol. GCL: Zelula granular geruza. GEFI: Gefitinib. KA: Azido kainikoa. SGZ: Gune azpigranularra. Eskala barra 20 µm-koa da. ***p<0.001. Bide bakarreko ANOVA Holm-Sidak post-hoc testaren bidezko binakako konparazio anizkoitzez jarraitua. Barrek batez-bestekoa ± errore estandarra erakusten dute. Puntuek datu indibidualak erakusten dituzte.*

6.7. Zn^{+2}aren rola MTLE egoeran NSCen aktibazioan eta React-NSC indukzioan

Behin EGFRren seinalizazio ibilbideak MTLE sagu modeloan gune neurogenikoaren eta NSCen erantzun goiztiarrean duen partaidetza demostraturik, bere aktibazioa eragin zezaketen mekanismo posibleak aztertzera jo genuen. Hala, geure begirada Zn^{+2}aren norabidean zuzendu genuen, zeina EGFR seinalizazioa bultzatzen duela deskribatu den, bai era zuzenean eta baita zeharka ere, HB-EGFaren askapena eraginez (Samet et al., 2003; Wu et al., 2004). Are gehiago, Zn^{+2} neurobabesle bezala deskribatua izan da, neurona zirkuitu orokorraren hiperaktibazioa ekidituz (Bancila et al., 2004; Takeda et al., 2003). Izan ere, konbultsio ostean, jarduera neuronala larriagotu egiten denean, Zn^{+2} HPFan areagotu egiten dela erakutsi da (Carrasco et al., 2000; Kasarskis et al., 1987; Mody and Miller, 1985). Nolanahi ere, zelula glialetan duen efetuak ezezagun dirau. Hala, konbultsio osteko aktibazio neuronalaren gainean Zn^{+2}aren rol posible bati buruz galdetu genion geure buruari eta neuronengan duen efektuaz aparte EGFRren bidezko aktibazio masiboa eta React-NSC indukzioa bultzatu zitzakeen mekanismo alternatibo bezala proposatu genuen.

6.7.1. MTLE egoeran Zn^{+2} areagotu egin zen gune neurogenikoan

Lehenik, deskribaturiko HPFan ematen den konbultsio osteko Zn^{+2} askapenak (Carrasco et al., 2000; Kasarskis et al., 1987; Mody and Miller, 1985) espezifikoki gune neurogenikoarengan eragiten duen ebaluatzea bilatuz, histokimikoki erreaktiboa (askea) zen Zn^{+2} maila neurtzeko asmotan Danscher tindaketara jo genuen. Danscher tindaketak sodio selenito injekzioa oso garai kontrolatuan behar du (sakrifizioa baino 30 minutu lehenago) granuloen tamaina aldatu barik Zn^{+2}a prezipitatu dadin kondizio guztietan (Danscher, 1981). Hala, disoluzio isotoniko edo KA administrazio intrahipokanpalaren ostean 72 ordutara, KA administrazioaren osteko ugaritzeak goia jotzen duenean (Sierra et al., 2015), GCL+SGZ zonaldean Nestin-GFP espresatzen zuten zelulekin gainjartzen zen Zn^{+2} kopurua neurtu genuen. Emaitzek disoluzio isotonikoarekin injektaturiko kontrol animalietan GCL+SGZ zonaldean Zn^{+2}ik ia ez zegoela erakutsi zuten, hau hilusera mugaturik aurkitzen zelarik, non MFek Zn^{+2}ez beteriko besikula sinaptikoak dituzten (Frederickson et al., 1983; Sindreu et al., 2003), eta beraz Nestin-GFP espresatzen zuten zelulekin gainjarpen oso txikia izanik. Kontrara, KA administrazioaren ostean Zn^{+2} granuluak GCL+SGZ zonaldetik sakabanaturik ageri ziren, Nestin-GFP espresatzen zuten NSCekin neurri batean gainjarriz **(R26 A Figura)**. Izan ere, Zn^{+2} granuluen kuantifikazioak, pixeletan neurtua, behaketa hauek konfirmatu zituen. Lehenbizi Danscher tindaketa teknikaren

kalitatearen neurri bezala Zn^{+2} granuluen tamaina egiaztatu genuen, disoluzio isotonikoarekin eta KArekin injektaturiko animalien artean ezberdintasun estatistikorik antzeman gabe eta beraz teknikaren aldakortasunak sor zitzakeen desberdintasun posibleak baztertuz **(R26 B Figura)**. Bestalde, KA administrazioa jasotako animalietan GCLean Nestin-GFP espresatzen zuten zelulekin gainjartzen zen Zn^{+2} granuluen kopuruak ia 2 aldiko areagotzea aurkeztu zuen, kontrol animaliekin alderatuz **(R26 C Figura)**. Honela, KAak induzituriko Zn^{+2} askapena gune neurogenikoan biltzen zela ondorioztatu genuen, NSCetatik gertu, bien arteko interakzio posible baten ateak irekiz.

Are gehiago, KA ostean Zn^{+2} kopurua HPFean eta espezifikoki gune neurogenikoan areagotzen zela izanik, MTen espresioa ere kondizio hauetan areagotu egingo zela hipotetizatu genuen. MTak Zn^{+2} zelulaz barneko maila gutxitzeaz arduratzen diren metaloproteinak dira, nerbio-sistema zentraleko (ingelesetik central nervous system; CNS) Zn^{+2} homeostasia kontrolatuz (Kägi and Schäffer, 1988; Vašák and Hasler, 2000). Gure hipotesia frogatzeko, aurreko esperimentuetan jarraituriko denbora-eskala jarraitu genuen, animaliak KA ostean denbora puntu ezberdinetan sakrifikatuz (1,5 h, 12 h, 24 h, 72 h) **(R26 D Figura)**. WB bidez MT1 eta MT2 proteina nibelak determinatu genituen eta emaitzek MT1 eta MT2 espresioa KA administratu eta 12 ordura igotzen hasten zela adierazi zuten, kontrol animaliekin konparatuta **(R26 E Figura)**. Era berean, RT-qPCR bitartez MT1, MT2 eta baita MT3 mRNA maila ere determinatu genuen. Kasu honetan, KA ostean MT1 mRNA nibelak areagotu egin ziren 24 ordutik aurrera esanguratsu bihurtuz. Gainera, nahiz eta estatistikoki esanguratsua ez izan, MT2rentzako tendentzia berdina ikusi zen. Ordea, MT3 nibelak KA administrazioaren osteko denbora-puntu guztietan aldakaitz mantendu ziren **(R26 E-F Figura)**. Hau dena kontuan harturik, emaitzek KA ostean HPFan Zn^{+2} askapen masibo bat ematen dela adierazi zuten, sistema eusten saiatzen den MT nibelak areagotu egiten direlarik baita ere. Gainera, GCLean gertatzen den akumulazioari so eginez, Zn^{+2}a NSCei eragiten egon zitekeen, euren MTLE hasierako erantzun goiztiarra bultzatuz.

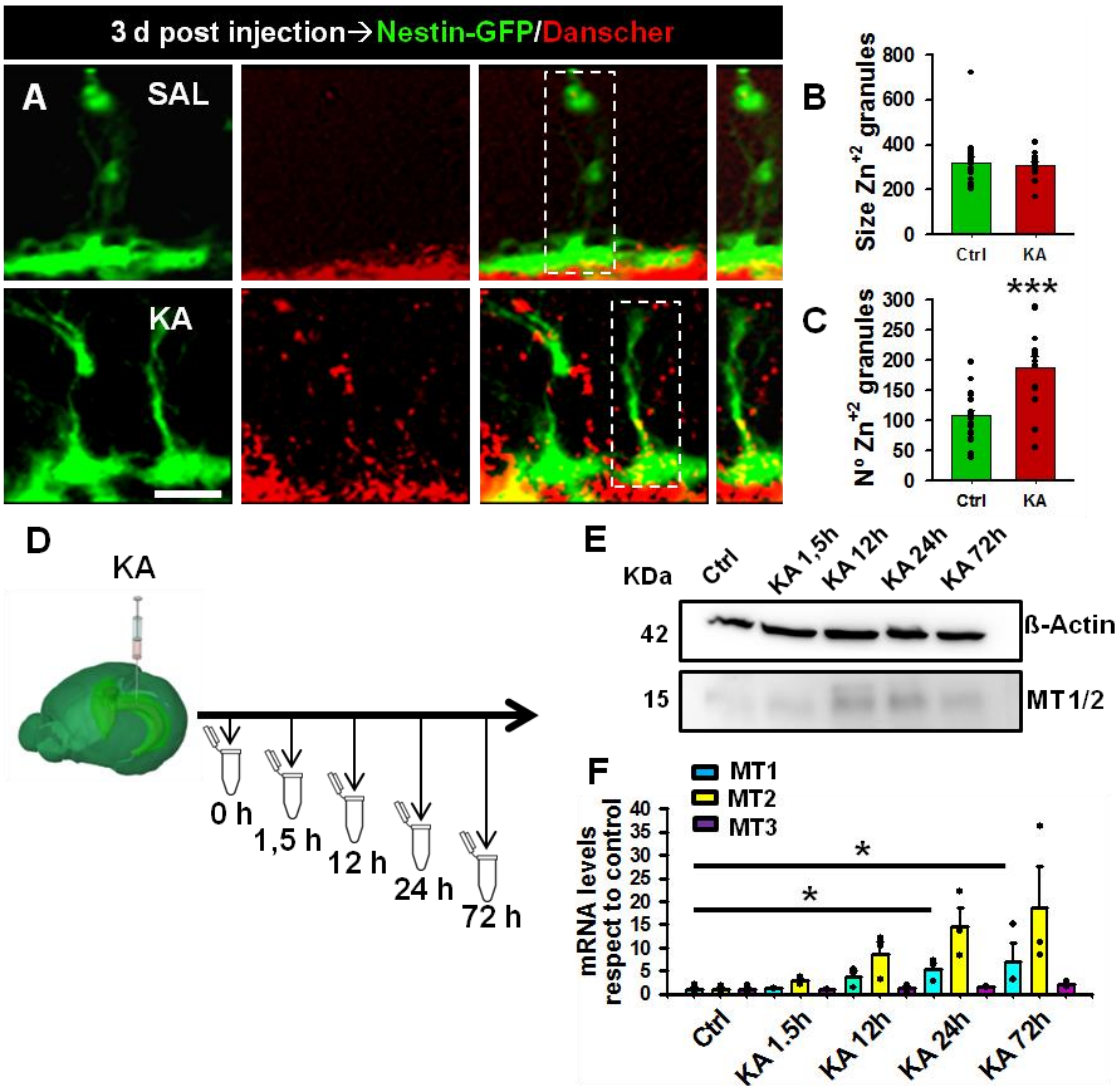

R26 Figura. Zn^{+2}a gune neurogenikoan bildu zen KA administrazioaren ostean. A) Mikroskopio fluoreszente irudi errepresentatiboak KA administrazio osteko 72 orduetan gune neurogenikoan gertatzen den Zn^{+2} igoera eta bere gainjarpena NSCekin erakutsiz. Irudiak pseudokoloreztatuak (Zn^{+2} gorriz) izan ziren irudikapen arrazoiengatik. **B)** Danscher teknikaren kalitatearen kontrol neurri modura, Zn^{+2} granuluen tamainaren kuantifikazioa. KA eta kontrol taldearen arteko diferentzia ezak teknikaren garapen eraginkorra adierazi zuen. **C)** Kuantifikazioa Zn^{+2} granuluek Nestin-GFP espresatzen zuten zelulekin zuten gainjarpenean KAren ostean zegoen areagotze esanguratsua erakutsiz. **D)** Denbora-eskala esperimentalaren eskema. Hipokanpoak KA administratu osteko denbora-puntu ezberdinetan bilduak izan ziren. **E)** KA administrazioaren ondoren denbora-puntu ezberdinetan bildutako hipokanpoen WBak KA eman eta 12 orduz geroztik MT1 eta MT2 espresioaren igoera erakutsi zuen. **F)** KA administrazioaren ondoren denbora-puntu ezberdinetan bildutako hipokanpoen RT-qPCRak KA administratu eta 12 orduz geroztik MT1 eta MT2 nibelen, baina ez MT3renak, areagotzeko tendentzia agertu zuen. Grafiko bakoitzeko datuak normalizatuak izan ziren CTRL+CTRL taldearen batez bestekoa 1 ± errore estandarra bezala hartuta. *SAL: Disoluzio isotonikoa. KA: Azido kainikoa. Eskala barra 20 µm-koa da. *p<0.05, ***p<0.001. Student's t testa (B-C)n. Kruskal Wallis Dunnet post hoc testaren bidezko kontrol taldearen aurkako konparazio anizkoitzez jarraitua MT1entzako eta MT3rentzako eta bide bakarreko ANOVA Dunnet post hoc testaren bidezko kontrol taldearen aurkako konparazio anizkoitzez jarraitua MT2rentzako*

(F)n. Barrek batez bestekoa ± errore estandarra erakusten dute. Puntuek datu indibidualak erakusten dituzte.

6.7.2. Zn^{+2}ak dosiaren araberako ugaritzea sustatu zuen NSPCetan

Ondoren, Zn^{+2}ak NSCen gainean izan zezakeen efektu posiblea ikertzeari ekin genion. Horretarako, NSPCetara jo genuen, ugaritze kondizioetan hauek manipulatzeko eta Zn^{+2} dosi ezberdinek eragindako efektua ebaluatzeko asmoz (0, 5, 10 and 400 µM). 25.000 NSPC hazi genituen lamininaz gainjantzitako estalkietan, Zn^{+2} dosi ezberdinekin tratatu eta finkatu baino ordubete lehenago BrdU pultsu bat eman genien, zelula ugaritzea determinatzeko xedez. Emaitzek erakutsi zutenez, NSPCak 5 µM Zn^{+2}ekin tratatu eta gero BrdUa bereganatu zuten zelulak 3 aldiz areagotu ziren **(R27 A-B Figura)**. Hala ere, Zn^{+2} dosiak igotzerakoan (10 µM and 400 µM) NSPCengan Nestin-GFP zitoplasmatikoaren galera eta heriotza zelularra iradokitzen zuten nukleo txiki eta argien presentzia eragin zituen efektu kaltegarri bat sortu zen **(R27 A-B Figura)**. Emaitza hauek Zn^{+2}ak dosi baxuetan NSPCen ugaritzea sustatzen zuela adierazi zuten, nahiz eta dosiak igotzerakoan heriotza zelularra eragiten zuen. Lorturiko emaitzen argitan, *in vivo* MTLE kondiziotan Zn^{+2}ak NSCengan eduki zezakeen rol posiblearen gainean galdetu genion geure buruari.

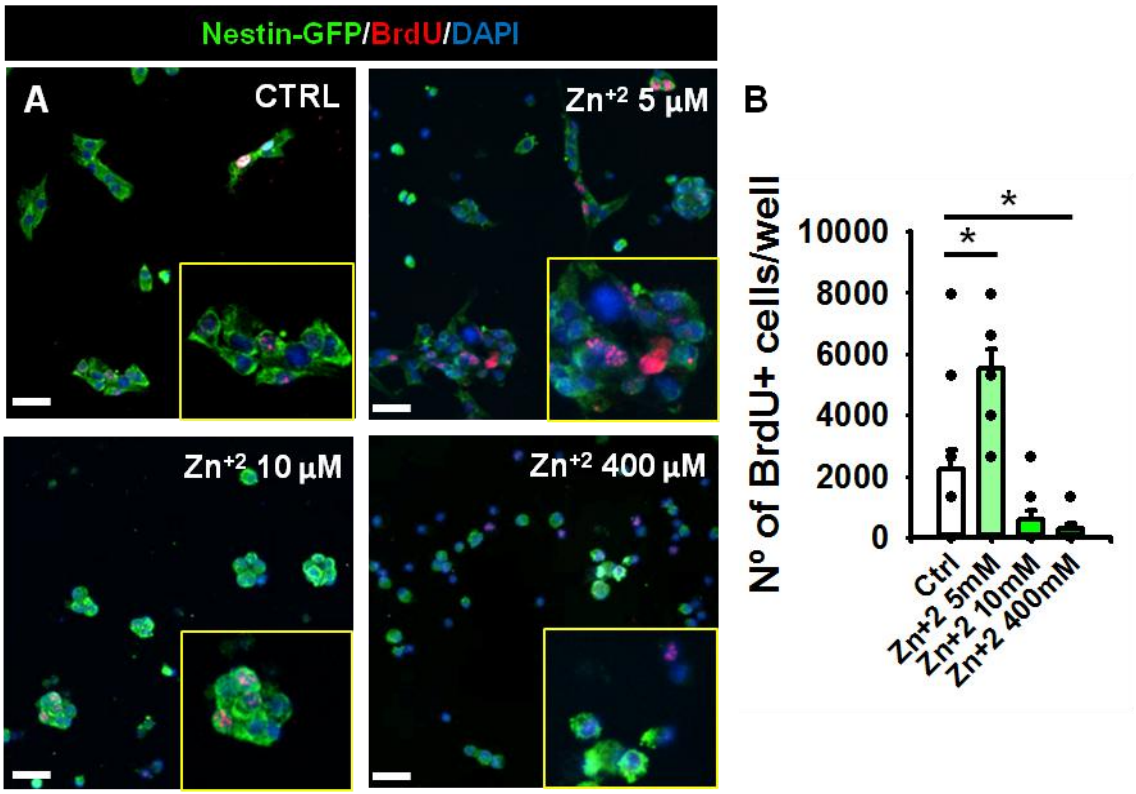

R27 Figura. Zn^{+2} administrazioak dosiaren arabera efektu desberdinak eragin zuen NSPCengan. A) Konfokal irudi errepresentatiboak ugaritzen ari ziren NSPCak erakutsiz. Irudiek erakutsi zuten 5 µM of Zn^{+2} eman ondoren BrdUa NSPC kopuru handiagoek bereganatzen zutela, dosi handiagoekin kopuru hau gutxitzen zelarik. Era berean, NSPCak 10 µMekin edo 400 µMekin tratatzen zirenean ikusitako nukleo txiki eta borobilduek Zn^{+2} dosi hauek heriotza zelularra sortzen zutela adierazi zuten. **B)** BrdUa bereganatu zuten NSPCen kopuru totala kondizio esperimental bakoitzean erakusten duen kuantifikazioa. Areagotze esanguratsua ikusi zen zelulak 5 µM Zn^{+2}ekin tratatu zirenean, kopurua murrizten joan zelarik dosia igo zen heinean. *CTRL: Kontrol. Zn^{+2}: Zinc. Eskala barra 20 µm-koa da. *p<0.05. Kruskal Wallis Dunn post hoc testaren bidezko kontrol taldearen aurkako konparazio anizkoitzez jarraitua. Barrek batez bestekoa ± errore estandarra erakusten dute. Puntuek datu indibidualak erakusten dituzte.*

6.7.3. Zn^{+2} administrazio intrahipokanpalak MTLEak gune neurogenikoan eragiten dituen alterazioen antzekoak sortu zituen

KA administrazioaren ostean Zn^{+2}a GCLean banatu egiten zela, Nestin-GFP espresatzen zuten zelulekin gainjarriz, eta *in vitro* hazitako NSPCetan ugaritzea sustatzen zuela kontuan harturik, *in vivo* Zn^{+2} administrazioaren efektua gune neurogenikoan ebaluatzeari ekin genion, konbultsio ostean ageri den aktibazio eta React-NSC indukzioan paper bat joka zezakeelakoan. Hau aztertzeko, disoluzio isotonikoa (kontrol taldea) edo Zn^{+2} dosi ezberdinak (5, 20 or 30 nM) injektatu genituen intrahipokanpalki eta hauen efektua gune neurogenikoaren eta NSCen gainean zazpi egun geroago ebaluatu genuen. Animaliak sakrifikatu baino 24 ordu lehenago BrdU injektatu genuen intraperitonealki, ugaritzen zeuden zelulak identifikatzeko asmoz **(R28 A Figura)**. Emaitzek Zn^{+2} 5 nMko dosiarekin diferentzia esanguratsurik ez zegoela adierazi zuten (erakutsi gabeko datuak). Aldiz, dosi altuagoek gune neurogenikoan dosiaren araberako efektu gogorra eragin zuten. 20 nM eta 30 nM dosiekin GCDa, BrdU zelula positiboen areagotzea eta NSCen morfologia erreaktiboa eta desplazamendua ikusarazi zitezkeen **(R28 B-D Figura)**, KA injekzioak eragindako gune neurogenikoaren erantzuna definitzen duten efektu nagusietako batzuk erreplikatuz.

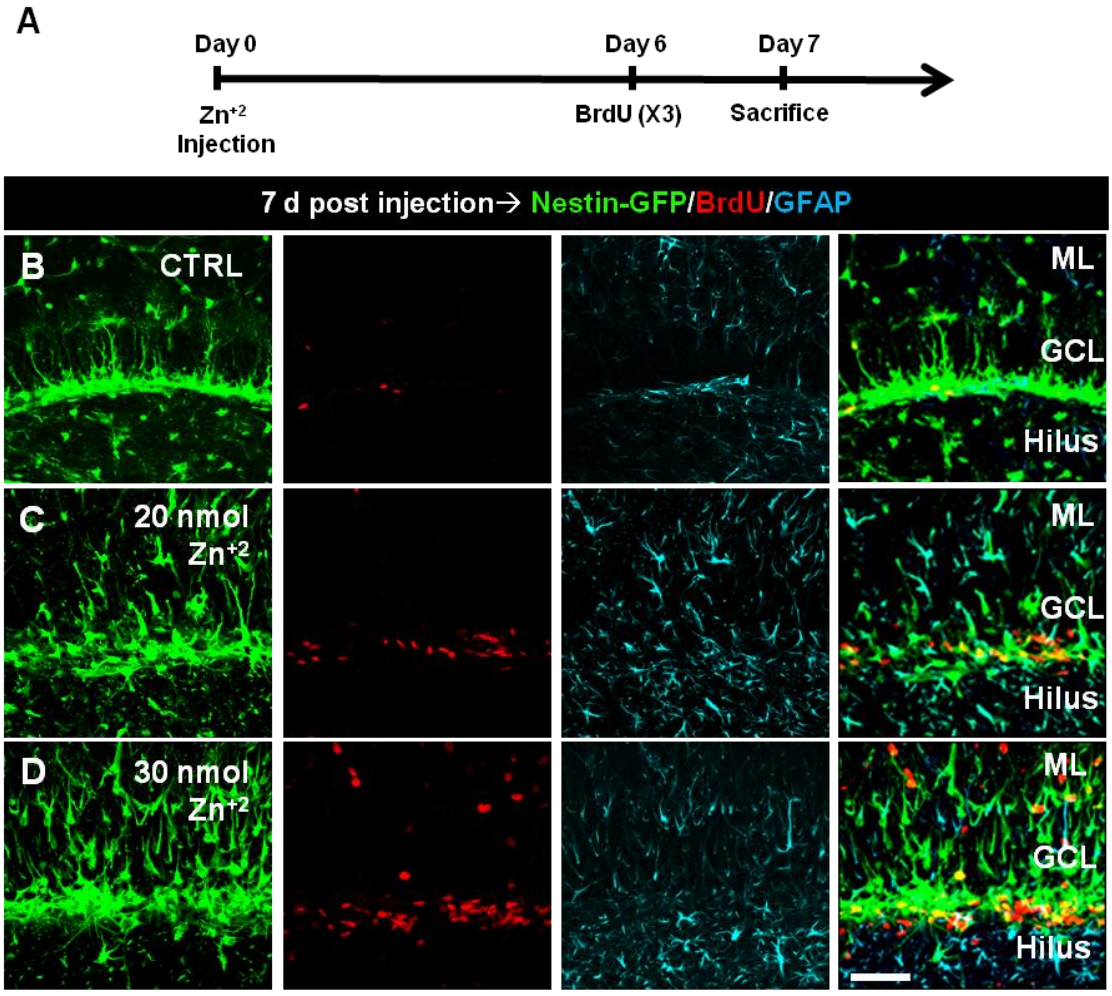

R28 Figura. Zn^{+2} intrahipokanpalak dosiaren araberako disrupzioa sortu zuen gune neurogenikoan. A) Denbora-eskala esperimentalaren eskema. Nestin-GFP saguak Zn^{+2} administrazio hipokanpala egin eta zazpi egunera sakrifikatuak izan ziren. Sakrifizioa baino egun bat lehenago hiru BrdU injekzio intraperitoneal administratu ziren, hiru orduz bananduak, ugaritzen zeuden zelulak markatzeko asmoz. **B-D)** Konfokal irudi errepresentatiboak disoluzio isotoniko (CTRL) (B), 20 nM Zn^{+2} (C) edo 30 nM Zn^{+2} (D) intrahipokanpal administrazioaren efektua erakutsiz. Zn^{+2} administrazioak gune neurogenikoan eragina izan zuela ikusi daiteke GCDa, BrdU zelula positiboen areagotzea eta NSCen alterazio morfologiko eta espazialak sortuz, azken hauek erreaktibo bilakatzen zirelarik SGZtik MLerantza alde egiten zutelarik. *GCL: Zelula granular geruza. ML: Geruza molekularra. Zn^{+2}: Zinc. Eskala barra 20 µm-koa da.*

Gure ikerketa aurrera eramateko eta Zn^{+2}aren efektua hobeto karakterizatzeko gune neurogenikoan alterazioak sortu zituen Zn^{+2} kopururik baxuena erabiltzea erabaki genuen. Aurretik erabilitako denbora-eskala berdina jarraitu genuen, saguak Zn^{+2} injekzio intrahipokanpala administratu eta zazpi egunera sakrifikatuz eta BrdU sakrifikazioa baino egun bat lehenago injektatuz **(R29 A-B Figura)**. Hala, konbultsio ostean gune neurogenikoaren etetea definitzen duten karakteristika nagusietako batzuen errepikapena ebaluatu genuen. Lehenik DAPI tindaketan oinarrituz eta

GCLaren lodiera neurtuz GCDa ebaluatu genuen (Houser, 1990) eta ondoren gune neurogenikoan BrdUa bereganatu zuten zelula kopurua ebaluatu genuen. Emaitzek Zn^{+2} injekzioa jaso zuten animalien GCLean nukleoen dispertsio esanguratsua erakutsi zuten, disoluzio isotonikoa jaso zutenekin alderatuta **(R29 D Figura)**. Are gehiago, Zn^{+2} administrazioaren ostean gune neurogenikoan BrdU bereganatu zuten zelulen dentsitatea lau aldiz areagotu zen **(R29 E Figura)**. Emaitza hauek Zn^{+2} administrazioak KA administrazioak gune neurogenikoan eragiten dituen efektu antzekoak sorrarazten dituela are gehago egiaztatu zuten.

Ondoren Zn^{+2} efektua zehazki NSCen gainean ebaluatzeari ekin genion. GCLean zegoen NSC dentsitatea eta BrdU bereganatu zuten NSCen proportzioa bi talde esperimentaletan kuantifikatu genituen. Era interesgarrian, Zn^{+2} eman eta zazpi egunera NSCen dentsitateak murrizteko tendentzia aurkeztu zuen **(R29 F Figura)**, nahiz eta NSC guztien artean BrdU positiboak ziren NSCen proportzioa aldaezin mantendu zen **(R29 G Figura)**. Honek gune neurogenikoaren gaineko Zn^{+2}aren efektua iradoki zuen, nahiz eta NSCen aktibazioan eraginik ez izan, zeina era diferentizialen erregulatuak egongo litekeen. Haatik, ezin genezake Zn^{+2} administraziotik gutxira NSCen aktibazio iragankor bat baztertu, zeina zazpi egunera jada itzalia egongo litzakeen, NSCak erregulatu eta bere kontrol aktibazio mailetara bueltatuz.

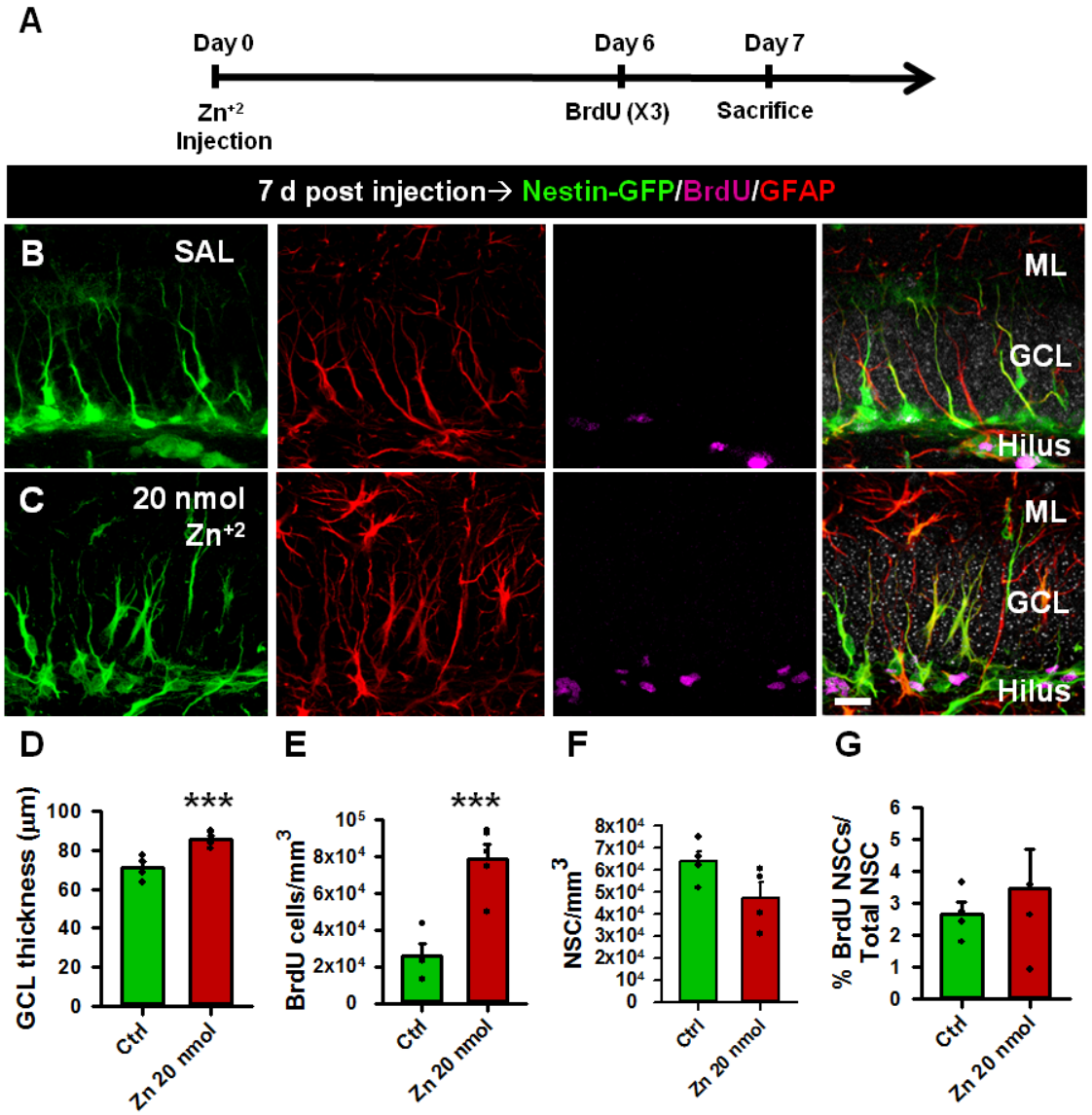

R29 Figura. Zn^{+2} administrazio intrahipokanpalak KA administrazioaren osteko alterazio antzekoak sortu zituen gune neurogenikoan. A) Denbora-eskala esperimentalaren eskema. Nestin-GFP saguak Zn^{+2}a administratu eta zazpi egunera sakrifikatuak izan ziren. Sakrifizioa baino egun bat lehenago hiru BrdU injekzio intraperitoneal administratu ziren, 3 orduz bananduak, ugaritzen zeuden zelulak markatzeko asmoz. **B-C)** Konfokal irudi errepresentatiboak gune neurogenikoa disoluzio isotoniko (CTRL) (B) edo 20 nM Zn^{+2} (C) injekzio intrahipokanpalen ostean erakutsiz. **D)** DAPI tindaketan oinarrituriko GCD kuantifikazioa. Emaitzek Zn^{+2} administrazioaren ostean GCLaren lodieran areagotze esanguratsua erakutsi zuten. **E)** Kuantifikazioa BrdU zelula positiboen areagotzea erakutsiz Zn^{+2} administrazioaren ostean. **F)** NSC dentsitatearen kuantifikazioa. Emaitzek Zn^{+2} administratu ondoren NSC dentsitatearen gutxitzeko tendentzia erakutsi zuten, nahiz eta ez zen esanguratsua. **G)** Kuantifikazioa aktibaturiko NSCen proportzioan aldaketarik ez zegoela erakutsiz. *GCL: Zelula granular geruza. ML: Geruza molekularra. Zn^{+2}: Zinc. Eskala barra 20 µm-koa da. ***p<0.001. Student's t testa. Barrek batez bestekoa ± errore estandarra erakusten dute. Puntuek datu indibidualak erakusten dituzte.*

6.7.4. Zn^{+2}ak NSCengan duen efektuan EGFR bitartekari izan zitekeen

Gure aurreko emaitzek Zn^{+2}a KA administrazioaren ostean era masiboan askatzen dela aurkeztu zuten, gune neurogenikoan bilduz eta honen etetea sorrarazteko kapaz izanik, MTLE modelo esperimentalean gertatzen den antzera. Are gehiago, beste ikerlan batzuek Zn^{+2}a EGFR seinalizazio ibilbidea estimulatzeko gai dela argitaratu izan dute (Samet et al., 2003; Wu et al., 2004), haien arteko elkarrekintzak konbultsio ostean gune neurogenikoan eta NSCetan ikusi daitekeen erantzunean parte har lezakeela adieraziz. Zn^{+2}aren presentziak NSCak EGFRren bitartez modulatu ahal litzakeen ikusteko, NSPCetara jo genuen berriz ere. Zn^{+2}ak EGFRren gainean izan zezakeen efektu potentziala ikusteko asmoz, lehenik hazkuntza faktoreen seinalizazioa itzali behar genuen, zeina normalean hazitako NSPCetan aktibo dagoen hazkuntza medioan EGFren eta FGFren erabilpenaren ondorioz. Helburu honetarako, hazkuntza faktoreak erantsi genituen NSPCak hazkuntza faktorerik gabeko medio batean haziz. Gure datu preliminarrek adierazi zutenez, fosforilaturiko ERK1/2ren galera esanguratsua gertatu zen hazkuntza faktoreak kendu eta bi ordura (erakutsi gabeko datuak). Honela, hazkuntza faktoreek eragindako EGFR seinalizazioaren aktibazioa itzaltzeko eta Zn^{+2}aren bitartezko hartzailearen aktibazio potentziala ganoraz neurtzeko esperimentua hasi baino lehen zelulei hazkuntza faktoreak bi orduz erantsi zitzaizkien.

EGFR aktibatzeko Zn^{+2}aren ahalmena aurretiaz deskribaturiko protokolo baten adaptazioa erabiliz ebaluatu genuen (Wu et al., 2004). Hazkuntza faktorerik gabeko taldeaz gain (Stvd), 100 ng/ml EGF, EGFRren aktibazioaren kontrol neurri bezala (EGF), edo 200 μM Zn^{+2} (Stvd+ Zn^{+2}) administratu genituen. Are gehiago, NSPCak 200 μM Zn^{+2} administratu baino lehen 60 minutuz 2 μM Gefitinibekin tratatuak izan ziren beste talde bat gehitu genuen (Stvd+ Zn^{+2}+Gef). Y845 eta Y1068 EGFRan, hala nola EGFR totalean ere, proteina estraktuen WBa gauzatu zen, hartzailearen fosforilazioaren ratioa burutzeko asmoz **(R30 A Figura)**. Interesgarria izan zen nola Zn^{+2} administrazioa NSPCetan Y845 hondakinaren fosforilazio leuna eragiteko kapaza izan zen, hazkuntza faktorerik gabeko taldearekin alderatuta (Stvd), eta nola Gefitiniben aurretiazko tratamenduarekin fosforilazio hau guztiz blokeatua izan zen **(R30 C Figura)**. Nolanahi ere, EGFren presentzian, baina ez Zn^{+2}en presentzian, Y1068 hondakinaren fosforilazioa eragin zen **(R30 D Figura)**. Hori gutxi balitz, EGFRren ERK1/2 ur beherako seinalizazio ibilbidea aztertu genuen, zelula ugaritzearekin nagusiki erlazionatua dagoena (Downward et al., 1984). Emaitzek erakutsi zuten Zn^{+2}aren presentzia hazkuntza faktorerik gabe fosforilaturiko ERK1/2

seinalizazioa areagotzeko kapaza zela eta garrantzitsuago dena, EGFRren inhibizioak fosforilazio maila jaitsi zuela **(R30 B; E Figura)**. Beraz, emaitzek adierazi zutenez Zn^{+2} EGFR zuzenean aktibatzeko kapaza izan zen bere Y845 fosforilazio hondakinean eta honen ERK1/2 ur beherako seinalizazio ibilbidea aktibatu zezakeen baita ere, EGFR-ren inhibizioa nahikoa izanik fosforilazio zirkuitu hau eten eta hartzailea gelditzeko.

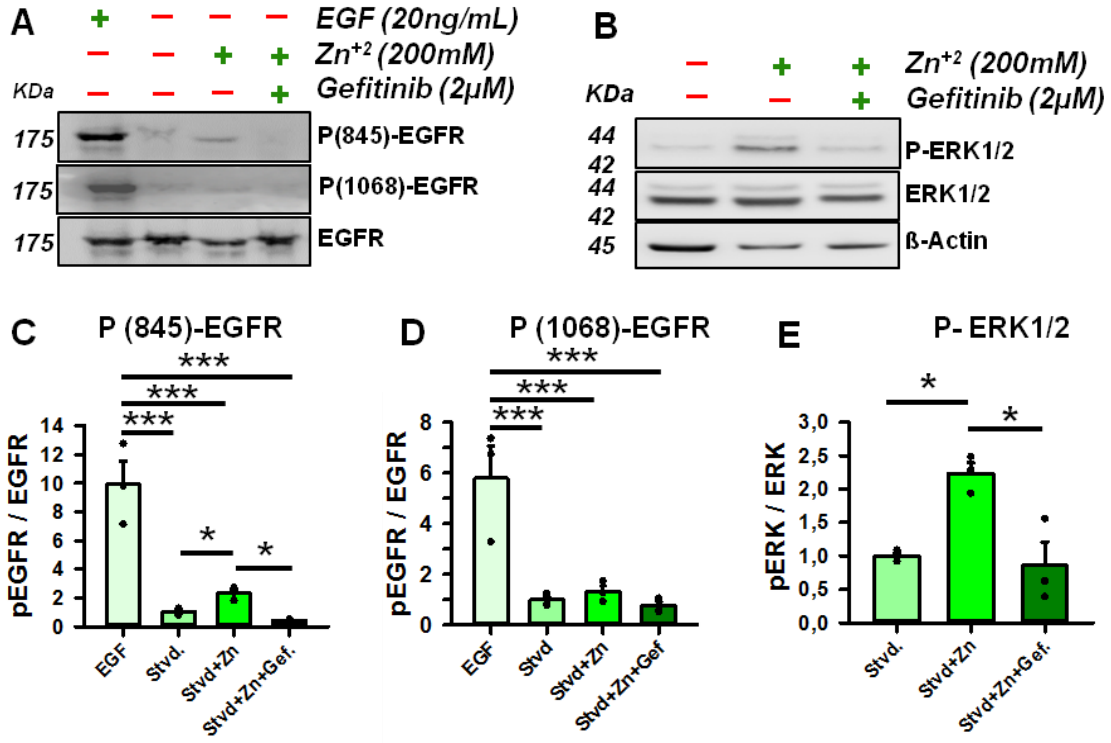

R30 Figura. Zn^{+2} NSPCetan EGFR seinalizazio ibilbidearen aktibazioa sustatzeko kapaza zen. A) WBak Y845 EGFR, 1068 EGFR eta EGFR totalarentzako EGFrekin estimulaturiko taldean, hazkuntza faktorerik gabeko taldean, Zn^{+2}arekin estimulaturiko taldean eta Gefitinibarekin tratatu ondoren Zn^{+2}arekin estimulaturiko taldean. **B)** WB P-ERK1/2entzako, ERK1/2 totalarentzako eta kontrol bezala ß-Actinarentzako hazkuntza faktorerik gabeko taldean, Zn^{+2}arekin estimulaturiko taldean eta Gefitinibarekin tratatu ondoren Zn^{+2}arekin estimulaturiko taldean. **C)** WBaren kuantifikazioa Y845 EGFRa EGFrekin trataturiko NSPCtan 10 aldiz areagotua zegoela erakutsiz, hazkuntza faktorerik gabeko zelulekin alderatuta. Era berean, Zn^{+2}a Y845 fosforilazioa era esanguratsuan areagotzeko kapaza zen eta aktibazio hau Gefitinib erabiliz blokeatzen zen. **D)** WBaren kuantifikazioa EGFrekin trataturiko NSPCetan EGFR totalaren arteko Y1068 EGFRa sei aldiz areagotua zegoela erakutsiz, hazkuntza faktorerik gabeko taldearekin alderatuta. Kasu honetan, Zn^{+2} ez zen Y1068 EGFRren aktibazioa sustatzeko gai izan, eta Gefitinibekin eginiko aurretiazko tratamenduak ez zuen alteraziorik eragin ezta. **E)** WBaren kuantifikazioa Zn^{+2}aren presentzian ERK1/2 totalaren arteko P-ERK1/2 fosforilazioa ratioa erakutsiz, hala nola bere inhibizioa Gefitinibekin egindako aurretiazko tratamenduaren ondorioz.**p<0.05 eta***p<0.001. Kruskal Wallis Student-Newman-Keuls post hoc testaren bidezko kontrol taldearen aurkako konparazio anizkoitzez jarraitua (C-D)n eta bide bakarreko ANOVA Holm-Sidak post hoc testaren bidezko binakako konparazio*

anizkoitzez jarraitua (E)n. Barrek batez bestekoa ± errore estandarra erakusten dute. Puntuek datu indibidualak erakusten dituzte.

Zn^{+2} NSPCtan EGFR estimulatzeko gai zela ikusiz, gutxienez Y845 fosforilazio lekuan, ondoren *in vivo* Zn^{+2} administrazioaren ostean ikusi genuen gune neurogenikoaren etetea Zn^{+2} bidezko EGFR aktibazioaren bitartez modulatua izan zitekeen ebaluatzera mugitu ginen. Helburu hau betetzeko, 20 nM Zn^{+2} dosi bakarra intrahipokanpalki jaso zuten Nestin-GFP saguetan EGFR inhibizioaren efektua aztertu genuen. KA administratu genuen esperimentuetan jarraituriko paradigma berdinarekin, lehen 72 orduetan zehar Gefitinib eman genuen sudurretik **(R23-R25 Figura)** eta ugaritzen zeuden zelulak jarraitzeko sakrifikatu baino egun bat lehenago animaliek hiru BrdU dosi intraperitoneal jaso zituzten **(R31 A Figura)**. Espero bezala, emaitzek Zn^{+2} administrazio intrahipokanpalak gune neurogenikoan BrdUa bereganatu zuten zelulen dentsitatea areagotzen zuela erakutsi zuten. Gainera, Gefitiniben bidezko EGFR inhibizioak Zn^{+2}ak gune neurogenikoan eragindako BrdU zelula positiboen areagotzea murrizten zuen, disoluzio isotonikoarekin injektaturiko animalietan aldaketarik eragiten ez zuen bitartean **(R31 B-C Figura)**. Emaitza hauen bitartez EGFRk Zn^{+2}aren eraginez gune neurogenikoan jazotzen den BrdU zelula positiboen areagotzean parte hartzen duela azaleratu zen, MTLE egoeran faktore bien arteko elkarreragitea iradokiz.

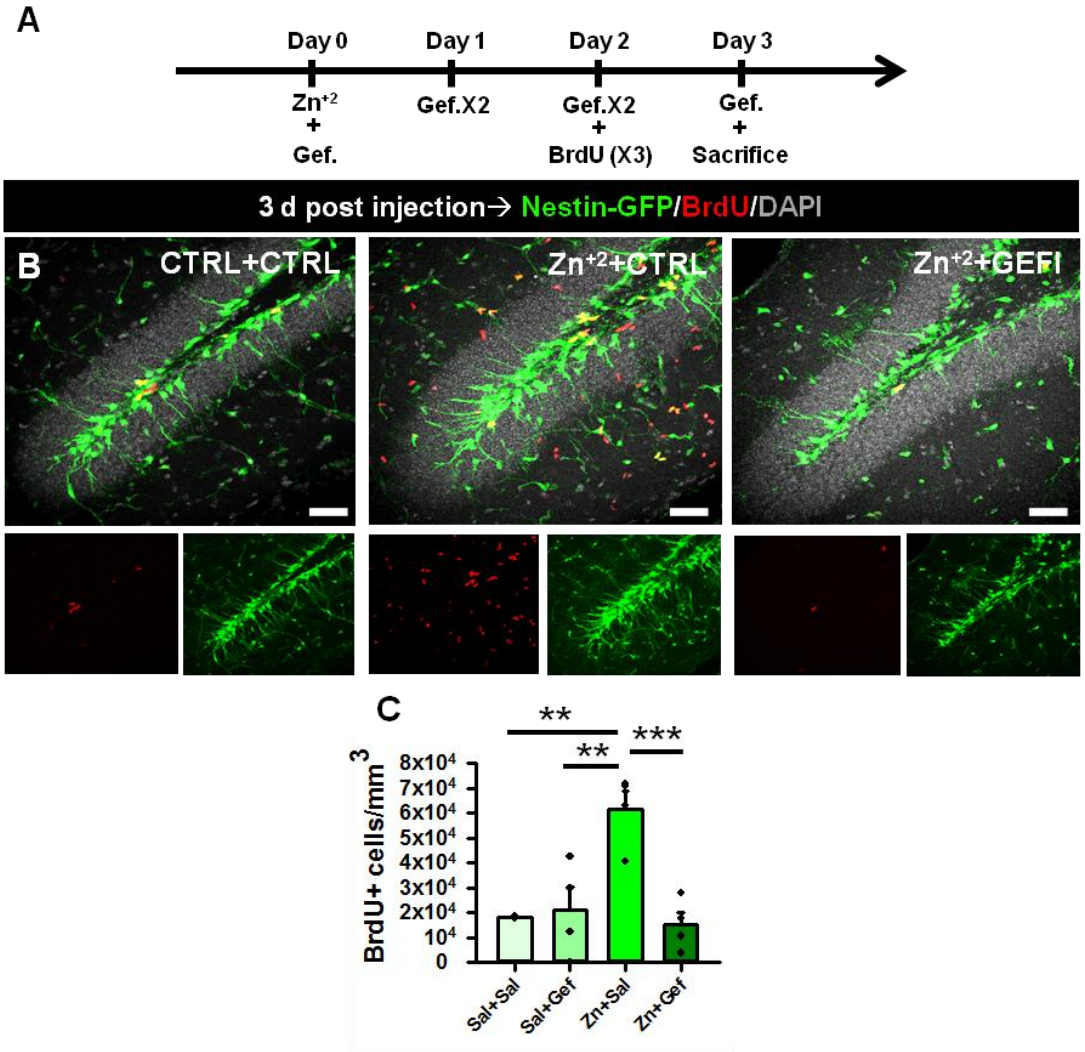

R31 Figura. Zn^{+2}ek DGko gune neurogenikoan ugaritzea sustatu zuen EGFRren bitartez. A) Denbora-eskala esperimentalaren eskema. Nestin-GFP saguak disoluzio isotoniko (CTRL) edo Zn^{+2} administrazioa egin eta 72 ordura sakrifikatuak izan ziren, 12 orduko tarteak utziz DMSOrekin (CTRL) edo Gefitinibekin sei sudurreko tratamendu jaso ostean. Sakrifizioa baino egun bat lehenago hiru BrdU injekzio intraperitoneal administratu ziren, 3 orduz bananduak, ugaritzen zeuden zelulak markatzeko asmoz. **B)** Konfokal irudi errepresentatiboak disoluzio isotoniko edo Zn^{+2} injekzio intrahipokanpalak eta sudurretik DMSO edo Gefitinib tratamendua jasotako saguen DGa erakutsiz. **C)** GCLean zegoen BrdU zelula positiboen dentsitatearen kuantifikazioa, Zn^{+2} administrazio intrahipokanpalaren ostean dentsitatearen areagotzea erakutsiz, disoluzio isotonikoarekin injektaturiko animaliekin konparatuz. Zn^{+2} administrazioaren ostean Gefitinib administratu zenean BrdU zelula positiboen areagotzea murriztu egin zen. CTRL: Kontrol. *SAL: Disoluzio isotonikoa. Zn^{+2}: Zinc. Eskala barra 20 µm-koa da. **p<0.01. ***p<0.001. bide bakarreko ANOVA Holm-Sidak post hoc testaren bidezko binakako konparazio anizkoitzez jarraitua. Barrek batez bestekoa ± errore estandarra erakusten dute. Puntuek datu indibidualak erakusten dituzte.*

6.7.5. Zn^{+2} kelazioak MTLE egoeran heriotza zelularra areagotu zuen GCLean

KA administrazioaren ostean 72 ordura GCLeanzegoen Zn^{+2} presentzia areagotua kontuan harturik, hala nola gune neurogenikoaren gainean honek duen EGFRren bitartezko efektua, gune neurogenikoan KA administrazioaren ostean ematen diren alterazioak murrizteko Zn^{+2} kelazioa estrategia baliagarria litzakeela espekulatu genuen. Hipotesi hau aztertzeko, disoluzio isotoniko (CTRL) edo KA injekzio intrahipokanpalak gauzatu genituen eta ondoren egunean birritan, zazpi egunez, azal azpitik 5 mg/Kg TPEN, Zn^{+2} kelazio agentea, edo bere ibilgailu den disoluzio isotonikoa (CTRL) administratu genituen aurretiaz deskribaturiko protokoloa jarraituz (Kim et al., 2012). TPENaren eraginkortasunaren neurri bezala GCLean zeuden zelula piknotikoen dentsitatea ebaluatu genuen. Emaitzek adierazi zutenez hiltzen zeuden zelulen kopuruak, DAPI tindaketa kondentsaketaren bitartez identifikatuak, gora egiteko tendentzia zuen KA administrazioaren ostean (KA+CTRL) disoluzio isotonikoarekin injektaturiko animaliekin alderatuz (CTRL+CTRL). Bestalde, disoluzio isotoniko injekzio intrahipokanpalaren osteko TPEN administrazioak (CTRL+TPEN) ez zuen eraginik izan GCLean. Ustekabean, KArekin injektaturiko animalietan TPEN administrazioaren ostean (KA+TPEN) hildako zelulek gora egin zuten kontrol taldeekin alderaturik (CTRL+CTRL; CTRL+TPEN) eta gora egiteko tendentzia agertu zuten KArekin injektaturiko eta ibilgailuarekin trataturiko animaliekin alderatuz (KA+CTRL) **(R32 A-B Figura)**. Hala, emaitza hauek argitu egin zuten Zn^{+2} kelazioak heriotza zelularra areagotu egiten zuela, estrategia hau MTLEn erabiltzeko ikuspegi terapeutiko bezala baztertuz.

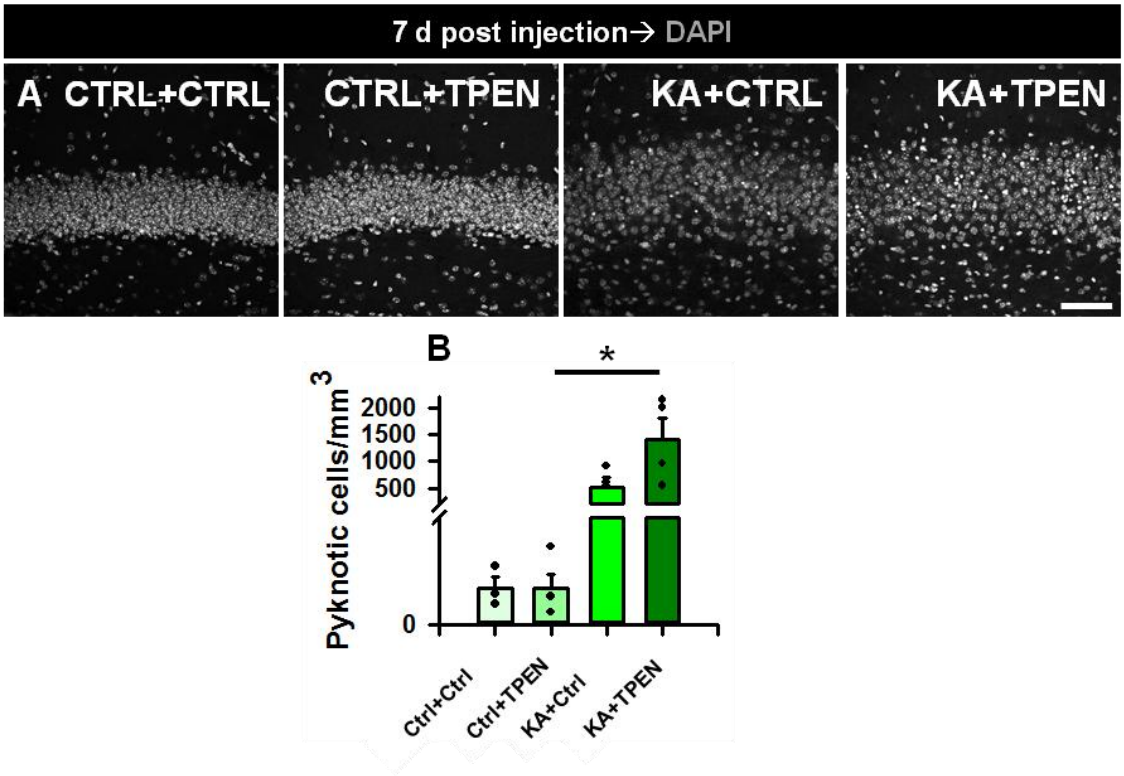

R32 Figura. Zn^{+2} kelazioak MTLEn jazotzen den heriotza zelularra areagotu egin zuen GCLean. A) Konfokal irudi errepresentatiboak disoluzio isotoniko edo KA injekzioen (CTRL edo KA) eta ibilgailu edo TPEN azal azpiko tratamenduen ostean (CTRL edo TPEN) GCLa erakutsiz. **B)** GCLean zeuden zelula apoptotikoen dentsitatearen kuantifikazioa. KA injekzioaren ostean zelula piknotikoen igoera jazo zen, TPEN tratamenduak areagotu zuena. *CTRL: Kontrol. KA: Azido kainikoa. SAL: Disoluzio isotonikoa. Eskala barra 20 µm-koa da. *p<0.05. Kruskal Wallis Dunn post hoc testaren bidezko binakako konparazio anizkoitzez jarraitua. Barrek bateznbestekoa ± errore estandarra erakusten dute. Puntuek datu indibidualak erakusten dituzte.*

Lortutako emaitzek EGFRk eta Zn^{+2}ek konbultsio ostean gune neurogenikoak ematen duen erantzunean parte hartzen dutela iradoki zuten. Izan ere, Zn^{+2} EGFRren fosforilazioa estimulatzeko gai zen bere Y845 tirosina lekuan, konbultsio ostean EGFRren aktibazioan lagunduko duen mekanismo bezala iradokiz. Era interesgarrian, Zn^{+2}aren barneratze zelularrak HB-EGFa mintz zelularretik askatzea sustatzen duela deskribatu da, azken hau EGFRren estekatzaile potente bat izanik (Samet et al., 2003; Wu et al., 2004). Hala, KA administrazioaren ostean HB-EGFk EGFR aktibazioan parte hartu zezakeen ikertzera jo genuen.

6.8. KA administrazioaren ostean HB-EGF DGan masiboki askatua izan zen

Aurreko emaitzek KA administrazioaren ostean jazotzen den erantzunean EGFR eta Zn^{+2}, bien, rol integratu bat iradokitzen zuten. Kontuan izanik Zn^{+2}aren

berreskuratze zelularrak mintz zelularretik HB-EGF askatzea susta dezakeela (Samet et al., 2003; Wu et al., 2004), eta konbultsio ostean Zn^{+2} GCLean masiboki askatua zela, HB-EGFk MTLEn ematen zen EGFRren bitartezko efektua sustatu zezakeen ikertzeari ekin genion. HB-EGFk hazitako astrogliaren ugaritzearengan, diferentziazioarengan eta morfologiarengan eragina izan dezakela (Jia et al., 2018; Kornblum et al., 1999; Puschmann et al., 2014) eta KA administrazio intraperitonealaren ostean areagotua izaten dela deskribatu da (Opanashuk et al., 1999). Are gehiago, HB-EGFk biziki estimulatzen du astrogliaren migrazioa (Faber-Elman et al., 1996). Honela, NSCek EGFR espresatzen zutela aurretiaz deskribatu genuelarik eta KA administratu ostean 14 egunera gaizki kokaturik eta nahasirik ageri zirela kontuan izanik, gure KA intrahipokanpal modeloan HB-EGF aldaketak karakterizatzera jo genuen.

Aurretiaz jarraituriko paradigma esperimental berdinarekin, KA administratu genuen intrahipokanpalki bi hilabeteko Nestin-GFP saguetan eta injektaturiko hipokanpoa denbora-puntu ezberdinetan bildu genuen (1.5 h, 12 h, 24 h, 72 h) **(R33 A Figura)**. HPFean askaturiko HB-EGF kopurua aztertzeko HB-EGFa ehunean KA osteko denbora ezberdinetan ELISA teknikaren bitartez neurtu genuen eta emaitzak disoluzio isotonikoarekin injektatuak izan ziren (Ctrl) animaliekin konparatu genituen. Emaitzek KA ostean 12 ordura %25 inguruko areagotze esanguratsua erakutsi zuten saguak disoluzio isotonikoarekin injektatuak izan ziren kontrol egoerarekin alderatuta. Nolanahi ere, areagotze honek goia jo zuen 24 ordura eta azkar egin zuen behera hortik aurrera **(R33 B Figura)**. ELISA teknikak gune neurogenikoan baino gehiago HPF guztian zegoen HB-EGF kopuruari buruzko informazioa eman zigunez gero, IHCra jo genuen estekatzailearen presentzia KA edo disoluzio isotonikoa administratu eta 72 ordura DGan neurtzeko. Emaitzek erakutsi zuten HB-EGF tindaketa aberasturik ageri zela goialdeko ML hurbilean eta hilusean, nahiz eta GCLak ez zuen aldaketa esanguratsurik aurkeztu kontrol taldearekin alderatuta **(R33 C Figura)**. Hala ere, ezin genezake KA administratu eta 72 ordu baino lehenago GCLean HB-EGFaren areagotze iragankor baten gertaera baztertu. Beraz, HB-EGFek rol bat joka lezake espezifikoki DGan. MLan ageri zen espresio altua eta bere deskribaturiko kimioerakartzaile rola kontuan izanik (Faber-Elman et al., 1996), konbultsio ostean NSCek MLrantz egiten duten migrazio prozesuan HB-EGFek rol bat izatea espekulatu genuen.

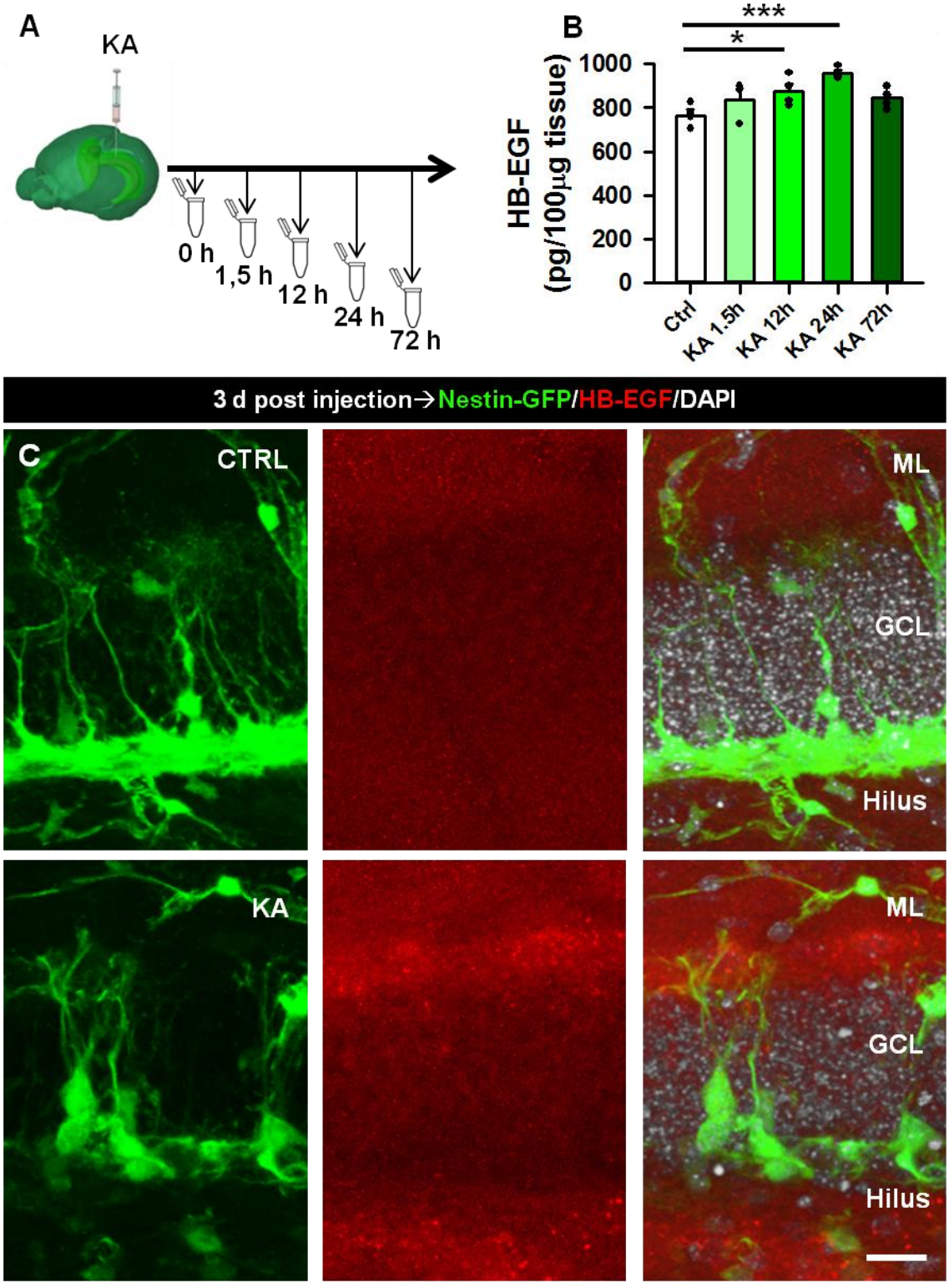

R33 Figura. HB-EGF azkar areagotu egin zen DGan KA administrazioaren ostean. A) Denbora-eskala esperimentalaren eskema. Hipokanpoak denbora-puntu ezberdinetan bilduak izan ziren KA administrazioaren ostean. **B)** ELISAren bidezko HB-EGF kopuruaren neurketa ehunean KA administratu eta denbora-puntu ezberdinetan. HB-EGFen pg/µg-en areagotze bat zegoen KA administratu eta 12-24 ordura, hortik aurrera murriztu egiten zena. **C)** Konfokal irudi errepresentatiboak DGan HB-EGF espresioa

erakutsiz. Tindaketak erakutsi zuenez, HB-EGFa MLan eta hilusean areagotu egiten zen bitartean, GCLak alteraziorik gabe zirauen disoluzio isotonikoarekin injektaturiko animaliekin alderatuz. *GCL: Zelula granular geruza. KA: Azido kainikoa. ML: Geruza molekularra. SAL: Disoluzio isotonikoa. Eskala barra 20 µm-koa da. ***p<0.001. Bide bakarreko ANOVA Holm-Sidak post hoc testaren bidezko kontrol taldearen aurkako konparazio anizkoitzez jarraitua. Barrek batez bestekoa ± errore estandarra erakusten dute. Puntuek datu indibidualak erakusten dituzte.*

KA administrazioaren ostean HB-EGF DGan askatua izaten zela kontuan harturik, HB-EGF askapen honetan NSCen kontribuzio potentziala ikertzeari ekin genion, hala nola hazitako NSPCtan EGFR eta bere ur beherako seinalizazio ibilbidean dagoen ERK1/2 HB-EGFren aktibatzeko ahalmena ikertzeari.

In vitro hazitako Nestin-GFP zelulak ugaritze egoeran mantendu genituen eta IHC bitartez NSPCetan zegoen HB-EGF presentzia ebaluatu genuen. Emaitzek adierazi zutenez, nahiz eta NSPC batzuetan HB-EGF espresioa zegoen HB-EGF antigorputz primariorik gabeko kontrolekin konparatuta, NSPCen gehiengoak ez zuen HB-EGF espresiorik agertzen **(R34 A Figura)**. Hala ere, NSPCak ugaritze egoera konstantean mantentzen zirela izanik, HB-EGF mintz zelularretik era konstantean askatua izatearen eta EGFRren estekatzaile bezala jardutearen aukera planteatu genuen. Hala, ELISAren bitartez HB-EGF kopurua neurtu genuen era bereizian NSPCetan (Pellet), euren hazkuntza medioan (Supernatant) eta emaitzak kontrol talde bezala NSPCrik ez zuen hazkuntza medio batekin (Media) konparatu genituen. Emaitzek HB-EGF kopuruaren %200 inguruko areagotze esanguratsua erakutsi zuten NSPCak zituen hazkuntza medioan (Supernatant) kontrol medio (Media) eta zelula alearekin (Pellet) alderaturik, NSPCak ugaritze egoeran HB-EGFa zelulaz kanpoko ingurura askatzeko kapazak zirela demostratuz **(R34 B Figura)**.

Ondoren, HB-EGF EGFR seinalizazio ibilbidearen aktibazioa probokatzeko gai bazen ikusteko, lehenik EGFR seinalizazio ibilbidea itzaltzeko NSPCak EGF eta FGF barik hazi genituen. Gero, hazkuntza faktorerik gabeko NSPCak HB-EGF eta baita HB.EGF gehi Zn^{+2} erabilita estimulatu genituen, ahalik eta *in vivo* egoeraren antzeko kondiziotan EGFR NSPCetan aktibatzeko HB-EGFaren kapazitatea neurtzeko asmoz. Are gehiago, beste talde esperimental bat gehitu genuen zeina Gefitinib erabiliz tratatu zen aurretiaz eta gero HB-EGF eta Zn^{+2} aplikatu zitzaizkion. EGFRren aktibazioa bere Y845 eta Y1068 fosforilazio lekuetan neurtu genuen eta baita EGFRren ur beherako seinalizazio bide den ERK1/2ren fosforilazioa. Emaitzek HB-EGF EGFR bere aztertutako bi fosforilazio hondakinetan (Y845 eta Y1068) fosforilatzeko gai zela adierazi zuten. Azpimarragarria da Zn^{+2} estimulazioak ez zuela aparteko efekturik

eragin, ziurrenik gehiegizko HB-EGF mailagatik gailendua. Azkenik, Gefitinib bitartezko aurretiazko tratamendua Y845 eta Y1068 bi fosforilazio lekuak blokeatzeko zein ERK1/2 fosforilazioa murrizteko gai izan zen, baita HB-EGF eta Zn^{+2} elkarrekin administratu zirenean ere. Emaitza hauek KA administrazioaren ostean gune neurogenikoan jazotzen diren efektuak HB-EGFren eta EGFRren elkarreraginak sustatu litzakeela adierazi zuten, beharbada Zn^{+2}aren bitartezko HB-EGF askapenak erregulaturik.

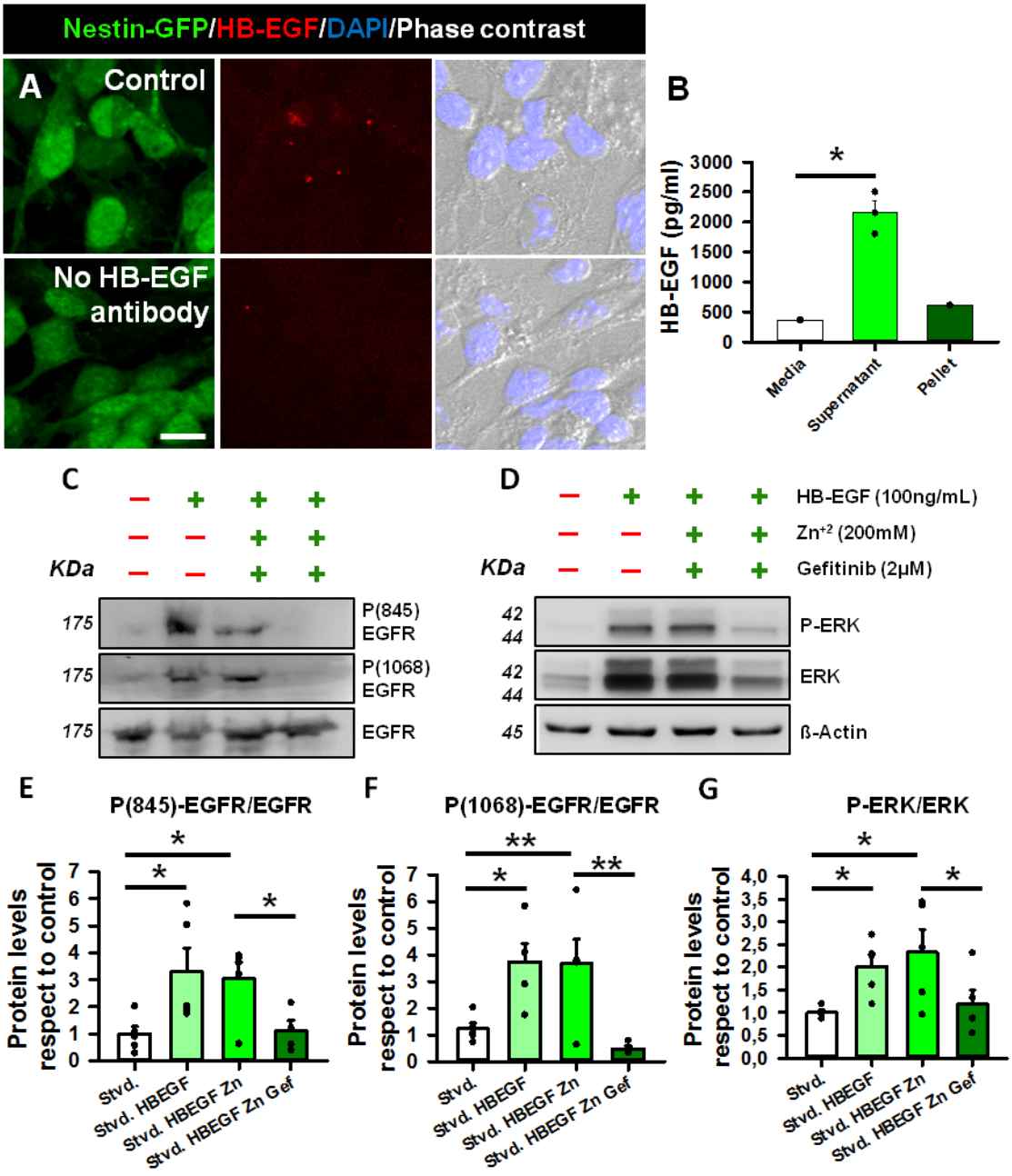

←Aurreko orrialdean. R34 Figura. HB-EGFek *in vitro* hazitako NSPCetan EGFRren aktibazioa sustatu zuen. A) Konfokal irudi errepresentatiboak *in vitro* hazitako NSPCak eta HB-EGF espresioa IHCaren ostean bai HB-EGF antigorputz primarioarekin zein antigorputz primariorik gabe erakutsiz. **B)** ELISAren bitartezko kuantifikazioa HB-EGF kopurua erakutsiz NSPCrik gabeko hazkuntza medioan (media), hazitako NSPCen medioan (supernatant) eta hazitako NSPCen zelula alean (pellet). Emaitzek areagotze esanguratsua erakutsi zuten hazitako NSPCen medioan zegoen HB-EGF kopuruan, NSPCak ugaritze egoeran estekatzailea askatzeko gai zirela erakutsiz. **C-D)** WBak areagotutako Y845 EGFR, Y1068 EGFR eta ur beherako seinalizazio ibilbidea den ERK1/2 maila erakutsi zuen HB-EGFrekin trataturiko kondizioetan. **E-G)** Proteina maila totalaren arteko fosforilazio mailaren kuantifikazioak EGFRrentzako (Y845 eta Y1068) eta bere ur beherako seinalizazio ibilbidea den ERK1/2rentzako. Grafiko bakoitzeko datuak normalizatuak izan ziren CTRL+CTRL taldearen batez bestekoa 100 ± errore estandarra bezala hartuta. *Eskala barra 20 µm-koa da. *p<0.05* eta ***p<0.01. Kruskal Wallis Tukey post hoc testaren bidezko kontrol taldearen aurkako konparazio anizkoitzez jarraitua in (B)n. Bide bakarreko ANOVA Holm-Sidak post hoc testaren bidezko kontrol taldearen aurkako konparazio anizkoitzez jarraitua (E)n, (F)n eta (G)n. Barrek batez bestekoa ± errore estandarra erakusten dute. Puntuek datu indibidualak erakusten dituzte.*

Tesi honen bigarren zatian lorturiko emaitzek konbultsio ostean DGan jazotzen den React-NSC transformazioan EGFR modulatzaile garrantzitsuetako bat bezala seinalatu zuten, ahalmen neurogeniko osoaren galera dakarrena. Gure lanak bide berri bat irekitzen du MTLEn hipokanpoak duen erantzunean EGFRren aktibazioa mekanismo alternatibo bezala adieraziz. Izan ere, Gefitiniben sudurreko administrazioa metodo baliagarria suertatu zen EGFR inhibitzeko, BBBa zeharkatuz eta konbultsioek hipokanpoarengan duten efektu latza leunduz (DCXen galera, GCDa eta React-NSC indukzioa). Horretaz gain, Zn^{+2}, HB-EGF eta haien arteko elkarreragina EGFRren aktibazioaren indukzioan partehartzaile bezala proposatzen ditugu, konbultsio ostean masiboki zelulaz kanpoko ingurunean askatuak izaten baitira. Buruan izanda konbultsio osteko erantzun hipokanpalean aktore bat baino gehiagok hartuko dutela parte, gure emaitzek argia igortzen dute React-NSC indukzioa eta neurogenesiaren galera antolatzen dituen mekanismo baten gainean. Aurkikuntza hauek bidea egiten dute beste seinalizazio ibilbide batzuetan oinarrituriko ikerketentzako, beste ErbB hartzaile batzuk barne, Zn^{+2}ak eta HB-EGFak modulatuak egon litezkeenak.

7. ONDORIOAK

7. ONDORIOAK

1. NSC helduak jaio ondoren sortuak izaten dira dNSCengandik independentea den populazio berri bat osatuz, DGaren garapenaren hondakin bezala iraun beharrean.

- NSC helduak jaio ondorengo etapa goiztiarrean zehar sortuak izaten dira cD2ren menpeko prozesu batean.

- Jaio ondorengo etapa goiztiarrean DGaren barruan kokaturik dauden sortzaileek NSC helduen erreserbara ekarpena egiten dute, DMStik datozen sortzaileak zeharo neurogenikoak diren bitartean.

- Jaio ondorengo LPA_1 espresioaren hasierak SGZan NSC helduak eta dNSCak ezberdintzen ditu.

2. Sortzaile matrizeen sorrera jarraiak (DNe, DMS, DG) ezaugarri antzekoak konpartitzen ditu giza eta sagu DGaren garapenean zehar.

- Giza haurdunaldi goiztiarraren garapenean (GW14) dNSC populazio heterogeneoek HPFko eremu ezberdinak betetzen dituzte (DNe, DMS, DG).

- Gizakietan, jaio aurretik Tbr2 espresioa duten sortzaileak eta Ki67 espresioa duten ugaritze fasean dauden zelulak hilusera mugaturik (GCLtik hurbil) agertzen dira.

- Nestin espresioa duten RGCak giza DGan mantentzen dira jaio ostean, nahiz eta ugaritze kapazitate arbuiagarria duten.

3. MTLEn gertatzen den aktibazio masiboa eta React-NSC indukzioa Zn^{+2}ek eta HB-EGFk sustatzen duten EGFRren aktibazioak erregulatzen du.

- EGFRk, baina ez FGFRk, parte hartzen du HPFan jazotzen den KA administrazioaren osteko erantzun azkarrean.

- EGFRren eta bere ur beherako seinalizazio ibilbidearen (STAT3, Akt, ERK1/2) espresioaren eta aktibazioaren areagotzea gertaera garrantzitsua da KA administrazioaren ondorengo hiru egunetan.

- Gefitinib kapaza da EGFR eta bere ur beherako seinalizazio ibilbidea den ERK1/2 NSPCetan *in vitro* inhibitzeko, euren ugaritzea era eraginkorrean blokeatuz.

- KAren osteko sudurreko Gefitinib administrazioak GCDa eta gune neurogenikoko ugaritzea murrizten ditu, hala nola NSCen aktibazioa eta transformazio erreaktiboa.

- Zn^{+2} masiboki askatua izaten da DGan KA administrazioaren ondoren, GCLean eta NSCetatik gertu akumulatuz.

- Zn^{+2}ek *in vitro* NSPCen ugaritzea estimulatu egiten du dosiaren arabera, dosi altuetan heriotza zelularra eraginez.

- Zn^{+2} injekzio intrahipokanpalak SGZan ugaritzea, GCDa eta NSCen transformazio erreaktiboa sustatzen ditu.

- Zn^{+2} administrazioak *in vitro* hazitako NSPCetan EGFRren fosforilazio zuzena eragiten du bere Y845 tirosina lekuan, baina ez Y1068 tirosina lekuan.

- Gefitiniben sudurreko administrazioak Zn^{+2} administrazio hipokanpalak sorrarazten duen SGZko ugaritze masiboa ekiditen du.

- Azal-azpiko TPEN injekzio errepikatuen bitartezko Zn^{+2} kelazioak KA administrazioak sorturiko heriotza zelularra areagotzen du, MTLE egoeran terapia potentzial bezala erabiltzeko edozein ideia baztertuz.

- KA administrazioaren ostean HB-EGF masiboki askatua izaten da DGan, MLan eta hilusean akumulatuz.

- HB-EGF administrazioak *in vitro* hazitako NSPCtan Y845 eta Y1068 EGFR tirosina kinasen eta bere ur beherako seinalizazio ibilbidea den ERK1/2ren aktibazioa biziki induzitzen du.

8. BIBLIOGRAFIA

8. BIBLIOGRAFIA

Altman, J., and Bayer, S.A. (1990). Migration and distribution of two populations of hippocampal granule cell precursors during the perinatal and postnatal periods. J. Comp. Neurol. *301*, 365–381.

Altman, J., and Das, G.D. (1965). Autoradiographic and histological evidence of postnatal hippocampal neurogenesis in rats. J Comp Neurol *124*, 319–335.

Ansorg, A., Witte, O.W., and Urbach, A. (2012). Age-dependent kinetics of dentate gyrus neurogenesis in the absence of cyclin D2. BMC Neurosci. *13*, 1–13.

Arantius, J.C. (1587). De humano foetu liber. Venetiis: Apud lacobum brechtanum.

Arnold, S.E., and Trojanowski, J.Q. (1996). Human fetal hippocampal development: I. Cytoarchitecture, myeloarchitecture, and neuronal morphologic features. J. Comp. Neurol. *367*, 274–292.

Arteaga, C.L. (2011). ERBB receptors in cancer: signaling from the inside. Breast Cancer Res. *13*, 304.

Bancila, V., Nikonenko, I., Dunant, Y., and Bloc, A. (2004). Zinc inhibits glutamate release via activation of pre-synaptic K ATP channels and reduces ischaemic damage in rat hippocampus. J. Neurochem. *90*, 1243–1250.

Barakat, N.S., Omar, S.A., and Ahmed, A.A.E. (2006). Carbamazepine uptake into rat brain following intra-olfactory transport. J. Pharm. Pharmacol. *58*, 63–72.

Berg, D.A., Su, Y., Jimenez-Cyrus, D., Patel, A., Huang, N., Morizet, D., Lee, S., Shah, R., Ringeling, F.R., Jain, R., et al. (2019). A Common Embryonic Origin of Stem Cells Drives Developmental and Adult Neurogenesis. Cell *177*, 654-668.e15.

Bessman, N.J., Freed, D.M., and Lemmon, M.A. (2014). Putting together structures of epidermal growth factor receptors. Curr. Opin. Struct. Biol. *29*, 95–101.

Biscardi, J.S., Maa, M.C., Tice, D.A., Cox, M.E., Leu, T.H., and Parsons, S.J. (1999). C-Src-mediated phosphorylation of the epidermal growth factor receptor on Tyr845 and Tyr1101 is associated with modulation of receptor function. J. Biol. Chem. *274*, 8335–8343.

Blümcke, I., Schewe, J.C., Normann, S., Brüstle, O., Schramm, J., Elger, C.E., and Wiestler, O.D. (2001). Increase of nestin-immunoreactive neural precursor cells in the dentate gyrus of pediatric patients with early-onset temporal lobe epilepsy. Hippocampus *11*, 311–321.

Bonaguidi, M.A., Wheeler, M.A., Shapiro, J.S., Stadel, R.P., Sun, G.J., Ming, G.L., and Song, H. (2011). In vivo clonal analysis reveals self-renewing and multipotent adult neural stem cell characteristics. Cell *145*, 1142–1155.

Bouilleret, V., Ridoux, V., Depaulis, A., Marescaux, C., Nehlig, A., and Le Gal La Salle, G. (1999). Recurrent seizures and hippocampal sclerosis following intrahippocampal kainate injection in adult mice: Electroencephalography, histopathology and synaptic reorganization similar to mesial temporal lobe epilepsy. Neuroscience *89*, 717–729.

Brunne, B., Franco, S., Bouché, E., Herz, J., Howell, B.W., Pahle, J., Müller, U., May, P., Frotscher, M., and Bock, H.H. (2013). Role of the postnatal erradial glial scaffold for the development of the dentate gyrus as revealed by Reelin signaling mutant mice. Glia *July*, 1347–1363.

Burgoyne, L. (1999). The Mechanisms of Pyknosis: Hypercondensation and death. Exp. Cell Res. *248*, 214–222.

Calof, A.L. (1995). Intrinsic and extrinsic factors regulating vertebrate neurogenesis. Curr. Opin. Neurobiol. *5*, 19–27.

Cameron, H.A., Woolley, C.S., McEwen, B.S., and Gould, E. (1993). Differentiation of newly born neurons and glia in the dentate gyrus of the adult rat. Neuroscience *56*, 337–344.

Carpenter, G., King, L., and Cohen, S. (1978). Epidermal growth factor stimulates phosphorylation in membrane preparations in vitro [21]. Nature *276*, 409–410.

Carrasco, J., Penkowa, M., Hadberg, H., Molinero, A., and Hidalgo, J. (2000). Enhanced seizures and hippocampal neurodegeneration following kainic acid-induced seizures in metallothionein-I + II-deficient mice. Eur. J. Neurosci. *12*, 2311–2322.

Chen, Y.M. (2013). Update of epidermal growth factor receptor-tyrosine kinase inhibitors in non-small-cell lung cancer. J. Chinese Med. Assoc. *76*, 249–257.

Cipriani, S., Journiac, N., Nardelli, J., Verney, C., Delezoide, A.L., Guimiot, F.,

Gressens, P., and Adle-Biassette, H. (2017). Dynamic Expression Patterns of Progenitor and Neuron Layer Markers in the Developing Human Dentate Gyrus and Fimbria. Cereb. Cortex *27*, 358–372.

Cipriani, S., Ferrer, I., Aronica, E., Kovacs, G.G., Verney, C., Nardelli, J., Khung, S., Delezoide, A.L., Milenkovic, I., Rasika, S., et al. (2018). Hippocampal erradial glial subtypes and their neurogenic potential in human fetuses and healthy and Alzheimer's disease adults. Cereb. Cortex *28*, 2458–2478.

Codega, P., Silva-Vargas, V., Paul, A., Maldonado-Soto, A.R., DeLeo, A.M., Pastrana, E., and Doetsch, F. (2014). Prospective Identification and Purification of Quiescent Adult Neural Stem Cells from Their In Vivo Niche. Neuron *82*, 545–559.

Cooper, J.M., Gadian, D.G., Jentschke, S., Goldman, A., Munoz, M., Pitts, G., Banks, T., Chong, W.K., Hoskote, A., Deanfield, J., et al. (2015). Neonatal hypoxia, hippocampal atrophy, and memory impairment: Evidence of a causal sequence. Cereb. Cortex *25*, 1469–1476.

Craig, C.G., Tropepe, V., Morshead, C.M., Reynolds, B.A., Weiss, S., and Van Der Kooy, D. (1996). In vivo growth factor expansion of endogenous subependymal neural precursor cell populations in the adult mouse brain. J. Neurosci. *16*, 2649–2658.

Crespel, A., Rigau, V., Coubes, P., Rousset, M.C., De Bock, F., Okano, H., Baldy-Moulinier, M., Bockaert, J., and Lerner-Natoli, M. (2005). Increased number of neural progenitors in human temporal lobe epilepsy. Neurobiol. Dis. *19*, 436–450.

Danscher, G. (1981). Histochemical demonstration of heavy metals - A revised version of the sulphide silver method suitable for both light and electronmicroscopy. Histochemistry *71*, 1–16.

Deisseroth, K., Singla, S., Toda, H., Monje, M., Palmer, T.D., and Malenka, R.C. (2004). Excitation-neurogenesis coupling in adult neural stem/progenitor cells. Neuron *42*, 535–552.

Dennis, C. V., Suh, L.S., Rodriguez, M.L., Kril, J.J., and Sutherland, G.T. (2017). Response to: Comment on 'Human adult neurogenesis across the ages: An immunohistochemical study.' Neuropathol. Appl. Neurobiol. *43*, 452–454.

Dionne, C.A., Crumley, G., Bellot, F., Kaplow, J.M., Searfoss, G., Ruta, M., Burgess,

W.H., Jaye, M., and Schlessinger, J. (1990). Cloning and expression of two distinct high-affinity receptors cross-reacting with acidic and basic fibroblast growth factors. EMBO J. *9*, 2685–2692.

Dorn, M., Lidzba, K., Bevot, A., Goelz, R., Hauser, T.K., and Wilke, M. (2014). Long-term neurobiological consequences of early postnatal hCMV-infection in former preterms: A Functional MRI study. Hum. Brain Mapp. *35*, 2594–2606.

Downward, J., Parker, P., and Waterfield, M.D. (1984). Autophosphorylation sites on the epidermal growth factor receptor. Nature *311*, 483–485.

Eckenhoff, M.F., and Rakic, P. (1984). Erradial organization of the hippocampal dentate gyrus: A Golgi, ultrastructural, and immunocytochemical analysis in the developing rhesus monkey. J. Comp. Neurol. *223*, 1–21.

Encinas, J.M., and Enikolopov, G. (2008). Identifying and Quantitating Neural Stem and Progenitor Cells in the Adult Brain. Methods Cell Biol. *85*, 243–272.

Encinas, J.M., and Sierra, A. (2012). Neural stem cell deforestation as the main force driving the age-related decline in adult hippocampal neurogenesis. Behav. Brain Res. *227*, 433–439.

Encinas, J.M., Vaahtokari, A., and Enikolopov, G. (2006). Fluoxetine targets early progenitor cells in the adult brain. Proc. Natl. Acad. Sci. U. S. A. *103*, 8233–8238.

Encinas, J.M., Michurina, T. V., Peunova, N., Park, J.H., Tordo, J., Peterson, D.A., Fishell, G., Koulakov, A., and Enikolopov, G. (2011). Division-coupled astrocytic differentiation and age-related depletion of neural stem cells in the adult hippocampus. Cell Stem Cell *8*, 566–579.

Estivill-Torrús, G., Llebrez-Zayas, P., Matas-Rico, E., Santín, L., Pedraza, C., De Diego, I., Del Arco, I., Fernández-Llebrez, P., Chun, J., and De Fonseca, F.R. (2008). Absence of LPA1 signaling results in defective cortical development. Cereb. Cortex *18*, 938–950.

Faber-Elman, A., Solomon, A., Abraham, J.A., Marikovsky, M., and Schwartz, M. (1996). Involvement of wound-associated factors in rat brain astrocyte migratory response to axonal injury: In vitro simulation. J. Clin. Invest. *97*, 162–171.

Fahrner, A., Kann, G., Flubacher, A., Heinrich, C., Freiman, T.M., Zentner, J.,

Frotscher, M., and Haas, C.A. (2007). Granule cell dispersion is not accompanied by enhanced neurogenesis in temporal lobe epilepsy patients. Exp. Neurol. *203*, 320–332.

Ferrer, I., Alcántara, S., Ballabriga, J., Olivé, M., Blanco, R., Rivera, R., Carmona, M., Berruezo, M., Pitarch, S., and Planas, A.M. (1996). Transforming growth factor-α (TGF-α) and epidermal growth factor-receptor (EGF-R) immunoreactivity in normal and pathologic brain. Prog. Neurobiol. *49*, 99–119.

Filippov, V., Kronenberg, G., Pivneva, T., Reuter, K., Steiner, B., Wang, L.P., Yamaguchi, M., Kettenmann, H., and Kempermann, G. (2003). Subpopulation of nestin-expressing progenitor cells in the adult murine hippocampus shows electrophysiological and morphological characteristics of astrocytes. Mol. Cell. Neurosci. *23*, 373–382.

Frederickson, C.J. (1989). Neurobiology of Zinc and Zinc-Containing Neurons. Int. Rev. Neurobiol. *31*, 145–238.

Frederickson, C.J., and Danscher, G. (1990). Zinc-containing neurons in hippocampus and related CNS structures. Prog. Brain Res. *83*, 71–84.

Frederickson, C.J., Klitenick, M.A., Manton, W.I., and Kirkpatrick, J.B. (1983). Cytoarchitectonic distribution of zinc in the hippocampus of man and the rat. Brain Res. *273*, 335–339.

Galichet, C., Guillemot, F., and Parras, C.M. (2008). Neurogenin 2 has an essential role in development of the dentate gyrus. Development *135*, 2031–2041.

Gall, C. (1993). Seizure-induced changes in neurotrophin expression: implications for epilepsy. Exp Neurol *124*, 150–166.

Gall, C., Lauterborn, J., Bundman, M., Murray, K., and Isackson, P. (1991). Seizures and the regulation of neurotrophic factor and neuropeptide gene expression in brain. Epilepsy Res Suppl *4*, 225–245.

de Garengeot, R.C. (1742). Splanchnologie ou, L'anatomie des viscères: avec de figures originales tirées d'apres les cadavres, suivle d'une dissertation sur l'origine de la chirurgie.

Gilley, J.A., Yang, C.P., and Kernie, S.G. (2011). Developmental profiling of postnatal dentate gyrus progenitors provides evidence for dynamic cell-autonomous regulation.

Hippocampus *21*, 33–47.

Goffin, J.R., and Zbuk, K. (2013). Epidermal growth factor receptor: Pathway, therapies, and pipeline. Clin. Ther. *35*, 1282–1303.

Golgi, C. (1886). Sulla fina anatomia degli organi centrali di sistema nervoso. V. Sulla anatomia di grande piede d'Hippocampo.

Gomez-Nicola, D., Riecken, K., Fehse, B., and Perry, V.H. (2014). In-vivo RGB marking and multicolour single-cell tracking in the adult brain. Sci. Rep. *4*, 1–10.

Gonçalves, J.T., Schafer, S.T., and Gage, F.H. (2016). Adult Neurogenesis in the Hippocampus: From Stem Cells to Behavior. Cell *167*, 897–914.

Gong, S., Zheng, C., Doughty, M.L., Losos, K., Didkovsky, N., Schambra, U.B., Nowak, N.J., Joyner, A., Leblanc, G., Hatten, M.E., et al. (2003). A gene expression atlas of the central nervous system based on bacterial artificial chromosomes. Nature *425*, 917–925.

Gould, E., Cameron, H.A., Daniels, D.C., Woolley, C.S., and McEwen, B.S. (1992). Adrenal hormones suppress cell division in the adult rat dentate gyrus. J. Neurosci. *12*, 3642–3650.

Gould, E., McEwen, B.S., Tanapat, P., Galea, L.A.M., and Fuchs, E. (1997). Neurogenesis in the dentate gyrus of the adult tree shrew is regulated by psychosocial stress and NMDA receptor activation. J. Neurosci. *17*, 2492–2498.

Gould, E., Reeves, A.J., Fallah, M., Tanapat, P., Gross, C.G., and Fuchs, E. (1999a). Hippocampal neurogenesis in adult Old World primates. Proc. Natl. Acad. Sci. U. S. A. *96*, 5263–5267.

Gould, E., Beylin, A., Tanapat, P., Reeves, A., and Shors, T.J. (1999b). Learning enhances adult neurogenesis in the hippocampal formation. Nat. Neurosci. *2*, 260–265.

Gould, E., Reeves, A.J., Graziano, M.S.A., and Gross, C.G. (1999c). Neurogenesis in the neocortex of adult primates. Science (80-.). *286*, 548–552.

Gray, W.P., and Sundstrom, L.E. (1998). Kainic acid increases the proliferation of granule cell progenitors in the dentate gyrus of the adult rat. Brain Res. *790*, 52–59.

Hanson, L.R., Fine, J.M., Svitak, A.L., and Faltesek, K.A. (2013). Intranasal administration of CNS therapeutics to awake mice. J. Vis. Exp. 2–7.

Hattiangady, B., Rao, M.S., and Shetty, A.K. (2004). Chronic temporal lobe epilepsy is associated with severely declined dentate neurogenesis in the adult hippocampus. Neurobiol. Dis. *17*, 473–490.

Heinrich, C., Nitta, N., Flubacher, A., Müller, M., Fahrner, A., Kirsch, M., Freiman, T., Suzuki, F., Depaulis, A., Frotscher, M., et al. (2006). Reelin deficiency and displacement of mature neurons, but not neurogenesis, underlie the formation of granule cell dispersion in the epileptic hippocampus. J. Neurosci. *26*, 4701–4713.

Herbst, R.S. (2004). Review of epidermal growth factor receptor biology. Int. J. Radiat. Oncol. Biol. Phys. *59*, S21–S26.

Hochgerner, H., Zeisel, A., Lönnerberg, P., and Linnarsson, S. (2018). Conserved properties of dentate gyrus neurogenesis across postnatal development revealed by single-cell RNA sequencing. Nat. Neurosci. *21*, 290–299.

Hodge, R.D., Kowalczyk, T.D., Wolf, S.A., Encinas, J.M., Rippey, C., Enikolopov, G., Kempermann, G., and Hevner, R.F. (2008). Intermediate progenitors in adult hippocampal neurogenesis: Tbr2 expression and coordinate regulation of neuronal output. J. Neurosci. *28*, 3707–3717.

Hodge, R.D., Nelson, B.R., Kahoud, R.J., Yang, R., Mussar, K.E., Reiner, S.L., and Hevner, R.F. (2012). Tbr2 is essential for hippocampal lineage progression from neural stem cells to intermediate progenitors and neurons. J. Neurosci. *32*, 6275–6287.

Hodge, R.D., Garcia, A.J., Elsen, G.E., Nelson, B.R., Mussar, K.E., Reiner, S.L., Ramirez, J.M., and Hevner, R.F. (2013). Tbr2 expression in Cajal-Retzius cells and intermediate neuronal progenitors is required for morphogenesis of the dentate gyrus. J. Neurosci. *33*, 4165–4180.

Houser, C.R. (1990). Granule cell dispersion in the dentate gyrus of humans with temporal lobe epilepsy. Brain Res. *535*, 195–204.

Humphrey, T. (1967). The development of the human hippocampal fissure. J. Anat. *101*, 655–676.

Hüttmann, K., Sadgrove, M., Wallraff, A., Hinterkeuser, S., Kirchhoff, F., Steinhäuser,

C., and Gray, W.P. (2003). Seizures preferentially stimulate proliferation of erradial glia-like astrocytes in the adult dentate gyrus: Functional and immunocytochemical analysis. Eur. J. Neurosci. *18*, 2769–2778.

Iglesias, J.E., Augustinack, J.C., Nguyen, K., Player, C.M., Player, A., Wright, M., Roy, N., and Frosch, M.P. (2015). A computational atlas of the hippocampal formation using ex vivo , ultra-high resolution MRI. Neuroimage 115–137.

Jhaveri, T.Z., Woo, J., Shang, X., Park, B.H., and Gabrielson, E. (2015). AMP-activated kinase (AMPK) regulates activity of HER2 and EGFR in breast cancer. Oncotarget *6*, 14754–14765.

Jia, M., Shi, Z., Yan, X., Xu, L., Dong, L., Li, J., Wang, Y., Yang, S., and Yuan, F. (2018). Insulin and heparin-binding epidermal growth factor-like growth factor synergistically promote astrocyte survival and proliferation in serum-free medium. J. Neurosci. Methods *307*, 240–247.

Jiang, M., Polepalli, J., Chen, L.Y., Zhang, B., Südhof, T.C., and Malenka, R.C. (2017). Conditional ablation of neuroligin-1 in CA1 pyramidal neurons blocks LTP by a cell-autonomous NMDA receptor-independent mechanism. Mol. Psychiatry *22*, 375–383.

Johnson, D.E., Lee, P.L., Lu, J., and Williams, L.T. (1990). Diverse forms of a receptor for acidic and basic fibroblast growth factors. Mol. Cell. Biol. *10*, 4728–4736.

Kägi, J.H.R., and Schäffer, A. (1988). Biochemistry of Metallothionein. Biochemistry *27*, 8509–8515.

Kambe, T., Tsuji, T., Hashimoto, A., and Itsumura, N. (2015). The physiological, biochemical, and molecular roles of zinc transporters in zinc homeostasis and metabolism. Physiol. Rev. *95*, 749–784.

Kaplan, M.S., and Bell, D.H. (1984). Mitotic neuroblasts in the 9-day-old and 11-month-old rodent hippocampus. J. Neurosci. *4*, 1429–1441.

Kasarskis, E.J., Forrester, T.M., and Slevin, J.T. (1987). Amygdalar kindling is associated with elevated zinc concentration in the cortex and hippocampus of rats. Epilepsy Res. *1*, 227–233.

Kempermann, G., Jessberger, S., Steiner, B., and Kronenberg, G. (2004). Milestones of neuronal development in the adult hippocampus. Trends Neurosci. *27*, 447–452.

Kim, J.H., Jang, B.G., Choi, B.Y., Kwon, L.M., Sohn, M., Song, H.K., and Suh, S.W. (2012). Zinc Chelation Reduces Hippocampal Neurogenesis after Pilocarpine-Induced Seizure. PLoS One *7*, 1–10.

Knoth, R., Singec, I., Ditter, M., Pantazis, G., Capetian, P., Meyer, R.P., Horvat, V., Volk, B., and Kempermann, G. (2010). Murine features of neurogenesis in the human hippocampus across the lifespan from 0 to 100 years. PLoS One *5*.

Kornack, D.R., and Rakic, P. (1999). Continuation of neurogenesis in the hippocampus of the adult macaque monkey. Proc. Natl. Acad. Sci. U. S. A. *96*, 5768–5773.

Kornack, D.R., and Rakic, P. (2001). The generation, migration, and differentiation of olfactory neurons in the adult primate brain. Proc. Natl. Acad. Sci. U. S. A. *98*, 4752–4757.

Kornblum, H.I., Zurcher, S.D., Werb, Z., Derynck, R., and Seroogy, K.B. (1999). Multiple trophic actions of heparin-binding epidermal growth factor (HB-EGF) in the central nervous system. Eur. J. Neurosci. *11*, 3236–3246.

Kosaka, T., and Hama, K. (1986). Three-dimensional structure of astrocytes in the rat dentate gyrus. J. Comp. Neurol. *249*, 242–260.

Kovacs, E., Zorn, J.A., Huang, Y., Barros, T., and Kuriyan, J. (2015). A Structural Perspective on the Regulation of the Epidermal Growth Factor Receptor. Annu. Rev. Biochem. *84*, 739–764.

Kralic, J.E., Ledergerber, D.A., and Fritschy, J.M. (2005). Disruption of the neurogenic potential of the dentate gyrus in a mouse model of temporal lobe epilepsy with focal seizures. Eur. J. Neurosci. *22*, 1916–1927.

Kraus, M.H., Issing, W., Miki, T., Popescu, N.P., and Aaronson, S.A. (1989). Isolation and characterization of ERBB3, a third member of the ERBB/epidermal growth factor receptor family: Evidence for overexpression in a subset of human mammary tumors. Proc. Natl. Acad. Sci. U. S. A. *86*, 9193–9197.

Kronenberg, G., Reuter, K., Steiner, B., Brandt, M.D., Jessberger, S., Yamaguchi, M., and Kempermann, G. (2003). Subpopulations of Proliferating Cells of the Adult Hippocampus Respond Differently to Physiologic Neurogenic Stimuli. J. Comp. Neurol. *467*, 455–463.

Kruglyakova, E.P., Khovryakov, A. V., Shikhanov, N.P., MacCann, G.M., Vaél', I., Kruglyakov, P.P., and Sosunov, A.A. (2005). Nestin-expressing cells in the human hippocampus. Neurosci. Behav. Physiol. *35*, 891–897.

Kuhn, H.G., Dickinson-Anson, H., and Gage, F.H. (1996). Neurogenesis in the dentate gyrus of the adult rat: Age-related decrease of neuronal progenitor proliferation. J. Neurosci. *16*, 2027–2033.

Kuhn, H.G., Winkler, J., Kempermann, G., Thal, L.J., and Gage, F.H. (1997). Epidermal growth factor and fibroblast growth factor-2 have different effects on neural progenitors in the adult rat brain. J. Neurosci. *17*, 5820–5829.

Kuruba, R., and Shetty, A. (2007). Could hippocampal neurogenesis be a future drug target for treating temporal lobe epilepsy? CNS Neurol Disord Drug Targets *6*, 342–357.

Lee, J., Auyeung, W.W., and Mattson, M.P. (2003). Interactive Effects of Excitotoxic Injury and Dietary Restriction on Microgliosis and Neurogenesis in the Hippocampus of Adult Mice. NeuroMolecular Med. *4*, 179–195.

Lee, J.C., Vivanco, I., Beroukhim, R., Huang, J.H.Y., Feng, W.L., DeBiasi, R.M., Yoshimoto, K., King, J.C., Nghiemphu, P., Yuza, Y., et al. (2006). Epidermal growth factor receptor activation in glioblastoma through novel missense mutations in the extracellular domain. PLoS Med. *3*, 2264–2273.

Lendahl, U., Zimmerman, L.B., and McKay, R.D.G. (1990). CNS stem cells express a new class of intermediate filament protein. Cell *60*, 585–595.

Levenson, C.W., and Morris, D. (2011). 22332038.Pdf. 96–100.

Li, D., Ambrogio, L., Shimamura, T., Kubo, S., Takahashi, M., Chirieac, L.R., Padera, R.F., Shapiro, G.I., Baum, A., Himmelsbach, F., et al. (2008). BIBW2992, an irreversible EGFR/HER2 inhibitor highly effective in preclinical lung cancer models. Oncogene *27*, 4702–4711.

Li, D., Takeda, N., Jain, R., Manderfield, L.J., Liu, F., Li, L., Anderson, S.A., and Epstein, J.A. (2015). Hopx distinguishes hippocampal from lateral ventricle neural stem cells. Stem Cell Res. *15*, 522–529.

Li, G., Kataoka, H., Coughlin, S.R., and Pleasure, S.J. (2009). Identification of a

transient subpial neurogenic zone in the developing dentate gyrus and its regulation by Cxcl12 and reelin signaling. Development *136*, 327–335.

Li, G., Fang, L., Fernández, G., and Pleasure, S.J. (2013). The ventral hippocampus is the embryonic origin for adult neural stem cells in the dentate gyrus. Neuron *78*, 658–672.

Li, Z.W., Li, J.J., Wang, L., Zhang, J.P., Wu, J.J., Mao, X.Q., Shi, G.F., Wang, Q., Wang, F., and Zou, J. (2014). Epidermal growth factor receptor inhibitor ameliorates excessive astrogliosis and improves the regeneration microenvironment and functional recovery in adult rats following spinal cord injury. J. Neuroinflammation *11*, 1–16.

Libermann, T., Nusbaum, H., Razon, N., Kris, R., Lax, I., Soreq, H., Whittle, N., Waterfield, M., Ullrich, A., and Schlessinger, J. (1985). Am Plification and Overexpression of T H E Egf R Ec Epto R Gene in Primary Hum an. J Cell Sci *3*, 161–172.

Lill, N.L., and Sever, N.I. (2012). Where EGF receptors transmit their signals. Sci. Signal. *5*.

Lin, S.Y., Makino, K., Xia, W., Matin, A., Wen, Y., Kwong, K.Y., Bourguignon, L., and Hung, M.C. (2001). Nuclear localization of EGF receptor and its potential new role as a transcription factor. Nat. Cell Biol. *3*, 802–808.

Liu, J.Y.W., Matarin, M., Reeves, C., McEvoy, A.W., Miserocchi, A., Thompson, P., Sisodiya, S.M., and Thom, M. (2018). Doublecortin-expressing cell types in temporal lobe epilepsy. Acta Neuropathol. Commun. *6*, 60.

López-García, C., Varea, E., Palop, J.J., Nacher, J., Ramirez, C., Ponsoda, X., and Molowny, A. (2002). Cytochemical techniques for zinc and heavy metals localization in nerve cells. Microsc. Res. Tech. *56*, 318–331.

Lorente de Nó, R. (1934). Studies on the strcuture of the cerebral cortex. II. Continuation of the study of the ammonic system. J Psychol Neurol *46*, 113–177.

Lugert, S., Basak, O., Knuckles, P., Haussler, U., Fabel, K., Götz, M., Haas, C.A., Kempermann, G., Taylor, V., and Giachino, C. (2010). Quiescent and active hippocampal neural stem cells with distinct morphologies respond selectively to physiological and pathological stimuli and aging. Cell Stem Cell *6*, 445–456.

Luzuriaga, J., Pineda, J.R., Irastorza, I., Uribe-Etxebarria, V., García-Gallastegui, P., Encinas, J.M., Chamero, P., Unda, F., and Ibarretxe, G. (2019). BDNF and NT3 reprogram human ectomesenchymal dental pulp stem cells to neurogenic and gliogenic neural crest progenitors cultured in serum-free medium. Cell. Physiol. Biochem. *52*, 1361–1380.

Maret, W. (2017). Zinc in cellular regulation: The nature and significance of “zinc signals.” Int. J. Mol. Sci. *18*.

Marucci, G. (2017). Commentary on human adult neurogenesis across the ages: An immunohistochemical study. Neuropathol. Appl. Neurobiol. *43*, 450–451.

Maske, H. (1955). Über den topochemischen Nachweis von Zink im Ammonshorn verschiedener Säugetiere. Naturwissenschaften *42*, 424.

Matas-Rico, E., García-Diaz, B., Llebrez-Zayas, P., López-Barroso, D., Santín, L., Pedraza, C., Smith-Fernández, A., Fernández-Llebrez, P., Tellez, T., Redondo, M., et al. (2008). Deletion of lysophosphatidic acid receptor LPA1 reduces neurogenesis in the mouse dentate gyrus. Mol. Cell. Neurosci. *39*, 342–355.

Matsue, K., Minakawa, S., Kashiwagi, T., Toda, K., Sato, T., Shioda, S., and Seki, T. (2018). Dentate granule progenitor cell properties are rapidly altered soon after birth. Brain Struct. Funct. *223*, 357–369.

Matsushime, H., Ewen, M.E., Strom, D.K., Kato, J.Y., Hanks, S.K., Roussel, M.F., and Sherr, C.J. (1992). Identification and properties of an atypical catalytic subunit (p34PSK-J3/cdk4) for mammalian D type G1 cyclins. Cell *71*, 323–334.

McKillop, D., Hutchison, M., Partridge, E.A., Bushby, N., Cooper, C.M.F., Clarkson-Jones, J.A., Herron, W., and Swaisland, H.C. (2004). Metabolic disposition of gefitinib, an epidermal growth factor receptor tyrosine kinase inhibitor, in rat, dog and man. Xenobiotica *34*, 917–934.

Meloche, S., and Pouysségur, J. (2007). The ERK1/2 mitogen-activated protein kinase pathway as a master regulator of the G1- to S-phase transition. Oncogene *26*, 3227–3239.

Meyerson, M., and Harlow, E. (1994). Identification of G1 kinase activity for cdk6, a novel cyclin D partner. Mol. Cell. Biol. *14*, 2077–2086.

Mignone, J.L., Kukekov, V., Chiang, A.S., Steindler, D., and Enikolopov, G. (2004). Neural Stem and Progenitor Cells in Nestin-GFP Transgenic Mice. J. Comp. Neurol. *469*, 311–324.

Mody, I., and Miller, J.J. (1985). Levels of hippocampal calcium and zinc following kindling-induced epilepsy. Can. J. Physiol. Pharmacol. *63*, 159–161.

Moreno-Jiménez, E.P., Flor-García, M., Terreros-Roncal, J., Rábano, A., Cafini, F., Pallas-Bazarra, N., Ávila, J., and Llorens-Martín, M. (2019). Adult hippocampal neurogenesis is abundant in neurologically healthy subjects and drops sharply in patients with Alzheimer's disease. Nat. Med. *25*, 554–560.

Muro-García, T., Martín-Suárez, S., Espinosa, N., Valcárcel-Martín, R., Marinas, A., Zaldumbide, L., Galbarriatu, L., Sierra, A., Fuentealba, P., and Encinas, J.M. (2019). Reactive Disruption of the Hippocampal Neurogenic Niche After Induction of Seizures by Injection of Kainic Acid in the Amygdala. Front. Cell Dev. Biol. *7*, 1–14.

Nakahira, E., and Yuasa, S. (2005). Neuronal generation, migration, and differentiation in the mouse hippocampal primoridium as revealed by enhanced green fluorescent protein gene transfer by means of in utero electroporation. J. Comp. Neurol. *483*, 329–340.

Namba, T., Mochizuki, H., Onodera, M., Mizuno, Y., Namiki, H., and Seki, T. (2005). The fate of neural progenitor cells expressing astrocytic and erradial glial markers in the postnatal rat dentate gyrus. Eur. J. Neurosci. *22*, 1928–1941.

Nicholson, R.I., Gee, J.M.W., and Harper, M.E. (2001). EGFR and cancer prognosis. Eur. J. Cancer *37*, 9.

Nicola, Z., Fabel, K., and Kempermann, G. (2015). Development of the adult neurogenic niche in the hippocampus of mice. Front. Neuroanat. *9*, 1–13.

Nieto-Sampedro, M., Gómez-Pinilla, F., Knauer, D.J., and Broderick, J.T. (1988). Epidermal growth factor receptor immunoreactivity in rat brain astrocytes. Response to injury. Neurosci. Lett. *91*, 276–282.

Nowakowski, R.S. (2000). New Neurons: Extraordinary Evidence or Extraordinary Conclusion? Science (80-.). *288*, 771a – 771.

Opanashuk, L.A., Mark, R.J., Porter, J., Damm, D., Mattson, M.P., and Seroogy, K.B.

(1999). Heparin-binding epidermal growth factor-like growth factor in hippocampus: Modulation of expression by seizures and anti-excitotoxic action. J. Neurosci. *19*, 133–146.

Palmer, T.D., Ray, J., and Gage, F.H. (1995). FGF-2-responsive neuronal progenitors reside in proliferative and quiescent regions of the adult rodent brain. Mol. Cell. Neurosci. *6*, 474–486.

Pastrana, E., Cheng, L.C., and Doetsch, F. (2009). Simultaneous prospective purification of adult subventricular zone neural stem cells and their progeny. Proc. Natl. Acad. Sci. U. S. A. *106*, 6387–6392.

Pedersen, M.W., Pedersen, N., Ottesen, L.H., and Poulsen, H.S. (2005). Differential response to gefitinib of cells expressing normal EGFR and the mutant EGFRvIII. Br. J. Cancer *93*, 915–923.

Pencea, V., Bingaman, K.D., Freedman, L.J., and Luskin, M.B. (2001). Neurogenesis in the subventricular zone and rostral migratory stream of the neonatal and adult primate forebrain. Exp. Neurol. *172*, 1–16.

Pilz, G.A., Bottes, S., Betizeau, M., Jörg, D.J., Carta, S., Simons, B.D., Helmchen, F., and Jessberger, S. (2018). Live imaging of neurogenesis in the adult mouse hippocampus. Science (80-.). *359*, 658–662.

Pineda, J.R., Daynac, M., Chicheportiche, A., Cebrian-Silla, A., Sii Felice, K., Garcia-Verdugo, J.M., Boussin, F.D., and Mouthon, M.A. (2013). Vascular-derived TGF-β increases in the stem cell niche and perturbs neurogenesis during aging and following irradiation in the adult mouse brain. EMBO Mol. Med. *5*, 548–562.

Pleasure, S.J., Collins, A.E., and Lowenstein, D.H. (2000). Unique expression patterns of cell fate molecules delineate sequential stages of dentate gyrus development. J. Neurosci. *20*, 6095–6105.

Plowman, G.D., Whitney, G.S., Neubauer, M.G., Green, J.M., McDonald, V.L., Todaro, G.J., and Shoyab, M. (1990). Molecular cloning and expression of an additional epidermal growth factor receptor-related gene. Proc. Natl. Acad. Sci. U. S. A. *87*, 4905–4909.

Priego, N., Zhu, L., Monteiro, C., Mulders, M., Wasilewski, D., Bindeman, W., Doglio,

L., Martínez, L., Martínez-Saez, E., Cajal, S.R.Y., et al. (2018). STAT3 labels a subpopulation of reactive astrocytes required for brain metastasis article. Nat. Med. *24*, 1024–1035.

Puschmann, T.B., Zandén, C., Lebkuechner, I., Philippot, C., De Pablo, Y., Liu, J., and Pekny, M. (2014). HB-EGF affects astrocyte morphology, proliferation, differentiation, and the expression of intermediate filament proteins. J. Neurochem. *128*, 878–889.

Qu, W. sheng, Tian, D. shi, Guo, Z. bao, Fang, J., Zhang, Q., Yu, Z. yuan, Xie, M. jie, Zhang, H. qiu, Lü, J. gao, and Wang, W. (2012). Inhibition of EGFR/MAPK signaling reduces microglial inflammatory response and the associated secondary damage in rats after spinal cord injury. J. Neuroinflammation *9*, 1–14.

Ramón y Cajal, S. (1893). Estructura del asta de Ammon. Anal Soc. Español Hist. Nat. *22*.

Ramón y Cajal, S. (1911). Histologie du système nerveux de l'homme et des vertébrés.

Rees, S., and Inder, T. (2005). Fetal and neonatal origins of altered brain development. Early Hum. Dev. *81*, 753–761.

Reynolds, B.A., and Weiss, S. (1992). Generation of neurons and astrocytes from isolated cells of the adult mammalian central nervous system. Science (80-.). *255*, 1707–1710.

Reynolds, B.A., Tetzlaff, W., and Weiss, S. (1992). A multipotent EGF-responsive striatal embryonic progenitor cell produces neurons and astrocytes. J. Neurosci. *12*, 4565–4574.

Rickmann, M., Amaral, D.G., and Cowan, W.M. (1987). Organization of erradial glial cells during the development of the rat dentate gyrus. J. Comp. Neurol. *264*, 449–479.

Riese, D.J., and Stern, D.F. (1998). Specificity within the EGF family/ErbB receptor family signaling network. BioEssays *20*, 41–48.

Río, C., Pérez-Cerdá, F., Matute, C., and Nieto-Sampedro, M. (1995). Preparation of a monoclonal antibody to a glycidic epitope of the epidermal growth factor receptor that recognizes inhibitors of astrocyte proliferation and reactive microglia. J. Neurosci. Res. *40*, 776–786.

Rodriguez, A., Ehlenberger, D.B., Hof, P.R., and Wearne, S.L. (2006). Rayburst sampling, an algorithm for automated three-dimensional shape analysis from laser scanning microscopy images. Nat. Protoc. *1*, 2152–2161.

Salomon, D.S., Brandt, R., Ciardiello, F., and Normanno, N. (1995). Epidermal growth factor-related peptides and their receptors in human malignancies. Crit. Rev. Oncol. Hematol. *19*, 183–232.

Samet, J.M., Dewar, B.J., Wu, W., and Graves, L.M. (2003). Mechanisms of Zn2+-induced signal initiation through the epidermal growth factor receptor. Toxicol. Appl. Pharmacol. *191*, 86–93.

Sandstead, H.H. (2012). Subclinical zinc deficiency impairs human brain function. J. Trace Elem. Med. Biol. *26*, 70–73.

Sandstead, H.H., Frederickson, C.J., and Penland, J.G. (2000). History of Zinc as Related to Brain Function. J. Nutr. *130*, 496S-502S.

Sasaki, H., Shimizu, S., Okuda, K., Kawano, O., Yukiue, H., Yano, M., and Fujii, Y. (2009). Epidermal growth factor receptor gene amplification in surgical resected Japanese lung cancer. Lung Cancer *64*, 295–300.

Sato, K.I., Sato, A., Aoto, M., and Fukami, Y. (1995). c-SRC phosphorylates epidermal growth factor receptor on tyrosine 845. Biochem. Biophys. Res. Commun. *215*, 1078–1087.

Segi-Nishida, E., Warner-Schmidt, J.L., and Duman, R.S. (2008). Electroconvulsive seizure and VEGF increase the proliferation of neural stem-like cells in rat hippocampus. Proc. Natl. Acad. Sci. U. S. A. *105*, 11352–11357.

Seki, T., and Arai, Y. (1993). Highly polysialylated neural cell adhesion molecule (NCAM-H) is expressed by newly generated granule cells in the dentate gyrus of the adult rat. J. Neurosci. *13*, 2351–2358.

Seki, T., Sato, T., Toda, K., Osumi, N., Imura, T., and Shioda, S. (2014). Distinctive population of Gfap-expressing neural progenitors arising around the dentate notch migrate and form the granule cell layer in the developing hippocampus. J. Comp. Neurol. *522*, 261–283.

Seki, T., Hori, T., Miyata, H., Maehara, M., and Namba, T. (2019). Analysis of

proliferating neuronal progenitors and immature neurons in the human hippocampus surgically removed from control and epileptic patients. Sci. Rep. *9*, 1–14.

Semba, K., Toyoshima, K., and Yamamoto, T. (1985). c-erbB-1/epidermal growth factor-receptor. *82*, 6497–6501.

Seress, L. (1988). Interspecies comparison of the hippocampal formation shows increased emphasis on the regio superior in the Ammon's horn of the human brain. J Hirnforsch *29*, 335–340.

Seress, L., Gulyás, A.I., and Freund, T.F. (1992). Pyramidal neurons are immunoreactive for calbindin D28k in the CA1 subfield of the human hippocampus. Neurosci. Lett. *138*, 257–260.

Seress, L., Ábrahám, H., Tornóczky, T., and Kosztolányi, G. (2001). Cell formation in the human hippocampal formation from mid-gestation to the late postnatal period. Neuroscience *105*, 831–843.

Seri, B., García-Verdugo, J.M., McEwen, B.S., and Alvarez-Buylla, A. (2001). Astrocytes give rise to new neurons in the adult mammalian hippocampus. J. Neurosci. *21*, 7153–7160.

Sharma, S. V., Bell, D.W., Settleman, J., and Haber, D.A. (2007). Epidermal growth factor receptor mutations in lung cancer. Nat. Rev. Cancer *7*, 169–181.

Sherr, C.J. (1995). Mammalian G1 cyclins and cell cycle progression. Proc. Assoc. Am. Physicians *107*, 181–186.

Shin, J., Berg, D.A., Zhu, Y., Shin, J.Y., Song, J., Bonaguidi, M.A., Enikolopov, G., Nauen, D.W., Christian, K.M., Ming, G.L., et al. (2015). Single-Cell RNA-Seq with Waterfall Reveals Molecular Cascades underlying Adult Neurogenesis. Cell Stem Cell *17*, 360–372.

Sierra, A., Martín-Suárez, S., Valcárcel-Martín, R., Pascual-Brazo, J., Aelvoet, S.A., Abiega, O., Deudero, J.J., Brewster, A.L., Bernales, I., Anderson, A.E., et al. (2015). Neuronal hyperactivity accelerates depletion of neural stem cells and impairs hippocampal neurogenesis. Cell Stem Cell *16*, 488–503.

Silvestre, F., Fissore, R.A., Tosti, E., and Boni, R. (2012). [Ca2+]i rise at in vitro maturation in bovine cumulus-oocyte complexes. Mol. Reprod. Dev. *79*, 369–379.

Simpson, D.L., Morrison, R., de Vellis, J., and Herschman, H.R. (1982). Epidermal growth factor binding and mitogenic activity on purified populations of cells from the central nervous system. J. Neurosci. Res. *8*, 453–462.

Sindreu, C.B., Varoqui, H., Erickson, J.D., and Pérez-Clausell, J. (2003). Boutons containing vesicular zinc define a subpopulation of synapses with low AMPAR content in rat hippocampus. Cereb. Cortex *13*, 823–829.

Slomianka, L. (1992). Neurons of origin of zinc-containing pathways and the distribution of zinc-containing boutons in the hippocampal region of the rat. Neuroscience *48*, 325–352.

Sofroniew, M. V. (2009). Molecular dissection of reactive astrogliosis and glial scar formation. Trends Neurosci. *32*, 638–647.

Sorrells, S.F., Paredes, M.F., Cebrian-Silla, A., Sandoval, K., Qi, D., Kelley, K.W., James, D., Mayer, S., Chang, J., Auguste, K.I., et al. (2018). Human hippocampal neurogenesis drops sharply in children to undetectable levels in adults. Nature *555*, 377–381.

Sugiyama, T., Osumi, N., and Katsuyama, Y. (2013). The germinal matrices in the developing dentate gyrus are composed of neuronal progenitors at distinct differentiation stages. Dev. Dyn. *242*, 1442–1453.

Takeda, A., and Tamano, H. (2009). Insight into zinc signaling from dietary zinc deficiency. Brain Res. Rev. *62*, 33–44.

Takeda, A., Minami, A., Seki, Y., and Oku, N. (2003). Inhibitory function of zinc against excitation of hippocampal glutamatergic neurons. Epilepsy Res. *57*, 169–174.

Tice, D.A., Biscardi, J.S., Nickles, A.L., and Parsons, S.J. (1999). Mechanism of biological synergy between cellular Src and epidermal growth factor receptor. Proc. Natl. Acad. Sci. U. S. A. *96*, 1415–1420.

Tropepe, V., Sibilia, M., Ciruna, B.G., Rossant, J., Wagner, E.F., and Van Der Kooy, D. (1999). Distinct neural stem cells proliferate in response to EGF and FGF in the developing mouse telencephalon. Dev. Biol. *208*, 166–188.

Ullrich, A., Coussens, L., Hayflick, J.S., Dull, T.J., Gray, A., Tam, A.W., Lee, J., Yarden, Y., Libermann, T.A., Schlessinger, J., et al. (1984). Human epidermal growth factor

receptor cDNA sequence and aberrant expression of the amplified gene in A431 epidermoid carcinoma cells. Nature *309*, 418–425.

Valcárcel-Martín, R., Martín-Suárez, S., Muro-García, T., Pastor-Alonso, O., Rodríguez de Fonseca, F., Estivill-Torrús, G., and Encinas, J.M. (2020). Lysophosphatidic acid receptor 1 specifically labels seizure-induced hippocampal reactive neural stem cells and controls their division. Front. Neurosci. - Neurogenes. *August*.

Vašák, M., and Hasler, D.W. (2000). Metallothioneins: New functional and structural insights. Curr. Opin. Chem. Biol. *4*, 177–183.

Verwer, R.W.H., Sluiter, A.A., Balesar, R.A., Baaijen, J.C., De Witt Hamer, P.C., Speijer, D., Li, Y., and Swaab, D.F. (2015). Injury Response of Resected Human Brain Tissue in Vitro. Brain Pathol. *25*, 454–468.

Vivanco, I., Ian Robins, H., Rohle, D., Campos, C., Grommes, C., Nghiemphu, P.L., Kubek, S., Oldrini, B., Chheda, M.G., Yannuzzi, N., et al. (2012). Differential sensitivity of glioma- versus lung cancer-specific EGFR mutations to EGFR kinase inhibitors. Cancer Discov. *2*, 458–471.

Wakeling, A.E., Guy, S.P., Woodburn, J.R., Ashton, S.E., Curry, B.J., Barker, A.J., and Gibson, K.H. (2002). ZD1839 (Iressa): An orally active inhibitor of epidermal growth factor signaling with potential for cancer therapy. Cancer Res. *62*, 5749–5754.

Van Der Wal, E.A., Gómez-Pinilla, F., and Cotman, C.W. (1994). Seizure-associated induction of basic fibroblast growth factor and its receptor in the rat brain. Neuroscience *60*, 311–323.

Walker, T.L., Overall, R.W., Vogler, S., Sykes, A.M., Ruhwald, S., Lasse, D., Ichwan, M., Fabel, K., and Kempermann, G. (2016). Lysophosphatidic Acid Receptor Is a Functional Marker of Adult Hippocampal Precursor Cells. Stem Cell Reports *6*, 552–565.

Watanabe, M., Oizumi, S., Kiuchi, S., Yamada, N., Yokouchi, H., Fukumoto, S., and Harada, M. (2018). The effectiveness of afatinib in a patient with advanced lung adenocarcinoma harboring rare G719X and S768I mutations. Intern. Med. *57*, 993–996.

Weber, K., Thomaschewski, M., Benten, D., and Fehse, B. (2012). RGB marking with

lentiviral vectors for multicolor clonal cell tracking. Nat. Protoc. *7*, 839–849.

Wu, W., Samet, J.M., Silbajoris, R., Dailey, L.A., Sheppard, D., Bromberg, P.A., and Graves, L.M. (2004). Heparin-binding epidermal growth factor cleavage mediates zinc-induced epidermal growth factor receptor phosphorylation. Am. J. Respir. Cell Mol. Biol. *30*, 540–547.

Xu, W., Morishita, W., Buckmaster, P.S., Pang, Z.P., Malenka, R.C., and Südhof, T.C. (2012). Distinct Neuronal Coding Schemes in Memory Revealed by Selective Erasure of Fast Synchronous Synaptic Transmission. Neuron *73*, 990–1001.

Yamaguchi, M., Saito, H., Suzuki, M., and Mori, K. (2000). Visualization of neurogenesis in the central nervous system using nestin promoter-GFP transgenic mice. Neuroreport *11*, 1991–1996.

Yang, J.C.H., Sequist, L. V., Geater, S.L., Tsai, C.M., Mok, T.S.K., Schuler, M., Yamamoto, N., Yu, C.J., Ou, S.H.I., Zhou, C., et al. (2015). Clinical activity of afatinib in patients with advanced non-small-cell lung cancer harbouring uncommon EGFR mutations: A combined post-hoc analysis of LUX-Lung 2, LUX-Lung 3, and LUX-Lung 6. Lancet Oncol. *16*, 830–838.

Yang, P., Zhang, J., Shi, H., Zhang, J., Xu, X., Xiao, X., and Liu, Y. (2014). Developmental profile of neurogenesis in prenatal human hippocampus: An immunohistochemical study. Int. J. Dev. Neurosci. *38*, 1–9.

Yarden, Y., and Sliwkowski, M.X. (2001). Untangling the ErbB signalling network. Nat. Rev. Mol. Cell Biol. *2*, 127–137.

BIBLIOGRAFIA

Hipokanpoko NSCak: Garapenetik Patologiara